Imperial College London

SHOCKWAVE FOR ABROGATION OF HEART FAILURE IN ISCHAEMIA-REPERFUSION INJURY

Dr Salomon Narodden
[Dr Mohamad Noorsalomon Narodden]

National Heart and Lung Institute
Faculty of Medicine
Imperial College London

A thesis submitted for the Clinical Medicine Research Degree of Doctor of Philosophy

Copyright Notice

The thesis is a work for a doctoral academic degree

Thesis design by Salomon Narodden

Published by Salomon Narodden

Dedication

This thesis is wholeheartedly dedicated to my beloved family, who has been the source of strength, who continually provide their moral, spiritual, and emotional support in this journey.

In memory of my beloved late father, who embarked on my path to study Medicine. Remembering you in spirit reminds me why I am doing this.

Declaration

I, Salomon Narodden declare that the Clinical Medicine PhD thesis entitled "Shockwave for the abrogation of heart failure in myocardial ischaemia-reperfusion injury" is the result of my own work (original idea, concept, design, conducted the experiments, collected and assembled data, performed data analysis and interpretation, and wrote the thesis) and includes nothing which is the outcome of work done in collaboration except as declared in the Acknowledgement and specified in the text. It is not substantially the same as any that I have submitted or being concurrently submitted for a degree or diploma or other qualification at the Imperial College London or any other University or similar institution except as declared in the Preface and specified in the text. It does not exceed the prescribed word limit for the relevant Degree Committee.

Acknowledgement

I cannot begin to express my thanks to MRI Physicist Dr Nicoleta Baxan who has precisely captured the imaging requirement of the project to a high standard from scratch, who has been instrumental in the CMR programming and data acquisition; and providing invaluable insight into MRI. The PhD would not have been possible without Nicoleta.

I'm extremely grateful to my primary supervisor, Professor Sian Harding, for the unrelenting support and belief in the project. The completion of the thesis would not have been possible without Professor Sian Harding who also has provided me with the invaluable tools of basic science, to develop and think like a scientist, and provided the conducive scientific training environment through lab meetings, academic seminars and the International Society for Heart Research conferences.

I'm incredibly grateful to my secondary supervisor, Professor Petros Nihoyannopoulos for the encouragement and patience and whose invaluable teachings had provided me with a solid foundation in cardiac imaging to allow me to take on the complexity of the project and who first introduced me to the concepts of stem cells for cardiac regeneration, cardiac shockwave and strain imaging. Professor Petros Nihoyannopoulos has provided the tool and training of post-processing of CMR cine using feature tracking. The PhD would not have been possible without Professor Petros Nihoyannopoulos.

I would like to extend my sincere thanks to my tertiary supervisor, Professor Prakash Punjabi, for the profound belief in my abilities and access to the

Hammersmith Imperial Private Healthcare as a PhD funding route, an initiative of Professor the Lord Darzi Of Denham. The PhD would not have been possible without the support of Professor Punjabi. Special thanks to the Hammersmith Imperial Private Healthcare and the consultants that I get to know; without their support, this PhD would not have been possible.

I'm incredibly grateful to Professor Dudley Pennell, my internal examiner, and Professor Derek Hausenloy, my external examiner, for an intellectually stimulating and enjoyable PhD viva voce.

I am also grateful to Professor Nadia Rosenthal and Professor Jane Evans, who played roles as reviewers during the early-stage and late-stage PhD reviews; their advice and inspiration cannot be underestimated.

I am indebted to Storz Medical of Switzerland that has kindly provided me with the shockwave equipment used in the *in vivo* research and to the British Heart Foundation, which donated the PCR equipment and, among other things at the centre that were used in the basic science experiments.

I also had the great pleasure of working with Mr Peter O'Gara, who was instrumental in rat cardiomyocytes isolation, troubleshooting laboratory issues and in the ordering of consumables.

I very much appreciate the help from Dr Catherine Mansfield, who helped in the early training of *in vivo* myocardial infarction; the practice has allowed for the evolution of the technique into the rat ischaemia-reperfusion model.

I’d like to recognise the assistance that I received from the Vets in their knowledge of animals’ scientific procedures. I gratefully acknowledge the staffs of Imperial Central Biomedical Services for their general support.

To my friends and colleagues who have provided me with useful, practical advice in my experiments. Especially to Dr Aida Di Gregorio-Pena and Dr Juan Miguel Sanchez Nieto to allow me to observe and learn the western blot technique, and to Dr Ana Abrunhosa-Carvalho-Limaiments, who troubleshot an issue in multi-colour flow cytometry. I very much appreciate Dr Matthew Tranter, who showed me how to set up the rat Langendorff Heart.

I gratefully acknowledge Mr Stephen Rothery for the induction to wide-field microscopy via the Facility for Imaging by Light Microscopy and Dr Pawel Tokarczuk for help in coding and provided insight into MRI physics.

Last but not least, special thanks to Professor Lan Zhao for looking after the staffs at the Imperial Biomedical Imaging Centre.

Conference Proceedings

1. **Poster:** *Different Ejection Fraction Methods Vary with Diseased State, Not Directly Comparable and Could Give Different Conclusion*.

   -**S Narodden**, et al. BHF Centre of Research Excellence and EPSRC **Centre for Mathematics of Precision Healthcare**. The Heart – Models, Measurement, Medicine. June 2017

2. **Poster:** *The feasibility and superiority of high frame rate strain imaging compared to ejection fraction in a rat model of ischemia-reperfusion myocardial infarction using cardiac MRI*.

   -**S Narodden**, et al.

   Presented at (Poster) **International Society of Heart Research. 2017 (Hamburg).**

3. *Segmental Longitudinal Myocardial Strains Can Distinguish the Healthy, Area-at-risk and Infarcted Myocardial Segments in Acute Ischaemia-Reperfusion Injury.*

   -**S Narodden**, et al.

   A. Oral presentation at the **EuroCMR 2018 (Barcelona):**

   1) Moderated ePoster Session: CMR in Acute Coronary Syndromes-named Best Moderated ePoster in Acute Coronary Syndromes.

   2) Oral presentation: Bests of Best Moderated ePoster abstracts

B. The abstract was refashioned into a printed poster and presented at the **NHLI Away Day 2019** (Queen Elizabeth II Conference Centre, Westminster)

4. *High-frame rate cine-MRI reveals systolic and diastolic functional abnormalities in the remote segments of ischaemia-reperfusion myocardial infarction.*

   -S Narodden, et al.

   Oral presentation at **ESC 2018 (Munich)** in the session "Innovative CMR **techniques ready** for clinical use"

5. *Longitudinal Exosomal and Tissue Expression of microRNA-208a and 208b in Acute and Chronic Rat Post-Myocardial Infarction Remodelling.*

   -Samuel C Guymer, **Salomon Narodden**, et al.

   Presented at **AHA scientific sessions 2018 (Chicago)** in the Poster session: Cardiac Failure and Remodeling

Publications

1. **Narodden, S**. *et al.* (2018) '*4384High-frame rate cine-MRI reveals systolic and diastolic functional abnormalities in the remote segments of ischaemia-reperfusion myocardial infarction*', *European Heart Journal*, 39(suppl_1). doi: 10.1093/eurheartj/ehy563.4384.
2. Samuel C Guymer, **Salomon Narodden**, et al. 2018. "*Abstract 15875: Longitudinal Exosomal and Tissue Expression of MicroRNA-208a and 208b in Acute and Chronic Rat Post-Myocardial Infarction Remodelling.*" *Circulation* 138 (Suppl_1): A15875–A15875. https://doi.org/10.1161/circ.138.suppl_1.15875.
3. **Salomon Narodden**, Samuel Guymer, Cesare Terracciano. Book chapter: *'Cardiomyopathies Molecular and Cellular Basis of Cardiomyopathies.'* in book "Heart of the Matter: Key concepts in cardiovascular science". Publisher: Springer (2019)
4. Inventor - **Salomon Narodden.** Patent WO2018096319 (A1) – 2018-05-31. *Treatments for Heart Failure and Cardiac Ischaemic Reperfusion Injury.*
5. Sintou, Amalia, Catherine Mansfield, Alma Iacob, Rasheda A. Chowdhury, **Salomon Narodden**, Stephen M. Rothery, Robert Podovei, et al. 2020. "Mediastinal Lymphadenopathy, Class-Switched Auto-Antibodies and Myocardial Immune-Complexes During Heart Failure in

Rodents and Humans." *Frontiers in Cell and Developmental Biology.* https://doi.org/10.3389/fcell.2020.00695

6. **Narodden, S**. et al. The feasibility and superiority of high frame rate strain imaging compared to ejection fraction in a rat model of ischemia-reperfusion myocardial infarction using cardiac MRI. Abstracts from the 34th Annual Meeting, European Section of the International Society for Heart Research, July 24–27, 2017, Hamburg, Germany. Journal of Molecular and Cellular Cardiology Volume 109, Supplement, July 2017, Pages 1-62.

Supervision of Students

1. Mr Samuel Guymer (Medical student at St George's University of London Medical School, London).
    a. Primary supervisor: BSc. in Medical Sciences with Cardiovascular Science (Intercalated with MBBS) at Imperial College London (2018). Sam was awarded a First-class honours for the study of the microRNAs of the tissue and plasma variants. He studied miR-21-5p expression (profibrotic), miR-208a-3p (pro-fibrotic), miR-208b-3p (anti-fibrotic) of the remote tissue, acute infarction tissue, chronic infarction tissue and the plasma exosomes. The abstract was presented at the AHA Scientific session 2018 (Chicago, Illinois) in session: Cardiac Failure and Remodelling. It demonstrated that the increase in pro-fibrotic miRs detected in the remote segments were also detectable in plasma exosomes. The study has provided a novel insight that the miRs of interest exist in the blood-derived exosomes and could be used as biomarker tools for monitoring of fibrotic process. (See **Figure 1 of Appendix 3** for graphical abstract of miR-21p results). MiR-21p could serve as a novel therapeutic target in the prevention of LV remodelling.
    b. Supervisor: Student Selected Component T year MBBS (2020). Poster module and data analysis.

2. Ms Rosheen Abaka-Wood, MSc Student Medical Ultrasound (Echocardiography) 2019/2020, Imperial College London
    a. Primary supervisor for the MSc research project: The Use of 2D Speckle Tracking to Classify the Degree of Adverse Left Ventricular Remodelling Post Myocardial Infarction: A Deformation Imaging Study.

       Rosheen investigated a new classification of LV remodelling after acute ST-elevation myocardial infarction as a more accurate method than the classical volumetric method in the phenotyping of LV remodelling. In the new classification, the patients would be stratified according to the severity of the global strain indices and the severity of volumetric changes. The research is useful for tighter patients' selection criteria in clinical trials and early identification of those at risk for LV remodelling.
3. MSc Students teaching [Medical Ultrasound (Echocardiography)]
    a. Cardiac segmentation
    b. Speckle tracking: left ventricle, right ventricle and atria
    c. Handling image data and analysis workflow
        I. Data protection on NHS computers
        II. anonymisation of DICOM image data: masking tool and removal of patients' identification metadata
        III. Systematic data organisation for retrieval and archive.
    d. Troubleshooting of post-processing, analysis and selection of imaging indices to use in answering research questions.

Abstract *

BACKGROUND: Although reperfusion of STEMI has markedly improved acute patients' survival, more patients are living with heart failure. Theoretically, more myocardial tissue is salvageable if reperfusion injury could be alleviated, limiting the risk of developing heart failure.

AIM: To assess the combination shockwave treatment with DPP4-inhibitor as a treatment adjunct for cardiac IR injury.

HYPOTHESIS: Shockwave provides cardioprotection from IR injury, improves cardiac function and cell-homing, and when shockwave used in conjunction with DPP4-inhibitor, the effects are augmented.

METHOD:

In-vivo: Surgical IR-rat models imaged using Bruker-BioSpec-9.4T. Multi-sequence CMR similar to clinical multi-planar acquisition using: (a) FLASH-CINE, (b) INTRAGATE-CINE, (c) MESE-T2-map, (d) T2-star, and (e) IR-LGE; in experimental groups: (1) Healthy versus IR-MI [a,b,c,e]; (2) Healthy versus Healthy-SW [a,b] ; (3) Healthy-SW versus Healthy-SW-inhibitor [a]; (4) IR-MI versus IR-MI-SW versus IR-MI-SW-inhibitor [a,b,c,e]; (5) iron pretreament then shockwave [c]; and (6) shockwave BOLD [d]. Segment(Medviso) post-processing to derive EDV, ESV, SV, CO, EF, T2-maps and T2star-maps; and Image-Arena(Tomtec) to derive GLS, GCS, GRS and segmental-strains; (6)

multi-colour-flow-cytometry CD45-CD90+ and CD45+CD34+ on PBMC after shockwave.

In-vitro: (7) Shockwave-treated HCF, HVT, HUVEC, and cardiomyocytes qPCR-assessed for SDF1. (8) Shockwave or SDF1-spiking treatment on oxygen-deprived cardiomyocytes and assessed for viability.

RESULTS: (1) Segmental-strains distinguished phenotypes of Healthy, AAR and Infarction; global-strains detected IR-MI better than EF. (2) Shockwave induced inotropy. (3) DPP4-inhibitor prolonged shockwave-inotropic effect. (4) Smaller infarction in shockwave group; reduced transmurality with DPP4-inhibitor; stronger GLS, GCS, GRS in IR-MI-SW than IR-MI; stronger GLS and GRS in IR-MI-SW-inhibitor had than IR-MI-SW while GCS was unchanged. (5) Shockwave reduced T2, signifying cell-homing. (6) Shockwave increased BOLD signifying angiogenesis. (7) SDF1 expression increased in HCF, HVT, HUVEC but not in cardiomyocytes. (8) Shockwave and SDF1-spiking improved cardiomyocytes viability.

CLINICAL CONTEXT: Shockwave with DPP4-inhibitor treatment in reperfused-STEMI could limit infarct size and improve cardiac function.

* This thesis contains abbreviations scattered throughout; a list of abbreviations is provided on page 63 as a single reference point to improve readability.

Thesis Introduction

1. Research Aims

The PhD thesis aims to investigate whether shockwave could be used as a treatment of myocardial ischemia-reperfusion injury and assess its efficacy when used in conjunction with a pharmacological DPP4 inhibitor. It also aims to explore the best imaging indices used to assess the experimental effects on cardiac function and answer the research questions.

2. **Research Questions (Problems)**

1. Does shockwave have a rescue effect on cell and tissue from anoxia/ischaemia; can the effect be enhanced using DPP4 inhibition?
2. As shockwave could induce SDF1 in tissue, what cell types in cardiac tissue are the key players, and what are the associated genes that could be expressed by shockwave?
3. As SDF1 is a chemokine, can shockwave be used to home progenitors to the heart and what is the effect of adding DPP4 inhibition?
4. What are the effects of shockwave on cardiac function, and the benefits of adding DPP4 inhibition?

5. Can strain imaging detect the effects of ischemia-reperfusion injury better than LV ejection fraction, if so, can strain imaging detects the functional changes of shockwave models of ischemia-reperfusion injury with and without DPP4 inhibition, and what are the novel effects on cardiac mechanic uncovered?
6. Can CMR be used to detect cell homing and angiogenesis in shockwave therapy?

3. Knowledge Contribution

The PhD thesis has contributed to new knowledge in the discovery of the rescue effect of shockwave on cardiomyocytes and heart tissue subjected to anoxia/ischaemia injury, an effect that could be enhanced by DPP4 inhibition. Shockwave treatment to ischaemia-reperfusion injury limited the infarct size and a new treatment avenue in the abrogation of heart failure and remodelling. The research informed the cells players involved, and the temporal expression of SDF1 gene expression (and other related genes of interest); discovered that SDF1 could be expressed in the endothelial cells and the fibroblasts, not in the cardiomyocytes, supporting the paradigm of the paracrine effects of SDF1, linking to the theory of cells homing. Through the discovery of the inotropic effect of shockwave without chronotropism, both in the hearts of the healthy and acute ischaemia-reperfusion injury, the positive

effect on the left ventricular systolic function by shockwave was explained in terms of global and regional strain indices, as well as in the classical indices of ventricular volume; and the contribution of DPP4 inhibition in the rapid establishment of inotropy and inotropy maintenance. The thesis also described the novel use of segmental strain in the distinguishment of segmental phenotypes after ischaemia injury — providing a solution to phenotype myocardial segments using high frame rate strain without using gadolinium contrast agent.

4. **Research Scope**

All experiments were performed in research laboratories and within the remit of a PhD thesis; performed *in vivo*, *in vitro*, and ex-vivo of healthy and diseased rat models, and human cardiac samples and cell lines, to discover whether shockwave and DPP4 inhibition could be used to treat ischaemic heart disease. The major focus was on the use of cardiac MR imaging, particularly strain imaging for the assessment of experimental effects of shockwave in cardiac ischaemia-reperfusion injury.

5. **Research Purpose**

The purpose of the research was to discover whether the proposed treatment could be translated into Human Medicine.

6. **Objectives**

1. The effects of experimental interventions were objectively assessed *in vivo* rat ischaemia-reperfusion myocardial (I/R MI) infarction models, quantified using cardiac magnetic resonance:
    i. cardiac function: global and regional indices: using true-volumes and tissue deformation imaging techniques; their performance compared;
    ii. area-at-risk (AAR): using T2 maps and early gadolinium enhancement;
    iii. scar volume: using late gadolinium enhancement;
2. Shockwave effects on:
    i. Inotropy
    ii. Cell homing using iron labelling detected using T2 map
    iii. Tissue SDF1 protein expression: immunohistochemistry
    iv. Tissue oxygenation as a surrogate for angiogenesis using T2* map BOLD signalling
    v. Peripheral blood progenitors using multi-colour flow cytometry

3. The effects of shockwave on SDF1 (and GOI) expression in cell types and cardiac tissue were assessed in human cardiac fibroblast, cardiomyocytes, endothelial cells (HUVEC) and human left ventricular tissue.
4. Shockwave and SDF1 effect on the viability of cardiomyocytes challenged with anoxia-reoxygenation

7. Summary of Findings

1. Rat groups of ischaemia-reperfusion injury (I/R-MI), ischaemia-reperfusion injury treated with shockwave (IR-MI-SW), and ischaemia-reperfusion injury treated with shockwave and DPP4 inhibition (IR-MI-SW-i) were compared:
   a. The LV volumetric indices showed: The end-diastolic-volume were not different between groups. The end-systolic volume decreased in the Healthy-SW group compared to Healthy, with no significant differences between the Healthy and IR/MI. In IR rats, SW decreased the ESV, and there was a negative linear trend between groups of IR-MI, IR-MI-SW, IR-MI-SW-i. The ejection fraction (derived from a stacked of LV short-axis images) increased in the Healthy-SW group compared to Healthy, with no significant differences between the Healthy and IR/MI. In IR-MI rats, shockwave increased the stacked-EF, and there was a positive

linear trend between groups of IR-MI, IR-MI-SW, IR-MI-SW-i. The stroke volumes (SV) were increased in the Healthy-SW group compared to both the Healthy and IR-MI, with no difference between the latter two. In IR rats, SW increased the SV, and there was a positive linear trend between groups of IR-MI, IR-MI-SW, IR-MI-SW-i.

b. There were no significant differences in the heart rate of the I/R-MI, I/R-MI-SW and I/R-MI-SW-i.

c. Myocardial salvage: In I/R MI, shockwave increased myocardial salvage mean by 50% compared to reperfusion alone and the addition of DPP4 inhibition to SW improved the salvage mean by 50% more. Myocardial salvage was calculated from area-at-risk (thresholding of whole heart T2-mapping for oedema) and late gadolinium enhancement for scar. The mean transmurality of the scar was reduced by 30% with the combination of shockwave and DPP4 inhibition. There were no significant differences in the LV masses and AAR between groups.

d. Global strain indices of endoGLS, myoGLS, GRS showed significant increasing improvement in the order of I/R-MI, IR-MI-SW and IR-MI-SWi. The endo and myoGCS were not different between IR-MI-SW than I/R-MI, although the endo and myoGCS were stronger IR-MI-SW than I/R-MI.

e. Segmental circumferential strain rate of the three short axes views to derive the strain-rate indices: S-SR (systolic function), E-SR (early diastolic lengthening rate of the fibre), A-SR (diastolic filling rate from atrial contraction) and the ratio of E-SR/A-SR. The remote segments were defined as segments with normal T2 values and no LGE; compared with the healthy segments. The abnormality of the function of the remote segments was demonstrated, consistent with a "restrictive" pattern, a predisposition for remodelling (partial data presented in ESC Munich 2018 in traditional oral abstract session: "CMR innovation for clinical use").

f. Torsion: The myo torsion of I/R-MI-SW and I/R-MI-SWi were both stronger than the epi torsion in both groups. Additionally, in the I/R-MI-SWi, the myo torsion was also stronger than the endo torsion.

2. Healthy rats compared with Healthy rats treated with shockwave:

   a. Time-series EF experiments on Healthy rats treated with shockwave showed the effect could be enhanced by DPP4 inhibition (stronger initial effect and longer lasting inotropy). Three doses of shockwave every three days were required to reach the steady state of inotropy, whereas one shockwave session with daily DPP4 inhibition could provide the same inotropic effect.

b. Global strain: the endoGLS and myoGLS were stronger in the Healthy-SW than the Healthy; the myoGCS were not different, while the endoGCS was stronger in Healthy-SW than the Healthy, indicating shockwave effect on contractility was layer selective favouring the endo layer.

c. EndoGCS and myoGCS were different between Healthy and Healthy-SW rats. The GRS did not significantly change between the healthy and Healthy-SW.

d. Basal versus apical rotation: at the base, the effect of shockwave on the rotation happened at the epicardial layer, while at the apex, the effect happened at the endocardial layer.

e. Torsion: the increase in torsion by shockwave happens predominantly at the myo and epi layers compared to Healthy control.

f. Rotational rate: the contractility exerted by shockwave happened at the base.

g. Cells homing: In rats pre-treated with intravenous iron, a decrease in whole heart T2-map was evident in the SW group, an indication of homing of cells; concordant with the increase in SDF1 shown in immunohistochemistry and the addition of DPP4 inhibition to shockwave could increase SDF1 signal. The Prussian-Blue histology confirmed iron deposition.

h. Angiogenesis: The effect was studied using Blood-oxygen-level dependent contrast imaging (BOLD-MRI) showed signals increase in the hearts that received shockwave. BOLD-MRI uses the contrasts of paramagnetic deoxyhaemoglobin (decreases T2*) and diamagnetic oxyhaemoglobin (increases T2*). As oxygenation blood in the myocardium is received during diastole, the difference in T2* between early diastole and late systole was the BOLD signal intensity. The gross appearance of the cardiac tissue showed an increase in vascularity in epicardial vessels in the shockwave treated hearts.

3. Rat groups of ischaemia-reperfusion injury and Healthy rats were compared, showing:
   a. Segmental longitudinal myocardial strains: can be used to distinguish the segments of Healthy, area-at-risk and infarcted myocardial segments in acute ischaemia-reperfusion injury (Best Moderated ePoster in Acute Coronary Syndromes - EuroCMR Barcelona 2018). An abnormal segmental longitudinal strain was an indication that the segment was diseased, associated with either one or both: abnormal T2 value and LGE. A positive (paradoxical) longitudinal segmental strain was associated with transmural LGE.

b. Global strain: using small animal numbers GLS, GCS and GRS could distinguish the Healthy and IR-MI, while EF could not. Feasibility data presented as a poster at ISHR 2017 (Hamburg) entitled "The feasibility and superiority of high frame rate strain imaging compared to ejection fraction in a rat model of ischemia-reperfusion myocardial infarction using cardiac MRI."

4. Cardiomyocytes challenged with anoxia-reoxygenation: both exogenous SDF1 and shockwave in independent groups exhibited a salvation effect on anoxic cardiomyocytes, suggest the mechanisms of salvation were via different routes and could be complementary.
5. SDF1 expression in cells and cardiac tissue: SDF1 could be induced by shockwave in all cells (endothelial cells and cardiac fibroblasts) except cardiomyocytes. The temporal expression of SDF1 in the fibroblasts lagged the expression of the endothelial cells to form an SDF1 gradient, and the temporal expression pattern is the opposite for VEGFA expression.

8. **The Overarching Topics**

The overarching topics are the "Shockwave", "DPP4 inhibitor", "Ischaemia-reperfusion", "SDF1", "Strain imaging", "Cardiac MR", "High frame rate cine", "Inotropy" and "Stem cells".

9. Detail Aims and Objectives

In respective thematic results chapters, detailed aims and objectives of the experiments will be presented after the introduction section of the chapter.

10. Prelude of Topic-Related Literature Review

After a myocardial ischaemia-reperfusion injury, a large proportion of cardiomyocytes would die despite successful revascularisation, leading to primary tissue loss, secondary cardiac remodelling with a progressive reduction in cardiac function. In this respect, therapeutic interventions that could limit the death of cardiomyocytes from reperfusion injury and delay the remodelling process could be beneficial for the patients' prognosis. It is estimated that 50% of the final infarct size is attributable to reperfusion injury [1] and the incidence of heart failure is around 25% of the acute cases.[2] Heart failure is a disease condition associated with low inotropic state when the heart is not able to commensurate the oxygen requirement of the body despite normal filling pressure.[3]

Low-energy shockwave is a non-linear mechanical wave (superposition principle does not apply, i.e. when two or more waves overlap in space, the resultant wave are not the sums of the individual waves) when applied to tissue, would cause rapid compression (few nanoseconds) and relatively slow hyper-expansion (milliseconds) at the wave-front. Through a biological effect

named mechanotransduction, the cells in the tissue could sense the physical forces and transduce biochemical signals to generate appropriate biological responses. Low-energy shockwave, when applied to tissue, could artificially induce SDF1, and the mechanism is independent of HIF-α activation and hypoxia.[4] Direct administration of SDF1 has been shown to preserve the cardiac function after myocardial infarction,[5] as well as in the case of SDF-1 expressing plasmid DNA as gene therapy in ischaemic cardiomyopathy.[67]

We have evidence that SDF1-α exerts a cardioprotective autocrine effect as well as a paracrine effect. The binding of SDF1-α to CXCR4 activates several G protein-mediated intracellular signalling cascades[8] (ERK-1/2, JAK, STAT, PI3K-AKT, PLC-PKC & RHO), induces Ca2+ influx, promotes cells trafficking, promotes homing of progenitors for initiation of angiogenesis and regeneration. Apoptosis is prevented via ERK and AKT kinases activation, production of BCL-XL protein and NO mechanism.

Cellular therapy using bone marrow progenitor cells, indeed, can produce functional improvement following myocardial infarction, and meta-analyses suggest potential mortality benefits; [9] however, the results from clinical trials so far are modest in magnitude. [10] This could be explained by poor cell homing, poor cell survival and the fact that a single dose might not be enough to promote sustained improvement in the left ventricular function. [11] Stem cells may exert their regenerative effect partly or mostly through paracrine

factors.[12] CXCR4 is the specific receptor for SDF1, and it is expressed in the haemopoietic and mesenchymal stem cells; and the endothelial progenitors. The interaction of SDF1/CXCR4 is known to activate the integrin and other attachment molecules that are essential for cells retention and survival.[13]

All stem clinical trials to date have used various forms of ejection fraction as the primary endpoint; and this might not be the most appropriate index as it is sensitive to loading conditions and does not assess the regional function where treatment is applied to and cannot evaluate the effects by compensatory mechanisms, which could also change as the disease progresses.

Imaging-based studies of stem cells tracking have demonstrated that cells retention in the heart, regardless of the methods of surgical delivery is poor, with most of the cells end up in the spleen and liver.[14] Homing of progenitors using shockwave is clinically advantageous over surgical cells delivery methods. Firstly, the procedure is non-invasive with good safety records. Secondly, a large diseased area in the human heart could be precisely treated, independent of prior knowledge of the blood supply (in the case of whether the same coronary territory supplies them or whether the disease is multi-vessels); a patent vessel is a prerequisite in intracoronary stem cells delivery, and it is not safe to do stop-flow intracoronary stem cells injections in multi-

vessels disease in one sitting. Thirdly is high in repeatability, where multi-dosing of autologous stem cells delivery is possible which make the treatment more affordable – all the stem cells clinical trial to date have used a single treatment only; and fourthly, the mobilisation of different types of stem cells and progenitors could provide a synergistic effect on cardiac regeneration. Such cells combination could not be easily replicated in GMP-produced cells. Lastly, the translation into clinical studies would be much shorter.

The intravascular half-life of SDF1-α is 25.6 min[15] and if administered as a single dose, has a very short physiological effect. The effect could be prolonged with a DPP4 inhibitor. The Dipeptidyl peptidase (DPP-4) inhibitor, Sitagliptin, is a drug for type-2 diabetes. It attenuates the degradation of incretin and GLP1, which enhance pancreatic insulin secretion and inhibit glucagon secretion, resulting in blood glucose lowering effect in diabetes. More importantly for this thesis, DPP4 inhibitor also acts to prolong the effect of endogenous substrates such as SDF1-α and substance P, a known stimulator of endothelium-derived nitric oxide release,[16] which is a vasodilator and inhibitor of atherosclerosis via inhibiting platelets adherence [17] translating into antiatherosclerotic and cardioprotective effects.

Imaging of small animal diseased model is challenging because of the size and heart rate. In the thesis, the rat hearts were assessed in ultra-high field MR to achieve the spatial resolution needed to visualise the small heart and assess small physiological changes at a high signal-to-noise ratio.

11. Definitions of the Terms and Scope of the Topic

"Shockwave" means extracorporeal pressure wave series generated artificially using a transducer; refers to either radial or focus shockwave depending on the transducer and generator used.

"DPP4 inhibitor" means a class of pharmacological inhibitor that blocks the exopeptidase (enzyme) that cleaves N-terminal dipeptides. In this thesis, Linagliptin was used, and DPP4 inhibitor refers to Linagliptin.

"Ischaemia-reperfusion" means an ischaemic event inducted by interruption of oxygenated blood supply followed by reestablishment of blood supply. *In vitro* cell model, the term anoxia-reoxygenation represents "Ischaemia-reperfusion".

"Strain imaging" means the post-processing method of cine images using feature tracking and refers to the Lagrangian strain method.

"Cardiac MR" means the acquisition of the *in vivo* heart image data using ultra high field 9.4T which covers FLASH and HFR cines, T2 mapping, T2* mapping, EGE and LGE.

"High frame rate cine" means the acquisition of dynamic images with a temporal resolution of ~3ms (effective repetition time) to capture motion using CMR.

"SDF1" means stromal derived factor 1, an important chemokine for stem cells homing.

"Inotropy" mean positive Inotropy unless indicated otherwise, refers to improvement in cardiac contractility

"Stem cells" means blood-derived progenitors that are capable to transform into other cells, secrete paracrine factor and modulate other cells' function. In the peripheral blood, it could be a heterogeneous mixture of endothelial progenitors, haematopoetic stem cells and mesenchymal stem cells. In this thesis, "stem cells" do not refer to embryonic stem cells or induced pluripotent stem cells.

"**Area at risk"** means the area or volume of myocardium distal to the occlusion of a coronary artery and represented by oedema measured using T2-mapping.

12. Evaluation of the Current State of the Literature on Research Topic

The effect of shockwave on *in vivo* myocardial infarction size after ischaemia-reperfusion, and cardiomyocytes viability after anoxia-reoxygenation, had not been previously assessed. Moreover, the combination treatment of shockwave and DPP4 inhibition has not been previously assessed in any

experimental and disease context, here, assessed in cardiac ischaemia-reperfusion injury. The assessment method studied in multi-strain domains using high frame rate strain imaging is novel in rat cardiac ischaemia-reperfusion model. The 'humanised' multi-planar MR scanning protocol and post-processing methods were reverse translated from "clinic" into "bench", has never been reported in a preclinical model to the extent. The discovery of the inotropic effects of shockwave is novel, so is the discovery that adding DPP4 inhibition to shockwave in improving the durability of the inotropic effect of shockwave. The shockwave inotropism was further explained in terms of myocardial layers and the differences in the contractility of the basal and apical levels. The research is broad, encompassing cross-disciplines of pharmacology, physiology, cardiac imaging, physics, cell and molecular biology, and human medicine. The research informed new knowledge on the cell types responsible for SDF1 expression and their temporal expression pattern. The assessment of cell homing using iron and shockwave has not been previously reported.

13. Stem Cells Translation Obstacles

This section summarises the possible causes why previous translations of stem cell therapy from animal models into human treatments have not been very successful. The thesis proposed a direct method of cell-homing (from the blood to the heart) which do not suffer from the disadvantages of surgical methods mentioned below:

- Poor bioretention of injected cells [see **section 1.7 and section 2.3**]
- Cell-homing mechanism was not active [see **section 1.4**]
- Cells have reduced ability to engraft (CXCR4 downregulated in culture,[18] heparin used as anticoagulant functionally disabled CXCR4) [see **section 1.6]**
- The timing of cell injection was not in synchrony with tissue homing signal (signal lag or absence or not activated) [see **section 1.4**]
- Paracrine factors removed during *ex vivo* cells processing [see **section 1.6**]
- Dose of cells lost (trapped) in the lungs, liver and spleen [see **section 2.3**]
- A shift from heterogeneous cell population to homogenous cell population; variation in potency. [19]
- One dose of cells used in clinical trials likely insufficient. [see **section 2.2**]
- Dose of injected cells arbitrarily determined, dose-escalation not performed leading to underdosing, and dose limited by the yield of cells achieved during harvest.
- Widespread use of heparin as an anticoagulant during cardiac angioplasty. Heparin binds to signalling proteins and angiogenic proteins. [see **section 1.6**]

- EF used as primary endpoints are not sensitive to detect small changes — masked by loading conditions and compensatory mechanisms in play. [see **section 1.9, chapter 5**]
- Cardiac imaging technology to assess for the regional function is still of insufficient fidelity, limiting detectability of small changes of experimental effects. [see **chapter 5**]
- Confounding factors in patients [diabetes, hypertension, concomitant drugs- see last **section 1.11** and **section 2.7**]

14. Outline of Research Importance and Contribution

- Cardiac ischaemia-reperfusion injury is a relevant topic to human disease, which carries a high socio-economic burden.
- Research on potential new treatment method to treat ischaemic heart disease.
- The discovery of the novel effect of shockwave on cardiac mechanics with and without DPP4 inhibition.
- The potential treatment is cheap and could be available for the mass market segment.

- A new non-invasive treatment method to enhance cells homing to be used as Human Medicine bypassing the GMP regulation, saving time in research and development.
- The research discoveries will lead to other hypothesis generations.
- The research will change the way myocardial function assessment in the preclinical setting.
- The discovery of the inotropic effect of shockwave is independent of the preload, which could be sustained for longer with DPP4 inhibition, paving the way for a new treatment in heart failure.

15. Outline of Epistemological and Ontological Positions

- Ejection fraction alone is not sufficient to assess cardiac function: strain imaging could be the solution to the problem.
- Stem cells have a regenerative effect.
- Stem cells homing to the heart is poor.
- Improvement of cells homing could be achieved by chemotaxis
- The heart is capable of responding to the mechanotransductive effect of shockwave inducing chemotaxis
- Migration of progenitors to the heart for regenerative effect
- DPP4 inhibition could enhance other important substrates

16. Hypotheses Statements

Rat groups of ischaemia-reperfusion injury, if immediately treated with shockwave, will have smaller infarct size and better cardiac function than without shockwave treatment. The addition of DPP4 inhibitor to shockwave will result in smaller infarct size and better cardiac function than shockwave treatment only. Cardiac function assessed using high frame rate strain will be able to detect IR injury better than ejection fraction can. The segmental strain and strain rate will be able to distinguish the tissue phenotype of IR injury and assess the diastology of remote segments of the experimental groups of IR rats, IR rats with shockwave and IR rats with shockwave and DPP4 inhibitor. SDF1 expression in cardiac tissue of healthy rats will increase with shockwave treatment than without treatment. In healthy rats treated with DPP4 inhibitor and shockwave, the abundance of SDF1 expression detected in cardiac tissue will be greater than in healthy rats treated with shockwave only and positively correlated with cell-homing in tissue, while inversely correlated with the abundance of progenitors in the blood.

Important Concepts and Variables

The key concepts are on the effectiveness of shockwave in cardioprotection, myocardial regeneration and repair. The key variables are the cardiac functional assessment, viability assessment, gene and protein expression, and markers of cell homing.

17. Brief Outline of Methodology

- Creation of ischaemia-reperfusion rat model
- CMR acquisition and post-processing: scout, planning, multi-planar cines, T2-mapping, T2*-map and LGE.
- The *in vivo* cardiac function was assessed using volumetric indices of the cine (LVEDV, LVESV, SV, CO, EF, FAC); and strain indices (LV GLS, GCS, GRS, segmental strain, torsion and twist; atrial strains) were derived using high frame rate cine MRI and post-processed using feature tracking
- The final infarct size was assessed using late gadolinium enhancement (inversion recovery), and the area at risk assessed using T2-mapping to derive salvage index.
- Segmental phenotype was classified according to the characteristic of LGE and T2-mapping results.

- Cell homing was assessed using intravenous iron and whole heart T2-mapping.
- Angiogenic effect was assessed using the BOLD signal of T2*.
- The gene expression of SDF1 (and GOI) in endothelial cells, cardiac fibroblast, cardiomyocytes, Langendorff heart and human cardiac tissue, was assessed using quantitative reverse transcriptase polymerisation chain reaction (qRT-PCR).
- Cardiomyocytes viability assessed using phase-contrast inverted light microscopy and manual cell counting.
- Immunohistochemistry was used to assess SDF1 expression on frozen tissue section.
- Multi-colour flow cytometry was used to quantify cell markers of interest in the peripheral blood mononuclear cells.
- *In vitro* culture of endothelial cells, cardiac fibroblasts, cardiomyocytes and human ventricular tissue.

18. Discussion of the Main Findings

The data presented support the hypotheses statement. Shockwave has a direct effect on cardiac contractility as evidenced by the ability to make the end-systolic volume smaller, hence increasing the stroke volume and the ejection fraction, as well as tissue deformation indices presented in multi-

strain domains, in the hearts of the healthy and IR-MI. The reaction of different tissue layers to shockwave, favouring the base to the apex for the enhancement of contractility is a novel discovery, and the effect is the opposite of inotropy by the adrenergic route. The enhancement of the cardiac function in shockwave by DPP4 inhibition was further supported the SDF1 paracrine theory. However, as DPP4 inhibitor also block the degradation of other paracrine factors (discussed in section 2.7), the effects cannot wholly be explained by SDF1. The *in vivo* cell labelling with iron demonstrated cardiac shockwave could home progenitors to the heart. The induction of inotropy by shockwave showed a fast onset and slow decline, extendable by DPP4 inhibition. Cell homing by shockwave is probably not required for the achievement of the inotropic effect; however, it could be useful for the other effects which manifest at a later stage when tissue vascularisation and remodelling are considered.

19. **Conclusion**

Together with the improvement of cardiac function, the salvation of tissue from ischaemia-reperfusion injury, and potential use to improve the blood supply, I believe shockwave is beneficial as a treatment for ischemic heart disease. The advanced imaging technology used has helped in answering the research questions.

20. The Brief Layout of the Thesis

1. Literature review on research topics
2. Theoretical framework: Epistemological and Ontological Positions
3. Methods:
    i) Surgical method in creating I/R rat model
    ii) CMR method
4. Thematic result chapters:
    i) *In vivo*: Ischaemia-reperfusion - proof of concept, volumetric indices, global strain, segmental strain, post-systolic shortening, atrial strain & volumes
    ii) *In vivo*: Inotropy- volumetric indices, global strain, rotational mechanics
    iii) *In vivo*: Inotropy with DPP4 inhibition
    iv) In-vivo: Ischaemia-reperfusion shockwave, DPP4 inhibition
    v) In-vivo: cells homing
    vi) *in vitro*: cells and tissue gene expression experiments
    vii) *in vitro*: anoxia/reoxygenation of cardiomyocytes
5. Conclusion
6. References
7. Appendices

21. Statement on Blinding Analysis

The analysis was not performed blinded throughout as the risk of errors from renaming, mislabelling and inadvertent mixing of images far outweighed the benefit of controlling for analysis bias. Furthermore, the data collection took some time to complete and partially analysed data were needed for progress meetings, PhD review reports, and conference abstracts.

Table of Content

List of Figures

Figure 1 of Appendix 3. A graphical abstract showing results of miR21-5p. (A) Healthy heart with no cardiac remodelling, (B) Acute-MI heart with no remodelling, (C) chronic-MI heart with remodelling. Exosomes from A, B and C collected. (D) a photograph of a healthy rat's heart, (E) a photograph of acute MI rat's heart with LAD ligation in situ, yellow circle indicating the remote area, orange circle indicating the acute infarcted area and the white broken line is the acute infarct border, (F) a photograph of a chronic-MI heart, pink circle indicating the remote area and red circle indicating the chronic-MI area and the white broken line is the chronic infarct border. (G) Exosome pallet extracted from rats' plasma using sedimentation method. (H) Roles of miR21 plays in pathways modulating proliferation, impaired apoptosis, angiogenesis, invasion, inflammation and genetic stability via molecular pathways, adapted from Melnik et a l [343] under the terms of the Creative Commons CC BY license , (I) miR-21-5p in tissue according to healthy, remote acute, infarct acute, chronic remote and chronic infarct plotted on a scatter dot plot axis on the left y-axis showing $\Delta\Delta$Ct/ath-miR159a overlay over fold changes on the right y-axis. (J) miR-21-5p in rats' plasma exosomes according to healthy, acute-MI and chronic-MI group plotted on a scatter dot plot axis on the left y-axis showing $\Delta\Delta$Ct/ath-miR159a overlay over fold changes on the right y-axis. **See overleaf for graphics.** _____515

List of Tables

List of Abbreviations

2CH	2 chamber view
3CH	3 chamber view
4CH	4 chamber view
4D	4 dimensional
AAR	Area at risk
ACE	Angiotensin-converting enzyme inhibitors
AHA	American Heart Association
AKT	Akt kinase aka. Protein kinase B
ANG1	Angiopoietin-1
ANOVA	Analysis of variance
ASE	American Society of Echocardiography
ASL	Arterial spin labelling
ASR	Diastolic strain rate of A wave
ATP	Adenosine triphosphate
AVC	Aortic valve closure
B1	The Perpendicular Radiofrequency Field Applied to B0
BHF	British Heart Foundation
BNP	Brain natriuretic peptide
BOLD	Blood oxygenation level dependant
BSA	Body surface area
BSA	Bovine serum albumin
CABG	Coronary artery by-pass operation
CAMP	Cyclic adenosine monophosphate
Cas9	Crispr associated protein 9
CBS	Central biomedical services
CD	Cluster of Differentiation
cDNA	Complementary DNA
CE	"Conformité Européenne"
CFU-S	Colony-forming-unit-spleen
CGMP	Cyclic GMP
CMR	Cardiac magnetic resonance
CO	Cardiac output
CRISPR	Clustered regularly interspaced short palindromic repeats
CT	Cycle threshold
CXCR4	Receptor to SDF1
DAB	3'-diaminobenzidine
DDP4	Dipeptidyl peptidase 4
DICOM	Digital Imaging and Communications in Medicine

DISC	Death reducing signalling complex
DNA	Deoxyribonucleic acid
DPP4i	DPP4 inhibitor
DTI	Diffusion tensor imaging
EACVI	European Association of Cardiovascular Imaging
ED	End-diastole
EDA	End diastolic area
EDV	End-diastolic volume
EF	Ejection fraction
En	End
endo	Endothelium
eNOS	Endothelial NOS
epi	Epicardium
ERK	Extracellular signal-regulated kinase
ESA	End systolic area
ESR	Diastolic strain rate of E wave
ESV	End-systole
ESV	End-systolic volume
FA	Flipped angle
FAC	Fractional area change
FDA	Federal Drug Administration of USA
FGF	Fibroblast growth factor
FISH	Fluorescence in-situ hybridisation
FLASH	Fast low angle shot
FMO	Florescence minus one
FOV	Field of view
FT	Feature tracking
GATA-4	Transcription factor gata-4
GCS	Global circumferential strain
GCSF	Granulocyte colony-stimulating factor
GCSF	Granulocyte colony-stimulating factor
GLP1	Glucagon-like peptide 1
GLS	Global longitudinal strain
GOI	Gene of interest
GRAPPA	Generalized Autocalibrating Partial Parallel Acquisition
GRS	Global radial strain
GS protein	G-Protein (Stimulative Mode)
GSK	Glycogen synthase kinase
hEGF	Human epidermal growth factor
HFmrEF	Heart failure with mid-range ejection fraction
HFPEF	Heart failure of preserved ejection fraction

HFR	High frame rate
HFREF	Heart failure of Reduced Ejection Fraction
HGF	Hepatic growth factor
HIF	Hypoxic-inducible factor
HIV	Human immune deficiency syndrome
HLA	Horizontal long axis
ICD	Intracardiac defibrillator
IGF1	Insulin-like growth factor 1
IR-MI	Ischaemia-reperfusion rat
IR-MI-SW	Ischaemia-reperfusion rat treated with shockwave
IR-MI-SWi	IR-MI-SW rats treated with DPP4 inhibitor
IL4	Interleukin 4
IV	Intravenous
IVRT	Interventricular relaxation time
LAD	Left anterior descending
LAScd	Left atrium conduit phase
LASct	Left atrium contraction phase
LASr	Left atrium reservoir strain
LFT	Low frame rate
LGE	Late gadolinium-enhanced MRI
LV	Left ventricle
LV	Left ventricle
LVAT	Left Ventricle assisted device
MCP1	Monocyte chemoattractant protein 1
MDR	Multidrug resistance
MEF2D	Myocyte Enhancer Factor 2d
miRNA	Micro ribonucleic acid
MMP	Matrix metallopeptidases
MRI	Magnetic resonance imaging
MSC	Mesenchymal stem cells
MESE	Multi-echo spin-echo
MUGA	Multiple gated acquisition scan (radionucleotide)
MVC	Mitral valve closure
MVO	Microvascular obstruction
myo	Myocardium
NICE	The National Institute for Health and Care Excellence
NK-1	Neurokinin-1
NO	Nitric oxide
NOGA	Cardiac navigation system
NOS	Nitric oxide synthase
OCT	Optimal cutting temperature compound

P	Passage of cells
PDE3	Phosphodiesterase 3
Pk	Peak
PKA	Protein kinase A
PSI	Post systolic index
PSI	Post systolic shortening
PSST	Time to peak of PSS
RAF	Proto-oncogene serine/threonine-protein kinase
RISK	Reperfusion injury salvage kinase pathway
RNA	Ribonucleic acid
ROI	Region of Interest
RR interval	ECG R to R interval
SAFE	Survivor activating factor enhancement pathway
SD	Standard deviation
SDF1	Stromal Derived Factor 1
SE	Standard Error
SGLT2	Sodium-Glucose Co-Transporter-2
SI	Sphericity Index
SLS	Segmental Longitudinal Strain
SSFP	Steady-State Free Precession
SSR	Systolic Strain Rate Of S
STAT3	Signal Transducer and Activator of Transcription 3
STEMI	ST Elevation Myocardial Infarction
SV	Stroke Volume
TI	Inversion Time
T1	MR Signal to Decay in The Longitudinal Plane
T2	MR Signal to Decay in The Transverse Plane
TAC1	Tachykinin Precursor 1
TE	Echo Time
TLR3	Toll-like receptors 3
TNF-α	Tumour necrosis factor alpha
TOF	Time of Flight
TR	Repetition Time
TTC	Triphenyltetrazolium chloride
USPION	Ultra-Small Super-Paramagnetic Iron Oxide Nanoparticles
VCAM	Vascular Cell Adhesion Molecule-1
VEGFA	Vascular Endothelial Growth Factor A
VEGFR	Receptor for VEGF
VLA	Vertical Long Axis
VO2 max	Maximal Oxygen Consumption
WNT	Wingless-Related Integration Site

Chapter One

LITERATURE REVIEW ON RESEARCH TOPICS

1.1 Healthy Priority of Ischaemic Heart Disease

Heart failure is a syndrome of multiple aetiologies. In the developed world, coronary artery disease and chronic obstructive pulmonary disease are the major causes, whereas, in low-income countries, rheumatic heart disease and hypertensive heart disease are the main causes. [20] Other heart failure causes are cardiomyopathies, valvular heart disease, metabolic, infiltrative causes (amyloidosis, sarcoidosis), pulmonary hypertension, infection (HIV), and toxicity (alcohol, chemotherapy, cocaine).

Heart failure affects 1-2% of the population in the UK, and it is increasing with age (frequency in those with coronary artery disease: 6.5% in 45-54 years old,

8.1% in 55-64 years old, 10.3% in 65-74 years old, and 16.5%). [21]. 70% of the causes of heart failure in the UK is due to coronary artery disease. [22] The syndrome carries significant health and economic burden and has adverse effects on the quality of life. The average life expectancy is three years after diagnosis (Royal College of Physicians 2005), which is worse than many forms of malignancy). 14% of heart failure patients die within six months of diagnosis.[23] It accounts for 5% of medical admissions and 1-2% of the NHS budget.[24] The hospital admissions with heart failure increase as the population ages. [24]

Contemporary reperfusion treatment of ST-elevation myocardial infarction with primary angioplasties and stents has markedly improved acute patients' survival; [25] paradoxically, however, more patients are living with heart failure. [26] A significant portion of myocardial tissue could be theoretically salvageable from ischaemia-reperfusion injury, if the treatment is applied early enough, and by doing so could limit the risk of developing heart failure.

1.2 Rationale for Novel Therapies

ACE inhibitors, beta-blockers and aldosterone antagonists are the backbones of heart failure treatment. However, NICE data indicates that prescribing of ACE inhibitors, beta-blockers and aldosterone antagonists remains suboptimal, and that improved use of these drugs has the potential to reduce hospitalisations and deaths caused by heart failure. Intolerance of the side

effects such as the deterioration in renal function, hypotensive crisis, hyperkalaemia, angioedema and cough could limit the use. Recently Sacubitril/valsartan and SGLT2 inhibitors have been shown to be efficacious. [27] [28] [29] [30]A radical treatment such as cardiac transplantation and circulatory assisted device (LVAT) could be considered, but there is a lack of available organs. The 10-year data on organ transplantation from 2008-2018 indicated that the number of patients on the transplant waiting lists increased out of proportion to the actual number of heart transplants. [31] The data from the publication were extracted and presented in **Figure 1-1**. With immunosuppressant, the risks for infection, atherosclerosis and cancer are increased. In the UK, the chance of survival after heart transplantation over ten years is 55.4%; [31] albeit better than 50% chance of survival in one year for patients with severe heart failure (NYHA class IV). [32] LVAT could be a bridge treatment to heart transplant or rarely as destination therapy, carries the complications of infection, thrombosis, stroke, arrhythmia, and pump failure.

Figure 1-1. UK Heart transplant statistics: biaxial plot of the number of patients versus the financial years; the data was extracted from an annual report document.[31] Symbols represents number of patients plotted with trendlines.

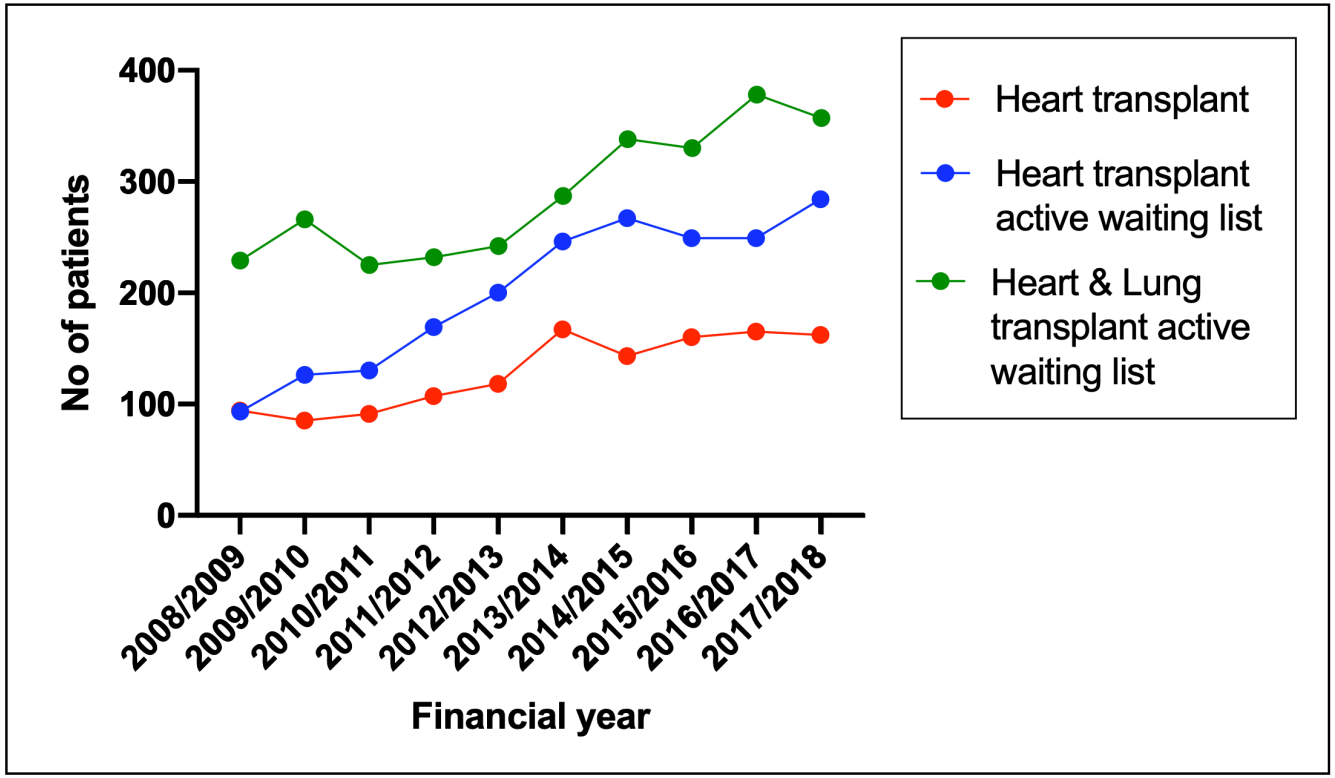

1.3 The Rationale for Studying Cardiac Ischaemia-Reperfusion Injury

In ST-elevation myocardial infarction treated with acute revascularisation with primary angioplasty, it is estimated that 50% of the final infarct size is attributable to reperfusion injury and the incidence of heart failure is around 25% of the acute cases. [33] [2] Limiting the infarct size could translate to better clinical outcome in terms of heart failure prevention. In human, reperfusion therapy is most effective when the treatment is applied < 90 minutes of symptoms onset. If a cardioprotection treatment adjunct is applied with reperfusion, there is a theoretical advantage in improving myocardial salvage beyond that what could be provided by reperfusion therapy only.

Myocardial IR injury has been extensively reviewed in these publications. [1] [34] [35] Briefly, myocardial IR injury refers to the concept that reperfusion of ischaemic myocardium could result in more tissue death of viable tissue at the moment of tissue reperfusion; however, less than the final infarct size of the heart without reperfusion. In theory, the total IR injury (infarct size) is the sums of the ischaemic component and the reperfusion component. The infarct size increases as the severity of ischaemia increase which correlates with the ischaemic time and the severity of blood supply reduction compared to baseline. Further, while the ischaemic component is salvageable by reperfusion treatment, there is a therapeutic window when exceeded, the

tissue injury becomes irreversible, [36] and when the ischaemic component becomes a greater contributor to final infarct size than the reperfusion component. [34] Within the therapeutic window as demonstrated in animal models, the reperfusion component contributes up to 50% of the final infarct size; [1 37] hence, it is an attractive therapeutic target for infarct size reduction. As the temporal evolution of tissue necrosis and AAR are challenging to assess accurately during reperfusion, the existence of lethal reperfusion is indirectly revealed in experimental models by the positive effects of infarct size reduction by cardioprotection treatments compared to untreated controls.[35] Adjunctive treatments such as ischaemic conditioning (applied pre or post), [38] [39] remote conditioning (applied pre, per or post), [39] and pharmacological agents (such as adenosine, cyclosporin and metoprolol) [40 41 42] applied per or post ischaemia, all have been shown to reduce infarct sizes than controls.

This thesis reports the novel use of shockwave treatment in myocardial IR. There is a gap in knowledge on the putative molecular mechanisms used by shockwave to mediate its cardioprotection effects compared to thousands of publications on ischaemic conditioning, where over one hundred signal molecules and mechanisms have been reported. [43] Very likely, shockwave uses some of these pathways in the mediation of cardioprotection. It is outside the scope of the thesis to review all the possible pathways; nevertheless, they could be deduced from the secretomes of shockwave induction, and these are

briefly discussed in section 11.8. Two major pathways that are linked to ischaemic conditioning treatments involve the activation of ERK 1/2 and AKT (collectively known as the RISK pathway); and the TNF-α and STAT3 pathways (collective known as the SAFE pathway). Both RISK and SAFE pathways could activate eNOS. Shockwave could access the RISK pathway via secreted ligands such as the SDF1 and VEGFA, and without ligand via mechanotransduction. As shockwave induces MCP1 expression (see chapter 10), which is known to be inducible by TNF-α, it is speculated that the SAFE pathway is quite likely involved.

Time is the essence in primary angioplasty. The phenomenon of ischaemia-reperfusion injury could be observed most in terms of survival benefits in those who are reperfused early— rationalises the call for cardioprotection treatment adjunct. In a study involving 1352 patients with STEMI, [25] it was demonstrated that the thirty-day-plus late cardiac mortality was the least in the group with reperfusion time of less than 2 hours, compared to groups with later reperfusion times (2-4 hours, 4-6 hours) and < 2hour group had the best the recovery of LV systolic function. (See **Figure 1-2**).

In another study involving 11,489 patients on the national Swedish Coronary Angiography and Angioplasty register who presented with STEMI comparing the 1-year mortality according to reperfusion time 0-30mins, 31-60mins, 61-90 mins, 91-120 mins and 121-360 mins; showing respective mortality hazard

ratio of 1.00, 1.08, 1.26, 1.41 and 1.51; and respective odds ratio of for severe heart failure of 1.00, 1.15, 1.74, 1.72 and 1.88.[44] The study showed reperfusion of STEMI after 90 minutes significant increase the odd ratio for severe heart failure.

In a CMR study[45] on STEMI patients evaluating myocardial salvage, infarct size, myocardial oedema and MVO (microvascular obstruction); comparing reperfusion times of 90mins, 90-150mins, 150-360mins and 360mins; it was discovered that myocardial salvage was significantly reduced in the groups of time to reperfusion >90 minutes, the effect was also associated with a progressive increase in the MVO and infarct size, while there was no difference in myocardial oedema size in the groups. The study suggests the efficacy of reperfusion therapy is time-limited to when myocardial salvage occurs. (See **Figure 1-3**)

Figure 1-2. Kaplan-Meier survival curves of 30-day-plus according to time of reperfusion in STEMI. [342] Reproduced with permission under license agreement no 4970230470250 in Appendix 4.

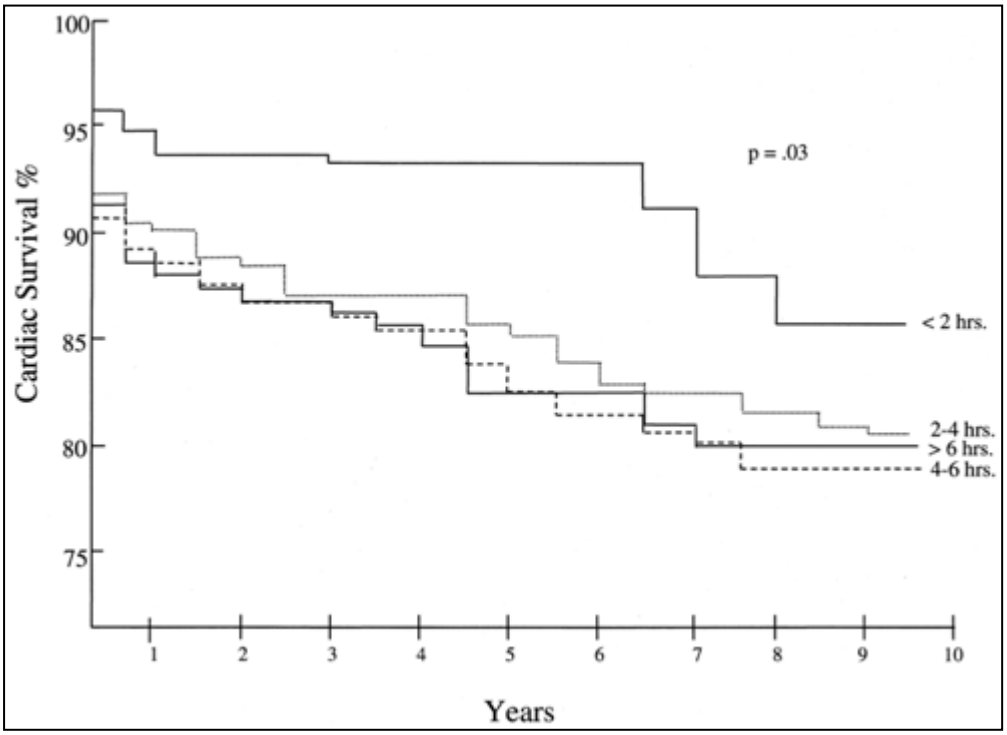

Figure 1-3. Bar charts (A) Infarction, (B) myocardial oedema, (C) myocardial salvage and (D) MVO. Data was expressed as the % to ventricular mass. [45] Reproduced with permission under license no 4970230731053 in Appendix 5.

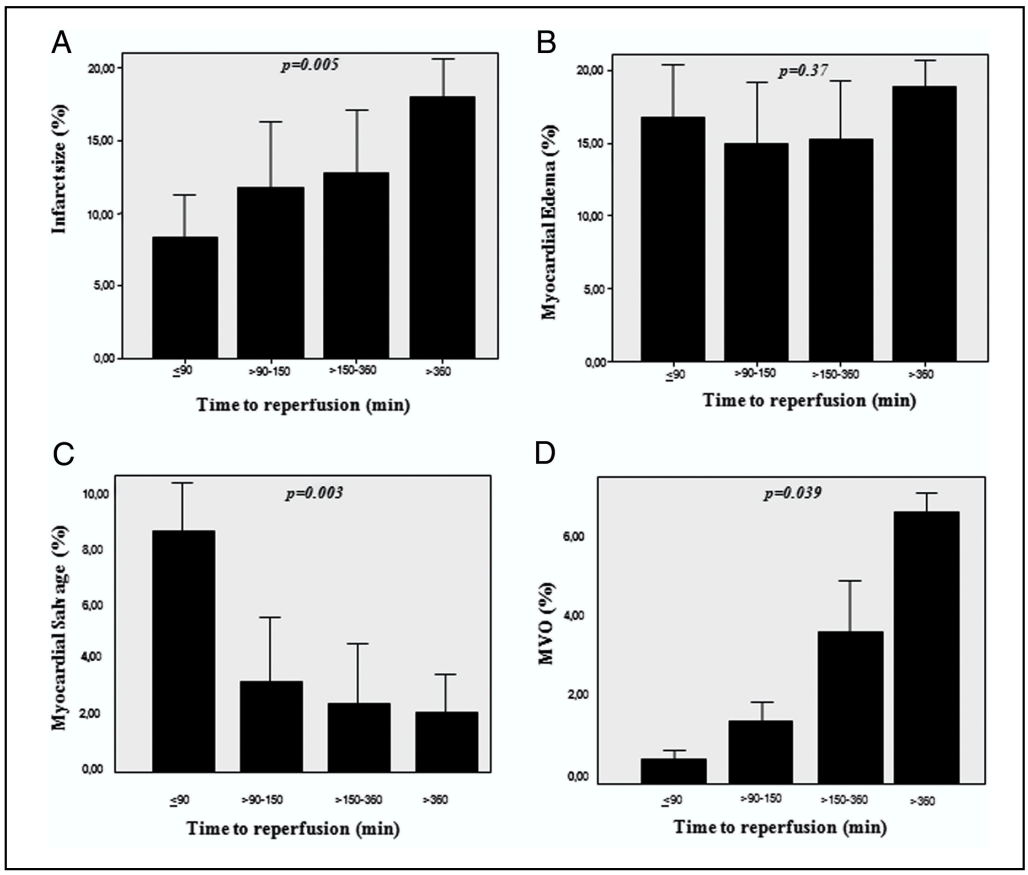

1.4 Rationale for SDF1 as a Target

SDF1/CXCR4 axis is one of the main axes in stem cell trafficking and homing. Oxygen tension in tissue regulates the expression of SDF1, such that with reduced oxygen tension, the transcription factor HIF-1 stabilises[46] then upregulates SDF1 expression.[47] In that way, the hypoxic gradient created in tissue with ischaemia would favour progenitor cell mobilisation towards ischaemic regions. Although SDF1 expression occurs immediately after MI, as hypoxia diminishes, the signal is lost at one week, hampering stem cell homing. [48] Whereas ischaemia requires HIF1 for SDF1 expression, shockwave induction of SDF1 in tissue is independent of HIF activation and hypoxia. [4] If SDF1 gradient were to be exploited for progenitor homing, it should be maintained. Furthermore, there is a limited supply of regenerative progenitors in the circulation, and these would need to be replenished first from the marrow. By the time the new progenitors are released into the circulation, the homing signal to the heart has faded away and is too late to effectively perform the rescue. The lag of mature CXCR4+ cells in the circulation to SDF1 expression in tissue could provide the explanation of inefficient homing of progenitors to the heart. The interaction of SDF1/CXCR4 is known to activate the integrin and other attachment molecules that are essential for cells retention and survival.[13]

A study of SDF1 biodistribution on normal rats using radiolabelled SDF1 in the form of [99mTc-MAS3]-SDF-1α showed the half-life of 25.8 ± 4.6 minutes, where after 2 hours of intravenous injection, 73.8 ± 6.1% of the injected dose was found in urine and faeces, very low uptake in all organs showing 0.1% radioactivity, except in the kidneys where the radioactivity was 0.5%. It was assessed further in rats that had ischaemia-reperfusion myocardial infarctions, 24 hours later injected with [99mTc-MAS3]-SDF-1α and assessed two hours after injection; compared to normal sham which also administered with [99mTc-MAS3]-SDF-1α, there was an increase in radioactivity only in the infarcted myocardium corresponding to an increase in CXCR4 expression. [15] The study has suggested that the half-life of SDF1 in the blood is very short, and the gradient of CXCR4 expression is higher in ischaemic tissue than in healthy tissue.

It is, however, debatable that SDF1 exist in the free form in the blood. A study of cytokine profiling of serum-derived exosomes revealed that abundance of detectable SDF1 was found at a higher level in aliquots of lysed exosomes than intact exosomes, suggesting that SDF1 exists inside exosomes. [49] Exosomes can also express CXCR4.[50] In a mouse study of multiple myeloma disease model, SDF1 and MCP1 were carried on exosomes, blocking with AMD3100 and CCR2 antagonist, reduced exosomes induced cell migration. [51] The existence of SDF1 in exosomes come as no surprise as exosomes are the novel mediators in cell-

cell communication, and recently exosomes have been reported to have specificity to target organs via the surface ligands. The modification of the surface of exosomes could be useful to control their pharmacokinetics. For example, exosomes with RVG-lamp2b surface molecule of dendritic cells has selective distribution to the brain[52] and exosomes with Integrin 64 of 4175 cells has selective distribution to the lungs. [53] MiR-19a-3p containing exosomes has been implicated as the effector of shockwave on angiogenesis and fibrosis reduction. [54] Three theories exist on exosomes uptake into cells, either by receptor-ligand interaction,[55] endocytosis via phagocytosis, [56] and fusion; [57] the specific receptors, however, remain elusive. Cue from HIV infection model has shown that platelets' derived particles could transfer CXCR4 receptor to CXCR4-null cells, making them susceptible to infection by X4-HIV and that exosomes can express CXCR4. [50]

1.5 Rationale for the use of DPP4 Inhibitor

In the intestinal epithelium resides the carbohydrate-sensing enteroendocrine L-cells and K-cells, respectively secreting the incretins GIP and GLP1 that have an insulinotropic effect on the pancreas. The half-life of GIP and GLP1 are in the order of a few minutes due to rapid proteolysis by the DPP4 enzyme ubiquitously expressed in the body, on the T cells, and could exist in soluble membrane-bound form from cells shedding. The DPP4 inhibition, hence, could

increase the bioavailability of the incretins and lowers glucose level via insulin secretion.

In a Langendorff heart experiment of prediabetic rats and control rats, with and without 4-week pretreatment with DPP4 inhibitor; the hearts were subjected to 35 mins coronary ligation; the infarct size of the control with and without DPP4 treatment was similar; however, the infarct size of the prediabetic rat without DPP4 treatment was larger than the infarct size of prediabetic rat with DPP4 treatment.[58] The phenomenon was attributed to the restoration of GLP1 in prediabetic rat to a normal level. This was shown not to be the case using GLP knock out mice of acute vascular injury model, where the treatment with Sitagliptin caused a faster carotid repair by an increase in the recruitment of CXCR4 endothelial progenitors to the injury site compared to control mice, indicating SDF-1/CXCR4 axis could function independently of gliptin route. [59]

SDF1/CXCR4 is the main target in the thesis. To name a few, other interesting substrates of DPP4 are the BNP, Substance P, IGF1 and Erythropoietin. The roles of these substrates will be discussed in **section 2.7**.

There are some evidence that DPP4 inhibition could artificially prolong SDF1 half-life and be used to enhance cell homing to enhance tissue repair. In patients treated with Sitagliptin, it was observed at 4-week, the circulating endothelial progenitors were increased, with a corresponding increase in

plasma SDF1. [60] Low level of endothelial progenitors has been implicated in micro and macrovascular complications in patients with metabolic syndrome and diabetes. [61] [62]

Indeed, when CXCR4 receptor antagonist AMD3100 was applied (below the threshold of cell mobilisation effect) with Diprotein A (a DPP4 inhibitor) and GCSF, the rescue effect on infarct size, cell homing, systolic and diastolic function were annulled. [63] GCSF was not considered in this thesis because GCSF-mobilised progenitors are mostly immature monocytes and granulocytes, often in G0/G1 of cell cycle and have a smaller proportion bearing CXCR4+. [64] Moreover, GCSF cleaves cells-surface adhesion molecules: CXCR4,[65] α-4-integrin and VCAM-1,[66] which are paramount for stem cells engraftment and myocardial regeneration function. Additionally, the drugs are expensive and not suitable for chronic administrations due to adverse effects, limiting their uses. AMD3100 was also not considered for the same reasons, it is only licensed for use with GCSF, and the fact that the competitive inhibition of CXCR4, exerted in the marrow for cell mobilisation, are also exerted in the upstream organ target impeding cell homing. [67] Via logic, releasing too many progenitors in abundance is probably not wise because there could be a limit in uptake capacity, then wasted, and the exhausted marrow then needs time to recover. It is, however, relevant if the cells were to be collected using

leukapheresis and to be processed further under GMP for maturing process and then reimplanted back into patients.

DPP4 inhibitor is a widely used antihyperglycaemic agent that can improve diabetic wound healing, independent of their beneficial effects on glycaemic control. In particular, DPP4 inhibitor promoted the migration and epithelial-mesenchymal transition of keratinocytes, directly and indirectly, by inducing SDF 1α production of fibroblasts *in vitro* and diabetic mice.[68]

1.6 Shockwave for Cell Homing

In the CELLWAVE trial, [11] a randomised control trial involving patients with chronic heart failure receiving either low-dose shockwave or high-dose shockwave administered 24 hours before intracoronary cells or placebo (saline) administration or placebo shockwave with intracoronary cells administration. After four months, the EF significantly increased by 3.5% in high-dose shockwave with marrow cells, where there was also a positive trend in the improvement of wall thickening, reduction of LGE volume and frequency of adverse event compared to shockwave with placebo. The marrow cells preparation in CELLWAVE trial was similar to the trial REPAIR-AMI, [69] where the marrow was aspirated from the pelvic bone; then it underwent a Ficoll–Hypaque gradient centrifugation for cell separation, a validated method to produce a heterogeneous cell population of hematopoietic, mesenchymal, and other progenitor cells, as well as mononuclear cells. The cells were resuspended in 10ml XVIVO 10 medium with 10% patient's own serum and then injected using intermittent stop flow intracoronary injection technique. The patients were pre-anticoagulated with intravenous heparin and abciximab (ReoPro).

The anticoagulant in the syringe for marrow aspiration in the CELLWAVE trial was heparin, a common method used in other similar trials.[70] [71] [72] As the

binding of heparin to proteins are covalent, heparin would not easily be washed off with repeated cell washing. Heparin is known to interfere with SDF1/CXCR4 axis by forming heparin-SDF1 complex limiting SDF1 bioavailability and preventing CXCR4 internalisation required for signal transduction.[73] Bivalirudin (anti-thrombin III inhibitor) could have been a better anticoagulant than heparin in these trials, and the use of acid citrate buffer in the syringe for marrow aspiration could have circumvented the problem of cells adhesion to cardiac tissue.

Heparin could also interfere with other cell communication[74] by binding to angiogenic ligands such as VEGF, HGF and FGF1/2; calcium ion channels, for example, in cardiomyocytes, heparin decreases calcium transient and contractility; [75] and to selectins and integrins, the adhesion cell molecules needed for cell migration. Indeed, heparin is a useful drug in the prevention of cancer metastases for these reasons.[76] The process of cell migration through the endothelium has been characterised in the steps of capture, rolling, activation, arrest and transmigration; [77] requires functional selectins and integrins.

In the CELLWAVE trial, shockwave could have been under-dosed by the fact that the reported maximum energy levels used were 0.051mJ/mm^2 and that only four spots applied at 750 pulses/spot. A spot is the focal area size of a focussed shockwave, and it is very small. The size of a spot within 90% of

energy-flux density is in the order of ~2mm in width and ~10mm in length. The shockwave treatment coverage was, therefore, too sparse for optimal induction of SDF1 expression in tissue. Moreover, there was no preplanning cardiac imaging to determine the tissue phenotype (infarction or hibernation), so the spots locations were inferred solely from the severity of regional wall motions abnormalities. Despite the limitations, the effect of marrow cells and shockwave on the EF was nonetheless evidently positive, albeit modest, and was also safe.

The effect of progenitors homing to tissue by shockwave was first reported in a hind-limb ischaemia nude rat model, [4] where shockwave facilitate homing of intravenously injected human endothelial progenitors cells to the treated leg compared to control untreated leg, corresponding to SDF1 expression in the treated tissue and improved tissue perfusion. Similar experiments have been performed in rabbits. [78] [79]

1.7 Stem cells

Through the seminal work of McCulloch and Till in the 50s, stem cells was discovered; they wanted to find a way to save military personnel who might sustain whole-body irradiation from nuclear weapons and determine marrow cells sensitivity to radiation. They experimented on lethally irradiated mice treated with bone marrow cells transplant and discovered splenic nodules

called colony-forming-unit-spleen (CFU-S), which later assayed to show that almost all of the individual CFU-S found to contain at least a few new colony-forming cells, each from a single cell. [80] The concepts of progeny, self-renewal and stem cells were born. By a different group of Lorenz et al., isologous bone marrow cells to lethally radiated mice were administered, and they discovered the mortality was reduced to 25% compared to 100% in non-treated mice. [81] The first successful human bone marrow transplant was performed in 1956 by Dr E. Donnall Thomas who took bone marrow from the healthy twin, and gave it to the other, who had leukaemia; he shared the Nobel Prize in Physiology or Medicine in 1990 for the method of bone marrow transplant using radiation and chemotherapy to kill own marrow cells, then treated with bone marrow cells from a donor.

The first stem cell cardiac trial was in 2002 in TOPCARE-AMI, on acute STEMI patients using the intracoronary injection of either marrow mononuclear cells or circulating blood-derived endothelial cells, wherein both, significant increase in the EF 51.6% to 60.1% was observed compared to matched-control showing EF of 51.1% to 53.5.8%, over four months period. Invasive stem cell delivery was employed rationalised by the belief that stem cells needed to be brought to the injury site in large quantities at the right moment. In the BOOST trial, in 2004, using intracoronary transfer of autologous bone-marrow cells within a few days of heart attacks, where the EF at six months increased by

6.7% in the cells group versus 0.7% in the control group. [82] Since these hallmark studies, there have been over 200 stem cells trials treating disease phenotypes of acute STEMI, ischaemic heart failure,[83] refractory angina[84] and non-ischaemic cardiomyopathy;[85] using variants of bone marrow mononuclear cells, marrow mesenchymal cells [86] and adipose mesenchymal cells;[87] using invasive delivery methods which later been shown to have little bioretention. Nonetheless, a meta-analysis and systematic reviews suggest, adult marrow cells treatment in acute, chronic ischaemic heart disease and heart failure is safe, delivers a modest effect on systolic function, and has potential on mortality benefits.[88] [9] The effects could be explained by paracrine mechanisms, which will be discussed in **section 2.6**. What is clear is that the SDF1/CXCR4 axis is the common effector to home stem cells to the heart.

Cardiomyocytes were viewed as terminally differentiated cells, once damaged irreplaceable; the belief has been refuted as there are some evidence of the existence of cardiomyocyte proliferation, deduced via methods of carbon-dating, genetic tracing, mathematical modelling and assumptions; the estimate of cardiomyocytes annual turnover is 1%, [89] [90] while some publications reporting higher estimates had been retracted. [91] It was also argued that bone marrow haematopoetic stem cell [92] and mesenchymal stem cells [93] could not differentiate into cardiomyocytes, leading to other research

routes to produce cardiomyocyte via direct-programming, [94] [95] using transcription factors, and miRNA. [95]

Putative cardiac stem cells took the spotlight for a decade, using markers such as Sca1+, Bmi1+, Isl1+ and ABCG2+, cardiosphere-derived: mesenchymal markers of CD90 and CD105, and c-kit. Results from preclinical cardiac stem cells studies were encouraging; however, the SCIPIO trial using c-kit cells in ischaemic cardiomyopathy was retracted from the Lancet,[96] and ALLSTAR trial using cardiosphere was abandoned at interim analysis over futility. [97]

Further, in mice knocked-in with interleaved and nested reporters inserted using CRISPR/Cas9, then injured with either doxorubicin or myocardial infarction, it was demonstrated that the contribution of putative stem cells to myocytes only happens in the embryonic stage but not in the adult heart, and new cardiomyocytes after injury were derived from preexisting cardiomyocytes, not from the endothelial cells, pericytes, fibroblasts etc. [98] The existence of c-kit cardiac stem cell was also refuted in another genetic-lineage mice study [99] and the paradigm-shift has been rescinded. [100]

In an earlier study on post mortem human male recipients of female-heart transplant, [101] sections of the left ventricle interrogated using fluorescence in-situ hybridisation (FISH) with markers of c-kit, MDR1, Sca-1, MEF2, GATA-4 and nestin; and the presence of Y chromosomes in the heart to indicate chimerism; showing 9±4% myocytes contains male chromosomes, of these, 17.2±4.2%

were Ki-67 compared to the rest of myocytes (from donors) were 1.0%±0.3 Ki-67; cells of Y chromosomes bearing MEF2D and GATA-4 were present, indicating a commitment to myogenic differentiation, also bearing nestin implying a more advanced stage of myocyte differentiation; there were significantly more MDR, c-kit and Sca-1 in the hearts of male recipients of female heart transplant than normal control, with a fraction contains Y chromosomes. Chimerism was also reported by another group, [102] detected in cardiac biopsies of living male patients of female cardiac transplantation.

1.8 Inotropy

Inotropy describes the state of contractility in the generation of force, where positive inotropy increases contractility, whereas negative inotropy decreases contractility. The pharmacological drugs that can modulate positive inotropy can be broadly classed into adrenergic agonists according to selectivity and have cross-reactivity to (adrenaline, noradrenaline, dobutamine, dopamine), PDE3 inhibitors (milrinone, levosimendan) and calcium desensitiser (omecamtiv, istaroxime).

β adrenergic agonists act via β receptor which is coupled with G_S protein and adenyl cyclase complex, converting ATP to CAMP to phosphorylates the PKA opening the L-type calcium channels causing calcium influx, in turn activating ryanodine-receptor-2 on the sarcoplasmic reticulum causing a large increase

in myoplasmic calcium. Calcium then binds to troponin, moving tropomyosin out of the way, exposing the binding sites on actin to myosin, free to form cross-bridges in the presence of ATP, resulting in contraction. In a low calcium state, this binding does not occur, so the presence of free calcium is an important regulator of muscle contraction.[103] PDE3 inhibitor prevents the degradation of CAMP and acts independently of the receptor.

The problems with inotropic agents are that the increase in contractility also counterintuitively increase the heart rate, energy expenditure and risk of arrhythmia. [104] With prolonged use, the receptors desensitised; increase the dose required to maintain the effect as toxicity increases. The patients could become dependent on inotropic support and become difficult to wean off the drugs. The use of such agents in heart failure are limited to specific emergency indications, in patients on a bridge to destination therapy (transplant, LVAT) and in the palliative setting. There are no clinically approved inotropic agents for mid and long-term use in heart failure. The general consensus is that the inotropic route via β agonist pathways could cause more harm than good in heart failure patients.

1.9 The Problems with Ejection Fraction

In a safe pair of hands, EF is relatively easy to perform. EF has widespread use in clinical guidelines in decision making on therapies selection and risk stratifications. For example, the MADIT-II trial showed a survival benefit of 23% to 31% of ICD recipients compared to patients without ICD treatment, where LVEF of <30% was used as an inclusion criterion.[105] Heart failure could be classed into HFREF, HFmrEF, HFPEF [3] with respective EF cut-off values of <40%, 40-49% and >50% when accompanied with symptoms and signs, and in the latter two categories, evidence of biomarker natriuretic peptide and other imaging biomarkers are required. However, there are several pitfalls in using volumetric LV measurement and ejection fraction; these argue the need to assess the cardiac function using multi-domain indices such as strain imaging; the feasibility of high frame rate strain imaging in a preclinical setting was explored using CMR in the thesis.

The stroke volume is calculated as the difference between LVEDV and LVESV. The ventricle of different sizes could have the same stroke volume, where the smallest ventricle would appear to be hyperdynamic in comparison to the largest ventricle; complicated further as the disease progressed and remodelling ensued, the cardiac mass could increase [106] and chambers dilate in order to maintain the stroke volume. To maintain comparability of EF

between, the measurements are indexed with the BSA, where normalisation error could be introduced in overweight and obese individuals,[107] [108] and in patients with cardiac cachexia, a wasting condition prevalent between 8-42% of heart failure populations.[109]

The contractile reserve in a failing heart is often unknown in human and difficult to assess without exercise; the assessment is virtually impossible to be performed longitudinally in the preclinical setting. Contractility is invasively assessed using dV/dt_{max}, an index of the myocardial contractile reserve with dobutamine stress, [110] which correlates with peak $VO_{2\ max}$.[111] Strain rate has been proposed as a non-invasive method to measure contractility. [112]

Furthermore, EF is still calculated using geometric assumptions: in the human biplane, the Simpson EF method could miss the effect of lateral infarction on the chamber volumes; and in LAD myocardial infarction models, the parasternal-long-axis view is often used by itself, consequently missing the effect on the anterior free wall not in view, then invalidates the assumptions based on the transformation of linear chamber dimensions into volume. Teichholz and Quinones EF methods are obsolete in clinics; however, they are still being used in pre-clinical cardiac imaging and accepted in scientific publications.[113] [114]

The ejection fraction could change because the loading conditions have changed, where an increase in stretch (preload) could increase the contraction

and EF, and in reverse, a decrease in afterload could increase the EF; via the Frank-Starling mechanism. For example, in mitral regurgitation when the afterload is reduced, the preoperative ejection fraction may be normal; however, in a third of the cases have a decrease postoperative EF affecting long-term survival. [115] Bloodletting and leaches had been used for centuries as treatments for acute decompensated heart failure before diuretics and nitrates became available, [116] all of these exert the positive effect via reduction of cardiac loading.

In acute myocardial infarction, normal EF value could be a false reassurance of health because of hypercontractility due to adrenergic stress response in the adjacent segment. [117] Conversely, impaired EF after reperfusion could be due to myocardial stunning, a phenomenon of transient dysfunction without evidence of necrosis which takes days to weeks to recover.[118] Moreover, EF being a global parameter, does not take into account of the regional function, when the treatment is often applied locally. The change in experimental intervention is often small; hence, a more sensitive detection method needs to be available or needs to be developed first. GLS is a predictor for adverse cardiac remodelling.[119]

There are many methods and modalities in deriving EF, for example, MUGA, X-Ray fluoroscopy LV ventriculogram (monoplane, biplane), echocardiography (biplane, triplane, 4D), different sequences in CMR for LV stack, different

segmentation methods, hence, the absolute EF values cannot be directly compared. The use of machine learning, semiautomatic segmentation and core lab reading in clinical trials have been proposed to negate the variability in human segmentation. [120] [121]

1.10 High Frame Rate Cine

In humans as per the Task Force of EACVI/ASE/Industry in standardisation of deformation imaging, a frame rate of 50-80 fps is required for the optimal assessment of strain, [122] [123] [124] and a higher frame rate of >100 fps may be required even at rest if all mechanical events are to be resolved, especially when time-dependent parameters, such as velocity and strain rate to be interrogated. There are six phases of mechanical events in a cardiac cycle: rapid ventricular filling (in diastole), diastasis (in diastole), atrial contraction (in diastole), isovolumetric contraction (in systole), ejection (in systole), and isovolumetric relaxation (in diastole). When myocardial tissue motions are concerned, during systole, there are pre-ejection velocity (S1), peak ejection velocity (S2) and post ejection velocity which could be biphasic, and during diastole, there are phases of early relaxation (E), diathesis (period of no contraction between E and A) and the late atrial filling (A). The systole begins when the aortic valve closes, and the diastole begins the mitral valve closes. In

rats, it is not possible to capture all these events in a low frame rate cine without introducing under sampling errors.

In clinical CMR, breath holdings during cine acquisition are used to avoid motions from respiration. Breath-holding is not practical in rodents, although not impossible to perform. It would involve endotracheal intubation, starting and stopping artificial ventilation whilst under anaesthesia; could increase the scan time, operator errors and injury to the animal. Respiratory gating is used instead in rodents when the cine image acquired during the respiratory plateau is detected using a balloon pressure sensor during prospective cine acquisition.

The heart rate of a rat is 320-500bpm, and the respiratory rate is 86bpm. As the mechanical events become shorter with increasing heart rate, it becomes a necessity to acquire cine images at a high frame rate to be able to resolve the desired events required in the thesis. In this thesis, a frame rate of 350Hz could be achieved via retrospective gating, when the data was continuously acquired then grouped to fill the k-space according to the phase of the cardiac cycle and in-slice navigator signal used to correct for in-slice motions.

1.11 The Pro and Cons using AAR using T2

In IR animal models, infarct size and AAR are often quantified in histology using Evans blue and TTC staining, or microspheres. Best performed *ex vivo* on a

perfusate system, Evans blue (or fluorescence labelled microspheres) infused after the coronary artery religation (suture left in situ) to demarcate the viable remote regions as blue (visualised under ultraviolet in the case of microspheres) and the AAR unstained. [125] Then, triphenyltetrazolium chloride (TTC) is infused whilst the ligature is off to stain the viable remote tissue as brick red and infarcted tissue left unstained as white. The heart cut from apex to base into short-axis cross-sections, then mounted on a plate and digitally photographed. The analysis could be performed in ImageJ for segmenting the white area as necrosis, the red brick area as AAR, and the blue area as remote. Despite the drawbacks of tissue shrinkage, dye bleaching and dye overrunning into other regions introducing errors in quantification, Evans blue-TCC histology has been validated in control animals to represent the AAR and infarct size, respectively using CMR T2-mapping and LGE. [126]

The application of T2 relaxation time for detection of myocardial oedema was first reported in the *ex vivo* NMR scans of myocardial infarction dog hearts, which showed that after 24 hours of LAD-ligation, the T2 value of the infarcted myocardium (48 ± 2ms) was higher than the normal region (42 ± 1 ms), and the tissue water content was significantly greater than the normal myocardium. [127] T2 techniques (GRASE or spin-echo) have been validated using MRI phantoms, showing a strong correlation with total water content with negligible systematic errors and random errors. [128] In this thesis, T2-map was

used to threshold for oedema, a surrogate for AAR, which was the area or volume of the myocardium distal to the coronary occlusion that would be infarcted had the blood supply not been re-established.

T2 map was adopted over T2W in the experiments in the thesis because at 9.4T, T2W had unacceptable variability from motion artefacts. Moreover, black blood cannot consistently be achieved, leading to errors during segmentation; and the variabilities in the contrasts between slices and between animals were difficult to control. T2-map was the best available quantitative MRI method available at the university, and it was adopted in the experiments with prior knowledge of the caveats. AAR after reperfusion injury had been reported to be not stable (displaying unimodal versus bimodal pattern). Furthermore, AAR could be affected by the intervention under study, the concomitant medications used and the coexisting pathological conditions. The change in T2 could be dependent or independent of conditions affecting T1 relaxation.[129]

Fernández-Jiménez et al. used pig models of cardiac ischemia-reperfusion injury to validate T2-mapping for oedema detection using gradient-spin-echo versus T2 turbo-spin-echo, which showed a strong agreement between the two sequences with the latter being three times faster. [130] Serial scans were taken at baseline, 2-hour, 24-hour, 4-day and 7-day post-reperfusion, showing the T2 in the ischaemic myocardium increased from baseline to 2-hours then dipped at 24- hour and to increase again to persist at 4-day and 7-day. Using a

T2 weighted sequence T2-STIR, the same group reproduced the same results in pigs [131] and STEMI patients treated with primary angioplasty.[132] However, in a retrospective multicentre CMR study using T2-STIR and CS-SSFP involving 215 patients from 17 centres, [133] the T2 bimodal pattern was not demonstrated either in size, quality of AAR, or detectability of the culprit artery; concluding that the diagnostic quality of AAR was constant over the first week.

The effect of bimodal pattern in reperfusion injury could be explained by the phenomenon of intramyocardial haemorrhage in acute myocardial infarction. Carrick et al. studied the time course of myocardial oedema using native T2 and T2* in STEMI patients treated with primary PCI; they discovered, the oedematous segments without haemorrhage displayed a unimodal pattern, whereas those with haemorrhage displayed a bimodal pattern.[134]

It is known that pigs have minimal collateral myocardial blood supplies,[135] a predisposition to haemorrhagic transformation in acute infarction. [136] This could explain the bimodality effect discovered by Fernández-Jiménez et al. In human, collateral blood supply is well developed compared to other species other than the Guinea pigs; [135] and in CAD patients with good collateral supply, ischaemia could be prevented after a brief occlusion in a third of individuals. [137] In STEMI patients with poor collateral blood supply, the MVO and infarct size were more extensive, and the clinical outcome was poorer than in patients with good collateral supply. [138] In the studied cohort of Patterson et al., the

risk for haemorrhage was increased as the size of the MVO and hypointensity score increased; and if the patient was on beta blocker on admission. As MVO was correlated with infarct size,[139] it was speculated that reperfused myocardial segments with poor blood supply had a higher risk of haemorrhagic transformation and hence, more readily detectable in pigs than in human. However, in a clinical study by Kim et al. on STEMI patients, even though there were more haemorrhagic transformations in those with poor collateral supply than those with good collateral blood supply, the effect was not significant. [140] Additionally, in a pig study by Hansen et al., the T2-STIR and T2-map could not distinguish MVO with and without haemorrhage. [141]

The effects of several experimental interventions on AAR and infarct size are briefly discussed here. In CHILL-MI trial [142] and MITO-CARE trial, [143] respectively, the AAR was not affected by therapeutic hypothermia and the MPTP opening inhibitor TRO40303. Another trial of note was the nitric oxide (NOMI) trial, which reported that timely reperfused MI treated with 4-hour inhalation of NO did not reduce the infarct size relative to absolute LV mass while the AAR measured using T2-STIR was not different between the NO treatment group and control.[144] Furthermore, the REFLO-STEMI trial involving STEMI PCI patients with study arms of control, adenosine and sodium nitroprusside revealed that the treatments did not reduce the infarct size, MVO, nor AAR. [145] However, AAR was affected by post-conditioning treatment.

For example, Thuny et al. discovered that T2-STIR AAR and LGE infarct size were smaller in the post-conditioned than untreated reperfused STEMI.[146] White et al. also found that remote ischemic conditioning could reduce myocardial oedema and infarct size, and increase myocardial salvage. [147] In ischaemic preconditioning mice, the read-out of AAR using T2-map was underestimated compared to the read-out of AAR using ASL. [126]

A few examples of concomitant medications that could affect the severity of reperfusion injury are nitro-glycerine nitric oxide, oxygen therapy and morphine. The sub-analysis of the NOMI trial on the use of intra-arterial nitro-glycerine nitric oxide in STEMI patients treated with PPCI discovered that those who had received intra-arterial nitro-glycerine nitric oxide had greater AAR and infarct size than the group without the drug. [144] Oxygen supplementation in STEMI patients without hypoxia could cause larger infarct sizes, greater arrhythmia frequency and recurrent myocardial infarctions than the group without oxygen; [148] possibly via the production of free radicals. In a multicentre study involving 734 STEMI patients, intravenous morphine treatment did not affect the overall MVO, infarct size and the difference in the 12-month survival compared to the group without morphine treatment; however, in the subgroup reperfused less than 120 minutes, the MVO and infarct sizes were smaller in the group with morphine than without morphine. [149] In the CIRCUS trial assessing the effect of cyclosporin in STEMI, there was no difference in all-

cause of mortality and infarct size assessed using peak CK between the groups with and without morphine. [150] Concomitant medications such as aspirin, GP IIb/ IIIa inhibitor, and P2Y12 ADP inhibitor that affect the platelets' function could negatively impact the attachment molecules needed to home progenitors.

Chapter Two

EPISTEMOLOGICAL AND ONTOLOGICAL POSITIONS

2.1 Ejection Fraction is not Sufficient to Assess Cardiac Function: Strain Imaging Could be the Answer

To the best of my knowledge, there has not been a proper GLS analysis performed in a preclinical model using the 3 AHA recommended long axis planes. There is one mice study using two long-axis planes, limited to 15 phases per one cardiac cycle using a 3 Tesla small animal MRI scanner. [151] Rodent's heart is very small, making the cardiac planning very challenging, requiring detailed knowledge in cardiac anatomy for correct planning to be applied, where a small error in angle can result in undesired anatomical structure included, and vice versa. To the unwary, the left ventricle slice could be

foreshortened; foreshortening has a significant impact on longitudinal strain measurement.[152] Because of these limitations, strain imaging is understudied in the preclinical model.

Cardiomyocytes are the building block of the heart, connected to each other by intercalated discs at their side-ends (which typically branched out), forming functional units of cardiac syncytium of four to six cells thick in continuous laminar sheets called sheetlets.[153] Transversely across the sheetlets, the myocardial fibres' helix angles change smoothly from about 60° on the inside to 0° on the mid-layer to about -60° on the outside. [154] [155] CMR diffusion tensor imaging (DTI) is a useful technique in assessing myofiber orientation. The Eigenvector of the largest diffusion tensor eigenvalue was shown to be parallel to the local fibre orientation.[156] Win-Yih et al. using DT CMR, reported that the directions of myocardial fibre, sheets and sheet normal correspond to the first, second and third eigenvectors. [157] The dynamic of sheetlets during left ventricular wall thickening has been characterised using DTI in human in the healthy and diseased states.

The helical fibre arrangements confer mechanical advantage such that the EF of 60% could be achieved from just 15-20% shortening of cardiomyocytes. [158] [159] Myocardial tissue excursion is often used to assess regional systolic function; however, there are no myocardial fibres in radial orientations, as it is a composite thickening effect of the myocardial layers. Using strain imaging,

myocardial contraction can be studied in any direction in the domains of strain, strain rate, displacement and velocity, beyond what can be achieved using ejection fraction. During systole, the basal segments rotate clockwise when viewed from the apex, termed twist and carry a negative value. The apical segments rotate anti-clockwise when viewed from the apex, termed untwist and carries a positive value.

The nomenclature and standardisation of strain imaging have been set by Imaging Societies, [160] [161] and have a stable ontology to be used in this thesis. Strain imaging could be useful in the study of ischaemia-reperfusion injury and the effect could be studied in myocardial layers and AHA segment models following coronary blood supply. It is recognised that the subendocardial layer is more susceptible to ischemia and fibrosis because the oxygenated blood is supplied in diastole by collapsible capillaries, and they are more compressed when the ventricle is dilated.[162] The change in the experimental intervention was expected to be small; hence a sensitive detection method needs to be available or needs to be developed first to serve as the foundation in the assessment methods of ischaemia-reperfusion injury.

There is a rat study using a phase-contrast MRI technique to assess myocardial motions achieving a temporal resolution of 3.2ms, using three separate acquisitions for each cardinal direction (x, y, z) for one slice, and these were reconstructed and normalised into one final image during post-processing. [163]

However, only the mid slice was interrogated, reflecting the limitation of the method in the practical sense.

2.2 Stem Cells Have Regenerative Effect

Cellular therapy using bone marrow progenitor cells indeed can produce functional improvement following myocardial infarction, and meta-analyses including thirty eight randomised controlled trials suggest potential mortality benefits;[88] however, the results from clinical trials so far are modest in magnitude. This could be explained by poor cell homing, poor cell survival and the fact that a single dose might not be enough to promote a sustained improvement in the left ventricular function. Stem cells may exert their regenerative effect partly or mostly through paracrine factors. Like drugs, paracrine factors have a half-life, likely need repeating dosing to maintain the desired therapeutic effect.

Stem cell regenerative effects are broadly based on four theories, and there are debates which theory holds true. In trans-differentiation theory, stem cells would differentiate into new cardiomyocytes. [164] In cell-fusion theory, stem cells would fuse with cardiomyocytes,[165] deducted from the phenomenon of binucleation and trinucleation in cardiomyocytes exist in synkaryon and heretokaryon. In the activation of resident cardiac stem cells theory, the exogenous stem cells would activate the stem cell niche via paracrine factors

for transformation into new cardiomyocytes.[166] In the proliferation of cardiomyocyte theory, the paracrine factors released by adult stem cell induces resident cardiomyocytes to proliferate.[167] The evidence of preclinical and clinical safety and efficacy using stem cell variants have been discussed in **section 1.7**.

2.3 Stem Cell Homing Is Poor

Imaging-based studies of stem cells tracking have demonstrated that cells retention in the heart, regardless of the methods of delivery is poor, with most of the cells eventually ending up in the spleen and liver. In a pig study, mesenchymal cells labelled with carboxyfluorescein succinimidyl ester then injected via into the mid myocardial layer via a pre-prepared catheter. The coronary sinus blood sampled before cells injection, immediately post-injection, 2 minutes and 4 minutes; it was observed via cytometric analysis, within a few heartbeats after injection, substantial cells quantities were wash-out in the coronary sinus.[168] In another pig study of ischaemic cardiomyopathy models, transendothelial and intracoronary infusion of ^{111}In-labelled MSC were compared between acute MI and chronic MI showing no difference, where the retention of the cells in the heart at 4 hours post-injection detected using whole body γ camera showing mean range 11-16% of the injected dose, ~20-30% detected in the lungs, 3-5% of the dose in the kidneys ~4-5% in the liver and ~1% of the dose in the spleen. [169] In a human study, intracoronary injection of marrow mononuclear cells labelled with ^{99}mTc revealed the retention of the cells was also poor, in which at 2 hours the cell retention in both acute and chronic myocardial infarction was in the order of a few per

cent; and at 20 hours the cell retention the acute was up to 1.3% and in chronic myocardial infarction was 0%, the cells end up in the liver and spleen. [14]

2.4 Improvement of Cells Homing could Be Achieved by Chemotaxis

Chemotaxis is a natural biological phenomenon when the cell could sense an external signal via the cell-surface receptor and move towards or away the gradient,[170] enabling the recruitment of cells in a guided direction. During chemotaxis, actin cytoskeletons rearrange forming lamellipodia, the ruffling of the membrane which anchors on the leading edge and withdraws from the trailing edge of the substrate for propulsion.[171] Several types of chemokine cell-surface receptor have been described in biology: G-protein, serpentine receptors, tyrosine kinase type;[172] however, all the 23 known human chemokine receptors are G-protein, and each receptor could have more than one ligand (pleiotropism), and there are 47 ligands have been discovered. [173] Of these, the SDF1/CXCR4 axis is the major route for progenitors' chemotaxis and homing.

2.5 The Heart Responds to Mechanotransductive Effect of Shockwave Inducing Chemotaxis

Shockwave is extracorporeal by nature; being a longitudinal wave, the energy travels in the direction of the motion where it could cause rapid symmetrical

compression and slower asymmetrical rarefaction in the media travelled. Through, miniaturisation; control of cycle repetitions; energy levels; reflective lens and focusing lens, the shape and distance of the over-pressure field could be controlled; to the desired therapeutic level. While natural shockwave has a frequency range of 150kHz to 100MHz and the wavelength could be as short to a few hundredth of nanoseconds, clinically applicable energy ranges are just in a few millijoules per millimetre square. The positive overpressure amplitude could be six-fold more than the negative overpressure amplitude, whereas the decay of the positive overpressure amplitude could be one-thousandth more rapid than the negative overpressure amplitude, in effect causing 'complex shear stress' and activate the mechanoreceptors at multiple sites. Mathematically, shear stress described only in one dimension is not sufficient to explain the mechanical properties of shockwave; shear stress is usually expressed in Dyn/cm^2, a unit measurement of accelerated weight in gram per square cm per second where 1 Dyn/cm^2 is equivalent to 0.1 Pa; and the negative and positive components and rate of decays are missing.

The tissue distortion translates into mechanotransduction, cellular mechanisms by which load-bearing cells sense physical forces, transduce the forces into biochemical signals, and generate appropriate responses leading to alterations in cellular structure and function, or release of signalling factors. The known sensors for mechanotransduction are cell-to-cell adhesions

(cadherins, gap junctions), cell-to-extracellular matrix adhesions (integrins, focal adhesions), cytoskeletons (microtubules, microfilaments and intermediate filaments) and surface processes (primary cilium, stereocilia). The heart contains cell types that have been described to possess mechanosensors. [174] The transduction of mechanical stimuli could also be initiated at the mechanosensitive ion channels, also known as the stretch-gated ion channels to cause an influx of ions such as calcium to act as a second messenger. Further, cells could communicate via gap junctions, hydrophilic channels path of cells interior known collectively as Connexin where an electrical coupling in cardiomyocytes happens, and passage of signals so that the cells coordinately respond as one unit, have a role in passing on death signal in ischaemia-reperfusion injury.[175] For example, Connexin type Cx46 is a mechanosensitive hemichannel and bipolar; when negative potential stress would open the gates and positive potential stress would close the gate.[176]

The molecular mechanisms of cardiac shockwave treatment are underreported, and the possible mechanisms, however, could be inferred from other cell types treated with shockwave. Shockwave treatment on neural stem cell promotes cell proliferation via P13K/AKT, which then phosphorylates FOXO3a leading to the upregulation of Cyclin D1; and promotes neurogenesis via Wnt/β-catenin and NOTCH pathways.[177] Shockwave treatment on mesenchymal stem cells *in vitro* induces proliferation, and self-renewal via

upregulating NANOG, OCT-4 and SOX-2.[178] YAP/TAZ have roles in mechanotransduction. [179] In subchondral stem cells, shockwave increases YAP expression and nuclear translocation with a proportional increase in the expression of NANOG and SOX-2. A specific YAP inhibitor, verteporfin, could only partially blocks self-renewal induced by shockwave, suggesting that other pathways regulate self-renewal. Further, the high-throughput sequencing data reveals changes of 600 genes compared to untreated controls. [180]

Another possible shockwave mechanism is sonoporation when the shockwave-treated cells display a transient permeability, and the effect appears to be dose-dependent; [181] [182] however, it is unclear whether sonoporation is distinct from the mechanotransductive effect of shockwave. It has been reported that shockwave increases intracellular calcium is mediated through plasma membrane calcium influx and PLC-IP3-IP3R pathway, and the effect is independent of sonoporation.[183] Sonoporation effects of shockwave are applicable in gene and drugs transfers and release of intracellular biomolecules into extracellular space. It was reported that in HUVEC, shockwave releases RNA activating Toll-like receptors 3 (TLR3), and arteriogenesis was detected in shockwave-treated wild-type mice and not in shockwave-treated TLR3 knockdown mice. [184] Further, shockwave has been reported to release exosomes from cells. While there are four sorting complexes have been described for exosomes biogenesis, [185] the relevant

mechanisms for exosomes biogenesis by shockwave is not known. Exosomes can contain chemokines such as SDF1 and MCP1 needed in the recruitment of stem cells and progenitors; exosomes can also contain miRNA that can downregulate the expression of SDF1 (miR-27b, miR-126, miR-126*) [186] [187] and CXCR4 (miR-150) impeding stem cells and progenitors recruitment.

2.6 Migration of Progenitors to the Heart for Regenerative Effect

A mouse lineage tracing study has refuted the existence of cardiac stem cells, [188] concluding that the heart is lacking endogenous stem cells and non-cardiac cells do not differentiate into cardiomyocytes. The contribution of putative stem cells to myocytes only happens in the embryonic but not in the adult heart. Using these paradigms, the exogenous progenitors from the blood and marrow are needed to exert the regenerative effect on the heart which mediated via paracrine effects.

Stem cells are known to secrete paracrine factors, and the putative secretomes have been described, [189] which have functional effects on cytoprotection, angiogenesis, cells proliferation, migration of progenitors not exclusively to stem cells, and modelling of tissue matrix and maturation, to name a few. Very likely that a combination of progenitor types is needed; each has specific roles and overall have a synergistic effect on cardiac regeneration. CXCR4, the

receptor for SDF1, is expressed in not only blood-derived stem cells but also B cells, and monocytes and most T lymphocyte subsets, but just weakly on NK cells.

Monocytes have been reported to have an important role in angiogenesis, first evidenced by the observation that in vascularised tumour in which there are plentiful monocytes.[190] There are subpopulations of bone-marrow-derived monocytes expressing VEGFR. The anti-angiogenic effect in cancer therapy using VEGFR blockade by Bevacizumab [191] could inhibit growth, neovascularisation and monocyte-macrophage recruitment; and the knockdown [192] of VEGFR receptor attenuates macrophages infiltration. Monocytes are marrow-derived, upon homing from the blood in tissue could transform into the M1/M2 macrophages phenotype; T-helper which were also homed by the SDF1 could secrete the IL4 needed for the polarisation of M1 phenotype into M2 phenotype.

Depending on the organ site, tissue-resident macrophages purported to originate from yolk sac progenitors [193] only, and also originated from the hematopoietic progenitor cells or passed through an intermediate monocyte stage. It is not yet clear the ontological roles. Several populations of monocytes have been described: Pro-angiogenic Tie-2 expressing monocytes recruited via Angiopoetin-2 to the site of injury could secrete VEGF, MMP9, COX2, and Wnt5A.[194] While Wnt5A could stimulate the endothelial cells to proliferate,

Angiopoetin-2 is released by the endothelial, and shockwave has been reported to be able to release Angiopoietin-2 from the endothelial cells.

The recruitment of circulating monocytes are required for angiogenesis — the circulating monocytes are the ancestors of endothelial cells, they provided the required inflammatory environment for repair.[195] Monocytes expressed VEGFR and could be mobilised by VEGF too. Ablating monocytes in the circulation using liposome-encapsulated clodronate impaired the blastema formation in adult salamander limb regeneration.[196]

Dendritic cells are antigen-presenting cells that would migrate to the lymph node and stimulate T cell proliferation.[197] T cells have a role in wound healing and survival after experimental myocardial infarction in mice. [198] However, SDF1 could directly recruit T-cell via CXCR4 and macrophages could secrete angiogenic factors such as VEGF. [199] Stem cells and blood progenitors also secrete miRNA, [200] paving another route in cardiac regeneration.

2.7 DPP4 Inhibition Could Enhance Other Important Substrates

SDF1 is not the only substrate for DPP4. To name a few, other interesting substrates of DPP4 are the BNP, Substance P, IGF1 and Erythropoietin; and DPP4 inhibition could increase their bioavailability by prolonging the half-life.

Shockwave treatment is associated with the release of Substance P, [201] a known stimulator of endothelium-derived nitric oxide release, and the vasodilating effect of Substance P is nitric oxide mediated. [202] A novel function of Substance P is a systemic chemotactic factor for bone marrow stromal-like cells CD29+ which participate in wound healing possibly via cells proliferation and epithelial transdifferentiation,[203] with an effect of enhanced repair. In cardioprotection, Substance P attenuates ischaemia- reperfusion injury via the NK-1 receptor and AKT reducing apoptosis,[204] inhibits platelets adherence translating into anti-atherosclerosis. The anti-apoptotic effect Substance P could also be mediated by Wnt signalling molecules such as β-catenin, p-GSK-3β, c-myc, and cyclin D1 in addition to β-catenin translocation to the nucleus supporting the fact that active Wnt signalling is involved in Substance P inhibition of apoptosis. [205] Morphine via opioid receptor could inhibit the release of Substance P into the circulation,[206] impeding mobilisation of NK-1 expressing progenitors from the marrow.[207] *In vitro*, substance P is shown to induce the biosynthesis of matrix metalloproteases[208] (MMP-1, MMP-2 and MMP-9), inhibits the synthesis of MMP inhibitors and is important for activation of ERK1/2. [209]

Shockwave has been associated with the release of Substance P and prostaglandin E2 on application to the rabbit femur. [201] The receptor for Substance P is NK1R. NK1R expressed in monocytes,[210] haemopoietic stem

cells,[211] lymphocytes[212]. NK1R is usually co-expressed with other receptors, CXCR4 and CCL2, respectively the receptors for SDF1 and MCP1. Substance P could increase cell cycle and proliferation, [213] and when injected into infarcted rats' hearts had higher c-Kit^{+} GATA4^{high} cell population was observed. Substance P has the ability to migrate monocytes. [214]

One study involving patients receiving shockwave for renal calculi showed shockwave could increase serum erythropoietin levels. [215] The shockwave energy dose in the renal application was tenfold higher than that used in cardiac application. It is not known whether cardiac shockwave treatment would affect erythropoietin level.

Chapter Three

METHOD: CREATION OF ISCHAEMIA-REPERFUSION RAT MODEL

3.1 Introduction

This chapter details the methods for setting up the rat cardiac ischaemia-reperfusion injury models, performed in a manner to ensure consistency and reproducibility of experimental read-outs.

3.2 Animal Characteristics and Housing

All laboratory rats used in the experiments, and presented in this thesis, were male Lewis rats sourced from Charles River UK. Lewis rats are syngeneic albino rats achieved through inbreeding. Only male rats were studied because females are intrinsically more variable because of cyclic reproductive hormones, have different mortality and heart failure development rates. It is

known that sex influences biological outcomes. [216] The rationale of using syngeneic rats was because cells transplantation may be carried out between Lewis rats in future experiments, and by using a syngeneic strain, the use of immunosuppression to negate graft rejection would be avoided, as well as the associated side-effects and confounding effects on results.

Before any experimental intervention was introduced, they were acclimatised for at least one week to allow for the physiological stress during transportation to recover and for the animals to adjust to a new housing environment. All experimental protocols conformed to The Animals (Scientific Procedures) Act 1986 Amendment Regulations 2012, and EU directive 2010/63/EU. The animals were housed at the Imperial Central Biomedical Services (CBS) under establishment license from the Home Office, where they have free access to drinking water and food, environmental enrichment, and 12-hour night and day cycle. The room temperature was regulated at a range of 20-24°C, and each cage received a regulated oxygen supply. Up to the day of surgery, the rats were caged in a group-housing in appropriately labelled cages. Up to cardiac MR scan, the rats were housed in Level 1 of CBS in an environment considered clean. It was recognised that infections may be asymptomatic and could interfere with research outcome and the interpretation of scientific results. After cardiac MR scan, the rats were housed in Level 2 of CBS for

animals that had been removed from Level 1. For the purpose of ischaemia-reperfusion experiments, the distinction between Level 1 or Level 2 is not important.

3.3 General Personal Preparation

All animal handlings required the use of personal protective equipment (PPE) consisting of a laboratory coat, hair net, a mask (Aura 9320+, 3M), a pair of gloves and overshoe covers; when in Level 2 of CBS. In addition to these, in Level 1 of CBS, a coverall was worn or a change of attire into surgical scrubs was mandated. The barrier time between the Level 1 and Level 2 was 48 hours, limiting how many surgeries and MRI scan could be performed in one week, as all the experimental interventions were performed by one person, also limiting instruments transfer between the units.

3.4 Table and Equipment Preparation

The equipment used, and the table setup are graphically presented on the top row of **Figure 3-1**

After handwashing, sterile gloves were worn throughout to maintain sterility of the items, that have been decontaminated and arranged on the table. The table decontamination was performed by spraying the surface with 70%

ethanol, then wiped with Clinell Universal Disinfectant Wipes (GAMA Healthcare) and then draped with a sterile surgical towel.

The heating platform was also wiped clean and then wrapped with a sterile surgical towel and placed on top of the draped table nearer the table edge facing the operator. The ventilator valve unit was placed on the other side of the heating platform, the ventilator main unit on its right, and iPM12Vet vital signs monitor to its left side. A sterile surgical tray was placed on the right side of the heating platform, also draped.

3.5 Preparation of Post-Operative Cage

To avoid the entrapment of nesting material into surgical wound causing infection, it was not included in the cage preparation. An absorbent paper was used instead of chopped wood as bedding, at least for the first few days until the thoracotomy wound had dried up. A paper tube and two gnawing sticks were supplied. Standard food pallets as well as grounded wet pallets were supplied for forty-eight hours.

3.6 Surgical Equipment

All surgical equipment must be sterile autoclaved prior to first use, consisted of:

- Disposable surgical blade size 15 (Swann Morton)
- Olsen-Hegar needle holder

- Iris Stitch Scissors - Straight 11.5cm
- Adson Serrated Dissecting Forceps
- Instrument box
- Fingered silicone insert
- Vi Ring Retractor (medium, Veterinary Instrumentation)
- Hooked retractor strips
- Surgical tray

An ultraviolet sterilizer cabinet was also used to decontaminate the surgical tools for surgeries performed in the same day.

Figure 3-1. Pictures showing the study materials and method for creation of rat ischaemia-reperfusion myocardial infarction. 1.Philips SONOS 5500; 2. Surgical tray for dirty equipment; 3. UV sterilizer; 4. Surgical tray for clean equipment, organised, draped. At rear, Povidone-iodine bottle and isoflurane bottle; 5. Oxygen flow meter and isoflurane vaporiser; 6. Ventilator main unit, 7. Sterile operating area, heating platform underneath, to its right, timer and pre-cut tape to length; 8. Mindray iPM12Vet, to its right, a sharp bin; 9. Recovery chamber; 10. Clinell wipes; 11. Oxygen concentrator; 12. Intubation platform, goose neck light and sterile ultrasound tube. Under heading Surgery, (left) showing steps undertaken, (right, top picture) showing ECG before LAD ligation, (right, middle picture) showing ST elevation ECG after LAD ligation. Under heading Echocardiography heading, (top picture) broken yellow line showing a segment with regional wall motion abnormalities during LAD ligation and (bottom picture) showing wall motion abnormalities had recovered. Under heading Shockwave showing a shockwave transducer being held and shockwave administered to the heart.

Study Materials

Echocardiography

Surgery

- General anaesthesia
- Endotracheal intubation
- Ventilation
- Thoracotomy
- LAD ligation
- Wound closure
- LAD release
- Recovery

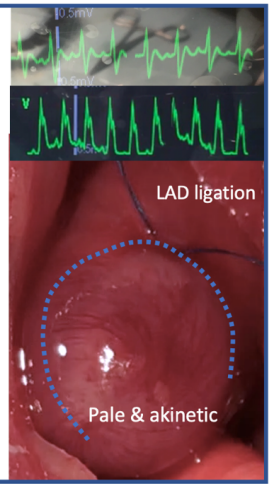

Shockwave

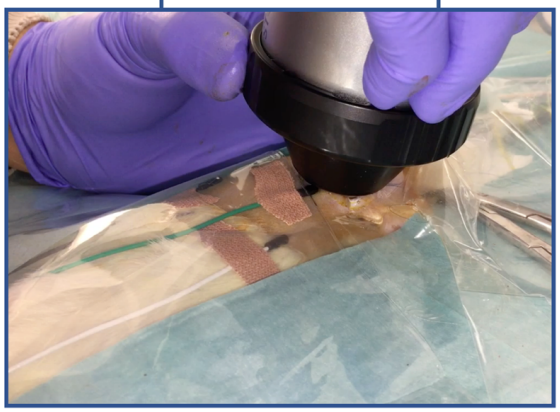

3.7 Ventilator

3.7.1 Description

A pressure cycled ventilator SAV04 (Vetronic UK) was used to ventilate the rats during surgery. It was chosen over volume cycled ventilator because of better ventilation profile; the decelerating expiration phase of a pressure cycle ventilator resulted in better gas exchanges; and over safety, as a valve system by design limiting the pressure, the risk of barotrauma was minimised.

SAV04 ventilator consisted of two units: the main unit and the valve unit. The main unit has the power switch, inspiratory positive pressure switch, control for expiratory time and ventilation pressure knobs. The valve unit connects to the main unit via a D-type socket, and it has one oxygen inlet from the vaporiser, one outlet to the animal and one outlet to the isoflurane scavenger. The valve unit controls the direction of flow, either only from the oxygen inlet to the animal or the animal to the scavenger outlet.

3.7.2 Ventilation Circuit

The oxygen was supplied by an oxygen concentrator delivering 100% oxygen to an Isoflurane vaporiser. The output from the vaporiser which would contain the desired concentration of isoflurane if any required, was circuited to the oxygen inlet port of the valve unit on the ventilator. The valve unit opened at

the oxygen outlet port, connected to the endotracheal tube via a short oxygen hose with a side port. The side port was connected to the end-tidal CO_2 monitor and the exhaust port connected to a tube to a scavenger unit.

3.7.3 Setup

As SAV04 ventilation rate was dependent on oxygen flow setting; how much flow to set on the flowmeter need to be determined first, calculated using the formula: sums of the tidal volume of the rat and the volume of the dead space in the circuit.

The tidal volume was determined using the formula 10ml/kg and the inspiratory flow rate calculated as follows: inspiratory flow rate (L/minute) = [Tidal Volume (in ml) x Respiratory rate x 3]/1000. A normal respiratory rate for an adult rat is 80-90/min. For example, for a 300g rat, the tidal volume is 3ml/breath, and the required oxygen flow rate is 0.72ml at 80 breaths/minute or 0.81ml at 90 breaths/minute.

The flow that was lost in the dead space was defined as the minimum flow of oxygen that would trigger the valve open, determined using the following method. A dead space is a volume in the ventilator circuit that does not participate in gas exchanges. With the ventilator circuit connected to the main unit and already switched on but without the animal, the final oxygen circuit to the animal - the endotracheal cannula's tip was occluded with a finger and

the oxygen flow was gradually increased until the ventilator started triggering. The flow volume identified was the “dead space’ flow rate (L/minute). The measured “dead space’ flow rate (L/minute) was then added to the calculated oxygen flow rate (L/minute) to give the final oxygen the flow rate required to ventilate the animal at the desired respiratory rate.

3.8 Heating Platform

A custom-make heating platform (Peco Services Ltd) with fine hemostatic control was used to maintain physiological temperature as the standard CBS provision caused ECG interference. Before use, it was sprayed with 70% ethanol and wiped off with tissues, then draped.

3.9 Pre-Surgery Animal Preparation

3.9.1 Weighing

The rats’ body weights were taken and serially measured throughout the experiment to monitor the animal wellbeing and for the calculation of drug doses to be administered. To maintain comparability and to avoid the need for normalisation of experimental readout indices, rats of similar weights were used. The rat was placed in a plastic container on a tared digital scale, and the values were recorded to the nearest gram. Animal weight is a good early

indicator of health; rats being prey species, are good at masking illness and may not show any sign until the disease is advanced.

3.9.2 Examination

Before removing the rat from its cage, it was visually assessed to display normal behaviour, eating and drinking normally. The stress level was assessed, and they should appear to breathe normally. The handling of a rat was performed by grasping around its shoulder whilst supporting the weight using the other hand.

3.9.3 Requirement for Fasting

Rats are not routinely fasted prior to anaesthesia due to their inability to vomit.

3.9.4 Pre-Medication

Pre-medication solely for the purpose of surgery was not administered. For rats that required pre-medication for the purpose of experimental intervention, depending on the group, the active substance and route of administrations will be detailed in the appropriate section. These could be administered as a pre-medication that might continue for a period after surgery, depending on the group the rat been allocated to.

3.10 Anaesthesia Induction

Isoflurane was used as an inhalant general anaesthetic gas. The rat was placed in a red see-through polycarbonate anaesthesia induction box, and the isoflurane vaporiser was adjusted to 3-5% delivered in 100% O_2. The respiratory rate was continuously monitored by visual counting as an indicator of the depth of the anaesthesia plane, becoming less rapid with increased depth. Usually, after a few minutes, the rat would fall asleep, then fell to one side. Pain reflexes are good indicators of anaesthetic depth; at light to the medium plane of anaesthesia, the tail pinch reflexes are lost, whereas, at a surgical plane of anaesthesia, pedal withdrawal reflexes are lost. [217] The rat was removed from the induction box, placed on a preheated mat in a ventral up position to a nose cone mask supplying 3% isoflurane so that the chest hair could be shaven off using an electric razor. At this juncture, preprepared subcutaneous enrofloxacin (Baytril, 5mg/kg) and Carprofen (Rimadyl, 5mg/kg) administered. The rat returned to the induction box and allowed it to reach a deeper anaesthetic plane to allow for intubation.

3.11 Endotracheal Intubation

There was no commercial rat endotracheal tube readily available, and a 16G intravenous winged cannula (Venflon, BD) for human was adapted for the purpose. The cannula was shortened by cutting its distal tip such that the overall length matched the length of oral-mid trachea length of the rat was to

be ventilated. For a large rat weighing more than 400g, a 14G might be necessary, or else the seal would leak, causing under ventilation, identified as a mismatch in the actual ventilation rate and animal's chest expansion.

Due to the small animal size, the procedure of endotracheal intubation can be very challenging to perform. As direct cannulation into the trachea often fails, a Seldinger technique using an optical cable wire was devised, performed as follows. The anaesthetised animal was hooked semi-tightly by its incisor tooth to an adjustable noose on an intubation platform angled in a vertical direction, and the rat allowed to gravitate to a vertical position whilst breathing freely. A flexible gooseneck arm shinning a bright LED light was placed in front of the trachea. The dressing forceps held in the right hand were used to pick up the rat's tongue. The left hand held a curved artery forceps which then advanced into the epiglottic vallecula (the space between the tongue and epiglottis) and at the same time used to push the tongue forward using the inside curvature of the forceps to allow direct visualisation of the trachea inlet. The opening and closing of the larynx with respiration have the appearance of blinking light when visualised from the mouth. The position of the LED light might need slight adjustments to achieve the best effect. Letting go of the forceps in the right hand, a fibre optic cable was guided into the trachea as the vocal cords were opening. The disappearance of the blinking lights indicated the correct placement of the optic cable inside the trachea; the fibre optic cable become

luminescent, and light could be seen seeping through between the space of the cable and the vocal cords. The fibre optic cable was advanced 3cm beyond the vocal cords. The artery forceps in the left hand was let go, the endotracheal cannula picked up and threaded over the fibre optic cable (Seldinger technique) until it passed slightly over its entire length whilst fixing the fibre optic cable in position. There should not be any resistance to the advancement. Whilst keeping the cannula secured inside the trachea, the fibre optic wire was removed, the rat unhooked from the noose and connected the animal to the ventilator. This modification has helped to achieve a 100% success rate of endotracheal intubation on the first attempt.

3.12 Ventilation

The endotracheal tube was carefully Luer-locked to the male counterpart of the outlet of the ventilator valve unit. The wing of the cannula behind was positioned behind the rat's incisor to reduce the likelihood of dislodgment. It was essential to ensure the tongue was pushed out to one side to avoid compression. The isoflurane was initially set between 3-5% in 100% oxygen depending on the depth of anaesthesia of the animal immediately post-intubation; higher setting when the anaesthetic plane appeared light, indicated by rapid spontaneous breathing and movement. The animal was observed to ventilate with good bilateral equal chest expansion, and that the

respiratory rate was matched the setting of the ventilator. Unilateral ventilation indicated that the endotracheal cannula was advanced too far and should be slightly withdrawn. The rat should appear well perfused by the colour of the mucous membrane, appear pink, not grey. When stabilisation was achieved, for maintenance of anaesthesia, 3% isoflurane was used. The end-tidal CO_2 was the second method to confirm the correct placement of the endotracheal tube was in the trachea such that the normal end-tidal CO_2 for a rodent should be 4.6 - 6 kPa. Overventilation would drop the value, under ventilation would increase the value, and no detection of CO_2 indicated oesophageal intubation.

3.13 Vital Signs Monitoring

Once the ventilation was secured, the rat was prepared with five ECG needle electrodes; two electrodes in the subcutaneous tissue near the shoulders, two electrodes in the pubis and one electrode in the mid sternum, and via Einthoven's bipolar, and unipolar configurations of ECG lead I, II, III, aVF, aVR, aVL and V could be continuously measured on Mindray iPM12Vet. An algorithm using impedance from ECG calculated the respiratory rate. The oxygen saturation probe fitted on the paw and a rectal temperature probe positioned in place. Capnography was achieved by sampling the CO_2 in the ventilatory circuit via a tube to a dehumidifier chamber on the iPM12Vet, and

the end-tidal CO_2 was partial pressure of the gas at the end of respiration. The ECG electrodes and all other cables were taped down as repositioning during surgery could prove difficult and would breach asepsis. The iPM12Vet monitor was set to alarm when the vital signs exceeded undesirable thresholds. The normal physiological measurements for rats are oxygen saturation of at least 95%, heart rate of 250-400bpm and core body temperature to 37˚C. These parameters must be achieved before the first incision to the chest took place, e.g., hypothermia compensated via increasing of heating mat temperature, subnormal oxygen saturation via adjustment of the respiratory rate and erratic heart rate by simply waiting for anaesthesia stability.

3.14 Marking the Incision Site and Eye Protection

The apical pulse was located using a finger and the site for incision marked on the skin using a permanent marker pen. As eye blinking was lost with anaesthesia, to prevent corneal ulceration, eye protection using paraffin-based ointment was applied to both eyes.

3.15 Surgical Light

The surgical light beam was adjusted to where the incision on the animal chest to be made to ensure good visibility throughout surgery and repositioned as appropriate.

3.16 Personal Preparation Before Animal Surgery

With the hands already scrubbed using Chlorhexidine gluconate 4.0% w/v (Hibisrub, Mölnlycke Health Care Limited) and towel-dried, a surgical gown was worn, and a pair of sterile gloves then put on. Henceforth, aseptic must be maintained. When a dirty area was inadvertently touched, a change to a new sterile pair of gloves was mandated.

3.17 Skin Sterilisation and Draping

The skin was sterilised with surgical gauzes soaked with 10% Povidone-iodine solution, applied three times from the centre outwards in a circular fashion by skin friction, each time with a new gauze. Excess Povidone-iodine was wiped off with clean gauze. The animal then draped with a transparent plastic sheet, pre-cut with a surgical window, and a self-adhesive incise drape (TEGADERM, 3M) then applied over the surgical window to the skin. The drape helped to create an isothermic sterile environment and defined the sterile field.

3.18 Thoracotomy

A left parasternal vertical incision of 1.5cm length was made using a surgical scalpel blade size 15 (Swann-Morton). A traumatic blunt tissue dissection was performed to find the surgical planes and to separate the muscle layers. Throughout surgery, haemostasis was maintained using cotton buds by direct pressure application. For maximisation of surgical access and field-of-view, a

ring retractor system with counter-traction elastic stays was used (See **Figure 3-2).** Upon reaching the ribs level, a pulsation on the intercostal muscle was sought which would indicate that the heart was just underneath, usually on the fourth intercostal space.

Thoracotomy was proceeded by opening the intercostal muscle using a small pair of scissors at the point before the ribs changed direction to upward direction (V point), and the ribs then retracted in the caudal-rostral directions by the elastic stays. The heart should be immediately insight, and if necessary, the lung and thymus gland might need to be pushed to one side to improve visual access.

3.19 Left Anterior Descending (LAD) Ligation-Release

The pericardium was gently lifted using a pair of forceps and it was cut opened to expose the anterior ventricular wall. In rats, the LAD was often not visible; therefore, the ligation entrance-exit points were based on anatomical landmarks where the vessel should lie its course. In human, the LAD runs its course in the interventricular grove to the apex, the furrow junction of the right and the left ventricle, above the septum. In rat, the heart surface is however smooth, that the interventricular grove is not useful for identification purpose. The junction of the right and the left ventricle was instead identified

by the colour of the ventricular tissue. The right ventricle contained deoxygenated blood and would appear darker than the left ventricle containing oxygenated blood. Underneath the interventricular border should where the septum be. The left atrial appendage was lifted, and the pulmonary conus and ascending aorta were identified. The origin of the LAD from the ascending aorta running along on top of the ventricular septum to the apex was conceptualised in mind.

A narrow semi-circular needle (Prolene 7/0, Ethicon, Johnson & Johnson) was used to ligate the LAD (if visible) at the point just after the second diagonal artery at the distal third of the ventricle. The needle should enter the left ventricular tissue adjacent to the desired LAD point of ligation, under the vessel and exit next to the other side of the vessel near the interventricular junction as previously described. Technically, it was not ligating the vessel per se; however, a method served to compress the surrounding tissue to stop the blood flow. It was important not to damage the vessel as the flow need to be re-established and not to exit the needle at the right ventricular wall because the wall was thin and could cause profuse bleeding. The ligation was secured using a double-loop releasable knot akin to tying up shoelaces. Successful ligation was indicated by blanching of the ventricular wall, visual impairment of contractile function and ST elevation on the ECG. (See **Figure 3-1)**. A 30-

minute timer countdown was then started. Photographs and video recordings were taken to record the ischaemic events as a measure of quality.

There are two methods of wound closure, depending on the requirement to wait for the 30 minutes to elapse: early versus late chest closure. In the early closure method, the wound was closed soon after the ligature was secured, and the knot was released from the outside of the chest. The suture loop and two ends were carefully separated and clipped to the drape so that they did not become entangled. In the end, the knot was released by pulling the two ends apart. Early wound closure allowed echocardiography to be performed during ischaemia, and the evidence of regional wall motions abnormalities and the return of contractile function after the relief from ischaemia recorded.

In the late closure method, the wound was not closed until 30 mins had elapsed and the ligature had been released. During this time, it was important to cover the heart with a surgical gauze soaked wet with sterile saline solution to maintain tissue hydration.

Bleeding during surgical skin incision was usually mild and would stop spontaneously; simple dabbing with a cotton bud would be sufficient. Larger bleeding on the heart required prolonged compression using a cotton bud, and if this could not be contained, the animal would be sacrificed.

Figure 3-2. An image showing a retractor with elastic stays on a thoracotomy wound on a rat cadaver.

3.20 Wound Closure

Wound closure was performed layer by layer as the elastic stays were unhooked. It was important to ensure the tissue tension was equally distributed to avoid the complication of wound dehiscence. Vicryl 6/0 (J&J) was used to close the ribs using simple interruption suturing technique. First, the separated ribs were approximated together, the needle entered the intercostal muscle in the above and exit one intercostal muscle below the thoracotomised intercostal space, avoiding the heart and lung tissue underneath, then secured using simple double-knotted suture. The procedure was repeated until the rib edges were completely closed and the stitches were equally spaced of ~7mm distance.

Even though no skeletal muscle was cut during entrance, the retraction had caused muscle stretching; a few sutures need to be inserted to orient the muscles into the original anatomical positions using 6/0 Vicryl. A few interrupted knots of 6/0 Vicryl were also inserted on the subcutaneous layer. Finally, the cutaneous layer closed with interrupted suture of Ethibond 6/0 (J&J). The suture line was checked for gaps and dehiscence; if present, these were immediately rectified. The exterior wound surface finally cleaned with 10% aqueous Povidone-iodine. No dressing was required.

3.21 Transthoracic Echocardiography

The scanning was performed using Philips SONOS 5500 with S12(12Mhz) sector transducer to acquire the parasternal long-axis view for visualisation of the basal to mid regions of interventricular septum; and the short-axes views at the basal, papillary and apex. The depth was set at 2cm, the focal point at the posterior wall level, fundamental imaging with tissue preset, adjustments of time gain compensation for uniform brightness and a narrow sector size to achieve the best temporal resolution. At best, a temporal resolution of 83Hz, equivalent to around 20 frames per R-R interval if the heart rate is 300bpm could be achieved. This was not sufficient for quantitative longitudinal measurements. It was, however, useful as a quality control step for assurance that large-enough infarction was consistently created and for localisation of the heart for shockwave treatment.

3.22 Post-operative Medication

1ml of subcutaneous normal saline for injection was administered to replace the fluid loss during surgery. If there was bleeding, an additional 1ml normal saline was administered at a different subcutaneous site. Buprenorphine (25-50mcg/kg) was administered subcutaneously as post-operative analgesia.

3.23 Recovery

The isoflurane was switched off, and the rat was allowed to regain consciousness. It usually took around 15 minutes before the animal could breathe spontaneously and safely extubated. This was cautiously performed by first switching off the ventilator, then disconnecting the Luer-locked to the endotracheal tube and watching for any sign of spontaneous chest expansion or limbs actions to indicate readiness. If not present, the rat was reconnected to the ventilator again, and the procedure was repeated again in a few minutes. Once successful, it was placed in a preheated recovery chamber at 30°C, and the respiration was supported with 100% oxygen administered via a nose cone. When the animal had recovered from the anaesthesia, indicated by an increase in mobility and non-compliant from oxygen, it was returned to its cage. For the next 48 hours, the rats received once-daily Carprofen (Rimadyl, 5mg/kg) as an analgesic, and the wound was inspected for any sign of infection.

3.24 Shockwave

Shockwave was generated by Duolith SD1 (Storz Medical, Switzerland) which delivered focal shockwave. The transducer was custom-made to have a very short focal point so that only the heart was treated. For those cohorts of animals allocated to receive shockwave, the administration was performed in

the following manner. A series of 2.5mJ/mm^2 x 500 pulses of focal shockwave was administered to the heart at 3Hz. As air reflected shockwave, it was important to couple the transducer contact to the skin with a liberal amount of ultrasound gel.

Chapter Four

METHOD: PREPARATION AND ACQUISITION OF CARDIAC MAGNETIC RESONANCE

4.1 Introduction

In this chapter, the methods of animals' preparation, CMR acquisition and image post-processing are detailed. These were maintained at a high standard to ensure reproducibility, consistency and reliability of data in the experiments.

4.2 Animal Preparation for MRI Scan

The animals were transported to the Biomedical Imaging Centre from the CBS for cardiac MRI and kept in temporary housing at the facility. After the scan,

they were housed at Level 1 of CBS if the scan was not terminal. All animals were weighed pre-scan for health monitoring and drug dosing.

The scans were performed whist the animals were continuously under anaesthesia; hence it was important to monitor the physiological health of the animal. If gadolinium injection was required, tail vein cannulation would be performed in the first instance before other preparations. The gadolinium and iv lines preparation are detailed in **section 4.3**.

(**Figure 4-1**) The rats were equipped with high fidelity sensors consisted of three-lead ECG, respiratory balloon pressure sensor, pulse oxymetry, and rectal temperature probe connected to a physiological monitor console (SA Instruments, Stony Brook, NY, USA) to respectively monitor the heart rate, respiratory waveforms, oxygen saturation and body temperature. The rats were scanned head-first in the prone position in a dedicated animal bed whilst continuously maintained under isoflurane anaesthesia. A heating pad was secured on the dorsal aspect of the animal to maintain physiological temperature during the scan.

4.3 IV Line Preparation

See **Figure 4-2.** IV lines were set up in the following configuration so that the gadolinium injection and saline flush could be independently injected from outside of the magnet bore to the cannulated tail vein during scanning. Two

1m polyethene Luer-lock iv extension tube (1mm internal diameter, Vygon) were used; one for gadolinium and one for the saline flush; both female ends bunged with anti-reflux needleless connectors (Vadsite, Vygon) and each male end connected to a lumen of double lumens octopus extension kit (Vygon) equipped with anti-reflux valves. The anti-reflux valves were essential because the injection volume was small, and they ensured the whole injected volume reached the tail vein as backflow was prevented and reduced the likelihood of air embolism.

4.4 Gadovist and Saline Flush Preparation

The brand of gadolinium contrast used was Gadovist (10 ml multi-use vial, 1mmol/ml) from Bayer. Prior to each use, Gadovist solution was inspected for cloudiness, discolouration, precipitation and breakage in the seal, which could indicate contamination, and in this situation, the drug must not be used. The dose of Gadovist used was 0.2mmol/kg, and for a 350g rat, 0.07mmol was required (70mcl of 1mmol/ml Gadovist); a volume difficult to inject, and hence Gadovist needed to be diluted first before use.

To prepare a concentration of 0.2mmol/ml of Gadovist, a 1:5 dilution was used such that 1ml of Gadovist was diluted with 4 ml of normal saline for injection in 5ml Luer-locked syringe to give a final volume of 5ml. At the dilution of

0.2mmol/ml Gadovist, a rat of 350g would require 350µl, which conveniently matched the weight of the animal per gram per µl per dose.

To obtain a homogenous mixture of diluted gadolinium, a small air bubble was left in the syringe, and it was inverted 10 times to help with the mixing. Before Luer-locking the syringe to Vadsite on the extension tube, the air bubble was gently expelled.

A 10ml saline for injection was prepared in a 10ml Luer-locked syringe, then connected to Vadsite on the second extension tubing. Different syringe sizes were used for easy identification. Nonetheless, the syringes were labelled.

4.5 Priming the Extension Tube

The tube was primed first with gadolinium by gentle injection to allow gadolinium to travel up to where the octopus arm adjoined the common reservoir where saline also pass. Next, the other tube was primed with saline by gentle injection to allow the saline to completely washed off gadolinium in the reservoir.

4.6 Connecting the Octopus to the Cannula

The connection of the octopus to the cannula was performed in a manner to avoid air bubble entrapment. The male-lock stopper was removed from the cannula and ~100mcl saline flush administered to check for patency. Two persons were needed for the next task. One person gently pushed the saline

syringe, and whilst the other person held the octopus end, allowing the saline to drip slowly and guiding its contact with the droplet of the tail vein cannula before Luer-locking the two connectors together in a closed system free from air bubbles. The extension tubes then unlooped and secured with sticky tapes along the length of the scanning bed.

Figure 4-2. Preparation of iv line with saline push for Gadolinium administration via iv extension and octopus.

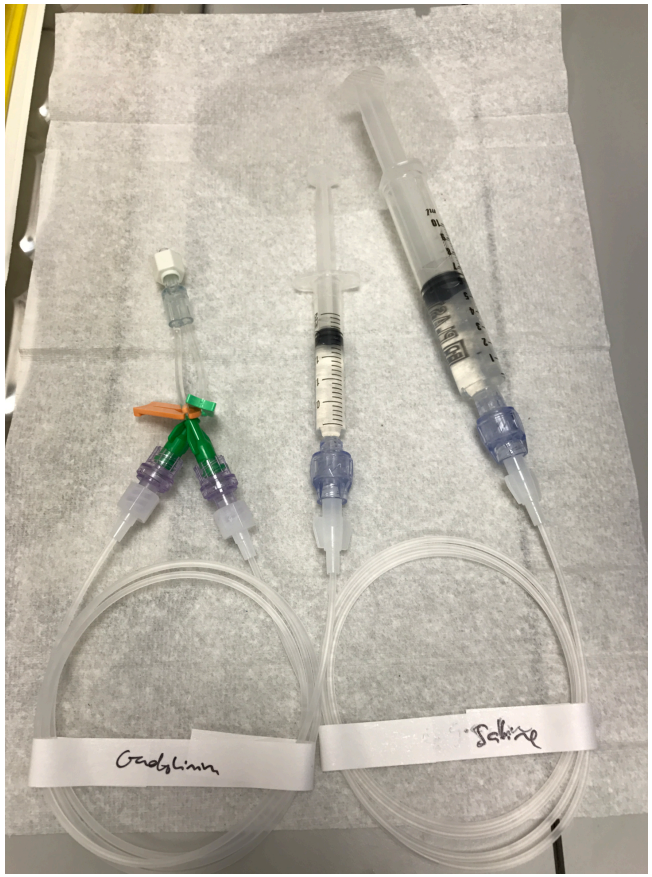

Figure 4-1. A Lewis rat lying in a prone position on a heating platform under isoflurane sedation via a nasal cone.

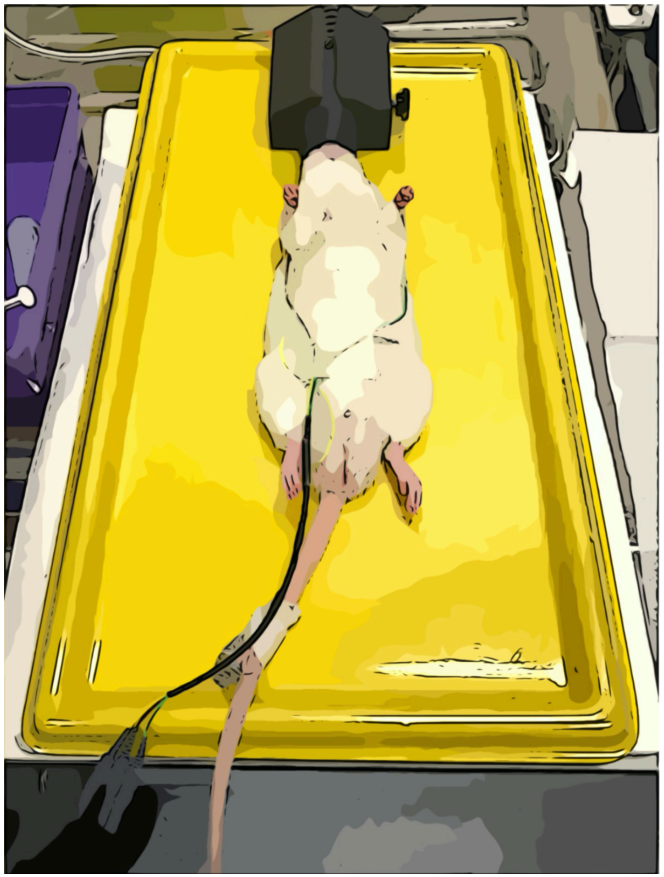

4.7 MRI Instrumentations

Cardiac MR scans were acquired on a Bruker Biospec 9.4 T scanner (94/20 USR Bruker BioSpec, Ettlingen, Germany) in a horizontal bore magnet with diameter clearance of 200mm, equipped with actively shielded gradients coil, integrated with shim setup to second order, gradient amplitude of 400mT/m and the maximum slew rate of 3440 T/m/s; and used in combination with a rat cardiac 1H 4×1 array receiver coil embedded in the cradle. The hardware was operated using Paravision 6.0.1 and stored in Digital Imaging and Communications in Medicine (DICOM) format version 3.0 for subsequent offline analysis.

4.8 Mounting Rat on Cradle

The rat with ECG leads and iv lines securely attached was transferred to the scanning room on a tray, and then carefully transferred to the cradle on the scanner, such that it was hooked by its incisor tooth to the ring at the tip of the tube supplying isoflurane and oxygen; and positioned horizontally. The tube passed through a conical mask that could slide in the caudal and cranial directions, such that the rat's head could advance to the mask to be locked in position, and that animal's heart could be adjusted to the centre of the receiver coil integrated on the cradle. All loose wires and iv lines were taped

down, and the cradle which sat on a slider was then advanced into the magnet's bore isocentre.

4.9 Scout and Nomenclature

A large field-of-view localiser was acquired for double-checking the animal's heart positioned at the magnet isocentre, where the homogeneity was the best; confirmed by the intersections of the vertical can horizontal black crosses on the body sagittal, coronal and transverse planes. A series of low-resolution transverse, sagittal and coronal scouts then acquired using FLASH-cine. These image series were then used for manual planning to derive the cardiac views as per AHA cardiac planes recommendation.[218] AHA cardiac imaging planes are the industry standard in clinical cardiac imaging. Although it is very challenging to perform in small animals, for translatability reason, it was the adopted standards for this thesis. Strict adherence to the imaging planes also allows the scans to be very reproducible and comparable between animals.

4.10 FLASH Cine Sequence

Henceforth, all FLASH-CINE were acquired using these parameters: repetition time (TR)=RR interval/number of frames (~6.2 ms for ~24 to 28 frames), TR Effective=RR interval, echo time (TE)=2.2 ms, flip angle 18°, slice thickness ≤1.2 mm, 13 to 14 slices, a field of view (28×28) mm^2, spatial in-plane resolution. Both respiration gating and R-wave based gating and triggering were used for

the acquisition of cine-based data, resolution (200 ×200) µm2, equally spaced frames to cover a full cardiac cycle.

4.11 Ventricular Long Axis (VLA) and Horizontal Long Axis (HLA)

The VLA slice was planned, using the transverse scout slice containing the mitral annulus; and the coronal scout slice containing the true apex; to prescribe the plane transecting the middle of the mitral annulus, the middle of the left ventricular cavity and the apex (Image 5 in **Figure 4-3**) The HLA slice was planned from the VLA, to prescribe the slice transecting the mitral annulus, the middle of the left ventricular cavity and the apex.

4.12 Mid-Slice

The mid-slice was defined as the short-axis slice of the mid-cavity of the left ventricle at the end-diastole, achieved by following these steps. From the VLA and HLA, five slices of equal thickness were prescribed from the apex to the base on their long axes (top row **Figure 4-4**). Then, the outer two slices were removed, leaving the three middle slices, namely from the direction of apex to base as the 'apical slice', the 'middle slice' and the 'basal slice' (see bottom row **Figure 4-4**).

4.13 Short-Axis Stack

The VLA and HLA were used to plan for the LV short-axis stack. Great care was taken to avoid foreshortening of the left ventricle and ensure the slices prescribed at both ends of the LV-stack were at the actual distal border, or else partial volume artefact would have been introduced. A contiguous short-axis stack of 0.9mm slices was prescribed covering the entire LV from the apex to the aortic root in the left atrioventricular plane, ensuring the final slice flush at the insertions of the aortic valve (left AV junction). It is acknowledged that they are three other variants on LV stack orientations, one when the slices are perpendicular to the septum, one when the slices are centred to the MV annulus and the other when the slices are parallel with the plane that cuts the right and left AV junctions. A human study has demonstrated that none of these significantly influences the results for LV only study. [219] As the rat valve leaflets were not visualisable at 9.4T; it was decided to centre the stack along the left atrioventricular plane for planning ease and consistency. (see **Figure 4-5**)

Figure 4-3. Planning from coronal scout, sagittal scout and coronal scout to obtain the VLA and HLA views

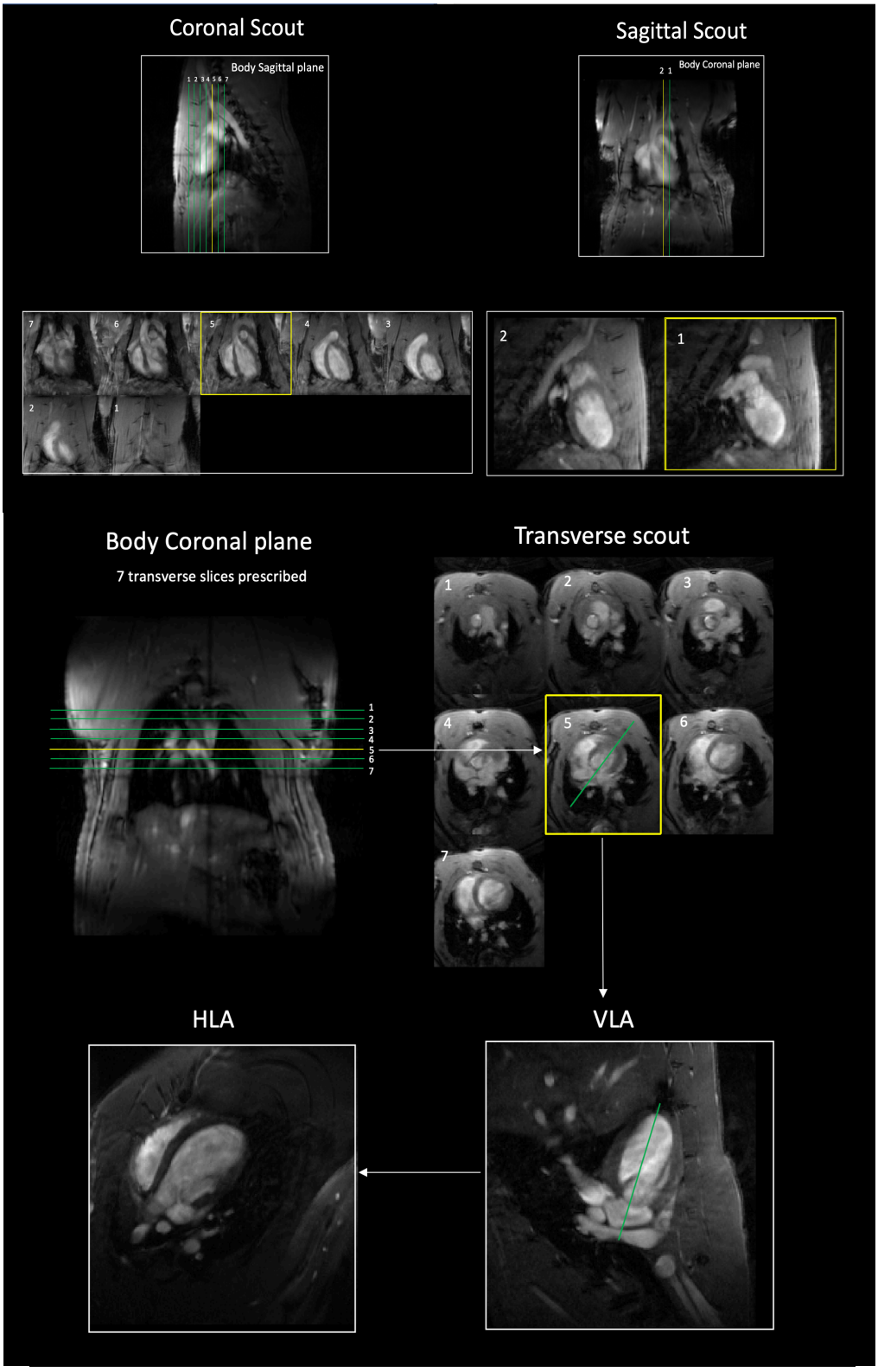

4.14 True 3-Chamber View

The VLA and the short-axis stack were used for planning for a true 3-chamber view. In the short-axis stack, the imaging plane must transect the aortic root in the direction that cut the anterior septum and the inferior lateral wall. Slight angulation of the long axis of the VLA at the base might be necessary to achieve the desired position.

4.15 True 2-Chamber

The true 3-chamber view, VLA and short-axis stack were used for planning for a true 3-chamber view. In the short-axis stack, the imaging plane must not transect the aortic root, and it passed the anterior wall and the inferior wall. In the HLA, the long axis was prescribed as the plane from the apex to the mitral valve and the left atrium. Slight angulation of the long axis of the VLA at the base might be necessary to achieve the desired position.

4.16 True 4-Chamber

The VLA, HLA and the short-axis stack were used for planning for the true 4-chamber. In the short-axis stack, the imaging plane just touched the lower border of the aortic root, transecting the atrial septum in the direction that cut the inferior septum and the anterior lateral walls. Slight angulation of the long axis of the VLA at the base might be necessary to achieve the desired position.

4.17 High Frame-Rate Cine

High frame rate cine was acquired using a self-gated FLASH sequence [220] (IntraGate™, Bruker Biospin, Ettlingen, Germany) with scanning parameters of TR/TE = 60/7 ms, FOV = (25×25) mm^2, spatial in-plane resolution (200×200) μm^2, 900 µm slice thickness, 60 cardiac frames, 10 min scan time per slice. Using the geometry already established during planning, the three short-axis slices (basal, mid-ventricular, apex) and three long-axis views (2CH, 3CH, 4CH) were acquired, and these conformed to AHA's planes recommendations and 16-segments model. The reconstruction method of the IntraGate cines is described in **section 6.5.4.**

Figure 4-4. Cardiac planning steps to derive the basal, mid and apical slices from the HLA and VLA

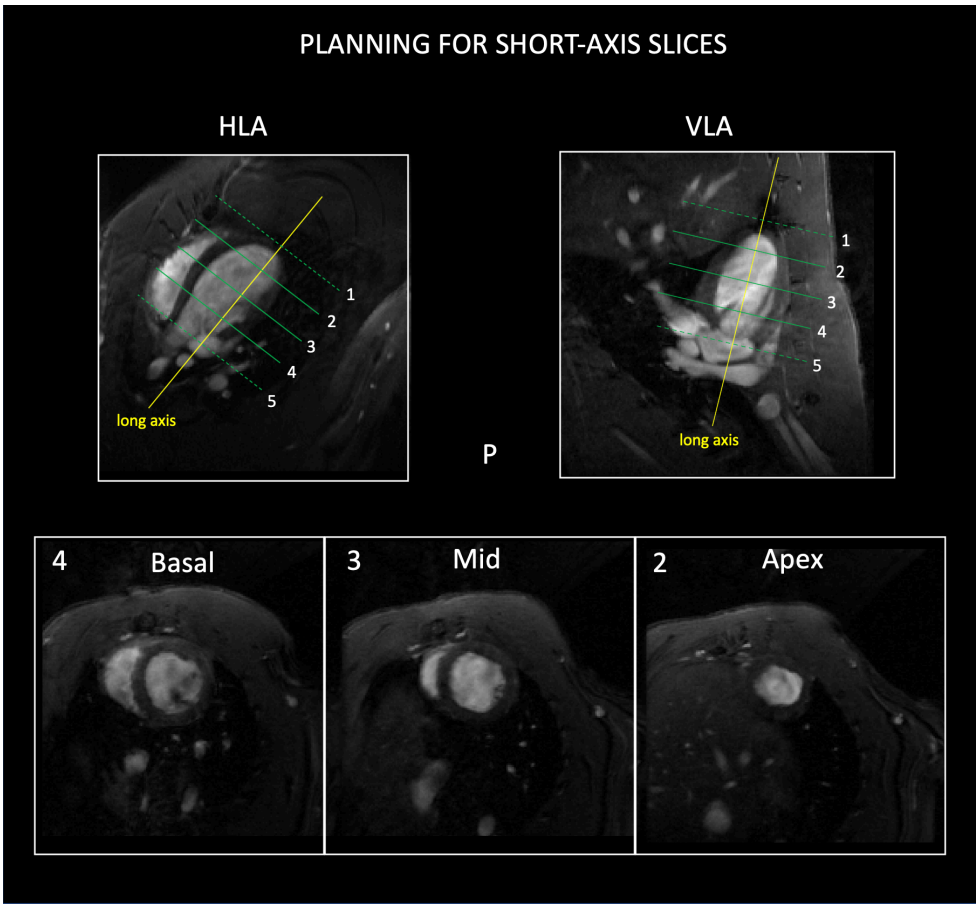

Figure 4-5. Cardiac planning steps to derive the short-axis stack. Bottom picture showing montage view of an LV short-axis stack

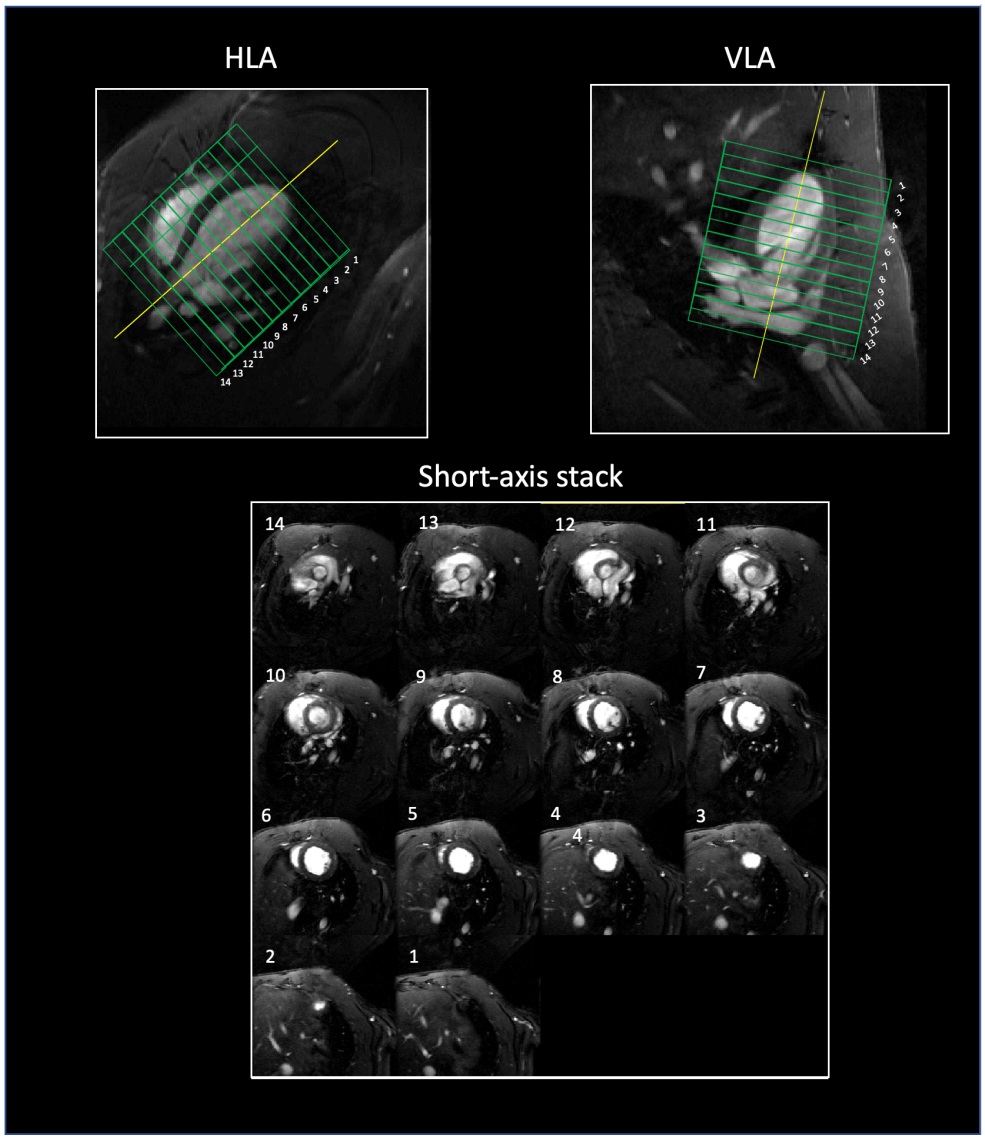

Figure 4-6. Cardiac planning steps to derive the 3-chamber view from the VLA

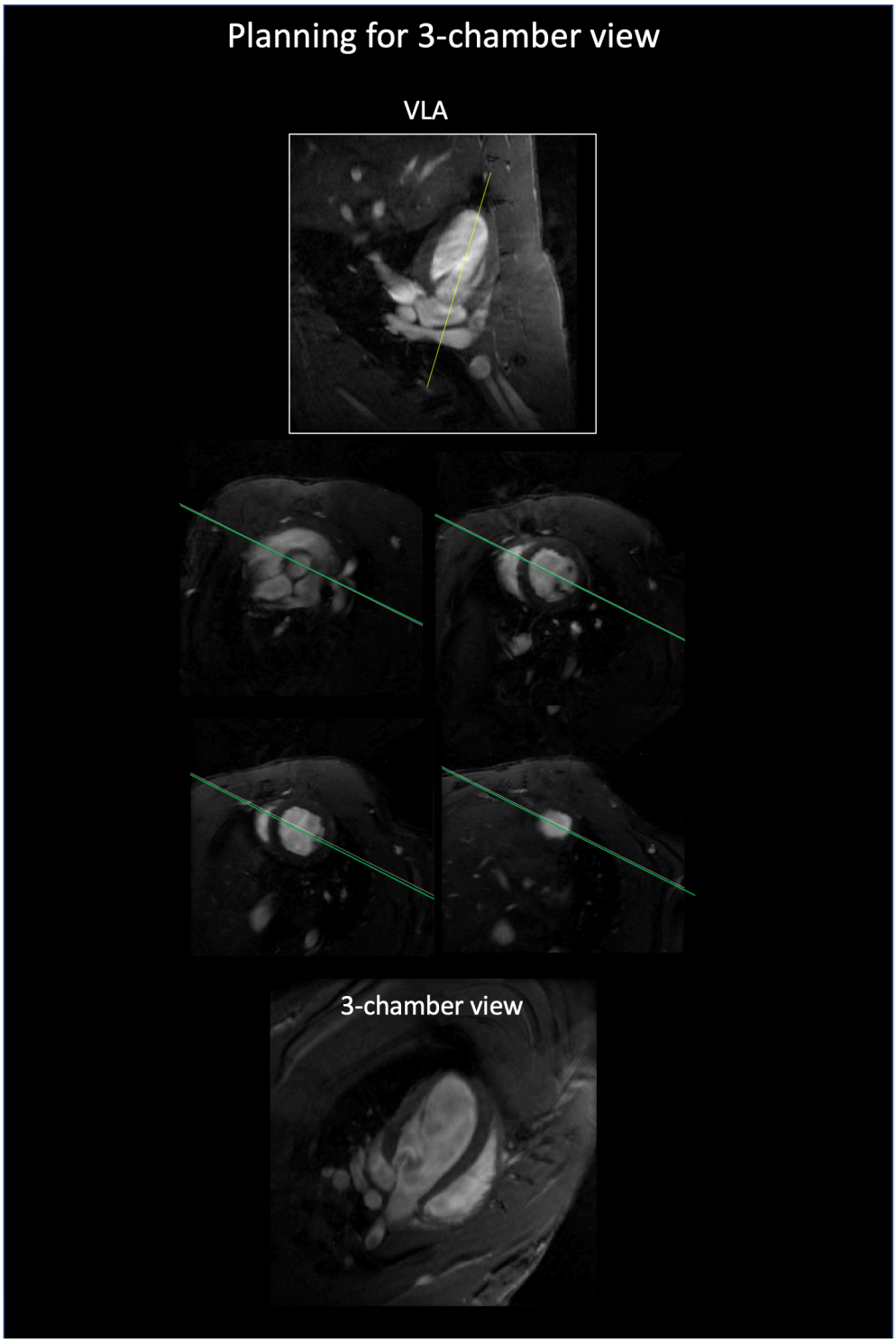

Figure 4-7. Cardiac planning steps to derive the 2-chamber view from the HLA and VLA

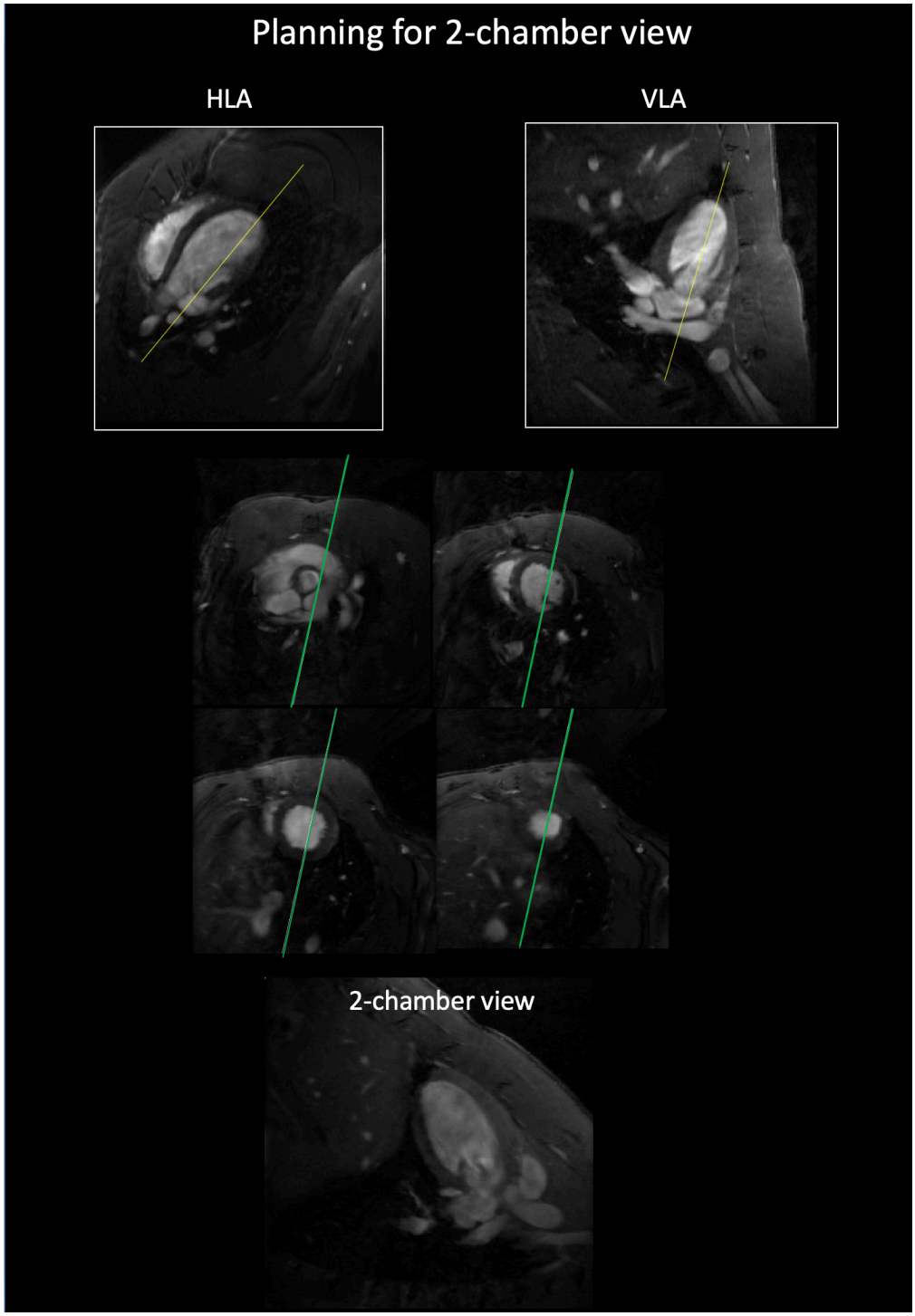

Figure 4-8. Cardiac planning step to derive 4-chamber view

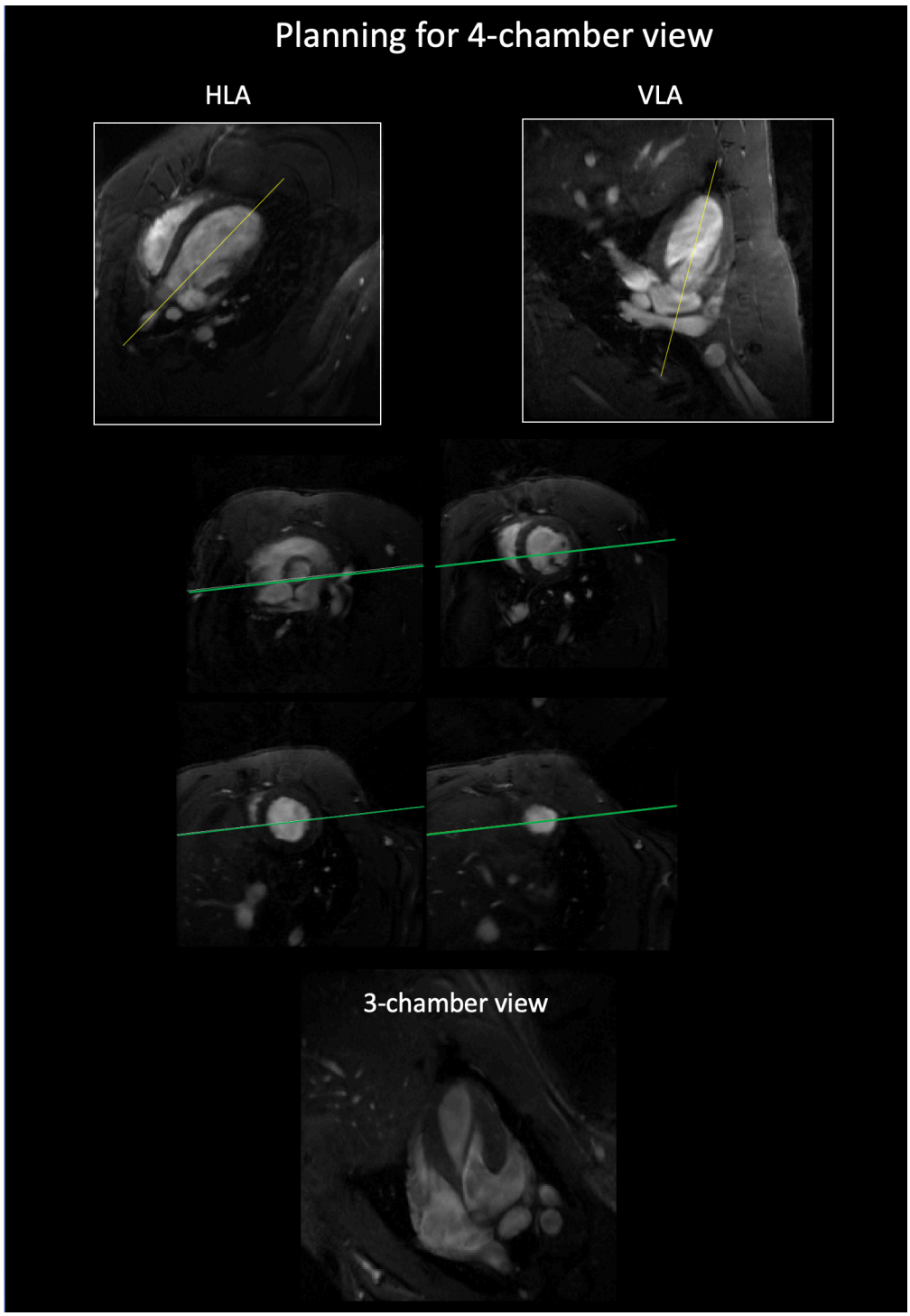

Figure 4-9. (A) Cardiac planning and scanning protocol. (B) AHA segmental nomenclature. (C) Cardiac tomography displaying the segment names. B and C adapted and used with permissions, [250, 161] respectively under license agreement no 4970780791522 and 4971080915551 in the Appendix.

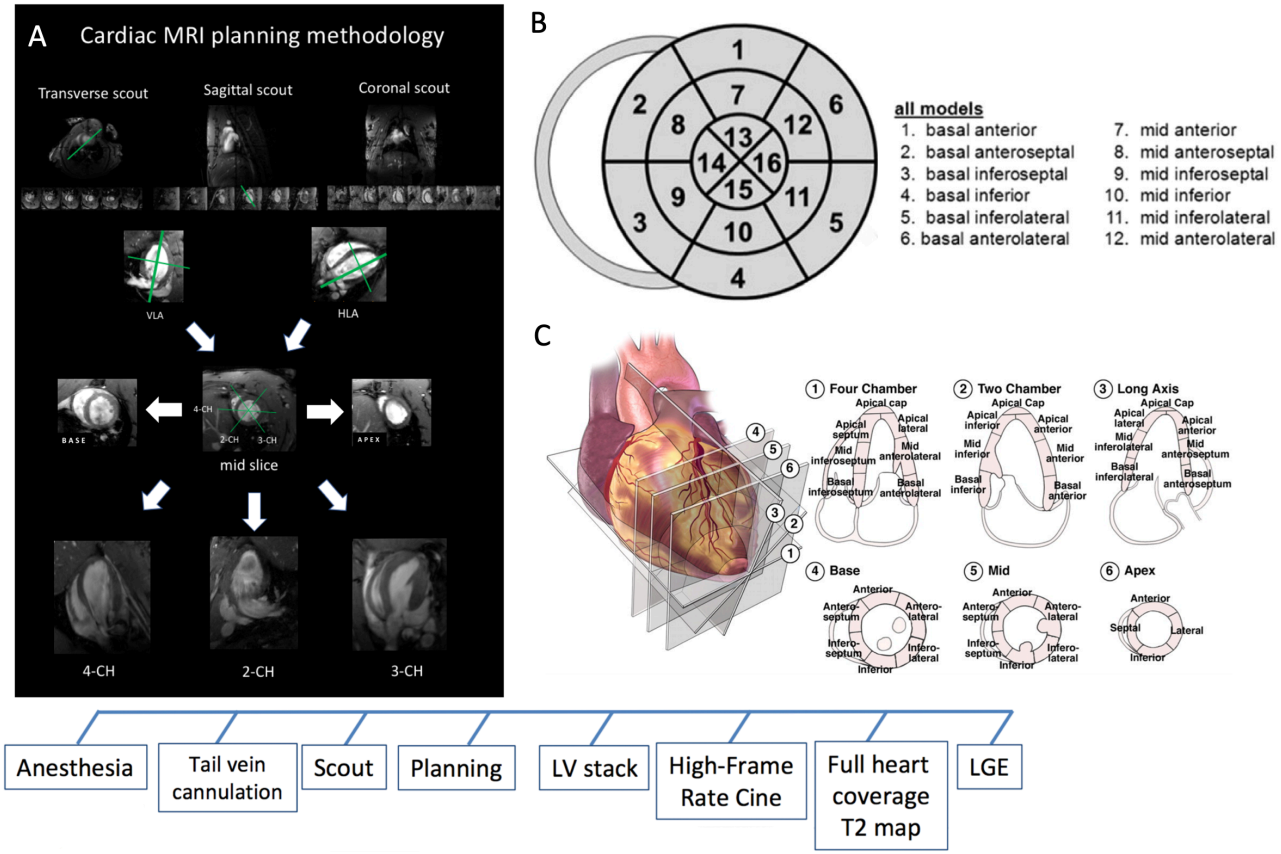

4.18 T2 Map Planning and Acquisition

The short-axis LV stack for T2-map consisted of seven contiguous short-axis slices; these were planned and positioned perpendicular to the long axis of the LV from the apex to the aortic root. In addition, three long axes views of the 2CH, 3CH and 4CH were also included.

T2 mapping was performed using a fat-suppressed multi-echo spin-echo (MESE) sequence with seven echo times, all acquired at the same moment of the cardiac cycle, just at the end of systole, during intraventricular relaxation time (IVRT) when the intraventricular flow was minimal. MESE allows for multiple echoes captured within one acquisition by a series of 180° refocusing pulses at different echo times within the same k-space. A pair of frequency-selective flow saturation bands were placed just proximal and distal of each imaging slice to minimise signal dropouts caused by flow artefacts and for attaining a 'black-blood' contrast. The acquisition parameters were TR/TE=3000/2.78, 5.47, 8.20, 10.93, 13.67 and 19.14ms; echo spacing 2.78 ms; a field of view (30×30) mm^2; spatial resolution (190×190) μm^2, slice thickness 0.9mm and GRAPPA acceleration factor 1.65. The immediate results visually checked for quality indicated by clear anatomical structures with minimal presence of artefacts, and that the image series should transition from bright

to dark with increasing echo times. If not meeting the quality control step, the scan would be repeated.

4.19 LGE Planning and Acquisition

The cardiac planning for LGE slices and slice geometry matched those used in T2 map so that both series could be used to determine the salvage index and in viability analysis.

The inversion time (T1) that nulled the myocardium was determined using the Look-Locker sequence. [221] TI was determined by scouting over a range of estimated T1 values, the T1 that nulled the myocardium; T1 that made it appeared darkened as the signal intensity was low, was the most appropriate selection.

When it was satisfied with the planning and T1, 0.2 mmol/kg Gadovist was administered and immediately followed by a saline flush to ensure the gadolinium arrived in the systemic circulation.

The LGE images were acquired 10 mins after gadolinium injection, using sequence multi-slice IR-FLASH with parameters: single T1 and a 90° flip angle, TR between each phase encoding pulse was 3.6 ms, TE=1.39 ms, FOV (36 × 36) mm^2, in-plane resolution (190×190) μm^2.

4.20 Image Analysis

4.20.1 Volumes, sphericity index and LV length

In Segment (Medviso, Lund), contiguous multi-slice short-axis cine images were merged into one stack, and all three long-axis images were used for cross-checking the LV segmentation. The same contrast and brightness were applied to all images. The endocardial and epicardial borders were contoured from the apex to the base in both end diastole and end systole phase (see **Figure 4-11**). The LV outflow tract was included in the LV blood volume to the level of aortic valve cusps. The papillary muscles and trabeculations were considered as part of the LV blood volume. Great care was taken to ensure that the mitral valve annulus and leaflets were correctly delineated. The ventricular mass and blood volume were computed by summation of the volume of each short-axis slice to derive the end-diastolic volume (EDV) and the end-systolic volume (ESV). The difference of EDV and ESV was the stroke volume (SV), and the percentage of SV/EDV was the ejection fraction (EF). The cardiac output (CO) was calculated as the SV times the heart rate observed during the LV stack acquisition. Sphericity index (SI)[222] was calculated by the ratio of the true LV volume derived from LV stack divided by the volume of a sphere from longitudinal dimension from the apex to the mitral annulus $LV(4/3\pi\ D/2)^3$ on the 4CH in diastole. D was calculated using three-point vector coordinates of

the apex and the mitral annulus at the end of diastole from the LV stack, where $D = ((x_2 - x_1)^2 + (y_2 - y_1)^2 + (z_2 - z_1)^2)^{1/2}$ and x, y, z were the annotated coordinates. The LV lengths at the ED and ES were also measured using three points vector annotated method. (see **Figure 4-12**)

4.20.2 Volumes, sphericity index and LV length

The analysis for LV mass was performed on the LV short-axis stack. The endocardial borders were segmented to exclude the papillary muscles and trabeculation, from the most apical endocardial slice to the aortic root. This is to maintain measurement consistency between animals as the papillary muscles could just partially end in the other slice, and the inclusion of that slice could cause an overestimation. The problem could be circumvented by using thinner slices; however, this would increase scan time. As the papillary muscles were not expected to change, it was decided not to include the papillary muscles. The epicardial borders were segmented from the slice containing the apical cap to the slice containing the aortic root. The LV mass was calculated by subtracting the LV volume of the epicardial borders with the LV volume of the endocardial borders at the end of diastole (see **Figure 4-12**).

Figure 4-10. Montage display of images of LV stack. Top: end diastole (ED) phase with 12 contagious stack numbered 1-12 from aortic root to apex. Bottom: end systole (ES) phase with 12 contagious stack numbered 1-12 from aortic root to apex.

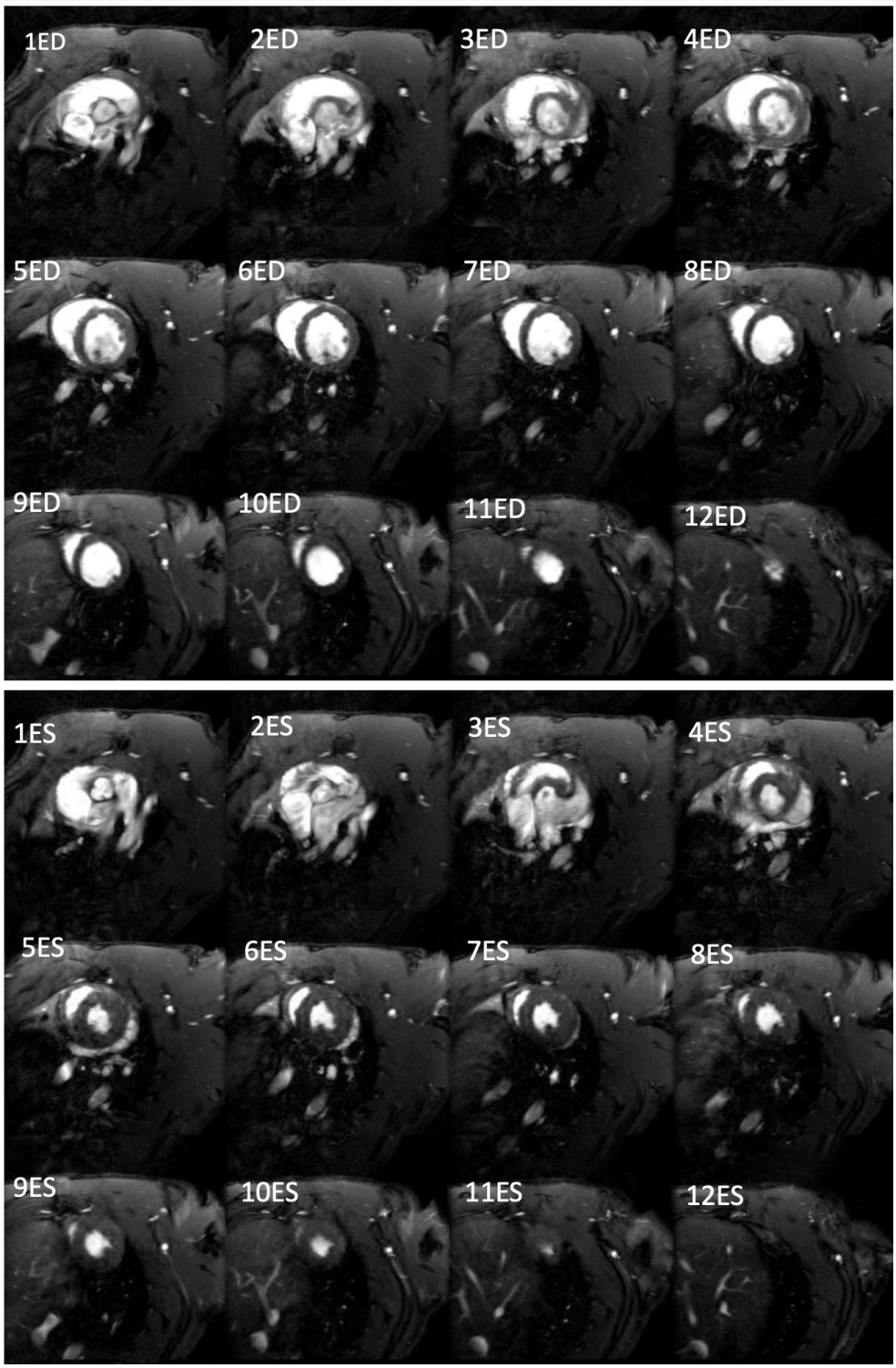

Figure 4-11. (A) Montage view of 12 short-axis LV stack at the end-diastole, (B) montage view of 12 short-axis LV stack at the end-systole, (C) 3D heart model constructed from A were red borders are the endocardium and green borders are the epicardium and (D) 3D heart model constructed from B were red borders are the endocardium and green borders are the epicardium. The volume between the red borders and green borders are the LV mass.

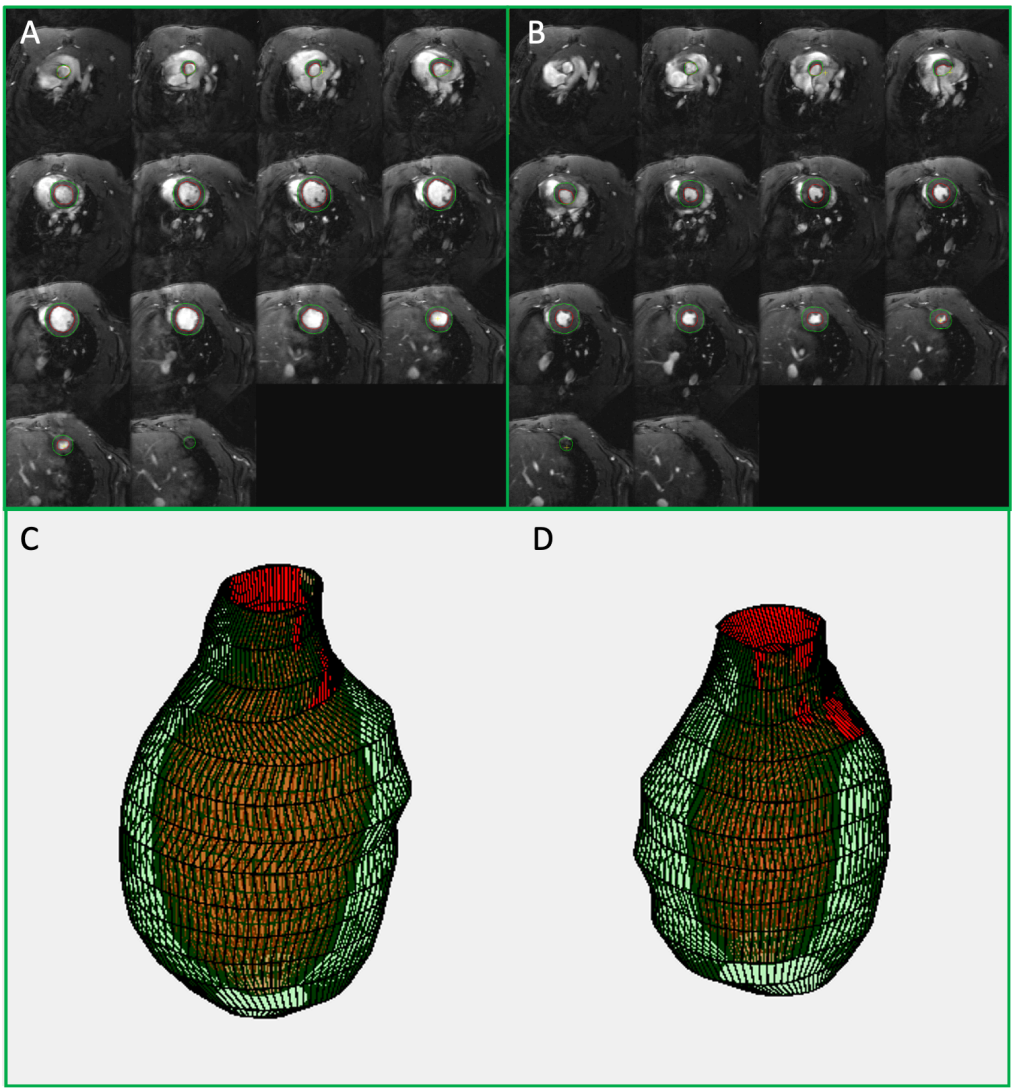

Figure 4-12. (A) A picture of sphere 'sitting' on the mitral annulus extending to the apex in a 4-chamber view at the end of diastole. (B) LV endocardial contour of short-axis LV stack: darker red is endocardial contour at the end systole with a vertical green bar representing the LV length at the end diastole, and transparent red is endocardial contour at the end diastole with a vertical blue bar representing the LV length at the end of systole. Bottom panel (left) showing the formula for 3D sphericity index and (right) 3-point vector length calculation.

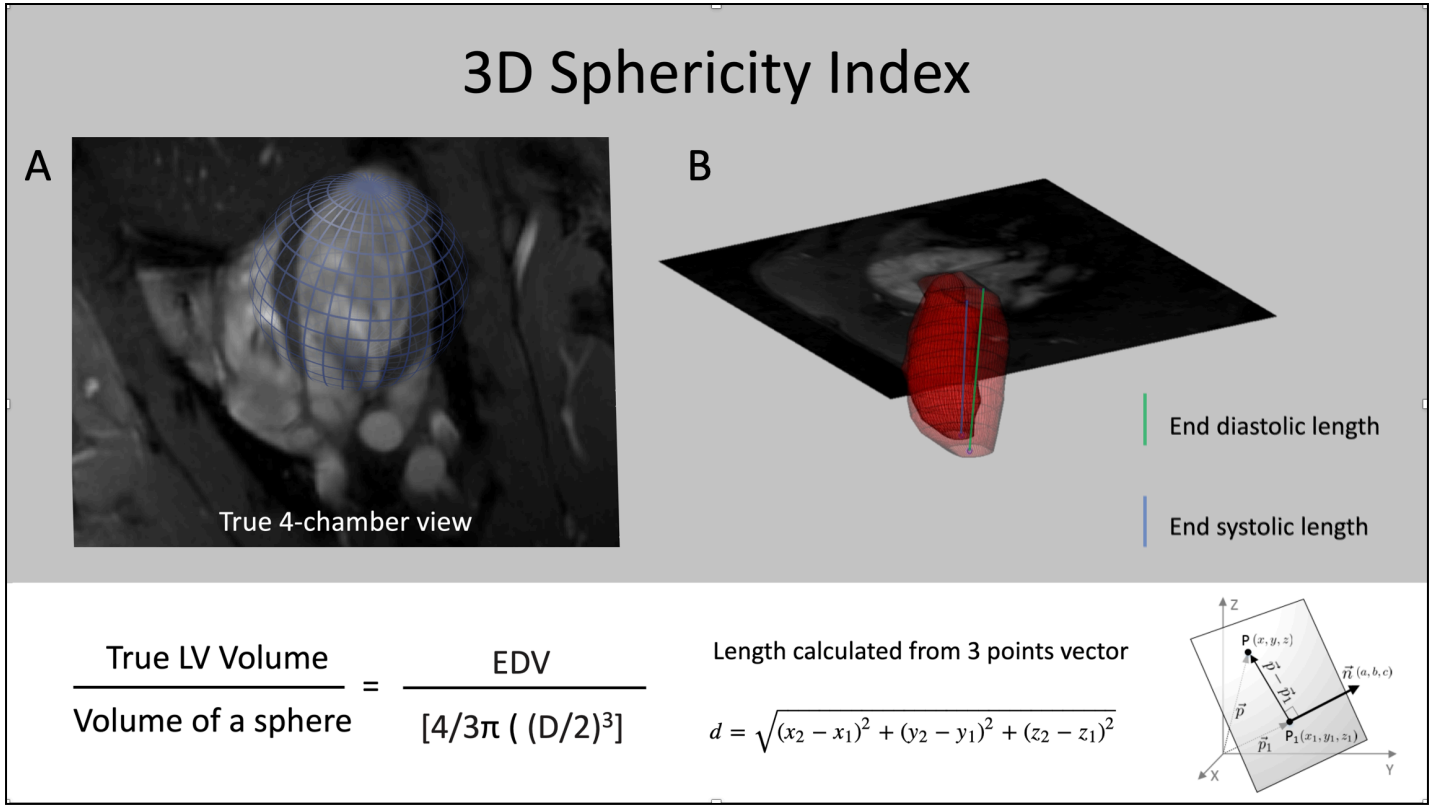

4.20.3 LGE analysis

Contiguous multi-slice short-axis LGE images were merged into one stack, and the endocardial and epicardial borders were manually delineated. The algorithm EWA [223] (Expectation-Maximisation, weighted intensity, a priori information) was used, and when needed, a manual correction was applied. (See **Figure 4-13**). The EWA algorithm automatically corrects the partial volume effects, and image contrast, particularly important in multi-slice IR-FLASH as the contrast could be slightly different between slices.

Figure 4-13. Short-axis LV stack of LGE images, green segmentation borders are the epicardium, red segmentation borders are the endocardium and yellow segmentation borders are the LGE regions, (B) 3D heart model of A, red borders are the endocardium, green borders are the epicardium, and the black borders are the LGE positive area.

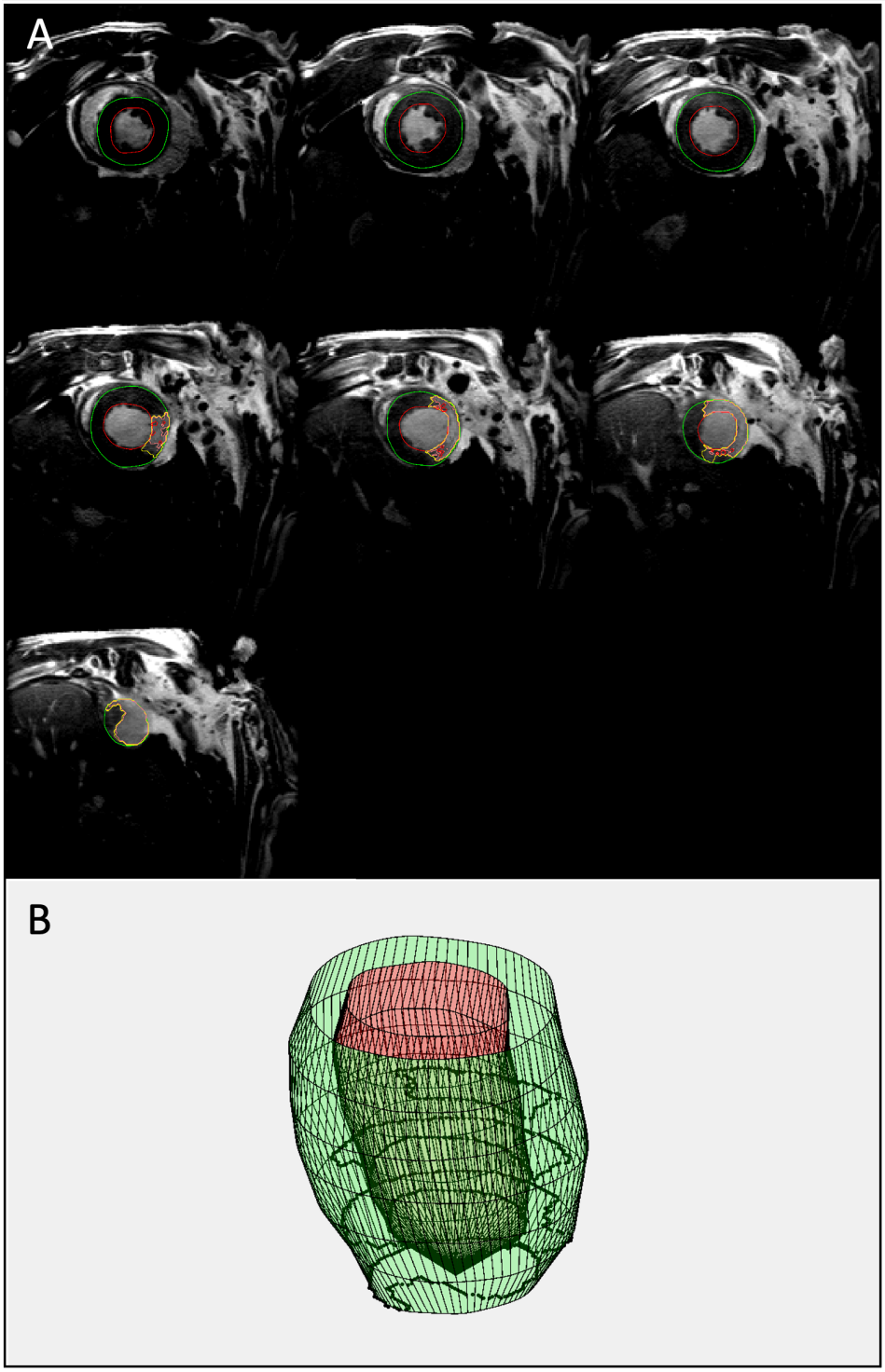

4.20.4 T2-maps

In Segment, the multi-slice short-axis slices of T2 echo images were merged into one stack. The first echo images in all echo series were discounted because they were susceptible to error, introduced by the imperfection of the excitation pulse of the low refocusing flip angle and B1 inhomogeneity. [224] [225] This method circumvented the systematic error that would have been introduced if they were included. [226] The endocardial and epicardial contours were segmented and sectored according to the AHA 16 segment model. A two-parameter pixel-wise T2 fit was carried out on a mono-exponential signal decay. Myocardial segmentation excluded the regions of bright signal caused by the stagnant subendocardial blood occasionally observed on T2 maps. The distribution of the pixel-wise T2 values would be inspected and statistically assessed for normality using D'Agostino and Pearson test where significant *P* values indicated non-Gaussian.

For the assessment of oedema, the mean of the medians of the upper 95% CI of the T2 value of each 16 AHA sector (n=7, Healthy rats) was used as a threshold to define whether the AHA segment is Healthy or 'diseased'. In the latter, the T2 values are increased and were used as the threshold to represent AAR (oedema) and/or myocardial infarction (LGE positive). For statistical analysis, the AHA myocardial segments were then grouped into the

aforementioned categories and paired with their corresponding segmental strain values.

4.20.5 Strain Post-Processing

Feature tracking-based strain analysis was performed using 2D-CPA-MR Image Arena version 4.6, a vendor-independent software with FDA 510(k) clearance and CE-marking, based on the three short-axis views and the three long axes views as per AHA 16 segment model. On each slice, the endocardial border was delineated, and ROI thickness adjusted to ensure appropriate coverage of the myocardium to the epicardium. The algorithm determined the centreline, solved the Laplace equation between the endo, mid and epicardial contours and tracked the 60 successive images within one complete cardiac cycle. The ED was defined as when the mitral valve leaflets had just closed (MVC) and when assessable in 3CH cine the ES when the aortic valve had just closed (AVC), otherwise respectively as the phase with the largest LV cavity and the smallest LV cavity. Correct placement of the time events was crucial to achieving a high level of accuracy of strain indices measurement. The quality of the wall tracking was manually checked in every 60 phases using the parametric overlay, and if errors found, the ROI borders were manually corrected, and the algorithm rerun to achieve the best possible wall tracking. ECG integration with DICOM images was not available.

4.21 Statistical method

All statistical analysis was performed in Graphpad Prism 8.4 for MacOS (GraphPad Software, San Diego) unless stated otherwise. For continuous variables, the central tendency of the data was reported by mean ± SD and 95%CI for Gaussian; or reported by median and interquartile range if non-Gaussian. For categorical variables, such as the number of subjects or segments per phenotypes groups, data were reported as relative frequencies and percentages. All continuous variables were checked for normality using D'Agostino and Pearson test (alpha=0.05), where non-significance test meant the spread was Gaussian.

Comparisons between two means were performed using Welch's t test between two Gaussian populations; otherwise, the Mann-Whitney U test was used to compare mean ranks. No logarithmic transformation was performed as strain data carry negative values.

Multi-groups mean comparisons were performed using one-way (between-subjects) ANOVA of Brown-Forsythe and Welch followed by Dunnett T3 multiple comparisons test; otherwise, the Kruskal-Wallis test with Dunn's multiple comparison test was used to compare mean ranks. Testing relationships between categorical variables and the assessment for linear

trend were performed using the Chi-Squared test; if significant, the effect size determined using Baptista-Pike's odd ratio.

The diagnostic performance of the indices for detecting I/R MI and phenotypes was assessed by using receiver-operating characteristic (ROC) curves, reporting sensitivity, specificity, with 95% confidence intervals (CIs) where appropriate. The area under the ROC for each parameter was used to determine performance using classification .90-1=excellent, .80-.90 =good, .70-.80=fair, .60-.70=poor and .50-.60=fail.

For the assessment of the reproducibility of sLS, the measurements were repeated twice in seven Healthy rats by one rater. The intraclass correlation coefficient (ICC) for two-way models[227] [228] and its 95% CI were calculated [229] and interpreted as excellent, good, moderate or poor reliability with the respective value of >0.90, 0.75-0.9, 0.5-0.75 and <0.5.[230]

Chapter Five

RESULTS: PROOF OF CONCEPT OF IN-VIVO STRAIN IMAGING IN ISCHAEMIA-REPERFUSION INJURY

5.1 Clinical perspective

Accurate phenotyping of myocardial segments is important for guiding clinical management and assessing the outcome of the experimental intervention in clinical trials. Myocardial motion characteristics are routinely used to infer segmental phenotype in echocardiography; however, in CMR, the method is limited by low temporal resolution. Established cardiac MRI methods for viability assessment such as T1, T2 mapping and late gadolinium-enhanced MRI (LGE) are commonly used to evaluate myocardial tissue viability. However, the multi-sequence examinations have the drawback of long

acquisition time, often difficult to perform on sick patients, carry the risk of brain gadolinium deposition, and risk of nephrogenic systemic fibrosis in patients with significant renal impairment. Furthermore, the post-processing analysis remains laborious. The utility of high frame rate CMR cine could open up diagnostic avenues with CMR having better spatial resolution than echocardiography. CMR based feature tracking (CMR-FT), an optical flow motion-tracking post-processing method is attractive for use because it is relatively quick to perform and does not require dedicated sequences, overcoming the error-prone laborious process of segmenting the LV wall borders semi-automatically. CMR-FT has not been assessed in high frame rate. In this chapter, the sLS-variants (peak-systolic, end-systolic and peak-sLS) in the endocardium and mid-layer, characterise the strain rate and post-systolic shortening (PSS) according to the segmental phenotypes of I/R-MI versus Healthy, as well as all the global strain and the classical volumetric measurements. HFR-CMR-FT is a useful tool to study cardiac mechanics and could distinguish the segmental phenotypes of I/R-MI.

5.2 Introduction

Ischaemic heart disease remains a major cause of death worldwide. Novel interventions to improve patients' outcome are actively being researched,[231,232,3] and active compounds would normally first undergo

mandatory pre-clinical testing[234] for demonstration of safety and efficacy.[235,236,237] The results from pre-clinical testing hence need to be robust to ensure appropriate translation of experimental interventions into human trials. In this pursuit, ultra-high-field MRI scanning dedicated for small animals was developed, enabling the study of heart disease models in unprecedented detail.

However, imaging of small animal left ventricle (LV) is technically challenging because of the size and fast heart rate, even more so when the stringent imaging planes are applied in order to match the standards of human cardiac tomography to ensure comparability. Despite the recent taskforce update to standardise protocols and simplify the patient-based approach to clinical CMR[238], these imaging planes were inconsistently applied in pre-clinical CMR protocols, hampering the appropriate translation to the clinic. These limitations argue for the establishment of robust CMR strategies capable of accurate phenotyping of the ischemic myocardium in a pre-clinical setting.

Myocardial wall motion characteristics have been used to infer segmental phenotypes in clinical practice. For example, both resting regional wall motions abnormalities[239] and post systolic shortening[240] are useful to diagnose coronary artery disease. A stimulation study with dobutamine[241] revealed patterns of myocardial contractility response either biphasic, blunted, or no

response that could respectively indicate hibernation, supplied by a significantly stenosed coronary or infarction. The observation can be, however, semi-quantitative and require high-level operator skills in order to achieve accurate interpretation.[242] Strain imaging is useful in prognostically important detection of global longitudinal GLS reduction in asymptomatic onco-cardiology[243] population and in ischaemic cohorts superior to ejection fraction[244], and identification of mild coronary artery disease[245] without stress and preceding clinical symptoms.[245]

5.3 Aims

The aim of this chapter was to assess whether the developed cardiac MR acquisition and post-processing methodology that was good enough to detect the experimental interventions, namely the Healthy rats versus I/R-rats, distinguish the segmental phenotypes of I/R-MI. If successful, the developed imaging methodology would be used to assess the experimental effects of shockwave on cardiac ischaemia-reperfusion injury using shockwave in combination with pharmacological DPP4 inhibition.

5.4 Objectives

In this chapter, a robust cardiac planning CMR strategy was performed, which enabled the establishment of high frame rate (HFR) CMR-FT in a rat model of ischemia-reperfusion (I/R). The HFR-CMR-FT was used to comprehensively

study the effects of I/R-MI versus Healthy rats, using both novel and classical indices to assess the global and regional cardiac left ventricular function. The index Segmental Longitudinal Strain (sLS) variants were used in distinguishing the phenotypes of I/R-MI. SLS variants consisted of the peak-systolic (Pk-Sys-sLS), the end-systolic (En-Sys-sLS)- and the peak (Pk-sLS). The HFR-CMR-FT was also used to study the global strains and was compared with EF and FLASH-cine. The HFR-CMR-FT was used to assess for post systolic shortening (PSS). The HFR-CMR-FT was also used to comprehensively study the apical and basal rotation, the twist and torsion in the endo, myo and epicardial layers between Healthy and I/R-MI.

As for global strain parameters, these would include the global longitudinal strain, global circumferential strain and global radial strain; examined in the layers of the endocardium and myocardium, respectively denoted with prefixed of endo and myo. The 3D Sphericity index was used to assess for left ventricular remodelling.

The parametric imaging such as T2-mapping will be used to assess area-at-risk, and the late gadolinium enhancement (LGE) was used to assess for the final infarct size.

The effects on volumetric and linear measurements were also characterised to assess the global systolic function such as the LVEDV, LVESV, SV, CO and EF.

The change in left ventricular volume rate during systole would derive *S*-dV/dt, and the change of the volume rate during diastole would derive indices of *E*-dV/dt and *A*-dV/dt. The cardiac physiology was assessed by heart rate expressed in beats per minute, and these were further divided into systolic and diastolic periods.

5.5 Methods

5.5.1 Experimental Design

The protocols carried out conformed to The Animals (Scientific Procedures) Act 1986 Amendment Regulations 2012, and EU directive 2010/63/EU.). Healthy rats (n=13) were compared with I/R-MI rats (n=9,), respectively defined as rats that had not received any experimental intervention by the time they were scanned with MRI and rats were rats that underwent surgical procedure for induction of ischaemia-reperfusion injury.

5.5.2 Ischaemia-Reperfusion Myocardial Infarction

The method of creation of ischaemia-reperfusion myocardial infarction has been detailed thoroughly in **chapter 3** of the thesis.

5.5.3 Cardiac MR Acquisition

The method of CMR instrumentals, in-vivo cardiac acquisition, animal preparation, cardiac planning and image modalities used have been thoroughly detailed in **chapter 4**. The use of FLASH sequence as opposed to

SSSP is rationalised here. FLASH was chosen because it is less sensitive to high-field related signal dropouts compared to SSFP, which is susceptible to severe banding artefacts at 9.4 T. It has been demonstrated that cardiac MR is feasible and highly reproducible using either FLASH or SSFP; therefore, the choice of using FLASH is justified in this study.[246]

5.5.4 Post-Processing for Volumetric Indices

5.5.4.1 Softwares

Segment (Medviso), freely available for research purposes and well-validated software, was used for MR image analysis of the LV volumes, T2 mapping and LGE. The feature tracking was performed on multi-frame cine FLASH images. TomTec-2D CPA-MR (Unterschleissheim, Germany) was used to perform multi-plane global strains; sLS-variants; strain rate (SR) analysis; post systolic index (PSI) and PSS time-to-peak (PSST); apical and basal rotation, twist and torsion; and atrial strains and volumes.

Microsoft Excel was used to compile the data output from Segment and TomTec-2D CPA-MR, then analysed in Prism.

5.5.5 Volumetric Indices, Sphericity Index and LV Length

The method for derivation of volumetric indices, Sphericity Index and LV length have been described in section **4.20.1.**

5.5.6 Peak Left Ventricular Systolic Ejection Rate and Diastolic Filling Rate

The rate of ventricular volume change, dV/dt was derived from the rate of change of LV volume curve. The three indices of interest are the *S*-dV/dt, *E*-dV/dt, *A*-dV/dt and *E/A*-dV/dt.

S-dV/dt denoted the peak ejection rate of the dV/dt during systole and was calculated as the average of peak systolic dv/dt for each of the long axis view of the 3-chamber, 2-chamber and 4-chamber views.

On the contrary, *E*-dV/dt denoted the peak of dV/dt during early diastole and was calculated as the average of early peak diastolic filling rate of dv/dt for each of the long axis view of the 3-chamber, 2-chamber and 4-chamber views, whereas the *A*-dV/dt denoted the peak of dV/dt during the late diastole and was calculated as the average of the late peak diastolic filling rate of each long axis view of the 3-chamber, 2-chamber and 4-chamber views.

The ratio of *E*-dV/dt and *A*-dV/dt denoted by *E/A*-dV/dt was used to assess the severity of diastolic dysfunction whether it had impaired relaxation, pseudonormal or restrictive.

5.5.7 LV Mass

The analysis for LV mass was performed on the LV short-axis stack. The endocardial borders were segmented to exclude the papillary muscles and trabeculation, from the most apical endocardial slice to the aortic root. This

was to maintain measurement consistency between animals as the papillary muscles could just partially end in the other slice, and the inclusion of that slice could cause an overestimation due to the phenomenon of partial thickness effect. The problem could be circumvented by using thinner slices; however, this would increase scan time. As the papillary muscles were not expected to change following I/R-MI, it was decided not to include the papillary muscles. The epicardial borders were segmented from the slice containing the apical cap to the slice containing the aortic root. The LV mass was calculated by subtracting the LV volume of the epicardial borders with the LV volume of the endocardial borders at the end of diastole

5.5.8 LGE Analysis

The method for derivation of LGE has been described in section **4.20.3.** The AHA myocardial segments with LGE were identified and then paired with the corresponding segmental strain values for statistical analysis**.**

5.5.9 T2-Maps Post Processing

The endocardial and epicardial contours were segmented and sectored according to the AHA 16 segment model. A two-parameter pixel-wise T2 fit was carried out, assuming a mono-exponential signal decay (See **Figure 5-1**). Stagnant blood near the endocardium may appear bright and could be confused with the myocardium. With careful myocardial segmentations, the

bright signals from stagnant blood occasionally observed on T2 maps were excluded.

The distribution of T2 values of each AHA sector typically showed a non-Gaussian distribution; hence the median values of the pixel-wise T2 was used for comparison (D'Agostino and Pearson test showing significant P-values). The mean of the medians of the upper 95% CI of the T2 value of each 16 AHA sector (n=7, Healthy rats) was used as a threshold to define whether the AHA segment is Healthy or 'diseased'. In the latter, the T2 values are increased and were used as a threshold to represent AAR (oedema) and/or myocardial infarction (LGE positive).

5.5.10 Quantification of AAR Using Parametric T2-Mapping

Area of risk was be calculated from a full LV stack of parametric T2-mapping using pixel-wise thresholding to compute the volume above and below the set threshold using the cumulative histogram method.

Figure 5-1. A representative result of T2 mapping was acquired using the multi echo spin echo method (Echo Times: 2.78, 5.47, 8.2, 10.93, 13.67, 16.40, 19.14ms; Repetition Time TR=3000ms) of a basal short axis slice of a normal rat. An exponential decay curve of each pixel was fitted using 2-parametric logistic regression to obtain the apparent T2 values from the equation $SI = \beta . e^{-TE/T2}$. By visual inspection as the echo time lengthens the images were progressively getting darker.

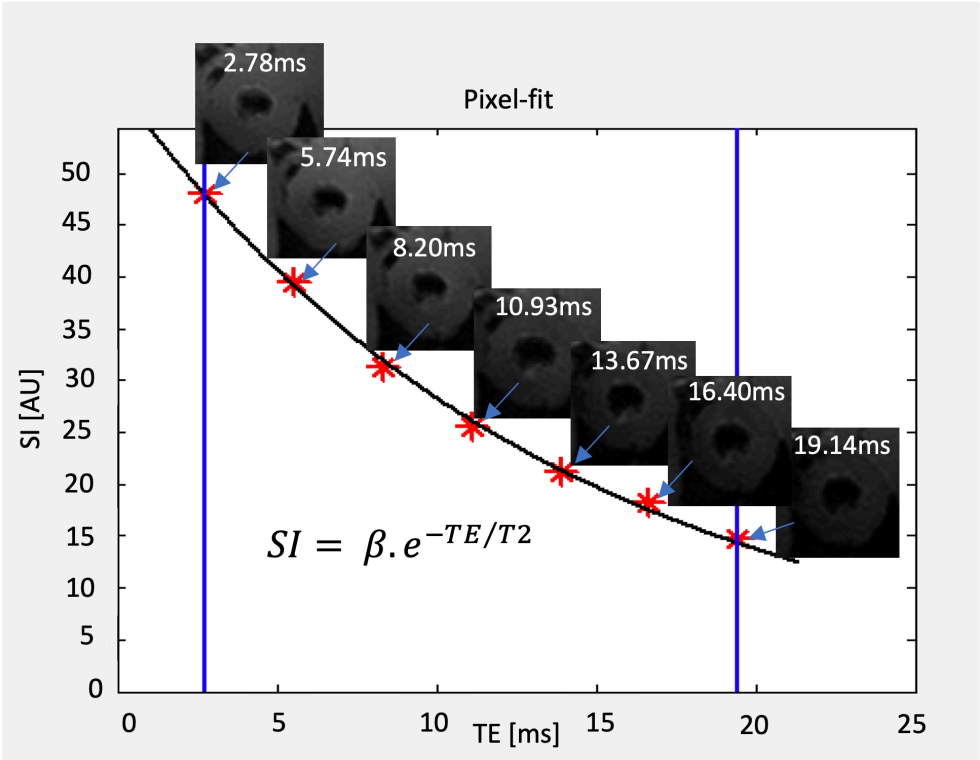

5.5.11 Global Strains Post-processing

Feature tracking-based strain analysis was performed using 2D CPA MR Image Arena version 4.6 (Tomtec, Unterschleissheim, Germany) based on the three short-axis views and the three long axes views as per AHA 16 segment model. 2D CPA MR is a vendor-independent software with FDA 510(k) clearance and CE-marking. For each slice, the endocardial borders were delineated, and the size of the epicardial contour adjusted to ensure appropriate coverage of the myocardium. The feature tracking algorithm determined the centreline for the left ventricle and solved the Laplace equation between the endo, mid and epicardial contours by tracking the 60 successive images within one complete cardiac cycle. The end-diastole was defined as the phase with the largest LV cavity and, when assessable, at the first occurrence of the coaptation of the mitral valve leaflets. The end-systole was defined as the phase with the smallest LV cavity and, when assessable, as the last phase before the mitral valve leaflets opening. Correct placement of the time events was crucial to determine the strain indices. The quality of the wall tracking was manually checked in every 60 phases, and if errors found, the contours were manually corrected, and the algorithm rerun to achieve the best possible wall tracking. The global longitudinal strain (GLS), global radial strain (GRS) and global circumferential strain (GCS) were derived from the three AHA long-axis views

and the sLS sectored according to the 16 AHA segment model. The peak-systolic (Pk-Sys-sLS), the end-systolic (En-Sys-sLS)- and the peak (Pk-sLS) segmental longitudinal strain values derived from the endo and mid-myocardial layers were used for comparison. Means of sLS values falling outside of the 95% confidence interval of the mean sLS of Healthy rats were used to distinguish between the 'Healthy' and the 'diseased'.

5.5.12 Sample calculation for EF, MyoGLS, myoGCS, GRS

The size effect for each EF, myoGLS, myoGCS and GRS was calculated using the method by Cohen in G*Power [247] (version 3.1.9.6) to compute sample sizes required when $\alpha = 0.05$, $(1 - \beta) = 0.8$, the sampling ratio of 1:1.

5.5.13 Segmental LV Strains Assignments

The AHA segments were assigned into groups in the I/R rats with three possible phenotypes: Infarcted, (2) salvaged myocardium or (3) Remote. The infarcted myocardial segments were defined as myocardial segments with LGE positive, the salvaged myocardial segments as segments with no LGE and high T2 values and the remote myocardial segments as segments with no LGE and normal T2 values. In medical imaging, the remote segments are commonly used as self-control representing "Healthy" myocardium, considered as a baseline for LGE quantification. In Healthy rats, all the segments are truly Healthy segments. Here, remote segments were defined as segments that were LGE negative and fell under normal T2- map. The thresholding of T2 cut-off values to distinguish

between Remote/Healthy and salvaged/infarcted segments are described in section 4.2.6.

5.5.14 Post-Processing of LV Cines For Rotation, Twist and Torsion

The methodology for the analysis of rotation, twist and torsion have been thoroughly detailed elsewhere in **section 6.5.5**.

5.5.14.1 LV Centroid for Short Axis Views

The endocardial, myocardial and epicardial contours were divided into 48 nodes, and their mean coordinate was used to calculate the LV centroid. If the nodal points are (x_1, y_1), (x_2, y_2), (x_3, y_3), …..(x_n, y_n), the formula for LV centroid is:

$$\left(\frac{x_1 + x_2 + x_3 + \ldots\ldots\ldots + x_n}{n}, \frac{y_1 + y_2 + y_3 + \ldots\ldots\ldots + y_n}{n}\right)$$

The LV centroid was then used as the reference point to determine the displacement and rotation. In trigonometry, anti-clockwise rotational angles in degrees are denoted a positive sign, whereas the clockwise rotation is denoted a negative sign in degree.

5.5.15 Atrial Strains

The atrial strain was quantified using the 4-chamber view and using the recommended nomenclatures as per task force. [248] Biplane strain algorithm and 4D atrial volume sequence were not available; hence only monoplane 4-chamber view was used to compute for the atrial volume. The left atrium

deforms in three phases, namely the reservoir phase (LASr), the conduit phase (LAScd) and the contraction phase (LASct). The reservoir phase starts from the mitral valve opening until mitral valve opening, and when compared with the left ventricle, the period includes the isovolumetric contraction, ejection and isovolumetric relaxation. The conduit phase starts from the mitral valve opening through the passive diastasis before the onset of atrial contraction. The contraction phase, also known as the booster phase, starts from the mitral valve opening through passive diastasis before the onset of atrial contraction until the end of mitral valve closure. In atrial fibrillation, the contraction phase is absent, and the conduit phase is the only phase after the peak atrial strain, and it ends on mitral valve closure. The zero baseline was set at the end of the left ventricular diastole, such that when the atrium fills and expands, the strain changes from zero to a positive peak. Careful segmentation was performed to exclude the pulmonary veins and the aorta. For segmental left atrial strain, the atrial walls are divided into the left wall, the roof and the right wall.

5.5.16 Atrial Volumes

The LA volume was computed using monoplane Simpson method on the 4-chamber view. The definition of ED and ES follow the timings of the left ventricle. The left atrium end-diastolic volume (LAEDV) measurement was taken on mitral valve closure. The left atrium end-systolic volume (LAESV)

measurement was taken on aortic valve closure and is also known as the atrial reservoir volume. Paradoxically, when compared with the LV the LAESV was larger than the LAEDV. The LAEF % was calculated using the formula $((LAESV - LAEDV)/LAESV * 100$. As the atrial appendage is very large in rat, it was included in the segmentation for the atria wall. The conduit volume was defined as the volume on the atrial volume-time curve that bears the same time coordinate of the booster strain. The booster volume was defined as the volume on the atrial volume-time curve that bears the same time coordinate of the booster strain. The fractional area change of the left atria was calculated as the percentage difference between the LAEDV and LAESV of LAEDV.

5.6 Results

5.6.1 Results of Global Strains

See overleaf for graphics. Figure 5-2 are the representative results of global strains achieved by following the AHA cardiac imaging planes, akin to what used in human cardiac tomography. It allows the cardiac MR scans to be very reproducible, comparable between animals, and to maintain translatability between human and animal.

See overleaf for graphics. Figure 5-2. (A1), (B1) and (C1) respectively represent the apical 4-chamber view, apical 3-chamber view and apical 2-chamber views; each overlaid with myocardial contours (in green) and to their right in (A2), (B2) and (C2) show their respective longitudinal strain curves where blue dots indicate endo longitudinal strain, red dot indicates myo longitudinal strain and each dot is a phase. (D1), (E1) and (F1) respectively represent the basal, mid and apical short-axes views overlaid with myocardial contour (in green) and to their left in (D2), (E2) and (F2) are their respective circumferential strain curves where the blue dots indicate endo circumferential strain, red dot indicate myo circumferential strain and the green dot indicate the radial strain and each dot is a phase. The isochronal average of (A2), (B2) and (C2) produces (H) and the isochronal average of (D2), (E2) and (F2) produces (I). (G) represents a graphical presentation of strain directions and depiction of the myocardial layers in the endothelial layer arranged in right helix, epi layer arranged in the left helix, the middle layer arranged in circumferential directions. There is no radially arranged fibres and radial strain is a composite strain of all the layers.

(Continue) Figure 5.2 See the previous page for text

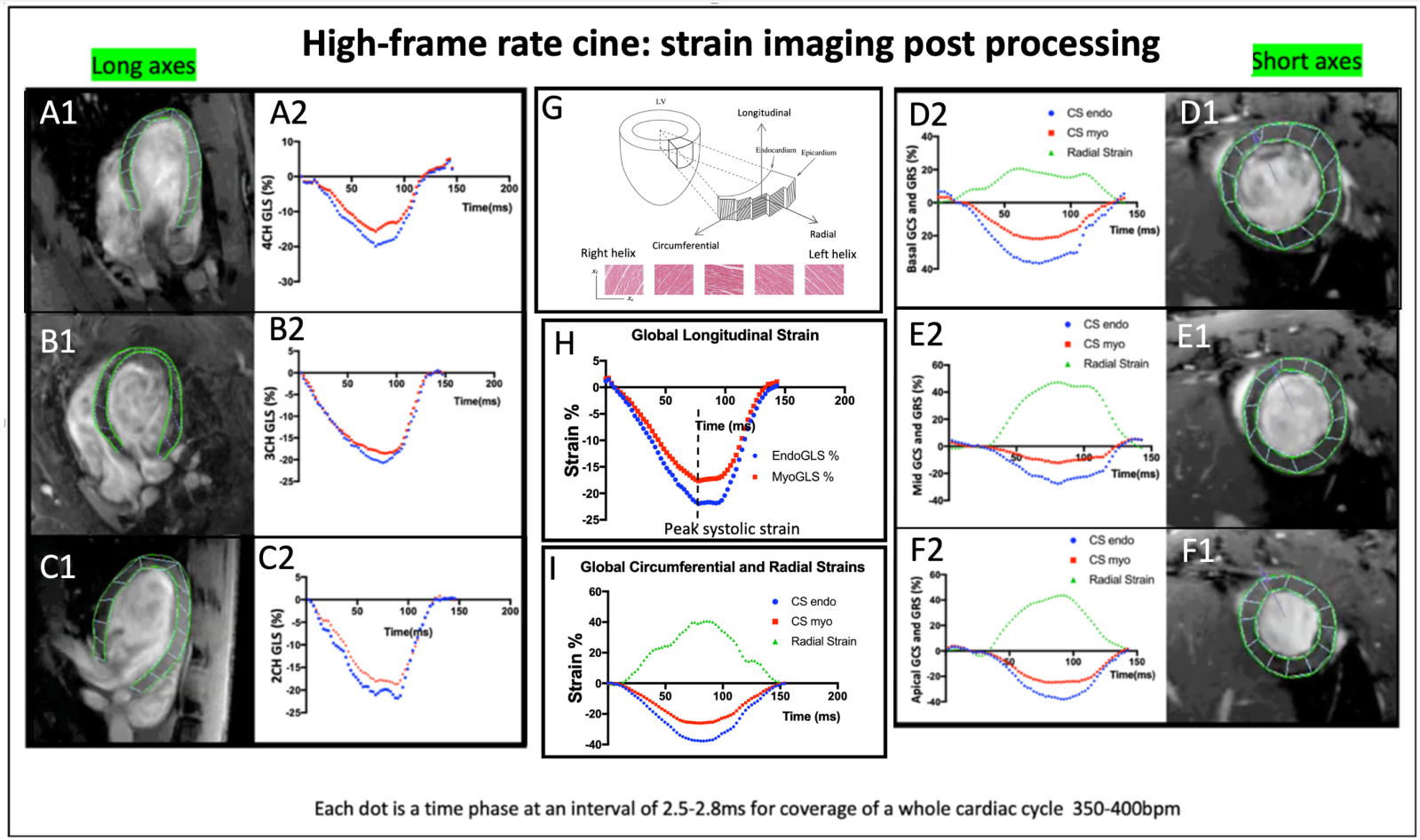

5.6.2 General Physiological and Animal Imaging Characteristics

The general physiological characteristics and global imaging results are summarised in **Table 5-1** and are presented in graphical plots in **Figure 5-3**.

5.6.3 The Effect on Chamber Volumes, Ejection Fraction, Stroke Volume, Sphericity Index and LV Lengths

See **Table 5-1** and **Figure 5-3**. The result on the effect of I/R MI status showed a significant increase in ESV in I/R MI **(**and **Figure 5-3B)** versus Healthy, P=.0176, While I/R MI EDV (596.8mcl±69.2) was slightly higher than the Healthy EDV (556.1mcl±31.7), the effect was not significant, *P* =.1517. Likewise, there was no significant difference in stroke volume **(Figure 5-3C)**, *P* = .4757, with I/R MI (338.7ml±46.2) attaining similar result to the Healthy rats (326.2ml ± 25.56), The effect on heart rate **(Figure 5-3E**), between Healthy rats (388.5bpm±29.0) and I/R MI (378.2bpm±21.5), was found to be not significant, *P*=.1517. Correspondingly, the cardiac output **(Figure 5-3D**), of I/R MI rats (127.0ml/min±17.8) and Healthy rats (127.9ml/min±11.3) showed no significant difference, *P*=.8902. Conversely, the effect of ejection fractions **(Figure 5-3F)**, between the Healthy (58.7%±1.7) and I/R MI rats (56.2%±2.2) showed a modest but significant difference, *P*= .162. A full LV stack LGE was performed in 6 rats which showed a mean LGE volume of 31.3%±5.3 and mean

EF 54.0%±6.7. These results suggest that with ~30% infarction when strictly confined mid-distal to the LAD territory, the effect on the cardiac function measured up to 7 days post I/R-MI assessed using EF showed a mild effect. The ED and ES LV lengths did not change with I/R-MI status. The sphericity index, however, was significantly larger in the I/R MI groups suggestive of the LV remodelling had occurred.

5.6.4 The Effect on Body Weight, LV Lengths AND DV/DT

See **Table 5-1**. There were no significant differences between the weight (*P* = .5366), ED length (*P* =.1072), and ES length (P = .4036) between the Healthy and I/R-MI rats, suggested the hearts of the animals between cohorts were of similar size. On the other hand, the mean was significantly smaller in I/R-MI versus the healthy, respectively showing S-DV/DT ± SD of -8.63ml/s ± 1.3 versus-9.89ml/s ± 0.78 in keeping with reduced systolic function (**Figure 5-4A)** following I/R-MI. The E-DV/DT was significantly smaller than in IR-MI than the Healthy **(Figure 5-4B),** whilst the A-DV/DT was similar (**Figure 5-4C)**, in keeping with significant impaired relaxation found in I/R-MI **(Figure 5-4D).**

Table 5-1. Summary of general physiological and imaging parameters between Healthy and I/R- MI, expressed in mean ± SD (95% CI) where † indicates Welch t test, significance $P < .05$.

Variable, unit	Healthy (n=13) Mean ± SD, (95%CI)	I/R MI (n=9) Mean ± SD, (95%CI)	† *P* value
Weight, g	323±26, (308, 339)	318±12, (309, 327)	.5366
HR, bpm	390.5±27.0, (374.2, 406.9)	375.3±20.7, (359.4, 391.3)	.1517
LVEDV, mcl	556.1±31.7, (536.9, 575.3)	596.8±69.2, (543.6, 650.0)	.1292
LVESV, mcl	229.9±14.1, (221.3, 238.4)	258.1±27.9, (236.6, 279.5)	.0176
SV, mcl	326.2±25.6, (310.8, 341.7)	338.7±46.2, (303.2, 374.2)	.4757
CO, ml/min	127.9±11.1, (121.2, 134.6)	127.0±17.8, (113.3, 140.7)	.8902
EF, %	58.7±1.7, (57.6, 59.7)	56.2±2.2, (54.5, 58.0)	.0167
S dV/dt, ml/s	-9.89±0.78, (-9.42, -10.36)	-8.63±1.30, (-7.63, -9.62)	.0225
E dV/dt, ml/s	8.25±0.87, (7.73, 8.78)	6.78±1.06, (5.96, 7.60)	.0037
A dV/dt, ml/s	7.66±1.73, (6.62, 8.71)	7.50±1.51, (6.34, 8.66)	.8168
E/A dV/dt	1.22±0.32, (1.02, 1.41)	0.95±0.22, (0.77, 1.14)	.0411
EndoGLS, %	-22.02±1.22 (-22.75, -21.28)	-12.10±4.69 (-15.70, -8.49)	.0002
MyoGLS, %	-18.25±0.35 (-18.46, -18.03)	-10.90±3.12 (-13.31, -8.49)	<.0001
EndoGCS, %	-35.98±2.45, (-37.39, -34.56)	-26.88±5.75, (-31.30, -22.46)	.0012
MyoGCS, %	-23.77±1.70 (-24.79, -22.74)	-17.59±4.43(-20.83.-14.18)	.0028
GRS	50.06±8.45, (44.95, 55.17)	34.87±9.66, (27.45, 42.30)	.0016
ED LV length, mm	14.2±0.8, (13.7, 14.6)	13.6±0.6, (13.1, 14.1)	.1072
ES LV length, mm	11.5±0.7, (11.0, 11.9)	11.7±0.7, (11.2, 12.3)	.4036
3D Sphericity index (SI)	0.38±0.05, (0.35, 0.41)	0.43±0.06, (0.38, 0.48)	.0414

5.6.5 The Effect on Global Strains

Using endoGLS **(Figure 5-6A)** and myoGLS **(Figure 5-6A)**, there was a strong significant difference for the Healthy and the I/R-MI, respective *P* = .0002 and *P* < .0001. The endoGCS **(Figure 5-6C)**, myoGCS **(Figure 5-6D)**, and GRS **(Figure 5-6E)**, showed significant differences in the Healthy and the I/R MI, respective *P* values of .0012, .0028 and .0016.

5.6.6 Performance Comparison Between EF And Global Strains

The AUC for ROC curve of diagnostic performance in the detection of systolic dysfunction after I/R MI for EndoGLS and MyoGLS were 1.0, 95%CI 1.0 to 1.0; EndoGCS was 0.94, 95%CI 0.83 to 1.00, MyoGCS was 0.97, 95%CI 0.92 to 1.00, GRS 0.88 95%CI 0.73 to 1.00 and EF was 0.81, 95%CI 0.63 to 1.00; **(Figure 5-6F)**. These results suggest that global strains are superior to EF in detecting changes in systolic function after I/R MI. The EndoGLS, MyoGLS, EndoGCS and MyoGCS were excellent performers, whereas the GRS was better than EF; nonetheless, both were good performers.

5.6.7 Power Calculation for Detection of the Differences Using Global Stains Versus EF

See **Figure 5-7.** The power calculation showed that using global strains, a smaller number of rats would be needed compared to when ejection fraction was used as an end-point index. When $\alpha=0.05$, with a range of Cohen's effect size, d; on t-test: difference between two independent means with ejection

fraction, 12 samples per group would be required as opposed to only 3 samples per group for MyoGLS: requires, 6 samples per group for myo GCS and 7 samples per group for GRS.

5.6.8 FLASH-Cine Versus IntraGate-Cine

5.6.8.1 EndoGLS

See **Figure 5-8. D**. Two-tailed paired t-test showed no significant difference between FLASH-cine endo GLS (-23.03%±2.1) and INTRAGATE endo GLS (-22.16±0.80), mean difference ± SEM between INTRAGATE endo GLS and FLASH-cine endo GLS 0.87±2.35, 95%CI -1.31% to 3.05%, t(df)=0.98(6), *P*<.3660, R2=0.1219. (See Endo FLASH-cine endo GLS variance (8.97%) was larger than INTRAGATE-cine endo GLS variance (3.62%), where the F test showed a significant difference; F, DFn, DFD = 6.6, 6, 6; *P*=.0367.

5.6.8.2 Bland Altman of IntraGate Endo GLS Versus Flash-Cine Endo GLS

See **Figure 5-8. B.** INTRAGATE endo GLS versus FLASH-cine endo showed % bias difference of -3.53%±10.83, 95% CI -24.77% to 17.70%. The differences are variable across the graph.

Figure 5-3. Scatter dot plot of all volumetric measurements, their derivatives and heart rate, where blue is Healthy, red is I/R MI, each dot represents an animal. (A) End diastolic volume (B) End systolic volume (C) Stroke volume (D) Cardiac output (E) Heart rate and (F) Ejection fraction. Middle bar is the mean, and the upper and lower bars are the 95% CI. NS is no significant, *<.05, ** $P < .01$, ***, $P < .001$, and **** $P < .0001$.

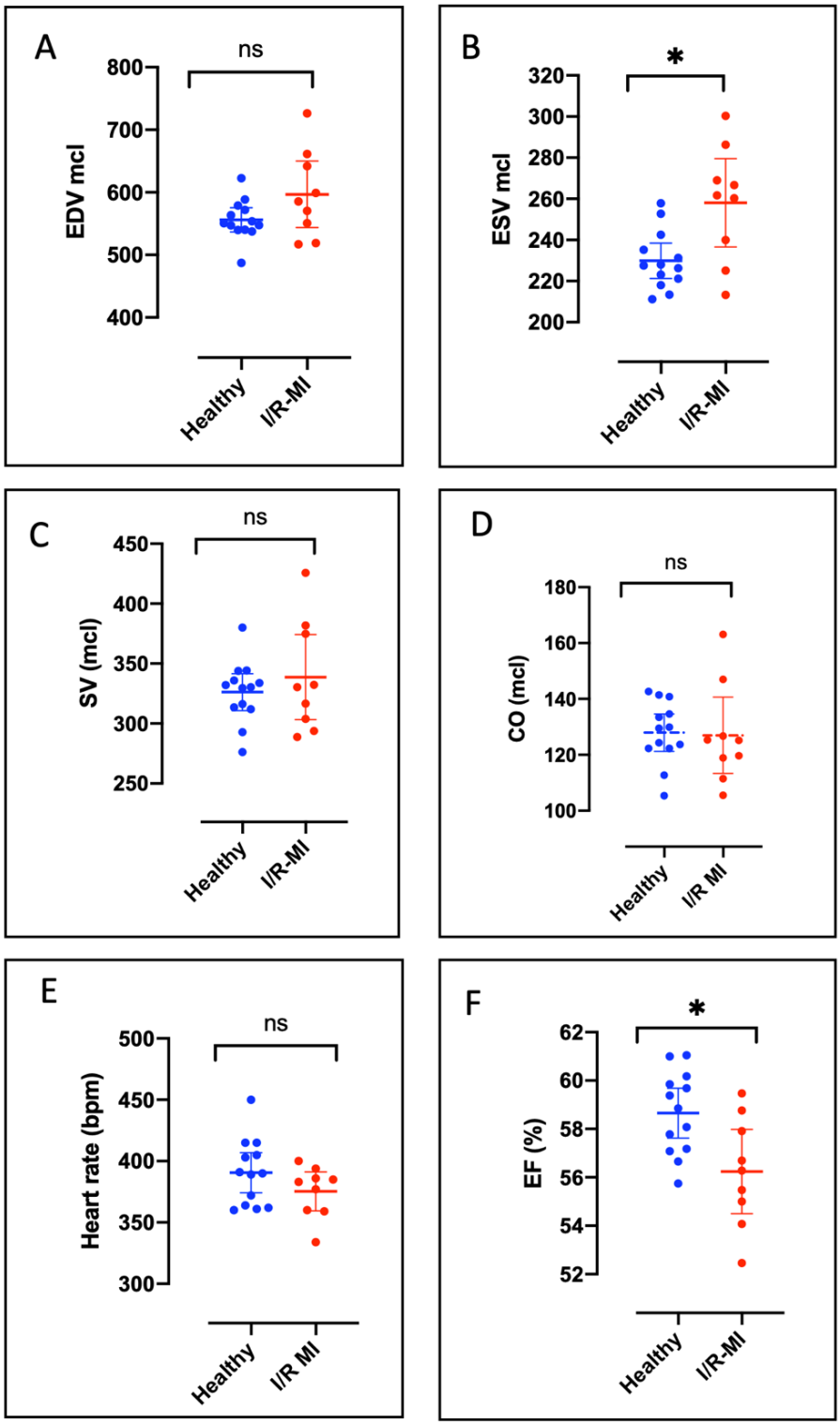

Figure 5-4. On the left-hand panel of (A), (B) and (C) respectively represent the silhouettes of the endocardial border at the end-systole and end diastole of apical 4 chamber view, apical 2 chamber view and apical 3 chamber view of a heart with I/R-MI. The thin silhouettes strips represent the infarcted territory. The magenta lines interconnect 48 pair of nodes on the ES and ED borders to indicate displacement. On the right-hand panel of (A), (B) and (C): the orange line curves are the volume curve over time and the blue line curves represent the rate of volume where indicated the peaks are *S*-DV/DT, *E*-DV/DT and *A*-DV/DT

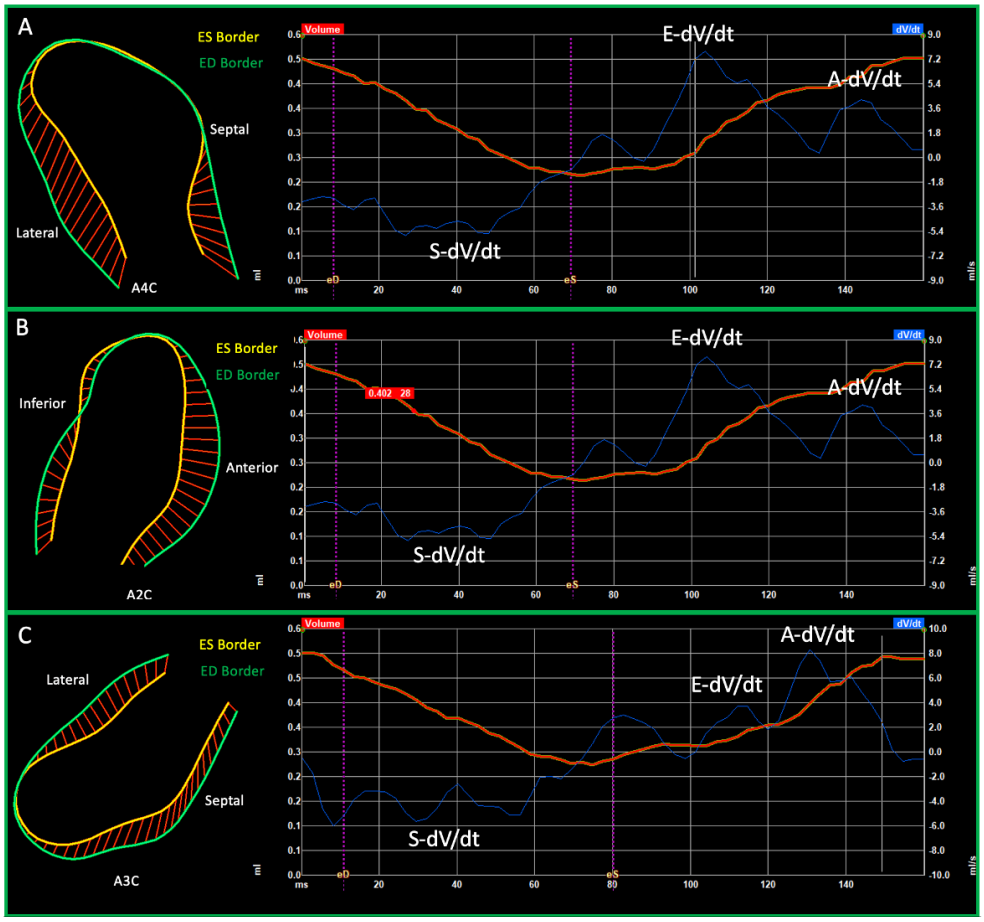

Figure 5-5. Scatter fdot plot of comparing Healthy versus I/R-MI, (A) S-dV/dt, (B) E-dV/dt, (C) A-dv/dt and (D) E-dv/dt

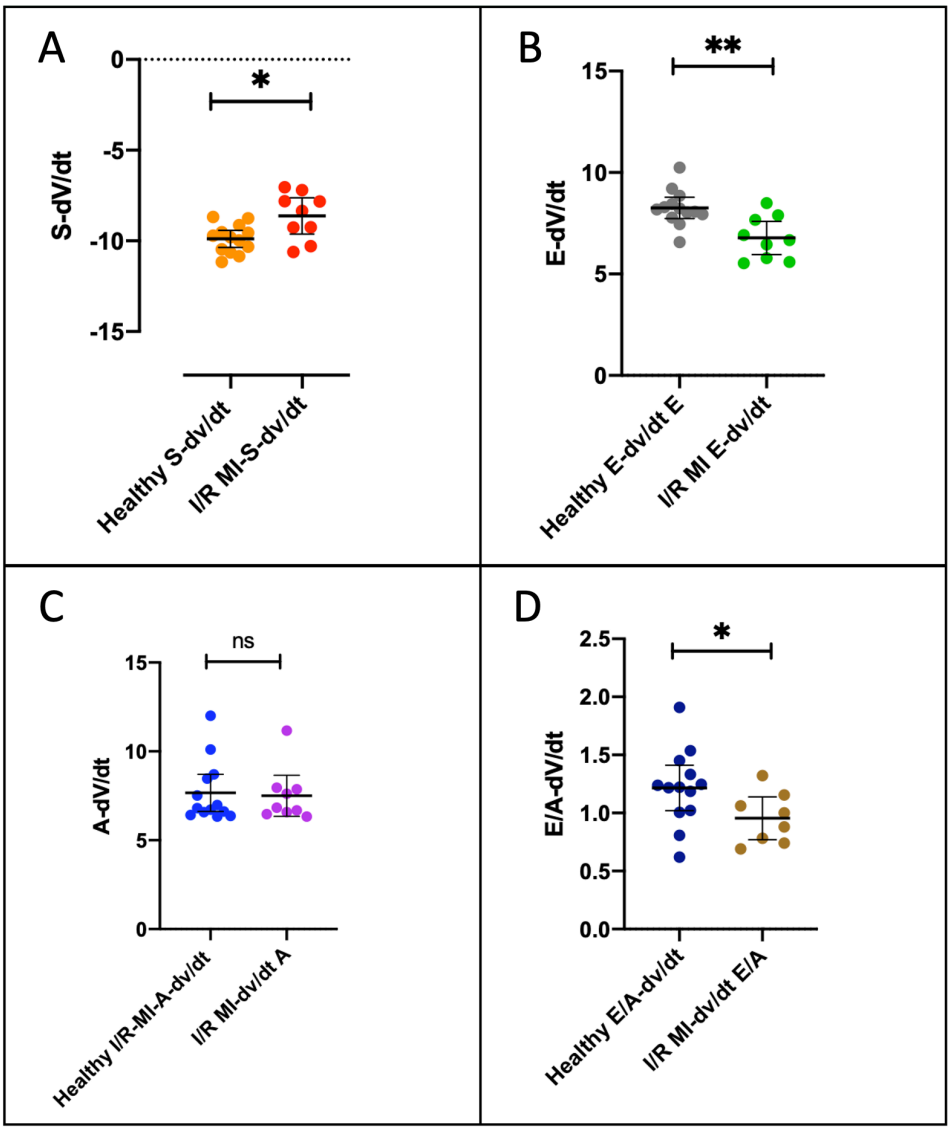

Figure 5-6. (A) Scatter dot plot of endoGLS of Healthy versus IR-MI, (B) scatter dot plot of Healthy vs. I/R MI, (C) scatter dot plot of endoGCS if Healthy vs I/R MI, (D) scatter dot plot of myoGCS of Healthy vs. I/R MI, (E) scatter dot plot of Healthy vs. I/R-MI, (F) Receiver operating characteristic (ROC) of myoGLS, myoGCS, GRS and EF plotted in one chart where the AUC are 1.0, 1.0, 0.94, 0.97, 0.91, 0.88 and 0.81 for the detection of systolic dysfunction after I/R-MI. The middle bar is the mean, and the upper and lower bars are the 95% CI. NS is no significant. * < .5, ** P < .01, *** P < .001 and **** P < .0001.

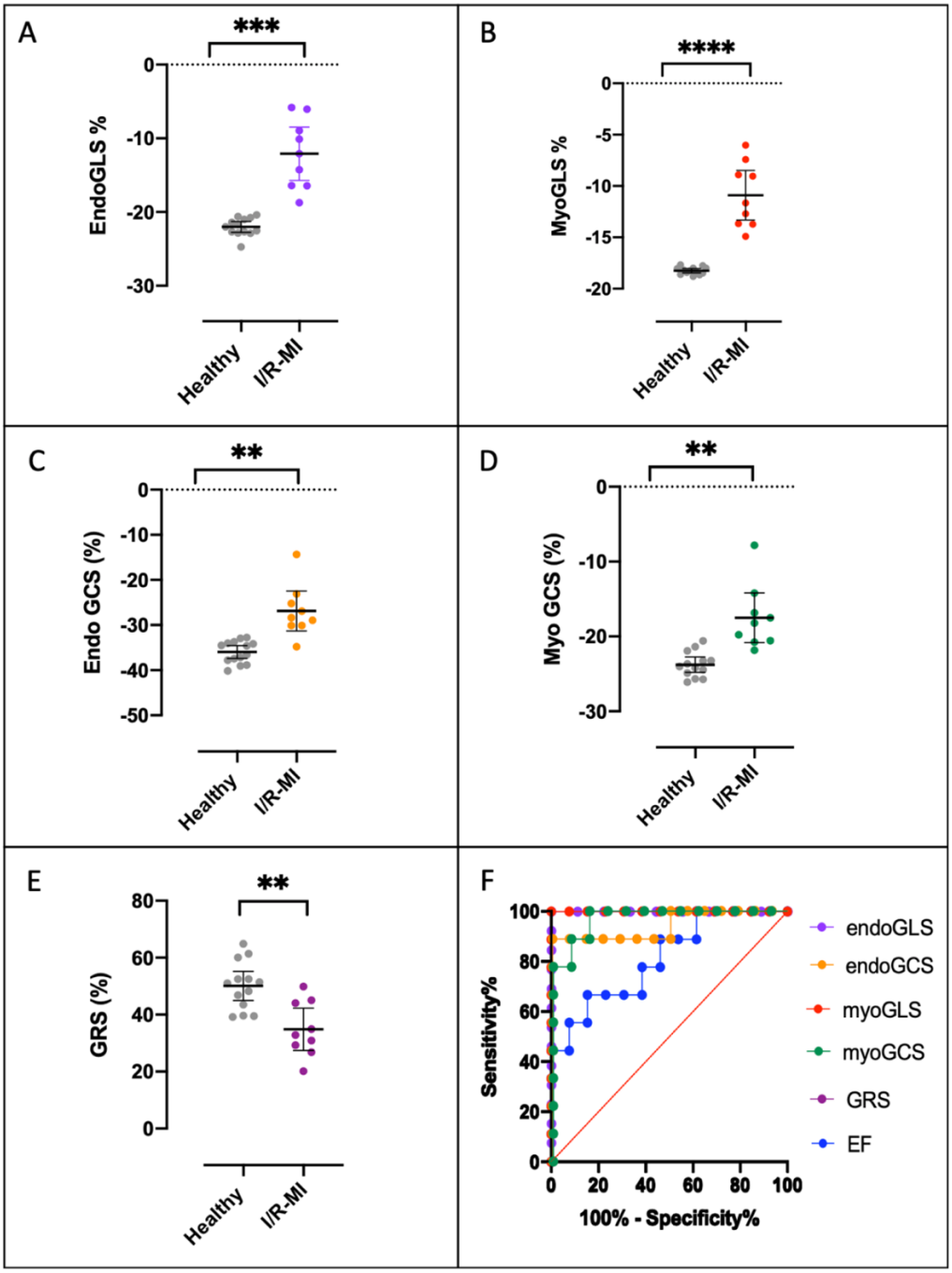

Figure 5-7. Charts showing total sample size required against $(1-\beta)$, when $\alpha = 0.05$, with a range of Cohen's effect size, d; on t-test: difference between two independent means. (A) Ejection fraction: requires 12 samples per group, (B) MyoGLS: requires 3 samples per group, (C) MyoGCS: requires 6 samples per group, (D) GRS: requires 7 samples per group.

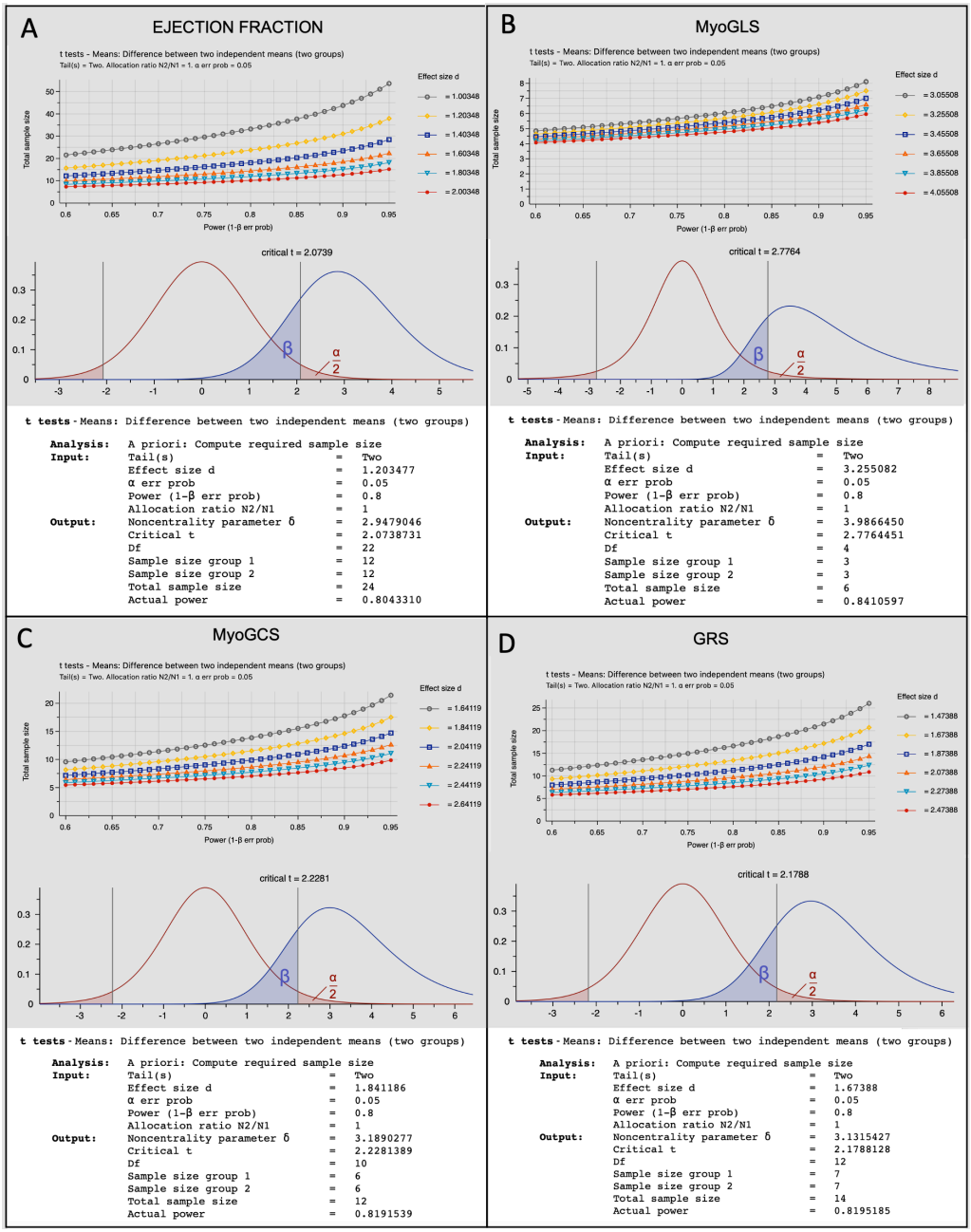

5.6.8.3 Myo Flash-Cine Versus IntraGate-Cine

See **Figure 5-8. C.** Two-tailed paired t-test showed a significant difference between FLASH-cine myoGLS (-19.37%±1.04) and INTRAGATE myoGLS (-18.32%±0.46), the mean difference ± SEM between INTRAGATE myoGLS and FLASH-cine myoGLS 1.05%±0.68, 95%CI 0.42% to 1.69%, t(df)=4.1(6), *P*=.0065, R2=0.4221. While the Endo FLASH-cine myoGLS variance (5.38%) was larger than INTRAGATE-cine myoGLS variance (2.50%), F test showed no significant difference; F, DFn, DFD =5.2, 6, 6; *P*=0.0648.

Bland Altman Of IntraGate Myo GLS Versus Flash-Cine

See **Figure 5-8. A.** INTRAGATE myoGLS versus FLASH-cine myoGLS showed % bias difference of -5.49%±3.56, 95% CI -12.48% to 1.49%. The differences tend to get smaller as the average increases (positive slope on best-fit values 4.24)

Figure 5-8. INTRAGATE EndoGLS versus FLASH-CINE EndoGLS, (C) scatter plot of myoGLS of Healthy rats of FLASH-cine versus INTRAGATE, (D) scatter plot of endoGLS of Healthy rats of FLASH-cine versus INTRAGATE. Middle bar is the mean, the upper and lower bars are the 95% CI. NS is no significant, *<.05, ** P < .01, ***, P < .001, and **** P< .0001.

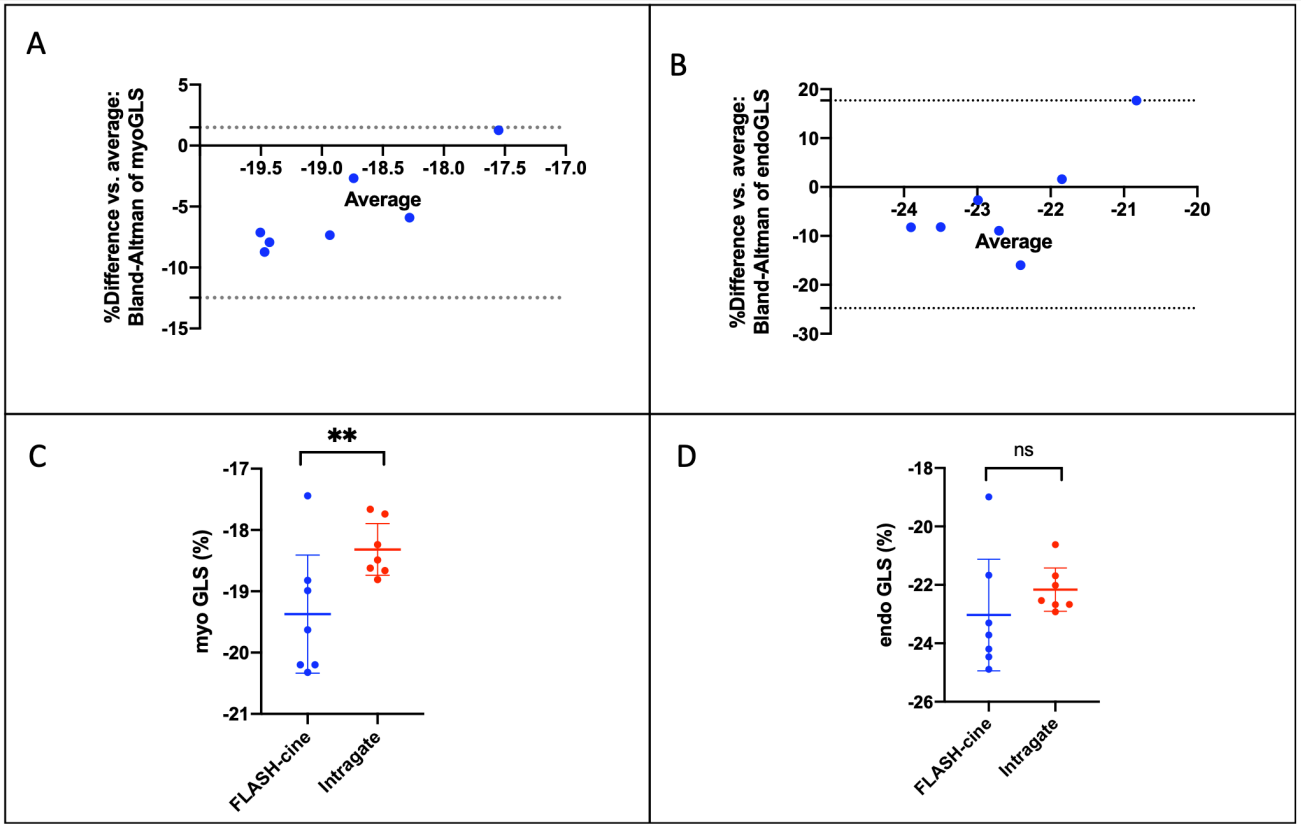

5.6.9 Results of Whole Heart Parametric T2 Mapping

The colour of each pixel in the parametric T2-map (**Figure 5-9A)** represents the apparent T2 value. With careful planning, equidistance short axis slices with no gaps between slices could be achieved in all animals, which allow the calculation of myocardial volume based on the set T2 threshold. The pixel-wise T2 values per 16 AHA sectors from each healthy animal (7 rats, 112 segments) was typically non-Gaussian; hence the upper limit of the 95%CI of the medians was used. The QQ plot of all the upper limit of the 95%CI of the 16 segments points (**Figure 5-9B)** follows a straight line that matches the line of identity, supportive of sampling from a Gaussian (normal) distribution. The mean of 23ms (mean of 16 upper 95%CI of the medians) and the value was used as a threshold to distinguish the Healthy versus 'diseased' (**Figure 5-9C).**

Figure 5-9. (A) Full-heart coverage Parametric T2-map displayed in 'donut' slices of the left ventricle from most basal to most apical, from left to right; each slice constructed from 6 images (echoes) of which the signal intensity decay fitted pixel-by-pixel on the 2-parameter-logistic regression to obtain the apparent T2 values of the pixels, then segmented, plotted in frequency distribution to obtain the median T2 value of the segment. (B) QQ plot line matches the straight line of identity indicated normal distribution. (C) scatter dot plot of upper 95% CI medians of T2 of Healthy heart segments.

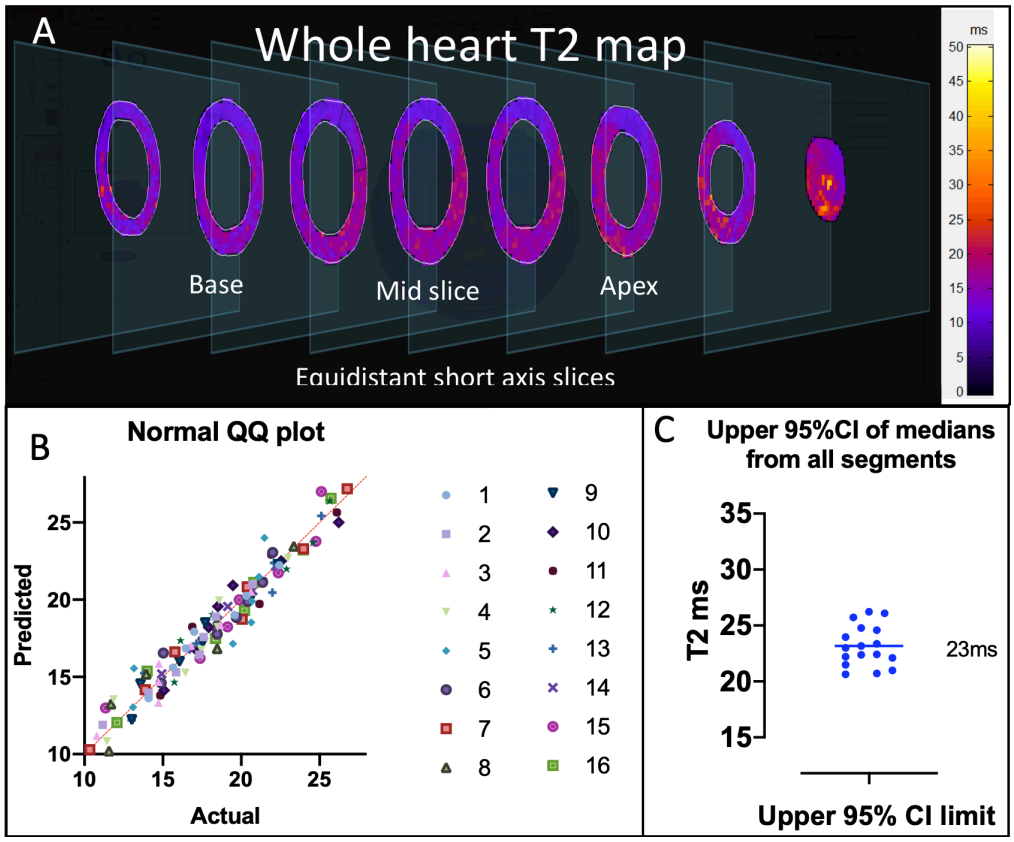

5.6.10 The Results of LV Segmental Strains

Figure 5-10 A, B, C are the representative results of segmental strains achieved by following the AHA cardiac imaging planes, akin to what used in human cardiac tomography. The heart was divided into 16 segments (**Figure 5-10 D, E, F),** and segments could be further clustered following its blood supply. It allows the cardiac MRI scans to be very reproducible, comparable between animals, and maintains translatability between animal and human. From the strain curves (**Figure 5-10 A, B, C)** three variants of peak strains could be identified; namely, the peak-systolic (Peak-sys-sLS), the end-systolic strain (En-Sys-sLS) and the peak strain (Pk-sLS), and the terms were pre-fixed with endo or myo to indicate the myocardial layer being interrogated. The peak strain is the peak value of the strain in the whole cardiac cycle, the sys-peak is the peak value during systole, whereas the end-systole stain is the strain at the end-systole. It is not clear which type of strain peaks are more useful than another and on which myocardial layers, and under what circumstances; hence these were investigated here.

Figure 5-10 J, K, L represent the long axis parametric T2- mapping and **Figure 5-10 M, N, O** represent the short-axis of the T2-mapping, where they are sectored into corresponding AHA nomenclature. **Figure 5-10 G, H, I** represent

the long axis LGE and **Figure 5-10 P, Q, R** represent the short axis of the LGE, where they are sectored into corresponding AHA nomenclature.

The combination of T2-mapping with LGE positivity allowed the myocardial segment to be phenotyped into either Healthy, Remote, area-at-risk (oedema) and permanently infarcted; such that a Healthy myocardium would have a normal T2 value and no LGE present, a Remote myocardium as the segments of an infarcted heart which was not in the affected coronary artery territory and no LGE was present, salvaged area-at-risk segments typically had a high T2 value and no LGE was present, and finally an infarcted segment had positive LGE. By matching the parametric characteristic of the segments with the segmental strains, it was hypothesised that the strain characteristics could be used to identify the segmental phenotype of IR injury.

5.6.11 All SLS Variants Could Distinguish the Three Relevant Imaging Phenotypes in I/R MI

The results of sLS variants are summarised in **Figure 5-11.** All sLS variants showed normal distribution, and there were no significant differences between the Healthy and Remote. In I/R MI rats, all sLS variants could detect the differences between the phenotypes. Between the Remote and AAR phenotypes, the endo Pk-Sys sLS showed the strongest significance difference ($P < .0006$), followed by myo Pk-Sys sLS ($P = .0022$), endo peak sLS ($P = .0117$),

myo En-Sys-Pk sLS (*P* =.0186), myo peak sLS (*P* = .0217) and endo En-Sys-Pk sLS (*P* =.0285).

Between the AAR and LGE phenotypes, all sLS variants showed strong differences (P < .0001). Likewise, between Remote and LGE phenotypes, all sLS variants showed strong significance differences (*P* < .0001). All sLS variants showed significant linear trends from left to right (P < .0001). This means the values of all sLS variants increases (more positive) from Remote, AAR and LGE phenotype.

The ROC charts of the sLS variants are presented in **Figure 5-12.** In all sLS variants, the endo versus their respective myo sLS variants showed no significant results. The best performing sLS variants for detecting AAR were the Endo Pk-sys-sLS and Endo Pk-sLS; however, the diagnostic performance in detecting AAR was fair with AUC of 0.71. The rest of the sLS variants were poor performers for detecting AAR. All sLS variants performed excellently in detecting LGE phenotype; the best sLS variants were Myo Pk-Sys-sLS, Myo En-Sys-sLS and Endo Pk-sLS with AUC of 0.94.

Figure 5-10. (A), (B) and (C) represent the respective longitudinal myo strain curves for (D), (E) and (F) which represent stills of high-frame rate cine overlaid with myocardial contours with AHA segments. (G), (H) and (I) represent the long axis LGE images whereas the (P), (Q) and (R) represent the short-axis LGE images. (J), (K) and (L) are the long axis of parametric T-2 map whereas M, N and O are the short axis of parametric T-2 map. All LGE and T2 parametric images are sectored according to AHA nomenclature.

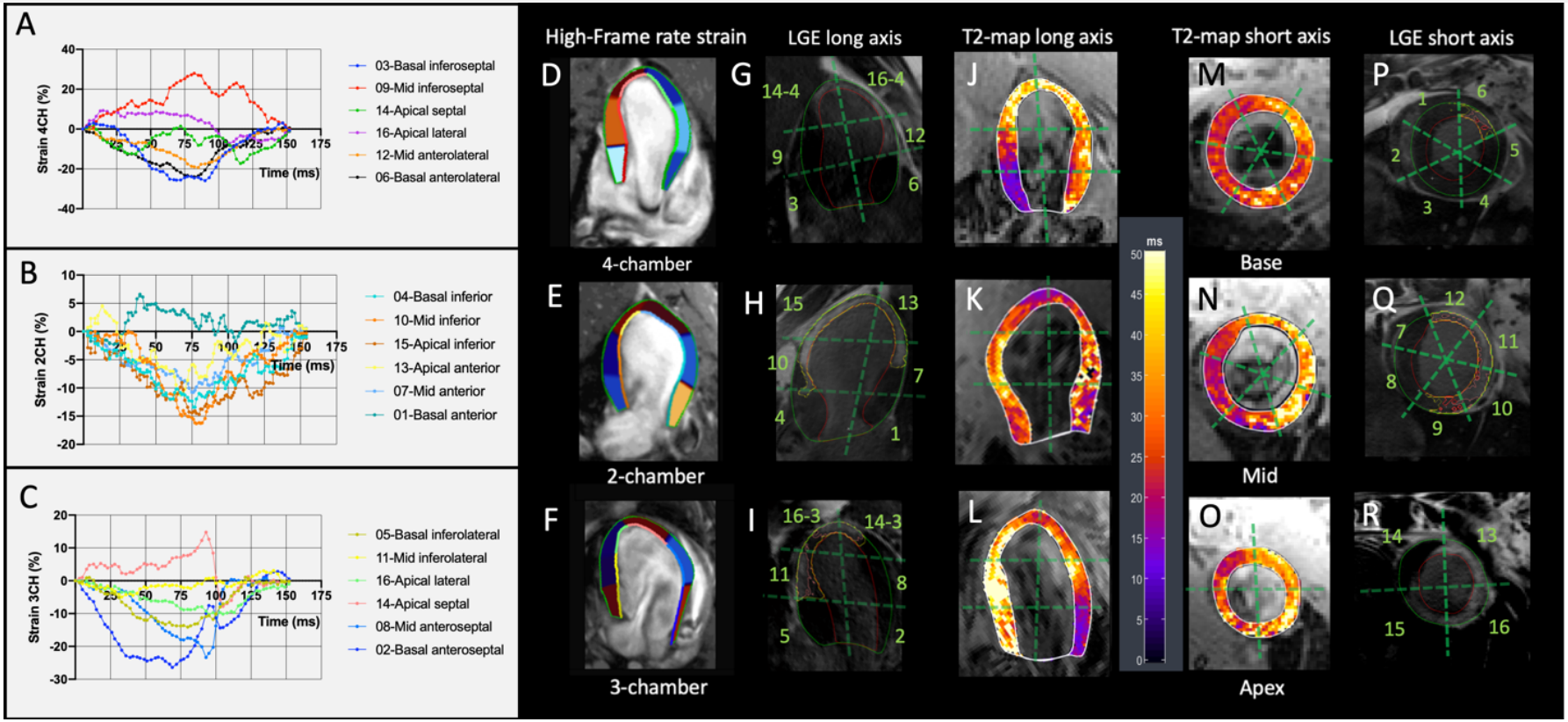

Figure 5-11. Dot plot of the variants of sLS according to imaging segmental phenotype: (A) Endo peak-systolic sLS, (B) Myo peak-systolic sLS, (C) Endo end-systolic sLS, (D) Myo end-systolic sLS, (E) Endo peak sLS, (F) Myo peak sLS. The middle bars indicate the mean, and the error bars indicate 95% confidence interval. NS is no significant, *<.05, ** P < .01, ***, P < .001, and **** P< .0001.

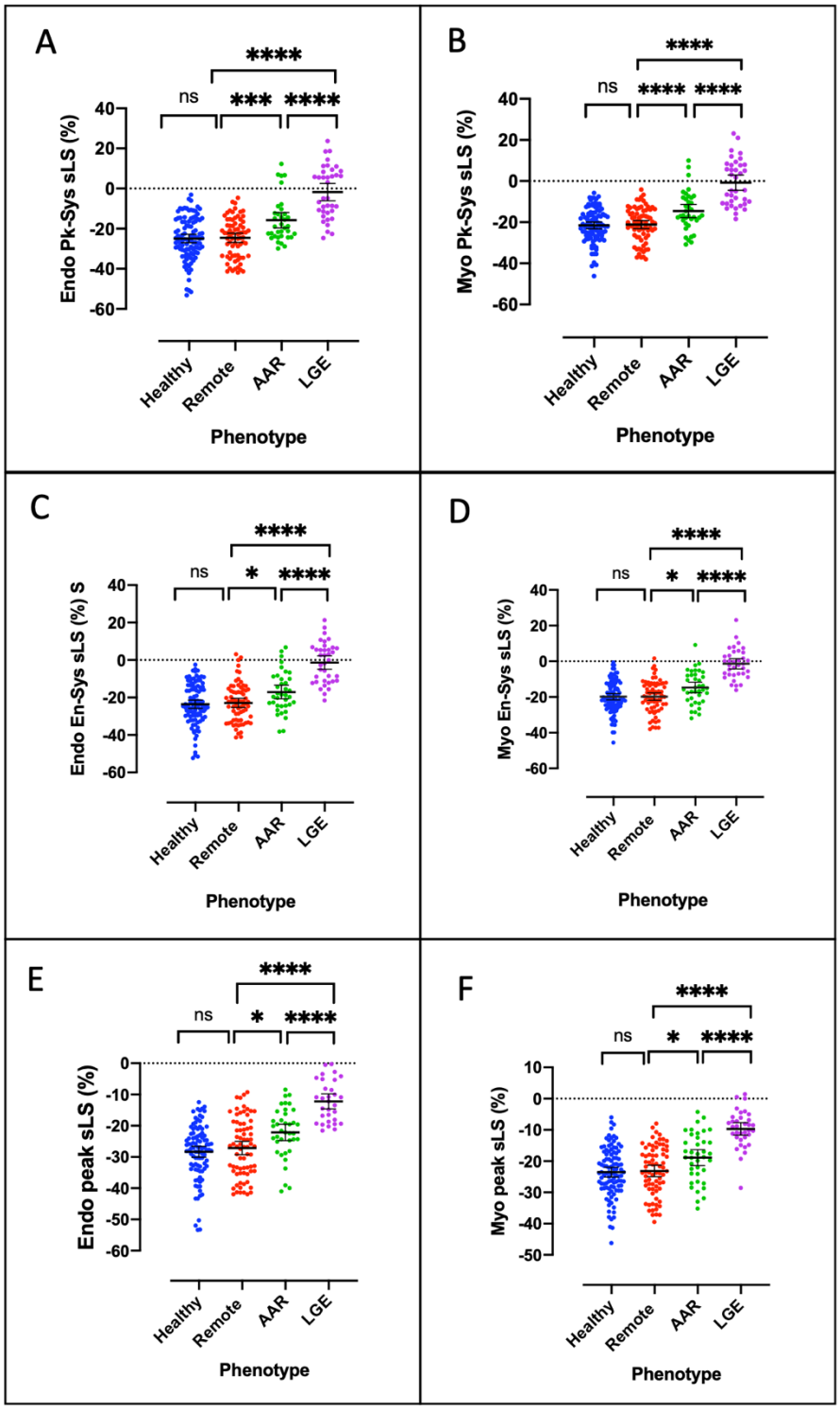

Figure 5-12. ROC curves with AUC±SEM of (A) Endo vs Myo Pk-Sys-sLS-AAR (respective Pk-Sys-sLS-Healthy as control), (B) Endo vs Myo EnS-sLS-AAR (respective EnS-sLS-Healthy as control), (C) Endo vs Myo Pk-sLS-AAR (respective Pk-sLS-Healthy as control), (D) Endo vs Myo Pk-Sys-sLS-LGE (respective Pk-Sys-sLS-Healthy as control), (F) Endo vs Myo EnS-sLS-LGE (respective EnS-sLS-Healthy as control), (G) Endo vs Myo Pk-sLS-LGE (respective Pk-sLS-Healthy as control)

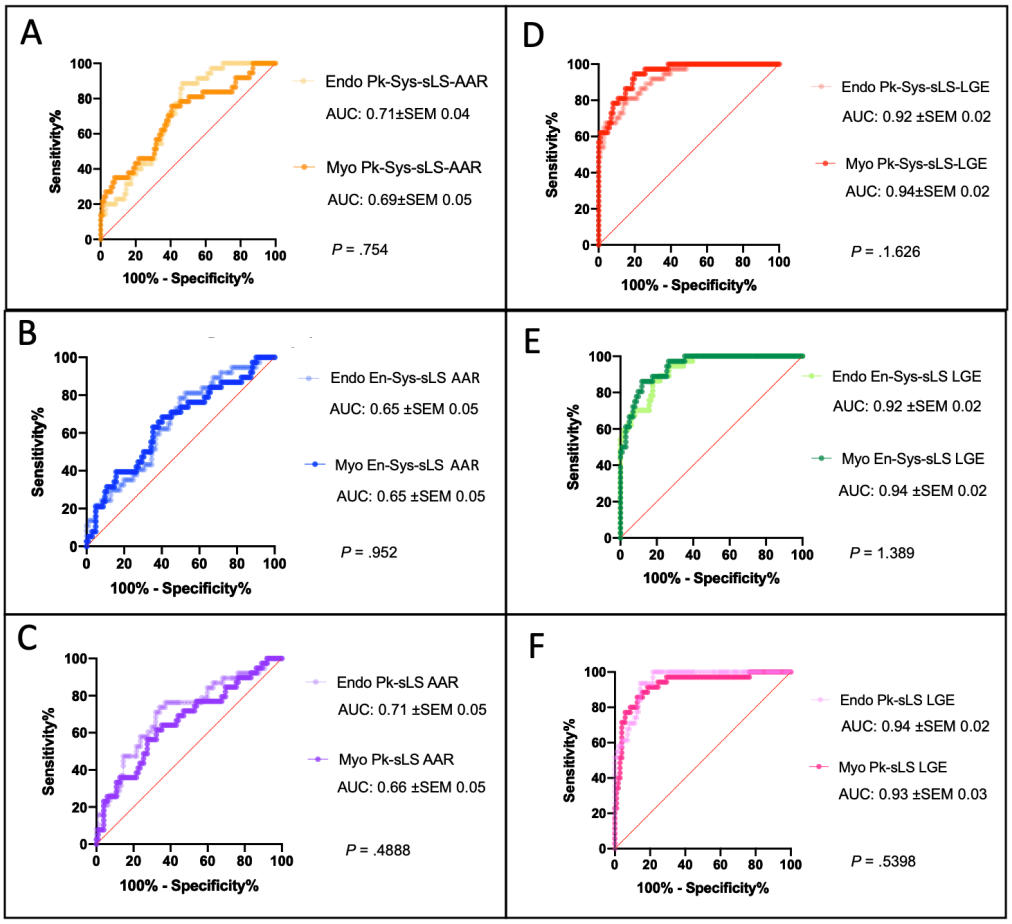

5.6.12 ICC intra-rater on sLS

Coefficients of Interrater Reliability and Agreement, Kappa[228] was computed using icc function in irr (version 0.84.1) running on R (version 3.22) [249] using the two-way random effect model and "single rater" unit; ICC(A,1). Kappa=0.9, 95% CI 0.856 to 0.931 showed a good-excellent absolute agreement between the two repeat measurements of segmental myoGLS (103 segments pairs, from 7 Healthy rats).

Moreover, the paired t-test between LS read 1 (mean±SEM 23.4%±0.79), LS read 2 (mean±SEM 22.9%±0.78) showed no significant difference, mean of differences 0.43±3.56, t(df)=1.24(103), *P*=.2166, mean diff ± SEM 0.35%±1.13, R2=0.0148. Correlation coefficient r =0.9, *P*<.0001.

5.6.13 Basal, Mid and Apical Myo Longitudinal Segmental Strains

One way Brown-Forsythe ANOVA test between basal segments (mean±SEM -21.16%±1.38, 42 segments), mid segments (mean±SEM -23.15%±1.24, 41 segments) and apical segments (mean±SEM -20.54%±1.53, 42 segments) from Healthy rats did not show significant difference, *P*=0.3894; basal vs. mid segments (mean diff 1.98% 95%CI -3.04% to 7.01%, *P*=.6380, basal vs. apical segments (mean diff -0.62% 95%CI -6.19% to 4.95%, *P*=.9866) and mid vs. apical segments (-2.61%, 95%CI -7.93% to 2.72%, *P*=0.4652).

5.6.14 Septal & Inferior Segments Vs. Anterior & Lateral Segments

Basal: Welch-corrected t-test comparing basal septal & inferior segments (mean±SEM -21.73%±2.00, 21 segments) versus basal anterior & lateral segments (-20.60%±1.96, 21 segments) of Healthy rats showed no significant difference; *P*=.6878, R2=0.0040, mean diff ±SEM 1.13%±2.8, 95%CI -4.52% to 6.78%.

Mid: Welch-corrected t-test comparing mid septal & inferior segments (mean±SEM -22.40%±1.87, 21 segments) versus mid anterior & lateral segments (-23.93%±1.57, 21 segments) of Healthy rats showed no significant difference), *P*=.5344, R2=0.0100, mean diff ±SEM -1.53%±2.44, 95%CI -6.47% to 3.41.

Apical: Welch-corrected t-test comparing apical septal & inferior segments (mean±SEM -20.20%±2.87, 21 segments) versus apical anterior & lateral segments (-20.88%±1.17, 21 segments) of Healthy rats showed no significant difference; *P*=.8278, R2=0.0018, mean diff ±SEM -0.68%±3.09, 95%CI -7.03% to 5.67%.

5.6.15 LV Systolic Strain Rate and Endo-Myo Strain Rate Gradient

The endo-myo gradient could be useful in the detection of infarct transmurality. In full transmural infarction, the gradient (the difference between endo and myo SR) would be expected to be around zero, whereas in partial infarction transmural infarction, the gradient would be reduced.

See **Figure 5-13** The Endo S_{SR} Healthy (median -9.81s^{-1}) versus Endo S_{SR} Remote (median -7.88 s^{-1}) showed significant difference, *P* = .0152. The Endo S_{SR} Remote (median -7.88 s^{-1}) versus endo S_{SR} AAR (median -7.67 s^{-1}) showed no significant difference, *P* > .999. The interaction between Endo S_{SR} Remote (median -7.88 s^{-1}) with Endo S_{SR} LGE (median 3.74 s^{-1}) was significant, *P* < .0001; and Endo S_{SR} AAR (median -7.67s^{-1}) versus Endo S_{SR} LGE (median 3.74 s^{-1}) was also significant, *P* < .0001.

See **Figure 5-13B.** The Myo S_{SR} Healthy (median -7.36s^{-1}) versus Myo S_{SR} Remote (median -7.25 s^{-1}) showed no significant difference, *P* = .3138. The Myo S_{SR} Remote (median -7.25 s^{-1}) versus Myo S_{SR} AAR (median -5.93 s^{-1}) showed no significant difference, *P* > .6065. The interaction between Myo S_{SR} Remote (median -7.25 s^{-1}) with Myo S_{SR} LGE (median 2.52 s^{-1}) was significant, *P* < .0001; and between myo S_{SR} AAR (median -5.93 s^{-1}) versus myo S_{SR} LGE (median 2.52 s^{-1}) was also significant, *P* < .0001.

The strain rate gradient in Healthy segments (-1.77^{-1} ± 2.27) in **Figure 5-13C**, Remote ($-1.23s^{-1}$ ± 1.76) **Figure 5-13D**, AAR (- 0.44 ±2.86) **Figure 5-E**, LGE ($1.45s^{-1}$ ± 2.93) in **Figure 5-F** showed a significant linear trend (P < .0001). The ΔS_{SR}-Rem versus ΔS_{SR} Healthy showed no significant difference, *P* = .1573. There was no significant difference between ΔS_{SR}-Remote versus ΔS_{SR} AAR, P = .4022; the difference between ΔS_{SR}-Remote versus ΔS_{SR} LGE was significant, *P* = .0001 and the difference between ΔS_{SR}-AAR versus ΔS_{SR} LGE was significant, *P* = .0288.

Figure 5-13. (A) Endo systolic strain rate, S_{SR} Endo and (B) Myo systolic strain rate, S_{SR} Myo according to segmental phenotype. Strain rate curves of segment with phenotype (C) Healthy, (D) Remote, (E) AAR, (F) LGE. The interrupted rings indicate the systolic strain rate gradient, mean ΔS_{SR} Healthy -1.77s^{-1}, ΔS_{SR} Remote -1.33s^{-1}, ΔS_{SR} AAR -1.04s^{-1}, ΔS_{SR} LGE 1.28s^{-1}.

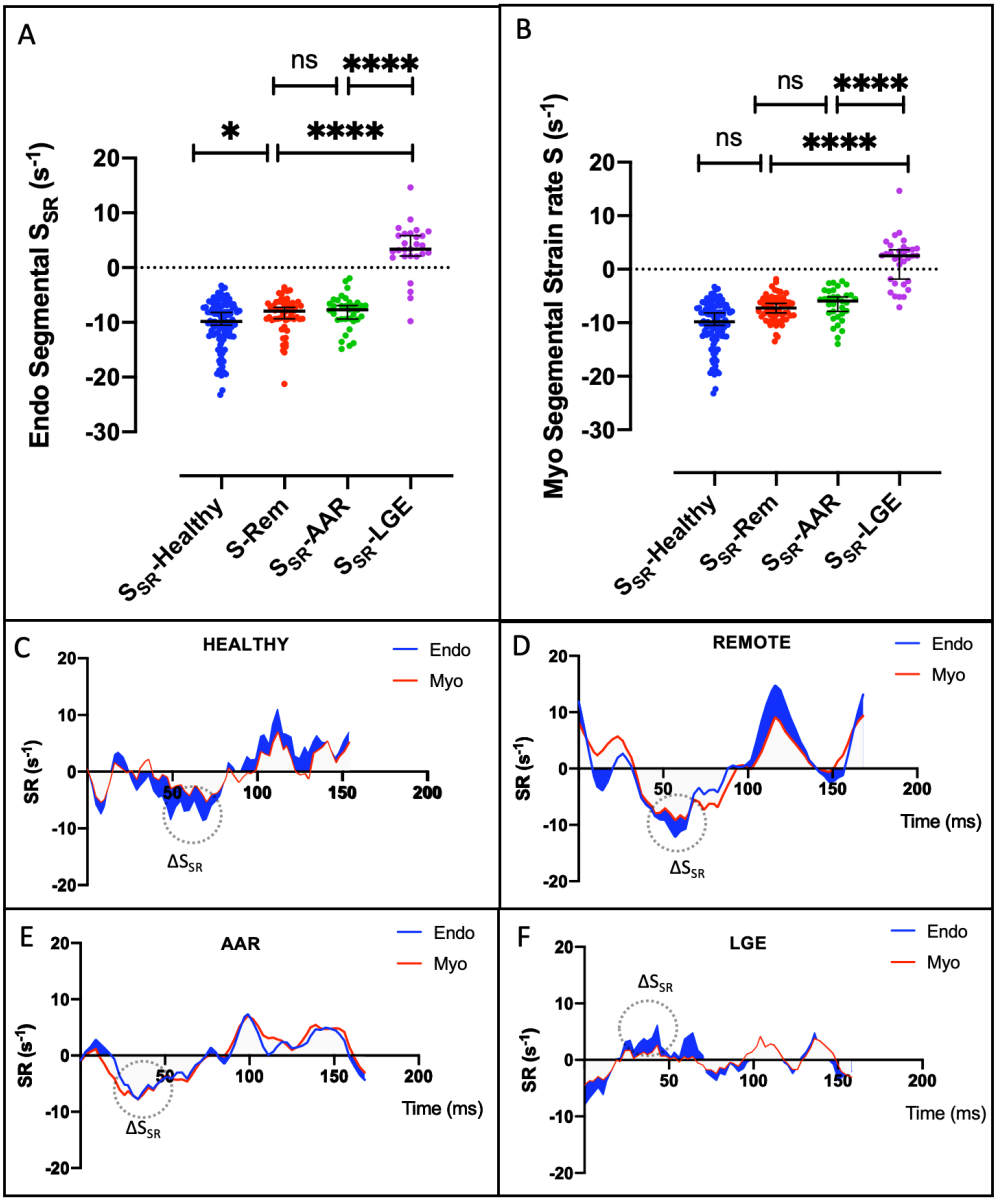

5.6.16 Post Systolic Shortenings were Proportionally More Frequent in Segments of I/R-MI Rats Than Healthy Rats

See **Figure 5-14**. PSS segment count according to segmental phenotype are reported in frequency in **Figure 5-14A and Table 1B** for endo, and **Figure 5-14** and **Table 1D** for myo. The two-sided Chi-Square test on endo PSS showed a significant linear trend, *P* = .0034. The Baptista-Pike odds ratio of IR-MI to Healthy for endo PSS was 1.78 with 95% CI (1.08, 2.97). The two-sided Chi-Square test on myo PSS also showed a significant linear trend, *P* = .0034. The Baptista-Pike odds ratio of IR-MI to Healthy for myo PSS was 2.39 with 95% CI (1.44, 3.98).

Figure 5-14A with table: Contingency chart (A) and table (B) of segmental endo with PSS according to phenotypes

A

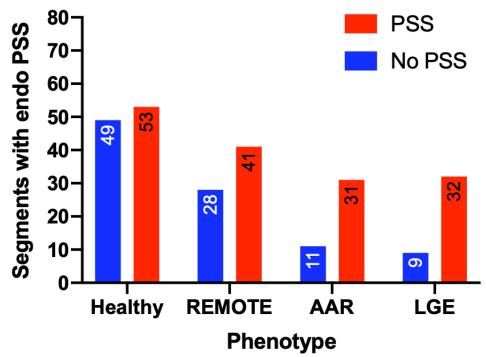

B

	No PSS count (%)	*PSS* count (%)	*Total*
Healthy	49 (48.04%)	53 (51.96%)	102(100%)
Remote	28 (40.58%)	41 (59.42%)	69 (100%)
AAR	11 (26.19%)	31 (73.81%)	42 (100%)
LGE	9 (21.95%)	32 (78.04%)	41 (100%)
Total	97	157	254

Figure 5-14B and table: Contingency chart (C) and table (D) of segmental endo with PSS according to phenotypes

C

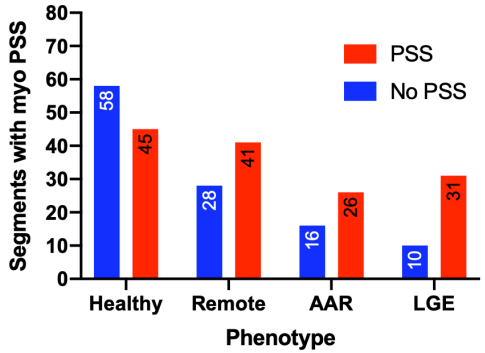

D

	No PSS count (%)	*PSS* count (%)	*Total*
Healthy	58 (56.31%)	45 (43.69%)	103(100%)
Remote	28(40.58%)	41 (59.42%)	69 (100%)
AAR	16 (38.10%)	26 (61.90%)	42 (100%)
LGE	10 (24.39%)	31 (75.61%)	41 (100%)
Total	112	143	255

5.6.17 Time-To-Peak Post Systolic Shortening Could Distinguish the Segmental Phenotypes

The Endo-TP-PSS-Remote (6.4±4.4) and Endo-Healthy-TP-PSS (5.4±3.9) were of similar duration, *P*=.2582. The TP-PSS of Remote-Endo, AAR-Endo and LGE-Endo were significantly different, *P* < .0001; also showing a significant linear trend with a positive slope, *P* < .0001. The Endo-TP-PSS-Remote (5.4±3.9) was shorter than Endo-TP-PSS-AAR (8.0±4.2), *P* = .0430; and Endo-TP-PSS-LGE (11.6±5.4), *P* < .0001. The Endo-TP-PSS-AAR was shorter than Endo-TP-PSS-LGE-, *P* = .0237.

The Myo-TP-PSS-Remote (6.5±4.3) was longer in duration than Endo-TP-PSS-Healthy (4.6±3.5), *P*=.0236. The TP-PSS of Remote-Myo, AAR-Myo and LGE-Myo were significantly different, *P*=0.0003; also showing a significant linear trend with a positive slope, *P*<.0001. The Myo-TP-PSS-Remote (4.6±3.6) was shorter than Myo-TP-PSS-AAR (7.7±4.1), *P*=.0065; and Myo-TP-PSS- LGE (10.1±6.2) *P*<.0014. The Myo-TP-PSS-AAR- was similar to LGE-Endo-TP-PSS (10.1±6.2), *P* =.3165.

5.6.18 Post Systolic Index

Between the Healthy and the Remote segments, the PSI was similar in both the endo and myo layers, where Endo-PSI-Remote (median=18%) and Endo-

PSI-Healthy (median=16%), *P*=.8385, U=1080; and Myo-PSI-Remote (median=15.3%) and Myo-PSI-Healthy (median=13.2%), *P*=.6469, U=975.

The Endo-PSI and Myo-PSI of IR/MI phenotypes were different, both showing *P*<.0001 by Kruskal-Wallis ANOVA. Dunn's multiple comparisons between Endo-PSI-Remote (median 18.0%) was similar to Endo-PSI-AAR (mean rank diff -8.33%, *P* =.6241) and was smaller than Endo-PSI-LGE (mean rank diff -39.65%, *P*<.0001). Endo-PSI-AAR was smaller than Endo-PSI-LGE (mean rank diff -31.32%, *P*<.0001). Dunn's multiple comparisons showed the Myo-PSI-Remote was smaller than Myo-PSI-AAR (mean rank diff -17.35%, *P*=0.0334) and was also smaller than Myo-PSI-LGE (mean rank difference -39.85%, *P*<.0001). The Myo-PSI-AAR was smaller than Myo-PSI-LGE (mean rank diff -22.50%, *P*<.0001).

5.6.19 The Effect of I/R Myocardial Infarction on Apical Rotation, Basal Rotation, Torsion and Twist in Myocardial Layers Between Healthy And I/R-MI

5.6.19.1 Apical Rotation

See **Figure 5-15A.** In the Healthy, the mean rank of the endo apical rotation was similar to the mean rank of myo apical rotation (*P* = .2136) but was greater than the mean rank of the epi apical rotation (*P*= .0454), respectively showing

rotation median ± IQR of 13.84° (5.01, 16.81), 6.92° (3.61, 8.70) and 5.38° (4.12, 5.80).

In I/R-MI, the mean endo apical rotation was similar to the mean of the myo apical rotation (*P* = 0.0798) but was greater than the mean of the epi apical rotation (*P* = .0330), respectively showing mean ± SD of 11.88° ± 5.79, 6.48° ± 3.07 and 5.02° ± 1.08.

The mean rank of the Healthy endo apical rotation (6.43) was similar to the mean rank of the I/R-MI endo apical rotation (7.67), respectively showing rotation median ± IQR of 6.54° (5.73, 11.53) and 16.86 (5.01,16.81), *P*= .6282, *U* = 17.

The mean of the Healthy myo apical rotation was similar to the mean I/R-MI myo apical rotation (*P* = 0.9145), respectively showing rotation mean ± SD of 6.64° ± 2.08 and 6.48° ± 3.07.

The mean rank of the Healthy epi apical rotation (7.50) was similar to the mean rank of the I/R-MI epi apical rotation (7.50), respectively showing rotation median ± IQR of 5.32° (4.79, 5.53) and 5.38 (4.11, 5.80), *P* > .9999, *U* = 24.

5.6.19.2 Basal Rotation

See Figure 5-15B. In the Healthy, the mean of the endo apical rotation was similar to the mean myo apical rotation and epi apical rotation in all

interactions (*P* = .3575), respectively showing rotation mean ± SD of -7.22° ± 2.63, -5.04° ± 2.86 and -5.61° ± 3.41.

The I/R-MI, the mean of the endo apical rotation was similar to the mean myo apical rotation and epi apical rotation in all interactions (*P* = .7832), respectively showing rotation mean ± SD of -11.67° ± 2.54, -11.43° ± 2.46 and -12.87° ± 4.20.

The mean of the Healthy endo basal rotation was significantly smaller than the I/R-MI endo basal rotation, respectively showing rotation mean ± SD of -7.22° ± 2.63 versus -11.67° ± 2.53, *P* = .0103.

The mean of the Healthy myo basal rotation was significantly smaller than the I/R-MI myo basal rotation, respectively showing rotation mean ± SD of -5.04° ± 2.86 versus -11.43° ± 2.46, *P* = .0012.

The mean of the Healthy epi basal rotation was significantly smaller than the I/R-MI epi basal rotation, respectively showing rotation mean ± SD of -5.61° ± 3.41 versus -12.87° ± 4.20, *P* = .0073.

5.6.20 Torsion

See **Figure 5-15C.** In the Healthy, the mean of endo torsion was significantly greater than the mean of myo torsion and mean of epi torsion, respectively showing mean torsion ± SD of 2.29°/mm ± 0.43 versus 1.53°/mm ± 0.21, *P* =

.0026; and versus 1.42°/mm ± 0.42, *P* = .0023. The Healthy myo torsion and I/R-MI epi torsion was similar, *P* = .5201.

In I/R-MI, the mean of endo torsion was similar to the mean of myo torsion, however significantly greater than the mean of epi torsion, respectively showing mean torsion ± SD of 3.70 ± 0.87 versus 4.52 ± 2.2, *P* = .4327; versus 2.59 ± 0.32, *P* = 0431. The mean I/R-MI myo torsion was similar to mean epi torsion, *P* = 0.845.

The mean Healthy endo torsion was significantly smaller to mean endo I/R-MI torsion, respectively showing mean torsion ± SD of 2.29 ±0.43 versus 3.70 ± 0.87, *P* = .0184.

The mean Healthy myo torsion was significantly smaller to mean myo I/R-MI torsion, respectively showing mean torsion ± SD of 1.53 ± 0.21 versus 4.51 ± 2.20, *P* = .0209.

The mean Healthy epi torsion was significantly smaller to mean epi I/R-MI torsion, respectively showing mean torsion ± SD of 1.42 ± 0.42 versus 2.59 ± 0.32, *P* = .0001.

5.6.21 Twist

See **Figure 5-15D**. In the Healthy, the mean of endo twist was significantly greater than the mean of myo twist and mean of torsion, respectively showing mean torsion ± SD of 15.37° ± 2.48 versus 11.21°± 2.79, *P* = .0091; and versus

9.56°/mm ± 2.82, *P* = .0015. The Healthy myo torsion and I/R-MI epi torsion was similar, *P* = .2784.

In I/R-MI, the mean of endo torsion, the mean of myo torsion and mean epi torsion were all similar in all interactions showing mean twist ± SD of 19.75° ± 7.56, 17.08° ± 4.8 and 16.56° ± 2.53.

The mean Healthy endo torsion was similar to the endo I/R-MI torsion, respectively showing mean torsion ± SD of 15.37 ± 2.48 versus 19.75 ± 7.76, *P* = .2337.

The mean Healthy myo torsion was significantly smaller than myo I/R-MI torsion, respectively showing mean torsion ± SD of 11.21 ± 2.79 versus 17.08 ± 4.06, *P* = .0149.

The mean Healthy epi torsion was significantly smaller than mean epi I/R-MI torsion, respectively showing mean torsion ± SD of 9.56 ± 2.82 versus 16.56 ± 2.53, *P* = .0006.

Figure 5-15. Scatter dot plots comparing layers in the apex and layers in basal, and between Healthy and I/R-MI in domain (A) apical rotation, (B) basal rotation, (C) torsion and (D) Twist.

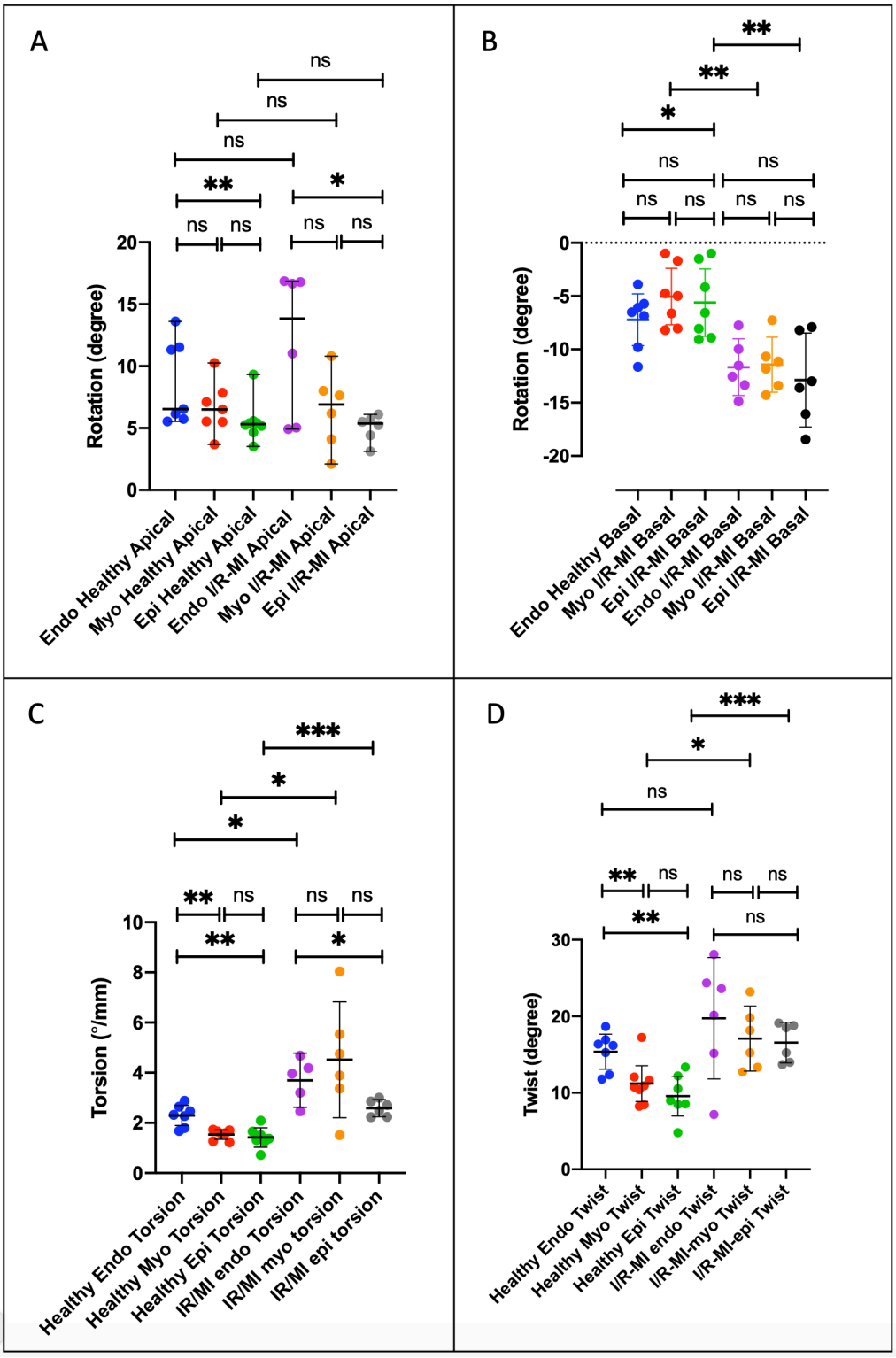

5.6.22 The Effect on Atrial Strains

5.6.22.1 Parametric Results

Results in **Figure 5-8** showed the tracking of the endocardial border of the left atrium for the derivation of longitudinal strain tracked from the end diastole to the end diastole frames. The zero-reference frame used was set at the end of left ventricular diastole, such that when the atrium fills and expands, the strain changes from zero to a positive peak, as indicated by the colour heatmap blue (less positive) and red (more positive). The result was used as a visual quality checking that the tracking of the motions of the atria wall was accurate.

Figure 5-8. (A) represents a cine of a 4-chamber at the diastole view at the end of diastolic frame of a Healthy rat, (B) represents a cine of a 4-chamber at the end of systole frame of a Healthy rat, and (C) represents the silhouettes of the endocardial borders of the left atrial wall at the end of systole (yellow) and end diastole (green border) and the magenta lines interconnect the 48 pair of nodes between ES border and ED border to indicate displacement.

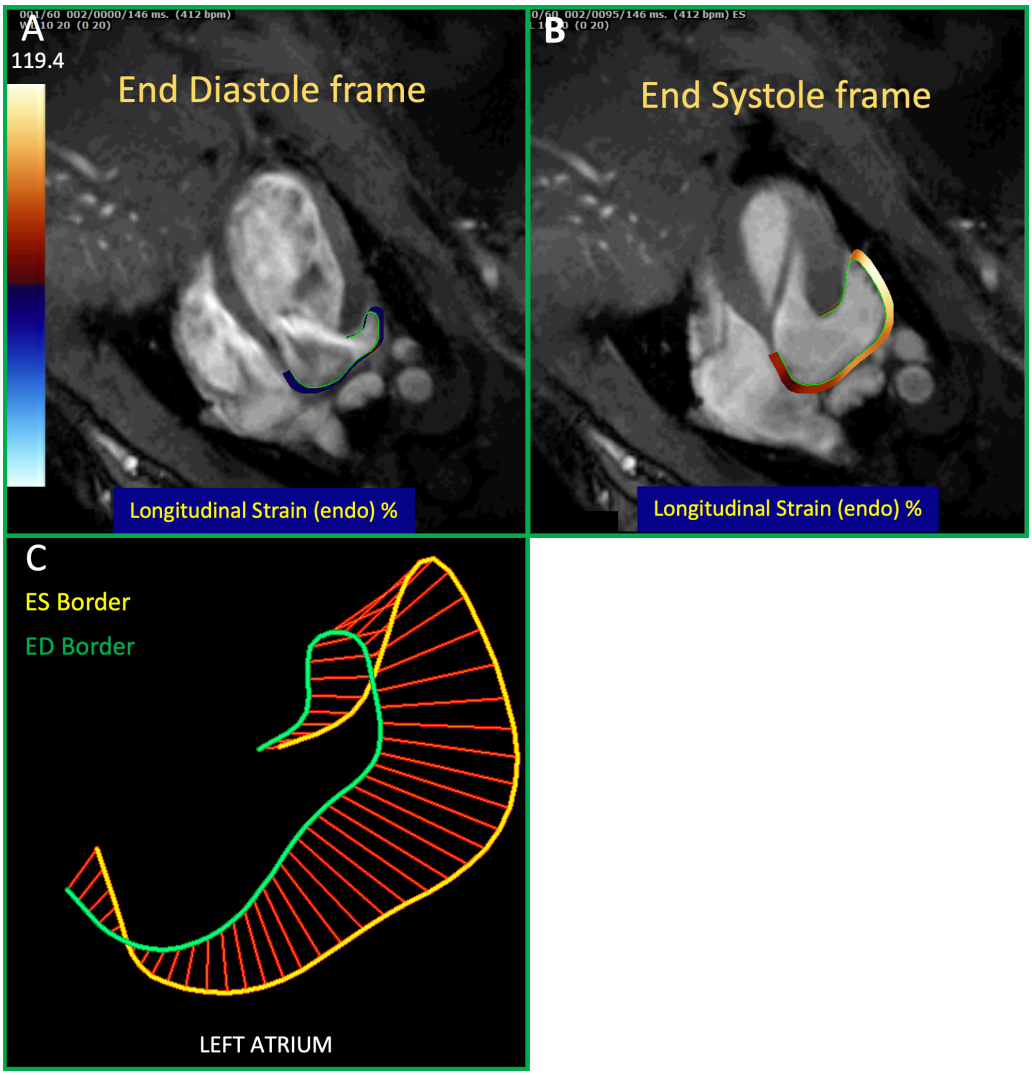

5.6.22.2 Results on Atrial Strain Indices

The indices of LASr, LASct, LAScd, LAEDV and LAESV are graphically shown in **Figure 5-9** and the results are summarised in **Figure 5-10**.

The means of LASr between the Healthy and I/R-MI were similar, respectively showing LASr ± SD of 34.85% ± 3.19 versus 33.94% ± 11.91, *P* = .8200 **(Figure 5-10A).**

The mean LAS-cd of the I/R-MI was significantly smaller than the mean of the LAS-cd of the Healthy, respectively showing LAS-cd ± SD of -14.44% ± 3.88 versus -21.21% ± 6.12, *P* = .0145. **(Figure 5-10B).**

The mean LAS-conduit of the I/R-MI was significantly larger (more negative) than the mean of the LAS-conduit of the Healthy, respectively showing LAS-conduit ± SD of -19.64% ± 8.06 versus -12.00% ± 6.05, *P* = .0424 **(Figure 5-10C).**

The means of pLASRr between the Healthy and I/R-MI were similar, respectively showing pLASRr ± SD of 12.43% ± 6.33 versus 10.17% ± 4.16, *P* = .1190 **(Figure 5-10D).**

The means of pLASRcd between the Healthy and I/R-MI were similar, respectively showing pLASRcd ± SD of -5.89% ± 1.95 versus -7.52% ± 3.93, *P* = .0.571 **(Figure 5-10E).**

The means of pLASRct between the Healthy and I/R-MI were similar, respectively showing pLASRct ± SD of -8.74% ± 4.22 versus -9.67% ± 5.08, *P* = .4941 **(Figure 5-10F).**

5.6.22.3 Results on Atrial Volumetric Indices

The mean of the left atrial EDV between the Healthy and I/R-MI were similar, respectively showing EDV ± SD of 101.4mcl ± 20.14 versus 123.2ml ± 53.55, *P* = .2524 (**Figure 5-11A).**

The mean of the left atrial ESV between the Healthy and I/R-MI were similar, respectively showing ESV ± SD of 214.9mcl ± 25.79 versus 209.1mcl ± 72.31, *P* =.8155 (**Figure 5-11B).**

The mean of the left atrial Booster volume between the Healthy and I/R-MI were similar, respectively showing Booster volume ± SD of 132.6mcl ± 28.19 versus 175.3mcl ± 75.59, *P* =.1212 (**Figure 5-11C).**

The mean of the left conduit volume between the I/R-M was significantly smaller mean of the Healthy conduit volume, respectively showing mean conduit volume ± SD of 33.80mcl ± 32.37 versus 82.3mcl ± 21.84, *P* =.0012 (**Figure 5-11D).**

The left atrial ejection fraction between the Healthy and I/R-MI were similar, respectively showing atrial EF ± SD of 47.60% ± 12.07 versus 47.60% ± 8.05, *P* =.6446 (**Figure 5-11E).**

The left atrial FAC between the Healthy and I/R-MI were similar, respectively showing atrial FAC ± SD of 40.67% ± 6.94 versus 40.67% ± 6.94, *P* =.4527 (**Figure 5-11F).**

Figure 5-9. (A) represents atrial strain curve over time and where indicated by the double-headed orange arrows showing where the measurements taken for LASr, LASct and LAScd indices. (B) the orange line represents atrial volume curve change over time and the blue line represents the rate of change of volume (dV/dt). The vertical purple segregated lines in (A) and (B) indicate where the ED and ES start and in (B) showed where the LAEDV and LAESV were taken from. (C) represents the segmental atrial strain rate curve over time, the colour indicated the atrial walls as indicated by the legend and the peaks of the waveforms where indicated show the measurements for pLASRr, pLASRcd and pLASRct indices were taken.

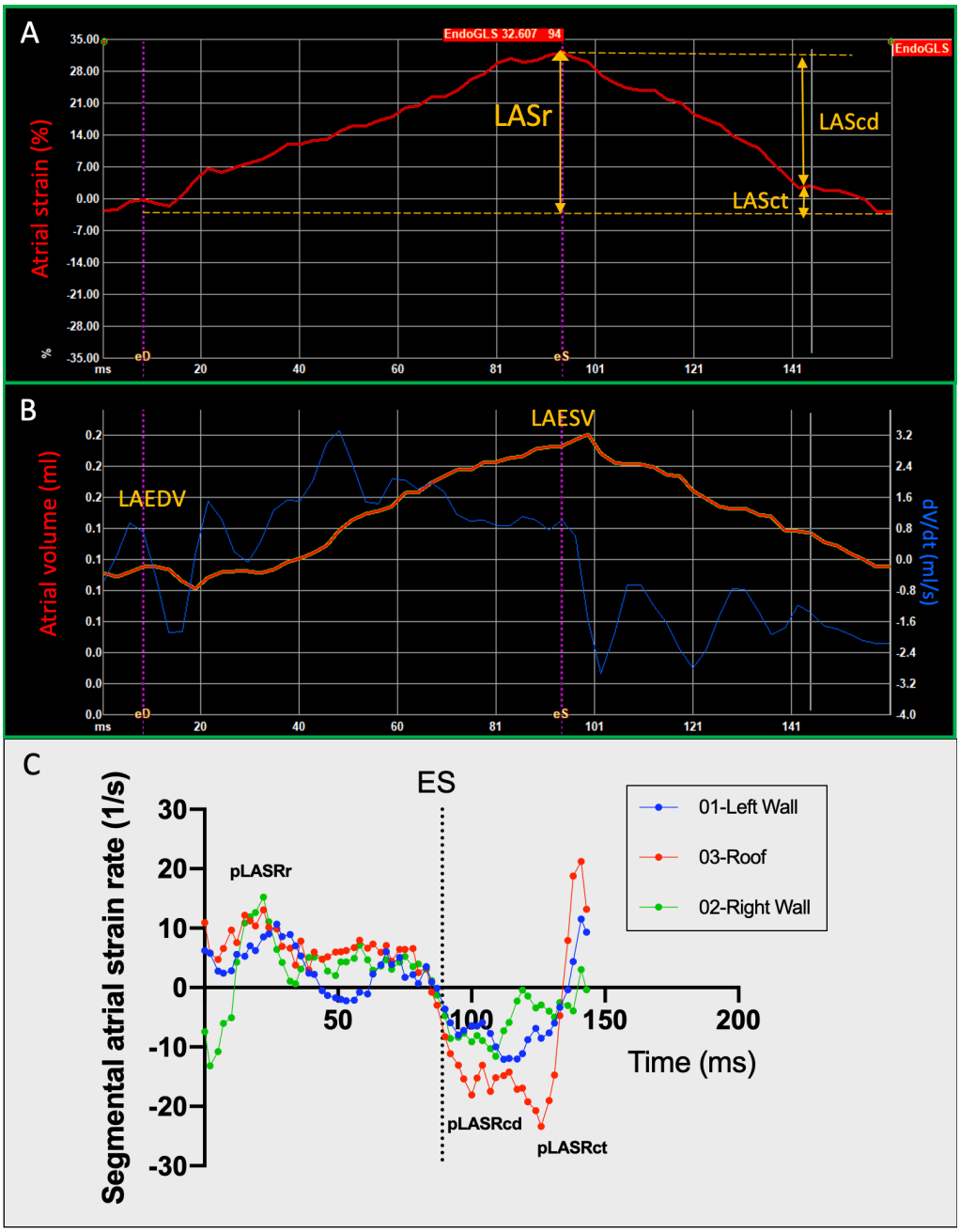

Figure 5-10. Scatter dot plots comparing Healthy versus I/R-MI for indices (A) LASr, (B) LAS-cd, (C) LAS-conduit, (D) pLASRr, (E) pLASRcd and (F) pLASRct

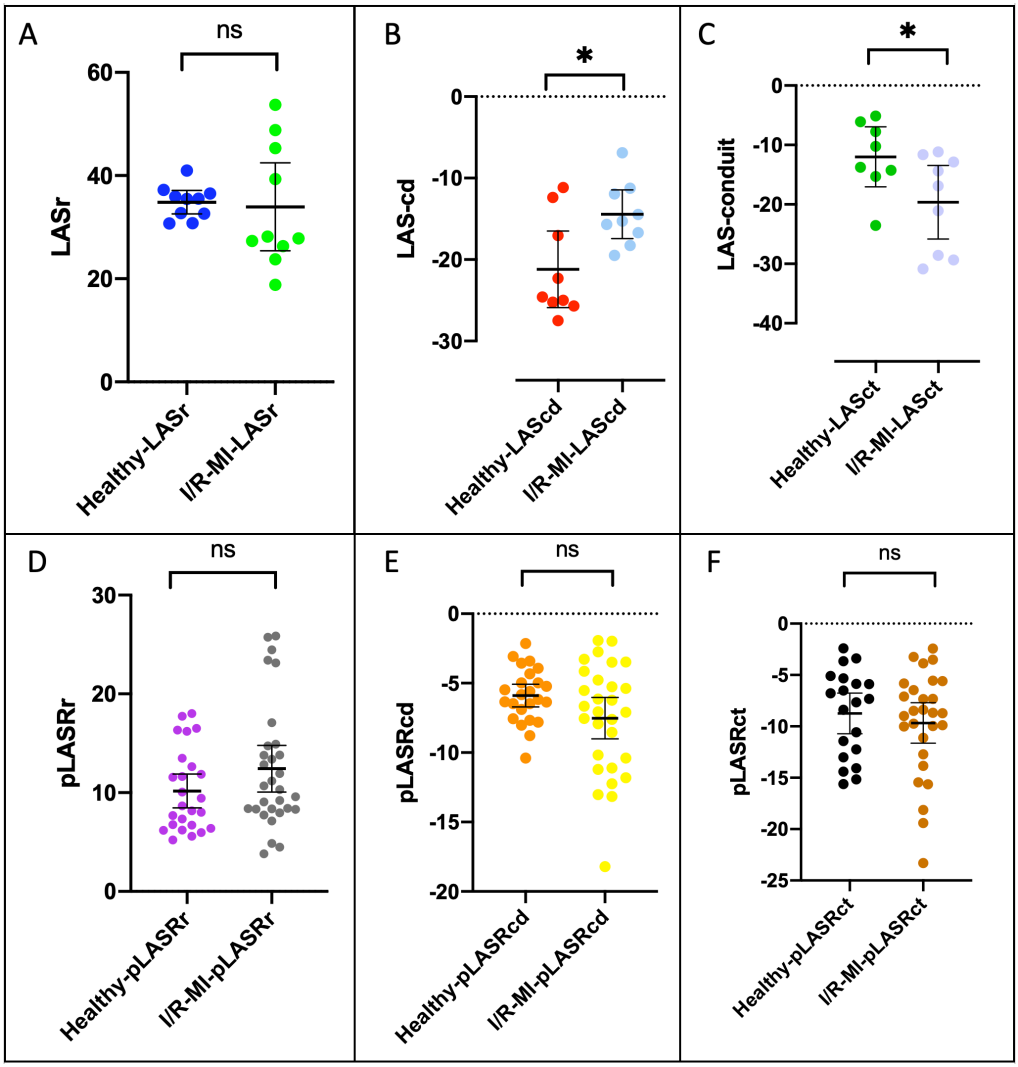

Figure 5-11. Scatter dot plots comparing Healthy versus I/R-MI for indices (A) atrial EDV, (B) atrial ESV, (C) Booster volume, (D) conduit volume (E) atrial ejection fraction and (F) LA FAC.

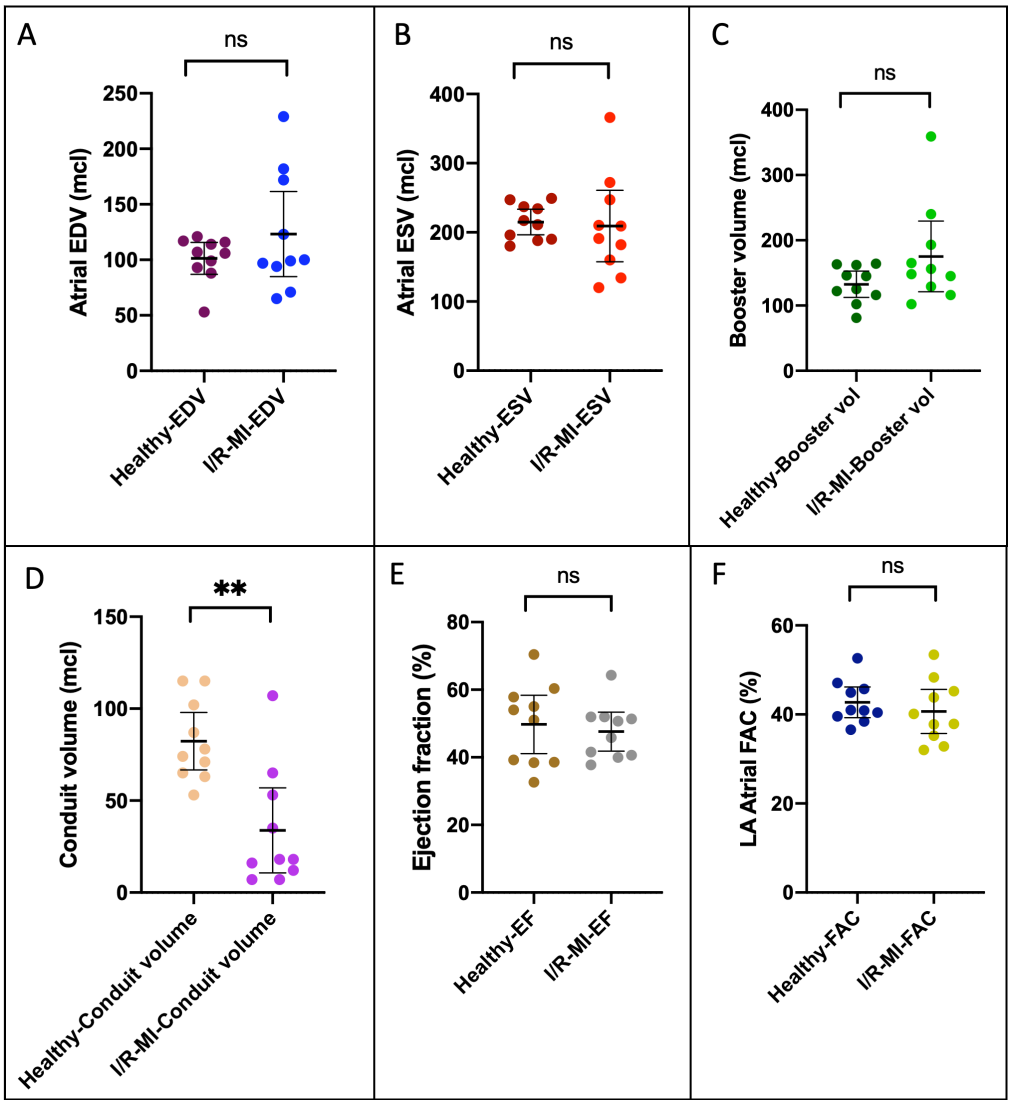

5.7 Discussion

In this proof-of-concept study, it was demonstrated that all the sLS variants of HFR-CMR-FT were able to detect all the relevant segmental phenotypes of cardiac ischaemia-reperfusion injury. A robust cardiac planning strategy was performed, which has enabled the establishment of HFR-CMR-FT and defined the segmental phenotypes using MRI gold standard methods for the assessment of viability using T2-mapping and LGE. The phenotypically categorised sLS variants then compared. An abnormal segmental longitudinal strain was an indication that the segment was diseased, associated with either abnormal T2 value with or without LGE. The former signifies salvaged myocardial segments, while the latter signifies necrotic myocardial segments. The sLS values of salvaged segments were weaker (more positive) than the Remote segments and stronger (more negative) than the LGE segments; all the sLS variants were exhibiting a significant linear trend from left to right.

It was observed that the LGE segments could have positive sLS values associated with transmural LGE, analogous to the dyskinetic movement of the wall by visual observation in wall motion score index[250] (WMSI), characterised by an outward movement of the myocardial wall during systole. SLS, however, benefits from a continuous quantifiable measure as opposed to discrete values of wall scoring in WMSI and sLS could be studied in the endo and myo layers.

Pk-Sys-sLS and En-Sys-sLS are considered more relevant than pk-sLS for the assessment of systolic as the measurements of the peaks happen within the systolic period. The En-Sys-sLS is recommended by the task force over the others, rationalised by the fact that that pk-sLS in diseased segments could have normal values due to the phenomenon of post systolic shortening. Here, it was demonstrated that this did not matter, as all sLS variants could still detect the phenotypes when compared as a group. It appears that the pk-sLS have more negative values, En-sys-sLS have intermediate negative values, and pk-Sys-sLS have the least negative values; an effect of moving the zero baselines upward.

Endo-Pk-Sys-sLS was better than En-Sys sLS in distinguishing Remote versus AAR phenotype with the respective mean differences of Remote-AAR were -8.7% and -5.7%. The Endo-Pk-sys-sLS-Remote was higher (more negative) than Endo-End-Sys-sLS-Remote as its peaks happened more frequently before the AVC and the strain curve crossed the AVC line at a lower value; whilst the mean Endo-Pk-Sys-sLS- AAR was lower (more positive) than Endo-End-Sys-sLS-AAR as its peaks could either be the same as Endo-End-Sys-sLS-AAR or crossed the AVC line at a value lower (more positive) before peaking again at post systolic shortening in diastole.

The diagnostic performance of the sLS variants in the endo and myo layers were compared, showing no significant differences. However, based on ROC AUC classification, the best performers for AAR detection are the Endo-Pk-sys-sLS and Endo-Pk-sLS against their respective Healthy controls. All sLS variants are excellent performers for LGE detection against their respective Healthy controls; the best performers are the Myo-Pk-Sys-sLS, Myo-En-Sys-sLS and Endo-Pk-sLS. The accuracies of En-Sys -LS and to a lesser extend of Pk-Sys-sLS are dependent on the correct placement of AVC, while the Pk-sLS is not. A recent recommendation from the task force recommends measurements from the mid layer.[152]

The relative values of all the Healthy-sLS variants were similar to the all Remote-sLS variants. However, when assessed using strain rate, the Remote endocardial layer was less negative than the Healthy endo; and the Remote myocardial layer SR was similar to Healthy in the myo layer SR. This demonstrates that there was subtle impairment in the Remote segmental function following I/R-MI. The abnormality in the Remote was also detected in T2-mapping, showing modest increase in the T2 values of the Remote segments in the I/R MI rats compared to the myocardial segments of the Healthy rats. The effect of myocardial infarction on the relaxation times T1 and T2 of the Remote segments were also observed in human. [251] The observation

that T2 was abnormal in the remote myocardium was supportive of an inflammatory process. Other studies have provided histological evidence of increased cell infiltration associated with inflammation[252] with the eventual outcome of fibrosis deposition via fibroblast activation[253] during LV remodelling. It is recognised that the subendocardial layer is more susceptible to ischemia and fibrosis because the blood supplied only in diastole by collapsible capillaries and are more compressed when the ventricle is dilated.[162]

It was demonstrated that the endo-myo strain rate gradient increased linearly (positive slope) from phenotype Healthy, Remote, AAR to LGE. All the interaction of ΔS_{SR} LGE with the other phenotypes were significant. The usefulness of strain rate gradient for the detection of ischaemia [254] and tissue velocity gradient for viability have been reported elsewhere. [255]

It was demonstrated that high frame rate strain could be used to quantify post systolic shortening in several ways. The proportional number of segments with PSS increased linearly with severity from the Healthy, Remote, AAR and LGE. The odds ratio of having endo PSS was 1.8-fold and Myo-PSS 2.4-fold in segments of I/R rats compared to the Healthy. The time to peak of PSS also increased with increasing disease severity, as well as the magnitude of PSS increased as quantified using PSI.

Even though 2% significant reduction in the EF was detected in I/R MI with the use of a moderate number of animals in order to achieve the statistical power, the ROC AUC for the stacked EF was merely good, whilst the AUCs for all the HFR-CMR-FT global strains were excellent in the order of the MyoGLS, MyoGCS and GRS using fewer animals. The global strains of HFR-CMR-FT have better sensitivity and specificity. To our knowledge, this was the first study to be able to perform multi-plane HFR-CMR-FT strains on the small animal disease model. It was observed that after acute I/R MI, there was preservation in the cardiac output and no change in the heart rate when the infarct size was 30% solely confined mid-distal to the LAD territory. The findings are congruent to that in human that a myocardial infarction of similar magnitude has a mild effect on the ejection fraction.[256,257] The stroke volume and cardiac output did not decrease, suggestive of a compensatory mechanism in play in maintaining the blood circulation post-myocardial infarction. An increase in the heart rate in the failing hearts is a known physiological compensatory response by the autonomic nervous system. It so does an increase in the end-diastolic volume as the means to increase the stroke volume via Frank-Starling mechanisms [258] and hence the cardiac output. An increase in heart rate was not observed, but the effect could have been blunted by anaesthesia. The end-diastolic volume was trending to increase although not reaching significance, which could indicate that that remodelling would ensue and the increased in the end-

diastolic volume with an increase in preload could also help maintain the cardiac output. Moreover, an increase in sphericity index in the I/R MI was observed, whilst the LV lengths were found to be similar between the Healthy and I/R MI rats. It is known that 60% of stroke volume is attributed to the long axis function of the atrioventricular plane.[259,260] Carlsson et al. have observed in heart failure the initial dilatation of the area of the upper base of the left ventricle could be a compensatory mechanism, such that the expanded epicardial area multiplied by the distance of the longitudinal atrioventricular plane displacement (AVDP) maintains the AVDP stroke volume contribution.

The rotation of all the layers in the apex followed the same pattern in both the Healthy and I/R-MI, where the endo rotation was stronger (more positive) than the epi, while the myo rotation was not different from the rotation of the endo and epi. On the contrary, the rotation in all layers in the basal slice were stronger (more negative) in the I/R-MI than their respective rotation in the layers of the Healthy. Within the groups, the rotations of all the layers were not different. These results suggest the status of I/R-MI increases the rotation at the base and preserves the rotation at the apex, signifying a compensatory mechanism. These findings are the opposite of the inotropic effect by adrenergic stimulation, where the basal rotation does not change with ascending doses of dobutamine, but the apical rotation does show a dose-

dependent increase. [261] Healthy human subjects infused with dobutamine exhibited the rotational response predominantly happening at the apex than the base when compared to the respective baseline. [262]

The torsions of all the layers in the I/R-MI were stronger than their respective torsion in all the layers in the Healthy. While the endo torsion was stronger than the myo and epi torsion in the Healthy, in the I/R-MI, the endo torsion was stronger than the torsion of the epi torsion, not the myo torsion, suggesting that the myo layer could be compensating proportionally more than the endo layer which was more sensitive to ischaemia. The increase in torsion resulted from the increase in the basal rotation as the apical rotation did not change in the rat LAD models of ischaemia-reperfusion injury, in keeping what has been reported in human. [263]

A compensatory mechanism was also exhibited by the fact that the peak atrial strain did not change after I/R-MI, even though the LAS-conduit strain was significantly smaller (decrease in the ratio by 1.4), compensated via an increase in LAS-Booster (contraction) strain by a ratio of 1.6 with a consequent of the maintenance of the Booster volume, atrial ejection fraction and fractional area change. It is known that the passive flow during LAS-conduit is dependent on the suction force by the left ventricle and LV relaxation. Despite the fact, the rats were scanned 3-7 days post I/R-MI, the mild reduction in the ratio of E/A dV/dt was detectable, supportive of global impairment in the LV relaxation. In

section **9.7.3**, the restrictive physiology was demonstrated in the remote segments, which also could explain the reduction in LAS-conduit strain in I/R-MI.

In clinics, segmental strains have not been showing consistent results so far and hence, are not recommended by societies for routine clinical use for scar in echocardiography [264,265] nor attempted for scar in cardiac MRI.[266] In this study, in-bred animals were used, which deliver highly reproducible surgical and biological models, and experiments performed in a highly controlled environment. For the thesis purpose, the reproducibility of sLS measurements using feature tracking showed good-excellent intra-class reliability, validated on the Healthy rats. It was also shown that all the sLS variants of the basal, mid and apex were not different. However, if sLS was compared only within per slice, the magnitude of sLS in the mid segment was more negative in the septum compared to the lateral wall, only if Endo-peak-sLS was used. The same trend was seen in mid segments septum-of Endo-pk-Sys and Endo-En-Sys, however not significant. The observation is in keeping with the fact that cardiac repolarisation starts from the left to the right, and from the endo to epicardium. As the distance travelled is very short in a small heart, the effect was negligible in the rat models. All the Myo-sLS variants did not show any difference between the septum and lateral walls.

There are some factors why segmental strains may not give consistent results in human are discussed here. There are many vendors and methods of strain quantification, and as a result of the lack of standardisation becomes an issue; the strain values cannot be directly comparable. Cardiac planning factors such as the placement of sample volume, number of nodes, layer placement, smoothing and averaging method are important in ensuring consistency and reproducibility. Vendor independent solution provided by feature-tracking is good for retrospective studies. However, when image acquisition was not performed using the same settings, using different frame rate, image resolution, quality, and small variation in image planning could cause small technical variations, which later become important. For example, apical foreshortening reduces the GLS [267,152], whereas ±20° basal/apical angulation errors did not significantly affect GCS measurement.[268] In our case, these confounding factors were kept constant throughout the experiments.

A retrospective gating and high frame rate cine were used to provide the high certainty of correct placements of timing events of end-diastole and end-systole during strain analysis and reducing errors. This was compared with LFR-CMR-FT prospectively gated cines containing 25-30 frames per R-R interval. The EndoGLS and MyoGLS values of healthy rats using LFT-CMR-FT were heterogeneous (high variance) compared to HFR-MRI-FT. The Myo-LFT-CMR-FT overestimated the MyoGLS, and as the average of HFR-CMR-FT and LFT-

CMR-FT got smaller in magnitude, the bias decreases with a stronger effect. The LFT-CMR-FT also overestimated the EndoGLS to a lesser degree than the MyoGLS, and there was a weak positive correlation between the average of HFR-CMR-FT and LFT-CMR-FT and the reduction in the size of bias. The most likely cause for the overestimation of LFT-CMR-FT was the incorrect placement of AVC. The number of frames per R-R in HFR-CMR-FT was fixed at 60 as opposed to fixing frame rate using TR that could be variable in the case of prospective gating. Typical native SSFP in clinical scanners without interpolation is 23-25 frames per RR, which could be too low and misregister the peaks from under-sampling. In addition, a high frame rate demands high resolution, or else the changes of displacement between pixels in successive frames becomes difficult to detect causing decorrelation errors [269] and therefore counterintuitive. The in-plane spatial resolution of 0.2 mm^2 was achieved in 9.4T versus 1-2mm^2 in 3T MRI systems, and our out-plane resolution was 0.9mm^2.

5.8 Study Limitations

The study has limitations. It was performed under general anaesthesia, which could mask the physiological measurements. The animals used were in-bred, producing good reproducibility using small animal numbers, compared to humans, where the population is heterogeneous. The use of retrospective high

frame rate cine, which is not yet routinely available in clinical scanners. Moreover, the sequence requires high RF and may not be suitable for human. The animal scanning and analysis require high technical skills, was performed manually; still very time-consuming to perform and not practical for routine clinical use. Only male rats were studied because female animals are intrinsically more variable because of cyclic reproductive hormones, have different mortality and heart failure development rate.

5.9 Conclusion

In conclusion, it was demonstrated that high frame rate global strain and sLS are useful in the quantitative assessment of myocardial phenotype after ischaemia-reperfusion injury for the distinction of permanent infarction, area at risk and Healthy myocardium. A number of compensatory mechanisms of ischaemia-reperfusion injury were reported comprehensively in rotational mechanics according to myocardial layers and atrial strains. The results in this chapter permit the use of the CMR assessment methods in the assessment of the efficacy of shockwave on experimental intervention in ischaemia-reperfusion injury.

Chapter Six

RESULTS: THE EFFECTS OF SHOCKWAVE ON GLOBAL CARDIAC MECHANICS

6.1 Clinical Perspective

The principal pathogenesis of heart failure is the reduction in the left ventricular contractile function associated with clinical deterioration of dyspnoea, orthopnoea, hypotension and shock leading to death. Intuitively, pharmacological inotropic agents that could improve contraction function could be beneficial to patients' prognosis. After over two decades since the first proposed use of inotropic agents, [270] the only agent recommended by the

ESC for chronic heart failure is digitalis.[271] All the other current approved agents are indicated only for short term use in acute heart failure patients who remain in shock despite all other medical interventions, and they have been shown to be futile beyond the short-term haemodynamic improvement. In other therapeutic avenues, such as in the case of cardiac resynchronisation therapy using biventricular pacing devices in heart failure, the improvement in LV systolic function could indeed halt the disease progression, reverse the remodelling, and improve patients' survival. [272]

6.2 Introduction

A pilot study performed on healthy rats having treated with shockwave and assessed using echocardiography has provided the inspiration to conduct the *in vivo* experiments in this chapter (**Appendix 1).** Immediately after the administration of shockwave, it was observed that the LVEDV was increased, LVESV was decreased, in effect, increased the stroke volume and the ejection fraction, suggesting that shockwave treatment to the heart could induce an inotropic effect. Interestingly, the immediate inotropic effect was associated with a transient reduction in the heart rate. These findings led us to study the effect of shockwave on cardiac mechanics in detail using strain imaging. To the best of our knowledge, the effect of shockwave on cardiac contractility has not

been previously described in the literature. If proven, it could path for a new treatment avenue for heart failure.

6.3 Aim

To assess in more detail using cardiac MR on the effect of shockwave on the cardiac mechanics to elucidate the mechanisms of inotropy.

6.4 Objectives

Objectively, the left ventricle functional parameters to be assessed could be broadly categorised into the following classifications:

(1) Physiology – heart rate per minute.

(2) Ventricular cavity area- the endocardial tracing of the blood/endocardial border per short-axis view;

(3) Ventricular chamber volume at ED and ES and their derivative indices for EF, SV and CO.

(4) Global strains: endo and myo GLS, endo and myo GCS and GRS

(5) Rotational mechanics – basal and apical rotation, basal and apical rotational rate, twist and torsion.

The definitions of the above measurements have been detailed in the method section.

6.5 Methods

6.5.1 Animal Characteristics

Healthy male Lewis rats were sourced from Charles River UK and used in the experiments in this chapter.

6.5.2 Experimental Design and Animals' Cohort

Healthy rats were defined as control rats that never received any experimental intervention up to the MRI scan. SW-Healthy rats were defined as rats that had been treated with shockwave three days before the MRI scan. The cardiac functional parameters of the Healthy rats were compared with SW-Healthy rats.

6.5.3 Shockwave Treatment

The full method of shockwave delivery to the rat's heart has been described in **section 3.24.** Briefly, focused shockwave 0.25mJ/mm^2 x 500 pulses were administered on SW-Healthy rats' hearts via precordial application whilst under light anaesthesia.

6.5.4 MRI Acquisition and Post-Processing in Paravision

The method of MRI instrumentations, in-vivo cardiac acquisition, animal preparation, cardiac planning and image modalities used have been thoroughly detailed in **chapter 4**.

A full LV stack using FLASH-cine was acquired in 14 Healthy rats and 10 SW-Healthy rats. High frame cine was acquired in 13 Healthy rats and 6 SW-Healthy

rats. The acquisition for high frame rate cine used the IntraGate sequence, which has been previously described in **section 4.17**. IntraGate cine used a retrospective gating where the data was continuously acquired and then sorted by software following an algorithm. A Navigator pulse was used to detect respiratory-cardiac motions and used by the algorithm to include or reject the acquired data during primary image construction. The placement of the first image frame depends on when the gate first opens and was impossible to be manually triggered to match the acquisition gate opening, and to start at the preferred phase of the cardiac cycle. There was an inevitable trigger delay when the sequence was initiated, complicated further by fast heart rate. So, the image would need to be reconstructed after the primary construction if the order of cardiac phases was not optimal for analysis. For systolic strain analysis, it was preferable to have the ED frame placed before the ES frame so that the systolic strain-time curve plot was not truncated. The secondary reconstruction was performed in Paravision to move the second frame series in front of the first frame series. If the ED frame was the preferred to be the first frame, the second frame series started from the ED frame inclusive to the last frame of the primary construction. The first frame series was defined as the frame series consisted of the ED frame to the last frame of the primary construction. The second frame series was defined as the frame series consisted of the first frame of the primary construction to the frame just

before the ED frame. As the ED and ES frame were identified by visual inspection; an underestimation of ED would require a new image reconstruction; hence, it was desirable to include a few offset frames in the front of the ED frame in the second series. The image data to be analysed was exported in DICOM 3.0 format.

6.5.5 Post-Processing of Cines for Rotation, Twist and Torsion

In 2D-CPA-MR, the short axis views of the basal and apical slices were post-processed to obtain the displacement coordinates over time, which then used to calculate the basal rotation, apical rotation, basal rotational rate, apical rotational rate, systolic twist and torsion.

The ED and ES were marked as previously described in **section** Error! Reference source not found.**.** In the basal slice, there were 6 AHA segments, and the six displacement curves plotted over time. In the apical slice, there were 4 AHA segments, and four displacement curves plotted over time. The coordinates were exported in the Comma Separated Values (CSV) format and Extensible Markup Language (XML) format. The files were analysed in Microsoft Excel where the segmental displacement coordinates for the apical and basal slices were sorted as such that the ED frame was placed at the first frame and all the phases in the cardiac cycle match with each other. The isochronal average of the segmental displacement for the slice was performed by averaging all the

segmental displacement values in the same phase to produce an average displacement plot over time. The peak value of the plot in systole was defined as the peak rotational angle. For determination of twist, it was imperative to ensure the ED frame for the apical and basal slices positioned on the first frame before isochronal summation of the net basal and apical rotation was performed or else the peak systolic twist could be underestimated. The method is summarised in **Figure 6-1**.

6.5.6 Definitions of Rotation, Rotational Rate, Systolic Twist and Torsion

The basal rotation was defined as the peak clockwise rotation expressed in degrees when viewed from the apex during systole. It was examined in the endocardial, myocardial and epicardial layers.

The apical rotation was defined as the peak anti-clockwise rotation expressed in degrees when viewed from the apex during systole. It was examined in the endocardial, myocardial and epicardial layers.

The basal rotational rate was defined as the peak velocity of the basal slice in clockwise rotation during systole. It was examined in the endocardial, myocardial and epicardial layers. The basal displacement coordinates carried negative values in systole.

The apical rotational rate was defined as the peak velocity of the apical slice in anti-clockwise rotation during systole. It would be examined in the

endocardial, myocardial and epicardial layers. The apical displacement coordinates carried positive values in systole.

The systolic twist was defined as the peak difference in the basal and apical rotation; and would be examined in the endocardial, myocardial and epicardial layers. The net isochronal difference of the coordinates of the apical displacement with the basal displacement produced the twist curve. The peak value of the twist curve during systole was used.

Torsion was defined as the angle of the twist divided by the distance between apical and basal short-axis slices. As the slice thickness could be slightly different between animals, and to maintain comparability, the distance from mid-slice thickness to mid-slice thickness was used as opposed to edge-to-edge distance. The DICOM tag (0020,1041) provided the information of the slice location, and the difference in the slice location values of the basal and apical slices was calculated as the distance of the basal and apical slice in mm.

All the rotation, twist, torsion and rotational rate plots were plot over time. To maintain comparability between animals, time was presented as the number of cine frames lapsed since ED (the first frame). The total number of frames in the cardiac cycle was fixed at 60 during acquisition, and the time duration between the two frames was 3ms.

Figure 6-1. S ental rotation cur pical endo averag . The procedure v

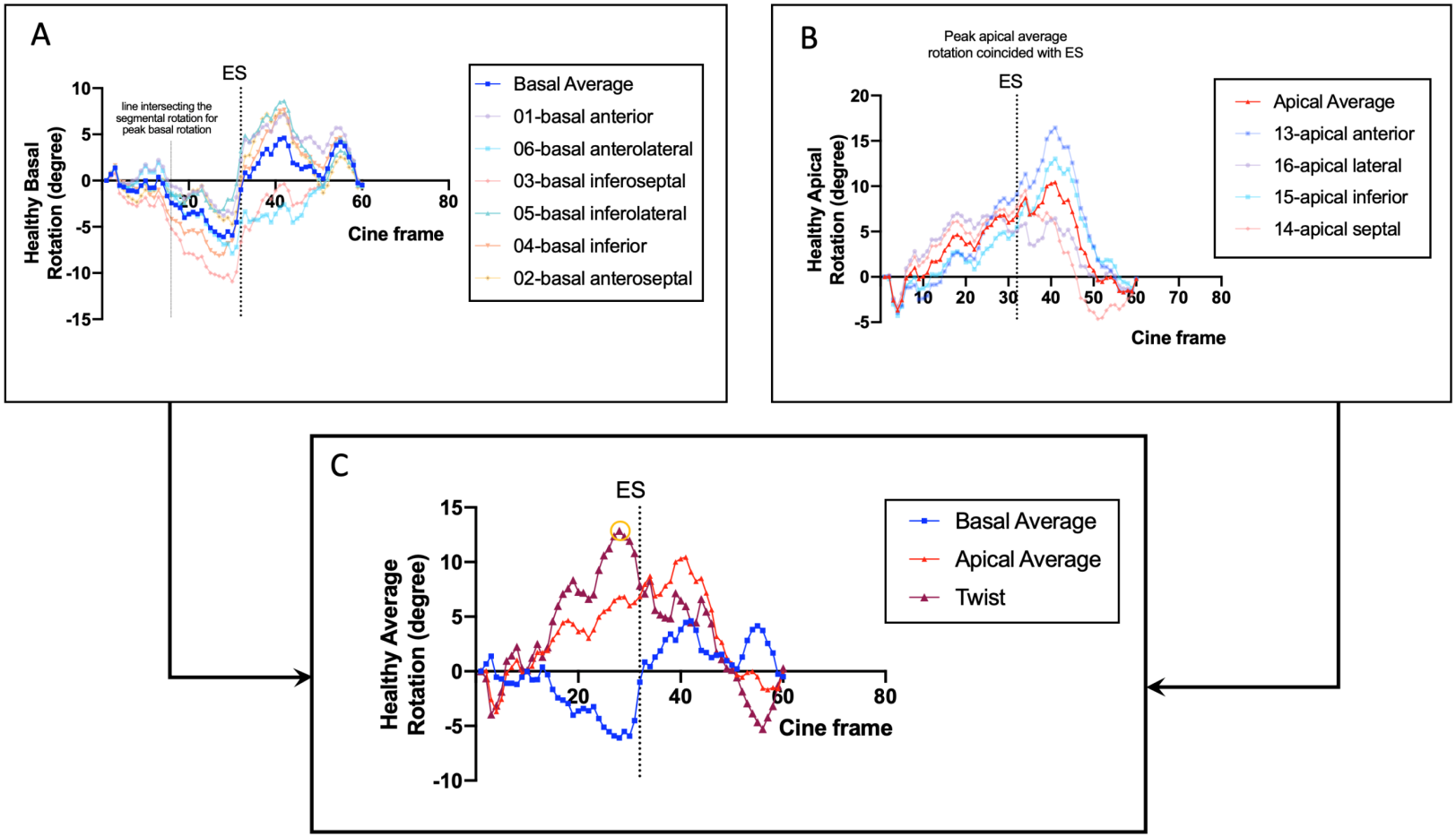

6.5.7 Post-Processing of Cines for Area and Volume

6.5.7.1 Short-Axis Basal, Apical Area and Fractional Area Change

The basal and systolic endocardial areas were derived from feature tracking measurements in 2D-CPA-MR, where the EDA was the largest area, and ESA was the smallest area. In CMR cine, no ECG information was stored in the image data. The FAC was calculated using the formula * 100 expressed in %.

6.5.7.2 LV Volume

The volumetric indices used were the LVEDV, LVESV, EF, SV, and CO measured from the LV stack. The definitions for these have been detailed elsewhere (chapter 5), and the analysis was performed in Segment (Medviso).

6.5.8 Heart Rate

The heart rate used was taken during LV cine stack when the observation was the longest and used to prospectively set the effective TR during analysis.

6.5.9 CS And RS According to Basal Slice and Apical Slice

The basal and apical circumferential strains were separately assessed according to slice to obtain the endo and myo CS, and the radial strain.

Figure 6-2. An illustration of apical rotation in anticlockwise direction (+) and basal rotation in clockwise direction (-) when viewed from the apex, where $\emptyset_A$ indicates apical rotational angle, $\emptyset_B$ indicates basal rotational angle, D is the distance between the apical and basal slice.

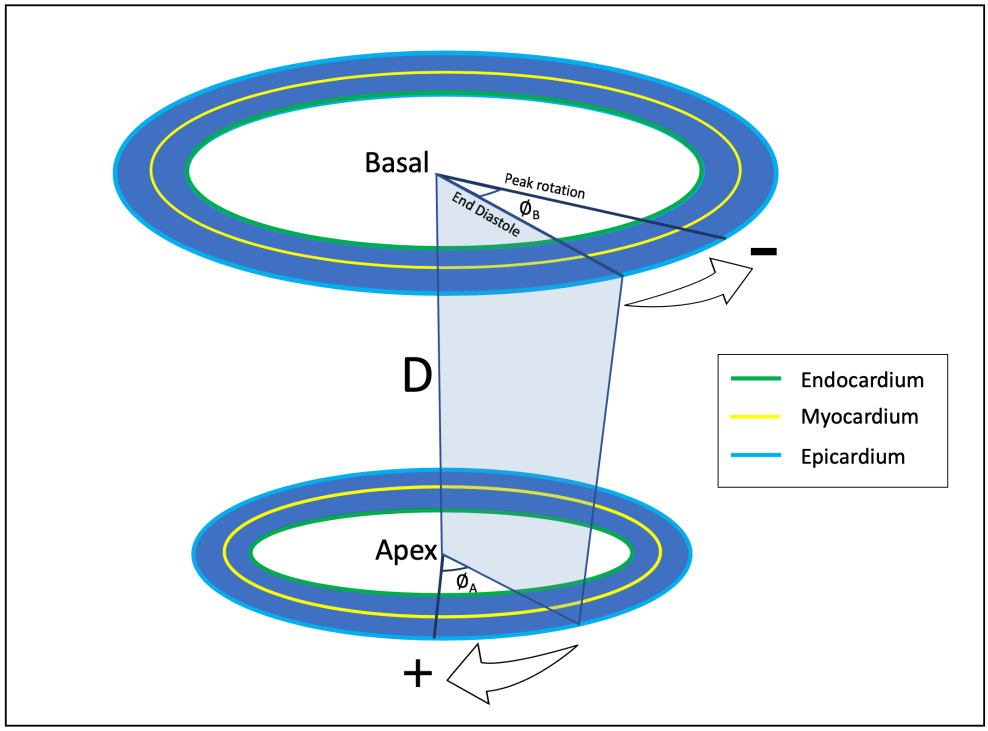

6.6 Results

6.6.1 Animals' Weight

There was no significant difference in animal weight between Healthy (n=14) versus SW-Healthy (n=10), respectively showing mean ± SD of 329.4g ± 29.9 versus 336.7g ± 30.94, *P* = .5697.

6.6.2 The Effect of Shockwave on Volumetric Parameters

The results for this section are graphically summarised in **Figure 6-2**.

The mean ejection fraction of SW-Healthy rats was significantly greater than the mean ejection fraction of Healthy rats, respectively showing EF±SD of 64.38% ± 2.19 versus 58.52% ± SD 2.20, *P* < .0001. **(Figure 6-3A)**

The mean end-diastolic volume of SW-Healthy rats was similar to the mean end-diastolic volume of Healthy rats, respectively showing EDV±SD of 585.0mcl ± 53.8 versus 556.4mcl ± SD 30.5, *P* = .1539. **(Figure 6-3B)**

The mean end-systolic volume of SW-Healthy rats was significantly smaller than the mean end systolic volume of Healthy rats, respectively showing ESV±SD of 208.4mcl ± 23.67 versus 231.2mcl ± 14.4, *P* = .0173. **(Figure 6-3C)**

The mean stroke volume of SW-Healthy rats was significantly larger than the mean stroke volume of Healthy rats, respectively showing SV±SD of 376.6ml ± 35.9 versus 325.3ml ± 24.8, *P* = .0014. **(Figure 6-3D)**

The mean heart rate of SW-Healthy rats was similar to the mean heart rate of Healthy rats, respectively showing heart rate ± SD of 382.1bpm ± 25.3 versus 390.1bpm ± 26.9, *P* = .4634. **(Figure 6-3E)**

The mean cardiac output of SW-Healthy rats was significantly larger than the mean cardiac output of Healthy rats, respectively showing CO±SD of 143.9ml/min ± 9.2 versus 126.8ml/min ± 11.2, *P* = .0005. **(Figure 6-3F)**

Figure 6-3. Scatter dot plots of (A) ejection fraction, (B) End diastolic volume, (C) end systolic volume, (D) stroke volume, (E) heart rate and (F) cardiac output. Middle bar is the mean, and the upper and lower bars are the 95% CI. NS is no significant, *<.05, ** $P < .01$, ***, $P < .001$, and **** $P < .0001$.

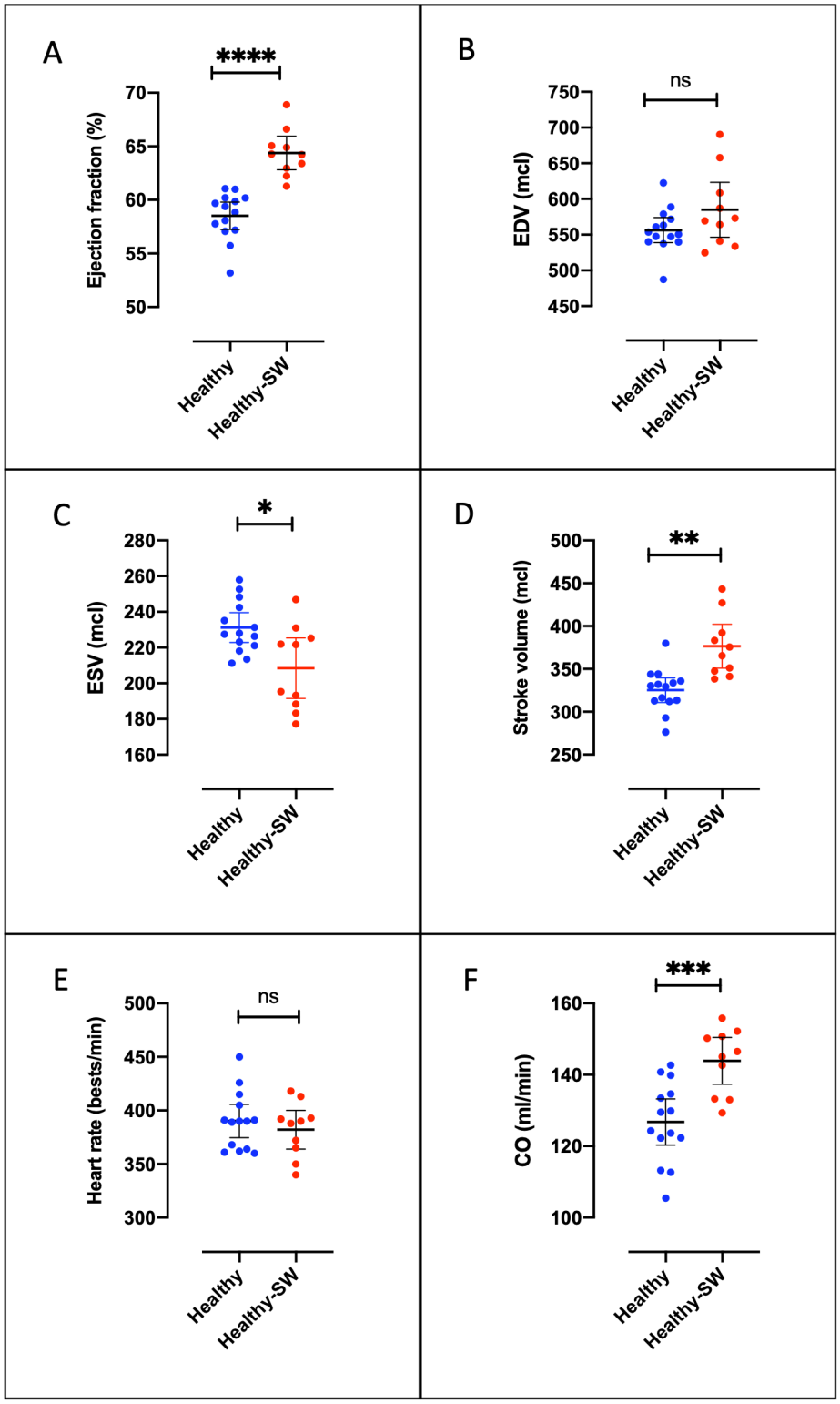

6.6.3 The Effect of Shockwave on Apical and Basal Area and Fractional Area Change

6.6.3.1 Animals' Weight

There was no significant difference in animal weight between Healthy (n=10) versus SW-Healthy (n=7), respectively showing mean ± SD of 318.5g ± 30.4 versus 320.0g ± 27.8, *P* = .9177.

6.6.4 Apical and Basal Area and Fractional Area Change

The results for this section are graphically summarised in **Figure 6-4.**

The mean basal diastolic area of the Healthy-SW rats was similar to the mean basal diastolic area of the Healthy rats, respectively showing EDA ± SD of 0.60cm^2 ± 0.04 versus 0.57cm^2 ± 0.09, *P* = .3477. The mean basal systolic area of the Healthy-SW rats was also similar to the mean basal systolic area of the Healthy rats, respectively showing ESA ± SD of 0.23cm^2 ± 0.02 versus 0.23cm^2 ± 0.04, *P* = .8372. (**Figure 6-4A)**

The mean basal fractional area change of the Healthy-SW rats was similar to the mean basal fractional area change of the Healthy rats, respectively showing FAC ± SD of 61.02% ± 2.08 versus 59.50% ± 2.65, *P* = .2266. **Figure 6-4B)**

The mean basal endo circumferential strain of the Healthy-SW rats was similar to the mean basal endo circumferential strain of the Healthy rats, respectively showing basal endoCS ± SD of -37.44% ± 1.58 versus -36.04% ± 2.05, *P* = .1481.

The mean basal myo circumferential strain of the Healthy-SW rats was similar to the mean basal myo circumferential strain of Healthy rats, respectively showing basal myoCS ± SD of -25.71% ± 1.35 versus -25.92% ± 1.99, *P* = .8105. (**Figure 6-4C)**

The mean basal radial strain of the Healthy-SW rats was similar to the mean basal radial strain of the Healthy rats, respectively showing basal RS of 62.82% ± 19.96 versus 58.62% ± 23.78, *P* = .7112. (**Figure 6-4D)**

The mean apical diastolic area of the Healthy-SW rats was significantly smaller than the mean apical diastolic area of the Healthy rats, respectively showing EDA ± SD of 0.31cm^2 ± 0.03 versus 0.36cm^2 ± 0.06, *P* = .0361. The mean apical systolic area of the Healthy-SW rats was significantly smaller than the mean apical systolic area of the Healthy rats, respectively showing ESA ± SD of 0.10cm^2 ± 0.01 versus 0.15cm^2 ± 0.04, *P* = .0031. (**Figure 6-4E)**

The mean apical fractional area change of the Healthy-SW rats was significantly larger than the mean apical fractional area change of the Healthy rats, respectively showing FAC ± SD of 66.38% ± 2.96 versus 59.34% ± 5.54, *P* = .0052. (**Figure 6-4F)**

The mean apical endo circumferential strain of the Healthy-SW rats was significantly stronger (more negative) than the mean apical endo circumferential strain of the Healthy rats, respectively showing apical endoCS ± SD of -41.90% ± 2.81 versus -36.38% ± 4.40, *P* = .0086. The mean apical myo

circumferential strain of the Healthy-SW rats was significantly stronger than the mean apical myo circumferential strain of Healthy rats, respectively showing apical myoCS ± SD of -28.15% ± 2.37 versus -23.96% ± 3.71, *P* = .0158. (**Figure 6-4G)**

The mean apical radial strain of the Healthy-SW rats was similar to the mean apical radial strain of the Healthy rats, respectively showing basal RS of 52.81% ± 20.00 versus 57.32% ± 18.03, *P* = .6603. (**Figure 6-4F)**

Figure 6-4. Scatter dot plot comparing Healthy versus Healthy-SW in A: Basal area, B: Basal FAC, C: Basal circumferential strain, D: basal radial strain, E: Apical area, F: apical fractional area change, G: apical circumferential strain and H: apical radial strain. Middle bar is the mean, and the upper and lower bars are the 95% CI. NS is no significant, *<.05, ** *P* < .01, ***, *P* < .001, and **** *P* < .0001.

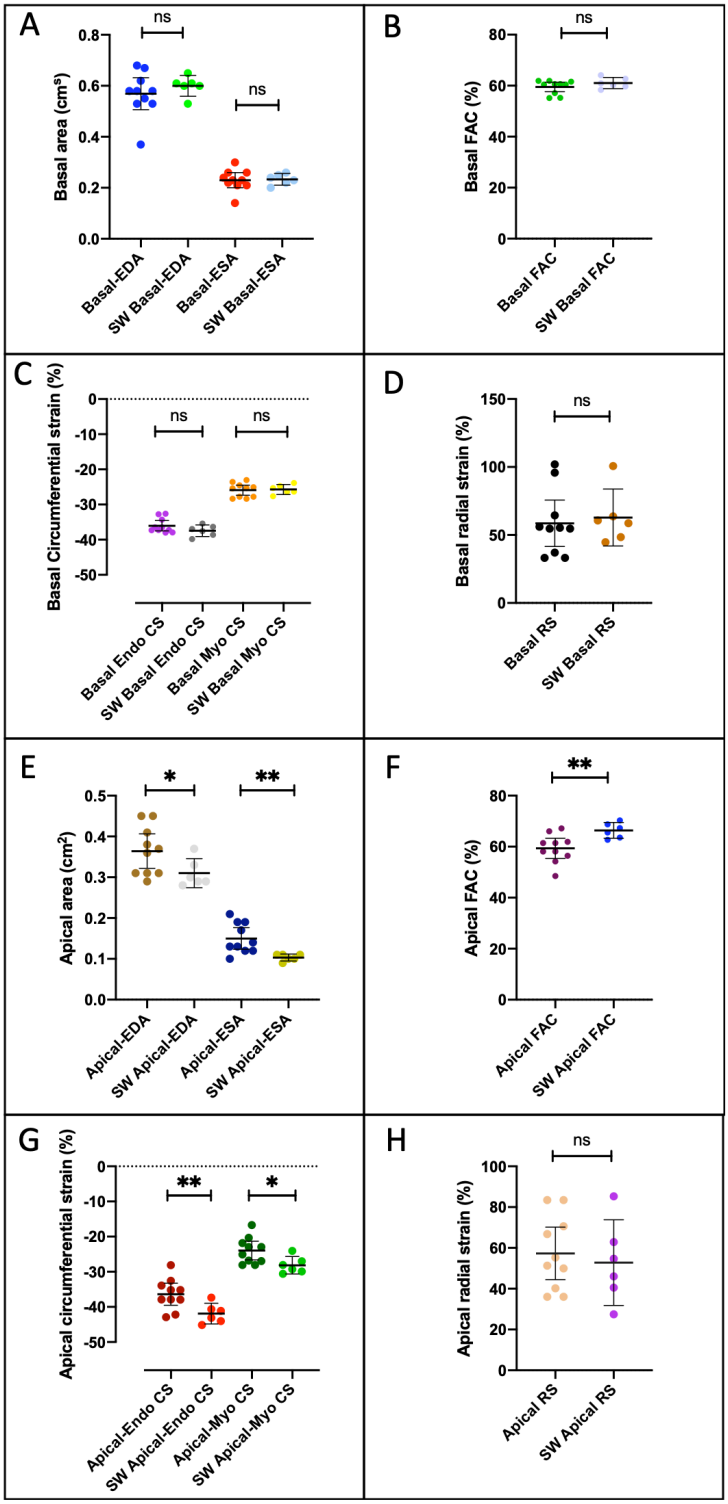

6.6.5 The Effect of Shockwave on Global Strains

The results for this section are graphically summarised in **Figure 6-5.**

The mean endoGLS Healthy-SW rats was significantly stronger (more negative) than the mean endoGLS of Healthy rats, respectively showing endoGLS ± SD of -25.15% ± 1.21 versus -21.72% ± 0.87, *P* = .0003. **(Figure 6-5A)**

The mean myoGLS Healthy-SW rats was significantly stronger (more negative) than the mean myoGLS of Healthy rats, respectively showing myoGLS ± SD of -20.37% ± 0.80 versus -18.32% ± 0.42, *P* = .0008. **(Figure 6-5B)**

The mean endoGCS Healthy-SW rats was significantly stronger (more negative) than the mean endoGCS of Healthy rats, respectively showing endoGCS ± SD of -39.47% ± 3.50 versus -35.23% ± 1.96, *P* = .0295. **(Figure 6-5C)**

The mean myoGCS Healthy-SW rats was similar to the mean myoGCS of Healthy rats, respectively showing myoGCS ± SD of -24.67% ± 2.76 versus -23.65% ± 1.78, *P* = .0295. **(Figure 6-5D)**

The mean GRS Healthy-SW rats was significantly stronger (more positive) than the mean GRS of Healthy rats, respectively showing GRS ± SD of 54.76% ± 5.72 versus 47.06% ± 7.12, *P* = .0295. **(Figure 6-5E)**

Figure 6-5. Scatter dot plot of (A) endoGLS, (B) myoGLS, (C) endoGCS and (D) myoGCS and (E) GRS. Middle bar is the mean, and the upper and lower bars are the 95% CI. NS is no significant, *<.05, ** *P* < .01, ***, *P* < .001, and **** *P* < .0001.

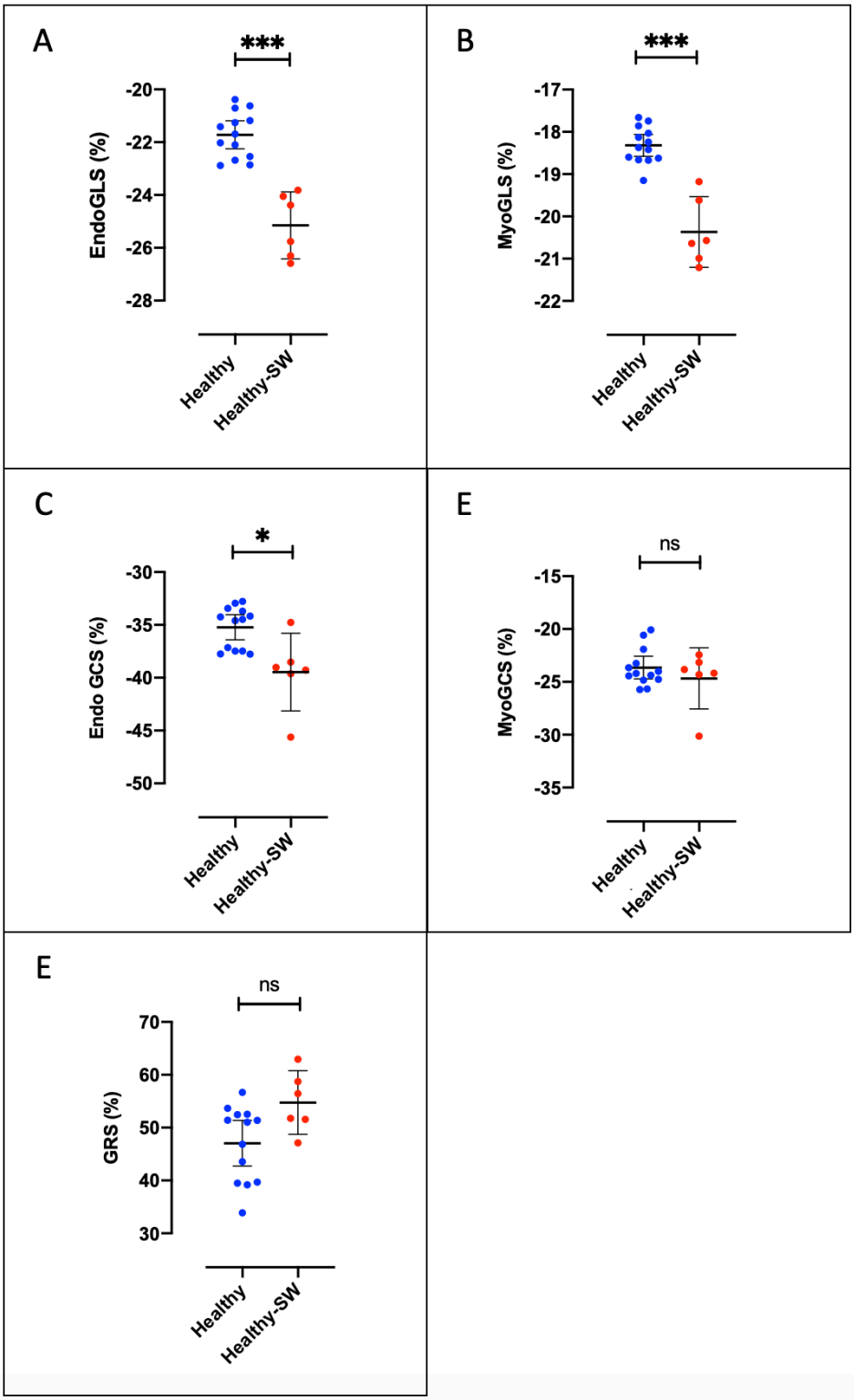

6.6.6 The Effect of Shockwave on Apical and Basal Rotation, Twist and Torsion in The Endo, Myo And Epicardial Layers

6.6.6.1 Animals' Weight

There was no significant difference in animal weight between Healthy (n=7) versus SW-Healthy (n=6), respectively showing mean ± SD of 326.4g ± 32.2 versus 323.3g ± 28.9, *P* = .8586. The same rat populations were used for analysis in section 2.6.

6.6.6.2 Rotational (Displacement) Curve Over Time

The peak rotation and peak torsion in systole were used and compared between Healthy rats and SW-Healthy rats, as illustrated in **Figure 6-6**.

6.6.6.3 Results of Apical and Basal Rotation, Torsion and Twist

The results are graphically summarised in **Figure 6-7**.

(See Figure 6-7A). While the mean SW-Healthy basal endo rotation was more negative than Healthy basal endo rotation, respectively showing basal endo rotation ± SD of -10.17° ± 3.22 versus -7.22° ± 2.63, the interaction was not significant, *P* = .1040. The mean rotation of basal myo SW-Healthy rats was significantly greater than the mean rotation of basal myo Healthy rats, however not reaching significance, respectively showing mean myo rotation ± SD of -8.53° ± 1.82 versus -5.04° ± 2.86, *P* = .0234. The mean rotation of basal epi SW-Healthy rats was significantly greater than the mean rotation of basal epi Healthy

rats, respectively showing mean epi rotation ± SD of -11.77° ± 1.65 versus -5.61 ± 3.41, *P* = .0022.

In Healthy rats, all the interactions between basal rotations of the endo, myo and epi layers were not significant, respectively showing mean rotation ± SD of -7.22° ± 2.63, -5.04° ± 2.86 and -5.61° ± 3.41; *P* = .3575. In SW-Healthy rats, the mean epi basal rotation was greater (more negative in clockwise displacement in systole) than myo basal rotation, respectively showing mean rotation ± SD of -11.77° ± 1.65 versus -8.53° ± 1.82, *P* = .0092. The mean endo basal rotation was similar to myo basal rotation and epi basal rotation, respectively showing -10.17° ± 3.22, -8.53° ± 1.82 and -11.77° ± 1.65, *P* = .3090 and *P* = .3131.

(See Figure 6-7B). The mean SW-Healthy apical endo rotation was significantly more positive than the mean Healthy apical endo rotation, respectively showing mean apical endo rotation ± SD of 12.59° ± 2.21 versus 8.63° ± 3.39, *P* = .0290. The mean SW-Healthy apical myo rotation was not different from the Healthy apical myo rotation, respectively showing mean apical myo rotation ± SD of 7.65° ± 1.93 versus 6.64° ± 2.08, *P* = .3846. The mean SW-healthy apical epi rotation was not different from the Healthy apical epi rotation, respectively showing mean apical epi rotation ± SD of 5.46° ± 1.06 versus 5.56° ± 1.80, P = .9070.

In Healthy rats, all the interactions between apical rotations of the endo, myo and epi layers were not significant, respectively showing mean rotation ± SD of 8.63° ± 3.39, 6.64° ± 2.08 and 5.56° ± 1.80; *P* = .1546. In SW-Healthy rats, the mean apical endo rotation was significantly more positive than the mean apical myo rotation and the mean apical epi rotation, respectively showing apical mean rotation ± SD of 12.59° ± 2.21 versus 7.65° ± 1.93, versus 5.46° ± 1.06, *P* = .0021 and *P* = .0002. The mean SW-Healthy myo apical rotation was significantly more positive than the mean SW-Healthy epi apical rotation, respectively showing mean rotation ± SD of 7.65° ± 1.93 versus 5.46° ± 1.06, *P* = .0420.

(See Figure 6-7C). The mean endo torsion in SW-Healthy rats was not different from the mean endo torsion in Healthy rats, respectively showing mean endo torsion ± SD of 2.72 °/mm ± 0.74 versus 2.29°/mm ± 0.43, *P* = .2500. The myo torsion in SW-Healthy rats was significantly greater than the myo torsion in Healthy rats, respectively showing mean myo torsion of 2.34°/mm ± 0.11 versus 1.53°/mm ± 0.21, *P* < .0001. The epi torsion in SW-Healthy rats was significantly greater than the epi torsion in Healthy rats, respectively showing mean myo torsion ± SD of 2.50°/mm ± 0.30 versus 1.42°/mm ± 0.42, *P* = .0002. In Healthy rats, the mean endo torsion was significantly greater than the mean myo torsion and epi torsion, respectively showing mean myo torsion ± SD of

2.29°/mm ± 0.43, 1.53°/mm ± 0.21 and 1.42°/mm ± 0. 42, *P* = .0026 and *P* = .0023. The Healthy mean myo torsion was similar to the mean epi torsion, respectively showing torsion ± SD of 1.53°/mm ± 0.21 versus 1.42°/mm ± 0.41, *P* = .5201. In SW-Healthy rats, all the interactions between torsions of the endo, myo and epi layers were not significant, respectively showing torsion ± SD of 2.72°/mm ± 0.74, 2.34°/mm ± 0.11 and 2.50°/mm ± 0.30, *P* = .3289.

(See Figure 6-7D). The mean endo twist in SW-Healthy rats was not different from the mean endo torsion in Healthy rats, respectively showing mean endo torsion ± SD of 19.34° ± 5.72 versus 15.37° ± 2.48, *P* = .1608. The myo twist in SW-Healthy rats was significantly greater than the myo twist in Healthy rats, respective showing mean myo torsion of 15.45° ± 1.12 versus 10.35° ± 1.48, *P* < .0001. The epi twist in SW-Healthy rats was significantly greater than the epi twist in Healthy rats, respectively showing mean myo twist ± SD of 16.49° ± 2.10 versus 9.56° ± 2.82, *P* = .0004.

In Healthy rats, the mean endo twist was significantly greater than the mean myo twist and epi twist; respective showing mean myo twist ± SD of 15.37° ± 2.48, 10.35° ± 1.48 and 9.56° ± 2.82, *P* = .0010 and *P* = .0015. The Healthy mean myo twist was similar to the mean epi twist, respectively showing twist ± SD of 10.35° ± 1.48 versus 9.56° ± 2.82, *P* = .5306. In SW-Healthy rats, all the interactions between twists of the endo, myo and epi layers were not

significant, respectively showing twist ± SD of 19.34° ± 5.72, 15.45° ± 1.12 and 16.49° ± 2.10, *P* = .2523.

Figure 6-6. Plots of the average basal and apical rotation (displacement) versus time; in the right column (A, C, E) is the plot for Healthy rats and in the right column is the plot for SW-Healthy rats (B, D, F). (A) Healthy endo rotation and endo twist, (B) SW-Healthy endo rotation and endo twist, (C) Healthy myo rotation and myo twist, (D) SW-Healthy myo rotation and myo twist, (E) Healthy Epi rotation and epi twist, (F) SW-Healthy Epi rotation and epi twist. Each dot symbol in the plot represents a phase and the colour as indicated by the legend.

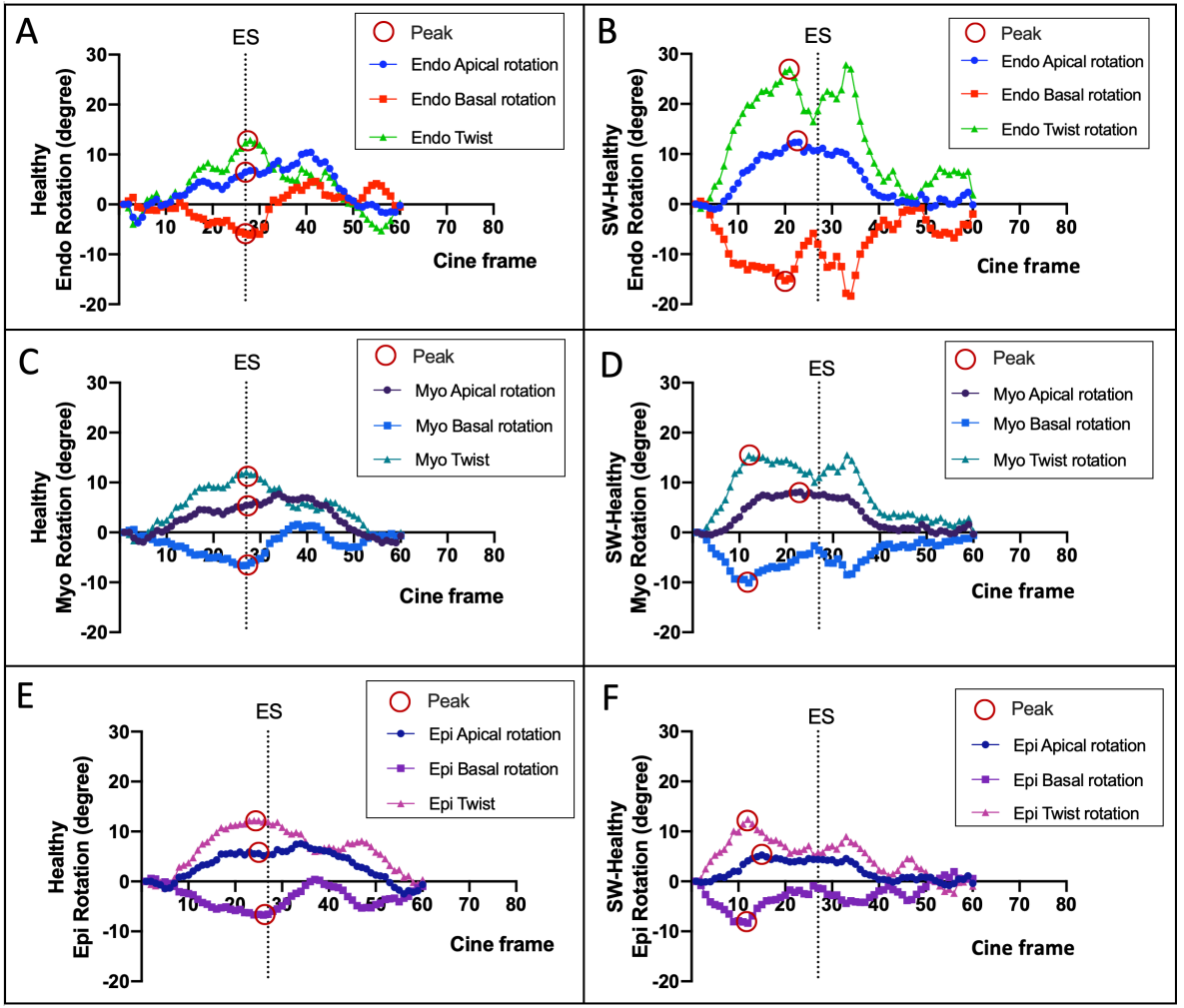

Figure 6-7. Scatter dot plot of (A) basal rotation of endo, myo and epi layers in Healthy and Healthy-SW, (B)apical rotation of endo, myo and epi layers in Healthy and Healthy-SW, (C) torsion of endo, myo and epi layers in Healthy and Healthy-SW, and (D) twist of endo, myo and epi layers in Healthy and Healthy-SW. Middle bar is the mean and the upper and lower bars are the 95% CI. NS is no significant, *<.05, ** $P < .01$, ***, $P < .001$, and **** $P < .0001$.

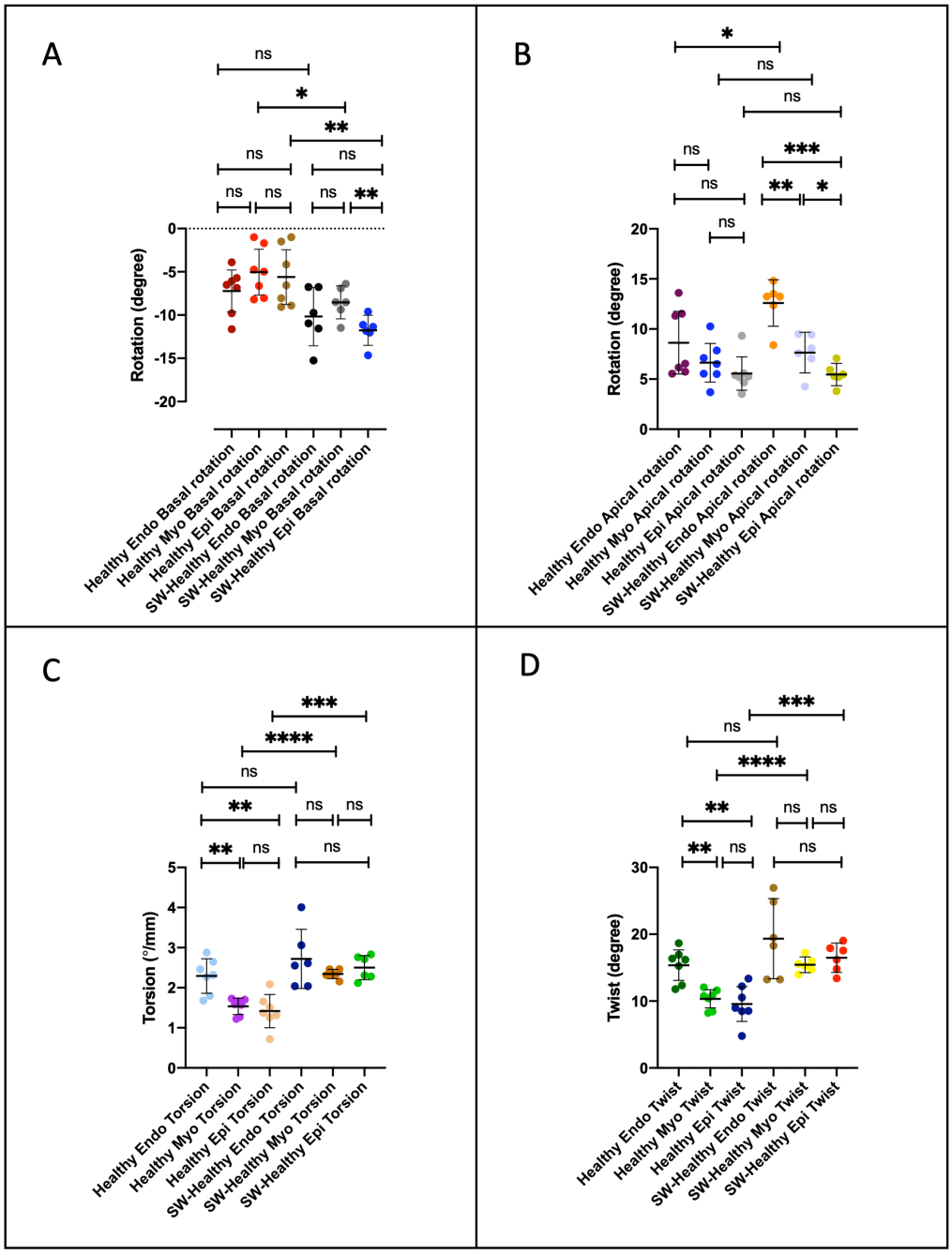

6.6.7 The Effect of Shockwave on Rotational Strain Rate in The Endo, Myo And Epicardial Layers

The results of the rotational rate curves are presented in **Figure 6-8,** where the peaks of the events in systole and diastole indicated. The mean apical rotational strain rates of the Healthy-SW in all layers were similar to their counterparts in the Healthy rats. The apical endo rotational rate of Healthy-SW was 366.4°/s ± 107.8 versus apical endo rotational rate of Healthy of 359.1°/s ± 114.4, *P* = .8154. The apical myo rotational rate of the Healthy-SW versus the Healthy was respectively 238.8°/s ± 91.2 versus 229.6°/s ± 71.9, *P* = .6977. The apical epi rotational rate of Healthy-SW was 231.8°/s ± 95.0 versus apical epi rotational rate of Healthy rats of 199.8°/s ± 83.8, *P* = .2164. In Healthy rats, the mean apical endo rotational rate was significantly greater than the mean apical myo rotational rate and the mean apical epi rotational rate, respectively showing rotational rate ± SD of 359.1°/s ± 114.4, 229.6°/s ± 71.9 and 199.8°/s ± 84.0, *P* < .0001 and *P* < .0001. The mean apical myo rotational rate and the mean apical epi rotational rate of the Healthy rats were not different, *P* = .1666. In SW-Healthy rats, the mean apical endo rotational rate was significantly greater than the mean apical myo rotational rate and the mean apical epi rotational rate, respectively showing rotational rate ± SD of 366.4°/s ± 107.8, 238.8°/s ± 91.2 and 231.8°/s ± 95.0, *P* < .0001 and *P* < .0001.

The mean apical myo rotational rate and the mean apical epi rotational rate of the SW-Healthy rats were not different, *P* = .8003. (**Figure 6-9A**).

The means basal rotational strain rate of the Healthy-SW in all layers were significantly different to their counterparts in the Healthy rats. The basal endo rotational rate of Healthy-SW was -410.0°/s ± 173.1 versus basal endo rotational rate of Healthy rats of -306.8°/s ± 153.6, *P* = .0075. The basal myo rotational rate of Healthy-SW was -259.4°/s ± 138.3 versus basal myo rotational rate of Healthy rats of -201.3°/s ± 103.3, *P* = .0439. The basal epi rotational rate of Healthy-SW was -336.7°/s ± 153.3 versus basal epi rotational rate of Healthy rats of -224.8°/s ± 107.8, *P* = .0005. In Healthy rats, the mean basal endo rotational rate was significantly greater than the mean basal myo rotational rate and the mean basal epi rotational rate, respectively showing rotational rate ± SD of -306.8°/s ± 153.6, -201.3°/s ± 103.3 and -224.8°/s ± 107.8, *P* = .0005 and *P* = .0068. The mean basal myo rotational rate and the mean basal epi rotational rate of the Healthy rats were not different, *P* = .3232. In SW-Healthy rats, the mean basal endo rotational rate was significantly greater than the mean basal myo rotational rate, respectively showing rotational rate ± SD of -410.0°/s ± 173.1 versus -259.4°/s ± 138.4, *P* = .0001. The mean basal epi rotational rate was similar to the mean basal endo rotational rate, respectively showing rotational rate ± SD of -336.7 °/s ± 153.3 versus -410.0°/s ± 173.1, *P* = .0614. The mean basal myo rotational rate was

significantly greater than the mean basal epi rotational rate, respectively showing rotational rate ± SD of -259.4°/s ± 138.3 versus -336.7°/s ± 153.3, *P* = .0274. **(See Figure 6-9B)**

Figure 6-8. Plots of rotational rate versus cine time, (A) Healthy endo apical segmental rotational rate, (B) SW-Healthy endo apical segmental rotational rate, (C) Healthy endo basal segmental rotational rate and (D) SW-Healthy endo basal segmental rotational rate. Cine time is the number of cine frames lapsed since the onset of cardiac cycle in end diastole. ES represents end systole.

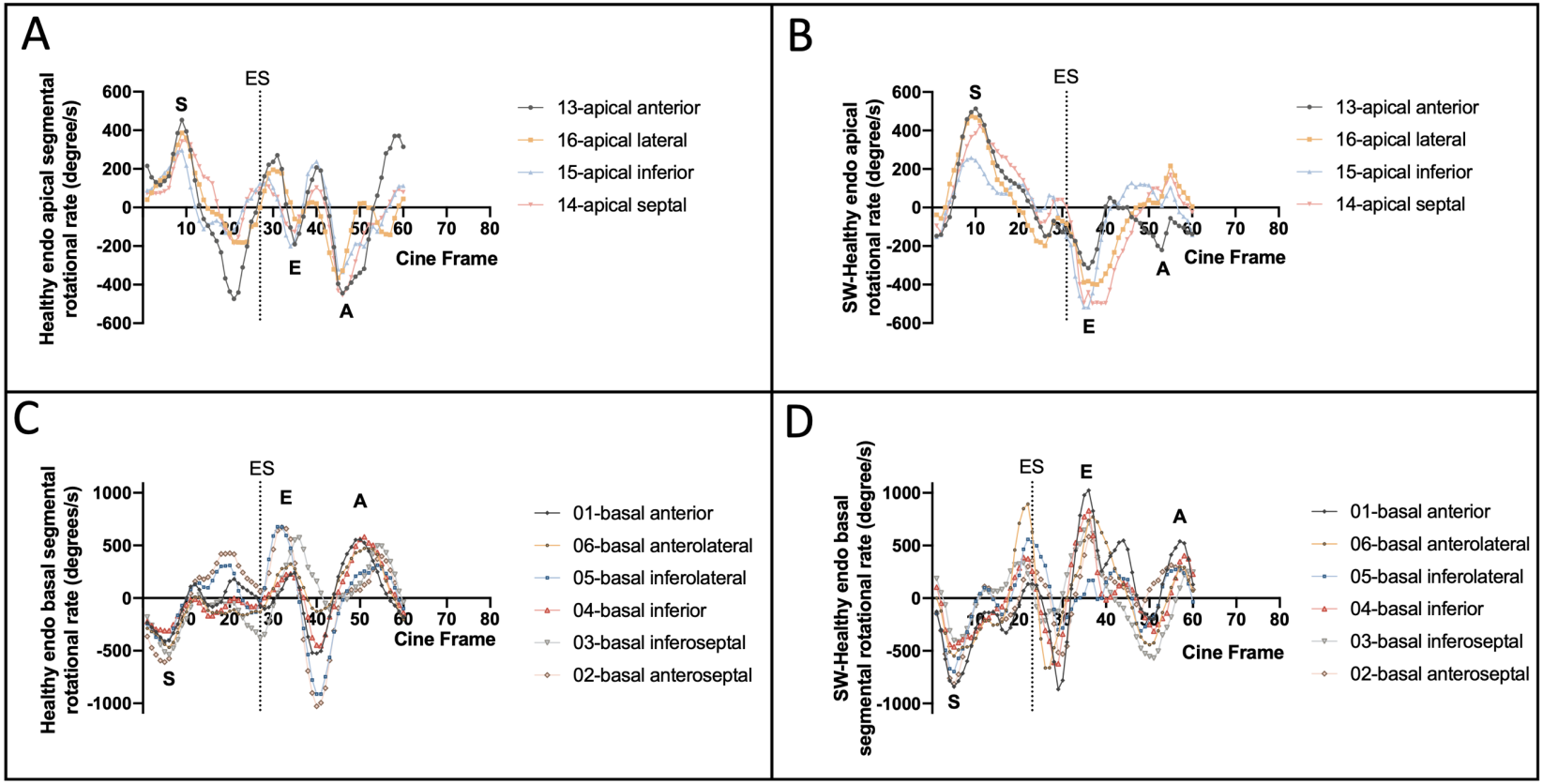

Figure 6-9. Scatter dot plot of (A) apical rotational rate of the endo, myo and epi layers of the Healthy and Healthy-SW rats and (B) basal rotational rate of the endo, myo and epi layers of the Healthy and Healthy-SW rats. Middle bar is the mean, and the upper and lower bars are the 95% CI. NS is no significant, *<.05, ** $P < .01$, ***, $P < .001$, and **** $P < .0001$.

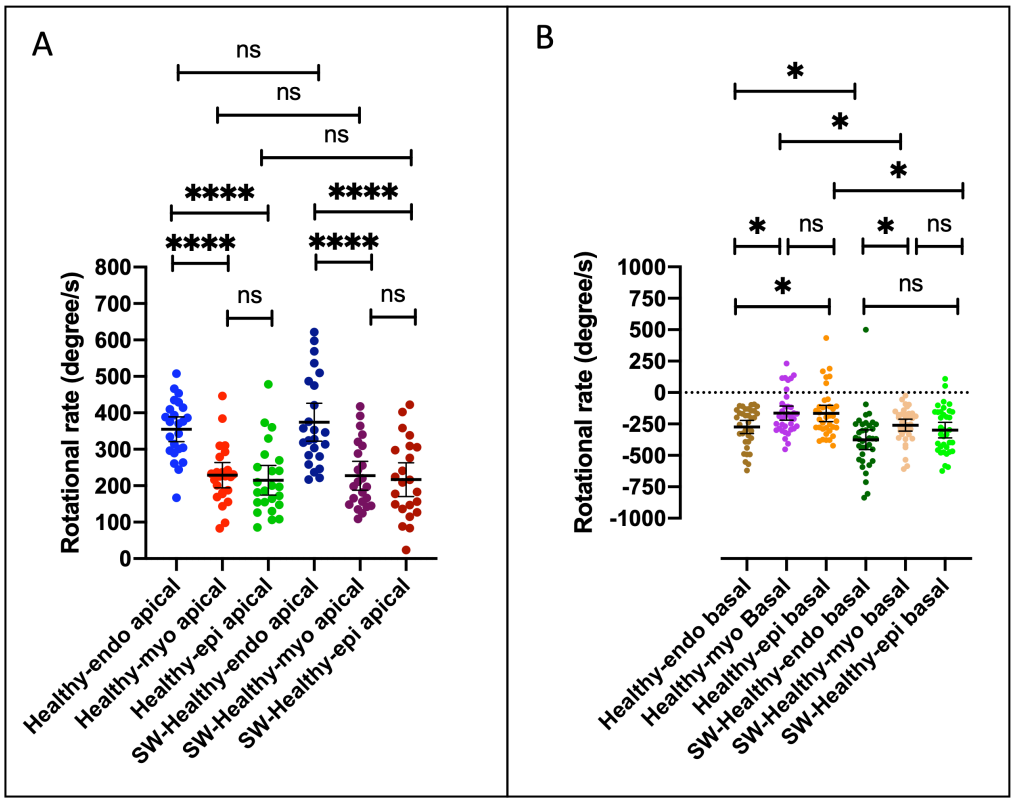

6.7 Discussion

In this chapter, the effects of shockwave on cardiac mechanics were assessed using volumetric indices; the areas and FAC of the base and apical slice; global longitudinal strain and circumferential strain of the endocardial and myocardial layer; global radial strain; basal rotation, apical rotation, twist and torsion in the endocardial, myocardial and epicardial layers; and the systolic rotational rate of the endocardial, myocardial and epicardial layers.

There was no difference in the EDV of the Healthy and Healthy-SW at three days post shockwave administration to the heart. However, the ESV was smaller in the Healthy-SW than the Healthy, indicating the SV was higher in the Healthy-SW than the Healthy. There was no effect on the heart rate by shockwave between the Healthy and Healthy-SW, while the CO was higher in Healthy-SW than Healthy, suggesting shockwave does have an effect on cardiac contractility. The EF was 5.9% higher in the Healthy-SW than the Healthy.

The basal areas in both phases of ED and ES, and the FAC were not different between the Healthy and Healthy-SW. These findings were echoed by the basal circumferential strain and basal radial strain, that they were not different between the Healthy and Healthy-SW.

On the other hand, the apical area of the ED and to a greater extend the ES was smaller than in the Healthy-SW than Healthy, translating to a higher FAC in Healthy-SW than the Healthy. The apical endo and myo CS was stronger (more negative) in Healthy-SW than the Healthy.

Compared to the echocardiography finding **(Appendix 1)**, showing evidence of immediate EDV dilatation post shockwave administration, however, by three days, as demonstrated here, the effect on EDV dilatation was lost. The endo and myo GLS was stronger (more negative) in the Healthy-SW than the Healthy. While the endo GCS was stronger (more negative) in Healthy-SW than Healthy, the myo GCS was not different between Healthy and Healthy-SW, suggesting that the effect of shockwave could be layer selective favouring the endo layer. The effect of shockwave on the GRS was minimal; not different between the Healthy and the Healthy-SW.

In Healthy, the basal rotations according to the layers of the endo, myo and epi were not different; and the apical rotations according to the layers of the endo, myo and epi were also not different. On the contrary, in the Healthy-SW, the epi basal rotation is stronger (more negative) than the myo rotation, while the myo and endo rotation was not different. The epi basal rotations and the myo basal rotation of the Healthy-SW were stronger (more negative) than their counterparts in the Healthy.

At the apex, the endo rotation was stronger (more positive) in the Healthy-SW than the Healthy. In the Healthy-SW, the endo rotation was stronger than the rotation in the myo and the epi layers, and the rotation in the myo layer was stronger than the rotation in the epi layers. These results indicate that at the base, the strongest effect of shockwave was on the rotation of the epicardial layer, while at the apex, the strongest effect was on the rotation of the endocardial layer. In I/R-MI reported in section **5.6.19**, the strength of the apical endo rotation after shockwave was not evident, reflecting that the inotropic mechanism by shockwave is different to the compensatory mechanisms of post ischaemia-reperfusion injury. Nonetheless, there are similarities in the inotropic effects on the basal rotations in Healthy-SW and I/R-MI. It is reiterated that agonist exerted the inotropic effect mainly at the apex as opposed to at the base. [261] [262]

The results of twist and torsion were similar in both the Healthy-SW than the Healthy, highlighting the fact that the rats' heart lengths were similar. Only torsion will be discussed as the comment also applies to the twist. In the Healthy-SW, the torsion of the endo, myo and epi layers were not different. In Healthy, the torsion of the endo was stronger (more positive) than the torsion of the myo and the epi, while the torsion of the myo and epi layers were not different. The torsion of the myo and epi of the Healthy-SW were respectively

stronger than their counterparts in the Healthy, while that of the endo layers were similar. These results indicate that the effect on torsion by shockwave happens predominantly at the myo and epi layers.

The systolic rotations rate at the apex in all layers were similar in both the Healthy-SW and the Healthy. The systolic rotational rates at the basal in all layers were stronger in all layers in Healthy-SW compared to their respective counterparts in the Healthy. These results provide further evidence that the contractility exerted by shockwave happens at the base.

6.8 Study Limitations

The limitations detailed in section 5.8 are also applicable to the experiments in this chapter, namely on the use of anaesthesia, in-bred rats and young male rats. The cardiac mechanical effects of shockwave in female could be different than in male. Sex differences in cardiac mechanics have been reported in human. Having smaller hearts, females have smaller ventricular volumes, higher EF, higher longitudinal and circumferential strains than males. [273] The higher EF detectable in female is secondary to higher SV for a given EDV. [274] Female use more LV twist (from apical rotation) to maintain the SV and CO than male when a large change in preload is applied; however, there are no differences between the sexes when afterload increased. [273] Females have longer heart compared to males, whereas males have larger hearts even after

allowance for body size (the BSA is larger in female than male). [275] The experiments were limited to young animals because an adult rat can grow to over 1 kg in weight, and the MRI cradle could only accommodate a rat of up to 0.5 kg. Moreover, the image quality would deteriorate with the increase in weight and obesity. Even with the use of fat suppression in MRI sequence, the compensation proved to be insufficient in obese animals.

6.9 Conclusion

In conclusion, the results in this chapter have shown that shockwave does have an inotropic effect on the heart. The underlying mechanisms were elucidated by the augmentations of the endo and myo GLS, the endo GCS and the twist contributed by the increase in the basal rotation.

Chapter Seven

RESULTS: THE EFFECTS OF DPP4 INHIBITION ON SHOCKWAVE

7.1 Clinical perspective

If cardiac shockwave were to be accepted as a treatment for patients with heart failure, the frequency of treatment (hospital attendance) should be accessible to many patients, and how to reduce the treatment burden must be researched. It was demonstrated in **chapter 6** that shockwave could induce inotropy. It was not known, however, how long the inotropic effect could last and whether repeated shockwave treatments could provide an additive effect on systolic function. The knowledge would help design shockwave treatment

and the dosing frequency. If the interval of shockwave dosing could be prolonged, the burden of treatment to the patients could be improved as well as patients' compliance.

7.2 Introduction

The in-vivo experiments presented in **chapter 6** and **chapter 8** have shown that shockwave has an inotropic effect on both the hearts of the healthy and of ischemia-reperfusion injury, assessed three days post shockwave treatment. In this chapter, cardiac function was assessed in time series.

The effect of shockwave on cardiac contractility could be partially explained by shockwave positive effects on SDF1 expression. As the half-life of SDF1 is short because of breakdown by Dipeptidyl-peptidase-4, if more SDF1 could be made available, the combination of shockwave with DPP4 inhibition could be the key to sustaining the effect of shockwave on contractility.

7.3 Purpose

The first purpose of the experiments in this chapter was to discover the durability of shockwave inotropic effect and, second, whether the addition of DPP4 inhibition to shockwave has a supportive effect on its sustainability. A drug that is able to enhance the inotropic effect of shockwave would be able to reduce the frequency of shockwave administrations and hence, the treatment burden to the patient.

7.4 Aims

This chapter aims to discover the longitudinal effect of shockwave on the systolic function and to discover whether DPP4 inhibition could be used as an adjunct with shockwave to enhance the said effect via discovering the trend on serial measurements.

7.5 Objectives

An increment in the EF was used as an indicator of the efficacy of shockwave treatment, and it was serially assessed over seven to ten days depending on the group for every three days in Healthy rats. The left ventricular ejection fraction of the group receiving only shockwave treatment was compared with the ejection fraction of the group receiving shockwave treatment and DPP4 inhibition, along their timelines to characterise the peaks and troughs, to compare the EF within the group, pre-treatment, post-treatment, and to assess the length of support DPP4 inhibition could deliver.

7.6 Rationale for using of Ejection Fraction

Ejection fraction has been shown in **chapter 6** to increase by 5.9% with shockwave treatment, and at this magnitude, EF deemed to be sensitive enough to follow through with the changes over time. It was also chosen because it was a simple and rapid index to acquire and measure, allowing more animals to be scanned per day. A gold standard LV-stacked ejection fraction

method was used, as described in **section 4.13**. If shown, a more detailed scan could be conducted in the future on different animal cohorts to discover other novel effects on cardiac mechanics.

7.7 Hypothesis

The inotropic effect of shockwave has a half-life, which could be prolonged using DPP4 inhibition.

7.8 Method

7.8.1 Animal Characteristics

All male Lewis rats used in the experiments were Healthy rats, and they were then subjected to experimental intervention as described below.

7.8.2 Experimental Design

Figure 7-1 summarises the time-series experimental design. In group A, the rats received multiple shockwave sessions administered on day 0, the third day and the seventh day, and the EF was assessed before and after each shockwave administration. In group B, the rats received DPP4 inhibitor via oral gavage one day before the first shockwave treatment, which to continue daily for a further ten days; received only one shockwave treatment on day 0; the EF was assessed before and after shockwave administration on day 0, the third day, seventh day and tenth day.

7.8.3 Drug Preparation and Oral Gavage Administration

Linagliptin 5mg (Trajenta, Boehringer Ingelheim) tablet was dissolved in 10ml water for injection in a 50ml conical tube to give a concentration of 2.5mg/5ml. A suitable curved gavage needle was preselected of sufficient length to cover the distance of the rat's mouth to just beyond the xiphoid process, then Luer-locked to a 5ml syringe. 3ml of the Linagliptin suspension was aspirated into the syringe via the gavage needle to include the needle's dead space. The oral gavage dose was administered using two hands technique. The left hand was used to restrain the rat held in an upright position by scuffing, immobilising the neck and head, creating a straight line from the mouth to the stomach. The right hand held the syringe, inserted the gavage needle to the left side of the mouth, along the hard palate to the back of the throat, into the oesophagus and the stomach. The drug was injected into the stomach, and the gavage needle was immediately withdrawn. Post-procedure, the rat was observed for any complications, e.g., difficulty in breathing, which could indicate lung dosing. Oral drug gavages were performed daily in the group of rats for DPP4 inhibition. No rats that had received oral gavage develop any complication of the procedure.

7.8.4 Control for confounding effects

All the animals used had not been subjected to any other experimental intervention other than described, e.g., intravenous or intraperitoneal

injections of fluid or bloodletting before or after the scan. These factors could affect the loading conditions affecting ejection fraction.

7.8.5 Shockwave Administration and MRI Preparation

General anaesthesia was induced in the rats using vaporised isoflurane as previously described in **chapter 4**. The precordial fur was removed by shaving. The rat was positioned in a supine position, the anaesthesia maintained via a nasal cone mask, and its four limbs taped down to a heating mat. The heartbeat was located by finger palpation for the location where the shockwave tip should be placed.

Shockwave was generated by Duolith SD1 (Storz Medical, Switzerland) equipped with a custom make transducer that has a very short focal point. The shockwave transducer tip was coupled with a liberal amount of ultrasound gel to the skin to ensure maximum transmission of energy as air bubbles reflected shockwave. A series of 2.5mJ/mm^2 x 500 pulses of focal shockwave administered to the heart at 3Hz (less than 3 minutes to complete). This dose had been previously shown to have an effect on ejection fraction. The respiratory rate was observed for suppression, and if it did happen, shockwave administration was interrupted and then resumed on recovery. The ultrasound gel wiped off, and the animal was prepared with ECG leads, then transferred to the MRI scanner where the rectal temperature monitor and heating pad were fitted. The MRI prep was identical to the method described in **chapter 4**.

No tail vein intravenous cannula was inserted. ECG monitoring and rectal temperature probe were applied.

7.8.6 Stacked-Ejection Fraction

The animal was scanned using Bruker Biospec 9.4 T scanner (94/20 USR Bruker BioSpec, Ettlingen, Germany). A multi-slice multi-frame FLASH was used to scout the left ventricle via multi-slice, tri-plane orthogonal imaging series covering the transverse, sagittal and coronal planes of the whole heart. Slices were oriented in short axis and covered the entire LV, making sure to include the apex to the aortic root. Both respiration and R-wave based triggering were used for the acquisition of cine-based data. The measurement parameters were: repetition time (TR)=RR interval/number of frames (~6.2 ms for ~24 to 28 frames), $TR_{Effective}$=RR interval, echo time (TE)=2.2 ms, flip angle 18°, slice thickness ≤1.2 mm, 13 to 14 slices, the field of view (28×28) mm^2, spatial in-plane resolution (200 ×200) μm^2, total scan time 18 minutes with triggering. The frames covered a full cardiac cycle. After the scan, the animal was recovered from anaesthesia and returned to the cage.

7.8.7 Image Analysis

As previously described, the following indices were measured from the LV stack images using Segment (Medviso) to measure the EDV, ESV to derive the EF. The results were compiled in Microsoft Excel and tabulated according to the groups.

7.8.8 Statistical Analysis

The statistical analysis was performed in Prism 8.4.3 for MacOS (Graphpad). Comparisons between matching time points of group A and group B means were performed using the Welch t test. Within group between time-series means, comparisons were performed using one-way (between-subjects) ANOVA of Brown-Forsythe and Welch. As the purpose of the time-series experiment was to screen the effect of shockwave, discover the trend for hypothesis generation, and because the number of animals used was very small, no *P* value adjustment was made to correct for type 1 error. *P* value < .05 considered significant. The data are expressed as Mean ± SD. ANOVA test for linear trend was used to assess EF means of preSW day 0, postSW day 0, post SW day 3 and post SW day 7, whether repeat shockwave sessions have an additive effect on EF.

7.9 Results

The results of comparison between A and B are presented first, then the time points within each Group A and B.

7.9.1 Comparison Between Time Points of Group A and Group B

Table 7-1 summarised the data on the EF of group A and B from day 0 to day 7. The trend lines between the two groups are presented in **Figure 7-5**. The mean EF of Day 0 (post) of group B was similar to the EF of Day 0 (post) of

Figure 7-1. S
and EF asses
assessment

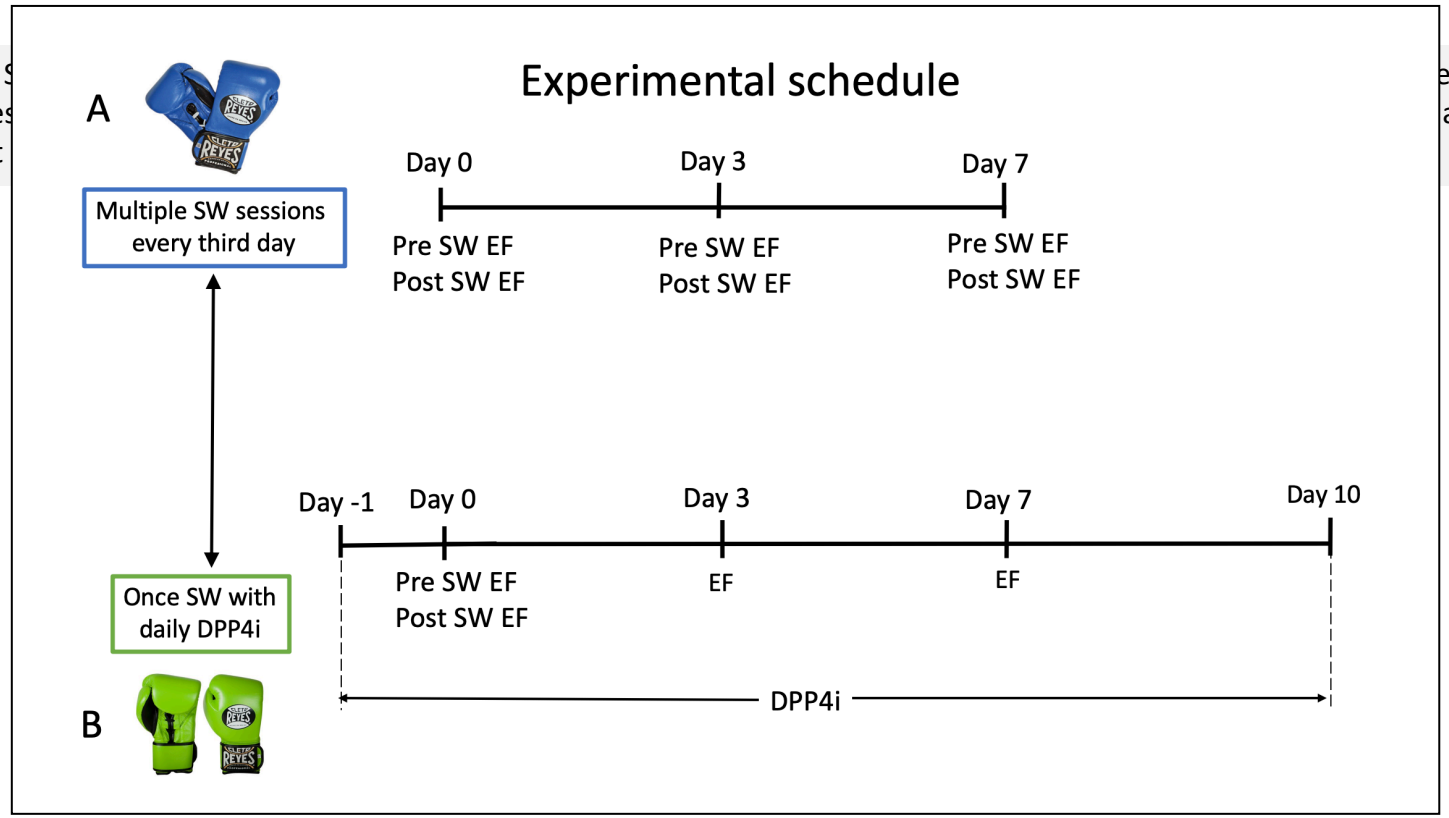

essions
and EF

group A, respectively showing EF ± SD of 67.3% ± 1.4 versus 65.0% ± 1.8, *P* = .1492. The mean EF of Day 3 (pre) of group B was significantly larger than the EF of Day 3 (pre) of group A, respectively showing EF ± SD of 66.0% ± 1.4 versus 63.9% ± 1.8, with a mean difference of 2.12%±SEM 0.80, R2=0.33, *P* = .0193. The mean EF of Day 7 (pre) of group B was similar to the EF of Day 7 (pre) of group A, respectively showing EF ± SD of 64.2% ± 0.8 versus 65.3% ± 1.7, *P* = .3941; and also similar to the mean EF of Day 7 (post) of group B, respectively showing EF ± SD of 64.2% ± 0.8 versus 68.0% ± 2.9, *P* = .0939.

7.9.2 Comparison of Time Points Within Group A

See **Figure 7-3** and **Table 7-2** for the summary of the results. Within group A, the ANOVA of Brown-Forsythe and Welch showed significant differences, *P* < .0001. Test for linear trend of EF means of preSW day 0, postSW day 0, post SW day 3 and post SW day 7 also showed significant results, *P* < .0001, slope 3.6 ±SE 0.04, 95%CI 2.8 to 4.4, R2 (effect size) 0.75.

In group A, the mean EF significantly increased from Day 0 (pre) to Day 0 (post); to Day 3 (pre); to Day 3 (post); to Day 7(pre); and to Day 7 (post), respectively showing *P* = .0080, *P* < .001, *P* = .002, *P* = .0060 and *P* = .0187. The mean EF of Day 0 (post) were not different with Day 3 (pre), Day 3 (post), Day 7(pre) and Day 7 (post), respectively showing *P* = .3964, P = .158, *P* = .8470, *P* = .2051. The mean EF of Day 3 (pre) was significantly smaller than Day 3 (post), *P* = .0136 and not different with Day 7 (pre) and Day 7 (post), respective *P* = .2903. *P* =

.1124. The EF of Day 3(post) was not different with Day 7(pre) and Day (7) post, respective *P* = .1985. *P* = .6724. Finally, the EF of Day 7 (pre) was not different with the EF of Day 7 (post), *P* = .2404.

7.9.3 Comparison of Time Points Within Group B

Within group B, the ANOVA of Brown-Forsythe and Welch showed significant differences, *P* < .0001. Test for linear trend of EF means of Day 0 (pre), Day 0 (post), Day 3 (pre) and Day 7 (pre) also showed significant results, *P* < .0001, slope 2.8 ±SE 0.32, 95%CI 2.14 to 3.46, R2 (effect size) 0.54.

See **Table 7-3** for the summary of the results. In group B, the mean EF was significantly increased from Day 0 (pre) to Day 0 (post), to Day 3 (pre) and to Day 7 (pre), respectively showing *P* = .0006, *P* < .0001 and *P* < .001. The mean EF of Day 0 (post) was not different to Day 3 (pre) but significantly larger than Day 7 (pre), respectively showing *P* = .2325 and *P* = .0384. Finally, the mean EF of Day 3 (pre) was significantly larger than the mean EF of Day 7 (pre)., *P* = .0441.

7.9.4 EF on the 10th Day

The EF of one rat of group B at day 10th post treatment showed an EF of 60.1% which fell into one SD range of Day 0 (pre-0).

7.9.5 Heart Rate

While group A (day 0) Post SW (n=3) heart rate was lower than (day 0) Pre SW (n=3) heart rate, the difference did not reach significance, *P* = .0681, respectively showing heart rate mean ± SD of 363.0bpm ± 26.89 versus 399.7bpm ± 29.4.

Group B (day 0) Post SW (n=3) heart rate was also similar to Pre SW (n=3) heart rate, showing heart rate mean ± SD of 366.3bpm ± 6.4 versus 384.3bpm ± 10.7, *P* = .1750.

The differences between pre- and post-SW (day) between group A and B was not significant, respectively showing a mean difference of -36.7bpm ± 17.5 versus -18.0bpm ± 15.1, *P* = .2354.

Table 7-1. Results of group A and group B.

† assessed using Welch t test

	A Mean±SD (n)	B Mean±SD (n)	*P* value †
Day 0 (pre)	58.4±2.2 (15)	58.4±2.2 (15)	-
Day 0 (post)	65.0±1.8 (3)	67.3±1.4 (3)	.1492
Day 3 (pre)	63.9±1.8 (9)	66.0±1.4 (7)	.0193
Day 3 (post)	67.2±1.2 (3)	-	-
Day 7 (pre)	65.3±1.7 (3)	64.2±0.8 (3)	.3941
Day 7 (post)	68.0±2.9 (3)	-	-
Day 10 (post)		60.1 (n=1)	-

Table 7-2. Group A mean differences within time-series group.

‡ Assessed using ANOVA of Brown-Forsythe and Welch

Comparison	Mean Diff.	95.00% CI of diff.	Significant?	Summary	*P* Value ‡
Day 0 (pre) vs. Day 0 (post)	-6.60	-10.10 to -3.11	Yes	**	.0080
Day 0 (pre) vs. Day 3 (pre)	-5.46	-7.17 to -3.75	Yes	****	<.0001
Day 0 (pre) vs. Day 3 (post)	-8.80	-11.09 to -6.52	Yes	***	.0002
Day 0 (pre) vs. Day 7(pre)	-6.90	-10.27 to -3.52	Yes	**	.0060
Day 0 (pre) vs. Day 7 (post)	-9.65	-15.90 to -3.40	Yes	*	.0187
Day 0 (post) vs. Day 3 (pre)	1.14	-2.33 to 4.61	No	ns	.3964
Day 0 (post) vs. Day 3 (post)	-2.20	-5.82 to 1.41	No	ns	.1588
Day 0 (post) vs. Day 7(pre)	-0.29	-4.24 to 3.66	No	ns	.8470
Day 0 (post) vs. Day 7 (post)	-3.05	-8.88 to 2.79	No	ns	.2051
Day 3 (pre) vs. Day 3 (post)	-3.34	-5.66 to -1.02	Yes	*	.0136
Day 3 (pre) vs. Day 7(pre)	-1.43	-4.79to 1.93	No	ns	.2903
Day 3 (pre) vs. Day 7 (post)	-4.19	-10.38 to 2.00	No	ns	.1124
Day 3 (post) vs. Day 7(pre)	1.91	-1.61 to 5.43	No	ns	.1985
Day 3 (post) vs. Day 7 (post)	-0.85	-6.93 to 5.24	No	ns	.6724
Day 7(pre) vs. Day 7 (post)	-2.75	-8.60 to 3.09	No	ns	.2404

Figure 7-2. Biaxial plot of EF versus days lapsed for group A with interconnecting lines to peaks and troughs. Changes in EF at Day 0 (pre), Day (post), Day 3 (pre), Day 3 (post), Day 7(pre) and Day 7(post). Arrows indicate shockwave dose administration. The symbols indicate the mean and upper/lower bars represent the SEM.

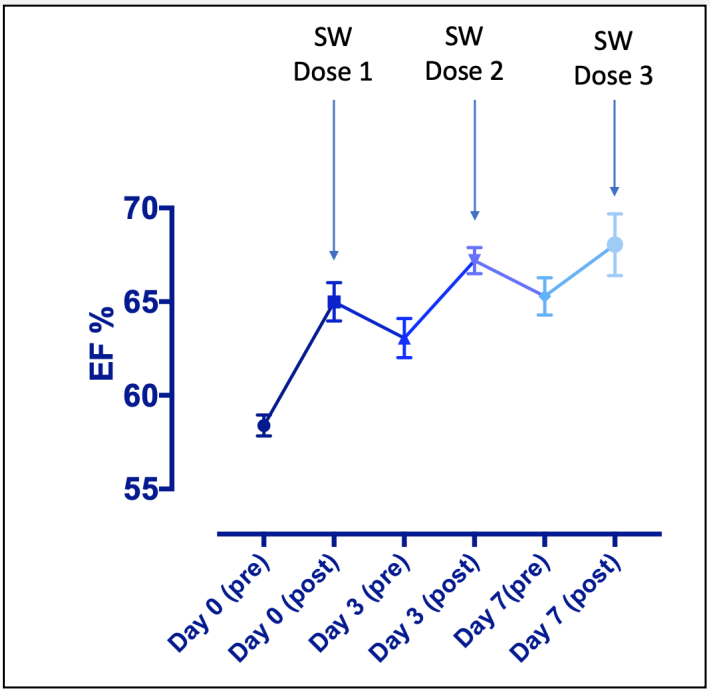

Figure 7-3. The same chart as in Figure 2 with a trend curve line to show changes in EF reaching a steady state at day 7. Horizontal bars indicate the statistical significance.

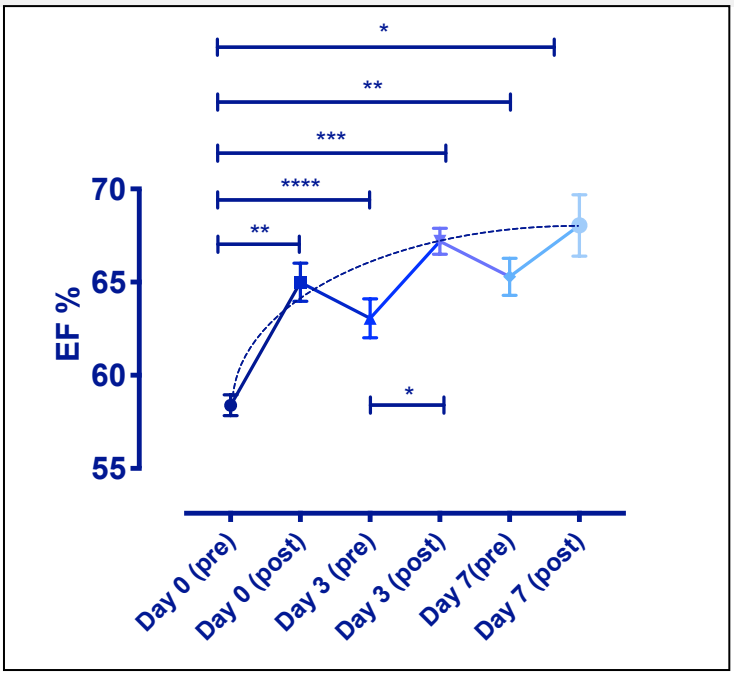

Table 7-3. Group B mean differences within time-series group.

‡ Assessed using ANOVA of Brown-Forsythe and Welch

Comparison	Mean Diff.	95.00% CI of diff.	Significant?	Summary	P Value‡
Day 0 (pre) vs. Day 0 (post)	-8.95	-11.60 to -6.29	Yes	***	.0006
Day 0 (pre) vs. Day 3 (pre)	-7.58	-9.22 to -5.95	Yes	****	<.0001
Day 0 (pre) vs. Day 7(pre)	-5.80	-7.47 to -4.12	Yes	****	<.0001
Day 0 (post) vs. Day 3 (pre)	1.37	-1.34 to 4.07	No	ns	.2325
Day 0 (post) vs. Day 7(pre)	3.15	0.30 to 6.00	Yes	*	.0384
Day 3 (pre) vs. Day 7(pre)	1.79	0.06 to 3.51	Yes	*	.0441

Figure 7-4. Biaxial plot of EF versus days lapsed for group B. Changes in EF in group B at Day 0 (pre), Day (post), Day 3 (pre), and Day 7 (pre). Arrows indicates shockwave dose administration. The EF peaked on Day 0 (post) and gradually reduces by Day 7, however remains higher than Day 0 (pre).

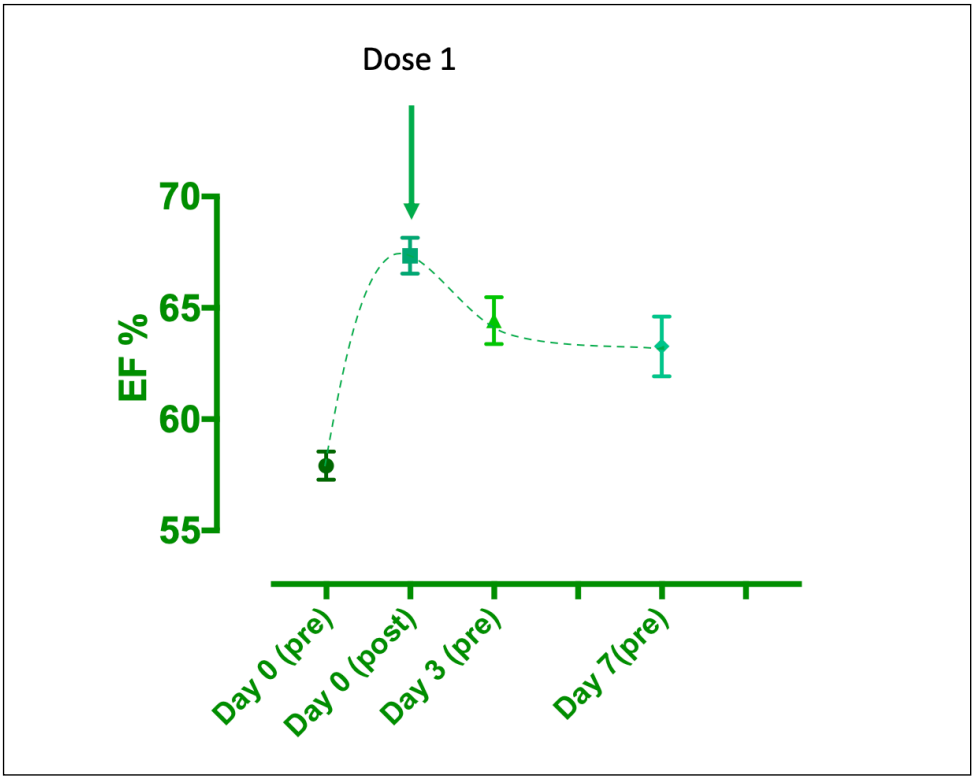

Figure 7-5. Comparison of EF trend curve lines of group A and group B.

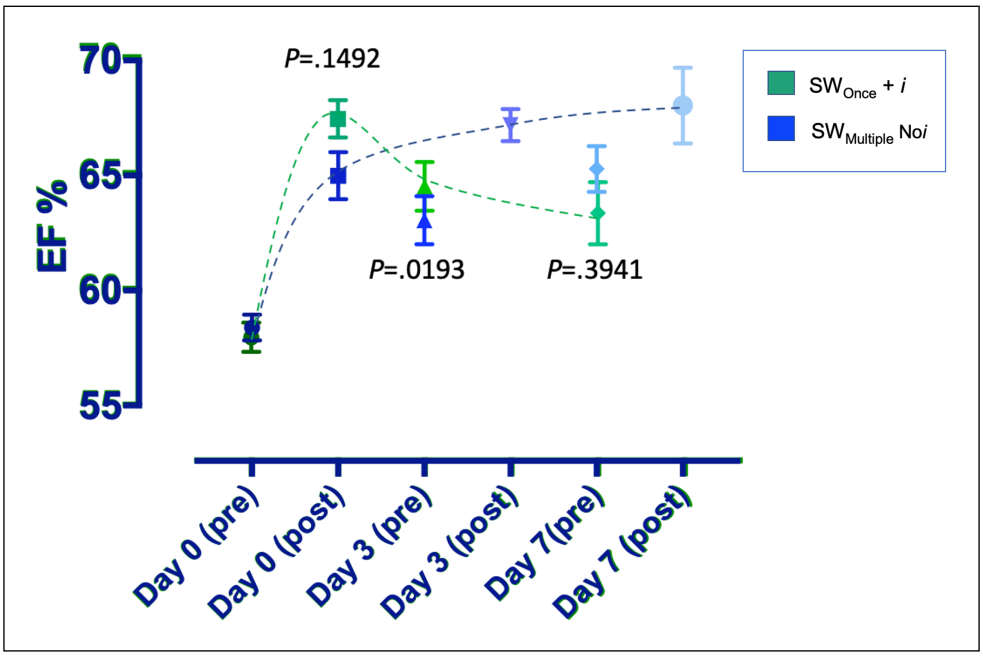

7.10 Discussion

In this chapter, two groups of Lewis rats were compared: rats that received shockwave every third day without DPP4 inhibition (Group A) versus rats that pre-treated with a DPP4 inhibitor then treated with only one session of shockwave (Group B). The efficacy was assessed using stacked-EF at Day 0, Day 3, Day 7, and Day 10 for Group B; assessed pre- and post- shockwave for Group A on Day 0, Day 3, Day 7. The use of stacked EF was justified because it has been validated to be a measurable read-out for shockwave, where in **chapter 6**, the EF increased by 5.9% with shockwave treatment. It was demonstrated that in Group A, the EF increased after each step of shockwave administration, reaching a plateau by Day 7 because the EF of Day 7 (post) was not different from the EF of Day 3 (post). While in Group B, the EF at Day 0 post shockwave was similar to the EF of Day 7 in Group B, followed by a gradual decay such that the EF between the two groups at day 7 (pre-shockwave for group A and B) were similar. The post-shockwave EF of group A was similar to the Day 7 EF of group B, although the mean of the former was higher than the mean of the latter (the number of animals used here was low). These results indicated that DPP4 inhibition enabled the establishment of rapid inotropy then decaying slowly, which otherwise require multiple shockwave treatment sessions to achieve the same magnitude.

The results in this chapter support the novel use of DPP4 inhibition with shockwave to reduce the frequency of shockwave administration for its inotropic effect. The acute increase in EF was confirmed in both shockwave-only group and shockwave with DPP4 inhibition group, and the first increment in EF in both groups were of a similar level. However, by Day 3, the effect on the EF in the shockwave-DPP4 inhibition group was significantly higher than shockwave-only Day 3 (pre) group, and by Day 7th, the EF in the shockwave-DPP4 inhibition group was similar to the EF of the shockwave-only group that had had two shockwave treatment every three successive days, suggesting that DPP4 inhibition could prolong the inotropic effect of shockwave. The results indicated that at least two-session shockwave treatment was equivalent to one shockwave treatment with DPP4 inhibition, and the effect on EF could be maintained for one week. By the 10^{th} day of the shockwave with DPP4 inhibition (Group B), the EF had returned to the baseline of the Day 0 pre-shockwave level.

Studying the peaks and troughs of the shockwave-only group from the (baseline) pre-treatment EF to the Day 7 (post) EF, when the rats had received three shockwave treatment every three successive days, showed the EF peaked after each shockwave dosing. The curved trendline suggested a steady state was reached by day 7^{th} post treatment when in group A, the EF of Day 7 (post) was not different from the EF of Day 3 (post). This observation was

supported by the fact that the EF of Day 3 (post) was significantly higher than the EF of Day 3 (pre), whilst EF of Day 3 (post) was not different to the EF on Day 7 (post), however, remained significantly higher than pre-treatment EF at Day 0.

The negative chronotropic effect of shockwave was not demonstrated during CMR compared to what had been observed during echocardiography suggesting the negative chronotropic effect of shockwave was brief, that beyond 20 minutes after shockwave, the effect on heart rate was no longer evident. It could be that anaesthesia had masked the effect on the heart rate; however, unlikely as anaesthesia usually slowed down the heart rate.

It is not clear how shockwave could induce inotropy but what can be deducted are that the effect has a shorter half-life than it would with DPP4 inhibition, and the cumulative effect on EF by serial shockwave administrations behave like a drug effect, suggesting a ligand-receptor interaction could be in play. As shockwave is known to increase SDF1 expression, which is known to have an effect on contractility, quite possibly SDF1 is one of the mediators of contractility enhancement observed here. Exogenous SDF1 in *ex vivo* hearts is known to have a positive effect on cardiac contractility [276] and blocking the CXCR4 receptor while administering exogenous SDF1 *in vivo* annuls the effect. [277] [278] Huang et al. experimented on ischaemia-reperfusion Langendorff mice model infused with exogenous SDF1, showing an improvement in the heart

contractility and relaxation, indicated by stronger magnitudes of LVDP, +dP/dt and -dp/dt, compared to hearts receiving vehicle. Further, infusing SDF1 with AMD3100 abolished the benefits of SDF1 on heart contractility and relaxation, indicated by similar LVDP, +dP/dt and -dP/dt compared to AMD3100 only, and to control vehicle.

DPP4 has neutral effects on the EF, heart rate, chambers volumes and cardiac masses as demonstrated by a subgroup analysis of PROLOGUE study [279] of sitagliptin in diabetic population. It was observed that the annual increase in E/e', signifying impairment in LV compliance and diastolic dysfunction, was attenuated in diabetics receiving sitagliptin compared to the conventional group not receiving sitagliptin.

AKT phosphorylation is known to increase cardiac contractility, [280] and there are several possible routes of AKT phosphorylation by shockwave. One that has been touched was via G-protein receptor activation by SDF1, and other possible ligands are growth factors such as IGF1,[281] and heat shock proteins. [282] [283]

7.11 Limitations

The limitations detailed in section 5.8 are also applicable to the experiments in this chapter, namely, on the use of anaesthesia, in-bred rats and male rats. In retrospect, to control for possible stress response confounding

experimental results, a group of rats receiving water gavage should have been performed. However, it was unlikely that a stress response playing a significant role as an increase in the apical rotation was not detected in the experiments reported in chapter 6. In the converse of adrenergic response, which was typically associated with an increase in apical rotation, shockwave increased basal rotation. While the effect of adrenergic response was expected to be short-lived, the effect of shockwave on the EF was additive. Furthermore, oral gavages have established use in chronic toxicology experiments and have acceptable effects on animals' behaviour and physiology.[284] It is unknown whether a fourth shockwave administration in group A would increase the EF further or whether it impacts the requirement for the maintenance and rate of decline; these could be explored in future experiments. To control for a possible direct effect of DPP4i on cardiac mechanics, a group of rats receiving only DPP4i could have been included. However, it was unlikely that DPP4i without shockwave affected the EF as the PROLOGUE study reported that sitagliptin had a neutral effect on the EF.

7.12 Conclusion

In conclusion, it was demonstrated in this chapter a novel use of DPP4 inhibitor in the rapid establishment and maintenance of the inotropic effect of shockwave.

Chapter Eight

RESULTS: SHOCKWAVE TREATMENT IN ANOXIC-REOXYGENATED CARDIOMYOCYTES

8.1 Introduction

Cardiomyocytes are the most abundant and metabolically active cells in the heart, hence, the most vulnerably affected by ischaemia-reperfusion injury. In acute myocardial infarction, a considerable loss of cardiomyocytes in the order of one billion cells, equivalent to 25% loss of the left ventricle, through the process of necrosis and apoptosis, [325] could progress to heart failure.[326] Half of final infarct size could be attributed to ischemia/reperfusion injury, and a significant portion of that cells death is caused by apoptosis process, [37] a relatively slow biological process that potentially could be reversed [327] [328] via

mechanisms that could tilt the balance in favour of anti-apoptotic over that of pro-apoptotic pathways.

The experiment in this chapter was motivated by the accidental discovery that cardiomyocytes in culture, having been treated by shockwave, could remain in viable shape and exhibited sporadic movements after 48 hours of platting. Here, the ischaemia-reperfusion injury was modelled *in vitro* using anoxia and reoxygenation challenge of cardiomyocytes. Anoxia and reoxygenation refer to the oxygen tension of the gas in the culture chamber.

8.2 Purpose

The purpose of this experiment was to assess whether shockwave could be used as a treatment for cardiac ischaemia-reperfusion injury.

8.3 Aims

It aims to assess whether shockwave could improve cardiomyocytes viability after anoxia-reoxygenation challenge.

8.4 Objectives

Objectively cardiomyocytes viability assessed by cells counting before and after anoxia-reoxygenation challenge in cells not treated with shockwave, cells treated with shockwave and cells treated with exogenous SDF.

8.5 Hypothesis

Shockwave rescues anoxic cardiomyocytes from death; doubling shockwave dose has a stronger effect on cardiomyocytes survival, and exogenous SDF1 had a similar effect to shockwave.

8.6 Method

8.6.1 Animals' Characteristics and Heart explanation

A Healthy adult Sprague Dawley rat (Charles River, UK) was anaesthetized with isoflurane, then euthanised by neck dislocation followed by secondary confirmation of death. The heart was rapidly removed via midline extended thoracotomy and, if necessary, during transport, left submerged in ice-cold heparinised (2units/ml) Krebs-Henseleit solution.

8.6.2 Cardiomyocytes Isolation Using Langendorff Preparation

Subsequently, the heart was hung by the ascending aorta to a perfusate needle of Langendorff device, secured using a suture and a clip. The perfusion began with warm Krebs-Henseleit solution to retrograde perfuse the heart from the aorta into coronaries and left ventricle to wash off the blood and rewarm up the heart that it began contracting. Then the perfusate was switched to 'low calcium solution', ran for 5 minutes, followed by 10 minutes perfusion of 'low calcium solution' containing enzymes (1mg/ml collagenase and 0.6mg/ml

hyaluronidase). The heart would appear swollen, then removed from the perfusate needle, transferred to a sterile petri dish where the atria, right ventricle and aorta cut out.

8.6.3 Sequential Enzymatic Tissue Dissociation

The left ventricle then aseptically minced into 1mm pieces using a blade, then transferred into a 50ml conical tube with a fresh 'low calcium solution' with enzymes. The mixture was gently agitated in a water bath maintained at 37°C under oxygen supplementation for 5 minutes, then sieved through a nylon mesh on a conical funnel to a collecting test tube. It was imperative to rinse the conical tube after each water bath and decontaminate the exterior with 70% ethanol. The first filtrate containing fibroblasts and some cardiomyocytes were set aside and not used for the experiment. The residue, a partially digested tissue, was retransferred to the 50ml conical tube, supplemented with a fresh 'low calcium solution' with enzymes. The second enzymatic digestion lasted for 30 minutes. The second filtrate contained mostly cardiomyocytes, allowed to sediment under gravity or centrifuged under a low gradient of 100G for 5 minutes. To remove the enzymes, the buffer was exchanged twice to a fresh low calcium solution. At this point, cells viability was assessed using a light microscope, where rod-shaped cardiomyocytes indicated viable cells, whereas rounded cells indicated non-viable cells. This

was performed as a quality control measure to assess the quality of the cardiomyocyte's isolation.

8.6.4 Cells Plating

For this experiment, as the cells need to be maintained for two days, the low calcium buffer was exchanged twice to M199 (Gibco, Thermofisher) supplemented with CCT, 0.5% BSA, 1% penicillin-streptomycin. On the last media exchange, it was supplemented with 1:100 Insulin-Transferrin-Selenium-Sodium Pyruvate (Gibco, Thermofisher).

High Grid-500 (Ibidi) 35mm µ-Dish was aseptically pre-coated with laminin (Engelbreth-Holm-Swarm murine sarcoma, Sigma) at concentration 1-2 µg/cm 50 mM Tris-HCl, pH 7.5, with 150 mM NaCl for at least two hours in 37°C in an incubator or left overnight at 4°C. Before use, the plate was washed with sterile PBS three times. The number of plates needed was determined as the product of the number of experimental conditions multiplied by three replicates; fifteen as detailed in experimental design.

The cells suspension was gently mixed to achieve a homogenous mixture of live and dead cells so that when plated, each replicate would have similar proportions of live/dead cells. The plating was performed in a biological safety cabinet where 1ml of cells suspension pipetted into each µ-Dish and topped with a further 1ml supplemented M199 to compensate for evaporation. With the lid covered, the µ-Dishes were swirled a few times to ensure the cells

distributed evenly on the plate, and this was visualised under light microscopy. The cells were allowed to adhere to the µ-Dishes bottom by incubation for a minimum of 1 hour in a 5% CO_2 incubator at 37°C. The adherence was confirmed under a microscope by flicking the µ-Dishes and witnessing stasis; and the dead floating cells, on the other hand, would move. Dead cells were removed by media exchange, performed in the hood, the µ-Dishes tilted, and the culture media was gently aspirated from the edge so that the plated cells were not disturbed. This was performed a few times to ensure virtually all the dead cells had been washed off. All the attachment surface area of the µ-Dishes was imaged using a digital pictomicroscope (Nikon Eclipse TE2000-E). The cells were left for two hours to equilibrate in a 5% CO_2 incubator 37°C before the experiment begun. As each experiment condition was performed in triplicate, for convenience and reduction of contamination risk, they were placed together in one round 100mm petri dish, lidded and appropriately labelled.

8.6.5 Experimental Design

The cardiomyocytes anoxia-reoxygenation experiment was assessed in five conditions:

1. Normoxia controls– defined as cells that did not receive shockwave treatment and did not receive anoxia-reoxygenation challenge. The cells remain in a 5% CO_2 incubator at 37°C or briefly outside the

incubator in normal room temperature and atmospheric oxygen concentration during pictomicroscopy. Condition 1 never received shockwave treatment.

2. Anoxia cells - defined as cells that had been placed in hypoxia chamber flushed with 100% N_2 and then sealed, returned to the incubator for 30 mins, and finally, the hypoxic chamber then opened to allow cells to breathe atmospheric oxygen. Condition 2 never received shockwave treatment.
3. Cells treated with SW 1 Bar x 1000 pulses – defined as cells experiencing condition 2 plus treatment with shockwave of 1Bar x 1000 pulses and then immediately returned to the incubator.
4. Cells treated with SW 2 Bar x 1000 pulses – defined as cells experiencing condition 2 plus treatment with shockwave of 2 Bar x 1000 pulses and then immediately returned to the incubator.
5. Cells spiked with exogenous rat SDF1 – defined as cells experiencing condition 2 plus exogenous SDF1. Rat SDF1-alpha was spiked into the media immediately after anoxia-reperfusion challenge (500pmol/ml) and then returned to the incubator. Condition 5 never received shockwave treatment.

Each condition was examined in replicates. For condition 1 and condition 2, the pictomicrographs were taken at Day 0 (after final media change on the day

of the experiment) and at Day 1 (the first event in day 1, 24 hours after Day 0). For condition 3, 4 and 5, the pictomicrographs were taken at Day 0 and Day 1 (24 hours after Day 1).

8.6.6 Anoxia Challenge

The procedure was performed in a hood to maintain sterility. The hypoxic chamber was pre-sterilised by 70% ethanol spray and let dry in the hood. The larger Petri dishes containing µ-Dishes for conditions 2 to 5 were transferred to the hypoxic chamber with their lid on, while the lids to the µ-Dishes inside were left open. This was to ensure exposure to anoxic ambient (after the chamber air had been replaced with 100% N_2 creating no oxygen ambient) and to maintain sterility. The hypoxic chamber then sealed, and purged with HEPA-filtered 100% nitrogen for 10 minutes. It was acknowledged that the anoxic ambient might not completely remove the dissolved oxygen in culture media and instead created a severe hypoxic environment in the culture media. For simplicity, the two terms here were used interchangeably. Then, both the inlet and outlet port clamped; and the hypoxic chamber returned to the incubator for 20 minutes, after which the anoxia was relieved simply by opening the outer shell in a hood. In effect, the cardiomyocytes in conditions 2, 3, 4 and 5 were exposed to anoxic ambient for 30 minutes in total. Additionally, the culture media for cells for condition 5 was spiked with SDF1. The lids to the µ-

Dishes were immediately put back on. Then, the μ-Dishes cells for conditions 2 to 4 would immediately proceed to shockwave treatment.

8.6.7 Shockwave Delivery

See **Figure 8-1**. The cardiomyocytes μ-Dishes for conditions 3 and 4 were treated with radial shockwave by Swiss Dolorclast classic (EMS, Switzerland) with Evo Blue handpiece. A radial shockwave is based on a ballistic principle, a pneumatic-accelerated ball bearing travelling in a piston column hitting the membrane on the tip of the applicator, producing shockwave that spread in a radial direction. The handpiece set up, as shown in Figure 1, held vertically by a clamp holder, tip facing upward, dressed in parafilm and ultrasound gel. To ensure sterility, the μ-Dishes were wrapped with parafilm, then placed on the ultrasound gel above the shockwave tip.

The ultrasound gel was used to couple the shockwave transmission from the tip to the cells. As air bubbles could reflect shockwave and reduce its efficacy, it was important to ensure the ultrasound gel was free of air bubbles. The energy level and the number of pulses delivered were as in condition 3 and condition 4. The pressure signified the peak of pressure amplitude measured in Bar, whereas the number of the pulses signified how many repetitions in the episode. Upon completion of shockwave treatment, the parafilm wrapper

removed, the μ-Dishes returned to their respective larger petri dish lid and finally to the incubator.

Figure 8-1. Preparation of shockwave hand piece treatment to the cells

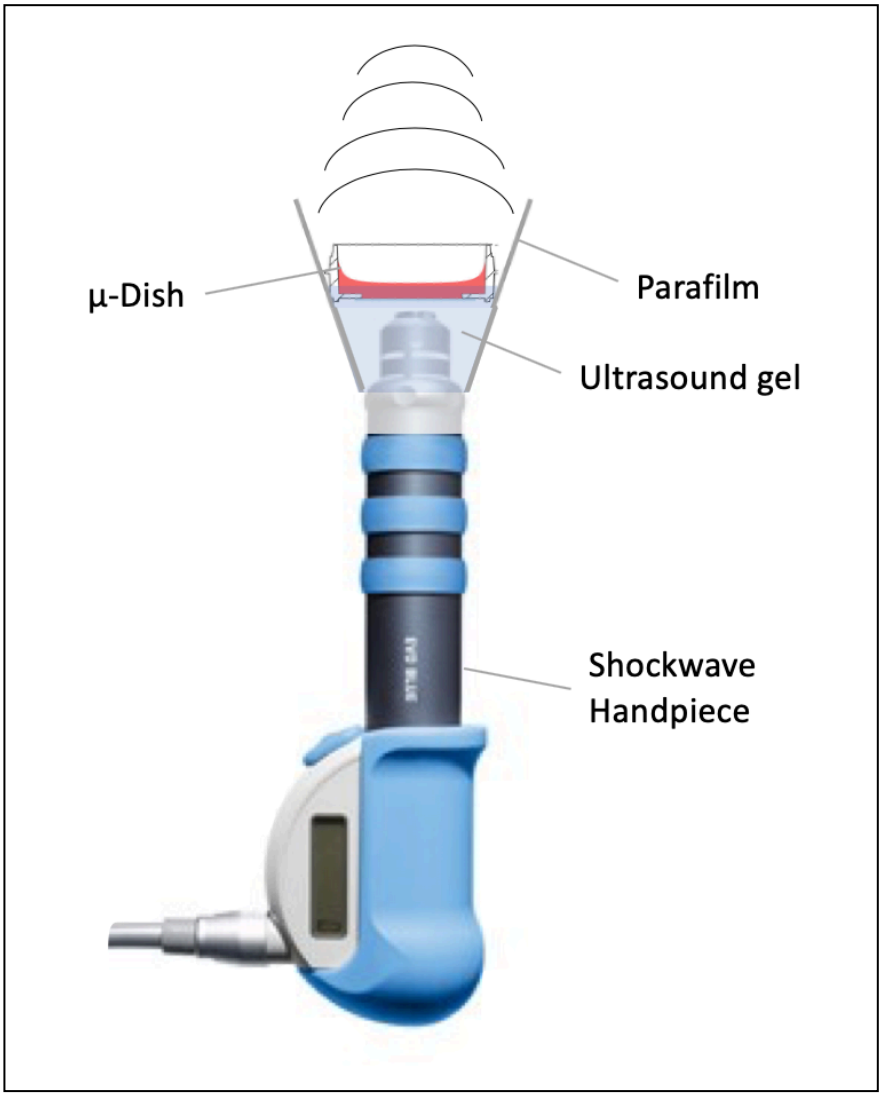

8.6.8 Cells Counting

Cardiomyocyte's viability was assessed by manual counting, performed offline on the photomicrographs using the 'cell counter' plugin in Fiji for MacOS (version 2.0.0-rc-43/1.52i), where rod-shaped cardiomyocytes indicated viable cells, whereas rounded cells with blebbing indicated apoptotic cells. The utility of morphological appearance for viability classification had been validated in a study [329] using a TUNEL assay; rod-shaped cardiomyocytes were TUNEL-negative, and rounded cells with blebbing were TUNEL-positive.

8.6.9 Statistical Analysis

The frequency of viable cells and apoptotic cells of the triplicates for each condition were expressed in percentage mean and standard deviation. The comparison between two condition groups was performed on the sums of absolute count of viable and non-viable cardiomyocytes per condition in 2x2 contingency table analysis using two-sided Fisher's exact test. *P* values < .5 were considered significant, and if significant in multiple comparisons, the *P* values would undergo Bonferroni correction. The relative risk was calculated using Koopman asymptomatic score. For linear trend, the Chi-Square test for trend was used to assess the trend of condition 2, 3 and 4.

8.7 Results

The results are summarized in **Figure 8-2**.

There was a small increase in the proportion of dead cells between normoxia day 0 (18.3%) versus normoxia day 1 (23.7%); however, the result was not significant, *P* = 0.0714, the relative risk of 1.1 (95%CI 1.1 to 1.4). The cell death in the anoxia group (58.1%) was significantly higher than normoxia day 1 (23.7%), *P* < .0001, relative risk 1.8 (95% CI 1.67 to 2.0); and with normoxia day 0 (18.3%), *P* < .0001, relative risk 2.0 (95%CI 1.8 to 2.1).

In cardiomyocytes receiving shockwave in condition 3, there were less cells death compared to the anoxia group (34.0% versus 58.1%, *P* < .0001, the relative risk of 0.6 (95% CI 0.6 to 0.7). In cardiomyocytes receiving shockwave in condition 4, there was less cells death compared to the anoxia group (32.4% versus 58.1%, *P* < .0001, the relative risk of 0.6 (95% CI 0.6 to 0.7). There was a 1.5% reduction in cells death with a higher dose of shockwave in cardiomyocytes in condition 4 compared to condition 3 (32.4% versus 34%); however, the effect was not significant, *P* =.6143. The anoxic cardiomyocytes spiked with SDF1 in condition 5 had less cells death compared to the anoxia group (35.2% versus 58.1%, *P* < .0001, relative risk of 06 to 0.7). The effect on cell death was not different between anoxic cardiomyocytes treated with SW-1Bar (34.0%) versus anoxic cardiomyocytes spiked with SDF1 (35.2%), *P*=.6774;

and between anoxic cardiomyocytes treated with SW-2Bar (32.4%) versus anoxic cardiomyocytes spiked with SDF1 (35.2%), *P*=.3466. There was a linear trend from condition 2, 3 and 4, *P* < .0001. There was less cell death in normoxia control day 1 (23.7%) versus SW-1Bar (34.0%), *P* < .0001, relative risk 1.2 (95%CI 1.1 to 1. 2). There was less cell death in normoxia control day 1 (23.7%) versus SW-2Bar (32.4%), *P*=.006, the relative risk of 1.1 (1.0 to 1.3). There was less cell death in normoxia control day 1 (23.7%) versus anoxic cardiomyocytes spiked with SDF1 (35.2%), *P* < .0001, the relative risk of 1.2 (1.1 to 1.3).

Figure 8-2. Bar chart of % rod-shaped cardiomyocytes versus cardiomyocytes experimental conditions. Error bars indicate standard deviation, middle bar indicates the mean. Experiments performed in triplicates. NS is no significant, *<.05, ** $P < .01$, ***, $P < .001$, and **** $P < .0001$.

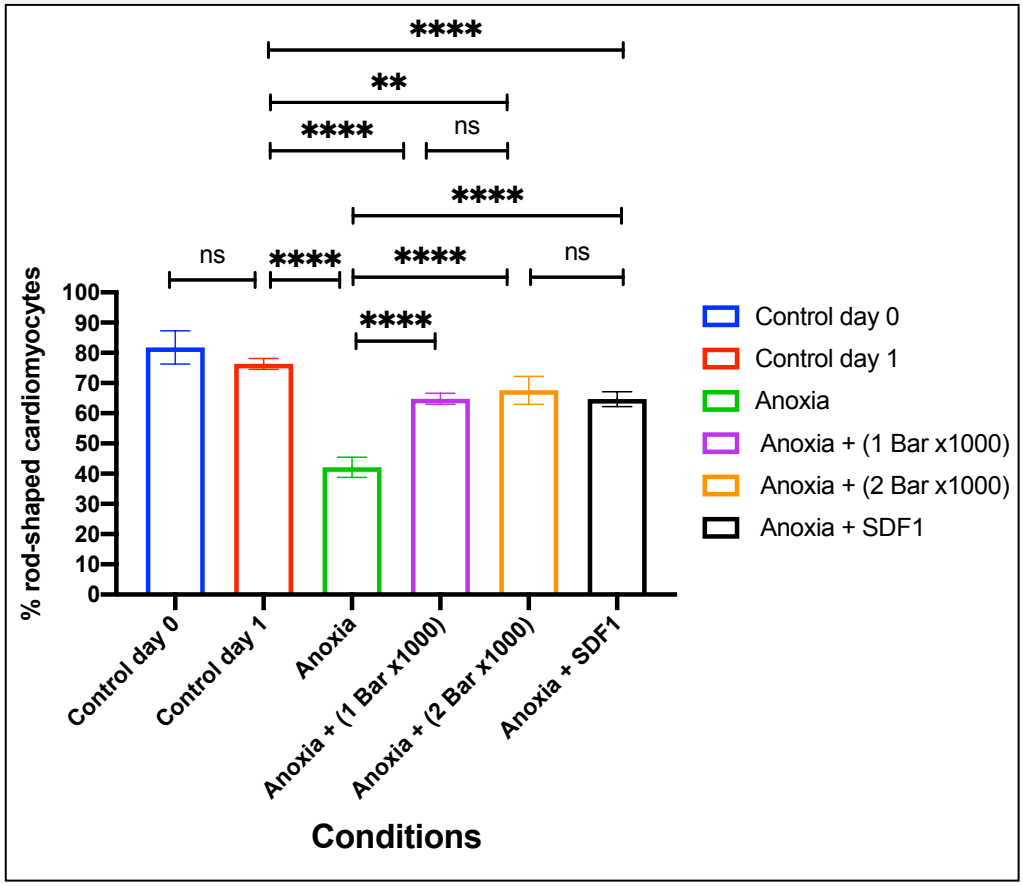

8.8 Discussion

In this chapter, plated cardiomyocytes were challenged with atmospheric anoxia for 30 minutes to mimic ischaemia, then reintroduced into room air to mimic reperfusion, and the cells were subjected to no treatment or shockwave (1 Bar x 1000 or 2 Bar x 1000) or exogenous SDF1 spiking; these were compared with normoxia untreated control and the viability was assessed 24 hours later. It was discovered that there were a higher proportion of viable cardiomyocytes in groups treated with shockwave or exogenous SDF1, compared to untreated anoxia cells. The results provide a proof-of-concept that shockwave application to anoxic cardiomyocytes could prevent the cells from death, and the discovery has motivated to assess the hypothesis further in rat models of ischaemia-reperfusion injury.

Here, it was shown that exogenous SDF1 alone has a positive effect in improving cardiomyocytes viability after they have been anoxically challenged, a finding consistent with other reports. In a study by Huang et al., SDF1 was infused in isolated mouse hearts subjected to ischaemia-reperfusion and displayed an anti-apoptotic effect. The cardioprotection mediated by SDF1 was via the activator of transcription 3 (STAT3), an effect that was cancelled by a CXCR4 blocker.[277] AMD3100-blocked isolated hearts, when treated with exogenous SDF1, did not attenuate cleaved caspase-8 and caspase-3 levels,

suggesting that CXCR4 was required for acute protection by SDF1. Interestingly, Huang et. el observed that SDF1 did not increase the AKT or ERK phosphorylation, in contrast to the direct effect of shockwave reported in other studies in cells and tissue. A study by Hatanaka et al., using the HUVEC, reported that shockwave could phosphorylate ERK 1/2 and AKT via mechanosensors properties of caveolin-1 and β1-integrin,[330] and via routes independent of activation by paracrine signalling factors such as the SDF1. These findings further support that the combination of SDF1 with shockwave could provide synergism in cardioprotection via at least two different anti-apoptotic pathways (the AKT and ERK via direct mechanotransduction, and SDF1 via paracrine signalling). In chapter 10, in section **11.9.1,** it was demonstrated that shockwave could not increase SDF1 expression in cardiomyocytes, so the SDF1 source must be from paracrine signalling (e.g., SDF1 from the fibroblasts as shown in section **11.11.1,** shockwave induces SDF1 expression in fibroblasts).

At excess doses of SDF1 and NO, which are of no biological relevance to shockwave, can induce apoptosis. In NO, the threshold was reported to be variable between cell types due to their different redox states, the amount of transition metal complexes, and the expression of survival genes across different cells types. SDF1 at 300ng/ml reported to be pro-apoptotic via production of the TNF-α. [331] Shockwave induction of SDF1 in tissue and cells

are unlikely to reach this concentration and hence of no concern. In this experiment, 500pg/ml of SDF1 was used, showing to have an anti-apoptotic effect.

To date, there have been no previous reports that shockwave could provide cardioprotection in ischaemia-reperfusion injury. Recently, however, shockwave has been reported to be able to protect cardiomyocytes from doxorubicin (DOX)-induced cell death, where it was demonstrated that shockwave phosphorylated the AKT via integrin/Integrin-linked kinase (ILK), upregulating survivin, resulting in the attenuation of apoptosis.[332] The ILK-mediated cell protection is not unique to shockwave as the mechanosensory mechanism is known to suppress cells apoptosis, such in the case of hyperglycemic osmotic stress. [333] These pieces of evidence further indicate that shockwave effects through both mechanotransductive mechanisms and ligand binding mechanisms can improve the survival of cells against stress-induced apoptosis.

SDF1 has two knowns receptors, the CXCR4 and CXCR7, and these have been reported to have a different downstream effect on AKT and ERK, and the effect on cells migration. In stem cells, CXCR4 knockdown decreased the phosphorylation of ERK but did not affect the phosphorylation of AKT and RAF. On the contrary, CXCR7 knockdown reduced the phosphorylation of AKT and RAF and did not affect the level of ERK's phosphorylation.[334] Transwell

migration assay showed that both CXCR4 and CXCR7 activations were required for cells migration. CXCR7 regulates CXCR4 via ligand internalisation, [335] via -arrestin-2. [336] Further, the co-expression of CXCR4 and CXCR7are not always present, dependent on other instructions and pathologic state. For example, oestrogen preferentially promotes the CXCR4 over CXCR7 expression in human breast cancer cell lines. The heterodimerisation of CXCR4/CXCR7 has been described, and there is crosstalk in the pathways. [337]

An important relevant downstream effect of PKC and AKT by shockwave is the phosphorylation of nitric oxide synthase. Mechanosensing ion channels too could affect the NO production via calcium influx,[338] via the formation of calcium-calmodulin complexes for the recruitment of eNOS from the Caveolin, and the rate of NO production could be increased by heat shock protein 90. The cascade effect of NO as an anti-apoptotic is vast. NO being lipophilic, mediate the action via diffusion and no cell surface receptor is required for cell entry. NO could cause shedding and reduce the expression of TNF receptor limiting inflammation, [339] and increase ceramide production in the reduction of DISC (death-inducing signalling complex). NO through the generation of cyclic GMP inhibits sphingomyelinases in the generation of ceramide-promoting apoptosis. [340] Cyclic GMP cascades effect on the release of cytochrome c from the mitochondria. NO nitrosylates the caspases impairing protein function at the protein binding sites in cardiomyocytes. [341]

8.9 Limitations

Even though the use of cardiomyocyte shape was a reliable sign of viability, it would have been best to include biochemical assays such as the LDH to assess for necrosis, other cellular markers of death and apoptosis. However, the latter would not have been straightforwardly performed on the same samples, as non-viable cardiomyocytes could become detached and lost during partial media exchange when introducing viability dye. For quantifying the caspase variants, the cardiomyocytes would need to be lysed first. With the limited quantity of cardiomyocytes per 35mm, the samples might need to be concentrated and performed using ultrasensitive assays. All of these could be performed in optimised different series of experiments.

8.10 Conclusion

In conclusion, this chapter reported the novel use of shockwave to rescue the cardiomyocytes from anoxia-reoxygenation cell death. The discovery has led to testing the hypothesis *in vivo* rat cardiac ischaemia-reperfusion injury, detailed in **chapter 9.**

Chapter Nine

RESULTS: THE EFFECTS OF SHOCKWAVE ON CARDIAC ISCHAEMIA-REPERFUSION INJURY

9.1 Clinical Perspective

After myocardial infarction, the remote myocardial segments may remodel and over time may become impaired as a consequence of cardiac remodelling. Early identification of segments at risk for remodelling could be important for prognostic reasons and for evaluation of novel therapeutic interventions for heart failure. The diastolic impairment usually precedes the systolic impairment where the pathogenesis on the ischaemic cascade run in the order of perfusion abnormalities, diastolic dysfunction, systolic dysfunction, ECG changes and finally clinical symptoms.

In ST-elevation myocardial infarction, early reperfusion limits the final infarction. After an ischemic threshold has been exceeded, a significant fraction of tissue will be lost from reperfusion injury. Currently, there is no approved therapy available to prevent the tissue loss of reperfusion injury.

9.2 Introduction

Cues from *in vitro* cardiomyocytes experiment (**Chapter 8**) revealed the novel use of shockwave in rescuing anoxic-challenged cardiomyocytes from apoptosis, and a similar effect could be achieved using exogenous SDF1, reaffirming that the paracrine effect of SDF1 in improving the viability of the cells likely to occur by a different route to that of shockwave. It was shown that shockwave could induce SDF1 in cardiac tissue **(section 10.7.9**) and in human cardiac fibroblast (section **11.11)** while the cardiomyocytes could not (**section 11.9.1**). In this chapter, the rescue effect of shockwave was assessed in a rat model of ischaemia-reperfusion injury treated with shockwave; DPP4 inhibition to enhance the effect of SDF1, and the functional outcomes and infarct size assessed using the CMR techniques described in **chapter 4** and **chapter 5**.

9.3 Aims

This chapter aims to investigate the rescue effect of shockwave on I/R-MI and to assess whether the combination of shockwave treatment with DPP4

inhibitor could enhance the rescue effect of shockwave further and study the rescue effect directly on the site of injury and in the remote segments.

9.4 Objectives

Objectively the following MRI imaging parameters were assessed in the groups, categorised into the domains of:

1) LV volumes: LVEDV, LVESV, SV, CO and EF;
2) Cardiac physiology: heart rate;
3) Global strains: endo and myo GLS, endo and myo GCS and GRS;
4) The effect on myocardial relaxation of the Remote using myo circumferential strain rate;
5) The effect on area at risk by T2-mapping;
6) The effect on final infarct size by LGE and infarct transmurality; and
7) The effect on rotational mechanics, twist and torsion

9.5 Hypothesis

Shockwave treatment on IR heart rescues the myocardium from ischaemia-reperfusion injury; the effect is enhanced by DPP4 inhibition (DPP4i), leading to better functional benefits, smaller infarct size, an increase in salvage index and reduction in infarct transmurality. Shockwave treatment improves the diastology of the remote segments in IR rats that received shockwave. The diastology of the remote segments of IR rats treated with shockwave and DPP4

inhibition is functionally more normal than the IR rat treated with shockwave only.

9.6 Methods

9.6.1 Experimental Design

9.6.1.1 Animal Characteristics and Groups

Healthy male Lewis rats were sourced from Charles River UK and used in all the experiments in this chapter. Three groups of animals were compared, I/R-MI, I/R-MI-SW and I/R-MI-SWi. I/R-MI rats were rats that underwent surgical procedure for induction of ischaemia-reperfusion injury. I/R-MI rats were rats that underwent surgical procedure for induction of ischaemia-reperfusion injury for 30 minutes. I/R-MI-SW rats were rats that underwent surgical procedure for induction of ischaemia-reperfusion injury and immediately treated with shockwave upon release of ligature. I/R-MI-SWi were rats that received the same treatment as I/R-MI-SW and additional linagliptin (Boehringer Ingelheim) pre-treatment of dose 10mg/kg via oral gavage daily for two doses prior to surgery. A shockwave dose of 0.25mJ/mm^2 x 500 pulses was administered to I/R-MI-SW and I/R-MI-SWi before the release of the ligature after 30 minutes of ischaemia.

9.6.2 CMR Scan Schedule

The I/R-MI, I/R-MI -SW and I/R-MI -SWi were scanned for up to 5 days post MI I/R.

9.6.3 Ischaemia-Reperfusion Myocardial Infarction

The methods of the creation of ischaemia-reperfusion myocardial infarction rat models have been detailed thoroughly in **chapter 3**.

9.6.4 Cardiac MR Acquisition

The method of MRI instrumentals, in-vivo cardiac acquisition, animal preparation, cardiac planning and image modalities used have been thoroughly detailed in **chapter 4.** MRI sequences used were INTRAGATE-cines, MESE-T2-mapping and IR-LGE.

9.6.5 Post-Processing for Volumetric Indices

The method for LV volumes: LVEDV, LVESV, SV, CO and EF have been detailed in earlier **section 5.5.4.**

9.6.6 Post-Processing for Global Strain

The method for post-processing for global strain has been detailed earlier in section Error! Reference source not found..

9.6.7 Assignments of Myocardial Segment

The AHA segments were assigned into phenotypes of either infarcted, Salvaged, Remote and Healthy; these were identical to that used in **section 5.5.8, 5.5.9, 0**; using a combination of parametric MR imaging of LGE and T2-

mapping thresholding. The infarcted myocardial segments were defined as myocardial segments with LGE positive, the salvaged myocardial segments as segments with no LGE and high T2 values and the remote myocardial segments as segments with no LGE and normal T2 values. T2 value of 23ms was used as the T2 threshold to define normal/abnormal as described in **section 5.6.9.**

9.6.8 Strain Rate

Segmental strain rate was used to study the effect of I/R-MI, shockwave and DPP4 inhibition on the Remote segments in the groups. The myo circumferential strain rate curves were constructed in 2D-CPA-MR, and the peak values of S_{SR}, E_{SR} and $A_{SR,}$ were manually identified and compiled in Microsoft Excel. S_{sr} was defined as the peak negative wave during systole, the E_{SR} was defined as the positive peak during early diastole, and A_{SR} was defined as the positive peak during late diastole. The $E_{SR}/A_{SR,}$ ratio was calculated. Each of the strain rate parameters was grouped into the phenotype infarcted, Salvaged, Remote and Healthy as described in the section above and statistically compared.

9.7 Results

9.7.1 The Effect of Shockwave and DPP4I on Volumetric Parameters

The results in this section are graphically summarised in **Figure 9-1**

9.7.1.1 LVEDV

The end-diastolic volume of the IR-MI, IR-MI-SW and IR-MI-i were similar, respectively showing EDV ± SD of 576.2mcl ± 49.7, 603.8mcl ± 50.7 and 608.2mcl ± 27.4, *P* = .3374. (**Figure 9-1A)**

9.7.1.2 LVESV

The end-systolic volume of IR-MI was significantly larger than IR-MI-SW and IR-MI-i, respectively showing ESV ± SD of 251.7mcl ± 24.0 versus 222.2mcl ± 19.7, *P* = .0493; versus 209.1mcl ± 16.5, *P* = .0070. The ESV of IR-MI-SW and IR-MI-i were similar, respectively showing EDV ± SD of 222.2mcl ± 19.7 versus 209.1mcl ± 16.5, *P* = .5329. (**Figure 9-1B)**

9.7.1.3 Stroke Volume

The stroke volume of IR-MI was significantly smaller than IR-MI-SW and IR-MI-i, receptively showing SV ± SD of 324.4mcl ± 34.2 versus 381.6mcl ± 35.4, *P* = .0181; and versus 399.1mcl ±15.8, *P* = .0004. The SV of IR-MI-SW and IR-MI-i were similar, respectively showing SV ± SD of versus 381.6mcl ± 35.4 versus 399.1mcl ± 15.8, *P* = .5944. (**Figure 9-1C)**

Figure 9-1. Scatter dot plot comparing volumetric parameters of I/R-MI, I/R-MI-SW, I/R-MI-SW-i, where (A) end diastolic volume, (B) end systolic volume, (C) stroke volume, (D) ejection fraction, (E) heart rate and (F) cardiac output.

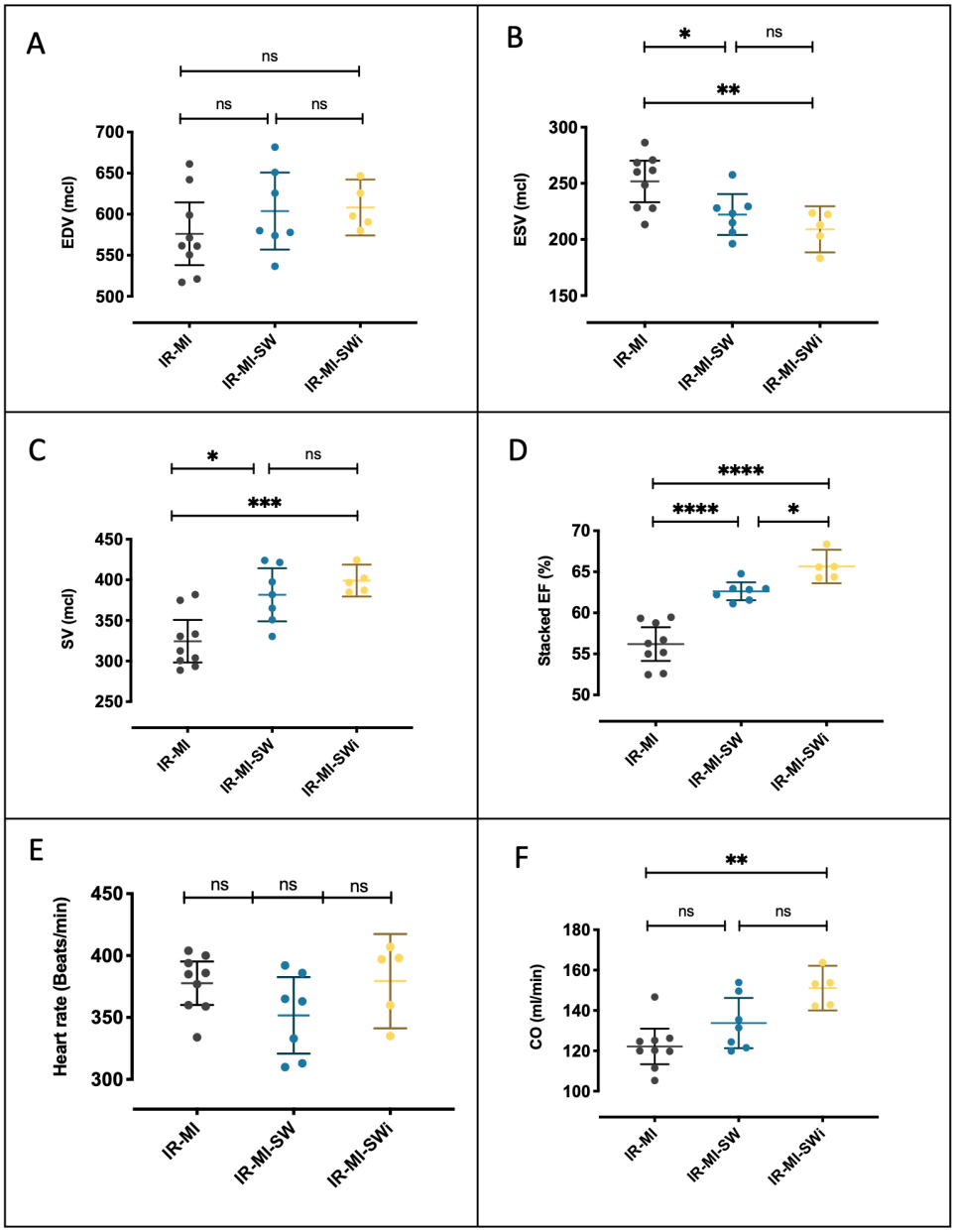

9.7.1.4 Ejection Fraction

The ejection fraction of IR-MI-SWi was significantly larger than IR-MI and IR-MI-SW, respectively showing EF ± SD of 64.3% ± 1.7 versus 62.6% ± 1.2, *P* < .0001; versus 56.2% ± 2.7, *P* = .0274. The ejection fraction of IR-MI-SW was significantly larger than IR-MI, respectively showing EF ± SD of 62.6% ± 1.2 versus 56.2% ± 2.7, *P* < .0001. The test for linear trend between column means from the left column to the right column showed a highly significant result, slope 4.9 ±SE 0.57, *P* < .0001. (**Figure 9-1D)**

9.7.1.5 Heart Rate

The heart rates of the IR-MI, IR-MI-SW and IR-MI-i were similar, respectively showing heart rate ± SD of 377.7bpm ± 22.8, 351.7bpm ± 33.4 and 379.4bpm ± 30.7, *P* = .2535. **Figure 9-1E)**

9.7.1.6 Cardiac Output

The cardiac output of the IR-MI-i was significantly larger than IR-MI, respectively showing CO ± SD of 151.1ml/min ± 8.9 versus 122.2ml/min ± 11.4, *P* = .0011. The CO of IR-MI-SW was similar with IR-MI and IR-MI-i, 133.8ml/min ± 13.5 versus 122.2ml/min ± 11.4, P = .2434; versus 151.1ml/min ± 8.9, *P* = .0637. (**Figure 9-1F)**

9.7.2 The Effect of Shockwave and DPP4i On Global Strains

The results in this section are summarised in **Figure 9-2**.

9.7.2.1 MyoGLS

The myoGLS of I/R-MI-SWi was significantly greater (more negative) than I/R-MI-SW and I/R-MI, respectively showing myoGLS ± SD of -18.29% ± 0.36 versus -15.36% ± 1.32, P = .0054; versus -10.81% ± 3.42, *P* = .0005. The endoGLS of I/R-MI-SW was significantly greater (more negative) than I/R-MI, *P*= .0119. The test for linear trend between column means from the left column to the right column showed a highly significant result, slope -3.81 ±SE -0.68, *P* < .0001. (**See Figure 9-2A)**

9.7.2.2 EndoGLS

The endoGLS of I/R-MI-SWi was significantly greater (more negative) than I/R-MI-SW and I/R-MI, respectively showing endoGLS ± SD of -21.04% ± 0.39 versus -17.44% ± 1.70, *P* = .0065; versus -12.96% ± 4.20, *P* = .0013. The endoGLS of I/R-MI-SW was significantly greater (more negative) than I/R-MI, *P* = .0430. The test for linear trend between column means from the left column to the right column showed a highly significant result, slope -4.08 ±SE -0.83, *P* = .0001. **(See Figure 9-2B)**

9.7.2.3 EndoGCS

The endoGCS of I/R-MI was significantly weaker (less negative) than I/R-MI-SW and I/R-MI-SWi, respectively showing endoGCS ± SD of -24.46% ± 5.50 versus -33.29% ± 2.35, *P* = .0064; versus -35.60% ± 1.35, *P* = .0017. The endoGCS of I/R-MI-SW and I/R-MI-SWi were similar, *P* = .1947**. (See Figure 9-2C)**

9.7.2.4 MyoGCS

The myoGCS of I/R-MI was significantly weaker (less negative) than I/R-MI-SW and I/R-MI-SWi, respectively showing myoGCS ± SD of -15.98% ± 4.24 versus -22.69% ± 1.80, *P* = .0071; versus -22.81% ± 1.45, *P* = .0068. The myoGCS of I/R-MI-SW and I/R-MI-SWi were similar, *P* = .9990. **(See Figure 9-2D).**

9.7.2.5 GRS

The GRS of I/R-MI-SWi was significantly greater (more positive) than I/R-MI-SW and I/R-MI, respectively showing GRS ± SD of 75.81% ± 7.16 versus 51.62% ± 10.69, P = .0045; versus 31.18% ± 6.83, *P* < .0001. The GRS of I/R-MI-SW was significantly greater (more positive) than I/R-MI, *P*= .0097. The test for linear trend between column means from the left column to the right column showed a highly significant result, slope 22.18 ±SE 2.35, *P* < .0001. **(See Figure 9-2E).**

Figure 9-2. Scatter dot plot comparing global strain parameters of I/R-MI, I/R-MI-SW, I/R-MI-SW-i, where (A) endoGLS, (B) myoGLS, (C) endoGCS, (D) myoGCS, (E) GRS.

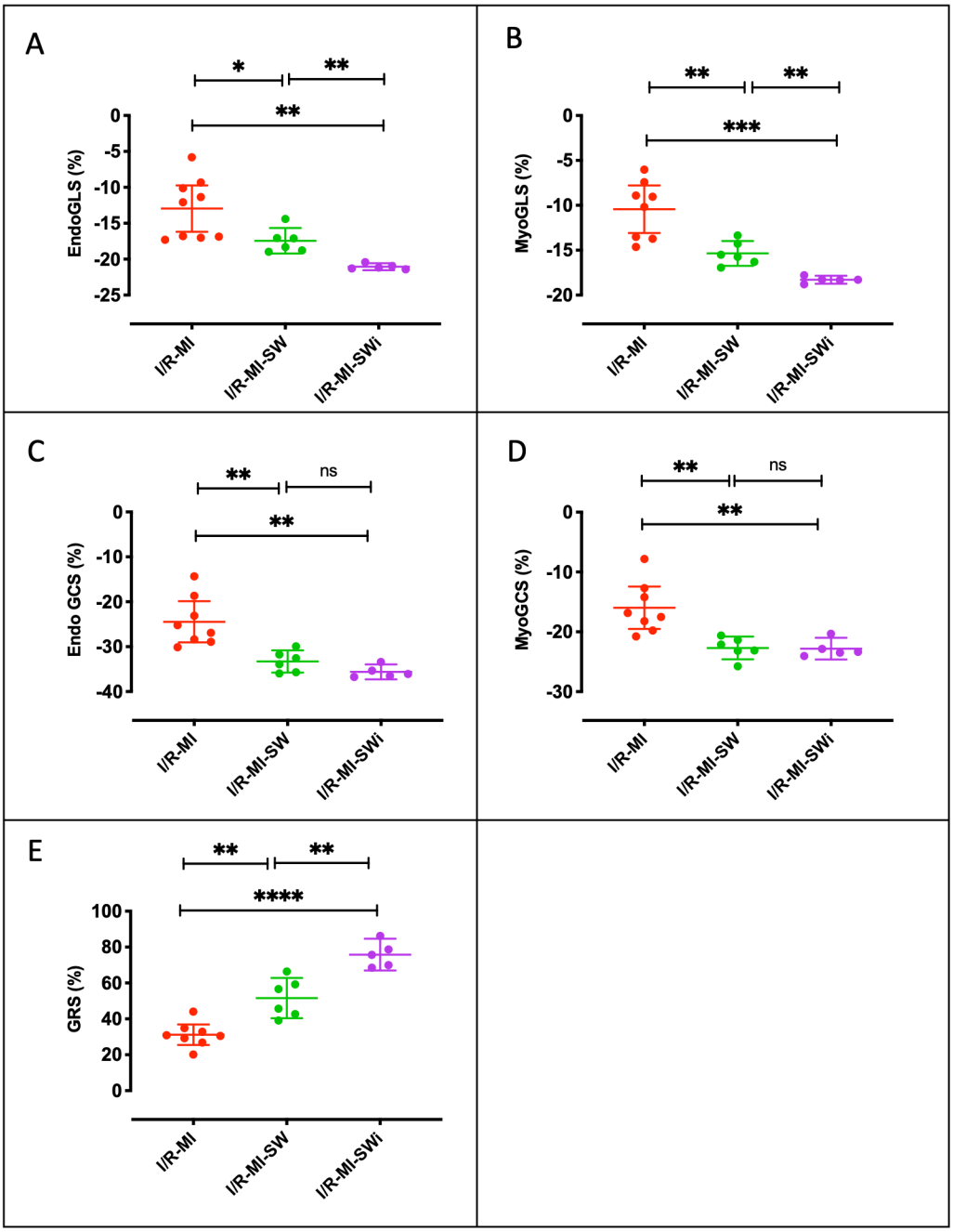

9.7.3 The Effect of Shockwave and DPP4i on Segmental Myo Circumferential Strain Rate

The results in this section are graphically summarised in **Figure 9-3**.

9.7.3.1 Circumferential Systolic Strain Rate (S_{SR})

The Ssr-Rem (n=36) was significantly weaker (less negative) than Ssr-Healthy (n=87), Ssr-Rem-SW (n=57) and Ssr-Rem-SWi (n=50), respectively showing Ssr ± SD of -6.63s^{-1} ± 2.71 versus -8.18 s^{-1} ± 2.40, *P* = .0041; versus -8.41 s^{-1} ± 2.88, *P* = .0034; and versus -8.99 s^{-1} ± 2.63, *P* = .0001. Ssr-Healthy, Ssr-Rem-SW and Ssr-Rem-SWi were similar, respectively showing Ssr ± SD of -8.18 s^{-1} ± 2.40, -8.41 s^{-1} ± 2.88 and -8.41 s^{-1} ± 2.88; Ssr-Healthy versus Ssr-Rem-SW, *P* = .6117; Ssr-Healthy versus Ssr-Rem-SWi, *P* = .0747; and versus Ssr-Rem-SW versus Ssr-Rem-SWi, *P* = .2786. (**See Figure 9-4A)**

9.7.3.2 Circumferential Diastolic E Strain Rate (E_{sr})

The Esr-Rem (n=37) mean rank was significantly reduced (less positive) compared to Esr-Rem-SWi (n=45), respectively showing Esr-median ± IQR of 7.11s^{-1} (4.84, 10.61) versus 9.60s^{-1} (7.70, 11.40), *P* = .0123. The differences between mean ranks of Esr-Rem versus Esr-Healthy (n=88) and Esr-Rem-SW (n=55) was not significant, both showing *P* > .9999 with respective Esr-median ± IQR of 7.11s^{-1} (4.84, 10.61), 8.40s^{-1} (5.81, 10.66) and 8.75 s^{-1} (6.96, 11.84). The mean ranks between Esr-Healthy, Esr-Rem-SW and Esr-Rem-SWi (n=45)

are similar, where Esr-Healthy versus Esr-Rem-SW, *P* = .3147; Healthy versus Esr-Rem-SWi, *P* = .0505; and Esr-Rem-SW versus Esr-Rem-SWi, *P* = .4313. (**See Figure 9-4B)**

9.7.3.3 Circumferential Diastolic A Strain Rate (A_{SR})

The mean rank of Asr-Rem (n=37) was significantly reduced (less positive) compared to the mean rank of Asr-Healthy (n=86), Asr-Rem-SW (n=52) and Asr-Rem-SWi (n=46), respectively showing Asr-median ± IQR of 3.20s^{-1} (2.33, 4.63) versus 6.56s^{-1} (4.61, 8.86), *P* < .0001; versus 7.06s^{-1} (4.49, 8.78), *P* < .0001; and versus 7.04s^{-1} (4.74, 10.47), *P* < .0001. The mean ranks of Asr-Healthy, Asr-Rem-SW and Asr-Rem-SWi were similar, where all interactions showed *P* > .9999. (**See Figure 9-4C)**

9.7.3.4 Circumferential Diastolic E/A Strain Rate

The mean rank of E_{SR}/A_{SR}-Rem (n=35) was significantly reduced (less positive) compared to the mean rank of E_{SR}/A_{SR}-Healthy (n=85), E_{SR}/A_{SR}-Rem-SW (n=47) and E_{SR}/A_{SR}-Rem-SWi (n=46), respectively showing E_{SR}/A_{SR}-median ± IQR of 2.39 (1.71, 3.21) versus 1.30 (0.77, 1.96), *P* < .0001; versus 1.32 (1.01, 1.76), *P* < .0001; and versus 1.17 (0.89, 2.05), *P* < .0001. The mean ranks of E_{SR}/A_{SR}-Healthy, E_{SR}/A_{SR}-Rem-SW and E_{SR}/A_{SR}-Rem-SWi were similar, where all interactions showed *P* > .9999. (**See Figure 9-4D)**

Figure 9-3. MRI images where in the first row represents the basal short axis, the second row represents the mid short axis, and the third row represents the apical short axis views. Columns (A), (B), (C) represent segmentation for feature tracking at early diastole; (D), (E) (F) represent colour-coded parametric T2-maps; and (G), (H), (I) represent the LGE.

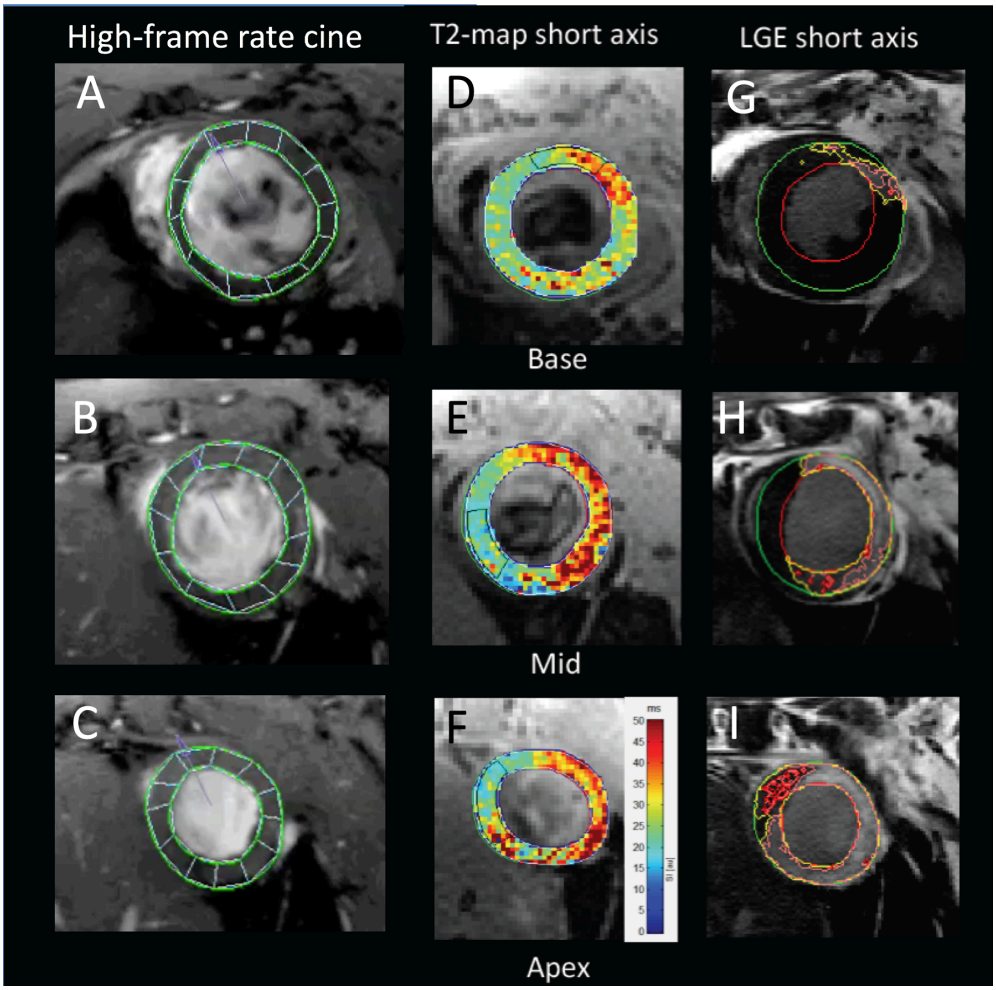

Figure 9-4. Myo Circumferential strain rate curve of (A) Healthy, (B) I/R-MI, (C) Healthy-SW and (D) Healthy-SWi, the Ssr, IVR_{SR}, E_{SR} and A_{SR} are where indicated on the waveforms. The double ended horizontal arrows indicated where the systole and diastole period. (E) Comparisons of Ssr, (F) comparison of E_{SR}, (G) comparison of A_{SR} and comparison of E_{SR}/A_{SR} amongst the Healthy, I/R-MI, Healthy-SW and Healthy-SWi.

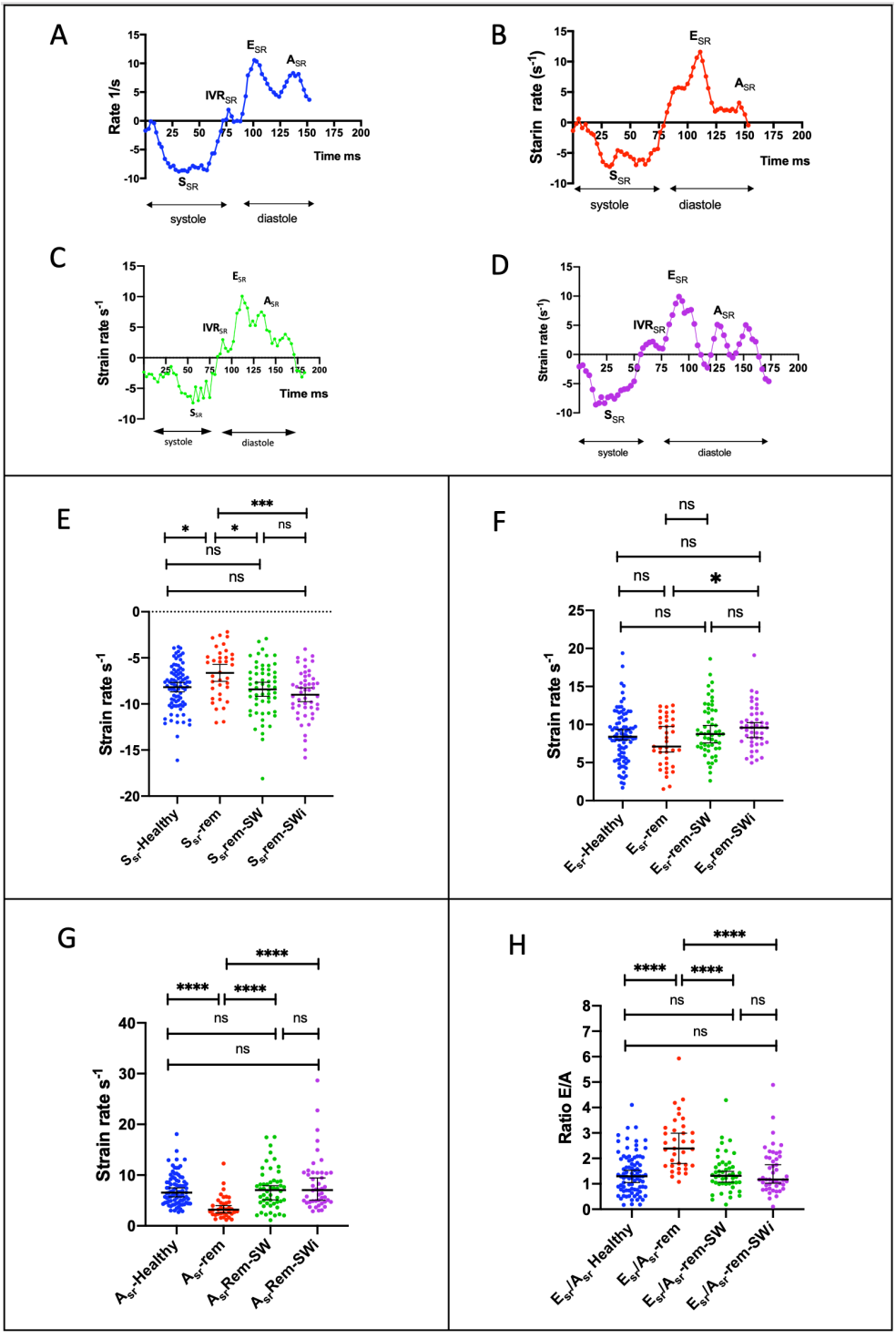

9.7.4 The Effect of **Shockwave and DPP4i On** Infarct Size, Area at Risk and Salvage Index

9.7.4.1 Visual Assessment of Infarct Size on Bullseye Plot

The bullseye plot constructed from LGE LV stacks showed the infarct size in the largest in I/R-MI, second largest in the I/R-MI-SW and smallest in the I/R-MI-SWi., respectively presented by **Figure 9-5A, Figure 9-5B and Figure 9-5C.** The colourmap signified infarct transmurality where dark red was the deepest infarct (100%), and dark blue was the shallowest (0%). **Figure 9-5D** presents a 3D model of the LV where the yellow contours are the segmented LGE volume**.**

9.7.4.2 LV Mass

See **Figure 9-5E.** The mean of LV masses of I/R-MI (n=6), I/R-MI-SW(n=5) and I/R-MI-SWi(n=6) were similar, respective mass ± SD were 400.5mg ± 37.7, 443.1mg ± 23.0 and 451.0mg ± 44.9, *P*=.0707.

9.7.4.3 Scar In µl

See **Figure 9-5F.** The mean of scar in ml in was the largest in the I/R-MI (n=6) compared to I/R-MI-SW (n=6) and I/R-MI-SWi (n=6), respectively showing LGE scar in ml ± SD of 117.6µl ± 19.2 versus 59.8µl ± 9.7, $P < .0001$, versus 32.4µl ± 9.2, $P < .0001$. The scar of I/R-MI-SWi was significantly smaller than I/R-MI-SW, $P = .0083$. Test for linear trend from the left column to the right column showed a significant negative slope of -42.59 ±SE -3.89, $P < .0001$.

9.7.4.4 LGE Volume %

See **Figure 9-5G.** The mean of LGE volume i.e., 'scar' in the I/R-MI (n=6) was the largest compared to I/R-MI-SW (n=6) and I/R-MI-SWi (n=6), respective showing LGE volume ± SD of 29.40% ± 5.02 versus 13.35% ± 1.80, *P* < .0001; and versus 7.10% ± 1.45, *P* < .0001. The LGE volume of I/R-MI-SWi was significantly smaller than I/R-MI-SW, *P* = .0106. Test for linear trend from the left column to the right column showed a significant negative slope of -11.15 ±SE -0.92, *P* < .0001.

9.7.4.5 Area at Risk Volume In %

See **Figure 9-5H**. Between I/R-MI (n=6), I/R-MI-SW (n=5) and I/R-MI-SWi (n=6), the mean of area at risk volume measured using T2-mapping were similar, respective AAR volume ± SD were 43.65% ± 12.32, 39.77% ± 12.89 and 41.11% ± 15.03, *P* = .8880.

9.7.4.6 Salvage Index

See **Figure 9-5I.** The mean of salvage index is the greatest in I/R-MI-SWi (n=6) compared to I/R-MI (n=6) and to I/R-MI-SW (n=5), respective SI ± SD of 0.79 ± 0.06 versus 0.26 ± 0.20, *P* = .0023; and versus 0.56 ± 0.10, *P* =.0112. The mean SI of the I/R-MI-SW was significantly greater than the mean of SI of I/R-MI, *P* = .0353. Test for linear trend from the left column to the right column showed a significant positive slope of 0.27 ±SE -0.04, *P* < .0001.

9.7.4.7 LGE Mean Transmurality

See **Figure 9-5J.** The mean transmurality of I/R-MI-SWi (n=6) was the smallest compared to I/R-MI (n=6) and I/R-MI-SW (n=6), respectively mean transmurality ± SD of 53.52% ± 12.92 versus 77.23% ± 3.79, *P* = .0045; and versus 72.08% ± 12.88, *P* = .0236. The mean transmurality of I/R-MI and I/R-MI-SW were similar, *P* = .6910.

9.7.4.8 LGE Total Extension

See **Figure 9-5K.** The mean LGE total extension of I/R-MI-SWi (n=6) was the smallest compared to I/R-MI (n=6) and I/R-MI-SW (n=6), respectively showing mean total extension ± SD of 10.56% ± 5.02 versus 49.3% ± 5.72, *P* < .0001; and versus 17.56% ± 6.81, *P* < .0001. The LGE total extension of the I/R-MI-SW and I/R-MI-SWi were similar, *P* = .1331.

9.7.4.9 Weighted LGE maximum transmurality

See **Figure 9-5L.** The mean of LGE maximum transmurality (n=6), I/R-MI-SW(n=6) and I/R-MI-SWi(n=6) were similar, respective weighed LGE maximum transmurality ± SD were 96.42% ± 2.93, 93.35% ± 5.72 and 87.50% ± 11.21, *P* = .2278.

Figure 9-5. Assessment of infarct size and salvage index in ischaemia-reperfusion myocardial infarction. LGE infarct transmurality displayed on bullseye plot of (A) I/R-MI, (B) I/R-MI-SW and (C) I/R-MI-SWi. (D) 3D model of LV (green is endocardium, red is epicardium, yellow is scar segmented from LGE) as viewed from the apex, (E) LV mass, (F) scar by volume, in mcl (G) % LGE scar to LV mass, (H) area-at risk, (I) salvage index, (J) LGE mean transmurality (K) scar total extension (L) maximum transmurality. **** P < 0.0001, *** P <0.001, ** P< 0.01, * P < 0.05, ns P > 0.05.

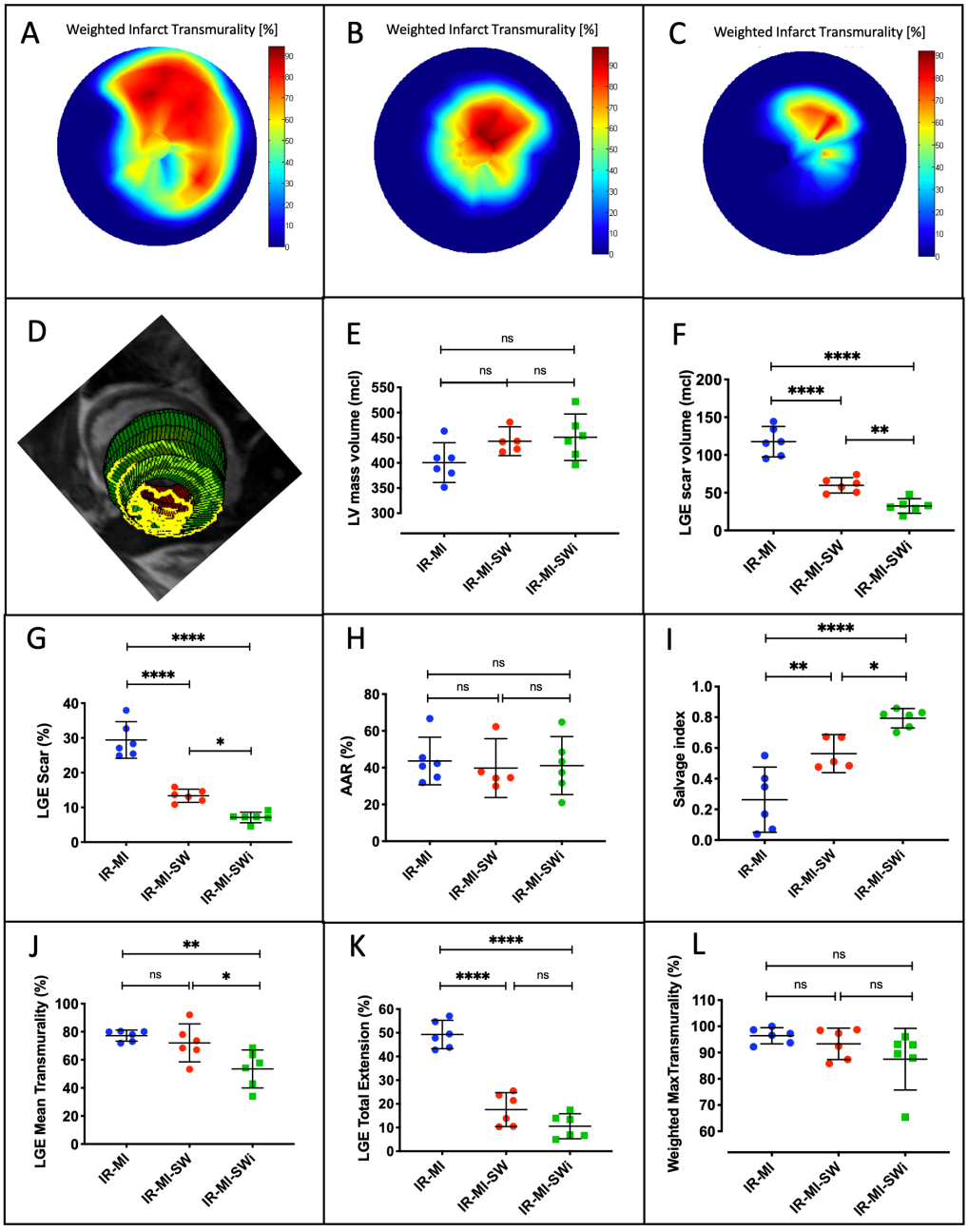

9.7.5 The Effect on Apical Rotation **Shockwave and DPP4i** on Segmental Myo Circumferential Strain Rate

9.7.5.1 Apical Rotation Between Layers of The Same Animal Group

9.7.5.1.1 I/R-MI

See **Figure 9-6A**. The mean apical rotation of the I/R-MI of the endo layer was significantly greater than the mean apical rotation of the I/R-MI of the epi layer, respectively showing mean ± SD of 11.88° ± 5.79 versus 5.02°± 1.08, *P* = .0330.

The mean apical rotation of the I/R-MI of the myo layer was similar to the mean apical rotation of the I/R-MI of the endo layer and the mean apical rotation of the I/R-MI of the epi layer, respectively showing mean ± SD of 6.48° ± 3.07 versus 11.88° ± 5.79 versus, *P* = .0798; versus 5.02°± 1.08, *P* = .3241.

9.7.5.1.2 I/R-MI-SW

See **Figure 9-6A.** The mean apical rotation of the I/R-MI-SW of the endo, myo and epi layers were similar, respectively showing mean ± SD of 8.42° ± 5.32, 5.58° ± 1.49 and 4.91°± 2.10, *P*= .4570.

9.7.5.1.3 I/R-MI-SWi

See **Figure 9-6A.** The mean apical rotation of the I/R-MI-SWi of the endo layer was significantly greater than the apical rotation of the I/R-MI-SWi of the epi

Figure 9-6. Scatter dot plot of comparing I/R-MI, IR-MI-SW and I/R-MI-SWi where (A) apical rotation according to layers within the same animal group, (B) apical rotation according to layers, (C) basal rotation according to layers within the same animal group, (D) basal rotation according to layers.

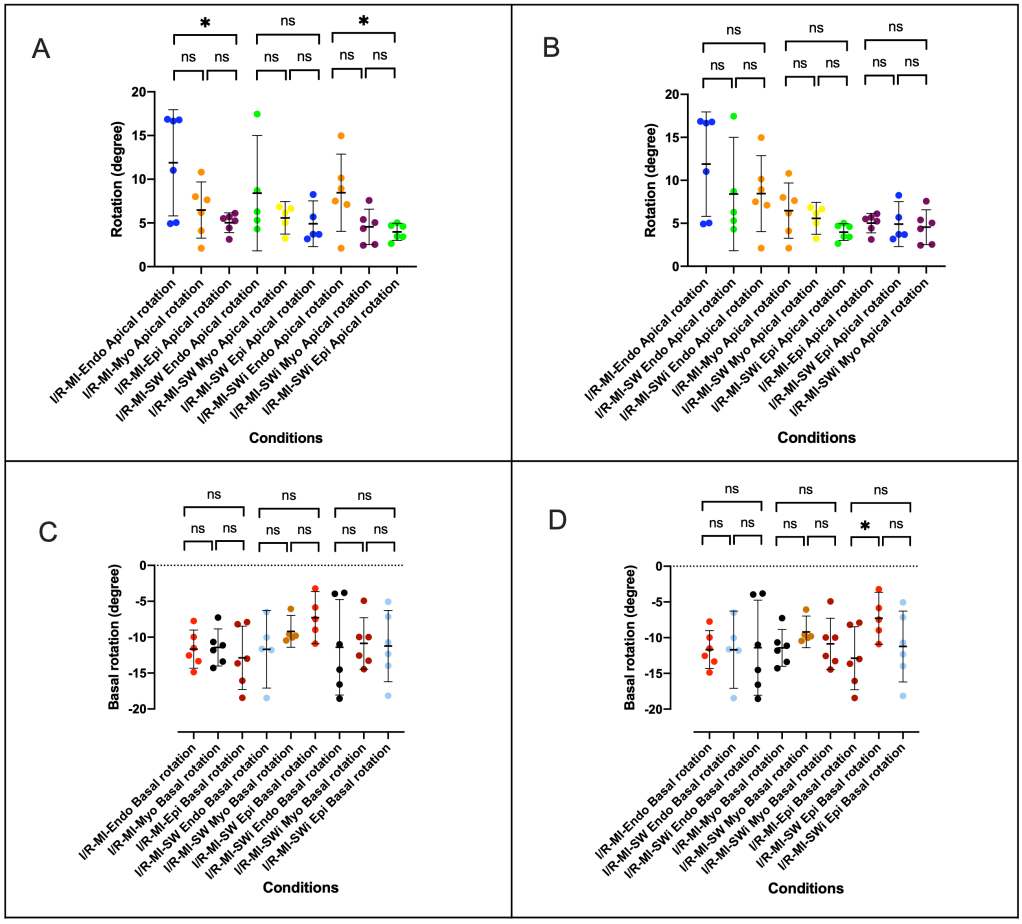

layer, respectively showing mean ± SD of 8.46° ± 4.21 versus 3.98°± 0.93, *P* = .0473.

The mean apical rotation of the I/R-MI-SWi of the myo layer was similar to the mean apical rotation of the I/R-MI-SWi of the endo layer and the mean apical rotation of the I/R-MI-SWi of the epi layer, respectively showing mean ± SD of 4.56° ± 1.93 versus 8.46° ± 4.21, *P* = .0796; versus 3.98°± 0.93, *P* = .5308.

9.7.6 Apical Rotation Comparison Between Layers

9.7.6.1 Endo

See **Figure 9-6B.** The mean endo apical rotation of the IR-MI, IR-MI-SW and IR-MI-SWi were similar, respectively showing endo apical rotation ± SD of 8.42° ± 5.32, 5.58° ± 1.49 and 4.91° ± 2.10, *P* = .4570

9.7.6.2 Myo

See **Figure 9-6B**. The mean myo apical rotation of the IR-MI, IR-MI-SW and IR-MI-SWi were similar, respectively showing myo apical rotation ± SD of 6.48° ± 3.07, 5.58° ± 1.49 and 4.56° ± 1.93, *P* = .4392.

9.7.6.3 Epi

See **Figure 9-6B**. The mean epi apical rotation of the IR-MI, IR-MI-SW and IR-MI-SWi were similar, respectively showing epi apical rotation ± SD of 5.02° ± 1.08, 4.91° ± 2.10 and 3.98° ± 0.93, *P* = .2648.

9.7.7 Basal Rotation Between Layers of The Same Animal Group

9.7.7.1 I/R-MI

See **Figure 9-6C**. The mean basal rotation of the endo, myo and epi layers of the I/R-MI were similar, respectively showing mean basal rotation ± SD of -11.67° ± 2.53, -11.43° ± 2.46 and -12.87° ± 4.21, *P* = .7820.

9.7.7.2 I/R-MI-SW

See **Figure 9-6C.** The mean basal rotation of the endo, myo and epi layers of the I/R-MI-SW were similar, respectively showing mean basal rotation ± SD of -11.68° ± 4.35, -9.19° ± 1.78 and -10.87° ± 3.42, *P* = .4213.

9.7.7.3 I/R-MI-SWi

See **Figure 9-6C.** The mean basal rotation of the endo, myo and epi layers of the I/R-MI-SW were similar, respectively showing mean basal rotation ± SD of -11.41° ± 6.34, -10.87° ± 3.42 and -11.23° ± 4.73, *P* = .9791.

9.7.8 Basal Rotation Comparison Between Layers

9.7.8.1 Endo

See **Figure 9-6D.** The endo basal rotation of the IR-MI, IR-MI-SW and IR-MI-SWi were similar, respectively showing endo basal rotation ± SD of -11.67° ± 2.53, -11.68° ± 4.35 and -11.41° ± 6.34, *P* = .9958.

9.7.8.2 Myo

See **Figure 9-6D**. The myo basal rotation of the IR-MI, IR-MI-SW and IR-MI-SWi were similar, respectively showing myo basal rotation ± SD of -11.43° ± 2.46, -9.19° ± 1.78 and -10.87° ± 3.42, *P* = .2625.

9.7.8.3 Epi

See **Figure 9-6D.** The mean epi basal rotation of the IR-MI was greater (more negative) than IR-MI-SW, respectively showing epi basal rotation ± SD of -12.87° ± 4.21 versus -7.28° ± 2.94, *P* = .0299.

The mean epi basal rotation of the IR-MI-SWi was similar to IR-MI and IR-MI-SW, respectively showing epi basal rotation ± SD of -11.23° ± 4.73 versus -12.87° ± 4.21, *P* = .5397; versus -7.28° ± 2.94, *P* = .1271.

The mean epi basal rotation of IR-MI-SW and IR-MI-SWi were similar, respectively showing epi basal rotation ± SD of -11.43° ± 2.46, -9.19° ± 1.78 and -10.87° ± 3.42, *P* = .2625.

9.7.9 Twist

9.7.9.1 Between Layers in The Same Animal Group

9.7.9.1.1 I/R-Mi

See **Figure 9-7E.** The means endo, myo and epi twist of I/R-MI were similar, respectively showing mean twist ± SD of 19.75°/mm ± 7.56, 17.08°/mm ± 4.06 and 16.56° ± 2.53, *P* = .6490.

9.7.9.1.2 I/R-MI-SW

See **Figure 9-7E.** The mean myo twist of I/R-MI-SW was significantly larger than the mean epi twist of the I/R-MI-SW, respectively showing twist ± SD of 13.12°/mm ± 2.39 versus 9.78° ± 1.52, *P* = .0345.

The mean endo twist of I/R-MI-SW was similar to the mean myo twist of I/R-MI-SW and mean epi twist of I/R-MI, respectively showing twist ± SD of 18.17° ± 7.09 versus 13.12°/mm ± 2.39, *P* = .1926; versus 9.78°/mm ± 1.52, *P* = .0057.

9.7.9.1.3 I/R-MI-SWi

See **Figure 9-7E**. The means endo, myo and epi twist of I/R-MI-SWi were similar, respectively showing mean twist ± SD of 18.83° ± 4.74, 14.09° ± 5.05 and 13.51° ± 3.97, *P* = .1526.

Figure 9-7. Scatter dot plot of comparing I/R-MI, IR-MI-SW and I/R-MI-SWi where (E) apical twist according to layers within the same animal group, (B) apical twist according to layers, (C) basal twist according to layers within the same animal group, (D) basal twist according to layers.

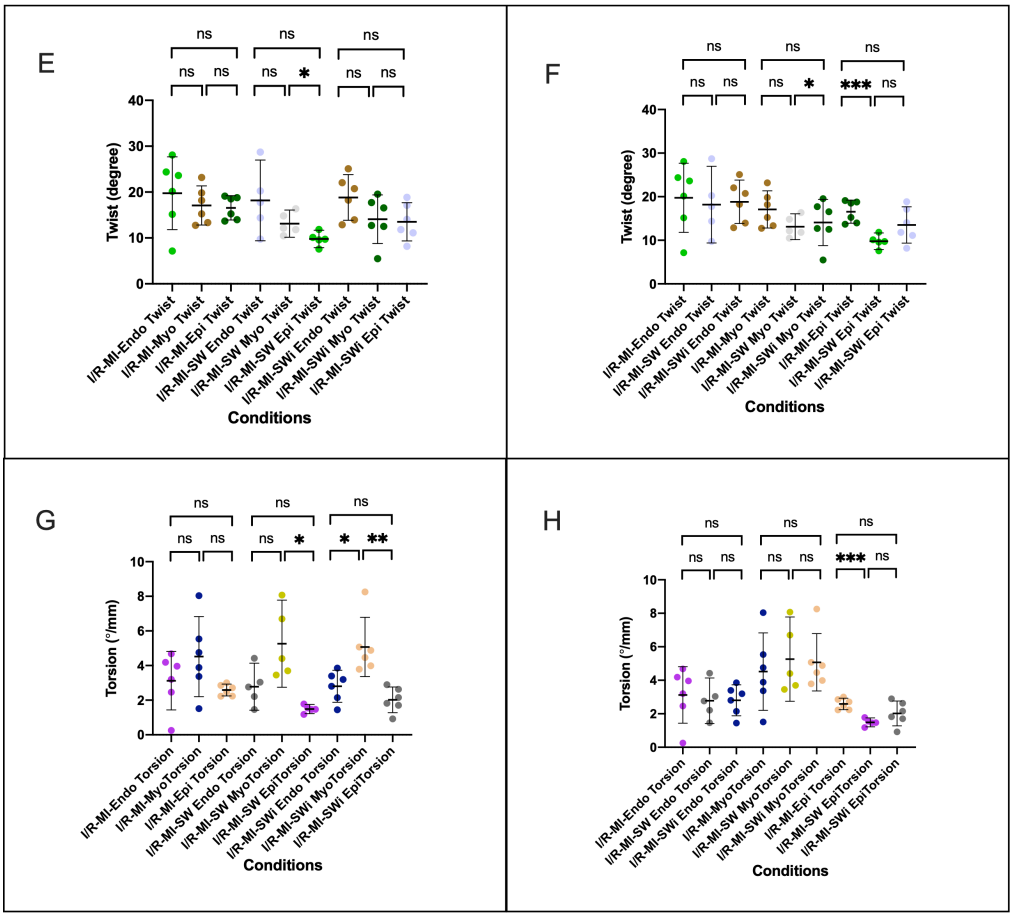

9.7.9.2 TWIST BY LAYERS BETWEEN ANIMAL GROUP

9.7.9.2.1 Endo

See **Figure 9-7F.** The mean endo twist of the I/R-MI, I/R-MI-SW and I/R-MI-SWi were similar, respectively showing mean twist ± SD of 19.75° ± 7.56, 18.17° ± 7.09 and 18.83° ± 4.74, P = .9416.

9.7.9.2.2 Myo

See **Figure 9-7F.** The mean myo twist of the I/R-MI, I/R-MI-SW and I/R-MI-SWi were similar, respectively showing mean twist ± SD of 17.08° ± 4.06, 13.12° ± 2.39 and 14.09° ± 5.05, *P* = .2069.

9.7.9.2.3 Epi

See **Figure 9-7F.** The mean epi twist of I/R-MI was significantly larger than the mean epi twist of I/R-MI-SW, respectively showing mean epi twist ± SD of 16.56° ± 2.53 versus 9.78° ± 1.52, *P* = .0005.

The mean epi twist of I/R-MI-SWi was similar to the mean epi twist of I/R-MI-SW and mean epi twist of I/R-MI, respectively showing epi twist ± SD of 13.51° ± 3.97 versus 9.78 ° ± 1.52, P = .0730; versus 16.56° ± 2.53, *P* =.1496.

9.7.10 Torsion

9.7.10.1 Between Layers in The Same Animal Group

9.7.10.1.1 I/R-MI

See **Figure 9-7G.** The means endo, myo and epi torsion of I/R-MI were similar, respectively showing mean torsion ± SD of 3.13°/mm ± 1.61, 4.52°/mm ± 2.20 and 2.59°/mm ± 0.32, *P* = .1683.

9.7.10.1.2 I/R-MI-SW

See **Figure 9-7G**. The mean myo torsion of I/R-MI-SW was significantly larger than the mean epi torsion of the I/R-MI-SW, respectively showing torsion ± SD of 5.27°/mm ± 2.03 versus 1.49°/mm ± 0.22. *P* = .0137.

The mean endo torsion of I/R-MI-SW was similar to the mean myo torsion of I/R-MI-SW and mean epi torsion of I/R-MI, respectively showing torsion ± SD of 2.78°/mm ± 1.10 versus 5.27°/mm ± 2.03, P = .0511; versus 1.49 °/mm ± 0.22, P = .0571.

9.7.10.1.3 I/R-MI-SWi

See **Figure 9-7G.** The mean endo torsion of I/R-MI-SWi was significantly smaller than the mean myo torsion of the I/R-MI-SWi, respectively showing torsion ± SD of 2.81°/mm ± 0.89 versus 5.08°/mm ± 1.63, P = .0181.

The mean myo torsion of I/R-MI-SWi was significantly smaller than the mean epi torsion of the I/R-MI-SWi, respectively showing torsion ± SD of 5.08°/mm ± 1.64 versus 2.02°/mm ± 0.71, P = .0043.

The mean endo torsion of I/R-MI-SWi was similar to the mean epi torsion of the I/R-MI-SWi, respectively showing torsion ± SD of 2.81°/mm ± 0.89 versus 2.02°/mm ± 0.71, P = .1214.

9.7.10.2 Torsion by Layers Between Animal Group

9.7.10.2.1 Endo

See **Figure 9-7H.** The mean endo torsion of I/R-MI, IR-MI-SW and I/R-MI-SWi were similar, respectively showing endo torsion of 3.13°/mm ± 1.61, 2.78°/mm ± 1.10 and 2.81°/mm ± 0.88, P = .9072.

9.7.10.2.2 Myo

See **Figure 9-7H.** The mean myo torsion of I/R-MI, IR-MI-SW and I/R-MI-SWi were similar, respectively showing myo torsion of 4.52°/mm ± 2.20, 5.27°/mm ± 2.03 and 5.08°/mm ± 1.64, P = .8391

9.7.10.2.3 Epi

See **Figure 9-7H.** The mean epi torsion of I/R-MI was significantly larger than I/R-MI-SW, respectively showing epi torsion ± SD of 2.59°/mm ± 0.32 versus 1.49°/mm ± 0.22, P = .0001.

The mean epi torsion of I/R-MI-SWi was similar to I/R-MI and I/R-MI-SW, respectively showing mean epi torsion ± SD of 2.02°/mm ± 0.71 versus 2.59 ± 0.33, P = .0097; versus 1.49°/mm ± 0.22, P = .1315.

9.8 Discussion

In this chapter, three groups of rats subjected to myocardial ischaemia-reperfusion injury were compared; the group either received no treatment (IR-MI) or treated with shockwave (IR-MI-SW) or treated with shockwave with DPP4 inhibition (IR-MI-SWi). The experimental treatment efficacy was assessed using CMR to quantify the volumetric indices, the global strains, circumferential strain rate, viability, and the rotational indices by myocardial layers.

The main finding of this chapter was the demonstration of the inotropic effect of shockwave in Healthy rats that could be reproduced in the diseased state of ischaemia-reperfusion injury. Furthermore, the inotropic effect of shockwave in ischaemia-reperfusion injury could be enhanced by DPP4 inhibition. Another major finding reported in this chapter is that shockwave have a rescue effect on the ischaemia-reperfusion injury, and the effect could too be further enhanced by DPP4 inhibition. The better functional outcome in treated groups was due to the effect on final infarct size, in addition to the inotropic effect.

On volumetric assessment, the LVEDV was not different by the status of IR-MI, IR-MI-SW and IR-MI-SWi. The status of IR-MI significantly increased the LVESV compared to IR-MI-SW and IR-MI-SWi. Conversely, the SV was reduced in the IR-MI compared to IR-MI-SW and IR-MI-SWi, whilst the SV between the IR-MI-

SW and IR-MI-SWi were not different. In effect, the EF of IR-MI-SWi was greater than that of IR-MI-SW and the least in the IR-MI. The heart rate was not different by the status of IR-MI, IR-MI-SW and IR-MI-SWi. The CO was less than the I/R-MI compared to IR-MI-SWi and not different between IR-MI-SW and IR-MI-SWi. The results indicate that the inotropic effect by shockwave was achieved without affecting chronotropy, which is a desirable approach in treating heart failure because of the associated mortality increase in the inotropic effect via adrenergic routes. [285] It is well established that adrenergic agonists could exert inotropy, however, accompanied by the unwanted chronotropic effect, which increases myocardial oxygen consumption and could worsen ischaemia. Further, the increase in systemic vascular resistance via the receptors would increase the afterload and, coupled with higher blood pressure, would put more stress on the diseased heart.

On global strain evaluation, which has better sensitivity than the volumetric indices, both the endo and myo GLS showed similar performance pattern, such that the I/R-MI has the least GLS (most positive), the I/R-MI-SWi was the highest GLS (most negative), and the I/R-MI-SW ranked in the middle. Both the endo and myo GCS also exhibited a similar pattern to GLS where the IR-MI was the least GCS compared to IR-MI-SW and IR-MI-SWi. However, the endo and myo GCS between IR-MI-SW and IR-MI-SWi were not different. The GRS

showed the strongest strain (most positive) in I/R-MI-SWi, followed by IR-MI-SW and IR-MI.

Strain rate imaging, being the least load dependent compared to other indices, evidently showed that the effect of shockwave on the intrinsic myocardial contractile was true. The results of the remote segment using myo circumferential strain rate showed the systolic regional function, S_{SR} was the weakest (less negative) in the Remote of IR-MI compared to the IR-MI-SW and IR-MI-SWi, while the S_{SR} of the IR-MI-SW and IR-MI-SWi were not different.

The regional diastolic function of the Remote was assessed using myo circumferential strain of $E_{SR,}$ A_{SR} and $E_{SR}/A_{SR.}$ The E_{SR} of the Remote in the of IR-MI was less than the E_{SR} of the Remote in the of IR-MI-SWi; on the other hand, the E_{SR} of the Remote of the Healthy, IR-MI and IR-MI-SW were similar. The A_{SR} of the Remote in the of IR-MI was the least, whist the A_{SR} of the IR-MI-SW and IR-MI-SWi were similar to the Healthy. The ratio of E_{SR}/ A_{SR} of the Remote in the IR-MI exhibited a restrictive pattern indicated by an increase in E_{SR}/ A_{SR} compared to the Healthy, IR-MI-SW and IR-MI-SWi, with the latter two carried similar values. The result indicated that shockwave treatment could preserve the regional systolic and diastolic function of the Remote.

The ability of shockwave to positively modulate both the systolic function and diastolic function simultaneously is unique and has not been described in the literature. The effect of known inotropic pharmacological agents on systolic

and diastolic function are discussed here. In normal human subjects, infusion of adrenaline increased indices of systolic function of the EF, SV and cardiac index in a dose-dependent manner; [286] however, could decrease in the atrial function and LV diastolic function. [287] Further, in heart failure patients infused with low dose dobutamine, even though the EF and SV had increased, the diastolic parameters did not improve.[288] On the other hand, noradrenaline administration on healthy volunteers reduced the stroke volume and cardiac output while elevating the blood pressure and systemic vascular resistance and impeded the diastolic function via prolonging the IVRT.[289] In patients with HFPEF, Sildenafil (PDE5 inhibitor) did not improve exercise capacity, LV systolic function, nor LV relaxation as demonstrated by RELAX trial. [290] A novel heart failure drug, myosin activator, omecamtiv was reported to exert an inotropic response via increasing the systolic ejection time with unchanged contractility (dP/dt) and diastolic function.[291]

In this chapter, the AAR was assessed using T2-mapping, where it was demonstrated that the size of oedema between the experimental groups of IR-MI, IR-MI-SW and IR-MI-SWi were not different. This was an important factor to control as the final infarct size could vary because the AAR were different, and it was controlled by perfecting the surgical technique in creating the models. It was reported in **chapter 9** that in the Healthy rats, shockwave did not change the T2 values. The discovery is unique to shockwave as

experimental cardioprotective drugs and preconditioning interventions in ischaemia-reperfusion injury have been reported to reduce AAR, minimising the positive effect. [292]

A second important factor to control was the LV masses, and this was achieved by using animals of similar weight. The LV masses between IR-MI, IR-MI-SW and IR-MI-SWi were not different. The LGE volume and percentage LGE to LV mass showed that the IR-MI has the strongest effect on LGE volume, while the IR-MI-SWi was less than the IR-MI-SW. Concordantly, the salvage index was the highest in the IR-MI-SWi and the least in the IR-MI. LGE transmurality reflected the depth of the scar/injury and an indication of severity. The LGE transmurality was less in the IR-MI-SWi compared to IR-MI-SW and the I/R-MI. The mean of LGE total extension both IR-MI-SW and IR-MI-SWi were around 10-15% compared to in I/R-MI when it was 50%. These results support the hypothesis that DPP4 inhibition to shockwave has an additive rescue effect in reducing ischaemia-reperfusion injury.

One of the mechanisms of inotropy was revealed by the study of torsion. The myo torsion of I/R-MI-SW and I/R-MI-SWi were both stronger than the epi torsion in both groups. Additionally, in the I/R-MI-SWi, the myo torsion was also stronger than the endo torsion. In I/R-MI, the torsion of the endo, myo and epi were not different. There was no difference in the endo, myo and epi torsion of the I/R-MI. The epi torsion of I/R-MI was stronger than the epi

torsion of the IR-MI-SW and IR-MI-SWi, while the epi torsion of the IR-MI-SW was not different to IR-MI-SWi.

The apical rotations within the same layer amongst groups of IR-MI, IR-MI-SW and IR-MI-SWi were not different. It is known from **chapter 6** that shockwave does not increase the apical rotation. However, between layers within the individual group of IR-MI, IR-MI-SW and IR-MI-SWi, the apical endo rotation was stronger in the IR-MI than the IR-MI-SWi, indicating the compensatory mechanism was activated in IR-MI for the maintenance of cardiac output. As the magnitude of the apical rotational of the layers in the IR-MI-SW and IR-MI-SWi were similar to that of the Healthy; it could be deduced that the requirement for the activation of the compensatory mechanism of the apex was not required and superfluous when the infarction sizes were already reduced in IR-MI-SW and IR-MI-SWi.

9.9 Limitations

The limitations detailed in section 5.8 are also applicable to the experiments in this chapter, namely on the use of anaesthesia, in-bred rats and male rats only. Even though IR-LGE has been validated in rats and mice myocardial infarction models by other groups, [293] [294] it would have been best had the infarct size also been assessed by histology for assurance that the models were robust and reliable. Superlatively, a control group for shockwave therapy could

have been included on the presumption that the treatment had the desired positive effects.

9.10 Conclusion

In conclusion, the results in this chapter are supportive of the application of shockwave in reducing final infarct size in ischaemia-reperfusion injury, and the effect could be further enhanced by DPP4 inhibition, leading to better functional outcome.

Chapter Ten

RESULTS: CELLS HOMING

10.1 Clinical Perspective

This research in this chapter was motivated by the desire to non-invasively home progenitors to the heart using shockwave via the SDF1/CXCR4 axis. All cellular therapy trials to date used cells that were first harvested from their niches (such as the marrow, adipose tissue, peripheral blood, cardiac explants), then purified in the laboratory under GMP, and some cell products were expanded before finally reinjected into the heart using various surgical methods (such as the intracoronary, intramuscular, open chested during

CABG, NOGA system). Imaging-based studies of stem cells tracking have demonstrated that cells retention in the heart, regardless of the methods of surgical delivery is poor, with most of the cells end up in the spleen and liver.[14] A therapeutic intervention that could home the cells better could deliver improved outcome for patients. It is rationalised that as the cells are already present in the patients' body, they simply need to be mobilised and homed to the heart, making obsolete the need of surgical means to artificially home the cells to the heart. The results from stem cells clinical trials are so far are modest in magnitude. [10] This could be explained by poor cell homing, poor cell survival and the fact that a single dose might not be enough to promote sustained improvement in the left ventricular function.[11] It is economically not viable to perform multiple sessions of cells injections using procedures that carry clinical risks.

10.2 Introduction

Shockwave as an inductor for SDF1 expression in tissue, could be specifically targeted to regions of interest on the heart, and via CXCR4, the receptor for SDF1 that are expressed in many stem cells and immune cells, could promote cells homing. The interaction of SDF1/CXCR4 is known to activate the integrin and other attachment molecules that are essential for cells retention and

survival.[13] Stem cells exert their regenerative effect partly or mostly through paracrine factors, [12] hence the importance to maximise the time of contact.

10.3 Purpose

The main purpose was to discover whether shockwave could be used to home progenitors to the heart.

10.4 Aims

The experiments aim to seek evidence of cells homing assessed using MRI, the effect on tissue oxygenation, to discover the effect of shockwave on the markers of interest in the PBMC and the effect on SDF1 expression in cardiac tissue.

10.5 Objectives

Objectively, cell homing was assessed by a drop in T2 MR relaxation, an indication that iron-loaded cells have migrated to the heart having been treated by shockwave. The angiogenic effect of shockwave was studied using T2* to derive the BOLD MRI signal when an increase in BOLD signal used as an indication of improved tissue perfusion. The expression of SDF1 in cardiac tissue was assessed using immunohistochemistry using DAB staining for detection of SDF1 in cardiac tissue. The effect on CD90, CD34 CD45 population on the peripheral blood was assessed using multi-colour flow cytometry.

10.6 Hypotheses

Cells homing to the heart can be detected using T2 MR relaxation when T2 decreases with shockwave treatment in rats pre-treated with iron, indicating cells homing. The angiogenic effect of shockwave can be detected using BOLD-MRI, detected as an increase in BOLD signal intensity in the shockwave group versus untreated controls. Shockwave therapy decreases the frequency of the CD markers of interest in the PBMC. Shockwave increases the abundance of SDF1 detected in cardiac tissue in rats with DPP4 inhibition than shockwave alone.

10.7 Methods

10.7.1 Experiment 1: Iron

10.7.2 Animal Characteristics

Healthy male Lewis rats were used in this experiment following the housing requirement stated in **section 3.2.**

10.7.3 Experimental Design

The experimental design is illustrated in **Figure 10-1** detailing the experimental timeline of Day 0, Day 3 and Day 6; and the five groups of animals, where group 1 defined Healthy untreated rats that had not received any experimental intervention up to MRI, group 2 defined as Healthy rats treated with shockwave only on day 3, group 3 defined as Healthy rats treated with

intravenous iron only on day 0, group 4 defined as Healthy rats treated with iv iron on day 0 and then treated with shockwave on day 3, and group 5 defined as Healthy rats treated iv iron on day 0 and daily DPP4 inhibition then shockwave. On day 3. All animals were scanned with MRI on day 7.

10.7.4 Personal Preparation

A white coat, a mask and a pair of nitrile gloves were worn during animal handling, as described in **section 3.3.**

10.7.5 Iron Administration

Light sedation was induced in the rats using isoflurane in an induction box, placed on a preheated mat, and the sedation was maintained with the animal breathing 2% isoflurane in 100% oxygen on the nasal cone. During tail warming, the animal was positioned in a supine, its tail dipped in warmed tap water for 5 minutes to induce hyperemia. The tail was wiped clean with a tissue, and it would appear pink after the dirt had been removed. The tail then sterilized with 2% chlorhexidine wipes (Clinell, GAMA Healthcare) and the animal was positioned to its side for easy access to the lateral vein. The base of the tail was taped down, gentle traction was applied, and the tail was slightly curved downward where the needle to be inserted. At the eye level, a winged 26g cannula over needle (Terumo, UK) was used to cannulate a lateral vein. The needle was initially inserted deep enough to withdraw a blood flashback

and then advanced very slightly by 1mm, and the needle then fixed whilst the rest of the cannula advanced into the vein. The needle was then withdrawn, and the cannula connected to a pre-prepared 1ml syringe containing the desired dose of Ferinject (50 mg iron/ml, Vifor Pharma UK Limited) to be administered. The dose of Ferinject for rats was 80mg/kg, given undiluted by slow iv injection, and immediately followed by a saline flush. The cannula was removed, and the puncture site applied pressure on for a few minutes to stop bleeding.

Figure 10-1. Experimental schedule showing timeline day 0, day 3 and day 6, when respectively iv iron, shockwave and MRI occurred. A tick sign in the table indicates treatment or test was administered and a cross sign indicates the treatment was not administered. 1 to 5 are groups of rats.

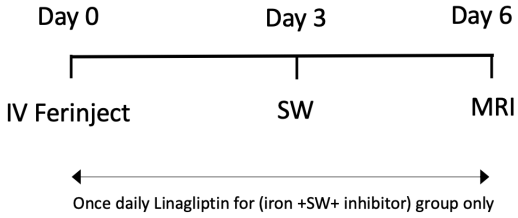

1. Untreated control	✗	✗	✓
2. SW only	✗	✓	✓
3. Iron only	✓	✗	✓
4. Iron + SW	✓	✓	✓
5. Iron + SW + inhibitor	✓	✓	✓

10.7.6 DPP4 Inhibition

In group 5, Linagliptin administered daily via oral gavage as previously described in **7.8.3.**

10.7.7 Shockwave

In group 2, 4 and 5, shockwave was administered 3 days before shockwave. The method has been previously described in **7.8.5.**

10.7.8 Cardiac MRI

The animal preparation for the MRI scan was as previously described in **7.8.5.** All MRI scans were performed three days 3 days after shockwave for group 2, 4, and 5; and three days after intravenous Ferinject for group 3.

10.7.8.1 T2-Mapping Acquisition and Analysis

Whole heart T2-mapping was performed using seven short-axis slices with no gaps, which covered the whole of the left ventricle. The MRI acquisition method has been described in **7.8.6.** Each T2 parametric short-axis slice image was constructed from 6 echo times images fitted to 2PL on the basis of pixels, divided into 6 segments except at the apex the slice divided into 4 segments. The median value for the pixels in the sector was used because the pixel spread was usually non-Gaussian. The segmental T2 values of the animal groups 1-5 were compared. The shortening of T2 value was an indication that more iron had been deposited in the heart.

10.7.9 Immunohistochemistry

10.7.10 Heart Preparation for Cryosection After Explantation

After a scan, when the animal was still under anaesthesia, it was euthanised by neck dislocation followed by a secondary confirmation of death by exsanguination of femoral bleed. The heart was rapidly removed via midline thoracotomy, placed in a 50ml conical tube, blood completely washed off via PBS exchanges, then into 4% PFA in PBS. The PFA was refreshed a few times, and the heart then left submerged overnight at 4°C in 4% PFA 20x its volume.

The next day, the PFA was replaced with sucrose solution in PBS for cryoprotection following these steps: 10% Sucrose (15 min or until sample drops to the bottom of the tube), 2:1 10% sucrose:30% sucrose (15 min or until sample drops to the bottom of the tube), 1:1 10% sucrose:30% Sucrose (15 min or until sample drops to the bottom of the tube), 1:2 10% Sucrose:30% Sucrose (15 min or until sample drops to the bottom of the tube), 30% Sucrose (15 min or until sample drops to the bottom of the tube) 30% sucrose (15 min or until sample drops to the bottom of the tube) and finally 30% sucrose (15 min or until sample drops to the bottom of the tube).

10.7.11 Embed the Heart in OCT

The heart was removed from the conical tube, the excess sucrose pad dried with tissue paper (Kimwipes), then transferred to a 5ml flat-bottom breakable

plastic Bijou containing 2.5ml OCT suspended vertically. The Bijou vial with OCT and the heart then placed in a pre-chilled Isopentane (Sigma-Aldrich) in a beaker under dry ice.

It was crucial to embed the heart vertically during freezing so that sectioning could be performed with ease in the same slope direction of the OCT block bottom, perpendicular to the long axis of the heart. The Bijou vial then screw-capped, appropriately labelled and transferred to a -80°C freezer until use.

10.7.12 Cryosection

The cryosection was performed using Leica CM1850 Cryostat. The Bijou vial was broken to retrieve the OCT block containing the heart, then left to equilibrate inside the Cryostat at 17°C for at least 30 minutes to soften the OCT for sectioning. The heart was sectioned at 5-10µm thickness, stuck onto a slide (SuperFrost® Plus), air dried, permeabilize in cold 100% methanol for 10 minutes and let dry in the chemical hood. If not used immediately, the slides were stored in a -80°C freezer.

10.7.13 Iron Staining and Imaging

For iron staining the slide, the was hydrated with deionized water, then submerged in pre-prepared iron staining solution (1:1 of 4% w/v Potassium Ferrocyanide Solution and 1.2mM Hydrochloric Acid Solution) for 10 mins, then rinsed in deionized water, stained further with Pararosaniline solution

(1:50 Pararosaniline hydrochloride, 1% w/v, in methanol) for 5 minutes, rinsed in deionized water, dehydrated through alcohol and xylene, and mount. The slides were allowed to dry up overnight. The tissue sections on slides were imaged using a wide-field microscope Zeiss Axio Observer (HWF1), the micrograph tiles stitched in Zen Blue software for edge-to-edge image reconstruction of a whole heart section and viewed in Fiji ImageJ for Mac version 2.0.

10.7.14 Experimental Design for Experiment 2 (BOLD)

10.7.14.1 Animals

3 Healthy Lewis rats that received extracorporeal shockwave therapy were compared with 3 untreated Healthy controls; the hearts imaged 3 days later using T2* imaging to derive BOLD signals.

10.7.14.2 BOLD Imaging

The concept of BOLD-MRI is graphically illustrated in **Figure 10-6A.** BOLD-MRI uses the contrast from paramagnetic Deoxyhaemoglobin (decreases T2*) and diamagnetic Oxyhaemoglobin (increases T2*). As oxygenation blood in the myocardium is received during diastole, the difference of in T2* between early diastole and late systole is the BOLD signal intensity. If shockwave on tissue had an angiogenic effect, the BOLD signal would increase as tissue oxygenation was expected to increase with better blood supply. As there was an inevitable

trigger delay, the end systole (EnS) and early diastole (ErD) were respectively set three frames before aortic valve closure, and three frames after aortic valve opening visualised on the three-chamber view.

10.7.15 BOLD MRI Method

Throughout the scan, the animals' oxygenation levels were monitored and kept constant. For each slice, T2* maps, using multi-gradient echo, were acquired in the end systole (EnS) and early diastole (ErD), analysed in Segment (Medviso-AB, Lund), to obtain the pixel-wise T2*-map using 2-PL curve fitting. BOLD SI was calculated as the difference of the median values of segmental T2* value of ErD–EnS.

10.7.16 Experimental Design for Experiment 3: Flow Cytometry

10.7.16.1 Animal

3 Healthy male Lewis rats (weight >500g) were used in the experiment for longitudinal assessment before and after shockwave.

10.7.16.2 Experimental Design

The timeline is illustrated in **Figure 10-2**. Blood was sampled before shockwave, three days after shockwave and seven days after shockwave.

Figure 10-2. Experimental timeline indicating number of days of blood sampling and shockwave events relative to each other.

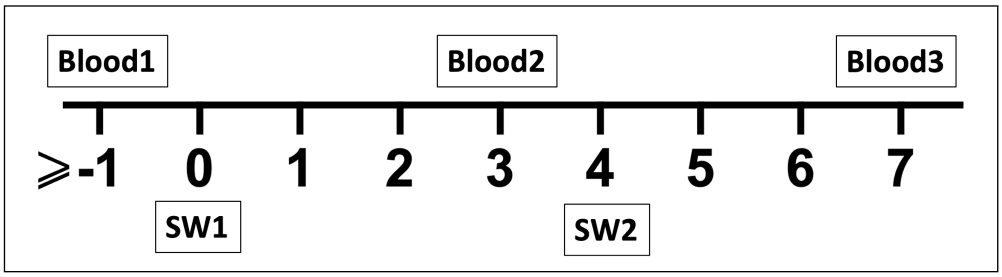

10.7.16.3 Blood Sampling

The technique was an extension of tail vail cannulation. After successful cannulation, the cannula was connected to a 1ml syringe prefilled with 3.2% buffered sodium citrate of volume ratio to blood 1:9 as an anti-coagulant. Blood was allowed to be passively withdrawn into the syringe to avoid haemolysis, to a predefined volume and homogeneously mixed with sodium

citrate by multiple gentle inversions. Blood was sampled at 3 days and 7 days after shockwave.

10.7.16.4 Separation for Mononuclear Cells

10.7.16.4.1 Gradient Centrifugation

The density of the peripheral density of mononuclear cells of rats is slightly higher than that from humans, and commercial gradient for human cannot be optimally be used without adjusting the osmolality first, or else issues of contamination from neutrophils and reduction in separation efficacy could ensue. The density barrier was prepared by diluting Iodixanol (Optiprep, Alere Technologies AS) to 1.077g/L by diluting 60% Iodixanol with buffered saline (prepared to 242mOSm) at a ratio of 2.7:9.3. Rat's blood was diluted with an equal volume of isosmotic buffered saline preprepared by mixing 0.85% of NaCl buffered n HEPES pH 7.4. The diluted blood then overlaid over a density barrier. The tube was centrifuged at 700G in a swing-out bucket at room temperature, which would separate the blood into four layers from the top diluted plasma, mononuclear cells, buffered saline and red blood cells. The top layer was aspirated and discarded. The mononuclear cells layer was harvested and washed in two volume of HEPES buffered saline, pelleting the cells by centrifugation at 400G.

10.7.16.5 Antibodies Conjugation

The pelleted cells were counted using LUNA-FL™ Dual Fluorescence Cell Counter, and the viability was assessed by staining an aliquot using AO/PI straining; orange colour indicated dead cells and green colour indicated non-viable cells. The cells concentration in aliquots adjusted using the formula $C_1V_1 = C_2V_{2.,}$ where C represents concentration and V represents volume. A Mastermix of antibodies CD45 (VioBlue), CD31 (VioBrightFITC), CD34 (APC) and CD90 (PerCPVio700; and a Mastermix of their respective isotype controls were prepared. All antibodies were sourced from Miltinyi, except for the CD34 antibody, which was sourced from Novus Biologicals.

Three tubes were prepared, each with 1 million viable cells: one tube of unstained cells for autofluorescence, one tube for antibodies panel of interest and one tube for isotype controls; the latter two processed as the following. The cells were suspended 100mcl PBS, and 1mcl Viobility dye (405/520) added. It was important to ensure the buffer was free of protein as the dye binds to free protein limiting its efficacy. It was incubated at room temperature for 15 minutes, then washed, pelleted down and resuspended in 60mcl PBS with 0.5% BSA and 2mM EDTA (Buffer). Then 20mcl FcR Blocking (BD) Reagent added to the cells, incubated for 10 minutes, then washed, pelleted down. The cells then added to antibodies Mastermix to a total adjusted volume of 50mcl using the Buffer, incubated at 4°C for 10 minutes, then washed, pelleted down and fixed using Inside Fix (contains 3.7% formaldehyde, Miltinyi).

10.7.16.6 Flow Cytometry

BD LSR II, a four-laser benchtop flow cytometer onlined to FACSDiva software was used to assess the cells using voltage and compensation settings determined during a validation run of single and combination cell staining compared with the isotype controls. At least 50,000 events were acquired. The data was exported in FCS format and analysed in FlowJo 10.6.1 for Mac.

10.7.16.7 Gating Strategy

The fluorescence spillover emissions were compensated using the settings of Fluorescence Minus One (FMO) determined during a validation run of single stains and combination cell staining. On the Forward Scatter (FSC) by Side Scatter (SSC), the cells were gated for singlets (gating out debris and non-viable cells) using the polygon tool to include cells along the diagonal line. Then, the time of flight (TOF) inspected to ensure only the events in a stable flow stream were included. The non-viable cells were gated out by positive selection. The axes of biaxial plots were displayed in biexponential transformation for better separation of the positive and negative populations than the standard logarithmic scale to ensure the width set high enough that all of the data in the histogram was visible. The cells of the biaxial plots were visualised in pseudocolour density mode and gated using quadrants; the boundaries decided upon from the inspection of the isotype controls indicating the

negative population. The cells were plotted CD90 by CD45. Q1 and Q2 quadrants were further interrogated, whether positive or negative for CD34. The samples population relative abundance of before shockwave, three days after shockwave and seven days after shockwave.

10.7.17 Experiment 4: SDF1 Tissue Staining

10.7.17.1 Animal

3 male Lewis rats in each group of treatment were used: a group with water gavage only; a group with pretreatment with water gavage and shockwave; a group with pretreatment with water gavage of Linagliptin and then shockwave. Two gavages before shockwave, and the animals were sacrificed the day after shockwave treatment.

10.7.17.2 Immunohistochemistry

The hearts were prepared for immunohistochemistry (frozen section) using similar methods described in section **10.7.10, 10.7.11 and 10.7.12.** After blocking with BSA (Sigma), the tissue sections were incubated with rabbit anti-rat SDF1 primary antibodies (Invitrogen) and goat anti-rabbit HRP-conjugated secondary antibodies (Vector Lab); rinsed in buffer and then incubated with DAB working solution (Vector Labs) and once developed, rinsed in water. The tissue sections were then counterstained using hematoxylin (Vector Lab), rinsed with buffer and then dehydrated with 100% ethanol. The slides were

mounted, allowed to dry overnight and imaged using microscope Zeiss Axio Observer. The DAB substrate used for chromogenic detection of HRP to yield insoluble brown bands if positive for SDF1. Hematoxylin stained all the tissue section. The HRP-DAB reaction is schematically presented in **Figure 10-3**.

10.7.18 Image Analysis

Using the plugin tool of Colour Deconvolution in Fiji, the RGB colour of the micrographs was deconvoluted into colour 1 (blue), colour 2 (brown) and colour 3 (green). Colour 3 (green) micrographs were not used in the analysis. Thresholding then applied to highlight the brown stain in colour 2 to red and hematoxylin colour 1 to black. ROI of similar sizes and coordinates applied both images to determine the percentage of the fractional area of DAB/ hematoxylin.

Figure 10-3. A schematic of SDF1 detection on frozen tissue section using HRP-DAB immunohistochemistry.

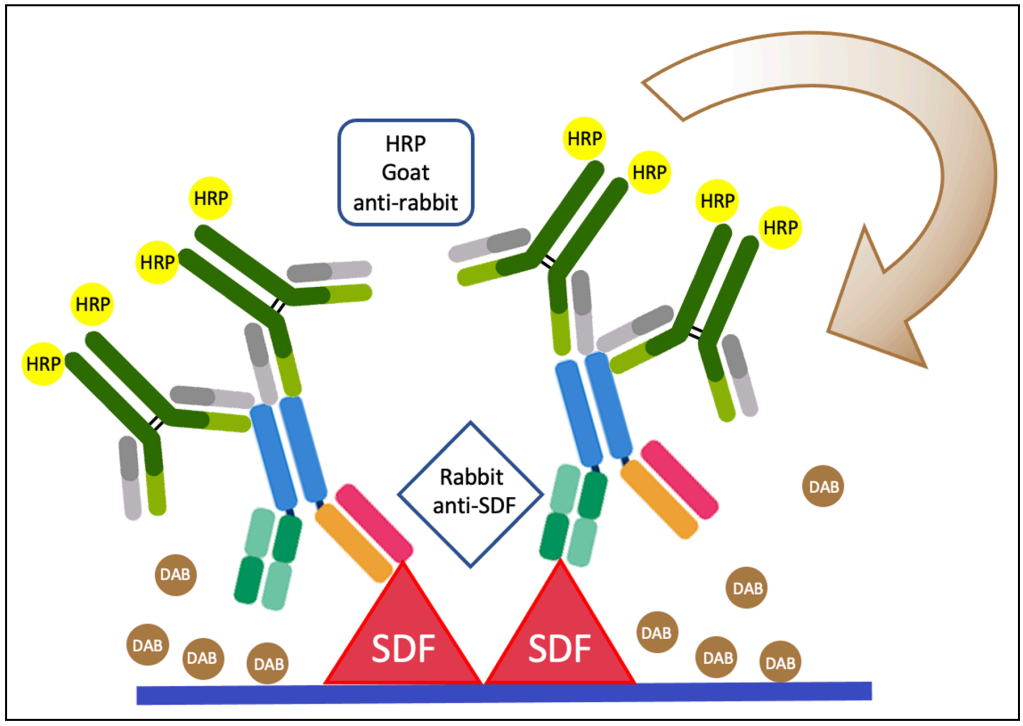

10.8 Results

10.8.1 Segmental T2-Mapping

The results are summarised in **Figure 10-4** and **Table 10-1**.

Brown-Forsythe and Welch ANOVA tests showed significant differences between subjects ($P < .0001$). There was no significant difference between the mean T2 values of the segments of the untreated Healthy rats and SW only rats ($P > .9999$), respectively showing mean T2 ± SD of 18.6ms ± 3.79 versus 19.1ms ± 4.3. The T2 values of the segments of Iron only group were significantly smaller than that of SW only rats ($P < .0001$) and untreated Healthy rats ($P < .0001$); respectively showing mean T2 ± SD of 16.6ms ± 1.9 versus 19.1ms ± 4.3; versus 18.6ms ± 3.8.

With the addition of SW treatment to iron, there was a further significant reduction in T2 values compared to iron only group ($P < .0001$); compared to SW only group ($P < .0001$); and compared to untreated Healthy rats ($P < .0001$), respectively showing mean T2 ± SD of 14.5ms ± 2.4, 19.1ms ± 4.3 and 18.6ms ± 3.8; and the test for trend showed a significant slope of 1.15 ± SEM 0.20, $P < .0001$. There was no significant difference between the Iron + SW group versus DPP4i iron + SW ($P=.2534$), respectively showing a mean T2 ± SD of 14.5ms ± 2.4 versus 15.3ms ± 2.5. The T2 values of the segments in the DPP4i + iron+SW group was smaller than untreated Healthy rats ($P < .0001$), SW only rats ($P <$

.0001) and iron only group (*P*=.0003); respectively showing mean T2 ± SD of 15.3ms ± 2.5, 19.1ms ± 4.3 and 16.6ms ± 1.

10.8.2 Immunohistochemistry

10.8.2.1 Iron Staining

The micrograph of the heart cross-sections showed signs of iron deposition by Prussian Blue, indicated by bright blue staining on the cytoplasm, stained light pink by Pararosaniline. See **Figure 10-5**.

Figure 10-4. Scatter dot plot Each dot is a myocardial segment according to experimental conditions group. The error bars are the 95%CI of mean. The middle bar is the mean. Untreated rats (4 rats, 129 segments), SW rats (4 rats, 138 segments), iron only rats (3 rats, 97 segments), iron+SW, (4 rats, 136 segments) and DPP4i+iron+SW (3 rats,102 segments). NS is no significant, *<.05, ** P < .01, ***, P < .001, and **** P < .0001.

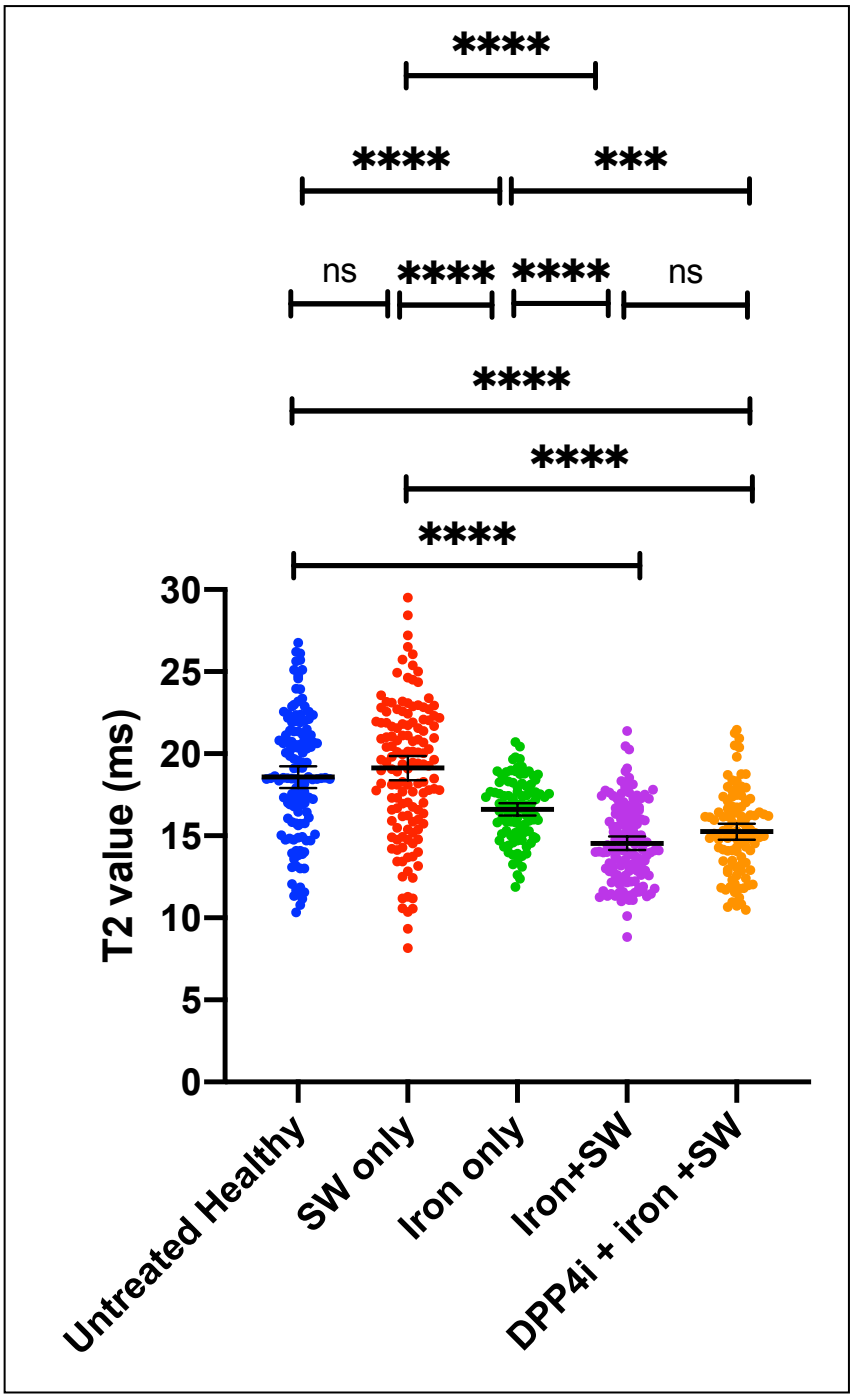

Table 10-1. Table showing multi-group comparisons of the experimental conditions, showing mean difference, 95% CI of difference, level of significance and the adjusted *P* value using † Dunnett's T3 multiple comparisons test. NS is no significant, *<.05, ** P < .01, ***, P < .001, and **** P < .0001.

Group comparisons	Mean Diff.	95.00% CI of diff.	Significant?	Summary	Adjusted *P* Value †
Iron only vs. Iron+SW	2.068	1.205 to 2.932	Yes	****	<.0001
Iron only vs. Untreated Healthy	-1.971	-3.151 to -0.791	Yes	****	<.0001
Iron only vs. DPP4i + iron +SW	1.358	0.395 to 2.322	Yes	***	.0003
Iron only vs. SW only	-2.515	-3.787 to -1.244	Yes	****	<.0001
Iron+SW vs. Untreated Healthy	-4.039	-5.239 to -2.840	Yes	****	<.0001
Iron+SW vs. DPP4i + iron +SW	-0.7100	-1.697 to 0.277	No	ns	.2534
Iron+SW vs. SW only	-4.584	-5.873 to -3.294	Yes	****	<.0001
Untreated Healthy vs. DPP4i + iron +SW	3.329	2.058 to 4.601	Yes	****	<.0001
Untreated Healthy vs. SW only	-0.5441	-2.059 to 0.971	No	ns	>.9999
DPP4i + iron +SW vs. SW only	-3.874	-5.230 to -2.517	Yes	****	<.0001

Figure 10-5. Prussian Blue (counterstained with Congo Red) histology of heart cryo-section of a rat pre-treated with iv iron and then shockwave showing iron deposition where iron pigments are bright blue, nuclei are red, and cytoplasm is light pink.

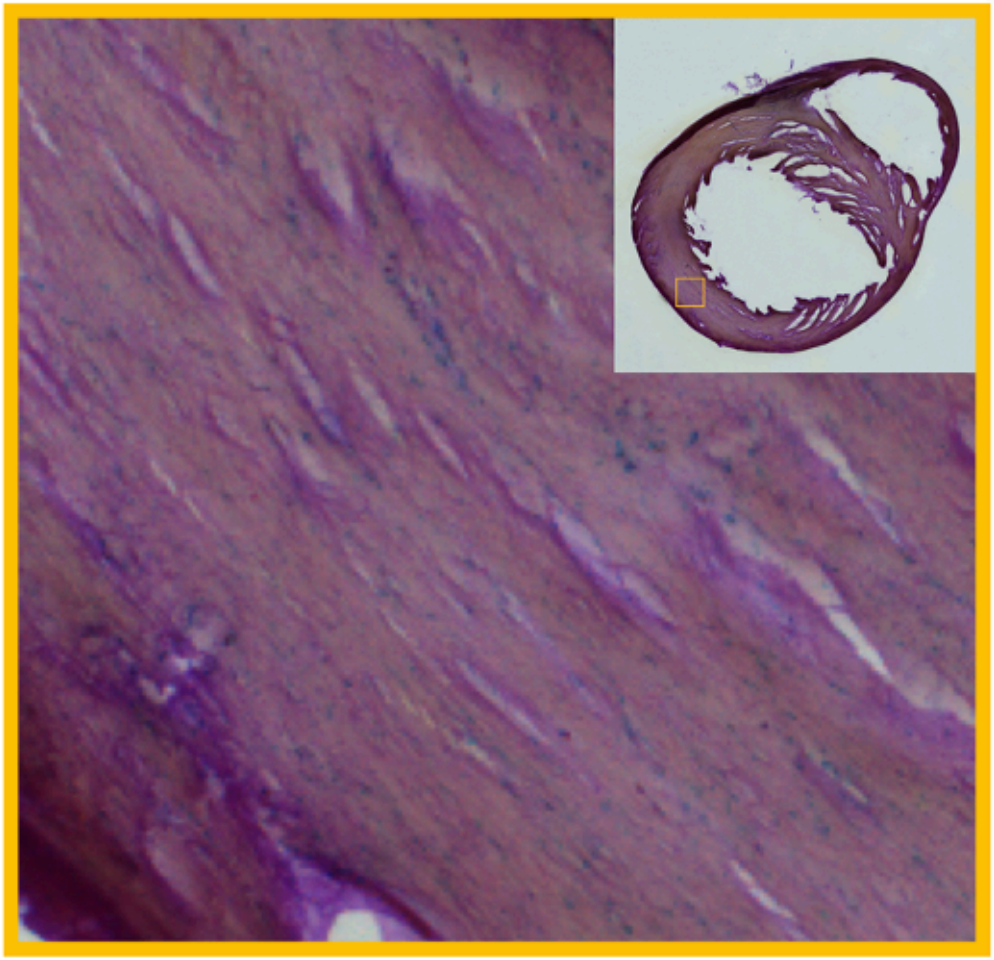

10.8.3 BOLD MRI

The results are graphically presented in **Figure 10-6B.** The BOLD signal intensity of the untreated controls had characteristics: 34 segment pairs, median 0.46ms, 95%CI 0.23-0.91ms, whereas the shockwave group have 28 segment pairs, median 1.56ms, 95%CI 1.03-2.59ms. Two-tailed Mann Whitney test comparing the two groups showed P = .0002, U=222.5 with a significant increase in a positive direction in the shockwave group. The photographs of the heart revealed an increase in epicardial vessel vascularity.

Figure 10-6. (A) Red dash lines conceptualise coronary flow which increases during diastole; the chart compares pixel-wise T2 star relaxation in a myocardial segment at the end systole and early diastole; the difference is the BOLD signal. The error bars in both charts indicate the 95% CI of the medians. (B) Bottom: Scatter dot plot chart comparing the BOLD signal in untreated control versus SW. (B) Top: Photographs of heart exterior immediately after euthanisation, showing increase vascularity of epicardial vessels.

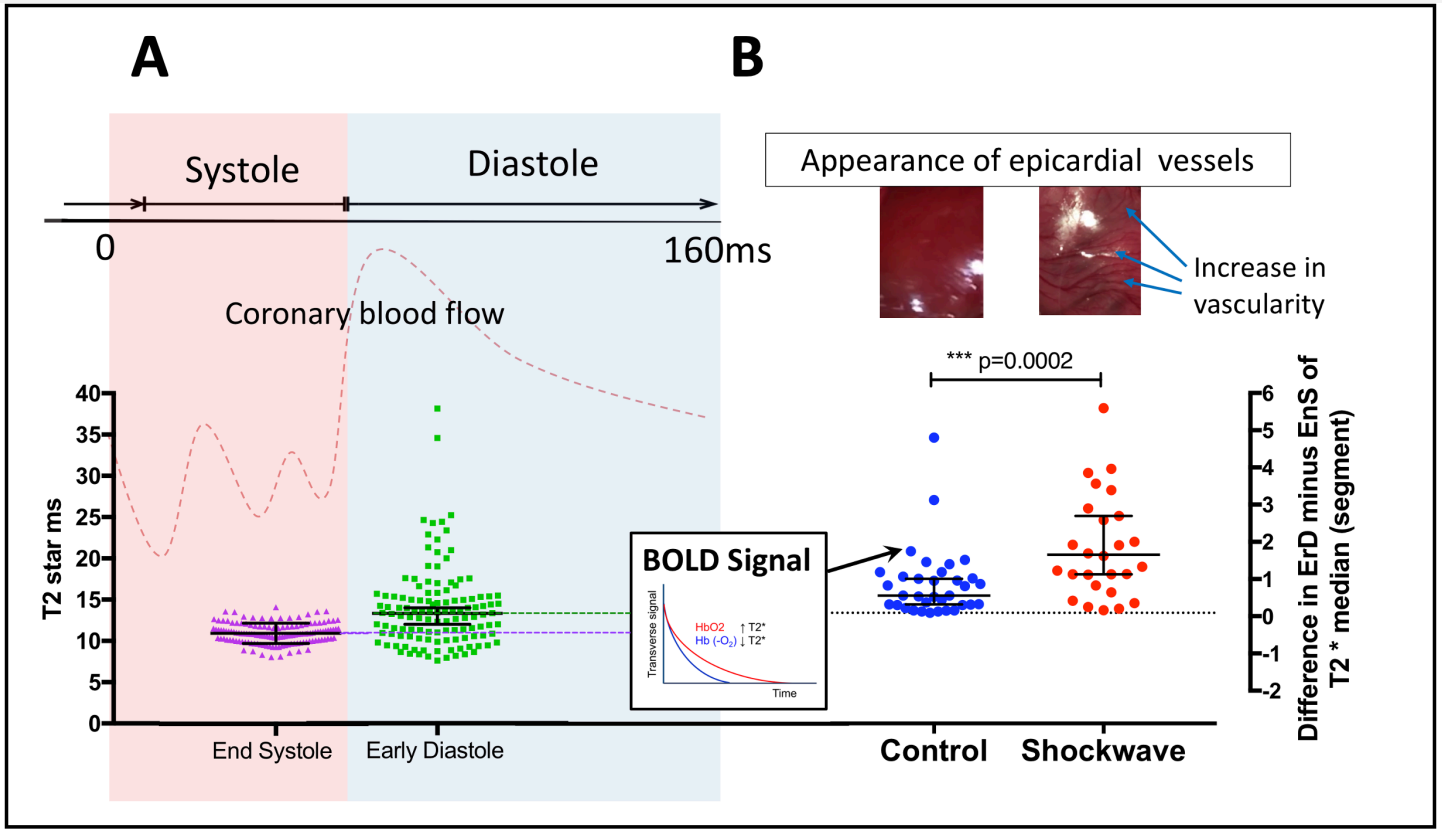

10.8.4 Multi-Colour Flow Cytometry

The results of density biaxial plots are presented in **Figure 10-7**

10.8.4.1 CD45- CD90+ (Q1)

See **Figure 10-8A.** The analysis of Q1 of plot CD90 by CD45 showed a significant drop in the relative abundance of CD45- CD90+ population of the pre-shockwave to Day-3 post shockwave (*P* = .0121) to Day-7 post shockwave (*P*= .0018), respectively showing relative abundance mean ± SD of 50.7% ± 7.6, 27.9% ± 7.3 and 17.0% ± 4.2. There was no significant difference between Day-3 post shockwave and Day-7 post shockwave, *P* = .1848.

10.8.4.2 CD45+ CD90+ CD34+

See **Figure 10-8B.** The analysis of Q2 for CD34 showed a significant drop in the relative abundance of CD45+ CD90+ CD34+ population of the pre-shockwave to Day-3 post shockwave (*P* = .0173) to Day-7 post shockwave (*P*= .0301), respectively showing relative abundance mean ± SD of 0.45% ± 0.09, 0.07% ± 0.05 and 0.04% ± 0.02. There was no significant difference between Day-3 post shockwave and Day-7 post shockwave, *P* = .6921.

Figure 10-7. Biaxial plot of CD90 vs CD45 at (A) pre shockwave, (B) 3 days post of shockwave, (C) 7 days post shockwave, (D) Q1 of A for CD34 marker, (E) isotype control for B, (F) isotype control for C, (G) unstained cells pre shockwave, (H) Q1 of C for CD34 marker, (I) unstained cells at 7 days

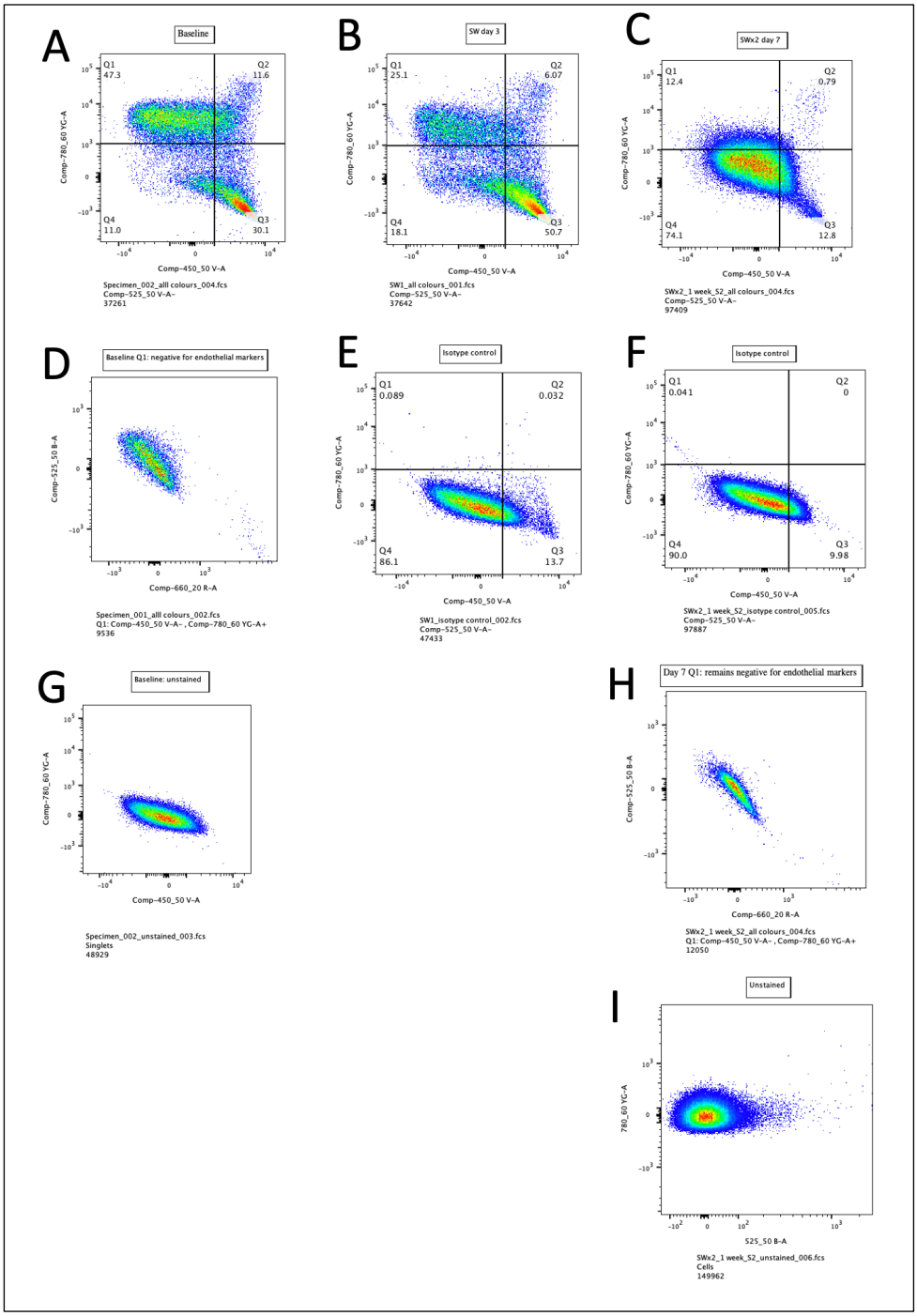

Figure 10-8. Scatter dot plot comparing the relative abundance of time course of baseline (pre-shockwave), Day-3 post shockwave and Day-7 post shockwave of (A) CD45+ CD34+ population and (B) CD45- CD90+ population. The middle bars indicate the mean, and the lower/upper bars indicate the SD.

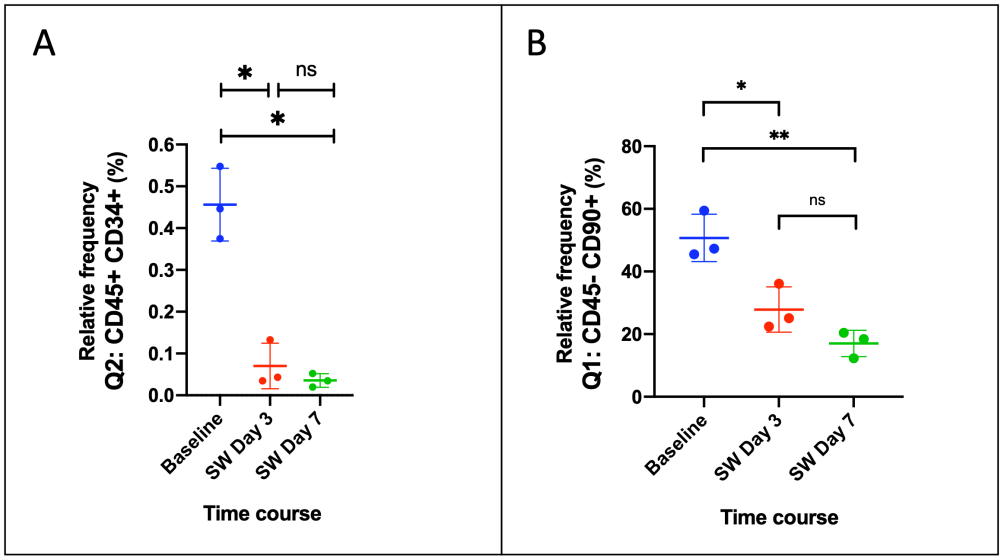

10.8.5 SDF1 Immunohistochemistry

The results are summarised in **Figure 10-9**. The median percentage of ROI fractional area of DAB/Hematoxylin in water gavage + SW group was significantly greater than water gavage only group (P = .0382) and significantly less than DPP4 inhibitor + SW (P = .0382), respectively showing median ± IQR of 12.53% (5.07, 20.00), 3.43% (1.42, 5.44) and 21.50% (15.88, 27.12). The median percentage of ROI fractional area of DAB/Hematoxylin of DPP4 inhibitor + SW group was significantly higher than the water gavage only group (P < .0001).

Figure 10-9. Micrographs of DAB/Haematoxylin stains of rats receiving (A) water gavage only, (B) water gavage and shockwave and (C) DPP4 inhibition and shockwave. (D), (E) and (F) respectively threshold of colour 1 in black of micrographs A, B and C. (G), (H) and (I) are respectively threshold of colour 2 in red of micrographs A, B and C Scatter. (J) Scatter dot plot of % of ROI fractional area of deconvolution of DAB/Haematoxylin. The bars signify the median with interquartile range. DAB staining indicates localisation of SDF1 expression.

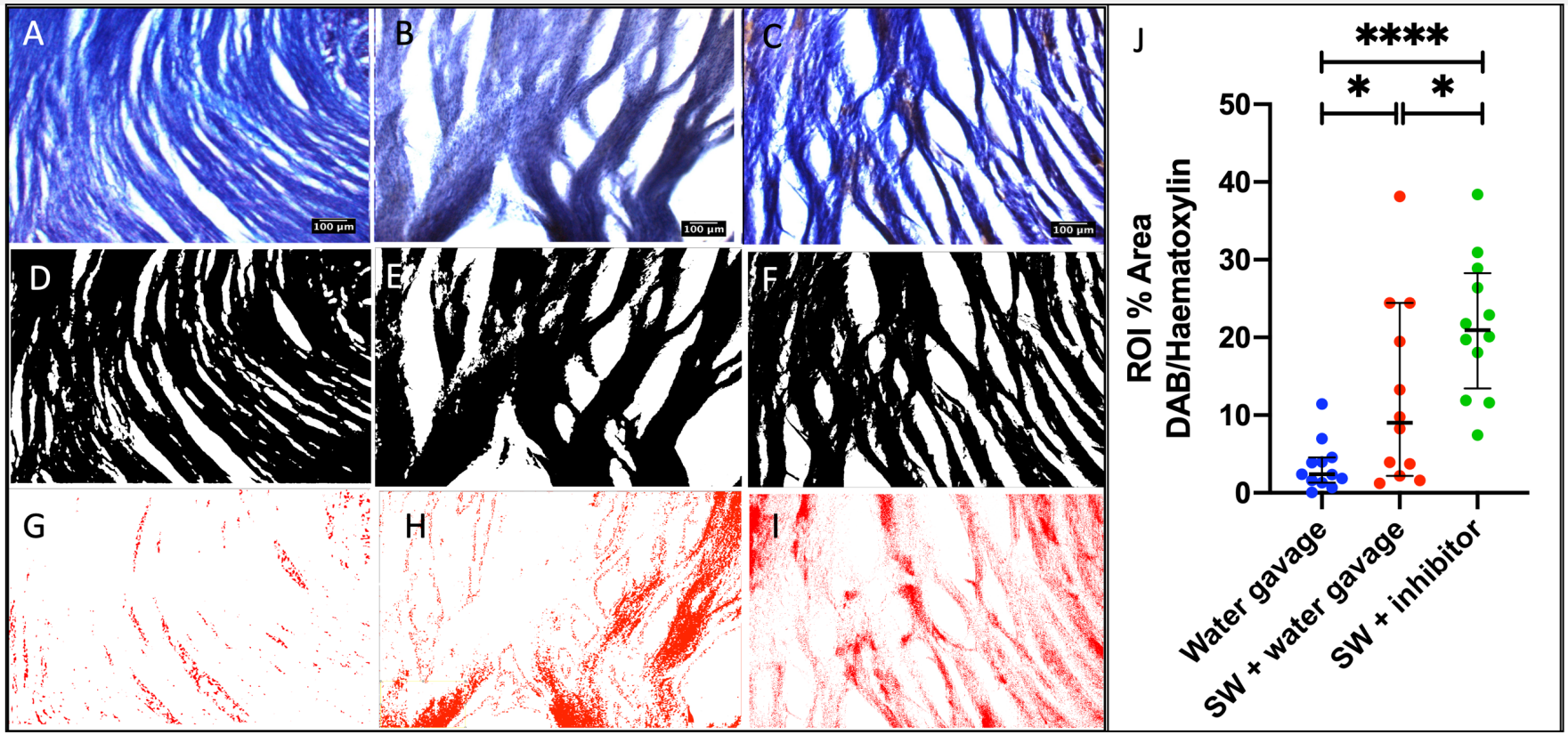

10.9 Discussion

In this chapter, iron was used to detect cell homing to the heart. The animals were intravenously injected with clinical-grade ferric carboxymaltose (Ferinject, VIFOR Pharma) for *in vivo* labelling of progenitors and used to create MRI contrast. The pharmacokinetics of the drug indicated the iron would be taken up by cells in the marrow and reticuloendothelial system. Ferric carboxymaltose is a clinically approved drug as a treatment for iron deficiency anaemia and classed as ultra-small super-paramagnetic iron oxide nanoparticles (USPION), being less than 50nm, allowing uptake into cells. Iron oxide has an unpaired extra electron which becomes aligned in the direction of a magnetic field. Consequently, iron itself became a magnet and attracted to another magnet, with an effect of paramagnetism when the T2 is shortened, which is the opposite of the effect of gadolinium which increases the T1.

Several studies have used *in vivo* iron labelling techniques, and they have indicated that iron could label stem cells and immune cells. For example, a study by Khurana et al. [295] has shown that *in vivo* intravenous injection of iron (ferumoxytol) could label marrow mesenchymal stem cells, and the iron could still be detected in the progeny of *ex vivo* expansion. The presence of iron in these cells were exhaustively demonstrated by electron microscopy, confocal microscopy and fluorescence microscopy and Prussian blue staining. The cells

then injected into the rats' knees and evaluated by MRI, showing shortening of the T2 signal, confirming detection. This study serves as a validation that one of the cell population that could be homed to the heart following shockwave could be marrow mesenchymal in origin.

In a study by Montet-Abou et al., [296] rats were pretreated with intravenous fluorescent iron oxide nanoparticles and ischaemia–reperfusion myocardial infarction was then induced. The dual labelling system allowed *in vivo* tracking of the cells by MRI and optical imaging. It was identified that the circulating monocytes before myocardial infarction contained iron, and after myocardial infarction, the MRI T2 signal had dropped, indicating that the iron-loaded monocytes or macrophages had infiltrated the infarcted cardiac tissue. Immunohistochemistry showed the presence of fluorescent and iron-loaded cells in infarcted territory against CD68. Furthermore, anti CCL5 reduced the frequency of CD68. This study supports the notion that the identity of the cell that one of the cell population that could be homed to the heart following shockwave could be monocytes or macrophages in origin. Iron oxide has been used to label haematopoietic stem cells, T cells and induced pluripotent stem cells. [297]

In this chapter, it was observed *in vivo* that the T2 values of the heart segments in rats receiving intravenous iron was lower than Healthy untreated rats, indicating iron uptake in the heart. Three days were allowed to pass after iron

injection to ensure blood T2 was not masking the readout. In the cardiac tissue, however, the background effect on T2 remained detectable at three days after intravenous iron injection. This could be explained by the fact that the heart is capable of iron storage, a role that could be undertaken by the Tissue-resident macrophages (Kupffer cells). [298] Most importantly, it was demonstrated that shockwave reduces the T2 beyond the T2 effect of the iron tissue background, indicating more iron deposition in the heart, a surrogate indicator cells containing iron had been homed to the heart. Furthermore, Prussian blue histology confirmed the presence of iron in the tissue matrix and verified that the drop in T2 MRI was because of iron deposition. DPP4 inhibition with shockwave did not lower the T2 values of myocardial segments beyond shockwave when assessed at day 3, and this could reflect the limited quantity of cells pre-labelled with iron or the new progenitors since iron injection did not contain iron and avoided detection. The identities of the progenitors that had migrated to the heart following shockwave were most likely were the combinations of marrow cell populations of mesenchymal and haemopoietic stem cells, and immune cells; the confirmation of their true identity would involve a large panel of markers ideally performed using a high-throughput technique such as the imaging mass cytometry, [299] or genetic lineage methods,[300] and these are outside the scope of the thesis.

It was not previously known what effect shockwave had on the MR T2 values of the heart. In cardiac ischaemia-reperfusion injury, an elevated T2 was used as a surrogate for oedema, used to quantify area at risk and in the calculation of salvage index **(Chapter 9**). An increase in T2 with shockwave, if it did, would cause an overestimation of AAR, and an underestimation of salvage index, preventing the usefulness of the method in AAR quantification in shockwave experiments. Here, it was demonstrated that shockwave did not increase the myocardial T2 but could instead increase the BOLD signal in the myocardial segments of rats receiving shockwave treatments. Deoxyhaemoglobin being paramagnetic resulted in the shortening of the T2*, and with oxygenation, the level of deoxyhaemoglobin decreased, causing the T2* to lengthen; the difference of the T2* acquired at the end of systole and early diastole was the BOLD signal, and this was used to assess for tissue oxygenation level which was dependent on the blood supply. It would have been more ideal if the acquisition of BOLD was performed in a slightly hypercapnic state; however, the setup was not possible in pre-clinical imaging. Here, it was demonstrated as a proof-of-concept that BOLD-MRI was a feasible method to quantify angiogenesis *in vivo*. Arterial Spin Labelling (ASL) could also have been useful, but the development time needed for the sequence was outside the timeframe of the project. It has been reported in a clinical study that the rest

and stress BOLD-CMR could be used to differentiate myocardial segments with and without ischaemia. [301]

This chapter reported an increase in the vascularity of the epicardial vessels in the shockwave treated hearts on gross tissue examination, in keeping with findings by other researchers that showed shockwave could induce angiogenesis. Zimplfer et al. performed a histological analysis of the anterior walls of LAD infarction rat models showing a significant increase in the microvascular density of the small, medium and large vessels, as well as the presence of more vWF+ endothelial cells in the shockwave-treated group compared to untreated control and untreated-posterior segments of rats with LAD infarction. [302] Holfeld et al. experimented on mice hind-limb ischaemia models treated with shockwave and discovered that there were more vessels per high-power field in shockwave treated limbs and better laser Doppler perfusion index compared to untreated controls. The phenomenon was attributed to the increase in angiogenic growth factors VEGF-A, VEGF-B and PlGF, observed 72 hours after shockwave treatment. [303]

The results of immunochemistry staining for SDF1 using DAB-HRP reaction has shown that more SDF could be detected in shockwave group with DPP4 compared to shockwave with water gavage, and the group with the water gavage only group exhibiting the least DAB staining. DAB was a chromogenic substrate which produced a brown reaction product in the presence of

peroxidase (HRP) enzyme, which was conjugated with SDF1 detection antibodies, so a proportional increase of SDF1 expression was indicated by stronger brown straining. The finding is in line with the fact that DPP4 inhibition reduces the breakdown of SDF1 and hence higher detectable abundance on DAB staining.

Multi-colour flow cytometry showed a drop in the relative abundance of CD45-CD90+ and CD45+ CD90+ CD34+ populations at Day-3 post shockwave and persisted by Day-7 post-shockwave compared to the pre-shockwave level. CD45 is a protein tyrosine phosphatase found on most haematopoetic cells except the erythrocytes and plasma cells, and the co-expression of CD35 with CD45 indicates haematopoetic progenitors. The CD45-CD90+ PBMC population represented non-haematopoetic progenitors inclusive of mesenchymal stem cells. It is acknowledged that there are other subgroups of CD45+ CD34+ and CD45-CD90+ that could be investigated, but for the purpose of this chapter, these markers have provided sufficient read-outs for the detection of the abundance of haematopoetic progenitor and mesenchymal stem cells in the peripheral blood circulation. Furthermore, there was a limit of blood volume that could be sampled *in vivo*, and a large panel of markers would require higher blood volume than permissible, or else the resolution of cell events required by statistical analysis could not be achievable. In human, the enumeration of mobilised haematopoetic stem cells for leukapheresis and

transplantation in haematological diseases uses the ISHAGE protocol, [304] which uses the *in vitro* diagnostic kit containing monoclonal antibodies of CD34 and CD45 (Stem-Kit, Beckman Coulter). Haematological reconstitution using CD45+ CD34+ cell product following marrow ablation has not been an issue and provides the reassurance that these markers truly represent haematopoietic stem cells. Here, a drop in the abundance of CD45+ CD34+ and CD45-CD90+ cells in the peripheral blood circulation indicated cell 'consumption'. As there was no other experimental intervention delivered to the rats except cardiac shockwave, it could be deduced that these cells, known to co-express CXCR4, had migrated to the heart via the chemotaxis action of SDF1, in line with the increase in DAB staining in the histological finding. Blood sampling on Day-7 post shockwave showed the populations had not recovered, indicating that the rate of cells consumption (homing) was greater than the rate of cells being released in the circulation. It cannot be excluded the possibility that the new progenitors since iron injection did not contain iron and avoided detection. In practical terms, cells overconsumption is unlikely to happen in human as shockwave focal size is very small and, in a rat, the focal size would cover the entire heart. Indeed, if this is true, and if the desire is to home more progenitors becomes necessary, for example, because the dose-effect was not sufficient, the problem could be mitigated by using a pharmacological cell mobiliser. Shockwave was reported in **chapter 6** to be able to induce inotropy.

As the inotropic effect was immediate, very unlikely homing of progenitors was required for the inotropic effect to occur, reflecting the many roles SDF1 could play, such as in the cardiac contractility, cell homing, and limiting infarction size in ischaemia-reperfusion injury. Cell homing is, however, relevant in the limitation of ischaemia-reperfusion injury and adverse cardiac remodelling.

A cell mobiliser of interest is the parathyroid hormone because of the side effects profile is good and reported efficacy. PTH, in addition to being an inhibitor to DPP4, can also activate osteoblasts with the effect to decrease osteopontin,[305] which is a negative regulator of marrow stem cell pool size. [306] Osteopontin deficiency results in increased stem cell numbers with enhanced expression of endothelial cell receptor tyrosine kinase Tie-2 and Notch ligand Jagged 1, and decreased level of stem-cell apoptosis. Studies using genetically modified OPN knock out (OPN−/−) mice have shown that OPN deficiency increases bone marrow stem-cell pool size. PTH directly stimulates angiogenesis on endothelial progenitor cells via the avβ3/P13-K/AKT/eNOS/NO signalling pathway.[307] PTH administration following myocardial infarction is known to attenuate ischemic cardiomyopathy via neovascularization, reduce infarct size independent of GCSF action and via recruitment of CXCR4+ stem cells to ischemic hearts. [308] The serum PTH level was positively correlated with the cells number, and there was an associated increase in serum SDF1-a and VEGF. Unlike GCSF, PTH mobilises a constant

level of lin-/Sca-1+/c-kit+ cells and CD45+/CD34+ subpopulations of the bone marrow without depleting the bone marrow.[309]

10.10 Limitation

The limitations detailed in section 5.8 are also applicable to the experiments in this chapter, namely on the use of anaesthesia, in-bred rats and male rats only. In retrospect, immunohistochemistry could have been performed to assess for cell homing directly. Immunohistochemistry, however, has limitations that immune and stem cell markers may not persist at the time point used for CMR, and different cohorts of animals would have been needed to screen for different populations of cells on different days. For example, the monocytes could transform into macrophages, and there are different types of macrophages (M1, M2a, M2b, M2c). Learning from the experience of the origin of c-kit and rebuttal of cardiac stem cells [310] over a decade which was first identified using immunohistochemistry,[311] it would not have been very straightforwardly to identify the cells using immunohistochemistry without genetic lineage tracing or cell-labelling technique. The histological technique demonstrated by Zimplfer et al. could have been applied to assess angiogenesis.

10.11 Conclusion

In conclusion, the results in this chapter are supportive of the use of shockwave as a non-invasive method to home progenitors to the heart. The demonstration of cell homing using iron labelling was highly effective, a fast and simple method in answering the research question. Non-invasive homing of progenitors using shockwave could provide a clinically advantageous therapeutic technique over surgical cells delivery methods.

Chapter Eleven

RESULTS: SDF1 EXPRESSION IN CELLS AND TISSUE

11.1 Clinical Perspective

There is no clear consensus on how to treat a diseased heart with mixed segmental phenotypes (such as viable tissue but ischaemic: stunned, hibernation; or non-viable: mostly scared) using shockwave, and whether to treat from the central core outwards or inward; and how often. The main compositions of cardiac tissue according to cell types are the cardiomyocytes (70-85%), [312] with the rest constitutes of endothelial cells (60%), fibroblasts (<20%) and hematopoietic-derived cells (5–10%). [313] In the diseased states, for example, in infarcted cardiac segments, there is fibrosis and a reduction in the capillary density. It is not clear what cell type would respond to shockwave and

temporal changes in gene expression after shockwave treatment; the knowledge would help rationalise shockwave treatment protocol. Gene expression experiment could help answer whether it is worthwhile to treat scar tissue if, for instance, no chemokines could be induced *in situ* by shockwave.

11.2 Introduction

SDF1 is of interest because of the positive effect on ischaemia-reperfusion injury and the effect on cells homing reported via SDF1/CXCR4 axis in hind limb ischaemia models. [314] [4] As the skeletal myocytes and cardiomyocytes are phenotypically and physiologically distinct, it was unclear whether shockwave could induce SDF1 expression in the heart tissue. If it could, it is not clear what cells types are responsible for SDF1 expression. Moreover, there could be other associated gene expression with SDF1 gene expression with shockwave. In this chapter, the cell types of relevance to cardiac tissue were assessed using quantitative polymerisation chain reaction (q-PCR) for SDF1 expression following exposure to radial shockwave of at least two energy levels.

The gene of interest (GOI) in this chapter are the CXCL12, VEGFA, MCP1, ANG1, TAC1 (substance P), NOS3 and IGF1, which transcripts were respectively responsible for the production of stromal derived factor 1 (SDF1), vascular

endothelial growth factor A, monocyte chemotactic factor 1, angiopoietin 1, substance P, nitric oxide synthase 3 and insulin derived factor 1.

11.3 Purpose

The purpose of the experiments in this chapter was to discover the cell types responsible for SDF1 (and other GOI) expression and to discover a suitable shockwave dose for the induction of SDF1 gene expression.

11.4 Aim

The experiments aimed to screen for SDF1 (and other GOI) expression on cell types relevant to cardiac tissue following shockwave treatment using qPCR.

11.5 Objectives

Objectively, samples from human umbilical vascular endothelial cells (HUVEC) were used to represent the endothelial cells, cardiomyocytes of both rat and human in origin, Langendorff of Spontaneously Hypertensive Rats and human cardiac fibroblast from explants of failing hearts, were assessed at several acute time points after exposure to shockwave depending on the experimental design laid out in the sections below.

11.6 Hypothesis

After shockwave treatment, the endothelial and fibroblast cells express SDF1 (and other GOIs) in a different temporal pattern. Shockwave increases SDF1 (and other GOIs) expression in whole cardiac human ventricular tissue and the rat Langendorff hearts.

11.7 Method

11.7.1 Personal Preparation

The personal protection equipment consisted of wearing a laboratory coat and a pair of clean gloves in the wet laboratory.

11.7.2 HUVEC

11.7.2.1 Culture

The HUVEC used in the experiments were kindly donated by the veterinarians of the Royal College of Veterinary Medicine. Cells from multiple donors were used to serve as biological replicates in the experiments. For assurance that the cells were in a proliferative state, only P3-P5 were used in the experiments. The HUVEC were grown in Lonza EGM2 (Lonza) supplemented with Bullet-kit containing: 0.5ml hEGF, 0.5ml Hydrocortisone, 0.50 mL Gentamicin with Amphotericin B, 2ml BBE, Ascorbic Acid and 10ml FCS. The exact composition of the supplements was not disclosed by the manufacturer.

HUVEC was grown in filter-capped TC treated flasks: T75 flasks (Falcon) to increase cells quantities and finally seeded in T15 flasks (VWR, UK) for shockwave experiments. The flasks were coated with 0.1% gelatin in PBS (Sigma) for at least 10 minutes at 37°C prior use to enhance cells attachment. The excess gelatin was removed by rinsing with PBS. The HUVEC were counted and seeded evenly at the density of 2-4x10^4 cells/cm^2. The culture media was exchanged 24 hours after seeding and every 2 days until reaching 80% confluency. The cells attachment and growth were observed under an inverted microscope and exhibited epithelial-like morphology.

The procedure for cells passaging was a common method for both the HUVEC and human cardiac fibroblasts. The flask was removed from the incubator, sprayed with 70% ethanol and transferred inside the hood. The media was emptied from the flask using a serological pipette to a beaker and to be discarded later. TrypLE™ Select Enzyme (1X), no phenol red (Gibco) was added to the culture flask and ensured to completely cover the whole monolayer. The flask was then incubated at 37°C in an incubator for 5 minutes, after which cells detachment was checked under a microscope. The flask was tapped a few times to help detach the cells, and then the cells suspension in TrypLE™ Select Enzyme transferred to a 15ml conical tube. The cells were sedimented under centrifugation at 400G, either washed

11.7.2.2 Cryopreservation

Excess cells were cryopreserved in 20% DMSO in supplemented EBM2 in cryovials, stored in Mr Frostie (Nalgene) at -80°C overnight and then transferred to the vapour phase in the nitrogen tank. When cells were required, the cells were thawed in 37°C water bath by swirling until only a small ice crystal present in the tube, then prewarmed EGM2 added dropwise, then transferred to a 15ml conical tube, topped up with EGM2 to 10ml and centrifuged for 5 mins at 400G. The supernatant aspirated out and discarded; the pellet resuspended with fresh EGM2, plated in a T75 flask and incubated in 5% CO_2 incubator at 37°C.

11.7.2.3 Experimental Design

The number of flasks with HUVEC needed to be prepared was determined from the experimental design. Each flask was for one time point and one shockwave dose only. There were three time points: time point 0, 2hrs, 4 hours, 6 hours, 24hours and 48 hours. The doses of shockwave used were: 1.0Bar x 1000, 1 Bar x 2000, 2.0 Bar X 1000, 2.0 Bar x 2000.

11.7.2.4 Shockwave Administration to Cells

Shockwave administration setup was similar to shockwave administration to the cardiomyocytes (see **chapter 8**, section **8.6.7**); the only difference was in place of the dish was a flask. Briefly, the flask was wrapped in Parafilm (Sigma)

and placed above a radial shockwave transducer and coupled with ultrasound gel (see **Figure 11-1**). Upon completing shockwave treatment, each flask was returned to the incubator until the desired time point was reached.

11.7.2.5 RNA Extraction

The method for RNA extraction for HUVEC was described in the RNA extraction **section 11.7.8**.

Figure 11-1. Shockwave administration to cells.

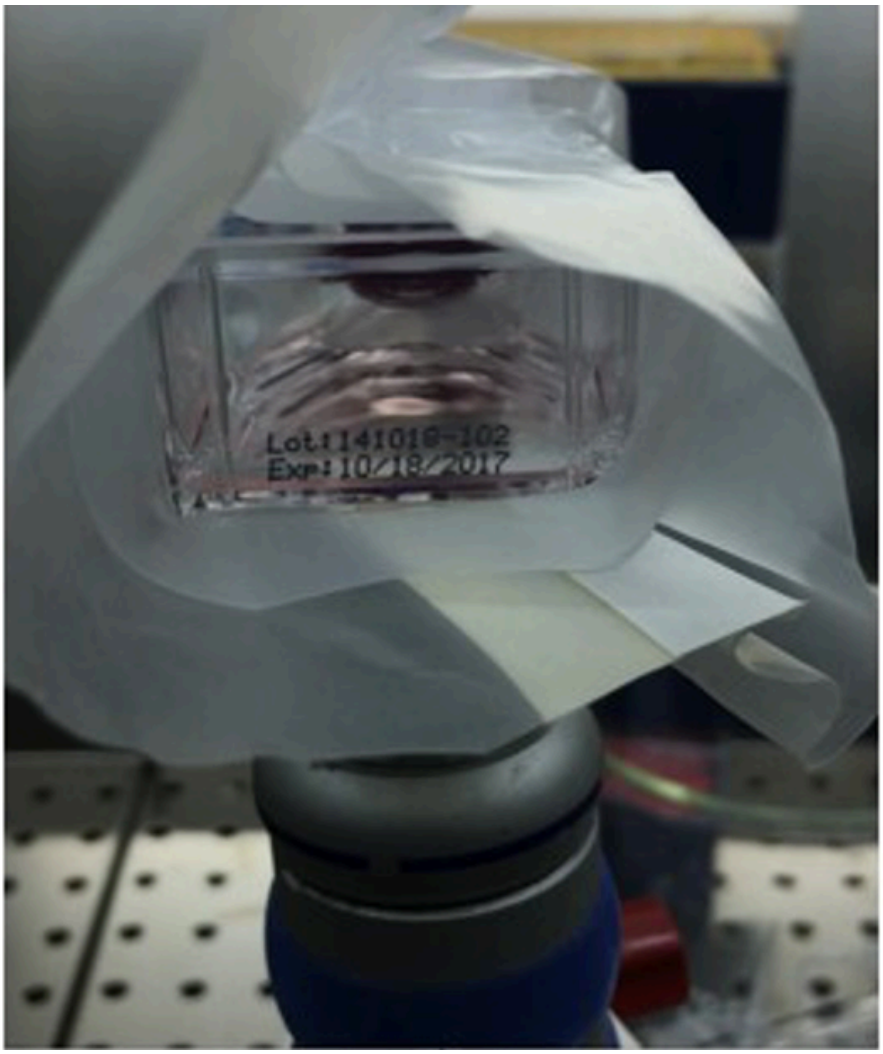

11.7.3 Human Cardiomyocytes

11.7.3.1 Isolation

Human ventricular tissue was aseptically handled. The tissue was cut into 1mm small pieces using a blade in a petri dish containing cardioplegia solution, then transferred into preoxygenated 'low calcium' solution in a 50ml conical tube, agitated for 10 minutes by a motorized shaker over a 37°C water bath.

'Low calcium' base ingredients: NaCl, KCl, MgSO4, K, HEPES, Taurine, NTA (calcium chelator). The 'low calcium' solution decanted and replaced with preoxygenated 'enzyme solution' with 1mg/ml collagenase and 0.5mg/ml protease, agitated for 10 minutes by a motorized shaker over a 37°C water bath. The 'enzyme solution' contained the same ingredients as 'low calcium' but without the NTA.

Then the samples sieved through a nylon mesh, the first decant contained mostly fibroblasts processed as described in the section below. The tissue residue was collected from the nylon mesh, transferred back into the conical tube, supplied with a fresh 'enzyme solution' with enzymes, agitated for 10 minutes by a motorized shaker over a 37°C water bath. The samples sieved through a nylon mesh; the second decant contained cardiomyocytes and fibroblast. It was either allowed to sediment under gravity or centrifuge at 100G for 5 minutes, the supernatant collected and processed similarly as the

first decant. The sediment containing cardiomyocytes resuspended in fresh enzyme solution without the enzymes. See **Figure 11-2**

For downstream application (e.g. shockwave experiment), the buffer was exchanged with M199 supplemented with CCT. CCT supplement contains creatine, taurine and carnitine. It was discovered that cardiomyocytes were not calcium tolerant and terminally contracted in M199. Several attempts of gradual recalcification were introduced to improve cardiomyocytes viability to no avail. As the experiment required good quantities of viable cardiomyocytes, the experiment was abandoned, and rats' cardiomyocytes used instead.

Figure 11-2. Human cardiomyocytes under light microscopy

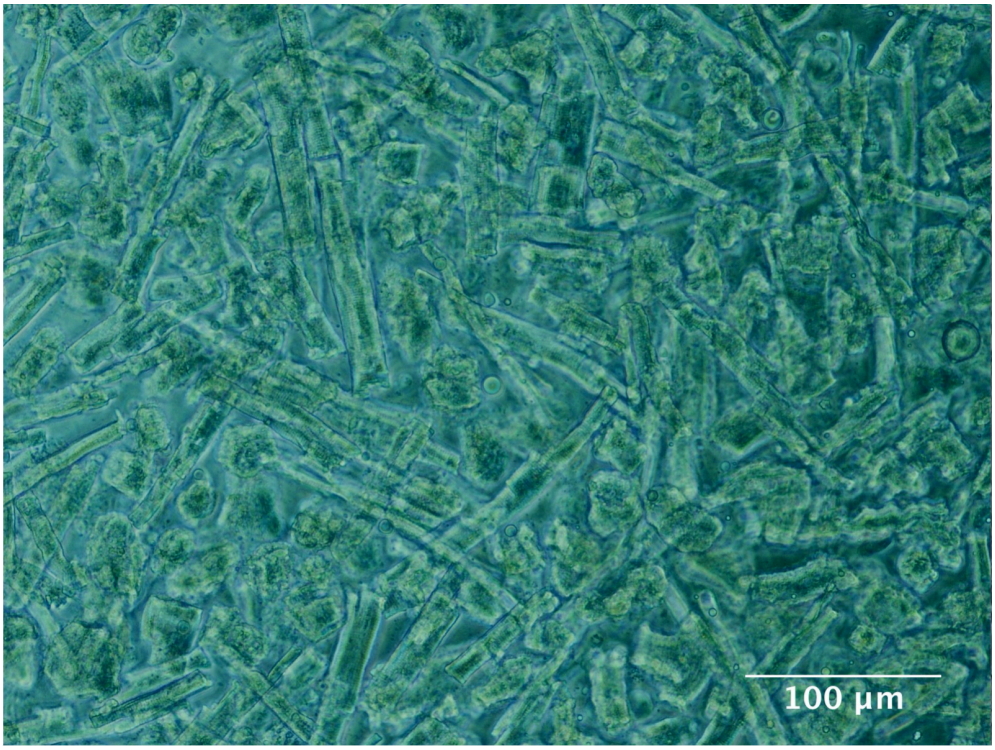

11.7.4 Rat Cardiomyocytes

11.7.4.1 Isolation and Culture

The method for rat cardiomyocytes isolation and culture was described in **section 8.6.2.** The cardiomyocytes were plated on 35mm µ-Dishes pre-coated with Laminin, cultured in M199 supplemented with CCT, and incubated in 5% CO_2 incubator.

11.7.4.2 Experimental Design

The number of µ-Dishes required was determined from the experimental design. In this experiment, there were two time points: time point 0 and 4 hours. Each µ-Dishes was for one time point and one shockwave dose only. The doses of shockwave used were: 1.0Bar x 1000 and 2 Bar x 1000.

11.7.4.3 Shockwave Administration to Cells

The shockwave administration setup was similar to the shockwave administration in the cardiomyocytes anoxia experiment (see **section 8.6.7**). Upon completing shockwave treatment, each flask was returned to the 5% CO_2 incubator until the desired time point was reached.

11.7.4.4 RNA Extraction

For RNA extraction, the M199 was aspirated out and saved in 1.5ml Eppendorf tubes, and 250mcl of TRI Reagent added to the dish, pipetted up and down until cells lysis completed, then transferred to 1.5ml Eppendorf tubes and

stored in -80°C until use. The subsequent method of RNA purification using Qiagen columns was identical with other cells and tissue types.

11.7.5 Human Cardiac Fibroblast

11.7.5.1 Isolation and Culture

The human cardiac fibroblasts were derived from human ventricular tissue via enzymatic dissociation. The method for enzymatic cardiomyocytes isolation has been described in **section 8.6.2** and **section 8.6.3**. The first and second filtrate from cardiomyocytes isolation were centrifuged at 100G for 5 minutes to sediment the cardiomyocytes and large debris. The top half of the supernatant containing fibroblasts were aspirated, transferred to a fresh 15ml conical tube (Falcon) and centrifuge at 400G for 10 minutes to obtain the cells pellet. The supernatant completely aspirated, and the cells pellet resuspended in 15ml DMEM advance containing Glutamax supplemented with 10% FCS, 1mcg/ml of basic FGF (Peprotech) and 50ng/ml Gentamicin (Sigma), and finally transferred to filter capped T75 TC flask (Falcon). The flask was incubated at 37°C in 5% CO_2 incubator overnight. The next day, the media was completely aspirated and fresh 15ml prewarmed supplemented DMEM pipetted into the flask. The flask was swirled to collect residual debris, and the media completely aspirated. A fresh 15ml prewarmed supplemented DMEM added to the flask, and the adherent cells viewed under the microscope HCF [insert HCF picture] having an appearance of spindle-shaped cells with thin processes extending out of the cell body (see **Figure 11-3**). The media was changed every 48 hours

until 80% confluency had been reached. The method of cells passaging and cryopreservation for human cardiac fibroblast was the same as for HUVEC.

11.7.5.2 Experimental Design

The number of flasks with human cardiac fibroblasts needed to be prepared was determined from the experimental design. Each flask was for one time point and one shockwave dose only. There were three time points: time point 0, 3hrs, 6 hours and 24hours. The doses of shockwave used were: 0.5 Bar x 1000, 0.5 Bar x 2000, 1.0 Bar x 1000, 1 Bar x 2000, 2.0 Bar x 1000 and 2.0 Bar x 2000.

11.7.5.3 Shockwave Administration to Cells

Shockwave administration setup was similar to shockwave administration to the cardiomyocytes (see **section 8.6.7**); the only difference was in place of the dish was a flask. Briefly, the flask was wrapped in Parafilm (Sigma) and placed above a radial shockwave transducer and coupled with ultrasound gel. Upon completing shockwave treatment, each flask was returned to the incubator until the desired time points been reached.

11.7.5.4 RNA Extraction

The method for RNA extraction for human cardiac fibroblasts was described in **section 11.7.8.1**.

Figure 11-3.Human cardiac fibroblast under light microscopy

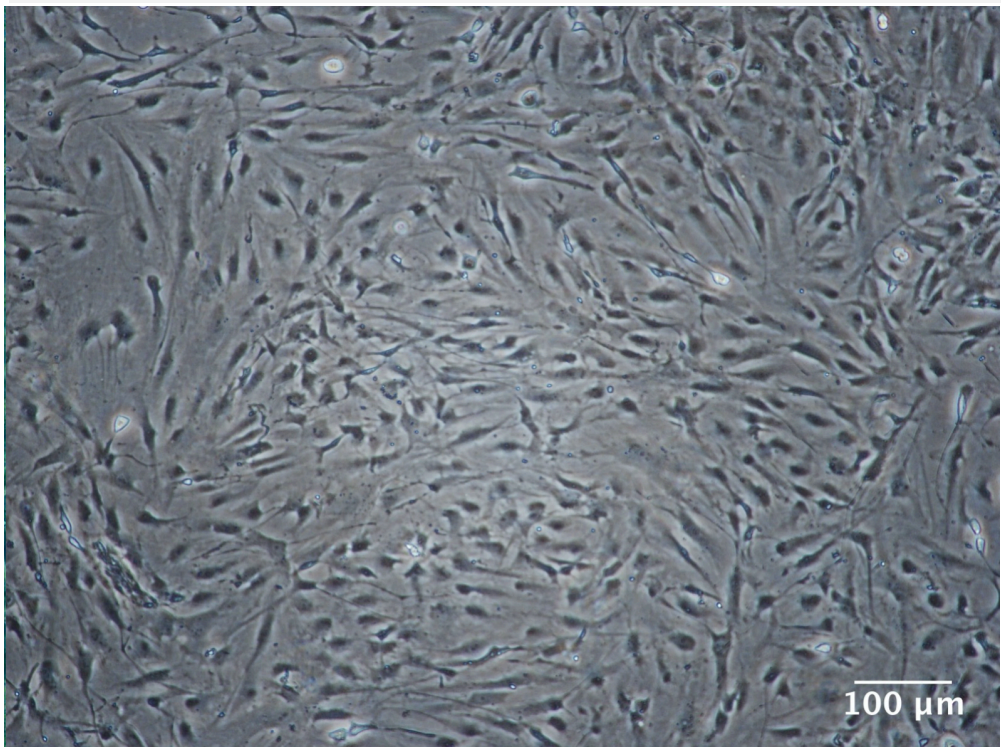

11.7.6 Rat Langendorff Heart

Spontaneously Hypertensive Rats (SHR) were used for all Langendorff heart experiments. The rats were kindly donated by Professor Cook.

11.7.6.1 Heart Explanation and Transport

The heart extraction method was a common procedure for all experiments that require beating hearts. The animal was humanely killed in steps of sedation with isoflurane, followed by a neck dislocation and a secondary confirmation of death by exsanguination of femoral bleed. To gain access to the heart, a horizontal incision was made across the subcostal regions using a scalpel to open into the upper abdominal cavity, then both hemidiaphragms cut opened, and a vertical cut performed from the xiphisternum to the upper sternum levels through the left parasternal ribs using a pair of surgical scissors. The resulting right and left chest flaps were folded opened, and the distal corners secured to the tissue underneath on their respective sides with artery forceps. The beating heart should be evident in the middle with the lungs on both sides.

The ascending aorta was clamped using arterial forceps, then cut distally, the heart then lifted with the arterial forceps; any connective tissue preventing the lift was carefully cut to avoid damaging the heart during removal, and the specimen would contain the heart, the lungs, the thymus and the ascending

aorta. It was crucial to submerse it in ice-cold heparinised (2units/ml) Krebs-Henseleit solution if prolonged transport was required.

11.7.6.2 Langendorff Preparation

The device consisted of a water bath; a roller pump circulating the heated water from the water bath to a heater jacket and to the outer lumen of a heat condenser, and back to the water bath; a top chamber filled with un-warmed Krebs-Henseleit solution where it was bubbled with 100% oxygen; an inner lumen (spiral glass) heat condenser through which the oxygenated KH passed through; and a cannula tip where the warmed and oxygenated KH solution dripped under gravity, and the flow was controlled using a tap.

The heart was attached to the cannula tip by the ascending aortic root secured using a crocodile clip and suture ligature. It would start beating after a few minutes. The lungs, thymus and atria were removed from the heart by cutting.

11.7.6.3 Shockwave Treatment to The Langendorff Hearts

The hearts received radial shockwave by Swiss Dolorclast classic (EMS, Switzerland) with Evo Blue handpiece. The doses of shockwave used were: 1.0 Bar x 1000, 2 Bar x 1000 and 3.0 Bar X 1000. Shockwave was administered via direct contact of the shockwave handpiece tip barriered with a cling film to the heart (**Figure 11-4**). The hearts were left beating for 4 hours on the

Langendorff apparatus encased by a heater jacket, then removed from the apparatus, cut in pieces, dried with Kim white and preserved in RNA Later. The method for RNA extraction was identical to that in human tissue (see **section 11.7.8**)

Figure 11-4. Rat Langendorff Heart administered with radial shockwave.

11.7.7 Human Ventricular Tissue

The experiments on human cardiac tissue were performed in compliance with the Human Tissue Act. The heart arrived in the laboratory from the donor hospital sites in ice-cold cardioplegia.

11.7.7.1 Isolation and Culture

A required amount was cut out from the heart, transferred to a 50ml Falcon tube containing fresh cardioplegia and put on ice. The work was performed under the hood to maintain sterility, and an aseptic technique was maintained throughout. The tissue was cut into small pieces on a petri dish; one piece of tissue was for one experiment condition and for one time point. See **Figure 11-5**. Each tissue piece was placed in a well of 16-well plate containing prewarmed M199 and left in the incubator for at least 10 minutes before shockwave treatment.

11.7.7.2 Shockwave Administration

To deliver shockwave, each tissue was transferred into a 2ml Eppendorf tube filled with M199 taken from the same well the tissue was taken. As air bubbles impeded the transmission of shockwave, M199 was filled to the brim, and the lid was locked whilst ensuring no air bubbles were trapped inside the tube. The shockwave transducer was directly put in contact with the Eppendorf tube held by hand in gauze, coupled with a good amount of ultrasound gel during

shockwave dose delivery. The dose applied were: 1 Bar x 1000, 1 Bar x 2000, 2 Bar x 1000 and 2 Bar x 2000. Once done, the tissue and M199 returned to the same well and incubated for 4 hours in the incubator.

11.7.7.3 Tissue Preservation

At the end of the timepoint, the tissue was removed from its well and excess M199 pat dry with Kim White. Then, it was transferred to a fresh 2ml Eppendorf tube containing RNA later (Invitrogen). It was important to ensure the tissue was completely submerged in RNA Later to ensure proper preservation of the RNA. The tissue samples were stored in -80°C until RNA extraction. RNA Later was preferred over snap freeze using N_2 because snap freezing would not prevent RNA degradation during thawing, but RNA Later could. The avoid the risk associated with liquid N_2 and the associated laborious process of RNA extraction using chilled mortar and pestle.

11.7.7.4 Tissue RNA Extraction

If frozen, the samples in RNA later thawed to room temperature, removed from the tube and the excess RNA pat dry with Kim White. They were weighed and transferred to 15ml round bottom test tubes with TRI Reagent, at a ratio of 1ml Tri Reagent to 100mg tissue for homogenization under the ice. A start-stop pulsating technique was used to avoid heating. Once satisfied, the tissue had been fully homogenised, the tubes were centrifuged for 5 mins at 400G to

sediment the debris; the clear TRI Reagent on top containing RNA was transferred to appropriately labelled fresh tubes. At this juncture, the samples could be frozen at -80°C until RNA extraction. Otherwise, proceed to RNA extraction using a combination of chloroform and spin-column RNAeasy as described in the above section.

Figure 11-5. Human left ventricular tissue of a failing heart cut into small pieces.

11.7.8 RNA Extraction

11.7.8.1 RNA Extraction for HUVEC and Cardiac Fibroblast

The method for RNA extraction for lysing cells was applicable for both HUVEC and human cardiac fibroblasts. The cells culture medium was aspirated from the flask and aliquoted in 1.5ml Eppendorf tubes containing cocktails of protease inhibitors (Sigma) for cryopreservation in -80°C. 400mcl of TRI Reagent (Sigma) was added to the flask, spread to ensure contact with the cells monolayer; the cells then scrapped using a cell scraper, the mixture pipetted up and down a few times to assist with cells lysis and finally transferred to a 2ml Eppendorf tube. At this juncture was the option to store cells lysate in TRI Reagent at -80°C until use, otherwise proceeded as below.

11.7.9 Column Method of RNA Purification

A method of RNA extraction using a combination of chloroform and spin-column RNAeasy (Qiagen) was used because of better RNA purity. The spin columns contained a silica membrane inside a spin-column. If started from frozen, the samples from section 10.7.8.1 were first thawed to room temperature and then mixed with a vortexer. 80mcl chloroform volume (20% of lysate volume) was added to the cell lysate, mixed using a vortexer and then incubated for a few minutes. The tubes were centrifuged for 15mins at 12,000G 4°C for 15mins which separated the mixture into red phenol-

chloroform at the bottom layer and a clear aqueous phase at the top layer. The aqueous layer was aspirated and transferred into a new tube. Then, an equal volume of 70% ethanol was added to the tube to precipitate the RNA. The mixture then transferred to a spin column, one column for one sample. Here, the processing of one spin column is described as it is applicable to many columns. The spin-column containing precipitated RNA mixture was spun for 15s at 8000G and the follow-through discarded. The precipitated RNA was trapped on the membrane and ready for washing. The spin-column (membrane) washed with 700mcl RW1 buffer and then spun for 15s at 8000G, and the follow-through discarded. After that, the membranes were washed with 500mcl RPE buffer, spun for 15s at 8000G twice, and the follow-through discarded. The spin-columns then placed into a fresh collecting tube and spun at 15000G to dry the membrane. Then, the collecting tubes were replaced with a 1.5ml Eppendorf tube. 30mcl RNAase-free water directly was directed pipetted onto the membrane and left for 1 minute to collect the RNA. The tubes were spun down for 1 minute at 15000G to elute the RNA in water. At this juncture, there was an option to store the RNA in -80°C until further analysis.

11.7.10 Nanodrop 8000 Spectrophotometer

The computer was switched on and ensured to be online with Nanodrop, and the software module was that was opened. The instrument has 8 channels, so up to 8 samples can be processed at one time. The pedestal was inspected to ensure it was clean. Following on-screen instruction, 2mcl deionized water was pipetted onto lower pedestals, the arm was closed, and the instrument initiated. The next step was blanking the spectrophotometer using the same diluent that was used to dilute the RNA, i.e., RNAase-free water.

The deionized water from the initiation step was wiped off from both the lower and upper pedestals with lint-free tissue paper (Kim White). Then 2mcl RNAase-free water was pipetted onto the lower pedestals. All channels were activated, and the measurement was run. A valid result was indicated by a flat spectrum with a baseline near zero on each channel. The blank samples were wiped off, the samples name and ID entered on the screen, and 1mcl, the RNA samples to be tested were pipetted on each pedestal. The RNA option was selected, and the measurement was initiated. When completed, table with results of absorbance values at 280, 260/280, 260/230 and estimated concentration of RNA in ng/mcl. An absorbance 260/280 ratio of ~2.0 is interpreted as “pure” for RNA, whereas a ratio of ~1.8 interpreted as “pure” DNA. 260/230 ratio was used as a secondary indicator of nucleic acid purity, usually in the range of 1.8-2.2, and lower values indicated the presence of

contaminants. Nanodrops calculated the RNA concentration using Beer's Law using Beer-Lambert equation, where A=E*b*c, A is the absorbance, E is the molar absorptive coefficient, b is the path length, and c is the analyte concentration in moles/litre. The path length for Nanodrop was 0.2mm, and the E for RNA is 40ng-cm/mcl.

11.7.11 Reverse Transcriptase PCR

This was performed after RNA quantification using Nanodrop. A two-step RT-qPCR method was used; first, the RNA was converted to cDNA; and the cDNA underwent quantitative PCR using Taqman assay. It was essential to use calibrated positive displacement pipettes as the volumes were very small. The bench workspace was thoroughly cleaned to remove carryover particles which could introduce errors in PCR experiments.

11.7.12 cDNA Preparation

High-Capacity cDNA Reverse Transcription Kits (Applied Biosystem) was used to convert the RNA to cDNA. In a 20mcl reaction, the kit could convert up to 2mcg of RNA to cDNA. The RNA samples were diluted to the same concertation using the formula $(CV)_1 = (CV)_2$, where C was the concentration of the RNA in ng/mcl, and V was the volume in mcl. The kit contains 10X RT Buffer, 10X RT Random Primers, 25X dNTP Mix and Multiscribe Reverse Transcriptase (50U/mcl) vials.

They were allowed to thaw on ice. Per 20mcl cDNA reaction consisted of 10mcl of diluted RNA of standardised concentration and 10mcl of 2X RT master mix, performed in 0.2ml MicroAmp Reaction Tube with Cap (Applied Biosystems). The number of reactions needed was determined from the number of samples in the experiment run, with 20% insensible loss through pipetting. One cDNA reaction of 2X RT master mix required 2mcl 10X RT Buffer, 0.8mcl 25X dNTP Mix, 2mcl 10X RT Random Primers, 1mcl 25X dNTP Mix and 3.2mcl nuclease-free water. If 10 reactions were required, 2X RT master mix sufficient for 12 reactions were reconstituted on ice in a 1.5ml Eppendorf tube. 10mcl of RT Master mix was pipetted into each MicroAmp Reaction Tubes containing 10mcl of pre-prepared standardised RNA samples. The reverse transcription reactions were performed on Eppendorf Motorcycler, programmed with step 1: 80°C for 10 minutes; step 2: 37°C for 120 minutes; step 3: 85°C for 5 minutes and step 4: 4°C for infinity. The cDNA was stored in -20 °C until use.

11.7.13 qPCR

TaqMan® Gene Expression Assays—single–tube assays were used to perform quantitative PCR. Taqman gene expression assay using the following probes. SDF1 and VEGF expression were assessed in all sample types. In addition to SDF1 (Hs03676656_mH) and VEGFA (Hs00900055_m1) in human cardiac fibroblast, MCP1 (Hs00234140_m1), TAC1 (Hs00243225_m1) and IGF1

(Hs01547656_m1) were also assessed. In addition to SDF1 and VEGFA in human ventricular tissue, MCP1, ANG1PT1 (Hs00919202_m1) and NOS3 (Hs01574665_m1) were also assessed. GAPDH (Hs00234140_m1) was used as a reference gene for all. The probe for rat samples were: CXCL12 (Rn00573260_m1), VEGFA, (Rn01511602_m1) and GAPDH (Rn01476455_m1).

11.7.14 Plate Planning and Mastermix

Singleplex one target gene was amplified per well in a 10mcl reaction performed in 10mcl volume in 384-well plate. The wells on the plate were preplanned to receive which sample type and which Singleplex Taqman gene reaction. The number of reactions needed was calculated, sufficient for three technical replicates per cDNA sample plus 20% insensible loss through pipetting. Per 10mcl reaction required 5mcl Taqman Gene expression Mastermix (2X); either 0.5mcl Taqman Assay or Taqman endogenous control and 4.5mcl of cDNA diluted in nuclease-free water. The latter should contain 5 to 50ng of cDNA standardised in all reactions.

First, a Mastermix of Taqman Gene expression Mastermix (2X) and Taqman Assay or Taqman endogenous control with nuclease-free water prepared on ice in a 2ml Eppendorf tube, in amount based on the number of reactions needed. The 4.5mcl cDNAs were pipetted into each 384-well plate, pre-planned to receive what sample type and what Singleplex Taqman gene

reaction. Then 5.5mcl of the Mastermix added to wells. The plate was sealed with an adhesive film (MicroAmp optical, Applied Biosystem). The plate was briefly centrifuged to bring the content to the bottom of the wells and inspected for bubbles.

11.7.14.1 QPCR Instrument

7900 HT Fast Real-Time PCR System (Applied Biosystems) was used to perform PCR reactions. The instrument was set up with the thermal cycling protocol, step 1: 50°C held for 2 minutes; step 2: 95°C held for 10 minutes; and step 3: 40 cycles of 95°C for 15 seconds for denaturing and 60°C for 60 seconds to anneal/extend. Upon completion of the programme, the amplification plot was viewed in log view mode. An auto baseline and auto threshold were set. If this was not satisfactory, a manual adjustment was performed to choose a baseline where it transected the amplification curves at the linear phases to derive the CT values. The CT values were exported to an Excel spreadsheet, and comparative analysis was performed.

11.7.14.2 Analysis of CT Values

The quantitative PCR analysis was performed using 2-ΔΔCT method,[315] where ΔCT = CT(a target gene)-CT(a reference gene) and ΔΔCT= ΔCT(a target sample)-ΔCT(a reference sample). To convert into fold change ΔΔCT, it was calculated using the formula $2^{-\Delta\Delta CT}$. The formula assumes 100% amplification efficiency.

As the Taqman assay was used, which has 100% efficiency, the efficiency calculation step was not necessary, and the formula remained valid without correction applied.

A CT value was calculated from an average of three technical replicates. In a situation there was only one successful reaction, the value from one CT value would be used, and if there were two successful reactions, the average CT value from the two reactions would be used.

As the PCRs were performed in multiple runs, in different plates and the data merged later, it became necessary to autoscale the fold changes using log transformation, perform mean centering and autoscaling to reduce interexperimental variations. The method used was described in this publication.[316] The plate design and time points were consistent in all the plates to be merged in the analysis. Briefly, the calculation was performed in Microsoft Excel, where all the data tabulated in the same spreadsheet. ΔCT values were determined using their respective reference gene, and ΔΔCT then obtained for all samples using the same reference sample, i.e., the first control. ΔΔCT values were converted into fold changes using the formula $2^{-\Delta\Delta CT}$. The fold changes values per one experimental run were transformed by log 10 and then mean centred by subtracting each of the log-transformed fold change with the average value of log-transformed fold changes for the group. The

procedure was repeated in the other experimental groups to be included in the analysis. The mean centred values were then autoscaled. This was performed by dividing the values by the standard deviation for the group and multiplied by the average of the standard deviations of mean centred values in all experimental groups to be included in the analysis. Then the autoscaled mean centred values of each sample types were averaged amongst themselves, and their standard errors calculated using the formula $SE=(SD)/(n)^2$. The 95% CI was calculated from the standard error using the TINV function, and then the autoscale mean centred values could be converted to the average fold change by antilog 10. For comparison, all the fold changes were divided by the control's fold change so that the average fold change and the control average became one and the other comparators were how many folds increase or decrease compared to the control's fold change.

11.8 Statistical Analysis

The autoscaled mean centred data were continuous variables and expressed as the mean ± SEM and their corresponding fold changes expressed as fold change±95%CI. The comparisons were performed on the autoscaled mean centred data as they were linear. Where possible, when the sample number was large enough, normality was assessed using D'Agostino and Pearson test (alpha=0.05), where non-significance test meant the spread was Gaussian.

Comparisons between two means were performed using Welch's t test. Multi-groups mean comparisons were performed using one-way (between-subjects) ANOVA of Brown-Forsythe and Welch.

As the purpose of the experiment was to discover the gene expression pattern, and it was not possible to know in advance the spread of gene expression in the controls which could be wide; also taking account of the fact that the number of time points groups was moderate with low biological replicates, no *P* value correction was applied.

11.9 Results

11.9.1 Cardiomyocytes

See **Figure 11-6**. There was no significant difference in SDF1 expression between cardiomyocytes control, 1 Bar x 1000 and 2 Bar x 1000, *P* =.6604.

See **Figure 11-7**. There was no significant difference in VEGFA expression between cardiomyocytes control, 1 Bar x 1000 and 2 Bar x 1000, *P* =.5126.

Figure 11-6. Left Y-Axis Is the Log 2(SDF1 ΔΔCT/GAPDH) For Dot Plot Where Each Dot Is A ΔΔCT Value, And the Blue Bar Is the Mean. Right Y-Axis Is the SDF1 Fold Change for The Box Plot where the Middle Bar Is the Mean and The Upper/Lower Borders Are the 95%CI.

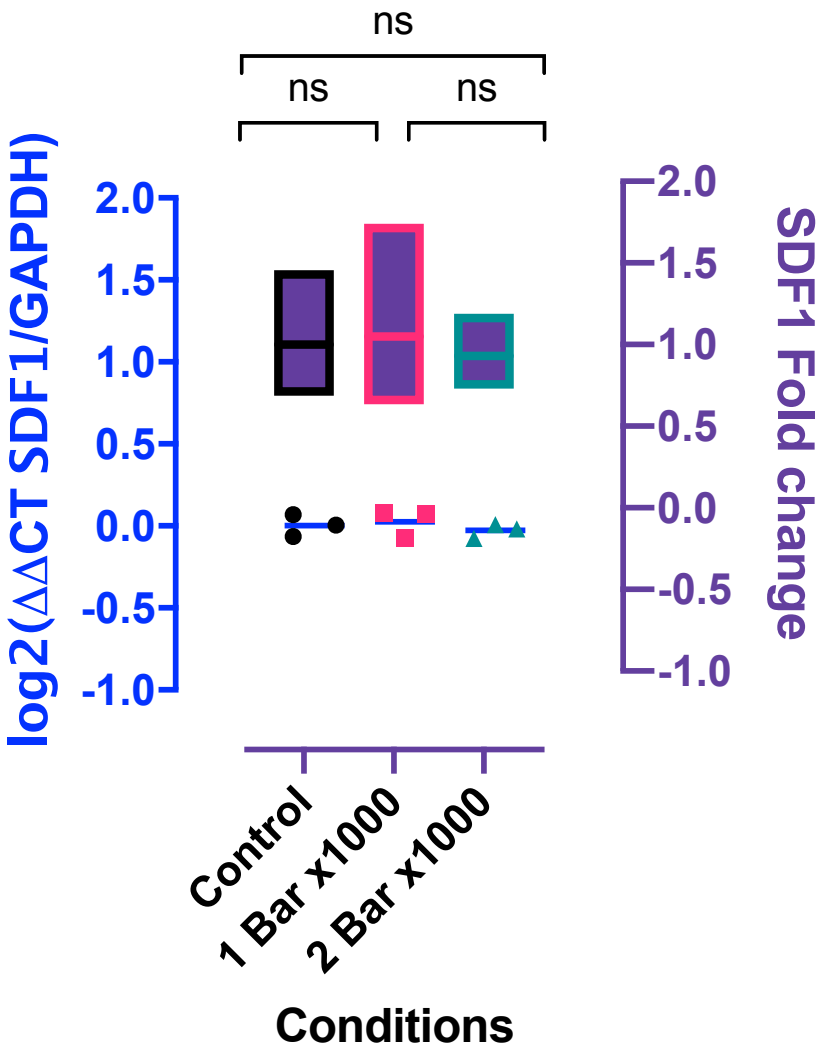

Figure 11-7. Left y-axis is the VEGF ΔΔCT/GAPDH for dot plot where each dot is a ΔΔCT value, and the blue bar is the mean. Right y-axis is the SDF1 fold change for the box plot where the middle bar is the mean, and the upper/lower borders are the 95%CI.

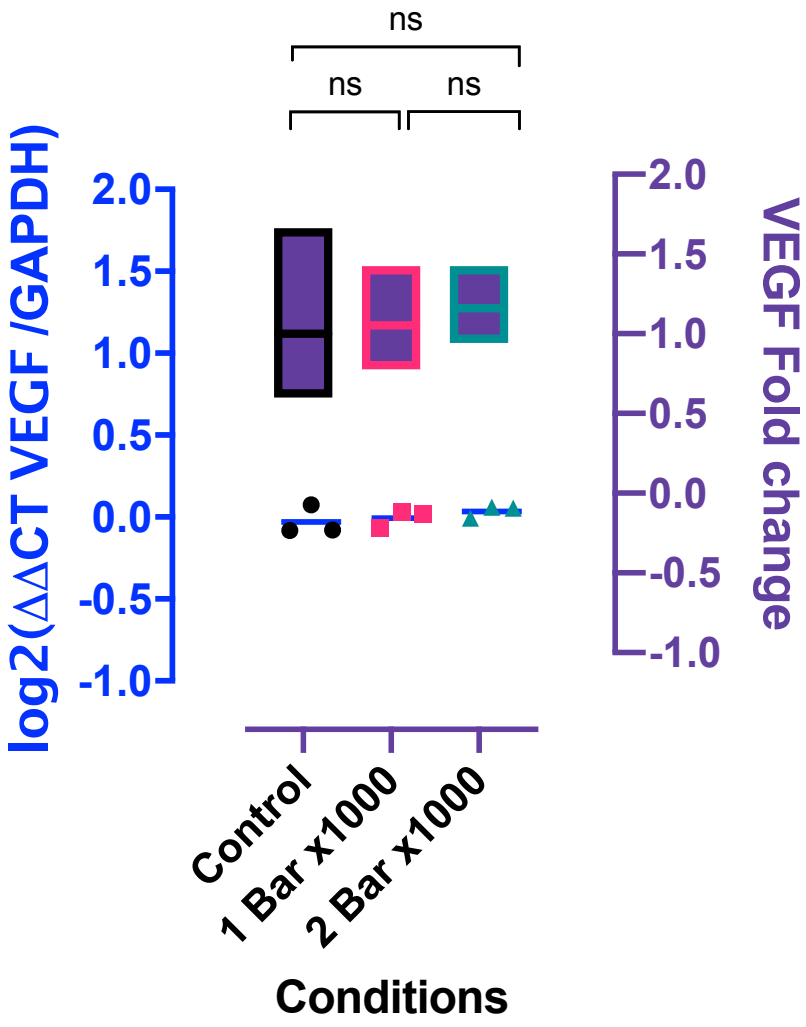

11.9.2 Langendorff Heart

11.9.2.1 SDF1 Gene Expression

See **Figure 11-8A.** Significant increase in SDF1 gene expression was observed only in 1 Bar x 1000 compared to control. The mean SDF1 fold change ± 95% CI increased in 1 Bar x 1000 to 1.47 (1.20, 1.81), unchanged in 2 Bar x 1000 at 0.97 (0.74, 1.28) and 3 Bar x 1000 at 1.20 (0.73, 1.99) compared to control 1.00 (0.61, 1.63)

11.9.2.2 VEGFA Gene Expression

See**Figure 11-8B.** The VEGFA fold change gene expression was similar across the groups with fold changes±95% CI of 1 Bar x 1000 1.33 (0.92, 1.93), 2 Bar x 1000 1.25 (0.99,1.57) and 3 Bar x 1000 1.12 (0.65, 1.44) compared to control 1.00 (0.35, 2.87).

Figure 11-8. (A) SDF1 gene expression in rat Langendorff heart following 4 hours of shockwave treatment. (B) VEGF gene expression in rat Langendorff heart following 4 hours of shockwave treatment. Charts on the left are the log2*(ΔΔCT GOI/GAPDH) versus shockwave doses of 1 Bar x 1000, 2 Bar x 1000 and 3 Bar x 1000. Error bars indicate the standard error and middle bars are the mean. Charts on the right are the fold changes of GOI and error bars are the 95%CI intervals. * indicates significant interactions $P < .05$ with

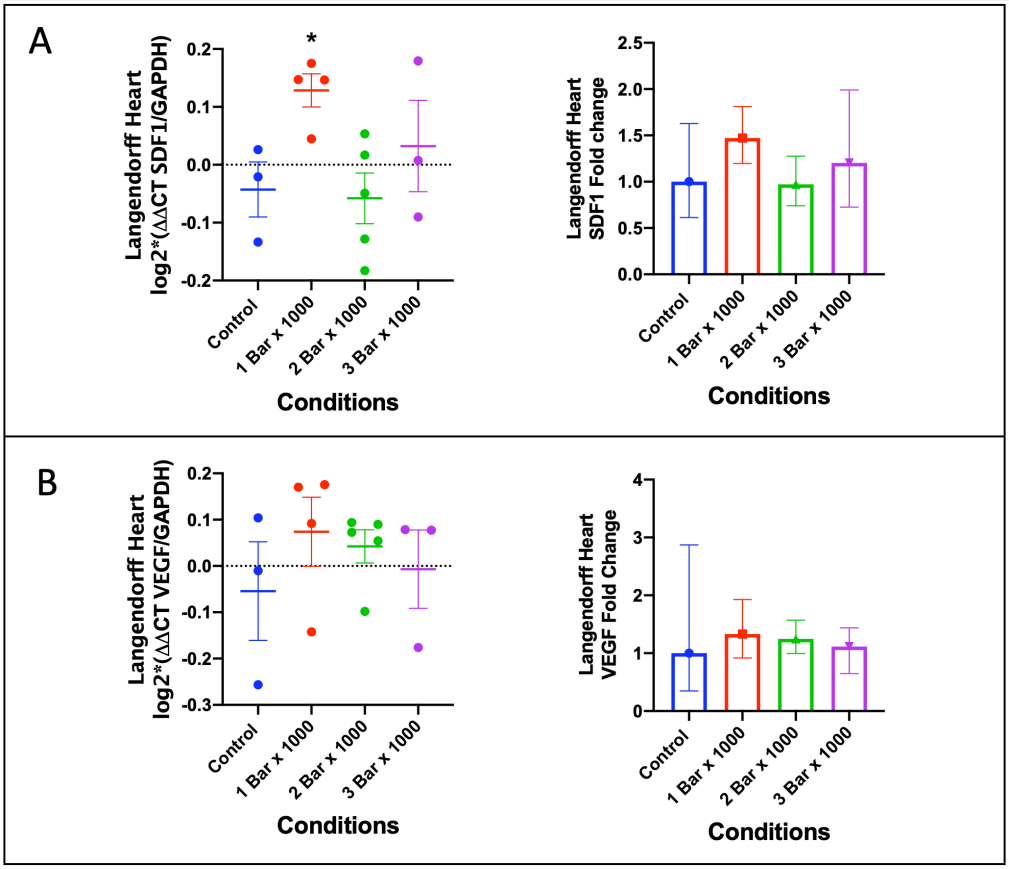

11.10 HUVEC

11.10.1 SDF1 Gene Expression

The means of SDF1 gene expression increased significantly in all energy level groups at 2 hours, 4 hours and 6 hours compared to 0 hours.

In group 1 Bar x 1000 (**Figure 11-9A**), the mean SDF1 gene expression peaked at 4 hours at 8.7-fold from 5.0-fold at 2 hours and dropped to 4.4-fold at 6 hours, compared to 0 hours. In group 1 Bar x 2000, the mean SDF1 gene expression stayed within the range of 4.3 to 4.9-fold for 2-6 hours compared to 0 hours. In group 2 Bar x 1000 (**Figure 11-9B**), the mean SDF1 gene expression peaked at 2 hours at 7.7-fold, then decreased to 3.7-fold at 4 hours and decreases further to 2.9-fold at 6 hours, compared to 0 hours. In group 2 Bar x 2000 (**Figure 11-9C**), the mean SDF1 gene expression stayed within the range of 4.5-4.2-fold for 2-4 hours and decreased to 2.5-fold at 6 hours, compared to 0 hours. In group 1 Bar x 1000 (**Figure 11-9D**), by 24 hours, the mean SDF1 gene expression had returned to the level of 0 hours and persisted at the same level at 48hours.

The SDF1 expression at 4 hours for 1 Bar x 1000 was 1.8-fold significantly greater than SDF1 expression at 4 hours for 2 Bar x 1000, P =.0439; 2.4-fold significantly greater than SDF1 expression at 4 hours for 2 Bar x 1000, P = .0422.

The SDF1 expression at 2 hours for 2 Bar x 2000 was 1.5-fold significantly greater than SDF1 expression at 2 hours for 2 Bar x 1000, *P* = .0186.

The AUC of 1 Bar x 1000 was the largest, decreased in the order of 2 Bar x 1000, 1 Bar x 2000 and 2 Bar x 2000. However, the overall effect on AUC was not significant, *P*=.4990.

The results indicated that low energy and low pulse number were sufficient for induction of SDF1. Higher energy and pulse number could have a retardation effect on SDF1 induction. It means shockwave treatment can be delivered quicker with less energy for a maximum effect of SDF1 induction, translating to improved treatment burden.

11.10.2 VEGFA Gene Expression

A significant increase in mean VEGFA gene expression was observed only in the time series group of 1.0 Bar x 1000 (**Figure 11-10A**) showing biphasic responses where it significantly peaked at 2 hours at 1.2-fold, then returned to baseline at 4 hours and significantly increased at 6 hours at 1.7-fold and then increased significantly furthermore at 24 hours at 2.0-fold compared to 0 hours. The increase in VEGFA expression from timepoints 2-hour to 6-hour to 24-hour was significant in all interactions suggests VEGFA peaked slower than SDF1 gene expression.

The VEGFA gene expression of time series in group 2.0 Bar x 1000 was similar throughout (**Figure 11-10B**), ANOVA *P* = .975.

The results indicated that only the lower energy shockwave of 1.0 Bar x 1000 was able to induce VEGFA expression in HUVEC, unlike for SDF1 expressions, which were inducible at all energy levels. 1.0 Bar x 1000 was the energy level that showed the greatest SDF1 fold changes, and it was able to induce VEGFA gene expression too.

Figure 11-9 SDF1 gene expression in HUVEC following shockwave treatment, in (A) 1 Bar x 1000; (B) 1 Bar x 2000; (C) 2 Bar x 1000; and (D) 2 Bar x 2000. Charts on the left are the log2*(ΔΔCT SDF1/GAPDH) versus time series from 0 hours to 6 hours captured at 2 hourly intervals. Error bars indicate the 95%CI, middle dots are the means. The AUC was calculated as the area above the mean of 0 hours (ΔΔCT -0.5). The charts on the right are the SDF1 fold changes of the chart on the left. Symbols pairs †, ‡ and ¤ indicates significant interactions $P < .05$.

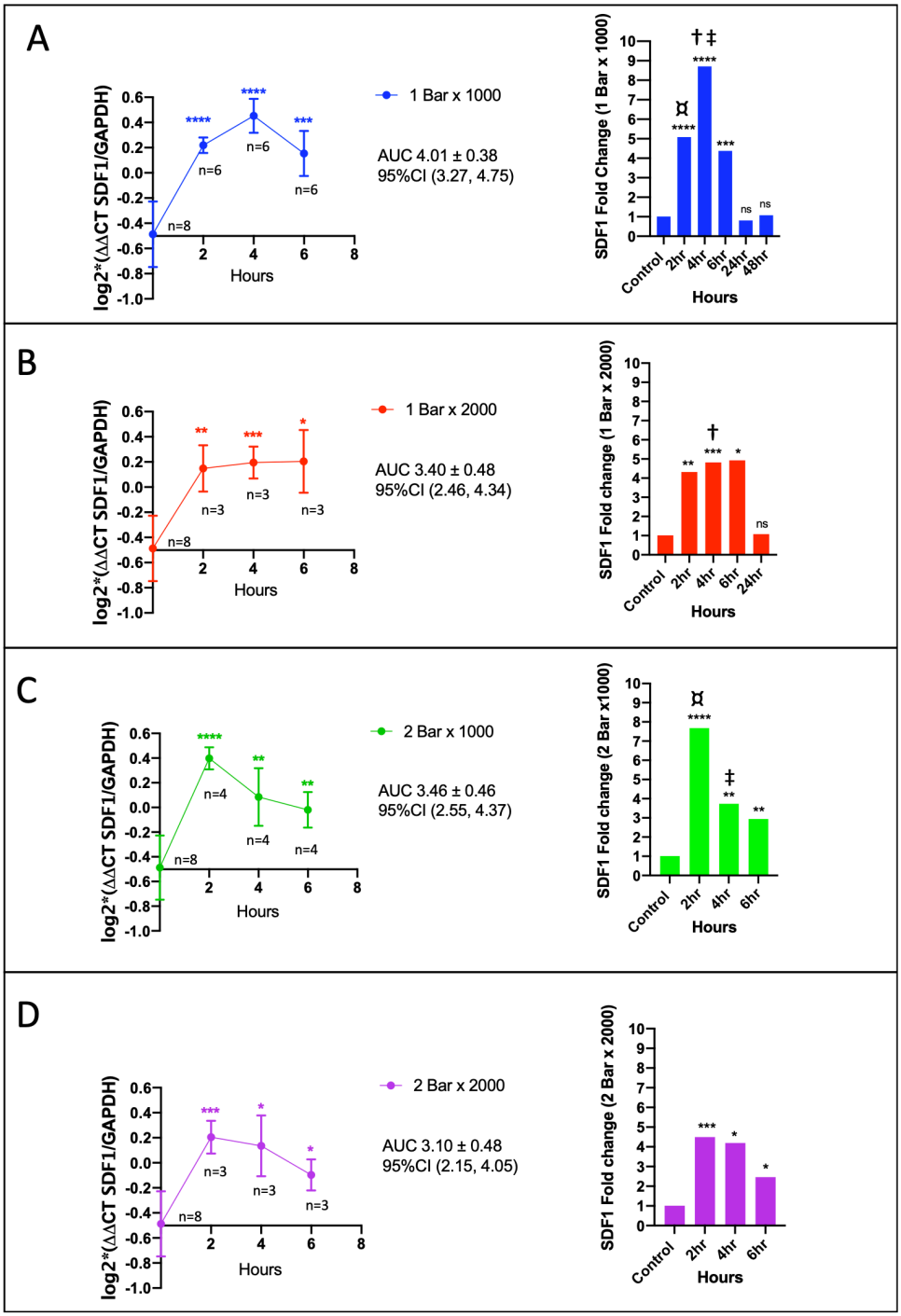

Figure 11-10. VEGF gene expression in HUVEC following shockwave treatment, (A) 1 Bar x 1000; (B) 2 Bar x 1000. Charts on the left are the log2*(ΔΔCT SDF1/GAPDH) versus time series from 0 hours to 6 hours captured at 2 hourly intervals and 24-hour, each dot is a biological replicate. Error bars indicate the 95%CI, middle bars (charts on the left) and dots (charts on the right) are the means. Symbol * means $P < .05$, ** mean $P < .01$ significant interaction with 0-hour. Pairs with matching symbols †, ‡ and

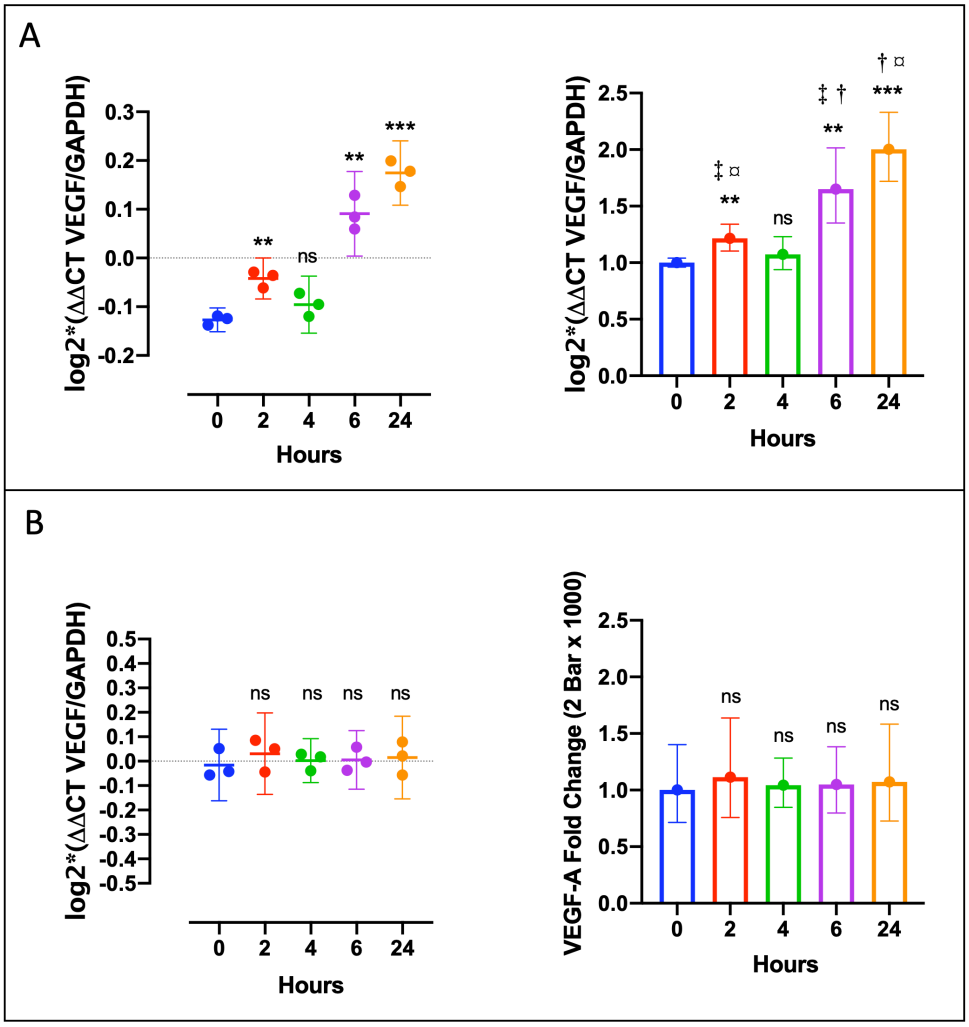

11.11 Human Cardiac Fibroblast

11.11.1 SDF1

See **Figure 11-11**. Shockwave doses of 0.5 Bar x 1000, 0.5 Bar x 2000, 1.0 Bar x 1000, 1 Bar x 2000, 2.0 Bar x 1000 and 2.0 Bar x 2000 were assessed for SDF1 gene expression. At 3-hour, all shockwave doses showed significant increase in the mean fold-change of SDF1 gene expression, respectively showing mean±95%CI of 1.29 (1.11,1.50), 1.22 (1.08,1.38), 1.27 (1.04, 1.56), 1.22 (1.13, 1.31), 1.20 (0.96, 1.52) and 1.14 (0.89, 1.45), compared to control 1.00 (0.88, 1.13). At 6-hour, only 1 Bar x 1000 showed significant increase in the mean fold-change of SDF1 gene expression showing mean±95%CI of 1.19 (0.89, 1.57) compared to control 1.00 (0.88, 1.13).

At 24hr, all shockwave doses showed strong significant increase in the mean fold-change of SDF1 gene expression showing mean±95%CI of 2.09 (1.54, 2.85), 2.45 (3.05, 1.97), 2.25 (1.91, 2.65), 2.08 (1.94, 2.23) and 2.09 (1.68, 2.59) compared to control 1.00 (0.88, 1.13). The overall results suggested that SDF1 gene expression in human cardiac fibroblast peaked later than HUVEC, at 24 hours versus 2-4 hours.

11.11.2 VEGFA

See **Figure 11-12**. The same shockwave doses as in SDF1 in the above were assessed for VEGFA expression. At 3-hour, all shockwave doses showed significant increase in the mean fold-change of VEGFA gene expression, respectively showing mean±95%CI of 2.43 (1.16, 5.09), 2.65 (1.79, 3.95), 2.74 (2.30, 3.26), 2.52 (2.09, 3.02), 2.59 (2.08, 3.22) and 2.59 (2.38, 2.82) compared to 1.00 (0.67, 1.48). At 6-hour, only 1 Bar x 2000 and 2 bar x 2000 showed a significant increase in the mean fold-change of VEGFA gene expression, respectively showing mean±95%CI of 1.44 (0.41, 5.07) and 1.75 (0.24, 12.84) At 24hr, all doses of shockwave were similar to control. The overall results suggested that VEGFA gene expression in human cardiac fibroblast earlier than HUVEC; at 3-hours versus 24 hours.

11.11.3 MCP1

See **Figure 11-13**. Shockwave doses of 0.5 Bar x 1000, 0.5 Bar x 2000, 1.0 Bar x 1000, 1 Bar x 2000, 2.0 Bar x 1000 and 2.0 Bar x 2000 were assessed for MCP1 gene expression. At 3-hour, all shockwave doses could significantly increase MCP1 gene expression in human cardiac fibroblast, respective showing fold-change mean±95%CI of 13.66 (4.55, 41.04), 14.14 (6.56, 30.49), 18.47 (11.15, 30.60), 14.42 (5.51, 37.75), 16.50 (10.30, 26.43), 13.86 (9.19, 20.90), compared to control 1.00 (0.31, 3.23). At 6-hour, only 2.0 Bar x 2000 showed a significant

increase in MCP1 gene expression in human cardiac fibroblast with fold-change mean±95%CI of 8.75 (6.35, 12.06) compared to control 1.00 (0.31, 3.23). The respective mean fold-change±95%CI of the rest were 5.83 (0.41, 83.07), 4.27 (0.27, 68.03), 4.54 (0.23, 90.05), 5.32 (0.48, 59.08) and 4.17 (0.18. 95.30). At 24-hour, all the shockwave doses showed similar MCP1 gene expression in human cardiac fibroblast compared to control 1.00 (0.31, 3.23). Their respective mean fold-change±95%CI were 1.92 (0.56, 6.60), 2.40 (0.42, 13.64), 1.87 (0.61, 5.87), 1.48 (0.42, 5.22), 2.08 (0.82, 5.27) and 1.61 (0.46, 5.63). The overall results suggested that MCP1 gene expression in human cardiac fibroblast earlier than HUVEC; at 3-hours similar trend to VEGFA gene expression.

11.11.4 TAC1

See **Figure 11-14**. Shockwave doses of 0.5 Bar x 1000, 0.5 Bar x 2000, 1.0 Bar x 1000, 1 Bar x 2000, 2.0 Bar x 1000 and 2.0 Bar x 2000 were assessed for TAC1 gene expression.

At 3-hour, all shockwave doses significantly increase TAC1 gene expression in human cardiac fibroblast, respective showing fold-change mean±95%CI of 22.53 (17.85, 28.43), 28.62 (13.59, 60.23), 27.44 (14.42, 52.20), 26.11 (13.55, 50.33), 18.15 (13.35, 24.67) and 22.30 (13.72, 36.25) compared to control 1.00 (0.39, 2.58).

At 6-hour, all shockwave doses significantly increase TAC1 gene expression in human cardiac fibroblast, respective showing fold-change mean±95%CI of 33.16 (23.62, 46.52), 32.84 (22.76, 47.38), 28.24 (16.61, 48.00), 31.03 (20.57, 46.81), 25.45 (17.94, 36.11) and 20.74 (17.17, 25.042) compared to control 1.00 (0.39, 2.58).

At 24-hour, all the shockwave doses showed similar TAC1 gene expression in human cardiac fibroblast compared to control 1.00 (0.31, 3.23). Their respective mean fold-change±95%CI were 1.83 (0.183, 18.36), 2.01 (0.946, 4.252), 0.81 (0.26, 2.52), 1.72 (0.39, 7.58), 1.19 (0.02, 93.98) and 1.52 (0.05, 46.77).

TAC1 gene expression in human cardiac fibroblast were at least sustained increase at 3-hours and 6 hours following shockwave treatment, and by 24-hour TAC1 gene expression had returned to baseline.

11.11.5 IGF1

See **Figure 11-15**. Shockwave doses of 0.5 Bar x 1000, 0.5 Bar x 2000, 1.0 Bar x 1000, 1 Bar x 2000, 2.0 Bar x 1000 and 2.0 Bar x 2000 were assessed for IGF1 gene expression. Although IGF1 expression pattern follows that of TAC1- an increase at 3-hour and 6-hour compared to control 1.00 (0.58, 1.72); the effect was not significant using samples of three. The analysis of the heat map

showed in one sample, the IGF expression started to increase later at 6-hour and remained persisted at 24-hour.

11.11.6 Heatmap

The heatmap of the SDF1, VEGFA, MCP1, TAC1 and IGF1 of qPCR results are presented in **Figure 11-16**.

Figure 11-11. SDF1 gene expression in human cardiac fibroblast following shockwave treatment, (A) 0.5 Bar x 1000; (B) 0.5 Bar x 2000; (C) 1.0 Bar x 1000; (D) 1 Bar x 2000; (E) 2.0 Bar x 1000; and (F) 2.0 Bar x 2000. Charts on the left are the log2*(ΔΔCT SDF1/GAPDH) versus time series from 0hr, 3-hr, 6-hr and 24-hr; error bars indicate the SEM and middle bars are the means. Charts on the on the right are the fold changes and error bars indicate 95% CI. Symbol * means $P < .05$, ** means $P < .01$, *** means $P < .001$ and **** means $P < .0001$ significant interaction with 0-hour. Symbols pairs †, ‡ and

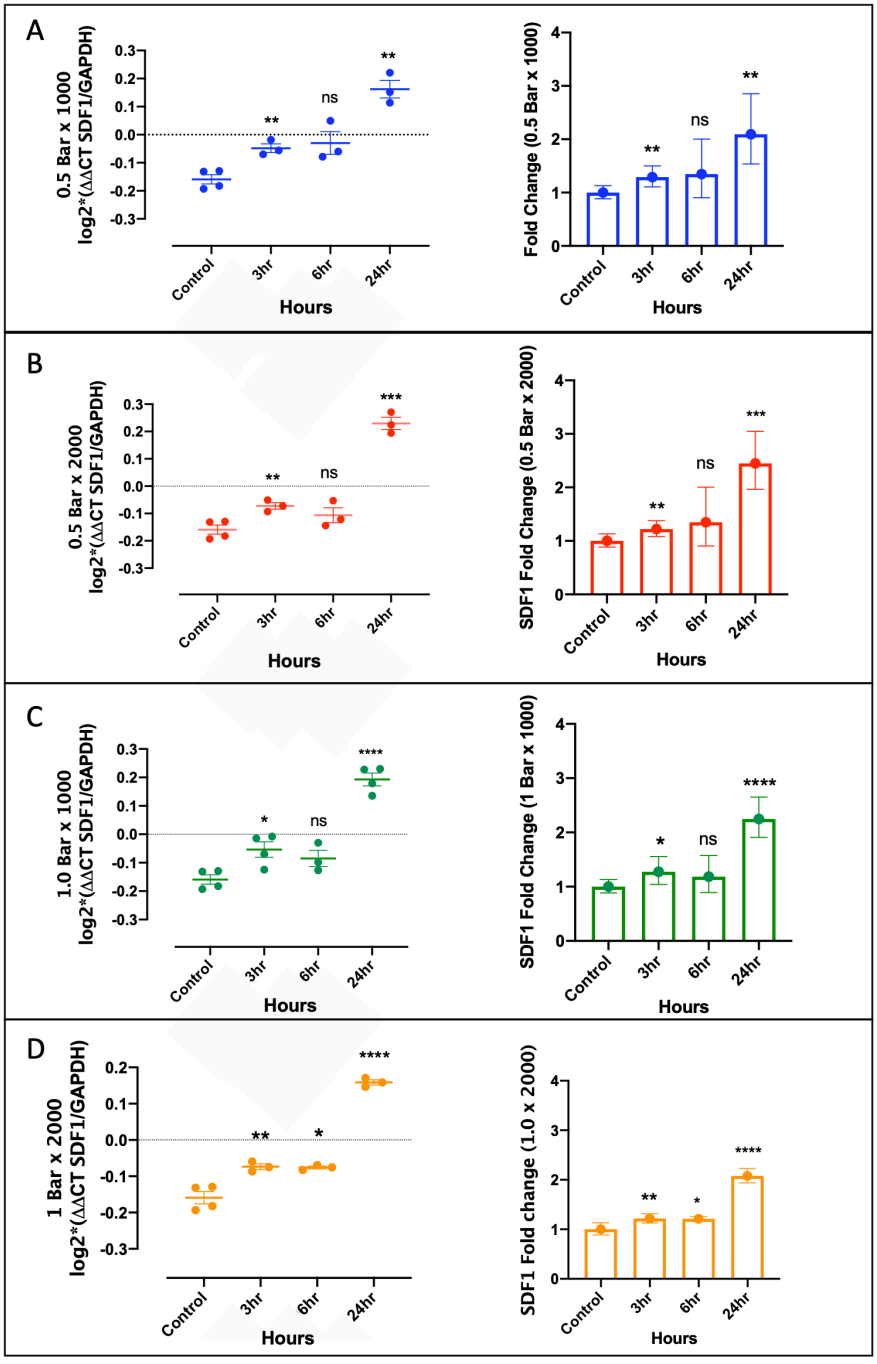

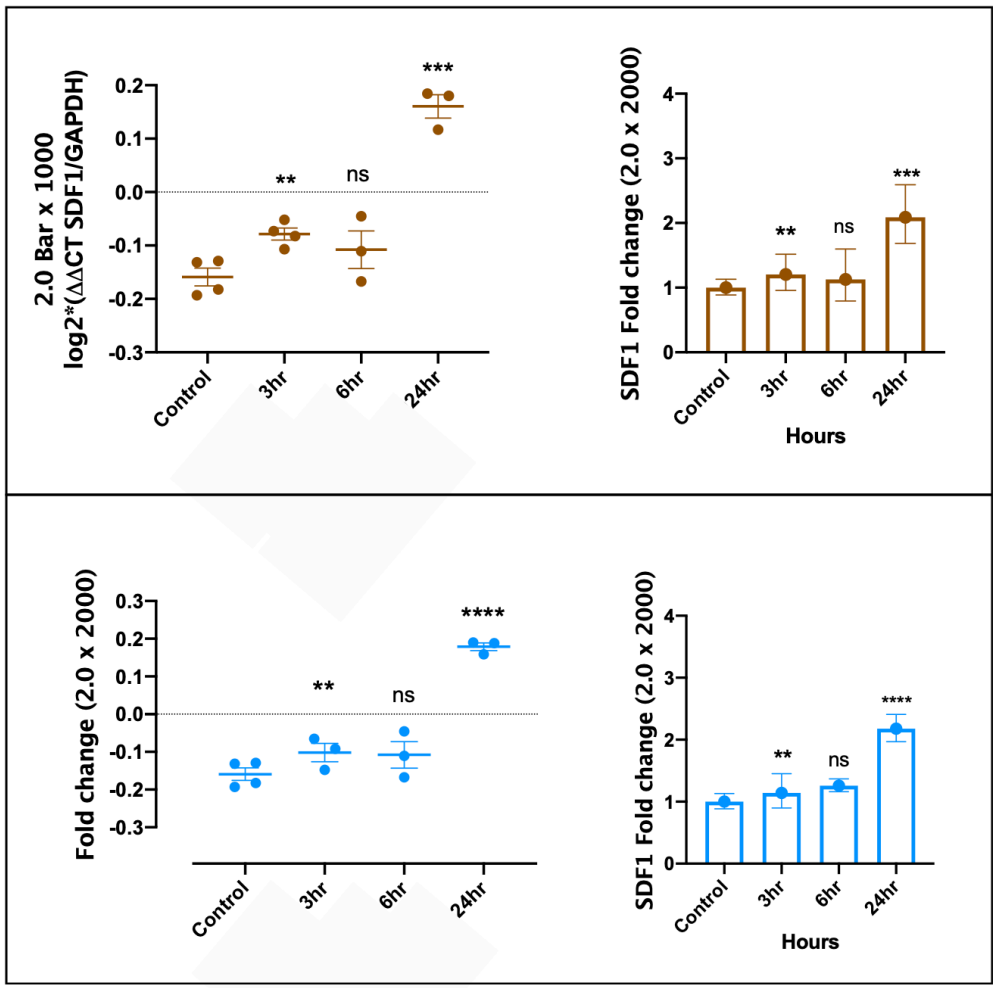
2.0 Bar x 1000
log2*(ΔΔCT SDF1/GAPDH)
0.2
0.1
0.0
-0.1
-0.2
-0.3
**
ns
***
Control
3hr
6hr
24hr
SDF1 Fold change (2.0 x 2000)
4
3
2
1
0
**
ns
***
Control
3hr
6hr
24hr
Hours
Fold change (2.0 x 2000)
0.3
0.2
0.1
0.0
-0.1
-0.2
-0.3
**
ns
****
Control
3hr
6hr
24hr
SDF1 Fold change (2.0 x 2000)
4
3
2
1
0
**
ns
****
Control
3hr
6hr
24hr
Hours

Figure 11-12. VEGF gene expression in human cardiac fibroblast following shockwave treatment, (A) 0.5 Bar x 1000; (B) 0.5 Bar x 1000; (C) 1.0 Bar x 1000; (D) 1 Bar x 2000; (E) 2.0 Bar x 1000; and (F) 2.0 Bar x 2000. Charts on the left are the log2*(ΔΔCT SDF1/GAPDH) versus time series from 0hr, 3-hr, 6-hr and 24-hr; error bars indicate the SEM and middle bars are the means. Charts on the on the right are the fold changes and error bars indicate 95% CI. Symbol * means $P < .05$, ** means $P < .01$, *** means $P < .001$ and **** means $P < .0001$ significant interaction with 0-hour. Symbols pairs †, ‡ and ¤ indicates significant interactions $P > .05$.

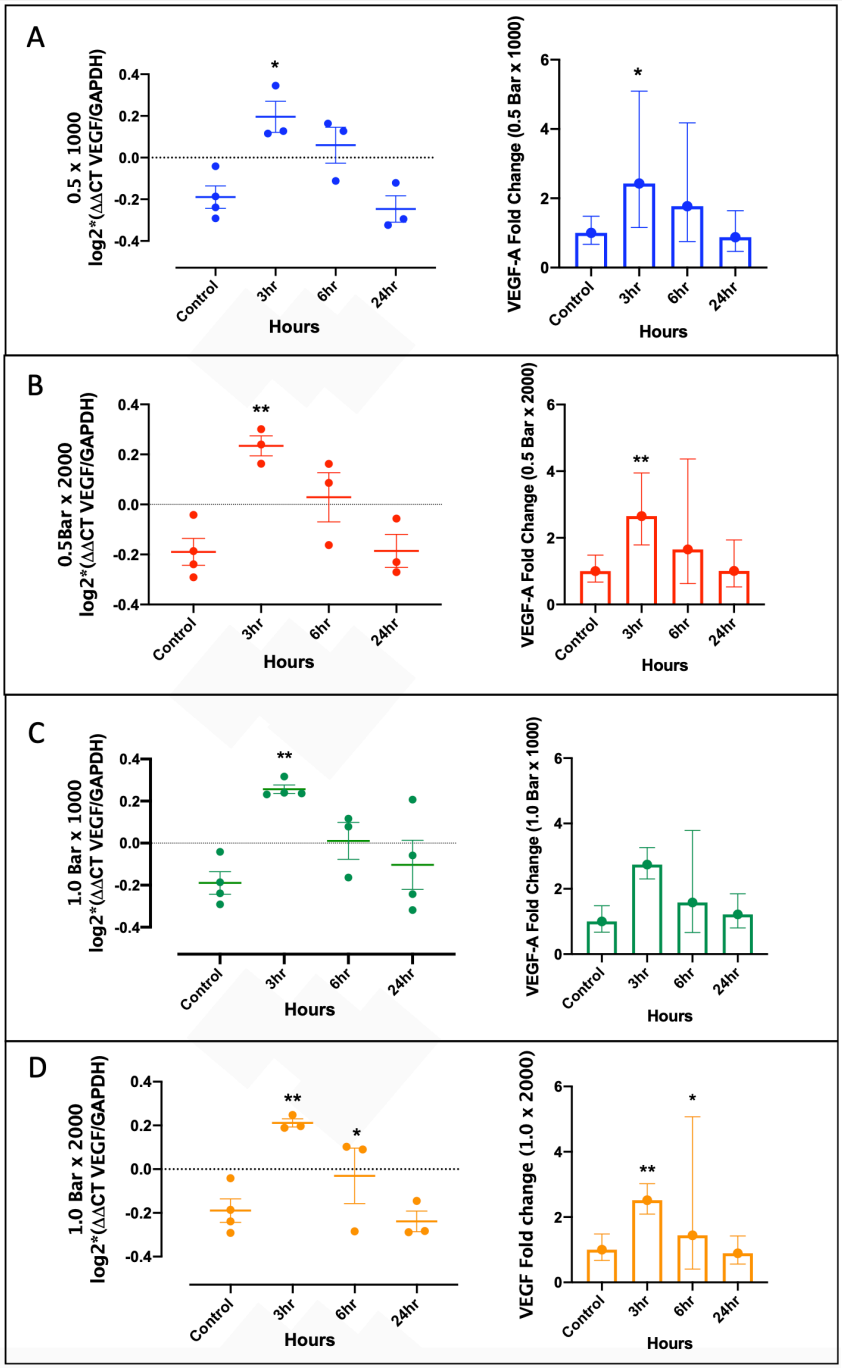

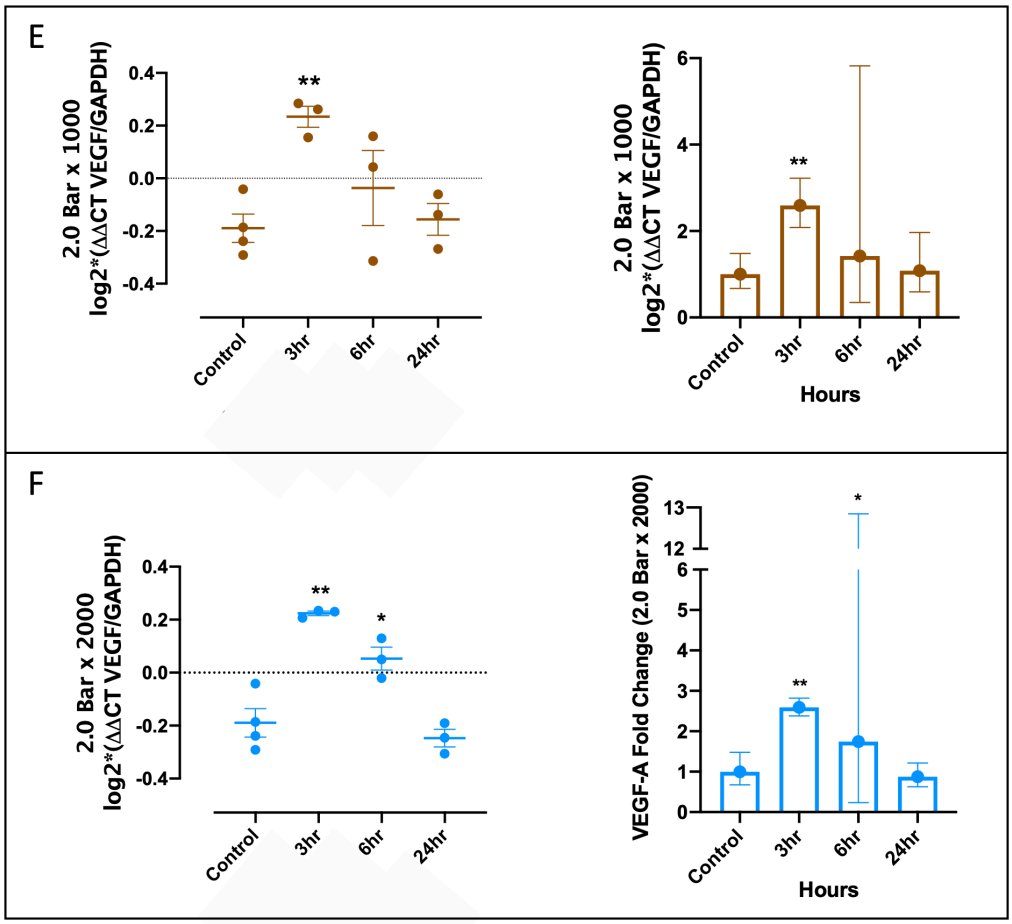
E
2.0 Bar x 1000
log2*(ΔΔCT VEGF/GAPDH)
0.4
0.2
0.0
-0.2
-0.4
**
Control
3hr
6hr
24hr
2.0 Bar x 1000
log2*(ΔΔCT VEGF/GAPDH)
6
4
2
0
**
Control
3hr
6hr
24hr
Hours
F
2.0 Bar x 2000
log2*(ΔΔCT VEGF/GAPDH)
0.4
0.2
0.0
-0.2
-0.4
**
*
Control
3hr
6hr
24hr
VEGF-A Fold Change (2.0 Bar x 2000)
13
12
6
5
4
3
2
1
0
**
*
Control
3hr
6hr
24hr
Hours

Figure 11-13. MCP1 gene expression in human cardiac fibroblast following shockwave treatment, (A) 0.5 Bar x 1000; (B) 0.5 Bar x 1000; (C) 1.0 Bar x 1000; (D) 1 Bar x 2000; (E) 2.0 Bar x 1000; and (F) 2.0 Bar x 2000. Charts on the left are the log2*(ΔΔCT MCP1/GAPDH) versus time series from 0hr, 3-hr, 6-hr and 24-hr; error bars indicate the SEM and middle bars are the means. Charts on the on the right are the fold changes and error bars indicate 95% CI. Symbol * means $P < .05$, ** means $P < .01$, *** means $P < .001$ and **** means $P < .0001$ significant interaction with 0-hour. Symbols pairs †, ‡ and ¤ indicates significant interactions $P > .05$.

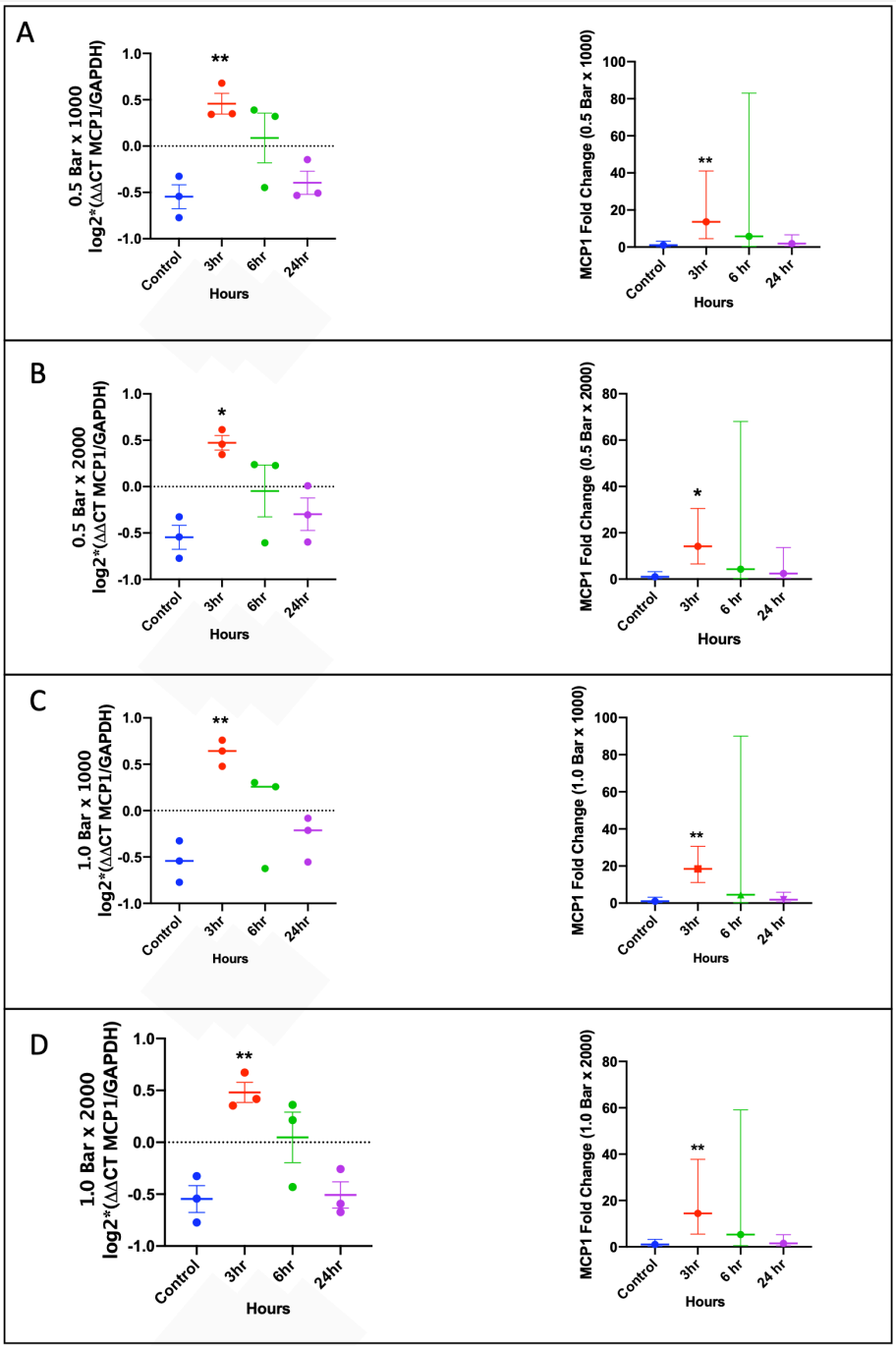

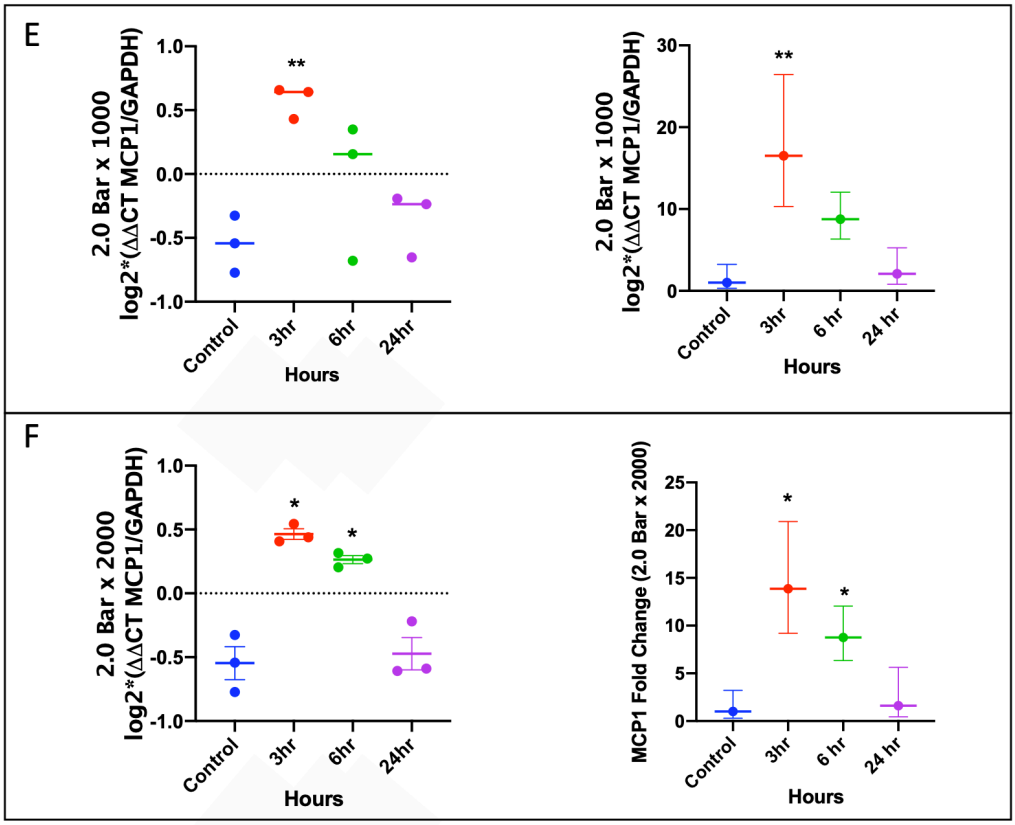
E
2.0 Bar x 1000
log2*(ΔΔCT MCP1/GAPDH)
1.0
0.5
0.0
-0.5
-1.0
**
Control
3hr
6hr
24hr
Hours
2.0 Bar x 1000
log2*(ΔΔCT MCP1/GAPDH)
30
20
10
0
**
Control
3hr
6 hr
24 hr
Hours
F
2.0 Bar x 2000
log2*(ΔΔCT MCP1/GAPDH)
1.0
0.5
0.0
-0.5
-1.0
*
*
Control
3hr
6hr
24hr
Hours
MCP1 Fold Change (2.0 Bar x 2000)
25
20
15
10
5
0
*
*
Control
3hr
6 hr
24 hr
Hours

Figure 11-14. TAC1 gene expression in human cardiac fibroblast following shockwave treatment, (A) 0.5 Bar x 1000; (B) 0.5 Bar x 1000; (C) 1.0 Bar x 1000; (D) 1 Bar x 2000; (E) 2.0 Bar x 1000; and (F) 2.0 Bar x 2000. Charts on the left are the log2*(ΔΔCT TAC1/GAPDH) versus time series from 0hr, 3-hr, 6-hr and 24-hr; error bars indicate the SEM and middle bars are the means. Charts on the on the right are the fold changes and error bars indicate 95% CI. Symbol * means $P < .05$, ** means $P < .01$, *** means $P < .001$ and **** means $P < .0001$ significant interaction with 0-hour. Symbols pairs †, ‡ and ¤ indicates significant interactions $P > .05$

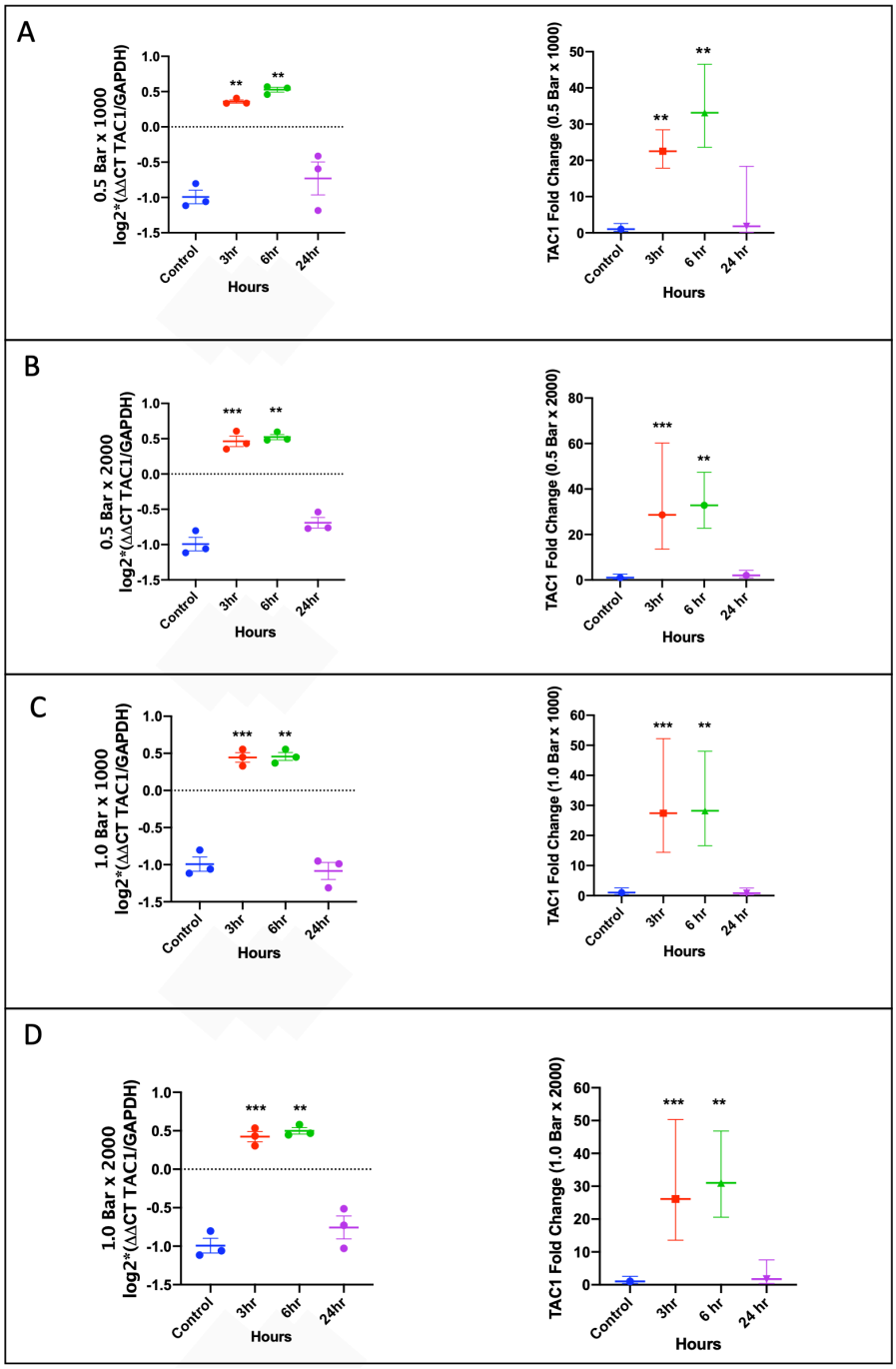

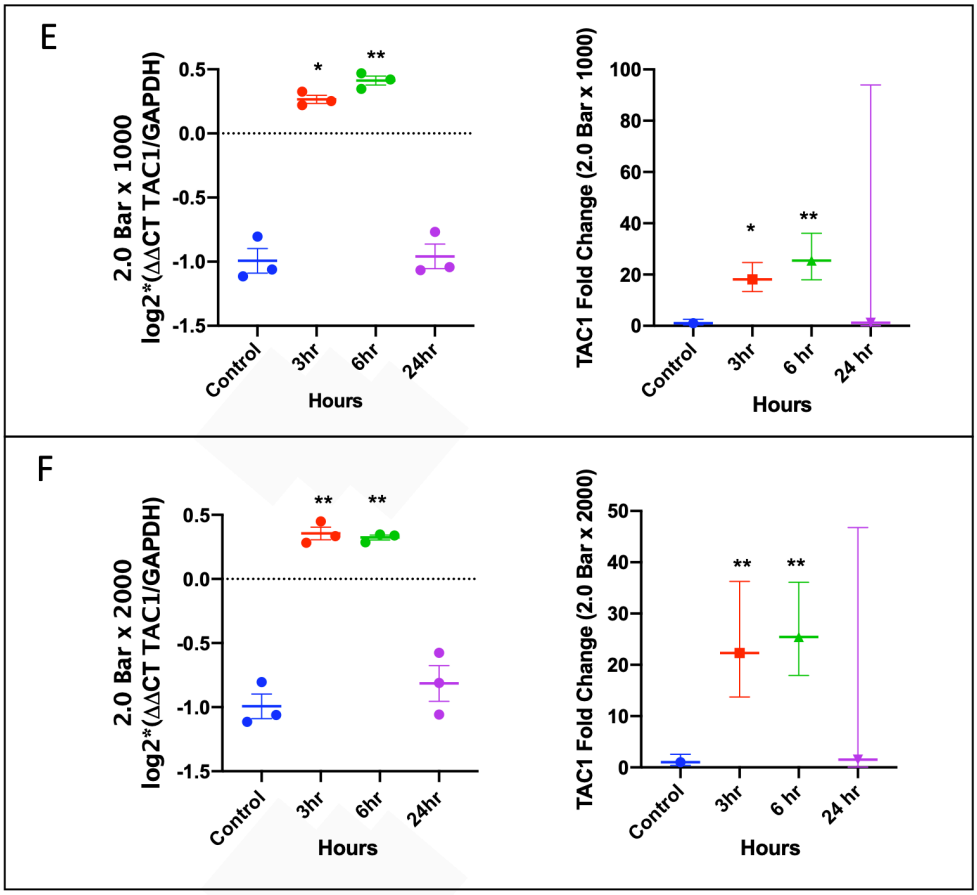
E
2.0 Bar x 1000
log2*(ΔΔCT TAC1/GAPDH)
0.5
0.0
-0.5
-1.0
-1.5
*
**
Control
3hr
6hr
24hr
Hours
TAC1 Fold Change (2.0 Bar x 1000)
100
80
60
40
20
0
*
**
Control
3hr
6 hr
24 hr
Hours
F
2.0 Bar x 2000
log2*(ΔΔCT TAC1/GAPDH)
0.5
0.0
-0.5
-1.0
-1.5
**
**
Control
3hr
6hr
24hr
Hours
TAC1 Fold Change (2.0 Bar x 2000)
50
40
30
20
10
0
**
**
Control
3hr
6 hr
24 hr
Hours

Figure 11-15. IGF1 gene expression in human cardiac fibroblast following shockwave treatment, (A) 0.5 Bar x 1000; (B) 0.5 Bar x 1000; (C) 1.0 Bar x 1000; (D) 1 Bar x 2000; (E) 2.0 Bar x 1000; and (F) 2.0 Bar x 2000. Charts on the left are the log2*(ΔΔCT TAC1/GAPDH) versus time series from 0hr, 3-hr, 6-hr and 24-hr; error bars indicate the SEM and middle bars are the means. Charts on the on the right are the fold changes and error bars indicate 95% CI. Symbol * means $P < .05$, ** means $P < .01$, *** means $P < .001$ and **** means $P < .0001$ significant interaction with 0-hour. Symbols pairs †, ‡ and

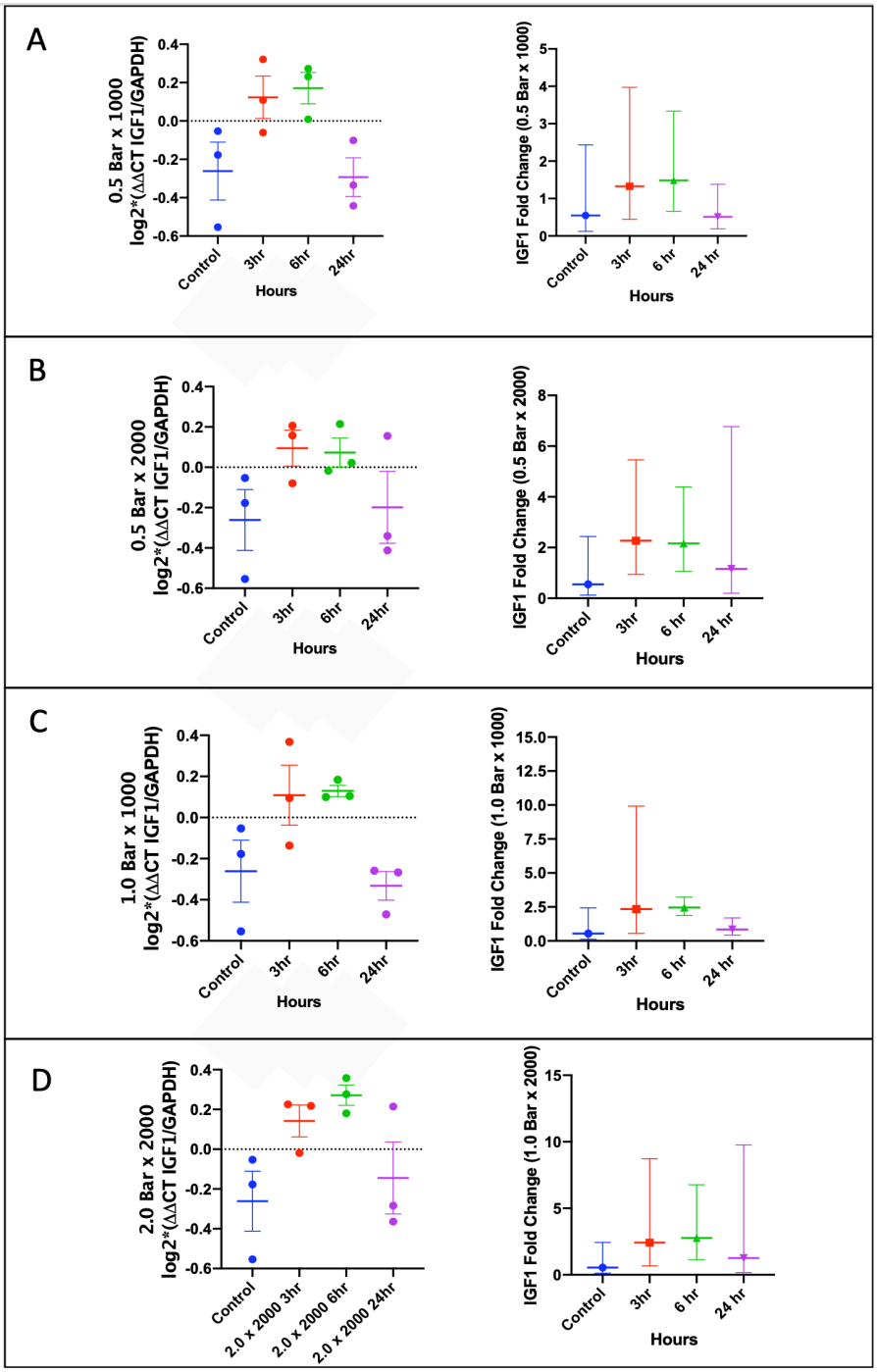

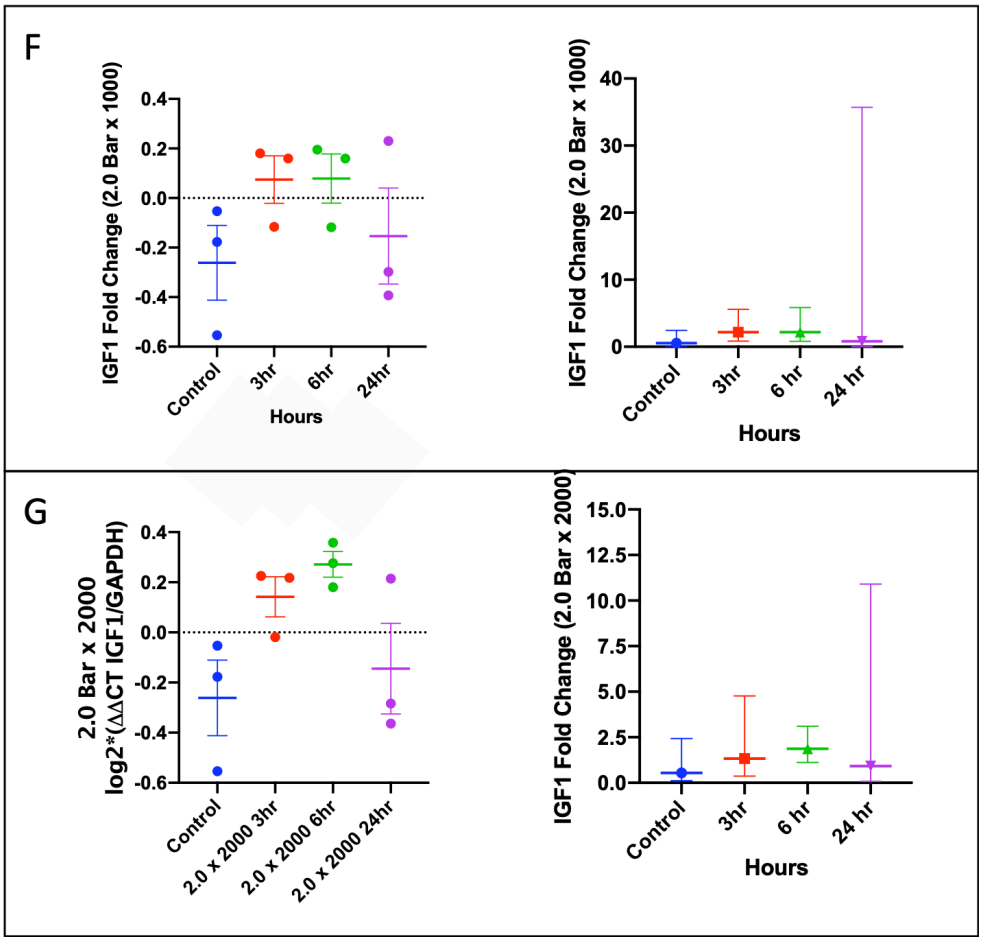
F
IGF1 Fold Change (2.0 Bar x 1000)
0.4
0.2
0.0
-0.2
-0.4
-0.6
Control
3hr
6hr
24hr
Hours
IGF1 Fold Change (2.0 Bar x 1000)
40
30
20
10
0
Control
3hr
6 hr
24 hr
Hours
G
2.0 Bar x 2000
log2*(ΔΔCT IGF1/GAPDH)
0.4
0.2
0.0
-0.2
-0.4
-0.6
Control
2.0 x 2000 3hr
2.0 x 2000 6hr
2.0 x 2000 24hr
IGF1 Fold Change (2.0 Bar x 2000)
15.0
12.5
10.0
7.5
5.0
2.5
0.0
Control
3hr
6 hr
24 hr
Hours

Figure 11-16. Heat map representation of gene expression changes of RT-qPCR data of human cardiac fibroblast treated with ascending shockwave doses (columns) and blocks of rows representing gene of interests (GOI): CXCL12, VEGF, MCP1, ANG1 and NOS3; and each cell is a biological replicate, an average from three technical replicates. The red and green colours correspond to low and high gene expression, respectively.

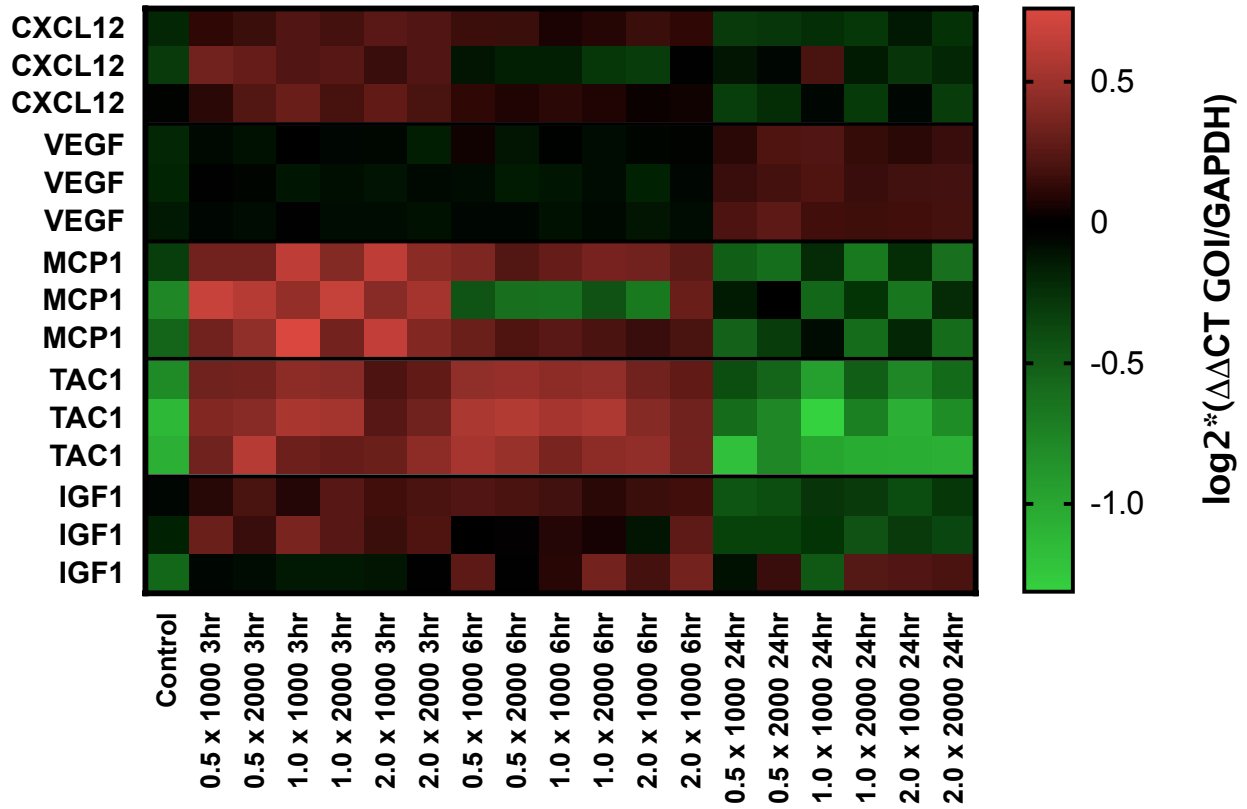

11.12 Human Ventricular Tissue

The results in this section are summarised in the heatmap in **Figure 11-17**.

11.12.1 SDF1

Shockwave doses of 1.0 Bar x 1000, 1.0 Bar x 2000, 2.0 Bar x 1000, 2.0 Bar x 2000 were assessed for SDF1 gene expression. Significant increases in the mean fold change of SDF1 gene expression was observed only in 1.0 Bar x 1000, 1.0 Bar x 2000, 2.0 Bar x 1000; showing respective mean fold change ± 95% CI of 1.84 (1.40, 2.42), 1.92 (1.10, 3.35) and 2.08 (1.69, 2.55); and *P* values of .0120, .0372 and .0013. The mean fold change of SDF1 gene expression for 2.0 Bar x 2000 was not significant, showing mean fold change ± 95% CI of 1.98 (0.90, 4.34); compared to untreated control 1.00 (0.90, 1.11).

11.12.2 VEGFA

Shockwave doses of 1.0 Bar x 1000, 1.0 Bar x 2000, 2.0 Bar x 1000, 2.0 Bar x 2000 were assessed for VEGFA gene expression. Significant increases in the mean fold change of VEGFA gene expression were observed in all tested shockwave doses, showing respective mean fold change ± 95% CI of 2.02 (1.85, 2.21), 1.64 (0.12, 22.03), 2.09 (1.73, 2.54), 1.50 (1.01, 2.23), 1.97 (1.47,2.65) and 2.94 (1.98, 4.35); and *P* values of .0002, .0005, .0005 and < .0001; compared to untreated control 1.00 (0.72, 1.38).

11.12.3 MCP1

Shockwave doses of 1.0 Bar x 1000, 1.0 Bar x 2000, 2.0 Bar x 1000, 2.0 Bar x 2000 were assessed for MCP1 gene expression. Significant increases in the mean fold change of MCP1 gene expression was observed in all tested shockwave doses, showing respective mean fold change ± 95% CI of 1.00 (0.85, 1.18), 3.54 (1.61, 7.78), 3.11 (2.25, 4.31), 3.35 (3.45, 3.82) and 4.03 (1.95, 9.82); and *P* values of .0074, < .0001, < .0001 and .0013; compared to untreated control 1.00 (0.85, 1.18).

11.12.4 ANG1

Shockwave doses of 1.0 Bar x 1000, 1.0 Bar x 2000, 2.0 Bar x 1000, 2.0 Bar x 2000 were assessed for ANG1 gene expression. Significant increases in the mean fold change of ANG1 gene expression was observed in all tested shockwave doses, showing respective mean fold change ± 95% CI of 2.38 (1.44, 3.93), 2.25 (1.73, 2.93), 2.67 (1.73, 4.12) and 2.86 (1.30, 6.28); *P* values of .0157, < .0001, .0079 and .0131; compared to untreated control 1.00 (0.81, 1.24)

11.12.5 NOS3

Shockwave doses of 1.0 Bar x 1000, 1.0 Bar x 2000, 2.0 Bar x 1000, 2.0 Bar x 2000 were assessed for NOS3 gene expression. Significant increases in the mean fold change of SDF1 gene expression was observed only in 1.0 Bar x 1000

and 2.0 Bar x 1000, showing respective mean fold change ± 95% CI of 1.49 (1.29, 1.72) and 1.33 (1.05, 1.68); and *P* values of < .0001 and .0209. Shockwave dose of 1.0 Bar x 2000 and 2.0 Bar x 2000 did not show significant increase in NOS3 gene expression showing respective mean fold change ± 95% CI of 1.29 (0.84, 1.95) and 1.27 (0.84, 1.92); and *P* values of .0588 and .0705.

Figure 11-17. Heat map representation of gene expression changes of RT-qPCR data of human ventricular tissue treated with ascending shockwave doses (columns) and blocks of rows representing gene of interests (GOI): SDF1, VEGF, MCP1, ANG1 and NOS3; and each cell is a biological replicate, an average from three technical replicates. The red and green colours correspond to low and high gene expression, respectively.

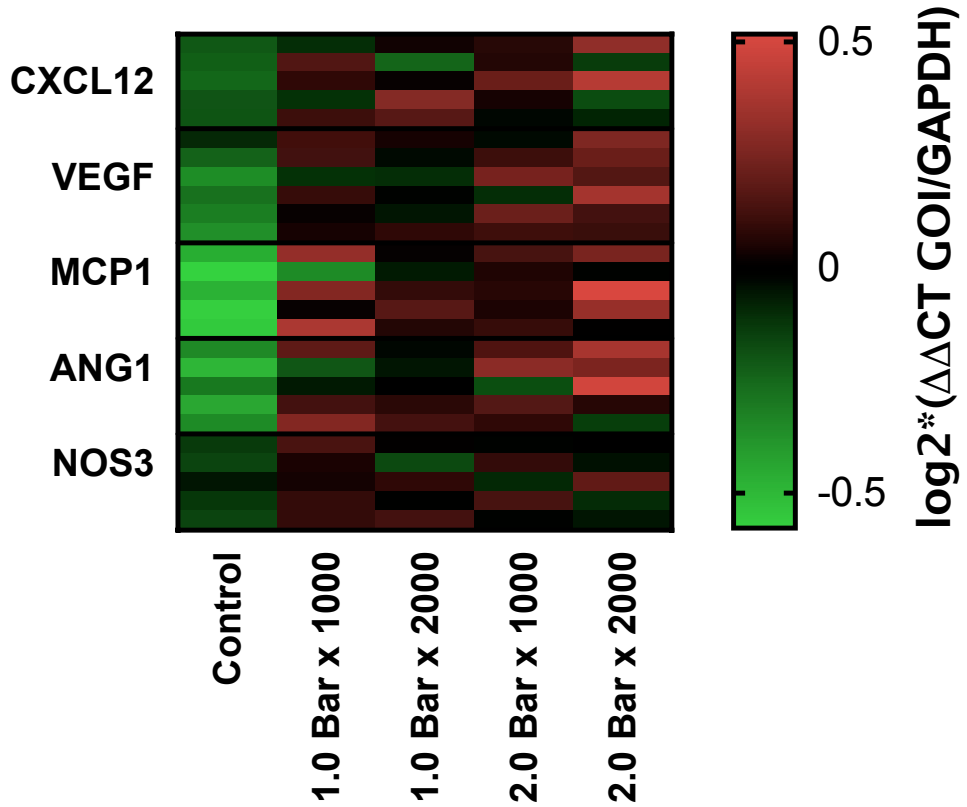

11.13 DISCUSSION

In this chapter, *in vitro* shockwave experiments were performed on human endothelial cells, human cardiac fibroblast, cardiomyocytes and human ventricular tissue; to discover which cell type have a role in SDF1 and VEGFA expression with shockwave, and to discover suitable shockwave dose.

It was discovered that shockwave could not induce SDF1 and VEGFA expression in the cardiomyocytes. However, both SDF1 and VEGFA expression could be induced in the endothelial cells and human cardiac fibroblast. In the endothelial cells, the SDF1 gene expression occurred within a few hours of exposure to shockwave, whereas in the fibroblasts, the SDF1 expression could take 24 hours after stimulation with shockwave. On the contrary, the VEGFA expression in the fibroblasts occurred within a few hours and returned to baseline at 24 hours, while in the endothelial cells, the VEGFA gene expression would take 24 hours after stimulation with shockwave. The natural lag of SDF1 expression in the fibroblasts compared to the endothelial cells could be for the creation of SDF1 gradient from the endothelial layer into the tissue to allow intravascular progenitors to migrate from the blood into the tissue. In the endothelial cells, shockwave could induce SDF1 at both 1 Bar x 1000 and 2 Bar x 1000, while VEGFA could only be induced with 1 Bar x 1000, which showed bimodal expression mild peaking at 2 hours, then a dip to baseline at 4 hours

to continue to increase at 6 hours and 24 hours. The purpose of bimodal expression of VEGFA was not clear; bimodality, however, has been reported to serve as a feedback loop. [317] In human cardiac fibroblast, shockwave could also induce MCP1, TAC1 and IGF1 expression.

In the Langendorff hearts of SHR, energy levels of 1 Bar x 1000, 2 Bar x 1000 and 3 Bar x 1000 were assessed; shockwave could only induce SDF1 expression only using 1 Bar x 1000, and no VEGFA in any of them in any of the shockwave setting. The Langendorff hearts method did not allow extended examination time, so it could not be excluded that the gene expression happening later and missed. It has been reported that VEGF expression is naturally increased in the SHR, [318] the high background could have been impeding the read-out.

In human ventricular tissue, all shockwave doses of 1.0 Bar x 1000, 1.0 Bar x 2000, 2.0 Bar x 1000, 2.0 Bar x 2000 could induce SDF1, VEGFA, MCP1, ANG1 and NOS3. The rationale for the other GOI will be discussed here. The VEGF and ANG1 are both potent proangiogenic factors. VEGF causes vascular permeability whilst ANG1 stabilises blood vessels and protects them from VEGF-induced plasma leakage. [319] The inductions of both proteins are essential for therapeutic angiogenesis, and they were shown to be inducible by shockwave. One of the possible routes of NO production by shockwave is via the AKT, as discussed in **section 8.8** (on page **319**), and here, the increase in NOS3 expression was demonstrated in human cardiac tissue. The NOS3 gene

encodes for nitric oxide synthase 3, the enzyme responsible for the synthesis of nitric oxide from L-arginine, and an increase in NOS3 expression could increase NO, which highly relevant in ischaemia-reperfusion injury as NO is known to confer cardioprotection by blocking mitochondrial permeability transition pore, [320] as one of the mechanisms.

MCP1 is interesting because not only it could home monocytes, it also displays the pleiotropic effects of chemoattractant to memory T-cells [321] and cardioprotection in ischaemia-reperfusion.[322] The significance of cardiac homing of monocytes has been discussed in **section 2.6.** Morimoto et al. [323] investigated the effect of overexpressing MCP1 in transgenic mice in cardiac ischaemia-reperfusion injury and discovered the mice had smaller infarction, better LV function compared to wild type. Furthermore, these transgenic mice exhibited macrophage infiltration, neovascularization, and myocardial IL-6 secretion, which with MCP1 synergistically activated STAT3 in cardiomyocytes, [324]exerting a cardioprotective effect. IL6 and MCP1 are on the fibroblast shockwave chemokine 'hits' list reported in **Appendix 2**. The role that MCP1 played in the angiogenesis process and limb regeneration was exemplified in the adult salamander, where the ablation of monocytes using clodronate liposomes impeded limb regeneration, and chemokines such as SDF1 and MCP1 were highly expressed. [196]

11.14 Limitations

The SHR was used not for a scientific reason but because of the availability of the animals at the time that would otherwise be culled and wasted. It would have been interesting to perform single-cell RNA-Seq to understand what genes were expressed, in what abundance, how the expression levels were spread across thousands of cells within a heterogeneous cell mixture, and what pathway and transcription factors were involved in shockwave therapy.

11.15 Conclusion

The results in this chapter have demonstrated that shockwave could induce SDF1 expression in the cardiac tissue, and according to cell type, the sources of SDF1 expression are the endothelial cells and fibroblasts, not the cardiomyocytes. The difference in the temporal expression of SDF1 between the endothelial cells and fibroblasts, which lags in the latter, could be for the purpose of a formation of SDF1 gradient to home intravascular progenitors into tissue. As the SDF1 is inducible in the fibroblast using shockwave, it is not improvident to treat tissue with a scar. The upregulation of other genes expression by shockwave reported here could be just the tip of the iceberg and warrant investigation using a high-throughput technique such as single-cell RNA-Seq.

Chapter Twelve

FINAL DISCUSSION

12.1 Overview

This thesis presents data that shockwave could be used as a treatment to reduce infarction size in cardiac ischaemic reperfusion injury, enhance cardiac contractility and promote cell homing to the heart. The addition of DPP4 inhibition to shockwave could limit the infarction size and improve cardiac contractility further. The research questions were answered using readouts from multi-sequence CMR, mostly the high-frame-rate strain for a comprehensive assessment of the experimental effects of shockwave in rat cardiac ischaemia-reperfusion injury. The CMR scanning protocols were

devised to be similar to CMR in human to ensure the translationalability of the data for human application. The summary of findings has been outlined in the thesis **introduction** in section seven. One of the mechanisms of inotropy was revealed by the increase in LV torsion due to the increase in the rotation of the base, not the apical rotation, the opposite of adrenergic stimulation. The improvement in the EF, ESV, CO with shockwave is congruent with the improvement in the global strain indices both in the Healthy and the diseased-state of ischaemia-reperfusion injury. The addition of DPP4 inhibition to shockwave in the diseased state could improve all the endo and myo global strain indices over what could be conferred by shockwave only, except in the endo and myo global circumferential strain, showing no further increment. DPP4 inhibition with shockwave enabled the establishment of rapid inotropy then decaying slowly, which otherwise required multiple shockwave treatment sessions to achieve the same magnitude, translating to a reduction in treatment burden. Shockwave could improve regional systolic function (S_{SR} - contractility) and preserve the diastolic function of the remote segments of the IR-MI hearts, which otherwise exhibited a restrictive pattern indicated by an increase in E_{SR}/ A_{SR} compared to the Healthy, IR-MI-SW and IR-MI-SWi. The evidence of cell homing by shockwave was demonstrated by the drop the T2 signal, an indication that iron-loaded cells had migrated to the heart having been shockwave-treated; the reduction of progenitors in peripheral blood

indicating consumption, and the increments in SDF1 expression in cardiac tissue treated with shockwave and shockwave with DPP4 inhibition. As the inotropic effect of shockwave was immediate, shockwave effect on cell homing was likely mechanistically distinct. Additionally, cell homing could be relevant in the improvement in tissue oxygenation and prevention of adverse cardiac remodelling in ischaemia-reperfusion injury. The thesis also reports on a proof-of-concept of the utility of segmental strain of high frame rate cine for the distinction of myocardial segment disease phenotypes that are relevant to cardiac ischaemia-reperfusion injury.

12.2 Clinical Relevance

The research output detailed in the thesis is highly relevant to human medicine and is translational. The proposed treatment tools have already received marketing authorisation, albeit for a different clinical indication; are inexpensive, could be available for the mass market of ischaemic heart disease, and most importantly, have good safety track records. There is no obstacle of GMP regulation of cell production, and the endogenous progenitors could be guided non-invasively to home to desired diseased segments of the heart. Most of the CMR readouts are already available in clinics, and this was done on purpose to ensure the translationability of the research.

12.3 Future work

A clinical trial (EudraCT no: 2013-004333-33) entitled: A phase I/II safety and efficacy of combination treatment of Shockwave, DPP4-inhibition and Parathyroid hormone for myocardial regeneration in ischemic heart failure; will be performed and is ready for recruitment. It will assess the safety of the combination treatment of shockwave with DPP4 inhibitor and parathyroid hormone. It aims to discover shockwave effects on cardiac mechanics, tissue perfusion, tissue viability, progenitors' markers in the blood, blood proteomics, and patients' ability to exercise.

12.4 Final Conclusion

The PhD thesis aims to investigate whether shockwave could be used as a treatment of myocardial ischemia-reperfusion injury and its efficacy when used in conjunction with a pharmacological DPP4 inhibitor, have been fulfilled. So does the aims to discover the best imaging indices for the assessment of the experimental effects on cardiac function in answering the research questions. Together with the improvement of cardiac function, the salvation of tissue from ischaemia-reperfusion injury, and potential use in improving the blood supply, I conclude that shockwave and DPP4 inhibition is beneficial as a treatment for ischemic heart disease and highly applicable for use in Human Medicine. The thesis has provided novel insights on the effect of shockwave

on cardiac mechanics, which would be explored in the clinical trial. The precision of the advanced imaging techniques used in CMR has rapidly helped in answering the research questions.

REFERENCES

1. Yellon DM, Hausenloy DJ. Myocardial Reperfusion Injury. *N Engl J Med*. 2007;357(11):1121-1135. doi:10.1056/NEJMra071667
2. Simonis G, Strasser RH, Ebner B. Reperfusion injury in acute myocardial infarction. *Crit Care*. 2012;16(2):A22. doi:10.1186/cc11280
3. Ponikowski P, Voors AA, Anker SD, et al. 2016 ESC Guidelines for the diagnosis and treatment of acute and chronic heart failure. *Eur Heart J*. Published online 2016. doi:10.1093/eurheartj/ehw128
4. Aicher A, Heeschen C, Sasaki K, Urbich C, Zeiher AM, Dimmeler S. Low-energy shock wave for enhancing recruitment of endothelial progenitor cells: a new modality to increase efficacy of cell therapy in chronic hind limb ischemia. *Circulation*. 2006;114(25):2823-2830. doi:10.1161/CIRCULATIONAHA.106.628623
5. Hajjar RJ, Hulot J-S. Myocardial delivery of stromal cell-derived factor 1 in patients with ischemic heart disease: safe and promising. *Circ Res*. 2013;112(5):746-747. doi:10.1161/CIRCRESAHA.113.300902
6. Penn MS, Mendelsohn FO, Schaer GL, et al. An open-label dose escalation study to evaluate the safety of administration of nonviral stromal cell-derived factor-1 plasmid to treat symptomatic ischemic heart failure. *Circ Res*. 2013;112(5):816-825. doi:10.1161/CIRCRESAHA.111.300440
7. Saxena A, Fish JE, White MD, et al. Stromal cell-derived factor-1alpha is cardioprotective after myocardial infarction. *Circulation*. 2008;117(17):2224-2231. doi:10.1161/CIRCULATIONAHA.107.694992
8. Busillo JM, Benovic JL. Regulation of CXCR4 signaling. *Biochim Biophys Acta - Biomembr*. 2007;1768(4):952-963. doi:10.1016/j.bbamem.2006.11.002
9. Abdel-Latif A, Bolli R, Tleyjeh IM, et al. Adult bone marrow-derived cells for cardiac repair: a systematic review and meta-analysis. *Arch Intern Med*. 2007;167(10):989-997. doi:167/10/989 [pii]\r10.1001/archinte.167.10.989 [doi]
10. Strauer BE, Steinhoff G. 10 years of intracoronary and intramyocardial bone marrow stem cell therapy of the heart: From the methodological origin to clinical practice. *J Am Coll Cardiol*. 2011;58(11):1095-1104. doi:10.1016/j.jacc.2011.06.016
11. Assmus B, Walter DH, Seeger FH, et al. Effect of Shock Wave–

Facilitated Intracoronary Cell Therapy on LVEF in Patients With Chronic Heart Failure. *Jama*. 2013;309(15):1622. doi:10.1001/jama.2013.3527
12. Baraniak PR, McDevitt TC. Stem cell paracrine actions and tissue regeneration. *Regen Med*. 2010;5(1):121-143. doi:10.2217/rme.09.74
13. Peled A, Kollet O, Ponomaryov T, et al. The chemokine SDF-1 activates the integrins LFA-1, VLA-4, and VLA-5 on immature human CD34(+) cells: role in transendothelial/stromal migration and engraftment of NOD/SCID mice. *Blood*. 2000;95(11):3289-3296.
14. Penicka M, Lang O, Widimsky P, et al. One-day kinetics of myocardial engraftment after intracoronary injection of bone marrow mononuclear cells in patients with acute and chronic myocardial infarction. *Heart*. 2007;93(7):837-841. doi:10.1136/hrt.2006.091934
15. Misra P, Lebeche D, Ly H, et al. Quantitation of CXCR4 expression in myocardial infarction using 99mTc-labeled SDF-1α. *J Nucl Med*. Published online 2008. doi:10.2967/jnumed.107.050054
16. Lüscher TF, Richard V, Tschudi M, Yang Z, Boulanger C. Endothelial control of vascular tone in large and small coronary arteries. *J Am Coll Cardiol*. Published online 1990. doi:10.1016/0735-1097(90)90619-Z
17. Napoli C, de Nigris F, Williams-Ignarro S, Pignalosa O, Sica V, Ignarro LJ. Nitric oxide and atherosclerosis: An update. *Nitric Oxide - Biol Chem*. 2006;15(4):265-279. doi:10.1016/j.niox.2006.03.011
18. Foguenne J, Di Stefano I, Giet O, Beguin Y, Gothot A. Ex vivo expansion of hematopoietic progenitor cells is associated with downregulation of alpha4 integrin- and CXCR4-mediated engraftment in NOD/SCID beta2-microglobulin-null mice. *Haematologica*. 2009;94(2):185-194. doi:10.3324/haematol.13206
19. Phinney DG. Functional heterogeneity of mesenchymal stem cells: implications for cell therapy. *J Cell Biochem*. 2012;113(9):2806-2812. doi:10.1002/jcb.24166
20. Ziaeian B, Fonarow GC. Epidemiology and aetiology of heart failure. *Nat Rev Cardiol*. Published online 2016. doi:10.1038/nrcardio.2016.25
21. BHF. Heart and Circulatory Disease Statistics 2019. *2019 Stat Compend*. 2019;(April):94-96. https://www.bhf.org.uk/what-we-do/our-research/heart-statistics/heart-statistics-publications/cardiovascular-disease-statistics-2019
22. Sutherland K. *Bridging the Quality Gap*.; 2010. doi:10.1080/14719030000000031
23. Mehta PA, Dubrey SW, McIntyre HF, et al. Improving survival in the 6 months after diagnosis of heart failure in the past decade: Population-based data from the UK. *Heart*. Published online 2009. doi:10.1136/hrt.2008.156034
24. NICE. Putting NICE guidance into practice. Resource impact report : Chronic heart failure in adults. 2018;(March). https://www.nice.org.uk/guidance/ng92/resources/resource-impact-report-pdf-4788823645

25. Brodie BR, Stuckey TD, Wall TC, et al. Importance of time to reperfusion for 30-day and late survival and recovery of left ventricular function after primary angioplasty for acute myocardial infarction. *J Am Coll Cardiol*. 1998;32(5):1312-1319. doi:10.1016/S0735-1097(98)00395-7
26. Conrad N, Judge A, Tran J, et al. Temporal trends and patterns in heart failure incidence: a population-based study of 4 million individuals. *Lancet (London, England)*. 2018;391(10120):572-580. doi:10.1016/S0140-6736(17)32520-5
27. Angiotensin-neprilysin inhibition versus enalapril in heart failure. *Kardiologiya*. Published online 2014. doi:10.5005/jp/books/12834_88
28. Desai AS, McMurray JJV, Packer M, et al. Effect of the angiotensin-receptor-neprilysin inhibitor LCZ696 compared with enalapril on mode of death in heart failure patients. *Eur Heart J*. Published online 2015. doi:10.1093/eurheartj/ehv186
29. Velazquez EJ, Morrow DA, DeVore AD, et al. Angiotensin–Neprilysin Inhibition in Acute Decompensated Heart Failure. *N Engl J Med*. Published online 2019. doi:10.1056/nejmoa1812851
30. McMurray JJV, Solomon SD, Inzucchi SE, et al. Dapagliflozin in Patients with Heart Failure and Reduced Ejection Fraction. *N Engl J Med*. Published online 2019. doi:10.1056/nejmoa1911303
31. Transplant NB and. Report on cardiothoracic organ transplantation. *NHS Blood Transpl*. 2018;2018(September 2018). https://nhsbtdbe.blob.core.windows.net/umbraco-assets-corp/12252/nhsbt-cardiothoracic-transplantation-annual-report-2017-2018.pdf
32. Effects of Enalapril on Mortality in Severe Congestive Heart Failure. *N Engl J Med*. Published online 1987. doi:10.1056/nejm198706043162301
33. Fraund S, Pethig K, Franke U, et al. Ten year survival after heart transplantation: palliative procedure or successful long term treatment? *Heart*. 1999;82(1):47-51. doi:10.1136/hrt.82.1.47
34. Heusch G. Myocardial ischaemia–reperfusion injury and cardioprotection in perspective. *Nat Rev Cardiol*. 2020;17(12):773-789. doi:10.1038/s41569-020-0403-y
35. Piper HM, Garcña-Dorado D, Ovize M. A fresh look at reperfusion injury1. *Cardiovasc Res*. 1998;38(2):291-300. doi:10.1016/S0008-6363(98)00033-9
36. Reimer KA, Lowe JE, Rasmussen MM, Jennings RB. The wavefront phenomenon of ischemic cell death. 1. Myocardial infarct size vs duration of coronary occlusion in dogs. *Circulation*. 1977;56(5):786-794. doi:10.1161/01.cir.56.5.786
37. Yellon DM, Hausenloy DJ. Myocardial Reperfusion Injury. *N Engl J Med*. 2007;357(11):1121-1135. doi:10.1056/NEJMra071667
38. Man C, Gong D, Zhou Y, Fan Y. Meta-analysis of remote ischemic

conditioning in patients with acute myocardial infarction. *Sci Rep*. 2017;7(1):43529. doi:10.1038/srep43529
39. Kleinbongard P, Amanakis G, Skyschally A, Heusch G. Reflection of Cardioprotection by Remote Ischemic Perconditioning in Attenuated ST-Segment Elevation During Ongoing Coronary Occlusion in Pigs: Evidence for Cardioprotection From Ischemic Injury. *Circ Res*. 2018;122(8):1102-1108. doi:10.1161/CIRCRESAHA.118.312784
40. Liu GS, Thornton J, Van Winkle DM, Stanley AW, Olsson RA, Downey JM. Protection against infarction afforded by preconditioning is mediated by A1 adenosine receptors in rabbit heart. *Circulation*. 1991;84(1):350-356. doi:10.1161/01.cir.84.1.350
41. Skyschally A, Schulz R, Heusch G. Cyclosporine A at reperfusion reduces infarct size in pigs. *Cardiovasc drugs Ther*. 2010;24(1):85-87. doi:10.1007/s10557-010-6219-y
42. García-Ruiz JM, Fernández-Jiménez R, García-Alvarez A, et al. Impact of the Timing of Metoprolol Administration During STEMI on Infarct\&\#xa0;Size and Ventricular Function. *J Am Coll Cardiol*. 2016;67(18):2093-2104. doi:10.1016/j.jacc.2016.02.050
43. Heusch G. Molecular Basis of Cardioprotection. *Circ Res*. 2015;116(4):674-699. doi:10.1161/CIRCRESAHA.116.305348
44. Koul S, Andell P, Martinsson A, et al. Delay from first medical contact to primary PCI and all-cause mortality: a nationwide study of patients with ST-elevation myocardial infarction. *J Am Heart Assoc*. 2014;3(2):e000486. doi:10.1161/JAHA.113.000486
45. Francone M, Bucciarelli-Ducci C, Carbone I, et al. Impact of Primary Coronary Angioplasty Delay on Myocardial Salvage, Infarct Size, and Microvascular Damage in Patients With ST-Segment Elevation Myocardial Infarction. Insight From Cardiovascular Magnetic Resonance. *J Am Coll Cardiol*. Published online 2009. doi:10.1016/j.jacc.2009.08.024
46. Koh MY, Powis G. Passing the baton: the HIF switch. *Trends Biochem Sci*. 2012;37(9):364-372. doi:10.1016/j.tibs.2012.06.004
47. Ceradini DJ, Kulkarni AR, Callaghan MJ, et al. Progenitor cell trafficking is regulated by hypoxic gradients through HIF-1 induction of SDF-1. *Nat Med*. Published online 2004. doi:10.1038/nm1075
48. Askari AT, Unzek S, Popovic ZB, et al. Effect of stromal-cell-derived factor 1 on stem-cell homing and tissue regeneration in ischaemic cardiomyopathy. *Lancet*. Published online 2003. doi:10.1016/S0140-6736(03)14232-8
49. Jung HH, Kim JY, Lim JE, Im YH. Cytokine profiling in serum-derived exosomes isolated by different methods. *Sci Rep*. Published online 2020. doi:10.1038/s41598-020-70584-z
50. Blanchard N, Lankar D, Faure F, et al. TCR Activation of Human T Cells Induces the Production of Exosomes Bearing the TCR/CD3/ζ Complex. *J Immunol*. Published online 2002. doi:10.4049/jimmunol.168.7.3235

51. Wang J, Hendrix A, Hernot S, et al. Bone marrow stromal cell-derived exosomes as communicators in drug resistance in multiple myeloma cells. *Blood*. 2014;124(4):555-566. doi:10.1182/blood-2014-03-562439
52. Alvarez-Erviti L, Seow Y, Yin H, Betts C, Lakhal S, Wood MJA. Delivery of siRNA to the mouse brain by systemic injection of targeted exosomes. *Nat Biotechnol*. Published online 2011. doi:10.1038/nbt.1807
53. Hoshino A, Costa-Silva B, Shen TL, et al. Tumour exosome integrins determine organotropic metastasis. *Nature*. Published online 2015. doi:10.1038/nature15756
54. Gollmann-Tepeköylü C, Pölzl L, Graber M, et al. miR-19a-3p containing exosomes improve function of ischaemic myocardium upon shock wave therapy. *Cardiovasc Res*. Published online 2020. doi:10.1093/cvr/cvz209
55. Miyanishi M, Tada K, Koike M, Uchiyama Y, Kitamura T, Nagata S. Identification of Tim4 as a phosphatidylserine receptor. *Nature*. Published online 2007. doi:10.1038/nature06307
56. Théry C, Zitvogel L, Amigorena S. Exosomes: Composition, biogenesis and function. *Nat Rev Immunol*. Published online 2002. doi:10.1038/nri855
57. Fader CM, Savina A, Sánchez D, Colombo MI. Exosome secretion and red cell maturation: Exploring molecular components involved in the docking and fusion of multivesicular bodies in K562 cells. *Blood Cells, Mol Dis*. Published online 2005. doi:10.1016/j.bcmd.2005.07.002
58. Huisamen B, Genis A, Marais E, Lochner A. Pre-treatment with a DPP-4 inhibitor is infarct sparing in hearts from obese, pre-diabetic rats. *Cardiovasc Drugs Ther*. Published online 2011. doi:10.1007/s10557-010-6271-7
59. Remm F, Kränkel N, Lener D, Drucker DJ, Sopper S, Brenner C. Sitagliptin Accelerates Endothelial Regeneration after Vascular Injury Independent from GLP1 Receptor Signaling. *Stem Cells Int*. Published online 2018. doi:10.1155/2018/5284963
60. Fadini GP, Boscaro E, Albiero M, et al. The oral dipeptidyl peptidase-4 inhibitor sitagliptin increases circulating endothelial progenitor cells in patients with type 2 diabetes: Possible role of stromal-derived factor-1α. *Diabetes Care*. Published online 2010. doi:10.2337/dc10-0187
61. Fadini GP, de Kreutzenberg S, Agostini C, et al. Low CD34+ cell count and metabolic syndrome synergistically increase the risk of adverse outcomes. *Atherosclerosis*. Published online 2009. doi:10.1016/j.atherosclerosis.2009.03.040
62. Werner N, Kosiol S, Schiegl T, et al. Circulating Endothelial Progenitor Cells and Cardiovascular Outcomes. *N Engl J Med*. Published online 2005. doi:10.1056/nejmoa043814
63. Theiss HD, Vallaster M, Rischpler C, et al. Dual stem cell therapy after myocardial infarction acts specifically by enhanced homing via the SDF-1/CXCR4 axis. *Stem Cell Res*. Published online 2011.

doi:10.1016/j.scr.2011.05.003
64. Dlubek D, Drabczak-Skrzypek D, Lange A. Low CXCR4 membrane expression on CD34+ cells characterizes cells mobilized to blood. *Bone Marrow Transplant*. Published online 2006. doi:10.1038/sj.bmt.1705198
65. Lévesque JP, Hendy J, Takamatsu Y, Simmons PJ, Bendall LJ. Disruption of the CXCR4/CXCL12 chemotactic interaction during hematopoietic stem cell mobilization induced by gcsf or cyclophosphamide. *J Clin Invest*. Published online 2003. doi:10.1172/JCI15994
66. Hill JM, Bartunek J. The end of granulocyte colony-stimulating factor in acute myocardial infarction? Reaping the benefits beyond cytokine mobilization. *Circulation*. Published online 2006. doi:10.1161/CIRCULATIONAHA.106.623777
67. Abbott JD, Huang Y, Liu D, Hickey R, Krause DS, Giordano FJ. Stromal cell-derived factor-1α plays a critical role in stem cell recruitment to the heart after myocardial infarction but is not sufficient to induce homing in the absence of injury. *Circulation*. Published online 2004. doi:10.1161/01.CIR.0000147780.30124.CF
68. Long M, Cai L, Li W, et al. DPP-4 inhibitors improve diabetic wound healing via direct and indirect promotion of epithelial-mesenchymal transition and reduction of scarring. *Diabetes*. Published online 2018. doi:10.2337/db17-0934
69. Schächinger V, Erbs S, Elsässer A, et al. Intracoronary Bone Marrow–Derived Progenitor Cells in Acute Myocardial Infarction. *N Engl J Med*. 2006;355(12):1210-1221. doi:10.1056/NEJMoa060186
70. Assmus B, Schächinger V, Teupe C, et al. Transplantation of progenitor cells and regeneration enhancement in acute myocardial infarction (TOPCARE-AMI). *Circulation*. Published online 2002. doi:10.1161/01.CIR.0000043246.74879.CD
71. Lunde K, Solheim S, Aakhus S, Arnesen H, Abdelnoor M, Forfang K. Autologous stem cell transplantation in acute myocardial infarction: The ASTAMI randomized controlled trial. Intracoronary transplantation of autologous mononuclear bone marrow cells, study design and safety aspects. *Scand Cardiovasc J*. Published online 2005. doi:10.1080/14017430510009131
72. Lunde K, Solheim S, Aakhus S, et al. Intracoronary Injection of Mononuclear Bone Marrow Cells in Acute Myocardial Infarction. *N Engl J Med*. Published online 2006. doi:10.1056/nejmoa055706
73. Seeger FH, Rasper T, Fischer A, et al. Heparin disrupts the CXCR4/SDF-1 axis and impairs the functional capacity of bone marrow-derived mononuclear cells used for cardiovascular repair. *Circ Res*. 2012;111(7):854-862. doi:10.1161/CIRCRESAHA.112.265678
74. Xu X, Dai Y. Heparin: An intervenor in cell communication. *J Cell Mol Med*. Published online 2010. doi:10.1111/j.1582-4934.2009.00871.x
75. Garcia MC, Sanchez JA, Sharma VK, Sheu S-S. Extracellular heparin

inhibits Ca2+ transients and contraction in mammalian cardiac myocytes. *Pflügers Arch*. 1995;431(1):84-90. doi:10.1007/BF00374380
76. Bendas G, Borsig L. Cancer cell adhesion and metastasis: Selectins, integrins, and the inhibitory potential of heparins. *Int J Cell Biol*. Published online 2012. doi:10.1155/2012/676731
77. Ley K. Molecular mechanisms of leukocyte recruitment in the inflammatory process. *Cardiovasc Res*. 1996;32(4):733-742.
78. Oi K, Fukumoto Y, Ito K, et al. Extracorporeal shock wave therapy ameliorates hindlimb ischemia in rabbits. *Tohoku J Exp Med*. Published online 2008. doi:10.1620/tjem.214.151
79. Fu M, Sun CK, Lin YC, et al. Extracorporeal shock wave therapy reverses ischemia-related left ventricular dysfunction and remodeling: Molecular-cellular and functional assessment. *PLoS One*. Published online 2011. doi:10.1371/journal.pone.0024342
80. Lorenz E, Uphoff D, Reid TR, Shelton E. Modification of irradiation injury in mice and guinea pigs by bone marrow injections. *J Natl Cancer Inst*. Published online 1951. doi:10.1093/jnci/12.1.197
81. McCulloch EA, Till JE. Perspectives on the properties of stem cells. *Nat Med*. Published online 2005. doi:10.1038/nm1005-1026
82. Wollert KC, Meyer GP, Lotz J, et al. Intracoronary autologous bone-marrow cell transfer after myocardial infarction: The BOOST randomised controlled clinical trial. *Lancet*. Published online 2004. doi:10.1016/S0140-6736(04)16626-9
83. Hendrikx M, Hensen K, Clijsters C, et al. Recovery of regional but not global contractile function by the direct intramyocardial autologous bone marrow transplantation: Results from a randomized controlled clinical trial. *Circulation*. Published online 2006. doi:10.1161/CIRCULATIONAHA.105.000505
84. Perin EC, Silva G V., Henry TD, et al. A randomized study of transendocardial injection of autologous bone marrow mononuclear cells and cell function analysis in ischemic heart failure (FOCUS-HF). *Am Heart J*. Published online 2011. doi:10.1016/j.ahj.2011.01.028
85. Seth S, Narang R, Bhargava B, et al. Percutaneous Intracoronary Cellular Cardiomyoplasty for Nonischemic Cardiomyopathy: Clinical and Histopathological Results: The First-in-Man ABCD (Autologous Bone Marrow Cells in Dilated Cardiomyopathy) Trial. *J Am Coll Cardiol*. Published online 2006. doi:10.1016/j.jacc.2006.07.057
86. Lee JW, Lee SH, Youn YJ, et al. A randomized, open-label, multicenter trial for the safety and efficacy of adult mesenchymal stem cells after acute myocardial infarction. *J Korean Med Sci*. Published online 2014. doi:10.3346/jkms.2014.29.1.23
87. Houtgraaf JH, Den Dekker WK, Van Dalen BM, et al. First experience in humans using adipose tissue-derived regenerative cells in the treatment of patients with ST-segment elevation myocardial infarction. *J Am Coll Cardiol*. Published online 2012.

doi:10.1016/j.jacc.2011.09.065
88. Fisher SA, Doree C, Mathur A, Taggart DP, Martin-Rendon E. Stem cell therapy for chronic ischaemic heart disease and congestive heart failure. *Cochrane Database Syst Rev*. Published online 2016. doi:10.1002/14651858.CD007888.pub3
89. Senyo SE, Steinhauser ML, Pizzimenti CL, et al. Mammalian heart renewal by pre-existing cardiomyocytes. *Nature*. Published online 2013. doi:10.1038/nature11682
90. Bergmann O, Bhardwaj RD, Bernard S, et al. Evidence for cardiomyocyte renewal in humans. *Science (80-)*. Published online 2009. doi:10.1126/science.1164680
91. Kajstura J, Gurusamy N, Ogórek B, et al. Myocyte turnover in the aging human heart. *Circ Res*. Published online 2010. doi:10.1161/CIRCRESAHA.110.231498
92. Murry CE, Soonpaa MH, Reinecke H, et al. Haematopoietic stem cells do not transdifferentiate into cardiac myocytes in myocardial infarcts. *Nature*. Published online 2004. doi:10.1038/nature02446
93. Grinnemo KH, Månsson-Broberg A, Leblanc K, et al. Human mesenchymal stem cells do not differentiate into cardiomyocytes in a cardiac ischemic xenomodel. *Ann Med*. Published online 2006. doi:10.1080/07853890500422982
94. Boon RA, Dimmeler S. MicroRNAs in myocardial infarction. *Nat Rev Cardiol*. Published online 2015. doi:10.1038/nrcardio.2014.207
95. Chen Y, Yang Z, Zhao ZA, Shen Z. Direct reprogramming of fibroblasts into cardiomyocytes. *Stem Cell Res Ther*. Published online 2017. doi:10.1186/s13287-017-0569-3
96. Bolli R, Chugh AR, D'Amario D, et al. Cardiac stem cells in patients with ischaemic cardiomyopathy (SCIPIO): Initial results of a randomised phase 1 trial. *Lancet*. Published online 2011. doi:10.1016/S0140-6736(11)61590-0
97. Makkar RR, Kereiakes DJ, Aguirre F, et al. Intracoronary ALLogeneic heart STem cells to Achieve myocardial Regeneration (ALLSTAR): a randomized, placebo-controlled, double-blinded trial. *Eur Heart J*. 2020;41(36):3451-3458. doi:10.1093/eurheartj/ehaa541
98. Li Y, He L, Huang X, et al. Genetic lineage tracing of nonmyocyte population by dual recombinases. *Circulation*. Published online 2018. doi:10.1161/CIRCULATIONAHA.118.034250
99. Liu Q, Yang R, Huang X, et al. Genetic lineage tracing identifies in situ Kit-expressing cardiomyocytes. *Cell Res*. Published online 2016. doi:10.1038/cr.2015.143
100. Leri A, Kajstura J, Anversa P. Role of cardiac stem cells in cardiac pathophysiology: A paradigm shift in human myocardial biology. *Circ Res*. Published online 2011. doi:10.1161/CIRCRESAHA.111.243154
101. Quaini F, Urbanek K, Beltrami AP, et al. Chimerism of the Transplanted Heart. *N Engl J Med*. Published online 2002.

doi:10.1056/nejmoa012081
102. Müller P, Pfeiffer P, Koglin J, et al. Cardiomyocytes of noncardiac origin in myocardial biopsies of human transplanted hearts. *Circulation*. 2002;106(1):31-35. doi:10.1161/01.cir.0000022405.68464.ca
103. Spudich JA. The myosin swinging cross-bridge model. *Nat Rev Mol Cell Biol*. Published online 2001. doi:10.1038/35073086
104. Ahmad T, Miller PE, McCullough M, et al. Why has positive inotropy failed in chronic heart failure? Lessons from prior inotrope trials. *Eur J Heart Fail*. Published online 2019. doi:10.1002/ejhf.1557
105. Moss AJ, Zareba W, Hall WJ, et al. Prophylactic Implantation of a Defibrillator in Patients with Myocardial Infarction and Reduced Ejection Fraction. *N Engl J Med*. Published online 2002. doi:10.1056/nejmoa013474
106. Kumar NT, Liestøl K, Løberg EM, Reims HM, Mæhlen J. Postmortem heart weight: Relation to body size and effects of cardiovascular disease and cancer. *Cardiovasc Pathol*. Published online 2014. doi:10.1016/j.carpath.2013.09.001
107. Finkelhor RS, Moallem M, Bahler RC. Characteristics and impact of obesity on the outpatient echocardiography laboratory. *Am J Cardiol*. Published online 2006. doi:10.1016/j.amjcard.2005.10.052
108. Singh M, Sethi A, Mishra AK, Subrayappa NK, Stapleton DD, Pellikka PA. Echocardiographic Imaging Challenges in Obesity: Guideline Recommendations and Limitations of Adjusting to Body Size. *J Am Heart Assoc*. Published online 2020. doi:10.1161/JAHA.119.014609
109. Okoshi MP, Capalbo RV, Romeiro FG, Okoshi K. Cardiac cachexia: Perspectives for prevention and treatment. *Arq Bras Cardiol*. Published online 2017. doi:10.5935/abc.20160142
110. Kobayashi M, Izawa H, Cheng XW, et al. Dobutamine Stress Testing as a Diagnostic Tool for Evaluation of Myocardial Contractile Reserve in Asymptomatic or Mildly Symptomatic Patients With Dilated Cardiomyopathy. *JACC Cardiovasc Imaging*. Published online 2008. doi:10.1016/j.jcmg.2008.04.012
111. Okumura T, Shimizu S, Fukaya K, et al. [Assessment of cardiac contractile reserve]. *Rinsho Byori*. 2013;61(10):917-923.
112. Greenberg NL, Firstenberg MS, Castro PL, et al. Doppler-derived myocardial systolic strain rate is a strong index of left ventricular contractility. *Circulation*. Published online 2002. doi:10.1161/hc0102.101396
113. Lucero CM, Andrade DC, Toledo C, et al. Cardiac remodeling and arrhythmogenesis are ameliorated by administration of Cx43 mimetic peptide Gap27 in heart failure rats. *Sci Rep*. Published online 2020. doi:10.1038/s41598-020-63336-6
114. Watanabe R, Suzuki JI, Wakayama K, et al. A peptide vaccine targeting angiotensin II attenuates the cardiac dysfunction induced by myocardial infarction. *Sci Rep*. Published online 2017.

doi:10.1038/srep43920
115. Quintana E, Suri RM, Thalji NM, et al. Left ventricular dysfunction after mitral valve repair - The fallacy of “normal” preoperative myocardial function. *J Thorac Cardiovasc Surg*. Published online 2014. doi:10.1016/j.jtcvs.2014.07.029
116. Davis RC, Hobbs FDR, Lip GYH. History and epidemiology. *BMJ*. 2000;320(7226):39-42. doi:10.1136/bmj.320.7226.39
117. Stamm RB, Gibson RS, Bishop HL, Carabello BA, Beller GA, Martin RP. Echocardiographic detection of infarct-localized asynergy and remote asynergy during acute myocardial infarction: Correlation with the extent of angiographic coronary disease. *Circulation*. Published online 1983. doi:10.1161/01.CIR.67.1.233
118. Barnes E, Khan MA. Myocardial stunning in man. *Heart Fail Rev*. 2003;8(2):155-160. doi:10.1023/a:1023092702389
119. Lacalzada J, de la Rosa A, Izquierdo MM, et al. Left ventricular global longitudinal systolic strain predicts adverse remodeling and subsequent cardiac events in patients with acute myocardial infarction treated with primary percutaneous coronary intervention. *Int J Cardiovasc Imaging*. Published online 2015. doi:10.1007/s10554-015-0593-2
120. Pellikka PA, She L, Holly TA, et al. Variability in Ejection Fraction Measured By Echocardiography, Gated Single-Photon Emission Computed Tomography, and Cardiac Magnetic Resonance in Patients With Coronary Artery Disease and Left Ventricular Dysfunction. *JAMA Netw open*. Published online 2018. doi:10.1001/jamanetworkopen.2018.1456
121. Bhuva AN, Bai W, Lau C, et al. A Multicenter, Scan-Rescan, Human and Machine Learning CMR Study to Test Generalizability and Precision in Imaging Biomarker Analysis. *Circ Cardiovasc Imaging*. Published online 2019. doi:10.1161/CIRCIMAGING.119.009214
122. Teske AJ, De Boeck BWL, Melman PG, Sieswerda GT, Doevendans PA, Cramer MJM. Echocardiographic quantification of myocardial function using tissue deformation imaging, a guide to image acquisition and analysis using tissue Doppler and speckle tracking. *Cardiovasc Ultrasound*. Published online 2007. doi:10.1186/1476-7120-5-27
123. Zhang J, Chen J, Cheong B, Pednekar A, Muthupillai R. High frame rate cardiac cine MRI for the evaluation of diastolic function and its direct correlation with echocardiography. *J Magn Reson Imaging*. Published online 2019. doi:10.1002/jmri.26791
124. Voigt JU, Pedrizzetti G, Lysyansky P, et al. Definitions for a common standard for 2D speckle tracking echocardiography: consensus document of the EACVI/ASE/Industry Task Force to standardize deformation imaging. *Eur Heart J Cardiovasc Imaging*. Published online 2015. doi:10.1093/ehjci/jeu184
125. Bohl S, Medway DJ, Schulz-Menger J, Schneider JE, Neubauer S, Lygate

CA. Refined approach for quantification of in vivo ischemia-reperfusion injury in the mouse heart. *Am J Physiol Heart Circ Physiol*. 2009;297(6):H2054-8. doi:10.1152/ajpheart.00836.2009
126. Dongworth RK, Campbell-Washburn AE, Cabrera-Fuentes HA, et al. Quantifying the area-at-risk of myocardial infarction in-vivo using arterial spin labeling cardiac magnetic resonance. *Sci Rep*. Published online 2017. doi:10.1038/s41598-017-02544-z
127. Higgins CB, Herfkens R, J. Lipton M, et al. Nuclear magnetic resonance imaging of acute myocardial infarction in dogs: Alterations in magnetic relaxation times. *Am J Cardiol*. Published online 1983. doi:10.1016/0002-9149(83)90093-0
128. Meyers SM, Kolind SH, Laule C, MacKay AL. Measuring water content using T2 relaxation at 3 T: Phantom validations and simulations. *Magn Reson Imaging*. Published online 2016. doi:10.1016/j.mri.2015.11.008
129. Bloch F. Nuclear induction. *Phys Rev*. Published online 1946. doi:10.1103/PhysRev.70.460
130. Fernández-Jiménez R, Sánchez-González J, Aguero J, et al. Fast T2 gradient-spin-echo (T2-GraSE) mapping for myocardial edema quantification: First in vivo validation in a porcine model of ischemia/reperfusion. *J Cardiovasc Magn Reson*. Published online 2015. doi:10.1186/s12968-015-0199-9
131. Fernández-Jiménez R, Sánchez-González J, Agüero J, et al. Myocardial edema after ischemia/reperfusion is not stable and follows a bimodal pattern: Imaging and histological tissue characterization. *J Am Coll Cardiol*. 2015;65(4):315-323. doi:10.1016/j.jacc.2014.11.004
132. Fernández-Jiménez R, Barreiro-Pérez M, Martin-García A, et al. Dynamic edematous response of the human heart to myocardial infarction: Implications for assessing myocardial area at risk and salvage. *Circulation*. Published online 2017. doi:10.1161/CIRCULATIONAHA.116.025582
133. Nordlund D, Klug G, Heiberg E, et al. Multi-vendor, multicentre comparison of contrast-enhanced SSFP and T2-STIR CMR for determining myocardium at risk in ST-elevation myocardial infarction. *Eur Heart J Cardiovasc Imaging*. Published online 2016. doi:10.1093/ehjci/jew027
134. Carrick D, Haig C, Ahmed N, et al. Temporal evolution of myocardial hemorrhage and edema in patients after acute st-segment elevation myocardial infarction: Pathophysiological insights and clinical implications. *J Am Heart Assoc*. Published online 2016. doi:10.1161/JAHA.115.002834
135. Maxwell MP, Hearse DJ, Yellon DM. Species variation in the coronary collateral circulation during regional myocardial ischaemia: a critical determinant of the rate of evolution and extent of myocardial infarction. *Cardiovasc Res*. 1987;21(10):737-746. doi:10.1093/cvr/21.10.737

136. Patterson RE, Kirk ES. Analysis of coronary collateral structure, function, and ischemic border zones in pigs. *Am J Physiol - Hear Circ Physiol*. Published online 1983. doi:10.1152/ajpheart.1983.244.1.h23
137. Seiler C, Stoller M, Pitt B, Meier P. The human coronary collateral circulation: Development and clinical importance. *Eur Heart J*. 2013;34(34):2674-2682. doi:10.1093/eurheartj/eht195
138. Freund A, Stiermaier T, de Waha-Thiele S, et al. Coronary collaterals in patients with ST-elevation myocardial infarction presenting late after symptom onset. *Clin Res Cardiol*. 2020;109(10):1307-1315. doi:10.1007/s00392-020-01625-w
139. De Waha S, Patel MR, Granger CB, et al. Relationship between microvascular obstruction and adverse events following primary percutaneous coronary intervention for ST-segment elevation myocardial infarction: An individual patient data pooled analysis from seven randomized trials. *Eur Heart J*. Published online 2017. doi:10.1093/eurheartj/ehx414
140. Kim EK, Choi JH, Song Y Bin, et al. A protective role of early collateral blood flow in patients with ST-segment elevation myocardial infarction. *Am Heart J*. Published online 2016. doi:10.1016/j.ahj.2015.10.016
141. Hansen ESS, Pedersen SF, Pedersen SB, et al. Cardiovascular MR T2-STIR imaging does not discriminate between intramyocardial haemorrhage and microvascular obstruction during the subacute phase of a reperfused myocardial infarction. *Open Hear*. Published online 2016. doi:10.1136/openhrt-2015-000346
142. Erlinge D, Götberg M, Lang I, et al. Rapid endovascular catheter core cooling combined with cold saline as an adjunct to percutaneous coronary intervention for the treatment of acute myocardial infarction: The CHILL-MI trial: A randomized controlled study of the use of central venous cathete. *J Am Coll Cardiol*. Published online 2014. doi:10.1016/j.jacc.2013.12.027
143. Atar D, Arheden H, Berdeaux A, Bonnet JL, Carlsson M, Clemmensen P. Effect of intravenous TRO40303 as an adjunct to primary percutaneous coronary intervention for acute ST-elevation myocardial infarction: MITOCARE study results. *Eur Hear J*. 2015;36. doi:10.1093/eurheartj/ehu331
144. Janssens SP, Bogaert J, Zalewski J, et al. Nitric oxide for inhalation in ST-elevation myocardial infarction (NOMI): A multicentre, double-blind, randomized controlled trial. *Eur Heart J*. Published online 2018. doi:10.1093/eurheartj/ehy232
145. Nazir SA, Khan JN, Mahmoud IZ, et al. The REFLO-STEMI trial comparing intracoronary adenosine, sodium nitroprusside and standard therapy for the attenuation of infarct size and microvascular obstruction during primary percutaneous coronary intervention: Study protocol for a randomised control. *Trials*. Published online 2014.

doi:10.1186/1745-6215-15-371
146. Thuny F, Lairez O, Roubille F, et al. Post-conditioning reduces infarct size and edema in patients with ST-segment elevation myocardial infarction. *J Am Coll Cardiol*. Published online 2012. doi:10.1016/j.jacc.2012.03.026
147. White SK, Frohlich GM, Sado DM, et al. Remote ischemic conditioning reduces myocardial infarct size and edema in patients with ST-segment elevation myocardial infarction. *JACC Cardiovasc Interv*. Published online 2015. doi:10.1016/j.jcin.2014.05.015
148. Stub D, Smith K, Bernard S, et al. Air Versus Oxygen in ST-Segment–Elevation Myocardial Infarction. *Circulation*. 2015;131(24):2143-2150. doi:10.1161/CIRCULATIONAHA.114.014494
149. Eitel I, Wang J, Stiermaier T, et al. Impact of Morphine Treatment on Infarct Size and Reperfusion Injury in Acute Reperfused ST-Elevation Myocardial Infarction. *J Clin Med*. 2020;9(3). doi:10.3390/jcm9030735
150. Bonin M, Mewton N, Roubille F, et al. Effect and Safety of Morphine Use in Acute Anterior ST-Segment Elevation Myocardial Infarction. *J Am Heart Assoc*. 2018;7(4). doi:10.1161/JAHA.117.006833
151. Lapinskas T, Grune J, Zamani SM, et al. Cardiovascular magnetic resonance feature tracking in small animals - a preliminary study on reproducibility and sample size calculation. *BMC Med Imaging*. Published online 2017. doi:10.1186/s12880-017-0223-7
152. Ünlü S, Duchenne J, Mirea O, et al. Impact of apical foreshortening on deformation measurements: a report from the EACVI-ASE Strain Standardization Task Force. *Eur Heart J Cardiovasc Imaging*. Published online 2020. doi:10.1093/ehjci/jez189
153. LeGrice IJ, Smaill BH, Chai LZ, Edgar SG, Gavin JB, Hunter PJ. Laminar structure of the heart: ventricular myocyte arrangement and connective tissue architecture in the dog. *Am J Physiol*. 1995;269(2 Pt 2):H571-82. doi:10.1152/ajpheart.1995.269.2.H571
154. STREETER DD, SPOTNITZ HM, PATEL DP, ROSS J, SONNENBLICK EH. Fiber Orientation in the Canine Left Ventricle during Diastole and Systole. *Circ Res*. 1969;24(3):339-347. doi:10.1161/01.RES.24.3.339
155. Novo Matos J, Garcia-Canadilla P, Simcock IC, et al. Micro-computed tomography (micro-CT) for the assessment of myocardial disarray, fibrosis and ventricular mass in a feline model of hypertrophic cardiomyopathy. *Sci Rep*. 2020;10(1):20169. doi:10.1038/s41598-020-76809-5
156. Hsu EW, Muzikant AL, Matulevicius SA, Penland RC, Henriquez CS. Magnetic resonance myocardial fiber-orientation mapping with direct histological correlation. *Am J Physiol*. 1998;274(5):H1627-34. doi:10.1152/ajpheart.1998.274.5.H1627
157. Tseng W-YI, Wedeen VJ, Reese TG, Smith RN, Halpern EF. Diffusion tensor MRI of myocardial fibers and sheets: correspondence with visible cut-face texture. *J Magn Reson Imaging*. 2003;17(1):31-42.

doi:10.1002/jmri.10223
158. Buckberg GD. Basic science review: The helix and the heart. *J Thorac Cardiovasc Surg*. Published online 2002. doi:10.1067/mtc.2002.122439
159. Sallin EA. Fiber Orientation and Ejection Fraction in the Human Left Ventricle. *Biophys J*. Published online 1969. doi:10.1016/S0006-3495(69)86429-5
160. Mor-Avi V, Lang RM, Badano LP, et al. Current and evolving echocardiographic techniques for the quantitative evaluation of cardiac mechanics: ASE/EAE consensus statement on methodology and indications endorsed by the Japanese society of echocardiography. *Eur J Echocardiogr*. 2011;12(3):167-205. doi:10.1093/ejechocard/jer021
161. Voigt JU, Pedrizzetti G, Lysyansky P, et al. Definitions for a common standard for 2D speckle tracking echocardiography: consensus document of the EACVI/ASE/Industry Task Force to standardize deformation imaging. *Eur Heart J Cardiovasc Imaging*. Published online 2015. doi:10.1093/ehjci/jeu184
162. Hoda SA. Underwood's Pathology: A Clinical Approach. *Am J Clin Pathol*. Published online 2019. doi:10.1093/ajcp/aqy140
163. Espe EK, Aronsen JM, Skårdal K, Schneider JE, Zhang L, Sjaastad I. Novel insight into the detailed myocardial motion and deformation of the rodent heart using high-resolution phase contrast cardiovascular magnetic resonance. *J Cardiovasc Magn Reson*. Published online 2013. doi:10.1186/1532-429X-15-82
164. Orlic D, Kajstura J, Chimenti S, et al. Bone marrow cells regenerate infarcted myocardium. *Nature*. Published online 2001. doi:10.1038/35070587
165. Alvarez-Dolado M, Pardal R, Garcia-Verdugo JM, et al. Fusion of bone-marrow-derived cells with Purkinje neurons, cardiomyocytes and hepatocytes. *Nature*. Published online 2003. doi:10.1038/nature02069
166. Amado LC, Saliaris AP, Schuleri KH, et al. Cardiac repair with intramyocardial injection of allogeneic mesenchymal stem cells after myocardial infarction. *Proc Natl Acad Sci U S A*. Published online 2005. doi:10.1073/pnas.0504388102
167. Yoon YS, Wecker A, Heyd L, et al. Clonally expanded novel multipotent stem cells from human bone marrow regenerate myocardium after myocardial infarction. *J Clin Invest*. Published online 2005. doi:10.1172/JCI200522326
168. van den Akker F, Feyen DAM, van den Hoogen P, et al. Intramyocardial stem cell injection: go(ne) with the flow. *Eur Heart J*. Published online 2016. doi:10.1093/eurheartj/ehw056
169. Van der Spoel TIG, Vrijsen KR, Koudstaal S, et al. Transendocardial cell injection is not superior to intracoronary infusion in a porcine model of ischaemic cardiomyopathy: A study on delivery efficiency. *J Cell Mol Med*. Published online 2012. doi:10.1111/j.1582-4934.2012.01594.x
170. Ridley AJ, Schwartz MA, Burridge K, et al. Cell Migration: Integrating

Signals from Front to Back. *Science (80-)*. Published online 2003. doi:10.1126/science.1092053
171. Alberts B, Johnson A, Lewis J et al. *Molecular Biology of the Cell, 4th Edition*. 4th ed. Garland Science; 2002. https://www.ncbi.nlm.nih.gov/books/NBK21054/
172. Affolter M, Weijer CJ. Signaling to cytoskeletal dynamics during chemotaxis. *Dev Cell*. Published online 2005. doi:10.1016/j.devcel.2005.06.003
173. Rot A, von Andrian UH. Chemokines in innate and adaptive host defense: basic chemokinese grammar for immune cells. *Annu Rev Immunol*. 2004;22:891-928. doi:10.1146/annurev.immunol.22.012703.104543
174. Dobner, Stephen. Amadi, Ovid C. Lee RT. Chapter 14 - Cardiovascular MechanotransductionTitle. In: *Muscle*. ; 2012:173-186. doi:https://doi.org/10.1016/B978-0-12-381510-1.00014-4
175. García-Dorado D, Rodríguez-Sinovas A, Ruiz-Meana M. Gap junction-mediated spread of cell injury and death during myocardial ischemia-reperfusion. *Cardiovasc Res*. Published online 2004. doi:10.1016/j.cardiores.2003.11.039
176. Bao L, Sachs F, Dahl G. Connexins are mechanosensitive. *Am J Physiol - Cell Physiol*. Published online 2004. doi:10.1152/ajpcell.00220.2004
177. Zhang J, Kang N, Yu X, Ma Y, Pang X. Radial Extracorporeal Shock Wave Therapy Enhances the Proliferation and Differentiation of Neural Stem Cells by Notch, PI3K/AKT, and Wnt/β-catenin Signaling. *Sci Rep*. 2017;7(1):15321. doi:10.1038/s41598-017-15662-5
178. Zhang H, Li Z-L, Yang F, et al. Radial shockwave treatment promotes human mesenchymal stem cell self-renewal and enhances cartilage healing. *Stem Cell Res Ther*. 2018;9(1):54. doi:10.1186/s13287-018-0805-5
179. Dupont S, Morsut L, Aragona M, et al. Role of YAP/TAZ in mechanotransduction. *Nature*. 2011;474(7350):179-183. doi:10.1038/nature10137
180. Zhao Z, Wang Y, Wang Q, et al. Radial extracorporeal shockwave promotes subchondral bone stem/progenitor cell self-renewal by activating YAP/TAZ and facilitates cartilage repair in vivo. *Stem Cell Res Ther*. 2021;12(1):19. doi:10.1186/s13287-020-02076-w
181. Lauer U, Bürgelt E, Squire Z, et al. Shock wave permeabilization as a new gene transfer method. *Gene Ther*. 1997;4(7):710-715. doi:10.1038/sj.gt.3300462
182. Kodama T, Hamblin MR, Doukas AG. Cytoplasmic molecular delivery with shock waves: importance of impulse. *Biophys J*. 2000;79(4):1821-1832. doi:10.1016/S0006-3495(00)76432-0
183. Takahashi T, Nakagawa K, Tada S, Tsukamoto A. Low-energy shock waves evoke intracellular Ca2+ increases independently of sonoporation. *Sci Rep*. 2019;9(1):3218. doi:10.1038/s41598-019-

39806-x
184. Holfeld J, Tepeköylü C, Reissig C, et al. Toll-like receptor 3 signalling mediates angiogenic response upon shock wave treatment of ischaemic muscle. *Cardiovasc Res*. 2016;109(2):331-343. doi:10.1093/cvr/cvv272
185. Kalluri R, LeBleu VS. The biology, function, and biomedical applications of exosomes. *Science*. 2020;367(6478). doi:10.1126/science.aau6977
186. Zhang Y, Yang P, Sun T, et al. miR-126 and miR-126* repress recruitment of mesenchymal stem cells and inflammatory monocytes to inhibit breast cancer metastasis. *Nat Cell Biol*. 2013;15(3):284-294. doi:10.1038/ncb2690
187. Lü M-H, Li C-Z, Hu C-J, et al. microRNA-27b suppresses mouse MSC migration to the liver by targeting SDF-1αin vitro. *Biochem Biophys Res Commun*. 2012;421(2):389-395. doi:10.1016/j.bbrc.2012.04.027
188. Maliken BD, Molkentin JD. Undeniable evidence that the adult mammalian heart lacks an endogenous regenerative stem cell. *Circulation*. Published online 2018. doi:10.1161/CIRCULATIONAHA.118.035186
189. Gnecchi M, Zhang Z, Ni A, Dzau VJ. Paracrine mechanisms in adult stem cell signaling and therapy. *Circ Res*. Published online 2008. doi:10.1161/CIRCRESAHA.108.176826
190. Condeelis J, Pollard JW. Macrophages: Obligate partners for tumor cell migration, invasion, and metastasis. *Cell*. Published online 2006. doi:10.1016/j.cell.2006.01.007
191. Cicatiello V, Apicella I, Tudisco L, et al. Powerful anti-tumor and anti-angiogenic activity of a new anti-vascular endothelial growth factor receptor 1 peptide in colorectal cancer models. *Oncotarget*. Published online 2015. doi:10.18632/oncotarget.3384
192. Li C, Liu B, Dai Z, Tao Y. Knockdown of VEGF receptor-1 (VEGFR-1) impairs macrophage infiltration, angiogenesis and growth of clear cell renal cell carcinoma (CRCC). *Cancer Biol Ther*. Published online 2011. doi:10.4161/cbt.12.10.17672
193. Gomez Perdiguero E, Klapproth K, Schulz C, et al. Tissue-resident macrophages originate from yolk-sac-derived erythro-myeloid progenitors. *Nature*. Published online 2015. doi:10.1038/nature13989
194. Murdoch C, Muthana M, Coffelt SB, Lewis CE. The role of myeloid cells in the promotion of tumour angiogenesis. *Nat Rev Cancer*. Published online 2008. doi:10.1038/nrc2444
195. Jaipersad AS, Lip GYH, Silverman S, Shantsila E. The role of monocytes in angiogenesis and atherosclerosis. *J Am Coll Cardiol*. Published online 2014. doi:10.1016/j.jacc.2013.09.019
196. Godwin JW, Pinto AR, Rosenthal NA. Macrophages are required for adult salamander limb regeneration. *Proc Natl Acad Sci U S A*. 2013;110(23):9415-9420. doi:10.1073/pnas.1300290110
197. Gordon S. Alternative activation of macrophages. *Nat Rev Immunol*.

Published online 2003. doi:10.1038/nri978
198. Hofmann U, Beyersdorf N, Weirather J, et al. Activation of CD4 + T lymphocytes improves wound healing and survival after experimental myocardial infarction in mice. *Circulation*. Published online 2012. doi:10.1161/CIRCULATIONAHA.111.044164
199. Zumsteg A, Christofori G. Corrupt policemen: Inflammatory cells promote tumor angiogenesis. *Curr Opin Oncol*. Published online 2009. doi:10.1097/CCO.0b013e32831bed7e
200. Lin L, Du L. The role of secreted factors in stem cells-mediated immune regulation. *Cell Immunol*. Published online 2018. doi:10.1016/j.cellimm.2017.07.010
201. Maier M, Averbeck B, Milz S, Refior HJ, Schmitz C. Substance P and prostaglandin E2 release after shock wave application to the rabbit femur. *Clin Orthop Relat Res*. 2003;(406):237-245. doi:10.1097/01.blo.0000030173.56585.8f
202. Newby DE, Boon NA, Webb DJ. Comparison of forearm vasodilatation to substance P and acetylcholine: Contribution of nitric oxide. *Clin Sci*. Published online 1997. doi:10.1042/cs0920133
203. Hong HS, Lee J, Lee E, et al. A new role of substance P as an injury-inducible messenger for mobilization of CD29 + stromal-like cells. *Nat Med*. 2009;15(4):425-435. doi:10.1038/nm.1909
204. Jubair S, Li J, Dehlin HM, et al. Substance P induces cardioprotection in ischemia-reperfusion via activation of AKT. *Am J Physiol - Hear Circ Physiol*. Published online 2015. doi:10.1152/ajpheart.00200.2015
205. Fu S, Jin D, Liu S, et al. Protective Effect of Neuropeptide Substance P on Bone Marrow Mesenchymal Stem Cells against Apoptosis Induced by Serum Deprivation. *Stem Cells Int*. Published online 2015. doi:10.1155/2015/270328
206. BRODIN E, GAZELIUS B, PANOPOULOS P, OLGART L. Morphine inhibits substance P release from peripheral sensory nerve endings. *Acta Physiol Scand*. Published online 1983. doi:10.1111/j.1748-1716.1983.tb07228.x
207. Amadesi S, Reni C, Katare R, et al. Role for substance P-based nociceptive signaling in progenitor cell activation and angiogenesis during ischemia in mice and in human subjects. *Circulation*. Published online 2012. doi:10.1161/CIRCULATIONAHA.111.089763
208. Cury PR, Canavez F, De Araújo VC, Furuse C, De Araújo NS. Substance P regulates the expression of matrix metalloproteinases and tissue inhibitors of metalloproteinase in cultured human gingival fibroblasts. *J Periodontal Res*. Published online 2008. doi:10.1111/j.1600-0765.2007.01022.x
209. DeFea KA, Vaughn ZD, O'Bryan EM, Nishijima D, Déry O, Bunnett NW. The proliferative and antiapoptotic effects of substance P are facilitated by formation of a β-arrestin-dependent scaffolding complex. *Proc Natl Acad Sci U S A*. Published online 2000.

doi:10.1073/pnas.190276697
210. Ho WZ, Lai JP, Zhu XH, Uvaydova M, Douglas SD. Human monocytes and macrophages express substance P and neurokinin-1 receptor. *J Immunol*. Published online 1997.
211. Li Y, Douglas SD, Ho W. Human stem cells express substance P gene and its receptor. *J Hematother Stem Cell Res*. 2000;9(4):445-452. doi:10.1089/152581600419107
212. Lai JP, Douglas SD, Ho WZ. Human lymphocytes express substance P and its receptor. *J Neuroimmunol*. Published online 1998. doi:10.1016/S0165-5728(98)00025-3
213. Dubon MJ, Park KS. Substance P enhances the proliferation and migration potential of murine bone marrow-derived mesenchymal stem cell-like cell lines. *Exp Ther Med*. Published online 2015. doi:10.3892/etm.2015.2291
214. Spitsin S, Meshki J, Winters A, Tuluc F, Benton TD, Douglas SD. Substance P–mediated chemokine production promotes monocyte migration. *J Leukoc Biol*. Published online 2017. doi:10.1189/jlb.1ab0416-188rr
215. Vögeli T, Schmitz-Dräger B, Mellin HE, Ackermann R. Changes in Erythropoietin Serum Levels by Extracorporeal Shock Wave Lithotripsy. *Urol Int*. 1990;45(2):92-94. doi:10.1159/000281677
216. Holdcroft A. Integrating the Dimensions of Sex and Gender into Basic Life Sciences Research: Methodologic and Ethical Issues. *Gend Med*. Published online 2007. doi:10.1016/S1550-8579(07)80048-9
217. Thomas JA, Lerche P, Pang D, Lawrence T. Anesthesia and Analgesia for Veterinary Technicians. *J Small Anim Pract*. Published online 2012.
218. Cerqueira MD, Weissman NJ, Dilsizian V, et al. Standardized Myocardial Segmentation and Nomenclature for Tomographic Imaging of the Heart. *J Cardiovasc Magn Reson*. 2002;4(2):203-210. doi:10.1081/JCMR-120003946
219. Marchesseau S, Ho JXM, Totman JJ. Influence of the short-axis cine acquisition protocol on the cardiac function evaluation: A reproducibility study. *Eur J Radiol Open*. 2016;3:60-66. doi:https://doi.org/10.1016/j.ejro.2016.03.003
220. Hoerr V, Nagelmann N, Nauerth A, Kuhlmann MT, Stypmann J, Faber C. Cardiac-respiratory self-gated cine ultra-short echo time (UTE) cardiovascular magnetic resonance for assessment of functional cardiac parameters at high magnetic fields. *J Cardiovasc Magn Reson*. Published online 2013. doi:10.1186/1532-429X-15-59
221. Look DC, Locker DR. Time saving in measurement of NMR and EPR relaxation times. *Rev Sci Instrum*. Published online 1970. doi:10.1063/1.1684482
222. Mannaerts HFJ, Van Der Heide JA, Kamp O, Stoel MG, Twisk J, Visser CA. Early identification of left ventricular remodelling after myocardial infarction, assessed by transthoracic 3D echocardiography. *Eur Heart J*.

Published online 2004. doi:10.1016/j.ehj.2004.02.030
223. Engblom H, Tufvesson J, Jablonowski R, et al. A new automatic algorithm for quantification of myocardial infarction imaged by late gadolinium enhancement cardiovascular magnetic resonance: experimental validation and comparison to expert delineations in multi-center, multi- vendor patient data. doi:10.1186/s12968-016-0242-5
224. Majumdar S, Orphanoudakis SC, Gmitro A, O'Donnell M, Gore JC. Errors in the measurements of T2 using multiple-echo MRI techniques. I. Effects of radiofrequency pulse imperfections. *Magn Reson Med*. Published online 1986. doi:10.1002/mrm.1910030305
225. Zelaya FO, Roffmann WU, Crozier S, Teed S, Gross D, Doddrell DM. Direct visualisation of B1 inhomogeneity by flip angle dependency. *Magn Reson Imaging*. Published online 1997. doi:10.1016/S0730-725X(96)00396-7
226. Milford D, Rosbach N, Bendszus M, Heiland S. Mono-exponential fitting in T2-relaxometry: Relevance of offset and first echo. *PLoS One*. Published online 2015. doi:10.1371/journal.pone.0145255
227. Bartko JJ. The intraclass correlation coefficient as a measure of reliability. *Psychol Rep*. Published online 1966. doi:10.2466/pr0.1966.19.1.3
228. Shrout PE, Fleiss JL. Intraclass correlations: Uses in assessing rater reliability. *Psychol Bull*. Published online 1979. doi:10.1037/0033-2909.86.2.420
229. Booth DS, Szmidt-Middleton H, King N, et al. RStudio: Integrated Development for R. *Nature*. Published online 2018. doi:10.1108/eb003648
230. Koo TK, Li MY. A Guideline of Selecting and Reporting Intraclass Correlation Coefficients for Reliability Research. *J Chiropr Med*. Published online 2016. doi:10.1016/j.jcm.2016.02.012
231. Mathur A, Arnold R, Assmus B, et al. The effect of intracoronary infusion of bone marrow-derived mononuclear cells on all-cause mortality in acute myocardial infarction: rationale and design of the BAMI trial. *Eur J Heart Fail*. Published online 2017. doi:10.1002/ejhf.829
232. Hausenloy DJ, Kharbanda RK, Møller UK, et al. Effect of remote ischaemic conditioning on clinical outcomes in patients with acute myocardial infarction (CONDI-2/ERIC-PPCI): a single-blind randomised controlled trial. *Lancet*. Published online 2019. doi:10.1016/S0140-6736(19)32039-2
233. Ridker PM, Everett BM, Thuren T, et al. Antiinflammatory therapy with canakinumab for atherosclerotic disease. *N Engl J Med*. Published online 2017. doi:10.1056/NEJMoa1707914
234. Sager HB, Heidt T, Hulsmans M, et al. Targeting interleukin-1β reduces leukocyte production after acute myocardial infarction. *Circulation*.

Published online 2015. doi:10.1161/CIRCULATIONAHA.115.016160
235. CDER, CBER. Product Development Under the Animal Rule. FDA Guidance for Industry. Published 2015. http://www.fda.gov/Drugs/GuidanceComplianceRegulatoryInformation/Guidances/default.htm%5Cnhttp://www.fda.gov/BiologicsBloodVaccines/GuidanceComplianceRegulatoryInformation/default.htm
236. DIRECTIVE 2001/83/EC OF THE EUROPEAN PARLIAMENT AND OF THE COUNCIL of 6 November 2001 Amended by: on the Community code relating to medicinal products for human use. https://ec.europa.eu/health/sites/health/files/files/eudralex/vol-1/dir_2001_83_consol_2012/dir_2001_83_cons_2012_en.pdf
237. Medicines Act 1968. http://www.legislation.gov.uk/ukpga/1968/67
238. Kramer CM, Barkhausen J, Bucciarelli-Ducci C, Flamm SD, Kim RJ, Nagel E. Standardized cardiovascular magnetic resonance imaging (CMR) protocols: 2020 update. *J Cardiovasc Magn Reson*. Published online 2020. doi:10.1186/s12968-020-00607-1
239. Cicala S, De Simone G, Roman MJ, et al. Prevalence and prognostic significance of wall-motion abnormalities in adults without clinically recognized cardiovascular disease: The strong heart study. *Circulation*. Published online 2007. doi:10.1161/CIRCULATIONAHA.106.652149
240. Brainin P, Biering-Sørensen SR, Møgelvang R, Søgaard P, Jensen JS, Biering-Sørensen T. Postsystolic shortening by speckle tracking echocardiography is an independent predictor of cardiovascular events and mortality in the general population. *J Am Heart Assoc*. Published online 2018. doi:10.1161/JAHA.117.008367
241. Chen C, Li L, Chen LL, et al. Incremental doses of dobutamine induce a biphasic response in dysfunctional left ventricular regions subtending coronary stenoses. *Circulation*. Published online 1995. doi:10.1161/01.CIR.92.4.756
242. Sicari R, Nihoyannopoulos P, Evangelista A, et al. Stress echocardiography expert consensus statement. In: *European Journal of Echocardiography*. Vol 9. ; 2008:415-437. doi:10.1093/ejechocard/jen175
243. Walker V, Lairez O, Fondard O, et al. Early detection of subclinical left ventricular dysfunction after breast cancer radiation therapy using speckle-tracking echocardiography: Association between cardiac exposure and longitudinal strain reduction (BACCARAT study). *Radiat Oncol*. Published online 2019. doi:10.1186/s13014-019-1408-8
244. Biering-Sørensen T, Biering-Sørensen SR, Olsen FJ, et al. Global Longitudinal Strain by Echocardiography Predicts Long-Term Risk of Cardiovascular Morbidity and Mortality in a Low-Risk General Population: The Copenhagen City Heart Study. *Circ Cardiovasc Imaging*. Published online 2017. doi:10.1161/CIRCIMAGING.116.005521
245. Montgomery DE, Puthumana JJ, Fox JM, Ogunyankin KO. Global

longitudinal strain aids the detection of non-obstructive coronary artery disease in the resting echocardiogram. *Eur Heart J Cardiovasc Imaging*. Published online 2012. doi:10.1093/ejechocard/jer282
246. Hudsmith LE, Petersen SE, Tyler DJ, et al. Determination of cardiac volumes and mass with FLASH and SSFP cine sequences at 1.5 vs. 3 Tesla: A validation study. *J Magn Reson Imaging*. Published online 2006. doi:10.1002/jmri.20638
247. Faul F, Erdfelder E, Lang AG, Buchner A. G*Power 3: A flexible statistical power analysis program for the social, behavioral, and biomedical sciences. In: *Behavior Research Methods*. ; 2007. doi:10.3758/BF03193146
248. Badano LP, Kolias TJ, Muraru D, et al. Standardization of left atrial, right ventricular, and right atrial deformation imaging using two-dimensional speckle tracking echocardiography: A consensus document of the EACVI/ASE/Industry Task Force to standardize deformation imaging. *Eur Heart J Cardiovasc Imaging*. Published online 2018. doi:10.1093/ehjci/jey042
249. Team RC. R: A Language and Environment for Statistical Computing. *Vienna, Austria*. Published online 2019.
250. Lang RM, Bierig M, Devereux RB, et al. Recommendations for chamber quantification: A report from the American Society of Echocardiography's guidelines and standards committee and the Chamber Quantification Writing Group, developed in conjunction with the European Association of Echocardiograph. *J Am Soc Echocardiogr*. Published online 2005. doi:10.1016/j.echo.2005.10.005
251. Biesbroek PS, Amier RP, Teunissen PFA, et al. Changes in remote myocardial tissue after acute myocardial infarction and its relation to cardiac remodeling: A CMR T1 mapping study. *PLoS One*. Published online 2017. doi:10.1371/journal.pone.0180115
252. Abbate A, Bonanno E, Mauriello A, et al. Widespread myocardial inflammation and infarct-related artery patency. *Circulation*. Published online 2004. doi:10.1161/01.CIR.0000133316.92316.81
253. Travers JG, Kamal FA, Robbins J, Yutzey KE, Blaxall BC. Cardiac fibrosis: The fibroblast awakens. *Circ Res*. Published online 2016. doi:10.1161/CIRCRESAHA.115.306565
254. Gallagher KP, Stirling MC, Choy M, et al. Dissociation between epicardial and transmural function during acute myocardial ischemia. *Circulation*. Published online 1985. doi:10.1161/01.CIR.71.6.1279
255. Hanekom L, Jenkins C, Jeffries L, et al. Incremental value of strain rate analysis as an adjunct to wall-motion scoring for assessment of myocardial viability by dobutamine echocardiography: A follow-up study after revascularization. *Circulation*. Published online 2005. doi:10.1161/CIRCULATIONAHA.104.489310
256. Roos ST, Timmers L, Biesbroek PS, et al. No benefit of additional treatment with exenatide in patients with an acute myocardial

infarction. *Int J Cardiol*. Published online 2016. doi:10.1016/j.ijcard.2016.06.283
257. Ott I, Schulz S, Mehilli J, et al. Erythropoietin in patients with acute st-segment elevation myocardial infarction undergoing primary : Percutaneous coronary intervention a randomized, double-blind trial. *Circ Cardiovasc Interv*. 2010;3(5):408-413. doi:10.1161/CIRCINTERVENTIONS.109.904425
258. Holubarsch C, Ruf T, Goldstein DJ, et al. Existence of the Frank-Starling mechanism in the failing human heart: Investigations on the organ, tissue, and sarcomere levels. *Circulation*. Published online 1996. doi:10.1161/01.CIR.94.4.683
259. Carlsson M, Ugander M, Mosén H, Buhre T, Arheden H. Atrioventricular plane displacement is the major contributor to left ventricular pumping in healthy adults, athletes, and patients with dilated cardiomyopathy. *Am J Physiol - Hear Circ Physiol*. Published online 2007. doi:10.1152/ajpheart.01148.2006
260. Carlsson M, Ugander M, Heiberg E, Arheden H. The quantitative relationship between longitudinal and radial function in left, right, and total heart pumping in humans. *https://doi.org/101152/ajpheart013762006*. 2007;293(1):H636-H644. doi:10.1152/AJPHEART.01376.2006
261. Kim WJ, Lee BH, Kim YJ, et al. Apical rotation assessed by speckle-tracking echocardiography as an index of global left ventricular contractility. *Circ Cardiovasc Imaging*. 2009;2(2):123-131. doi:10.1161/CIRCIMAGING.108.794719
262. Akagawa E, Murata K, Tanaka N, et al. Augmentation of left ventricular apical endocardial rotation with inotropic stimulation contributes to increased left ventricular torsion and radial strain in normal subjects - Quantitative assessment utilizing a novel automated tissue tracking technique. *Circ J*. Published online 2007. doi:10.1253/circj.71.661
263. Park S-M, Hong S-J, Ahn C-M, et al. Different impacts of acute myocardial infarction on left ventricular apical and basal rotation. *Eur Hear J - Cardiovasc Imaging*. Published online 2012. doi:10.1093/ejechocard/jer272
264. Ünlü S, Mirea O, Pagourelias ED, et al. Layer-Specific Segmental Longitudinal Strain Measurements: Capability of Detecting Myocardial Scar and Differences in Feasibility, Accuracy, and Reproducibility, Among Four Vendors A Report From the EACVI-ASE Strain Standardization Task Force. *J Am Soc Echocardiogr*. Published online 2019. doi:10.1016/j.echo.2019.01.010
265. Mirea O, Pagourelias ED, Duchenne J, et al. Variability and Reproducibility of Segmental Longitudinal Strain Measurement: A Report From the EACVI-ASE Strain Standardization Task Force. *JACC Cardiovasc Imaging*. Published online 2018. doi:10.1016/j.jcmg.2017.01.027

266. Erley J, Genovese D, Tapaskar N, et al. Echocardiography and cardiovascular magnetic resonance based evaluation of myocardial strain and relationship with late gadolinium enhancement. *J Cardiovasc Magn Reson*. Published online 2019. doi:10.1186/s12968-019-0559-y
267. Forsha D, Risum N, Rajagopal S, et al. The influence of angle of insonation and target depth on speckle-tracking strain. *J Am Soc Echocardiogr*. Published online 2015. doi:10.1016/j.echo.2014.12.015
268. Grabskaya E, Spira C, Hoffmann R, et al. Myocardial rotation but not circumferential strain is transducer angle dependent: A speckle tracking echocardiography study. *Echocardiography*. Published online 2010. doi:10.1111/j.1540-8175.2010.01158.x
269. Liang T, Yung L, Yu W. On feature motion decorrelation in ultrasound speckle tracking. *IEEE Trans Med Imaging*. Published online 2013. doi:10.1109/TMI.2012.2230016
270. Colucci WS, Wright RF, Braunwald E. New Positive Inotropic Agents in the Treatment of Congestive Heart Failure. *N Engl J Med*. 1986;314(6):349-358. doi:10.1056/NEJM198602063140605
271. Dickstein K, Cohen-Solal A, Filippatos G, et al. ESC Guidelines for the diagnosis and treatment of acute and chronic heart failure 2008. The Task Force for the Diagnosis and Treatment of Acute and Chronic Heart Failure 2008 of the European Society of Cardiology. Developed in collaboration with the Heart. *Eur J Heart Fail*. Published online 2008. doi:10.1016/j.ejheart.2008.08.005
272. Kramer DG, Trikalinos TA, Kent DM, Antonopoulos G V., Konstam MA, Udelson JE. Quantitative evaluation of drug or device effects on ventricular remodeling as predictors of therapeutic effects on mortality in patients with heart failure and reduced ejection fraction: A meta-analytic approach. *J Am Coll Cardiol*. Published online 2010. doi:10.1016/j.jacc.2010.05.011
273. Williams AM, Shave RE, Stembridge M, Eves ND. Females have greater left ventricular twist mechanics than males during acute reductions to preload. *Am J Physiol Heart Circ Physiol*. 2016;311(1):H76-84. doi:10.1152/ajpheart.00057.2016
274. Chung AK, Das SR, Leonard D, et al. Women have higher left ventricular ejection fractions than men independent of differences in left ventricular volume: the Dallas Heart Study. *Circulation*. 2006;113(12):1597-1604. doi:10.1161/CIRCULATIONAHA.105.574400
275. Grüner Sveälv B, Fritzon G, Andersson B. Gender and age related differences in left ventricular function and geometry with focus on the long axis. *Eur J Echocardiogr*. 2006;7(4):298-307. doi:10.1016/j.euje.2005.06.008
276. Hu X, Dai S, Wu WJ, et al. Stromal cell-derived factor-1α confers protection against myocardial ischemia/reperfusion injury: Role of the cardiac stromal cell-derived factor-1α-CXCR4 axis. *Circulation*.

2007;116(6):654-663. doi:10.1161/CIRCULATIONAHA.106.672451
277. Huang C, Gu H, Zhang W, Manukyan MC, Shou W, Wang M. SDF-1/CXCR4 mediates acute protection of cardiac function through myocardial STAT3 signaling following global ischemia/reperfusion injury. *Am J Physiol - Hear Circ Physiol*. 2011;301(4):1496-1505. doi:10.1152/ajpheart.00365.2011
278. Malik A, Bromage DI, He Z, et al. Exogenous SDF-1α Protects Human Myocardium from Hypoxia-Reoxygenation Injury via CXCR4. *Cardiovasc Drugs Ther*. Published online 2015. doi:10.1007/s10557-015-6622-5
279. Yamada H, Tanaka A, Kusunose K, et al. Effect of sitagliptin on the echocardiographic parameters of left ventricular diastolic function in patients with type 2 diabetes: A subgroup analysis of the PROLOGUE study. *Cardiovasc Diabetol*. Published online 2017. doi:10.1186/s12933-017-0546-2
280. Catalucci D, Condorelli G. Effects of Akt on cardiac myocytes: Location counts. *Circ Res*. Published online 2006. doi:10.1161/01.RES.0000239409.90634.a9
281. Cittadini A, Monti MG, Iaccarino G, et al. Adenoviral gene transfer of Akt enhances myocardial contractility and intracellular calcium handling. *Gene Ther*. Published online 2006. doi:10.1038/sj.gt.3302589
282. Basoli V, Chaudary S, Cruciani S, et al. Mechanical Stimulation of Fibroblasts by Extracorporeal Shock Waves: Modulation of Cell Activation and Proliferation Through a Transient Proinflammatory Milieu. *Cell Transplant*. Published online 2020. doi:10.1177/0963689720916175
283. Bang OS, Ha BG, Park EK, Kang SS. Activation of Akt is induced by heat shock and involved in suppression of heat-shock-induced apoptosis of NIH3T3 cells. *Biochem Biophys Res Commun*. Published online 2000. doi:10.1006/bbrc.2000.3805
284. Turner P V, Vaughn E, Sunohara-Neilson J, Ovari J, Leri F. Oral gavage in rats: animal welfare evaluation. *J Am Assoc Lab Anim Sci*. 2012;51(1):25-30.
285. Bristow MR. Treatment of chronic heart failure with β-adrenergic receptor antagonists: A convergence of receptor pharmacology and clinical cardiology. *Circ Res*. Published online 2011. doi:10.1161/CIRCRESAHA.111.245092
286. Stratton JR, Pfeifer MA, Ritchie JL, Halter JB. Hemodynamic effects of epinephrine: Concentration-effect study in humans. *J Appl Physiol*. Published online 1985. doi:10.1152/jappl.1985.58.4.1199
287. Fuenmayor AJ, Solórzano MI, Gómez L. Epinephrine and left atrial and left ventricular diastolic function decrease in normal subjects. *Int J Cardiol*. Published online 2016. doi:10.1016/j.ijcard.2016.06.139
288. Ulucam M, Korkmaz ME, Muderrisoglu H, et al. Effects of a single, 24-hour, low-dose intravenous dobutamine infusion on left ventricular myocardial performance index in congestive heart failure: A

prospective, nonrandomized study. *Curr Ther Res - Clin Exp*. Published online 2005. doi:10.1016/j.curtheres.2005.03.002
289. Niwa H, Hirota Y, Sibutani T, et al. The effects of epinephrine and norepinephrine administered during local anesthesia on left ventricular diastolic function. *Anesth Prog*. Published online 1991.
290. Redfield MM, Chen HH, Borlaug BA, et al. Effect of phosphodiesterase-5 inhibition on exercise capacity and clinical status in heart failure with preserved ejection fraction: A randomized clinical trial. *JAMA - J Am Med Assoc*. Published online 2013. doi:10.1001/jama.2013.2024
291. Obata K, Morita H, Takaki M. The energy-saving effect of a new myosin activator, omecamtiv mecarbil, on LV mechanoenergetics in rat hearts with blood-perfused isovolumic contraction model. *Naunyn Schmiedebergs Arch Pharmacol*. Published online 2019. doi:10.1007/s00210-019-01685-4
292. Dongworth RK, Campbell-Washburn AE, Cabrera-Fuentes HA, et al. Quantifying the area-at-risk of myocardial infarction in-vivo using arterial spin labeling cardiac magnetic resonance. *Sci Rep*. Published online 2017. doi:10.1038/s41598-017-02544-z
293. Price AN, Cheung KK, Lim SY, Hausenloy DJ, Yellon DM, Lythgoe MF. Late gadolinium enhanced MRI in small animal models of myocardial infarction. *J Cardiovasc Magn Reson*. 2010;12(1):P98. doi:10.1186/1532-429X-12-S1-P98
294. Protti A, Sirker A, Shah AM, Botnar R. Late gadolinium enhancement of acute myocardial infarction in mice at 7T: cine-FLASH versus inversion recovery. *J Magn Reson Imaging*. 2010;32(4):878-886. doi:10.1002/jmri.22325
295. Khurana A, Chapelin F, Beck G, et al. Iron administration before stem cell harvest enables MR imaging tracking after transplantation. *Radiology*. Published online 2013. doi:10.1148/radiol.13130858
296. Montet-Abou K, Daire JL, Hyacinthe JN, et al. In vivo labelling of resting monocytes in the reticuloendothelial system with fluorescent iron oxide nanoparticles prior to injury reveals that they are mobilized to infarcted myocardium. *Eur Heart J*. Published online 2010. doi:10.1093/eurheartj/ehp547
297. Kim SJ, Lewis B, Steiner MS, Bissa U V., Dose C, Frank JA. Superparamagnetic iron oxide nanoparticles for direct labeling of stem cells and in vivo MRI tracking. *Contrast Media Mol Imaging*. 2016;11(1):55-64. doi:10.1002/cmmi.1658
298. Frantz S, Nahrendorf M. Cardiac macrophages and their role in ischaemic heart disease. *Cardiovasc Res*. Published online 2014. doi:10.1093/cvr/cvu025
299. Ali HR, Jackson HW, Zanotelli VRT, et al. Imaging mass cytometry and multiplatform genomics define the phenogenomic landscape of breast cancer. *Nat Cancer*. Published online 2020. doi:10.1038/s43018-020-0026-6

300. Baron CS, van Oudenaarden A. Unravelling cellular relationships during development and regeneration using genetic lineage tracing. *Nat Rev Mol Cell Biol*. Published online 2019. doi:10.1038/s41580-019-0186-3
301. Manka R, Paetsch I, Schnackenburg B, Gebker R, Fleck E, Jahnke C. BOLD cardiovascular magnetic resonance at 3.0 tesla in myocardial ischemia.
302. Zimpfer D, Aharinejad S, Holfeld J, et al. Direct epicardial shock wave therapy improves ventricular function and induces angiogenesis in ischemic heart failure. *J Thorac Cardiovasc Surg*. Published online 2009. doi:10.1016/j.jtcvs.2008.11.006
303. Holfeld J, Tepeköylü C, Blunder S, et al. Low energy shock wave therapy induces angiogenesis in acute hind-limb ischemia via VEGF receptor 2 phosphorylation. *PLoS One*. Published online 2014. doi:10.1371/journal.pone.0103982
304. SUTHERLAND DR, ANDERSON L, KEENEY M, NAYAR R, CHIN-YEE I. The ISHAGE Guidelines for CD34+ Cell Determination by Flow Cytometry. *J Hematother*. Published online 1996. doi:10.1089/scd.1.1996.5.213
305. Noda M, Rodan GA. Transcriptional regulation of osteopontin production in rat osteoblast-like cells by parathyroid hormone. *J Cell Biol*. Published online 1989. doi:10.1083/jcb.108.2.713
306. Stier S, Ko Y, Forkert R, et al. Osteopontin is a hematopoietic stem cell niche component that negatively regulates stem cell pool size. *J Exp Med*. Published online 2005. doi:10.1084/jem.20041992
307. Nilsson SK, Johnston HM, Whitty GA, et al. Osteopontin, a key component of the hematopoietic stem cell niche and regulator of primitive hematopoietic progenitor cells. *Blood*. Published online 2005. doi:10.1182/blood-2004-11-4422
308. Zaruba MM, Huber BC, Brunner S, et al. Parathyroid hormone treatment after myocardial infarction promotes cardiac repair by enhanced neovascularization and cell survival. *Cardiovasc Res*. Published online 2008. doi:10.1093/cvr/cvm080
309. Brunner S, Zaruba MM, Huber B, et al. Parathyroid hormone effectively induces mobilization of progenitor cells without depletion of bone marrow. *Exp Hematol*. Published online 2008. doi:10.1016/j.exphem.2008.03.014
310. Sultana N, Zhang L, Yan J, et al. Resident c-kit + cells in the heart are not cardiac stem cells. *Nat Commun*. Published online 2015. doi:10.1038/ncomms9701
311. Beltrami AP, Barlucchi L, Torella D, et al. Adult cardiac stem cells are multipotent and support myocardial regeneration. *Cell*. 2003;114(6):763-776. doi:10.1016/s0092-8674(03)00687-1
312. Zhou P, Pu WT. Recounting cardiac cellular composition. *Circ Res*. Published online 2016. doi:10.1161/CIRCRESAHA.116.308139
313. Pinto AR, Ilinykh A, Ivey MJ, et al. Revisiting cardiac cellular composition. *Circ Res*. Published online 2016.

doi:10.1161/CIRCRESAHA.115.307778
314. Tepeköylü C, Wang F-S, Kozaryn R, et al. Shock wave treatment induces angiogenesis and mobilizes endogenous CD31/CD34-positive endothelial cells in a hindlimb ischemia model: implications for angiogenesis and vasculogenesis. *J Thorac Cardiovasc Surg*. 2013;146(4):971—978. doi:10.1016/j.jtcvs.2013.01.017
315. Livak KJ, Schmittgen TD. Analysis of Relative Gene Expression Data Using Real-Time Quantitative PCR and the 2−ΔΔCT Method. *Methods*. 2001;25(4):402-408. doi:10.1006/METH.2001.1262
316. Willems E, Leyns L, Vandesompele J. Standardization of real-time PCR gene expression data from independent biological replicates. *Anal Biochem*. Published online 2008. doi:10.1016/j.ab.2008.04.036
317. Gamba P, Jonker MJ, Hamoen LW. A Novel Feedback Loop That Controls Bimodal Expression of Genetic Competence. *PLoS Genet*. Published online 2015. doi:10.1371/journal.pgen.1005047
318. Jesmin S, Hattori Y, Togashi H, Ueno KI, Yoshioka M, Sakuma I. Age-related changes in cardiac expression of VEGF and its angiogenic receptor KDR in stroke-prone spontaneously hypertensive rats. *Mol Cell Biochem*. Published online 2005. doi:10.1007/s11010-005-7635-3
319. Gavard J, Patel V, Gutkind JS. Angiopoietin-1 Prevents VEGF-Induced Endothelial Permeability by Sequestering Src through mDia. *Dev Cell*. Published online 2008. doi:10.1016/j.devcel.2007.10.019
320. Wang G, Liem DA, Vondriska TM, et al. Nitric oxide donors protect murine myocardium against infarction via modulation of mitochondrial permeability transition. *Am J Physiol - Hear Circ Physiol*. Published online 2005. doi:10.1152/ajpheart.00796.2004
321. Carr MW, Roth SJ, Luther E, Rose SS, Springer TA. Monocyte chemoattractant protein 1 acts as a T-lymphocyte chemoattractant. *Proc Natl Acad Sci U S A*. Published online 1994. doi:10.1073/pnas.91.9.3652
322. Morimoto H, Hirose M, Takahashi M, et al. MCP-1 induces cardioprotection against ischaemia/reperfusion injury: role of reactive oxygen species. *Cardiovasc Res*. 2008;78(3):554-562. doi:10.1093/cvr/cvn035
323. Morimoto H, Takahashi M, Izawa A, et al. Cardiac overexpression of monocyte chemoattractant protein-1 in transgenic mice prevents cardiac dysfunction and remodeling after myocardial infarction. *Circ Res*. Published online 2006. doi:10.1161/01.RES.0000246113.82111.2d
324. Yamauchi-Takihara K, Kishimoto T. Cytokines and their receptors in cardiovascular diseases - Role of gp130 signalling pathway in cardiac myocyte growth and maintenance. *Int J Exp Pathol*. Published online 2000. doi:10.1046/j.1365-2613.2000.00139.x
325. Zhao ZQ, Vinten-Johansen J. Myocardial apoptosis and ischemic preconditioning. *Cardiovasc Res*. Published online 2002. doi:10.1016/S0008-6363(02)00442-X

326. Murry CE, Reinecke H, Pabon LM. Regeneration Gaps. Observations on Stem Cells and Cardiac Repair. *J Am Coll Cardiol*. Published online 2006. doi:10.1016/j.jacc.2006.02.002
327. Green DR, Kroemer G. The pathophysiology of mitochondrial cell death. *Science*. 2004;305(5684):626-629. doi:10.1126/science.1099320
328. Taylor RC, Cullen SP, Martin SJ. Apoptosis: Controlled demolition at the cellular level. *Nat Rev Mol Cell Biol*. Published online 2008. doi:10.1038/nrm2312
329. Kang PM, Haunstetter A, Aoki H, Usheva A, Izumo S. Morphological and molecular characterization of adult cardiomyocyte apoptosis during hypoxia and reoxygenation. *Circ Res*. Published online 2000. doi:10.1161/01.RES.87.2.118
330. Hatanaka K, Ito K, Shindo T, et al. Molecular mechanisms of the angiogenic effects of low-energy shock wave therapy: roles of mechanotransduction. *Am J Physiol Physiol*. 2016;311(3):C378-C385. doi:10.1152/ajpcell.00152.2016
331. Jarrah AA, Schwarskopf M, Wang ER, et al. SDF-1 induces TNF-mediated apoptosis in cardiac myocytes. *Apoptosis*. Published online 2018. doi:10.1007/s10495-017-1438-3
332. Yoon Lee J, Chung J, Hwa Kim K, et al. Extracorporeal shock waves protect cardiomyocytes from doxorubicin-induced cardiomyopathy by upregulating survivin via the integrin-ILK-Akt-Sp1/p53 axis. *Sci Rep*. Published online 2019. doi:10.1038/s41598-019-48470-0
333. Ohnishi M, Hasegawa G, Yamasaki M, et al. Integrin-linked kinase acts as a pro-survival factor against high glucose-associated osmotic stress in human mesangial cells. *Nephrol Dial Transplant*. Published online 2006. doi:10.1093/ndt/gfl120
334. Chen D, Xia Y, Zuo K, et al. Crosstalk between SDF-1/CXCR4 and SDF-1/CXCR7 in cardiac stem cell migration. *Sci Rep*. 2015;5:16813. doi:10.1038/srep16813
335. Naumann U, Cameroni E, Pruenster M, et al. CXCR7 functions as a scavenger for CXCL12 and CXCL11. *PLoS One*. Published online 2010. doi:10.1371/journal.pone.0009175
336. Coggins NL, Trakimas D, Chang SL, et al. CXCR7 controls competition for recruitment of β-arrestin 2 in cells expressing both CXCR4 and CXCR7. *PLoS One*. Published online 2014. doi:10.1371/journal.pone.0098328
337. Levoye A, Balabanian K, Baleux F, Bachelerie F, Lagane B. CXCR7 heterodimerizes with CXCR4 and regulates CXCL12-mediated G protein signaling. *Blood*. Published online 2009. doi:10.1182/blood-2008-12-196618
338. Martinac B. Mechanosensitive ion channels: Molecules of mechanotransduction. *J Cell Sci*. Published online 2004. doi:10.1242/jcs.01232
339. Bzowska M, Jura N, Lassak A, Black RA, Bereta J. Tumour necrosis

factor-α stimulates expression of TNF-α converting enzyme in endothelial cells. *Eur J Biochem*. Published online 2004. doi:10.1111/j.1432-1033.2004.04215.x

340. Barsacchi R, Perrotta C, Sestili P, Cantoni O, Moncada S, Clementi E. Cyclic GMP-dependent inhibition of acid sphingomyelinase by nitric oxide: An early step in protection against apoptosis. *Cell Death Differ*. Published online 2002. doi:10.1038/sj.cdd.4401095
341. Maejima Y, Adachi S, Morikawa K, Ito H, Isobe M. Nitric oxide inhibits myocardial apoptosis by preventing caspase-3 activity via S-nitrosylation. *J Mol Cell Cardiol*. Published online 2005. doi:10.1016/j.yjmcc.2004.10.012
342. Brodie BR, Stuckey TD, Wall TC, et al. Importance of time to reperfusion for 30-day and late survival and recovery of left ventricular function after primary angioplasty for acute myocardial infarction. *J Am Coll Cardiol*. 1998;32(5):1312-1319. doi:10.1016/S0735-1097(98)00395-7
343. Melnik BC. MiR-21: An environmental driver of malignant melanoma? *J Transl Med*. Published online 2015. doi:10.1186/s12967-015-0570-5

APPENDIX 1

Echo Assessment of LV Function After Shockwave Treatment

1. Purpose

This is a pilot experiment for hypothesis generating.

2. Aims

2.1. To learn whether shockwave have any adverse effect on the animal

2.2. To screen the acute effect of shockwave on the heart using echocardiography

3. Objectives

3.1. Evaluation of chamber sizes using basal, mid and apical views to derive area at ED and ES, and FAC.

4. **Method**

4.1. Animal Preparation, Echo Acquisition and Shockwave

A rat underwent anaesthesia induction using isoflurane as previously described, and precordial air removed by shaving. Light anesthesia was maintained throughout the scan using a nasal cone whilst the animal positioned in a dorsal position on a heating mat. The echo machine (Philips SONOS 5500, 12Mhz sector transducer) was prepared with the appropriate depth, gain, frequency settings to achieve the best resolution and frame rate.

The image was further optimised using TGC, focusing and sector size adjustment. ECG was not available. A pre-shockwave scans were acquired at the basal, mid and apical levels. Shockwave was applied to the heart using setting 2.5mJ/mm^2 x 500 pulses at 3Hz. Immediately after that, post-SW scans were repeated at the basal, mid and apical levels. The isoflurane was stopped, and the animal was allowed to recover from anaesthesia and returned to the cage. The animal was observed daily for the next few days

4.2. Image Analysis

The analogue videos were digitalized. The full-motion video could be watched using this link. Still image clips were acquired at the end-diastole and end-systole, respectively defined as the largest LV diameter and the smallest LV diameter, for each the basal, mid, apical level for pre-SW and post-SW. Images are imported to Fiji (version 2.0.0-rc-43/1.52i) was used to measure the area. To allow for measurements the distance between two calipers was calibrated to the acquisition length on the image; the distance between two markers was 1cm.Using freehand tool, the end-diastolic and end-systolic blood borders were traced using planimetry method, to derive ED area (EDA) and ES area (ESA) in all images. FAC (%) was calculated as (EDA-ESA)/EDA*100. The heart rate was semi-qualitatively assessed using from the interval between ED and ES.

4.2.1. FAC result

(See **Figure 1A of Appendix 1**)

Basal: Increase from 19.3% to 81.6%, =62.3%

Mid: increase from 20.1% to 64.5%, =44.4%

Apex: increase from 28.4% to 48.7%, =20.3%

All post-SW FACs at all levels were greater than their respective pre-SW FACs. The absolute difference in % of post-SW FAC to % of pre-SW FAC from the greatest to the least were in the order of basal, mid and apical level.

4.2.2. EDA

(**See Figure 1C of Appendix 1)**

Basal: Increase from 0.35cm^2 to 0.67cm^2, =0.32 cm^2

Mid: Increase from 030 cm^2 to 0.44 cm^2, =0.132 cm^2

Apex: increase from 0.168 cm^2 to 0.23 cm^2, =0.06 cm^2

It was observed that all post-SW EDAs at all levels were greater than their respective pre-SW FACs. The absolute difference in area change of cm^2 pre-SW FAC to post-SW FAC from the least to the greatest were in the order of apex, mid and basal level. The fold difference in absolute area change due to SW treatment from apex: mid: Basal = 1: 2.2: 5.

4.2.3. ESA

(**See Figure 1E of Appendix 1**)

Base: Decrease from 0.28 cm^2 to 0.129 cm^2, diff=0.15cm^2

Mid: Decrease from 0.24 cm^2 to 0.15 cm^2, diff=0.09 cm^2

Apex: Decrease from 0.119 cm^2 to 0.022 cm^2, diff=0.10 cm^2

The post-SW ESA at the basal and mid-levels were smaller after SW treatment than their respective pre-SW ESA. The was a very small increase at the apex in post-SW ESA compared to the post-SW ESA. The fold difference in absolute area change from apex: mid: Basal = 1:1: 1.5

4.2.4. Heart rate

It was observed shockwave had an acute effect on the heart rate. The heart rate of the animal was noticeably lower during shockwave than before SW.

4.2.5. Daily observations post SW

The animal was observed to behave normally in the days after shockwave treatment.

4.2.6. Conclusion

Shockwave dilated EDA more at the basal level compared to the apical level. Shockwave contracted ESA more at the basal level compared to the apical level. In effect the FAC post-shockwave to pre- shockwave was the greatest the base (62%) versus the apex (20%). As FAC is positively correlated to the stroke volume, shockwave have a positive effect on the stroke volume. The effects could be summarised as positively inotropic and negatively chronotropic. The contribution of inotropy by SW was by modulation of basal

level > apical level. At 2. 5mJ/mm^2 x 500 pulses at 3Hz, SW did not have an adverse outcome to the rat.

4.2.7. Discussion

The change in EDV could be because of bradycardia, increase in preload causing increase in EDV. On the other hand, the preferential inotropic effect on the basal than the apex cannot be explained only by bradycardia alone. Shockwave hence likely could modulate the systolic function and have different effect between basal and apical.

4.2.8. Further Research Questions

- Is it bradycardia or direct effect on cardiac muscles?
- How long bradycardia last for? How long does the effect last for?
- Mechanism of inotropy?

4.2.9. Hypothesis generated

Shockwave to the heart could induce inotropy

4.2.10. Future Plan

Detail scanning using CMR is warranted.

Figure 1 of Appendix 1. Green Box: preshockwave, Red Box: Post shockwave. In each box the first row is basal, the second row mid and third row apical, first column is end diastole, second column is end systole. (A) The change of FAC in the basal, mid and apical pre- and post-shockwave, (B) A line chart showing the difference in FAC post minus pre shockwave of the basal, mid and apex, (C) A line chart showing the difference EDA between pre- and post-shockwave at the basal, mid and apical, (D) The change in EDA in the basal, mid and apical pre- and post-shockwave. (E) The change in ESA in the basal, mid and apical pre- and post-shockwave. (F) A line chart showing the difference between pre- and post-shockwave at the basal, mid and apical.

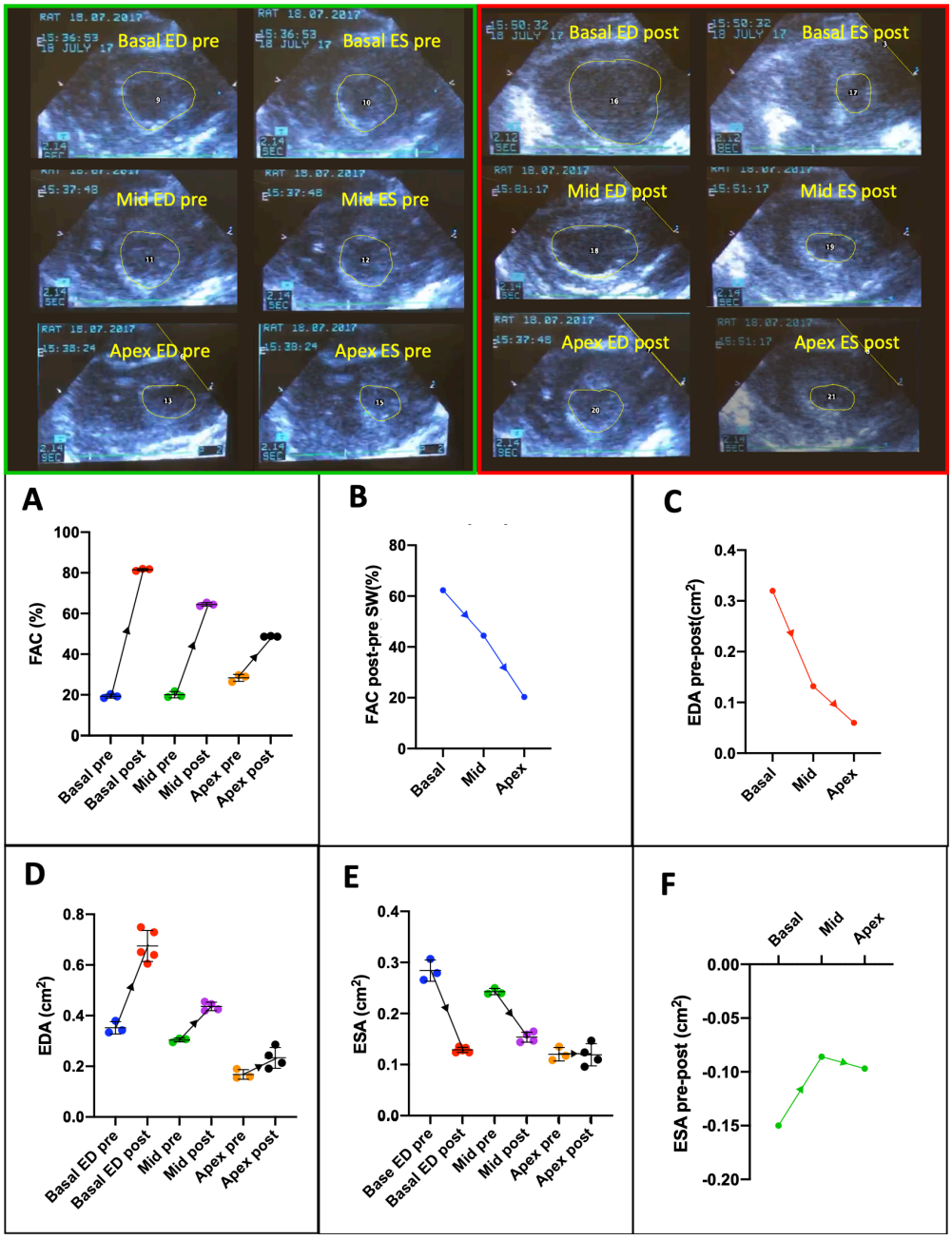

APPENDIX 2

Chemokine Released by Human Cardiac Fibroblast with Shockwave

1. Purpose

Screening for possible chemokines for hypothesis generating.

2. Aims

To learn whether shockwave have an effect on other proteins expression

3. Objectives

To screen for "hits" of the chemokines in **Figure 1 of Appendix 2.**

4. Method

4.1. Fibroblast Culture

Human cardiac fibroblasts of equal cells concentration were seeded in T12.5 TC-treated flask (VWR), cultured in DMEM Glutamax (Gibco) supplemented with 10% FCS (Thermofisher), 1mcg/ml basic FGF (Peprotech) and 50ng/ml Gentamicin (Sigma). The media changed every 2 days and cells grown to confluency. On the day of experiment, the media was completely aspirated, rinsed and exchanged three times with the same DMEM containing all the additives except the FCS which was replaced with 1% BSA (Sigma). It was ensured that all flasks contained identical culture media volume.

4.2. Shockwave

The method of shockwave administration to cells was administered as described in chapter 11. The culture supernatant was collected 48 hours after shockwave administration to maximise hit identification, although it is recognised that there could be proteins degradation whilst in culture, proteins have different temporal expression and half-life.

4.3. Dot Blot Assay

The relative levels of chemokine of human cardiac fibroblast secretome were determined in parallel using dot blot arrays (RnD Systems). Three arrays used to interrogate samples of the baseline, 1 Bar x 1000 (48hr), and 1 Bar x 1000 (48hr). The nitrocellulose membranes were pre-blotted with capture antibodies and their location on the membranes were known. The membranes were placed in a well, blocked to reduce non-specific binding, incubated for 1 hour on a rocker at room temperature. The culture supernatant thawed from -80˚C, vortexed mix, then placed on ice and used undiluted. Biotin-conjugated antibodies cocktail then added to three samples, mixed well and left to incubate for 1 hour at room temperature. The blocking buffer then pipetted out from the wells with membrane in situ and the samples-antibodies mixture added to the well and left to incubate overnight at 4˚C on platform shaker. The next day, the membranes were washed 3 times with a wash buffer, then

drained and Streptavidin-HRP buffer added to the wells, left to incubate for 30 minutes on a rocker. Again, the membranes were washed 3 times with a wash buffer, drained, and 1ml chemiluminescent reagent added to each well, left to incubated for 1 minute. The membranes were removed from the wells using a pair of flat-tip tweezers and placed in between transparent protective plastic sheets. The plastic sheets were flattened out to remove air bubbles and excess chemiluminescent reagent. The light signal intensities were read using a G-Box (Syngene) and the imaged analysed in Image Studio Lite (Licor).

5. Results

The results are graphically reported in **Figure 2 of Appendix 2** comparing the conditions at baseline, 1 Bar x 1000 and 2 Bar x 1000; presented in multiple charts because of different proteins have different dynamic range.

6. Conclusion

It was demonstrated that there are other chemokines that be induced by shockwave and human cardiac fibroblast could be the main player.

7. Hypothesis generated

Shockwave to the heart could induce inotropy

8. Future plan

High-throughput screening in a shockwave clinical study.

Figure 1 of Appendix 2. Dot blot chemokines	
C5/C5a Complement Component 5/5a	MCP-1 CCL2
CD40 Ligand CD154	MIF GIF, DER6
G-CSF CSFβ, CSF-3	MIP-1α CCL3
GM-CSF CSFα, CSF-2	MIP-1β CCL4
GROα CXCL1	Serpin E1 PAI-1
I-309 CCL1	RANTES CCL5
sICAM-1 CD54	SDF-1 CXCL12
IFN-γ Type II IFN	TNF-α TNFSF1A
IL-1α IL-1F1	sTREM-1
IL-1β IL-1F2	IL-13
L-1ra IL-1F3	IL-16 LCF
IL-2	IL-17
IL-4	IL-17E
IL-5	IL-23
IL-6	IL-27
IL-8 CXCL8	IL-32α
IL-10	IP-10 CXCL10
IL-12 p70	I-TAC CXCL11
IL-13	MCP-1 CCL2
IL-16 LCF	MIF GIF, DER6
IL-17	MIP-1α CCL3
IL-17E	MIP-1β CCL4
IL-23	Serpin E1 PAI-1
IL-27	RANTES CCL5
IL-32α	SDF-1 CXCL12
IP-10 CXCL10	TNF-α TNFSF1A
I-TAC CXCL11	sTREM-1

Figure 2 of Appendix 2. (A) Dot blot of chemokine screen of human cardiac fibroblast secretome comparing baseline (preshockwave), 1 Bar x 1000 and 2 Bar x 2000. **(B)**, **(C)**, **(D)** and **(E)** are the bar charts of protein expression displaying signal intensity (y-axis), separated in different chart because the dynamic range is wide, and all signal intensities cannot all be visualised in one chart.

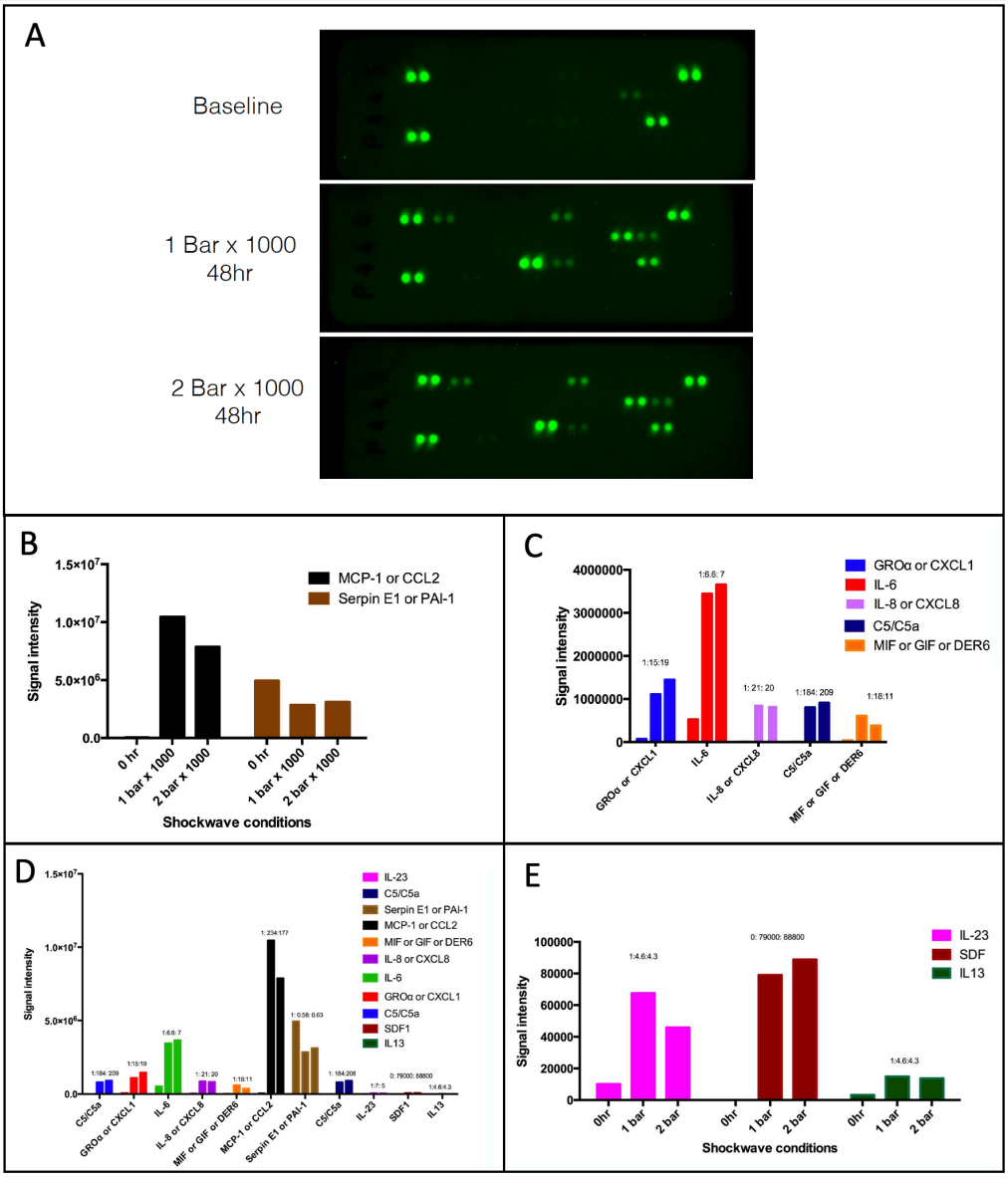

APPENDIX 3

Figure 1 of Appendix 3. A graphical abstract showing results of miR21-5p. (A) Healthy heart with no cardiac remodelling, (B) Acute-MI heart with no remodelling, (C) chronic-MI heart with remodelling. Exosomes from A, B and C collected. (D) a photograph of a healthy rat's heart, (E) a photograph of acute MI rat's heart with LAD ligation in situ, yellow circle indicating the remote area, orange circle indicating the acute infarcted area and the white broken line is the acute infarct border, (F) a photograph of a chronic-MI heart, pink circle indicating the remote area and red circle indicating the chronic-MI area and the white broken line is the chronic infarct border. (G) Exosome pallet extracted from rats' plasma using sedimentation method. (H) Roles of miR21 plays in pathways modulating proliferation, impaired apoptosis, angiogenesis, invasion, inflammation and genetic stability via molecular pathways, adapted from Melnik et a l [343] under the terms of the Creative Commons CC BY license , (I) miR-21-5p in tissue according to healthy, remote acute, infarct acute, chronic remote and chronic infarct plotted on a scatter dot plot axis on the left y-axis showing $\Delta\Delta$Ct/ath-miR159a overlay over fold changes on the right y-axis. (J) miR-21-5p in rats' plasma exosomes according to healthy, acute-MI and chronic-MI group plotted on a scatter dot plot axis on the left y-axis showing $\Delta\Delta$Ct/ath-miR159a overlay over fold changes on the right y-axis. **See overleaf for graphics.**

Results: miR-21-5p increased in the Healthy remote, acute infarction and chronic infarction

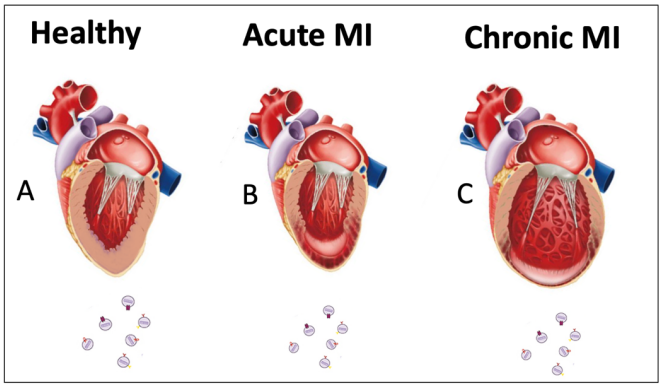

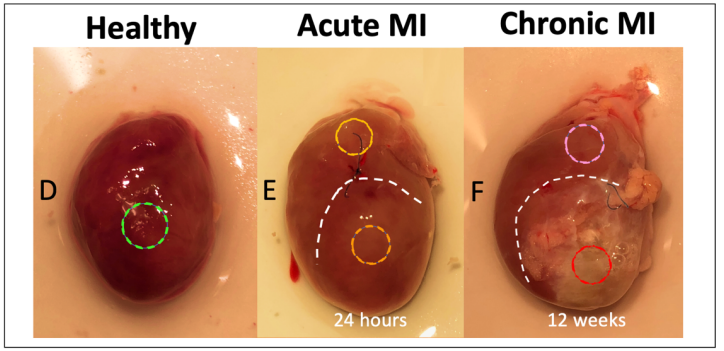

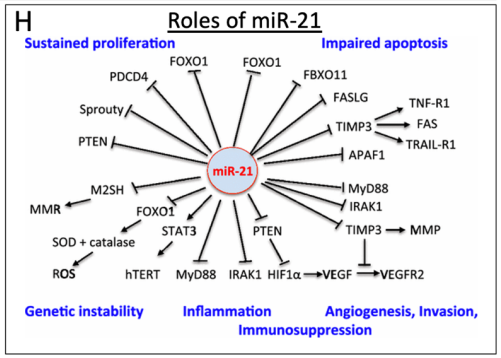

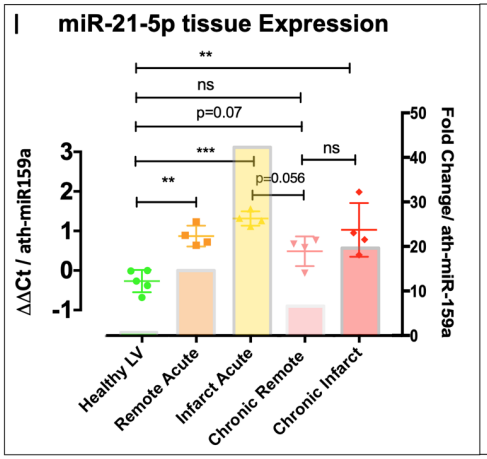

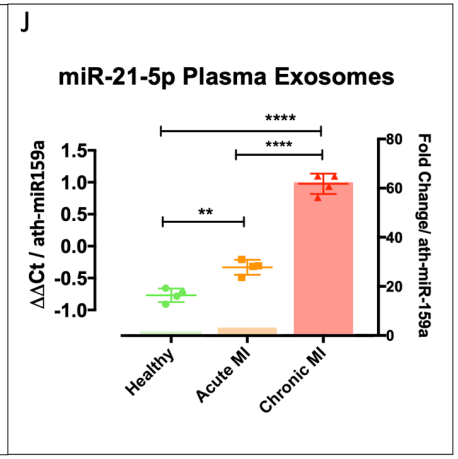

(Sam Guymer, BSc medical student)

ELSEVIER LICENSE
TERMS AND CONDITIONS

APPENDIX 4

Dec 16, 2020

This Agreement between Imperial College London -- Salomon Narodden ("You") and Elsevier ("Elsevier") consists of your license details and the terms and conditions provided by Elsevier and Copyright Clearance Center.

License Number	4970230470250
License date	Dec 15, 2020
Licensed Content Publisher	Elsevier
Licensed Content Publication	Journal of the American College of Cardiology
Licensed Content Title	Importance of time to reperfusion for 30-day and late survival and recovery of left ventricular function after primary angioplasty for acute myocardial infarction
Licensed Content Author	Bruce R Brodie,Thomas D Stuckey,Thomas C Wall,Grace Kissling,Charles J Hansen,Denise B Muncy,Richard A Weintraub,Thomas A Kelly
Licensed Content Date	Nov 1, 1998
Licensed Content Volume	32
Licensed Content Issue	5
Licensed Content Pages	8
Start Page	1312

End Page	1319
Type of Use	reuse in a thesis/dissertation
Portion	figures/tables/illustrations
Number of figures/tables/illustrations	3
Format	both print and electronic
Are you the author of this Elsevier article?	No
Will you be translating?	No
Title	PhD Thesis: Shockwave for the abrogation of heart failure in myocardial ischaemia-reperfusion injury
Institution name	Imperial College London
Expected presentation date	Jan 2021
Portions	Figure 3, page 1316
Requestor Location	Imperial College London NHLI, Hammersmith Campus Du Cane Road London London, W12 0NN United Kingdom Attn: Imperial College London
Publisher Tax ID	GB 494 6272 12
Total	0.00 GBP

Terms and Conditions

INTRODUCTION

1. The publisher for this copyrighted material is Elsevier. By clicking "accept" in connection with completing this licensing transaction, you agree that the following terms and conditions apply to this transaction (along with the Billing and Payment terms and conditions established by Copyright Clearance Center, Inc. ("CCC"), at the time that you opened your Rightslink account and that are available at any time at http://myaccount.copyright.com).

GENERAL TERMS

2. Elsevier hereby grants you permission to reproduce the aforementioned material subject to the terms and conditions indicated.

3. Acknowledgement: If any part of the material to be used (for example, figures) has appeared in our publication with credit or acknowledgement to another source, permission must also be sought from that source. If such permission is not obtained then that material may not be included in your publication/copies. Suitable acknowledgement to the source must be made, either as a footnote or in a reference list at the end of your publication, as follows:

"Reprinted from Publication title, Vol /edition number, Author(s), Title of article / title of chapter, Pages No., Copyright (Year), with permission from Elsevier [OR APPLICABLE SOCIETY COPYRIGHT OWNER]." Also Lancet special credit - "Reprinted from The Lancet, Vol. number, Author(s), Title of article, Pages No., Copyright (Year), with permission from Elsevier."

4. Reproduction of this material is confined to the purpose and/or media for which permission is hereby given.

5. Altering/Modifying Material: Not Permitted. However figures and illustrations may be altered/adapted minimally to serve your work. Any other abbreviations, additions, deletions and/or any other alterations shall be made only with prior written authorization of Elsevier Ltd. (Please contact Elsevier's permissions helpdesk here). No modifications can be made to any Lancet figures/tables and they must be reproduced in full.

6. If the permission fee for the requested use of our material is waived in this instance, please be advised that your future requests for Elsevier materials may attract a fee.

7. Reservation of Rights: Publisher reserves all rights not specifically granted in the combination of (i) the license details provided by you and accepted in the course of this licensing transaction, (ii) these terms and conditions and (iii) CCC's Billing and Payment terms and conditions.

8. License Contingent Upon Payment: While you may exercise the rights licensed immediately upon issuance of the license at the end of the licensing process for the transaction, provided that you have disclosed complete and accurate details of your proposed use, no license is finally effective unless and until full payment is received from you (either by publisher or by CCC) as provided in CCC's Billing and Payment terms and conditions. If full payment is not received on a timely basis, then any license preliminarily granted shall be deemed automatically revoked and shall be void as if never granted. Further, in the event that you breach any of these terms and conditions or any of CCC's Billing and Payment terms and conditions, the license is automatically revoked and shall be void as if never

granted. Use of materials as described in a revoked license, as well as any use of the materials beyond the scope of an unrevoked license, may constitute copyright infringement and publisher reserves the right to take any and all action to protect its copyright in the materials.

9. Warranties: Publisher makes no representations or warranties with respect to the licensed material.

10. Indemnity: You hereby indemnify and agree to hold harmless publisher and CCC, and their respective officers, directors, employees and agents, from and against any and all claims arising out of your use of the licensed material other than as specifically authorized pursuant to this license.

11. No Transfer of License: This license is personal to you and may not be sublicensed, assigned, or transferred by you to any other person without publisher's written permission.

12. No Amendment Except in Writing: This license may not be amended except in a writing signed by both parties (or, in the case of publisher, by CCC on publisher's behalf).

13. Objection to Contrary Terms: Publisher hereby objects to any terms contained in any purchase order, acknowledgment, check endorsement or other writing prepared by you, which terms are inconsistent with these terms and conditions or CCC's Billing and Payment terms and conditions. These terms and conditions, together with CCC's Billing and Payment terms and conditions (which are incorporated herein), comprise the entire agreement between you and publisher (and CCC) concerning this licensing transaction. In the event of any conflict between your obligations established by these terms and conditions and those established by CCC's Billing and Payment terms and conditions, these terms and conditions shall control.

14. Revocation: Elsevier or Copyright Clearance Center may deny the permissions described in this License at their sole discretion, for any reason or no reason, with a full refund payable to you. Notice of such denial will be made using the contact information provided by you. Failure to receive such notice will not alter or invalidate the denial. In no event will Elsevier or Copyright Clearance Center be responsible or liable for any costs, expenses or damage incurred by you as a result of a denial of your permission request, other than a refund of the amount(s) paid by you to Elsevier and/or Copyright Clearance Center for denied permissions.

LIMITED LICENSE

The following terms and conditions apply only to specific license types:

15. **Translation**: This permission is granted for non-exclusive world **English** rights only unless your license was granted for translation rights. If you licensed translation rights you may only translate this content into the languages you requested. A professional translator must perform all translations and reproduce the content word for word preserving the integrity of the article.

16. **Posting licensed content on any Website**: The following terms and conditions apply as follows: Licensing material from an Elsevier journal: All content posted to the web site must maintain the copyright information line on the bottom of each image; A hyper-text must be included to the Homepage of the journal from which you are licensing at http://www.sciencedirect.com/science/journal/xxxxx or the Elsevier homepage for books at http://www.elsevier.com; Central Storage: This license does not include permission for a scanned version of the material to be stored in a central repository such as that provided by

Heron/XanEdu.

Licensing material from an Elsevier book: A hyper-text link must be included to the Elsevier homepage at http://www.elsevier.com . All content posted to the web site must maintain the copyright information line on the bottom of each image.

Posting licensed content on Electronic reserve: In addition to the above the following clauses are applicable: The web site must be password-protected and made available only to bona fide students registered on a relevant course. This permission is granted for 1 year only. You may obtain a new license for future website posting.

17. **For journal authors:** the following clauses are applicable in addition to the above:

Preprints:

A preprint is an author's own write-up of research results and analysis, it has not been peer-reviewed, nor has it had any other value added to it by a publisher (such as formatting, copyright, technical enhancement etc.).

Authors can share their preprints anywhere at any time. Preprints should not be added to or enhanced in any way in order to appear more like, or to substitute for, the final versions of articles however authors can update their preprints on arXiv or RePEc with their Accepted Author Manuscript (see below).

If accepted for publication, we encourage authors to link from the preprint to their formal publication via its DOI. Millions of researchers have access to the formal publications on ScienceDirect, and so links will help users to find, access, cite and use the best available version. Please note that Cell Press, The Lancet and some society-owned have different preprint policies. Information on these policies is available on the journal homepage.

Accepted Author Manuscripts: An accepted author manuscript is the manuscript of an article that has been accepted for publication and which typically includes author-incorporated changes suggested during submission, peer review and editor-author communications.

Authors can share their accepted author manuscript:

- immediately
    - via their non-commercial person homepage or blog
    - by updating a preprint in arXiv or RePEc with the accepted manuscript
    - via their research institute or institutional repository for internal institutional uses or as part of an invitation-only research collaboration work-group
    - directly by providing copies to their students or to research collaborators for their personal use
    - for private scholarly sharing as part of an invitation-only work group on commercial sites with which Elsevier has an agreement
- After the embargo period
    - via non-commercial hosting platforms such as their institutional repository
    - via commercial sites with which Elsevier has an agreement

In all cases accepted manuscripts should:

- link to the formal publication via its DOI
- bear a CC-BY-NC-ND license - this is easy to do

- if aggregated with other manuscripts, for example in a repository or other site, be shared in alignment with our hosting policy not be added to or enhanced in any way to appear more like, or to substitute for, the published journal article.

Published journal article (JPA): A published journal article (PJA) is the definitive final record of published research that appears or will appear in the journal and embodies all value-adding publishing activities including peer review co-ordination, copy-editing, formatting, (if relevant) pagination and online enrichment.

Policies for sharing publishing journal articles differ for subscription and gold open access articles:

Subscription Articles: If you are an author, please share a link to your article rather than the full-text. Millions of researchers have access to the formal publications on ScienceDirect, and so links will help your users to find, access, cite, and use the best available version.

Theses and dissertations which contain embedded PJAs as part of the formal submission can be posted publicly by the awarding institution with DOI links back to the formal publications on ScienceDirect.

If you are affiliated with a library that subscribes to ScienceDirect you have additional private sharing rights for others' research accessed under that agreement. This includes use for classroom teaching and internal training at the institution (including use in course packs and courseware programs), and inclusion of the article for grant funding purposes.

Gold Open Access Articles: May be shared according to the author-selected end-user license and should contain a CrossMark logo, the end user license, and a DOI link to the formal publication on ScienceDirect.

Please refer to Elsevier's posting policy for further information.

18. **For book authors** the following clauses are applicable in addition to the above: Authors are permitted to place a brief summary of their work online only. You are not allowed to download and post the published electronic version of your chapter, nor may you scan the printed edition to create an electronic version. **Posting to a repository:** Authors are permitted to post a summary of their chapter only in their institution's repository.

19. **Thesis/Dissertation**: If your license is for use in a thesis/dissertation your thesis may be submitted to your institution in either print or electronic form. Should your thesis be published commercially, please reapply for permission. These requirements include permission for the Library and Archives of Canada to supply single copies, on demand, of the complete thesis and include permission for Proquest/UMI to supply single copies, on demand, of the complete thesis. Should your thesis be published commercially, please reapply for permission. Theses and dissertations which contain embedded PJAs as part of the formal submission can be posted publicly by the awarding institution with DOI links back to the formal publications on ScienceDirect.

Elsevier Open Access Terms and Conditions

You can publish open access with Elsevier in hundreds of open access journals or in nearly 2000 established subscription journals that support open access publishing. Permitted third party re-use of these open access articles is defined by the author's choice of Creative Commons user license. See our open access license policy for more information.

Terms & Conditions applicable to all Open Access articles published with Elsevier:

Any reuse of the article must not represent the author as endorsing the adaptation of the article nor should the article be modified in such a way as to damage the author's honour or reputation. If any changes have been made, such changes must be clearly indicated.

The author(s) must be appropriately credited and we ask that you include the end user license and a DOI link to the formal publication on ScienceDirect.

If any part of the material to be used (for example, figures) has appeared in our publication with credit or acknowledgement to another source it is the responsibility of the user to ensure their reuse complies with the terms and conditions determined by the rights holder.

Additional Terms & Conditions applicable to each Creative Commons user license:

CC BY: The CC-BY license allows users to copy, to create extracts, abstracts and new works from the Article, to alter and revise the Article and to make commercial use of the Article (including reuse and/or resale of the Article by commercial entities), provided the user gives appropriate credit (with a link to the formal publication through the relevant DOI), provides a link to the license, indicates if changes were made and the licensor is not represented as endorsing the use made of the work. The full details of the license are available at http://creativecommons.org/licenses/by/4.0.

CC BY NC SA: The CC BY-NC-SA license allows users to copy, to create extracts, abstracts and new works from the Article, to alter and revise the Article, provided this is not done for commercial purposes, and that the user gives appropriate credit (with a link to the formal publication through the relevant DOI), provides a link to the license, indicates if changes were made and the licensor is not represented as endorsing the use made of the work. Further, any new works must be made available on the same conditions. The full details of the license are available at http://creativecommons.org/licenses/by-nc-sa/4.0.

CC BY NC ND: The CC BY-NC-ND license allows users to copy and distribute the Article, provided this is not done for commercial purposes and further does not permit distribution of the Article if it is changed or edited in any way, and provided the user gives appropriate credit (with a link to the formal publication through the relevant DOI), provides a link to the license, and that the licensor is not represented as endorsing the use made of the work. The full details of the license are available at http://creativecommons.org/licenses/by-nc-nd/4.0. Any commercial reuse of Open Access articles published with a CC BY NC SA or CC BY NC ND license requires permission from Elsevier and will be subject to a fee.

Commercial reuse includes:

- Associating advertising with the full text of the Article
- Charging fees for document delivery or access
- Article aggregation
- Systematic distribution via e-mail lists or share buttons

Posting or linking by commercial companies for use by customers of those companies.

20. **Other Conditions**:

ELSEVIER LICENSE
TERMS AND CONDITIONS

APPENDIX 5

Dec 16, 2020

This Agreement between Imperial College London -- Salomon Narodden ("You") and Elsevier ("Elsevier") consists of your license details and the terms and conditions provided by Elsevier and Copyright Clearance Center.

License Number	4970230731053
License date	Dec 15, 2020
Licensed Content Publisher	Elsevier
Licensed Content Publication	Journal of the American College of Cardiology
Licensed Content Title	Impact of Primary Coronary Angioplasty Delay on Myocardial Salvage, Infarct Size, and Microvascular Damage in Patients With ST-Segment Elevation Myocardial Infarction Insight From Cardiovascular Magnetic Resonance
Licensed Content Author	Marco Francone,Chiara Bucciarelli-Ducci,Iacopo Carbone,Emanuele Canali,Raffaele Scardala,Francesca A. Calabrese,Gennaro Sardella,Massimo Mancone,Carlo Catalano,Francesco Fedele,Roberto Passariello,Jan Bogaert,Luciano Agati
Licensed Content Date	Dec 1, 2009
Licensed Content Volume	54
Licensed Content Issue	23
Licensed Content Pages	9

Start Page	2145
End Page	2153
Type of Use	reuse in a thesis/dissertation
Portion	figures/tables/illustrations
Number of figures/tables/illustrations	1
Format	both print and electronic
Are you the author of this Elsevier article?	No
Will you be translating?	No
Title	PhD Thesis: Shockwave for the abrogation of heart failure in myocardial ischaemia-reperfusion injury
Institution name	Imperial College London
Expected presentation date	Jan 2021
Portions	Figure 1, page 2149
Requestor Location	Imperial College London NHLI, Hammersmith Campus Du Cane Road London London, W12 0NN United Kingdom Attn: Imperial College London
Publisher Tax ID	GB 494 6272 12
Total	0.00 GBP

Terms and Conditions

INTRODUCTION

1. The publisher for this copyrighted material is Elsevier. By clicking "accept" in connection with completing this licensing transaction, you agree that the following terms and conditions apply to this transaction (along with the Billing and Payment terms and conditions established by Copyright Clearance Center, Inc. ("CCC"), at the time that you opened your Rightslink account and that are available at any time at http://myaccount.copyright.com).

GENERAL TERMS

2. Elsevier hereby grants you permission to reproduce the aforementioned material subject to the terms and conditions indicated.

3. Acknowledgement: If any part of the material to be used (for example, figures) has appeared in our publication with credit or acknowledgement to another source, permission must also be sought from that source. If such permission is not obtained then that material may not be included in your publication/copies. Suitable acknowledgement to the source must be made, either as a footnote or in a reference list at the end of your publication, as follows:

"Reprinted from Publication title, Vol /edition number, Author(s), Title of article / title of chapter, Pages No., Copyright (Year), with permission from Elsevier [OR APPLICABLE SOCIETY COPYRIGHT OWNER]." Also Lancet special credit - "Reprinted from The Lancet, Vol. number, Author(s), Title of article, Pages No., Copyright (Year), with permission from Elsevier."

4. Reproduction of this material is confined to the purpose and/or media for which permission is hereby given.

5. Altering/Modifying Material: Not Permitted. However figures and illustrations may be altered/adapted minimally to serve your work. Any other abbreviations, additions, deletions and/or any other alterations shall be made only with prior written authorization of Elsevier Ltd. (Please contact Elsevier's permissions helpdesk here). No modifications can be made to any Lancet figures/tables and they must be reproduced in full.

6. If the permission fee for the requested use of our material is waived in this instance, please be advised that your future requests for Elsevier materials may attract a fee.

7. Reservation of Rights: Publisher reserves all rights not specifically granted in the combination of (i) the license details provided by you and accepted in the course of this licensing transaction, (ii) these terms and conditions and (iii) CCC's Billing and Payment terms and conditions.

8. License Contingent Upon Payment: While you may exercise the rights licensed immediately upon issuance of the license at the end of the licensing process for the transaction, provided that you have disclosed complete and accurate details of your proposed use, no license is finally effective unless and until full payment is received from you (either by publisher or by CCC) as provided in CCC's Billing and Payment terms and conditions. If full payment is not received on a timely basis, then any license preliminarily granted shall be

deemed automatically revoked and shall be void as if never granted. Further, in the event that you breach any of these terms and conditions or any of CCC's Billing and Payment terms and conditions, the license is automatically revoked and shall be void as if never granted. Use of materials as described in a revoked license, as well as any use of the materials beyond the scope of an unrevoked license, may constitute copyright infringement and publisher reserves the right to take any and all action to protect its copyright in the materials.

9. Warranties: Publisher makes no representations or warranties with respect to the licensed material.

10. Indemnity: You hereby indemnify and agree to hold harmless publisher and CCC, and their respective officers, directors, employees and agents, from and against any and all claims arising out of your use of the licensed material other than as specifically authorized pursuant to this license.

11. No Transfer of License: This license is personal to you and may not be sublicensed, assigned, or transferred by you to any other person without publisher's written permission.

12. No Amendment Except in Writing: This license may not be amended except in a writing signed by both parties (or, in the case of publisher, by CCC on publisher's behalf).

13. Objection to Contrary Terms: Publisher hereby objects to any terms contained in any purchase order, acknowledgment, check endorsement or other writing prepared by you, which terms are inconsistent with these terms and conditions or CCC's Billing and Payment terms and conditions. These terms and conditions, together with CCC's Billing and Payment terms and conditions (which are incorporated herein), comprise the entire agreement between you and publisher (and CCC) concerning this licensing transaction. In the event of any conflict between your obligations established by these terms and conditions and those established by CCC's Billing and Payment terms and conditions, these terms and conditions shall control.

14. Revocation: Elsevier or Copyright Clearance Center may deny the permissions described in this License at their sole discretion, for any reason or no reason, with a full refund payable to you. Notice of such denial will be made using the contact information provided by you. Failure to receive such notice will not alter or invalidate the denial. In no event will Elsevier or Copyright Clearance Center be responsible or liable for any costs, expenses or damage incurred by you as a result of a denial of your permission request, other than a refund of the amount(s) paid by you to Elsevier and/or Copyright Clearance Center for denied permissions.

LIMITED LICENSE

The following terms and conditions apply only to specific license types:

15. **Translation**: This permission is granted for non-exclusive world **English** rights only unless your license was granted for translation rights. If you licensed translation rights you may only translate this content into the languages you requested. A professional translator must perform all translations and reproduce the content word for word preserving the integrity of the article.

16. **Posting licensed content on any Website**: The following terms and conditions apply as follows: Licensing material from an Elsevier journal: All content posted to the web site must maintain the copyright information line on the bottom of each image; A hyper-text must be included to the Homepage of the journal from which you are licensing at

http://www.sciencedirect.com/science/journal/xxxxx or the Elsevier homepage for books at http://www.elsevier.com; Central Storage: This license does not include permission for a scanned version of the material to be stored in a central repository such as that provided by Heron/XanEdu.

Licensing material from an Elsevier book: A hyper-text link must be included to the Elsevier homepage at http://www.elsevier.com . All content posted to the web site must maintain the copyright information line on the bottom of each image.

Posting licensed content on Electronic reserve: In addition to the above the following clauses are applicable: The web site must be password-protected and made available only to bona fide students registered on a relevant course. This permission is granted for 1 year only. You may obtain a new license for future website posting.

17. **For journal authors:** the following clauses are applicable in addition to the above:

Preprints:

A preprint is an author's own write-up of research results and analysis, it has not been peer-reviewed, nor has it had any other value added to it by a publisher (such as formatting, copyright, technical enhancement etc.).

Authors can share their preprints anywhere at any time. Preprints should not be added to or enhanced in any way in order to appear more like, or to substitute for, the final versions of articles however authors can update their preprints on arXiv or RePEc with their Accepted Author Manuscript (see below).

If accepted for publication, we encourage authors to link from the preprint to their formal publication via its DOI. Millions of researchers have access to the formal publications on ScienceDirect, and so links will help users to find, access, cite and use the best available version. Please note that Cell Press, The Lancet and some society-owned have different preprint policies. Information on these policies is available on the journal homepage.

Accepted Author Manuscripts: An accepted author manuscript is the manuscript of an article that has been accepted for publication and which typically includes author-incorporated changes suggested during submission, peer review and editor-author communications.

Authors can share their accepted author manuscript:

- immediately
    - via their non-commercial person homepage or blog
    - by updating a preprint in arXiv or RePEc with the accepted manuscript
    - via their research institute or institutional repository for internal institutional uses or as part of an invitation-only research collaboration work-group
    - directly by providing copies to their students or to research collaborators for their personal use
    - for private scholarly sharing as part of an invitation-only work group on commercial sites with which Elsevier has an agreement
- After the embargo period
    - via non-commercial hosting platforms such as their institutional repository
    - via commercial sites with which Elsevier has an agreement

In all cases accepted manuscripts should:

- link to the formal publication via its DOI
- bear a CC-BY-NC-ND license - this is easy to do
- if aggregated with other manuscripts, for example in a repository or other site, be shared in alignment with our hosting policy not be added to or enhanced in any way to appear more like, or to substitute for, the published journal article.

Published journal article (JPA): A published journal article (PJA) is the definitive final record of published research that appears or will appear in the journal and embodies all value-adding publishing activities including peer review co-ordination, copy-editing, formatting, (if relevant) pagination and online enrichment.

Policies for sharing publishing journal articles differ for subscription and gold open access articles:

Subscription Articles: If you are an author, please share a link to your article rather than the full-text. Millions of researchers have access to the formal publications on ScienceDirect, and so links will help your users to find, access, cite, and use the best available version.

Theses and dissertations which contain embedded PJAs as part of the formal submission can be posted publicly by the awarding institution with DOI links back to the formal publications on ScienceDirect.

If you are affiliated with a library that subscribes to ScienceDirect you have additional private sharing rights for others' research accessed under that agreement. This includes use for classroom teaching and internal training at the institution (including use in course packs and courseware programs), and inclusion of the article for grant funding purposes.

Gold Open Access Articles: May be shared according to the author-selected end-user license and should contain a CrossMark logo, the end user license, and a DOI link to the formal publication on ScienceDirect.

Please refer to Elsevier's posting policy for further information.

18. **For book authors** the following clauses are applicable in addition to the above: Authors are permitted to place a brief summary of their work online only. You are not allowed to download and post the published electronic version of your chapter, nor may you scan the printed edition to create an electronic version. **Posting to a repository:** Authors are permitted to post a summary of their chapter only in their institution's repository.

19. **Thesis/Dissertation**: If your license is for use in a thesis/dissertation your thesis may be submitted to your institution in either print or electronic form. Should your thesis be published commercially, please reapply for permission. These requirements include permission for the Library and Archives of Canada to supply single copies, on demand, of the complete thesis and include permission for Proquest/UMI to supply single copies, on demand, of the complete thesis. Should your thesis be published commercially, please reapply for permission. Theses and dissertations which contain embedded PJAs as part of the formal submission can be posted publicly by the awarding institution with DOI links back to the formal publications on ScienceDirect.

Elsevier Open Access Terms and Conditions

You can publish open access with Elsevier in hundreds of open access journals or in nearly 2000 established subscription journals that support open access publishing. Permitted third

party re-use of these open access articles is defined by the author's choice of Creative Commons user license. See our open access license policy for more information.

Terms & Conditions applicable to all Open Access articles published with Elsevier:

Any reuse of the article must not represent the author as endorsing the adaptation of the article nor should the article be modified in such a way as to damage the author's honour or reputation. If any changes have been made, such changes must be clearly indicated.

The author(s) must be appropriately credited and we ask that you include the end user license and a DOI link to the formal publication on ScienceDirect.

If any part of the material to be used (for example, figures) has appeared in our publication with credit or acknowledgement to another source it is the responsibility of the user to ensure their reuse complies with the terms and conditions determined by the rights holder.

Additional Terms & Conditions applicable to each Creative Commons user license:

CC BY: The CC-BY license allows users to copy, to create extracts, abstracts and new works from the Article, to alter and revise the Article and to make commercial use of the Article (including reuse and/or resale of the Article by commercial entities), provided the user gives appropriate credit (with a link to the formal publication through the relevant DOI), provides a link to the license, indicates if changes were made and the licensor is not represented as endorsing the use made of the work. The full details of the license are available at http://creativecommons.org/licenses/by/4.0.

CC BY NC SA: The CC BY-NC-SA license allows users to copy, to create extracts, abstracts and new works from the Article, to alter and revise the Article, provided this is not done for commercial purposes, and that the user gives appropriate credit (with a link to the formal publication through the relevant DOI), provides a link to the license, indicates if changes were made and the licensor is not represented as endorsing the use made of the work. Further, any new works must be made available on the same conditions. The full details of the license are available at http://creativecommons.org/licenses/by-nc-sa/4.0.

CC BY NC ND: The CC BY-NC-ND license allows users to copy and distribute the Article, provided this is not done for commercial purposes and further does not permit distribution of the Article if it is changed or edited in any way, and provided the user gives appropriate credit (with a link to the formal publication through the relevant DOI), provides a link to the license, and that the licensor is not represented as endorsing the use made of the work. The full details of the license are available at http://creativecommons.org/licenses/by-nc-nd/4.0. Any commercial reuse of Open Access articles published with a CC BY NC SA or CC BY NC ND license requires permission from Elsevier and will be subject to a fee.

Commercial reuse includes:

- Associating advertising with the full text of the Article
- Charging fees for document delivery or access
- Article aggregation
- Systematic distribution via e-mail lists or share buttons

Posting or linking by commercial companies for use by customers of those companies.

20. **Other Conditions**:

ELSEVIER LICENSE
TERMS AND CONDITIONS

APPENDIX 6

Dec 16, 2020

This Agreement between Imperial College London -- Salomon Narodden ("You") and Elsevier ("Elsevier") consists of your license details and the terms and conditions provided by Elsevier and Copyright Clearance Center.

License Number	4970780791522
License date	Dec 16, 2020
Licensed Content Publisher	Elsevier
Licensed Content Publication	Journal of the American Society of Echocardiography
Licensed Content Title	Recommendations for Chamber Quantification: A Report from the American Society of Echocardiography's Guidelines and Standards Committee and the Chamber Quantification Writing Group, Developed in Conjunction with the European Association of Echocardiography, a Branch of the European Society of Cardiology
Licensed Content Author	Roberto M. Lang,Michelle Bierig,Richard B. Devereux,Frank A. Flachskampf,Elyse Foster,Patricia A. Pellikka,Michael H. Picard,Mary J. Roman,James Seward,Jack S. Shanewise,Scott D. Solomon,Kirk T. Spencer,Martin St John Sutton,William J. Stewart
Licensed Content Date	Dec 1, 2005
Licensed Content Volume	18
Licensed Content Issue	12

Licensed Content Pages	24
Start Page	1440
End Page	1463
Type of Use	reuse in a thesis/dissertation
Portion	figures/tables/illustrations
Number of figures/tables/illustrations	9
Format	both print and electronic
Are you the author of this Elsevier article?	No
Will you be translating?	No
Title	PhD Thesis: Shockwave for the abrogation of heart failure in myocardial ischaemia-reperfusion injury
Institution name	Imperial College London
Expected presentation date	Jan 2021
Portions	Figure 9, page 1449
Requestor Location	Imperial College London NHLI, Hammersmith Campus Du Cane Road London London, W12 0NN United Kingdom Attn: Imperial College London
Publisher Tax ID	GB 494 6272 12

Total 0.00 GBP

Terms and Conditions

INTRODUCTION

1. The publisher for this copyrighted material is Elsevier. By clicking "accept" in connection with completing this licensing transaction, you agree that the following terms and conditions apply to this transaction (along with the Billing and Payment terms and conditions established by Copyright Clearance Center, Inc. ("CCC"), at the time that you opened your Rightslink account and that are available at any time at http://myaccount.copyright.com).

GENERAL TERMS

2. Elsevier hereby grants you permission to reproduce the aforementioned material subject to the terms and conditions indicated.

3. Acknowledgement: If any part of the material to be used (for example, figures) has appeared in our publication with credit or acknowledgement to another source, permission must also be sought from that source. If such permission is not obtained then that material may not be included in your publication/copies. Suitable acknowledgement to the source must be made, either as a footnote or in a reference list at the end of your publication, as follows:

"Reprinted from Publication title, Vol /edition number, Author(s), Title of article / title of chapter, Pages No., Copyright (Year), with permission from Elsevier [OR APPLICABLE SOCIETY COPYRIGHT OWNER]." Also Lancet special credit - "Reprinted from The Lancet, Vol. number, Author(s), Title of article, Pages No., Copyright (Year), with permission from Elsevier."

4. Reproduction of this material is confined to the purpose and/or media for which permission is hereby given.

5. Altering/Modifying Material: Not Permitted. However figures and illustrations may be altered/adapted minimally to serve your work. Any other abbreviations, additions, deletions and/or any other alterations shall be made only with prior written authorization of Elsevier Ltd. (Please contact Elsevier's permissions helpdesk here). No modifications can be made to any Lancet figures/tables and they must be reproduced in full.

6. If the permission fee for the requested use of our material is waived in this instance, please be advised that your future requests for Elsevier materials may attract a fee.

7. Reservation of Rights: Publisher reserves all rights not specifically granted in the combination of (i) the license details provided by you and accepted in the course of this licensing transaction, (ii) these terms and conditions and (iii) CCC's Billing and Payment terms and conditions.

8. License Contingent Upon Payment: While you may exercise the rights licensed immediately upon issuance of the license at the end of the licensing process for the transaction, provided that you have disclosed complete and accurate details of your proposed use, no license is finally effective unless and until full payment is received from you (either by publisher or by CCC) as provided in CCC's Billing and Payment terms and conditions. If

full payment is not received on a timely basis, then any license preliminarily granted shall be deemed automatically revoked and shall be void as if never granted. Further, in the event that you breach any of these terms and conditions or any of CCC's Billing and Payment terms and conditions, the license is automatically revoked and shall be void as if never granted. Use of materials as described in a revoked license, as well as any use of the materials beyond the scope of an unrevoked license, may constitute copyright infringement and publisher reserves the right to take any and all action to protect its copyright in the materials.

9. Warranties: Publisher makes no representations or warranties with respect to the licensed material.

10. Indemnity: You hereby indemnify and agree to hold harmless publisher and CCC, and their respective officers, directors, employees and agents, from and against any and all claims arising out of your use of the licensed material other than as specifically authorized pursuant to this license.

11. No Transfer of License: This license is personal to you and may not be sublicensed, assigned, or transferred by you to any other person without publisher's written permission.

12. No Amendment Except in Writing: This license may not be amended except in a writing signed by both parties (or, in the case of publisher, by CCC on publisher's behalf).

13. Objection to Contrary Terms: Publisher hereby objects to any terms contained in any purchase order, acknowledgment, check endorsement or other writing prepared by you, which terms are inconsistent with these terms and conditions or CCC's Billing and Payment terms and conditions. These terms and conditions, together with CCC's Billing and Payment terms and conditions (which are incorporated herein), comprise the entire agreement between you and publisher (and CCC) concerning this licensing transaction. In the event of any conflict between your obligations established by these terms and conditions and those established by CCC's Billing and Payment terms and conditions, these terms and conditions shall control.

14. Revocation: Elsevier or Copyright Clearance Center may deny the permissions described in this License at their sole discretion, for any reason or no reason, with a full refund payable to you. Notice of such denial will be made using the contact information provided by you. Failure to receive such notice will not alter or invalidate the denial. In no event will Elsevier or Copyright Clearance Center be responsible or liable for any costs, expenses or damage incurred by you as a result of a denial of your permission request, other than a refund of the amount(s) paid by you to Elsevier and/or Copyright Clearance Center for denied permissions.

LIMITED LICENSE

The following terms and conditions apply only to specific license types:

15. **Translation**: This permission is granted for non-exclusive world **English** rights only unless your license was granted for translation rights. If you licensed translation rights you may only translate this content into the languages you requested. A professional translator must perform all translations and reproduce the content word for word preserving the integrity of the article.

16. **Posting licensed content on any Website**: The following terms and conditions apply as follows: Licensing material from an Elsevier journal: All content posted to the web site must maintain the copyright information line on the bottom of each image; A hyper-text must be

included to the Homepage of the journal from which you are licensing at http://www.sciencedirect.com/science/journal/xxxxx or the Elsevier homepage for books at http://www.elsevier.com; Central Storage: This license does not include permission for a scanned version of the material to be stored in a central repository such as that provided by Heron/XanEdu.

Licensing material from an Elsevier book: A hyper-text link must be included to the Elsevier homepage at http://www.elsevier.com . All content posted to the web site must maintain the copyright information line on the bottom of each image.

Posting licensed content on Electronic reserve: In addition to the above the following clauses are applicable: The web site must be password-protected and made available only to bona fide students registered on a relevant course. This permission is granted for 1 year only. You may obtain a new license for future website posting.

17. **For journal authors:** the following clauses are applicable in addition to the above:

Preprints:

A preprint is an author's own write-up of research results and analysis, it has not been peer-reviewed, nor has it had any other value added to it by a publisher (such as formatting, copyright, technical enhancement etc.).

Authors can share their preprints anywhere at any time. Preprints should not be added to or enhanced in any way in order to appear more like, or to substitute for, the final versions of articles however authors can update their preprints on arXiv or RePEc with their Accepted Author Manuscript (see below).

If accepted for publication, we encourage authors to link from the preprint to their formal publication via its DOI. Millions of researchers have access to the formal publications on ScienceDirect, and so links will help users to find, access, cite and use the best available version. Please note that Cell Press, The Lancet and some society-owned have different preprint policies. Information on these policies is available on the journal homepage.

Accepted Author Manuscripts: An accepted author manuscript is the manuscript of an article that has been accepted for publication and which typically includes author-incorporated changes suggested during submission, peer review and editor-author communications.

Authors can share their accepted author manuscript:

- immediately
    - via their non-commercial person homepage or blog
    - by updating a preprint in arXiv or RePEc with the accepted manuscript
    - via their research institute or institutional repository for internal institutional uses or as part of an invitation-only research collaboration work-group
    - directly by providing copies to their students or to research collaborators for their personal use
    - for private scholarly sharing as part of an invitation-only work group on commercial sites with which Elsevier has an agreement
- After the embargo period
    - via non-commercial hosting platforms such as their institutional repository
    - via commercial sites with which Elsevier has an agreement

In all cases accepted manuscripts should:

- link to the formal publication via its DOI
- bear a CC-BY-NC-ND license - this is easy to do
- if aggregated with other manuscripts, for example in a repository or other site, be shared in alignment with our hosting policy not be added to or enhanced in any way to appear more like, or to substitute for, the published journal article.

Published journal article (JPA): A published journal article (PJA) is the definitive final record of published research that appears or will appear in the journal and embodies all value-adding publishing activities including peer review co-ordination, copy-editing, formatting, (if relevant) pagination and online enrichment.

Policies for sharing publishing journal articles differ for subscription and gold open access articles:

Subscription Articles: If you are an author, please share a link to your article rather than the full-text. Millions of researchers have access to the formal publications on ScienceDirect, and so links will help your users to find, access, cite, and use the best available version.

Theses and dissertations which contain embedded PJAs as part of the formal submission can be posted publicly by the awarding institution with DOI links back to the formal publications on ScienceDirect.

If you are affiliated with a library that subscribes to ScienceDirect you have additional private sharing rights for others' research accessed under that agreement. This includes use for classroom teaching and internal training at the institution (including use in course packs and courseware programs), and inclusion of the article for grant funding purposes.

Gold Open Access Articles: May be shared according to the author-selected end-user license and should contain a CrossMark logo, the end user license, and a DOI link to the formal publication on ScienceDirect.

Please refer to Elsevier's posting policy for further information.

18. **For book authors** the following clauses are applicable in addition to the above: Authors are permitted to place a brief summary of their work online only. You are not allowed to download and post the published electronic version of your chapter, nor may you scan the printed edition to create an electronic version. **Posting to a repository:** Authors are permitted to post a summary of their chapter only in their institution's repository.

19. **Thesis/Dissertation**: If your license is for use in a thesis/dissertation your thesis may be submitted to your institution in either print or electronic form. Should your thesis be published commercially, please reapply for permission. These requirements include permission for the Library and Archives of Canada to supply single copies, on demand, of the complete thesis and include permission for Proquest/UMI to supply single copies, on demand, of the complete thesis. Should your thesis be published commercially, please reapply for permission. Theses and dissertations which contain embedded PJAs as part of the formal submission can be posted publicly by the awarding institution with DOI links back to the formal publications on ScienceDirect.

Elsevier Open Access Terms and Conditions

20. **Other Conditions**:

v1.10

Questions? customercare@copyright.com or +1-855-239-3415 (toll free in the US) or +1-978-646-2777.

ELSEVIER LICENSE
TERMS AND CONDITIONS

APPENDIX 7

Dec 17, 2020

This Agreement between Imperial College London -- Salomon Narodden ("You") and Elsevier ("Elsevier") consists of your license details and the terms and conditions provided by Elsevier and Copyright Clearance Center.

License Number	4971080915551
License date	Dec 16, 2020
Licensed Content Publisher	Elsevier
Licensed Content Publication	Journal of the American Society of Echocardiography
Licensed Content Title	Definitions for a Common Standard for 2D Speckle Tracking Echocardiography: Consensus Document of the EACVI/ASE/Industry Task Force to Standardize Deformation Imaging
Licensed Content Author	Jens-Uwe Voigt,Gianni Pedrizzetti,Peter Lysyansky,Tom H. Marwick,Hélène Houle,Rolf Baumann,Stefano Pedri,Yasuhiro Ito,Yasuhiko Abe,Stephen Metz,Joo Hyun Song,Jamie Hamilton,Partho P. Sengupta,Theodore J. Kolias,Jan d'Hooge,Gerard P. Aurigemma et al.
Licensed Content Date	Feb 1, 2015
Licensed Content Volume	28
Licensed Content Issue	2
Licensed Content Pages	11

Start Page	183
End Page	193
Type of Use	reuse in a thesis/dissertation
Portion	figures/tables/illustrations
Number of figures/tables/illustrations	3
Format	both print and electronic
Are you the author of this Elsevier article?	No
Will you be translating?	No
Title	PhD Thesis: Shockwave for the abrogation of heart failure in myocardial ischaemia-reperfusion injury
Institution name	Imperial College London
Expected presentation date	Jan 2021
Portions	Figure 3/page186
Requestor Location	Imperial College London NHLI, Hammersmith Campus Du Cane Road London London, W12 0NN United Kingdom Attn: Imperial College London
Publisher Tax ID	GB 494 6272 12
Total	0.00 GBP

Terms and Conditions

INTRODUCTION

1. The publisher for this copyrighted material is Elsevier. By clicking "accept" in connection with completing this licensing transaction, you agree that the following terms and conditions apply to this transaction (along with the Billing and Payment terms and conditions established by Copyright Clearance Center, Inc. ("CCC"), at the time that you opened your Rightslink account and that are available at any time at http://myaccount.copyright.com).

GENERAL TERMS

2. Elsevier hereby grants you permission to reproduce the aforementioned material subject to the terms and conditions indicated.

3. Acknowledgement: If any part of the material to be used (for example, figures) has appeared in our publication with credit or acknowledgement to another source, permission must also be sought from that source. If such permission is not obtained then that material may not be included in your publication/copies. Suitable acknowledgement to the source must be made, either as a footnote or in a reference list at the end of your publication, as follows:

"Reprinted from Publication title, Vol /edition number, Author(s), Title of article / title of chapter, Pages No., Copyright (Year), with permission from Elsevier [OR APPLICABLE SOCIETY COPYRIGHT OWNER]." Also Lancet special credit - "Reprinted from The Lancet, Vol. number, Author(s), Title of article, Pages No., Copyright (Year), with permission from Elsevier."

4. Reproduction of this material is confined to the purpose and/or media for which permission is hereby given.

5. Altering/Modifying Material: Not Permitted. However figures and illustrations may be altered/adapted minimally to serve your work. Any other abbreviations, additions, deletions and/or any other alterations shall be made only with prior written authorization of Elsevier Ltd. (Please contact Elsevier's permissions helpdesk here). No modifications can be made to any Lancet figures/tables and they must be reproduced in full.

6. If the permission fee for the requested use of our material is waived in this instance, please be advised that your future requests for Elsevier materials may attract a fee.

7. Reservation of Rights: Publisher reserves all rights not specifically granted in the combination of (i) the license details provided by you and accepted in the course of this licensing transaction, (ii) these terms and conditions and (iii) CCC's Billing and Payment terms and conditions.

8. License Contingent Upon Payment: While you may exercise the rights licensed immediately upon issuance of the license at the end of the licensing process for the transaction, provided that you have disclosed complete and accurate details of your proposed use, no license is finally effective unless and until full payment is received from you (either by publisher or by CCC) as provided in CCC's Billing and Payment terms and conditions. If full payment is not received on a timely basis, then any license preliminarily granted shall be

deemed automatically revoked and shall be void as if never granted. Further, in the event that you breach any of these terms and conditions or any of CCC's Billing and Payment terms and conditions, the license is automatically revoked and shall be void as if never granted. Use of materials as described in a revoked license, as well as any use of the materials beyond the scope of an unrevoked license, may constitute copyright infringement and publisher reserves the right to take any and all action to protect its copyright in the materials.

9. Warranties: Publisher makes no representations or warranties with respect to the licensed material.

10. Indemnity: You hereby indemnify and agree to hold harmless publisher and CCC, and their respective officers, directors, employees and agents, from and against any and all claims arising out of your use of the licensed material other than as specifically authorized pursuant to this license.

11. No Transfer of License: This license is personal to you and may not be sublicensed, assigned, or transferred by you to any other person without publisher's written permission.

12. No Amendment Except in Writing: This license may not be amended except in a writing signed by both parties (or, in the case of publisher, by CCC on publisher's behalf).

13. Objection to Contrary Terms: Publisher hereby objects to any terms contained in any purchase order, acknowledgment, check endorsement or other writing prepared by you, which terms are inconsistent with these terms and conditions or CCC's Billing and Payment terms and conditions. These terms and conditions, together with CCC's Billing and Payment terms and conditions (which are incorporated herein), comprise the entire agreement between you and publisher (and CCC) concerning this licensing transaction. In the event of any conflict between your obligations established by these terms and conditions and those established by CCC's Billing and Payment terms and conditions, these terms and conditions shall control.

14. Revocation: Elsevier or Copyright Clearance Center may deny the permissions described in this License at their sole discretion, for any reason or no reason, with a full refund payable to you. Notice of such denial will be made using the contact information provided by you. Failure to receive such notice will not alter or invalidate the denial. In no event will Elsevier or Copyright Clearance Center be responsible or liable for any costs, expenses or damage incurred by you as a result of a denial of your permission request, other than a refund of the amount(s) paid by you to Elsevier and/or Copyright Clearance Center for denied permissions.

LIMITED LICENSE

The following terms and conditions apply only to specific license types:

15. **Translation**: This permission is granted for non-exclusive world **English** rights only unless your license was granted for translation rights. If you licensed translation rights you may only translate this content into the languages you requested. A professional translator must perform all translations and reproduce the content word for word preserving the integrity of the article.

16. **Posting licensed content on any Website**: The following terms and conditions apply as follows: Licensing material from an Elsevier journal: All content posted to the web site must maintain the copyright information line on the bottom of each image; A hyper-text must be included to the Homepage of the journal from which you are licensing at

http://www.sciencedirect.com/science/journal/xxxxx or the Elsevier homepage for books at http://www.elsevier.com; Central Storage: This license does not include permission for a scanned version of the material to be stored in a central repository such as that provided by Heron/XanEdu.

Licensing material from an Elsevier book: A hyper-text link must be included to the Elsevier homepage at http://www.elsevier.com . All content posted to the web site must maintain the copyright information line on the bottom of each image.

Posting licensed content on Electronic reserve: In addition to the above the following clauses are applicable: The web site must be password-protected and made available only to bona fide students registered on a relevant course. This permission is granted for 1 year only. You may obtain a new license for future website posting.

17. **For journal authors:** the following clauses are applicable in addition to the above:

Preprints:

A preprint is an author's own write-up of research results and analysis, it has not been peer-reviewed, nor has it had any other value added to it by a publisher (such as formatting, copyright, technical enhancement etc.).

Authors can share their preprints anywhere at any time. Preprints should not be added to or enhanced in any way in order to appear more like, or to substitute for, the final versions of articles however authors can update their preprints on arXiv or RePEc with their Accepted Author Manuscript (see below).

If accepted for publication, we encourage authors to link from the preprint to their formal publication via its DOI. Millions of researchers have access to the formal publications on ScienceDirect, and so links will help users to find, access, cite and use the best available version. Please note that Cell Press, The Lancet and some society-owned have different preprint policies. Information on these policies is available on the journal homepage.

Accepted Author Manuscripts: An accepted author manuscript is the manuscript of an article that has been accepted for publication and which typically includes author-incorporated changes suggested during submission, peer review and editor-author communications.

Authors can share their accepted author manuscript:

- immediately
    - via their non-commercial person homepage or blog
    - by updating a preprint in arXiv or RePEc with the accepted manuscript
    - via their research institute or institutional repository for internal institutional uses or as part of an invitation-only research collaboration work-group
    - directly by providing copies to their students or to research collaborators for their personal use
    - for private scholarly sharing as part of an invitation-only work group on commercial sites with which Elsevier has an agreement
- After the embargo period
    - via non-commercial hosting platforms such as their institutional repository
    - via commercial sites with which Elsevier has an agreement

In all cases accepted manuscripts should:

- link to the formal publication via its DOI
- bear a CC-BY-NC-ND license - this is easy to do
- if aggregated with other manuscripts, for example in a repository or other site, be shared in alignment with our hosting policy not be added to or enhanced in any way to appear more like, or to substitute for, the published journal article.

Published journal article (JPA): A published journal article (PJA) is the definitive final record of published research that appears or will appear in the journal and embodies all value-adding publishing activities including peer review co-ordination, copy-editing, formatting, (if relevant) pagination and online enrichment.

Policies for sharing publishing journal articles differ for subscription and gold open access articles:

Subscription Articles: If you are an author, please share a link to your article rather than the full-text. Millions of researchers have access to the formal publications on ScienceDirect, and so links will help your users to find, access, cite, and use the best available version.

Theses and dissertations which contain embedded PJAs as part of the formal submission can be posted publicly by the awarding institution with DOI links back to the formal publications on ScienceDirect.

If you are affiliated with a library that subscribes to ScienceDirect you have additional private sharing rights for others' research accessed under that agreement. This includes use for classroom teaching and internal training at the institution (including use in course packs and courseware programs), and inclusion of the article for grant funding purposes.

Gold Open Access Articles: May be shared according to the author-selected end-user license and should contain a CrossMark logo, the end user license, and a DOI link to the formal publication on ScienceDirect.

Please refer to Elsevier's posting policy for further information.

18. **For book authors** the following clauses are applicable in addition to the above: Authors are permitted to place a brief summary of their work online only. You are not allowed to download and post the published electronic version of your chapter, nor may you scan the printed edition to create an electronic version. **Posting to a repository:** Authors are permitted to post a summary of their chapter only in their institution's repository.

19. **Thesis/Dissertation**: If your license is for use in a thesis/dissertation your thesis may be submitted to your institution in either print or electronic form. Should your thesis be published commercially, please reapply for permission. These requirements include permission for the Library and Archives of Canada to supply single copies, on demand, of the complete thesis and include permission for Proquest/UMI to supply single copies, on demand, of the complete thesis. Should your thesis be published commercially, please reapply for permission. Theses and dissertations which contain embedded PJAs as part of the formal submission can be posted publicly by the awarding institution with DOI links back to the formal publications on ScienceDirect.

Elsevier Open Access Terms and Conditions

You can publish open access with Elsevier in hundreds of open access journals or in nearly 2000 established subscription journals that support open access publishing. Permitted third

party re-use of these open access articles is defined by the author's choice of Creative Commons user license. See our open access license policy for more information.

Terms & Conditions applicable to all Open Access articles published with Elsevier:

Any reuse of the article must not represent the author as endorsing the adaptation of the article nor should the article be modified in such a way as to damage the author's honour or reputation. If any changes have been made, such changes must be clearly indicated.

The author(s) must be appropriately credited and we ask that you include the end user license and a DOI link to the formal publication on ScienceDirect.

If any part of the material to be used (for example, figures) has appeared in our publication with credit or acknowledgement to another source it is the responsibility of the user to ensure their reuse complies with the terms and conditions determined by the rights holder.

Additional Terms & Conditions applicable to each Creative Commons user license:

CC BY: The CC-BY license allows users to copy, to create extracts, abstracts and new works from the Article, to alter and revise the Article and to make commercial use of the Article (including reuse and/or resale of the Article by commercial entities), provided the user gives appropriate credit (with a link to the formal publication through the relevant DOI), provides a link to the license, indicates if changes were made and the licensor is not represented as endorsing the use made of the work. The full details of the license are available at http://creativecommons.org/licenses/by/4.0.

CC BY NC SA: The CC BY-NC-SA license allows users to copy, to create extracts, abstracts and new works from the Article, to alter and revise the Article, provided this is not done for commercial purposes, and that the user gives appropriate credit (with a link to the formal publication through the relevant DOI), provides a link to the license, indicates if changes were made and the licensor is not represented as endorsing the use made of the work. Further, any new works must be made available on the same conditions. The full details of the license are available at http://creativecommons.org/licenses/by-nc-sa/4.0.

CC BY NC ND: The CC BY-NC-ND license allows users to copy and distribute the Article, provided this is not done for commercial purposes and further does not permit distribution of the Article if it is changed or edited in any way, and provided the user gives appropriate credit (with a link to the formal publication through the relevant DOI), provides a link to the license, and that the licensor is not represented as endorsing the use made of the work. The full details of the license are available at http://creativecommons.org/licenses/by-nc-nd/4.0. Any commercial reuse of Open Access articles published with a CC BY NC SA or CC BY NC ND license requires permission from Elsevier and will be subject to a fee.

Commercial reuse includes:

- Associating advertising with the full text of the Article
- Charging fees for document delivery or access
- Article aggregation
- Systematic distribution via e-mail lists or share buttons

Posting or linking by commercial companies for use by customers of those companies.

20. **Other Conditions**:

v1.10

THIS PAGE IS A BLANK PAGE

Copyright Notice

Thesis design by Salomon Narodden

Published by Salomon Narodden